JOINT EUROPEAN TORUS JET

JET JOINT UNDERTAKING

PROGRESS REPORT 1990

Volume I

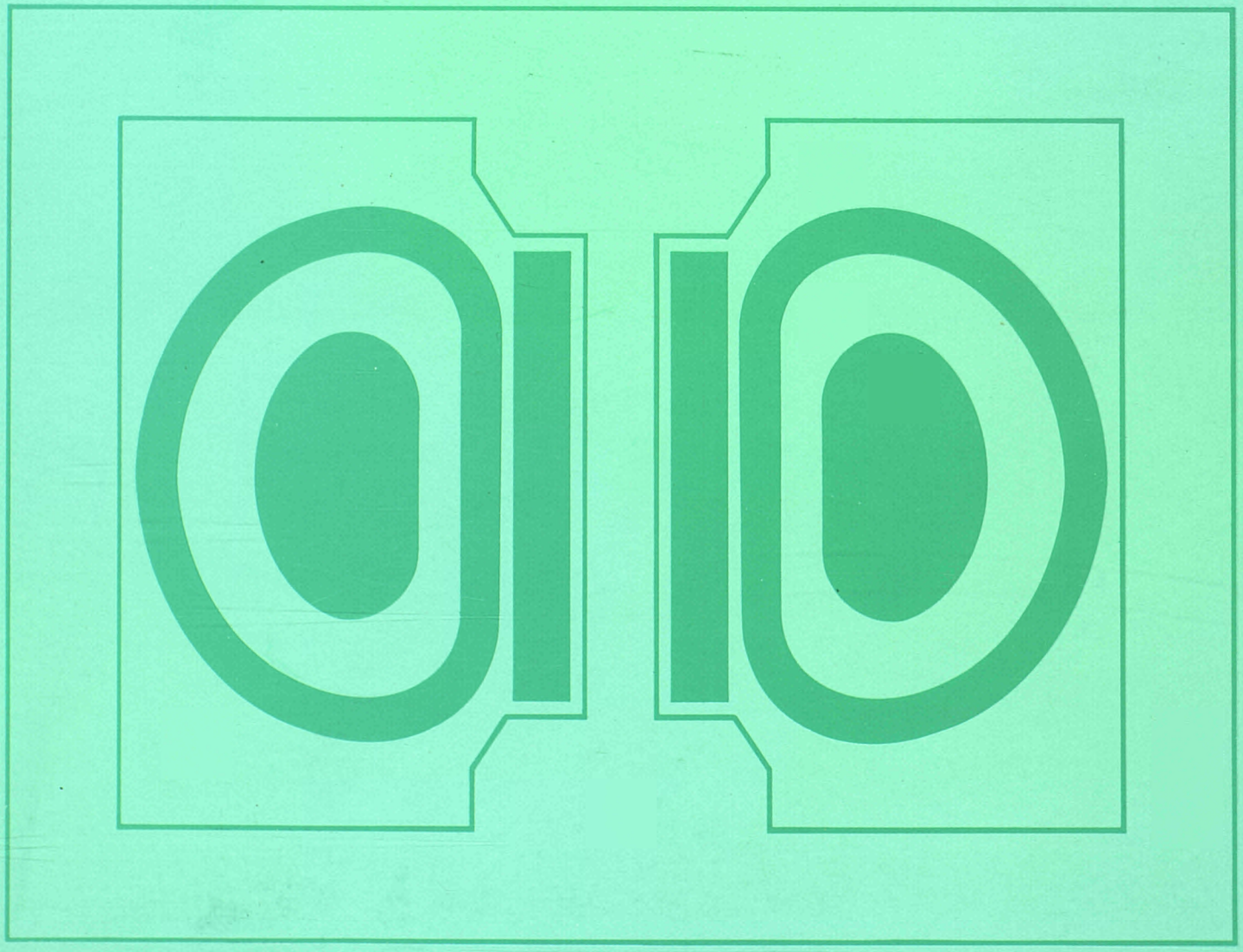

EUR 13493 EN
EUR-JET-PR8

JET JOINT UNDERTAKING

PROGRESS REPORT 1990

Volume I

March 1991

This document is intended for information only
and should not be used as a technical reference

EUR13493 EN (EUR-JET-PR8)March 1991.
Editorial work on this report was carried out by B.E.Keen.
The preparation for publication was undertaken by JET
Reprographic Service, JET Joint Undertaking, Abingdon, UK.

Catalogue number : CD-NA-13493-EN-C for the report EUR 13493 Volume I

Printed in England

Contents

Volume I

Volume II

Reprints of JET Papers

* Copies of these papers can be obtained from JET Publications Office, K1/1/20a, Ext. 4646

Foreword

This is the eighth of the JET Progress Reports, which provides an overview summary and puts into context the scientific and technical advances made on JET during 1990. In addition, the Report is supplemented by appendices of contributions (in preprint form) of the more important JET articles published during the year, which set out the details of JET activities.

This Report provides a more detailed account of JET's scientific and technical progress than that contained in the JET Annual Reports. It is aimed not only at specialists and experts engaged in nuclear fusion and plasma physics, but also to the more general scientific community. To meet these general aims, the Report contains a brief summary of the background to the Project, and describes the basic objectives of JET and the principal design aspects of the machine. In addition, the Project Team structure is included as it is within this structure that the activities and responsibilities for machine operation are carried out and the scientific programme is executed.

1990 proved to be another successful year for the Project. This period spanned the mid-stage of Phase III of the planned operational programme on Full Power Optimization Studies. The main aims of the experimental programme in 1990 were to improve plasma performance in operations with high reliability. This was carried out in material limiter configuration with currents up to 7MA with high energy content, and at up to 6MA in magnetic limiter plasmas, in order to exploit the high confinement H-mode regime of operations. Profile effects and related physics issues were also particular areas of study using RF, Neutral Beam and the prototype LHCD systems and using pellet injection.

Up to May 1990, the machine was in a scheduled shutdown period. The main tasks of the shutdown, which started in October 1989, were to replace a faulty toroidal field coil, install beryllium screens for the ICRF antennae and assemble the prototype Lower Hybrid launcher and waveguides. Following the successful replacement of the faulty toroidal field coil with a spare one, the re-assembly of the machine proceeded smoothly. One particularly critical operation was the rewelding of the internal strengthening rings of the vacuum vessel. Due to excellent preparation work, no particular difficulty was experienced and mechanical surveys confirmed that the vessel octant had been reassembled within 1-2mm of its original location. This was a major engineering achievement.

The shutdown from October 1989 to May 1990 involved work in two shifts, six days per week for about seven months. A total of 8000 man-hours was spent inside the beryllium-contaminated vessel. Throughout this period, there were no safety incidents involving beryllium. This must be considered a major success and a consequence of the considerable effort made at JET in both organisation and the provision of support teams and facilities for beryllium handling and contamination control. Between January and March 1990, in-vessel work was able to proceed without full protective suits. Face masks were found to be sufficient in view of the low residual beryllium contamination.

The experimental programme restarted in June 1990. Then, operation was mainly devoted to the introduction and exploitation of new facilities; further improvement in plasma performance; improvements in understanding key areas of tokamak physics (such as, particle and impurity transport; physics of the H-mode; energy transport and confinement; and experiments relevant to Next Step devices). Impurity control in JET, as for other long-pulse high power tokamaks, is of fundamental importance and therefore significant effort has been devoted to this area of study.

The number of pulses in 1990 was 2500 (compared with 2244 in 1989), bringing the total number of cumulative JET pulses to 23,530. A significant feature was the increasing number of discharges with plasma current exceeding 3MA, which for 1990, brought the cumulative total to about 7450.

A comparison between the current pulse distributions for 1989 and 1990 shows a continued movement to operation at higher current values in 1990 and a reduction in the number of low current values (<1 MA). In spite of the limited time available for operation, 1990 was a year in which high performance operation was repeatedly achieved and in which most systems performed satisfactorily. Of most concern were the in-vessel components which became damaged as a result of the large forces associated with disruptions during high performance plasma operation. Improvements in fixing such components will be carried out during 1991 and methods for improving the control of disruptions are being considered.

The successful operation of both the Octant No: 4 and Octant No:8 neutral beam injection systems was maintained throughout 1990, with high levels of both reliability and availability. Prior to the start of the operations programme, the conversion of the Octant No: 4 system to 140 kV was completed to give one injection system at 140 kV plus one at 80 kV. Although the change to 140 kV operation provided lower total power (7.8 MW compared with ~ 10.5MW at 80 kV), this was offset by enhanced beam penetration and, hence, more efficient heating of the central plasma region. Furthermore, the voltage of the Octant No: 8 system was progressively increased beyond its 80 kV design value to 85 kV, resulting in ~11.5 MW power without decrease in reliability. These modifications resulted in the record values for plasma parameters, achieved with NB heating in 1989, being marginally increased during the 1990 experimental campaign. The flexibility and usefulness of neutral particle injection was further enhanced by the successful use of Octant No:4 system to inject beams of ^{4}He and also of ^{3}He (at 120 kV) into the plasma during the final weeks of operation. This was advantageous in reducing the beam-plasma neutron production and eliminated the complication of measuring the thermonuclear neutron production.

The upgrading of the eight generators for the Radio Frequency (RF) heating systems was completed at the start of 1990 (3 MW to 4 MW each). RF power of 21 MW (for 1.75s) was subsequently coupled to the plasma, which was within 5% of the theoretical limit taking losses and reflection into account. A number of enhancements to the power plant and antennae system were commissioned during the year. Most notable was the use of a feedback system to automatically control the plasma position to maintain constant loading resistance despite L-mode to H-mode transitions. The enhancements combined with the beneficial effects of the new beryllium antennae increased the availability of high RF power and allowed important contributions to various aspects of the JET experimental programme.

In addition, the prototype lower hybrid current drive (LHCD) launcher compromising one third of the number of waveguides of the full system was tested and installed on the torus. The eight klystrons and associated drive, phase control and power transmission system were installed and commissioned, and the system used in operation during the experiment campaign. In the limited experimental and commissioning period, the prototype system operated at 1.5 MW for 20s and 1.6 MW for 10s. Initial coupling studies in X-point plasmas were performed. Useful data was obtained on assembly and operation of the system, which will be invaluable in the replacement by the full system.

The use of small pellets of solid deuterium is one of the possible methods of fuelling a fusion reactor. Experiments have been carried out with a multi-pellet injector which JET and the US Department of Energy (USDoE) have jointly installed and are jointly operating under the umbrella of the Bilateral Agreement on Fusion Research. Using 2.7 and 4mm deuterium pellets at speeds up to 1.4 x 10^3ms^{-1}, the injector was extensively used in experiments of all categories for various purposes of fuelling, and was particularly helpful in providing peaked density profiles for the Pellet Enhanced Performance (PEP) in the H-mode. A further pellet launcher has been developed to provide pellet speeds up to 4 x 10^3ms^{-1}, which should allow pellets to penetrate to the centre of a hot plasma at temperatures of a few keV. A prototype launcher is being installed ready for 1991 operation, in parallel with the existing pellet injector.

During the first few years of JET's operation, extensive areas of the torus walls, including the belt limiters, inner wall and X-point interaction regions, were covered with carbon tiles, and other surfaces were carbonized. Beryllium was introduced in 1989, first as a thin layer evaporated onto the carbon surfaces from four sources equally spaced around the torus mid-plane, and later with solid beryllium tiles on the belt limiters. Oxygen and carbon impurity concentrations in the plasma were strongly reduced, leading to lower Z_{eff} and higher fuel concentrations, n_D/n_e. Density control was previously a problem with all-carbon surfaces, but beryllium pumped both hydrogen and helium, giving better density control and the possibility of strong gas puffing to maintain a low edge temperature with reduced beryllium influx.

Operating experience in 1990 confirmed the benefits in terms of lower Z_{eff} and higher n_D/n_e, in using beryllium as

a first wall material. The replacement of nickel by beryllium on the ICRF antennae screens has allowed an extension in the operational range of H-mode with ICRF heating in both dipole and monopole antennae configurations. Further improvement to ICRF heating in the X-point configuration was obtained with a new position feedback system that maintained a constant plasma coupling impedance. This was effective in allowing high ICRF power (up to 10MW) to be maintained throughout the transition from L to H-mode. H-modes with ICRF heating now have confinement properties comparable to those with neutral beam heating

The change from graphite to beryllium for the lower X-point protection tiles was carried out by using tiles originally intended for the ICRF antennae frames. H-mode discharges were obtained with similar power thresholds and comparable confinement properties to discharges on the upper set of carbon tiles. However, a quantitative comparison between H-modes with carbon and beryllium X-point operation, prevented subsequent establishment of H-modes on the damaged tiles. As with carbon as a first wall material, high performance pulses with beryllium are terminated by an impurity "bloom". This confirms the need for active impurity control to sustain pulses in reactor relevant conditions.

Operating experience during 1990 indicated that, with the higher levels of plasma purity and performance being achieved, larger mechanical forces are acting on the wall protection tiles during disruptions and vertical instabilities. These forces result from currents flowing in the poloidal directions along the rails or plates used to support the tiles and have damaged mechanical support and brought protection tiles out of alignment causing some tiles to fracture or detach. Measures are being taken to strengthen the supports and accommodate these forces.

Another feature of 1990 operation was the demonstration of Helium neutral beam injection. Up to 5MW of ^{3}He and 7MW of ^{4}He at 120keV have been injected into 5MA limiter and 3.5MA double-null plasmas for up to 3s. Although a low level of localized heating was observed on the lower belt limiter, there were no indications of serious problems such as increased impurities or limiter heating due to the ionization of metastable neutrons in the beam. Beam penetration at these energies was excellent over the typical range of plasma densities. Preliminary results show that stored plasma energy and global energy confinement with He beams are comparable to those with D beams. The elimination of beam-beam and beam-plasma reactions resulted in significant reductions in neutron yield, which was advantageous in reducing vessel activation and in permitting a more direct interpretation of neutron diagnostic measurements of thermal neutrons.

He beam injection has been used as a precise particle source to simulate alpha-particle diffusion in L- and H-modes. The time and space resolved profiles of helium densities showing the evolution of the injected helium and the subsequent recycling have been measured. In L-mode discharges, the central helium density decayed promptly after the helium source was switched-off. In H-mode discharges, the helium concentration decreased more slowly and in some cases accumulated in the plasma core.

During 1990, substantial progress was made towards reaching reactor conditions, in that very high values of the fusion product ($n_i\tau_E T_i$) of ~9×10^{20}m^{-3}keVs were achieved. These high values were obtained within an H-mode X-point configuration; both with a hot-ion H-mode and with a Pellet Enhanced Performance (PEP) H-mode. The neutron yield for this hot-ion discharge was the highest ever achieved on JET at 3.8×10^{16}ns^{-1}, producing 50kW of fusion power with a $Q_{DD} = 2.5\times10^{-3}$. A full D-T simulation of this pulse showed that ~13MW of fusion power could have been obtained transiently with the 18MW of injected NB power, giving a fusion product value ($n_i\tau_E T_i$), which was within a factor of 5-8 of that required in a D-T reactor. In addition, fusion powers of ≈140kW were measured from the D-^{3}He fusion reaction. These experiments used ion cyclotron heating of the ^{3}He minority and best results were obtained with low ^{3}He concentrations admitted by gas puffing.

Other aspects of improved plasma performance, resulting largely from reduced impurity levels included:

- more efficient pumping and improved density control permitted low density and high temperature (up to 30keV) operation for times exceeding 1s;
- increased density limits lead to a record peak density of 4×10^{20}m^{-3};
- sawteeth oscillations were stabilised for periods exceeding 7.5s.

The plasma temperatures, plasma densities and confinement times obtained in JET, have now reached individually those needed in a reactor, but not simultaneously. JET is the only machine in the world to have reached this stage. However, these impressive results were achieved in a transient state and could not be sustained in the steady state. Ultimately, the influx of impurities caused a degradation in plasma parameters. However, by virtue of its size, its plasma performance and its long pulse capability, JET is in a unique

position to address the problem of impurity control in the basic geometry for the next step tokamak. Consequently, a new phase is planned for JET to demonstrate effective methods of impurity control in operating conditions close to those of a next step tokamak in an axi-symmetric pumped divertor configuration. The objectives of the pumped divertor in JET are to control impurities in the plasma, decrease the heat load on the target plates, control the plasma density, and demonstrate exhaust capabilities.

The schedule for the JET programme in the new phase should allow for a pump divertor in JET in 1992. To provide time for the new phase, the use of tritium in JET would be postponed until the end-1994. At this stage, all information on particle transport, exhaust and fuelling, first wall requirements and enhanced confinement regimes needed to construct the next step, should be available. Final tests with tritium, including alpha-particle heating studies could be performed in the two years following, leading to the completion of the JET programme by end 1996. The JET Council agreed the proposed prolongations on JET. In addition, a European Fusion Programme Evaluation Board (under the Chairmanship of Prof. U. Colombo) strongly supported the extension of the JET Project. A final decision of the Council of Ministers is awaited.

Much of JET's efforts during 1990 has been directed to preparations for the future, in particular to pursuing in parallel the two programme paths:

- preparations for the new pumped divertor phase in the frame of a proposed programme to 1996;
- completion of a JET programme by the end of 1992 with the final phase of tritium operations.

In the context of preparing for D-T operations, installation of the main sub-systems of the active gas handling system has proceeded as the components have been delivered and sub-system commissioning has started. Some important components have suffered delays and this has put back the date at which overall plant process commissioning can start. At present, it is still considered possible to undertake a limited campaign of D-T operations before the end of 1992. At the same time, the Project has pressed ahead strenuously with design and procurements for the new pumped divertor phase. The design of the main components - the divertor elements and the internal coils - evolved during the course of the year. The Project has been able to maintain the dual programme stance required pending the decision of the Council of Ministers on a revised Fusion Programme and in particular on the proposed prolongation of the JET Programme. However, this position cannot be maintained during 1991 for both programmatic and resource reasons.

JET is also providing an important input into the collaboration on the International Thermonuclear Experimental Reactor (ITER) Project. The ITER Conceptual Design Activities (CDA) were completed in December 1990 and JET is involved in a European Study Group set up to look at the proposal for a next phase of Experimental Design Activity (EDA) comprising a single machine. It is the JET view that a single Next Step facility (ITER) is a high risk strategy in terms of physics, technology and management, since it does not provide a sufficiently sound foundation for a demonstration reactor (DEMO). A Next Step Programme is proposed, which could comprise several complementary facilities, each optimised with respect to specific clear objectives. In a minimum programme, there could be two Next Step tokamaks, and a Materials Test Facility. Such a programme would allow division of effort and sharing of risk across the various scientific and technical problems, permit cross comparison and ensure continuity of results. It could even be accomplished without a significant increase in world funding. JET management has publicly expressed its opinion that the best way forward for Europe could be for it to take the lead in building the core of a fusion reactor as one of several complementary devices in the frame of a coherent world ITER programme.

The most impressive advances made so far by JET are a tribute to the dedication and skill of all those working on the Project. They also reflect the continuous co-operation and assistance received from the Associated Laboratories and from the Commission of the European Communities. I am confident that with such dedication of the staff and the support and guidance of the JET Council, JET Scientific Council and the JET Executive Committee, the Project will be able to meet all likely challenges to be encountered in future years and contribute substantially to crucial information for Next Step devices on the route to a fusion reactor.

Dr. P-H. Rebut
Director
March 1991

Introduction, Background and Report Summary

Introduction

JET Progress Reports are aimed both at specialists in plasma physics and nuclear fusion research and at the more general scientific community. This contrasts with the JET Annual Reports, which provide overview descriptions of the scientific, technical and administrative status of the JET programme, and is directed to the average member of the public.

To meet these general aims, the Progress Report contains a brief summary of the background to the Project, describes the basic objectives of JET and sets out the principal design aspects of the machine. In addition, the Project Team structure is detailed, since it is within this framework that machine activities and responsibilities are organized and the scientific programme is executed.

The main part of the 1990 Report provides overview summaries of scientific and technical advances made during the year, supplemented by appendices of detailed contributions (in preprint form) of the most important JET scientific and technical articles produced during the year. The final part of the Report briefly sets out developments underway to further improve JET's performance and plans for future experiments through to its foreseen completion.

Background

Objectives of JET

The Joint European Torus (JET) is the largest single project of the nuclear fusion research programme of theEuropean Atomic Energy Community (EURATOM). The project was designed with the essential objectives of obtaining and studying plasma in conditions and with dimensions approaching those needed in a fusion reactor.

The studies are aimed at:

(a) investigating plasma processes and scaling laws, as plasma dimensions and parameters approach those necessary for a fusion reactor;

(b) examining and controlling plasma wall interactions and impurity fluxes in near reactor conditions;

(c) demonstrating effective heating techniques (particularly, RF and Neutral Beam Heating), capable of approaching reactor temperatures in JET, in the presence of the prevailing loss processes;

(d) studying alpha particle production, confinement and subsequent plasma interaction and heating produced as a result of fusion between deuterium and tritium.

Two of the key technological issues in the subsequent development of a fusion reactor are faced for the first time in JET. These are the use of tritium and the application of remote maintenance and repair techniques. The physics basis of the post JET programme will be greatly strengthened if other fusion experiments currently in progress are successful. The way should then be clear to concentrate on the engineering and technical problems involved in progressing from an advanced experimental device like JET to a prototype power reactor.

Basic JET Design

To meet these overall aims, the basic JET apparatus was designed as a large tokamak device with overall dimensions of about 15m in diameter and 12m in height. A diagram of the apparatus is shown in Fig.1 and its principal parameters are given in Table I. At the heart of the machine, there is a toroidal vacuum vessel of major radius 2.96m having a D shaped cross section 2.5m wide by 4.2m high. During operation of the machine, a small quantity of gas (hydrogen, deuterium or tritium) is introduced into the vacuum chamber and is heated by passing a large current through the gas. Originally, the machine was designed to carry 4.8MA, but

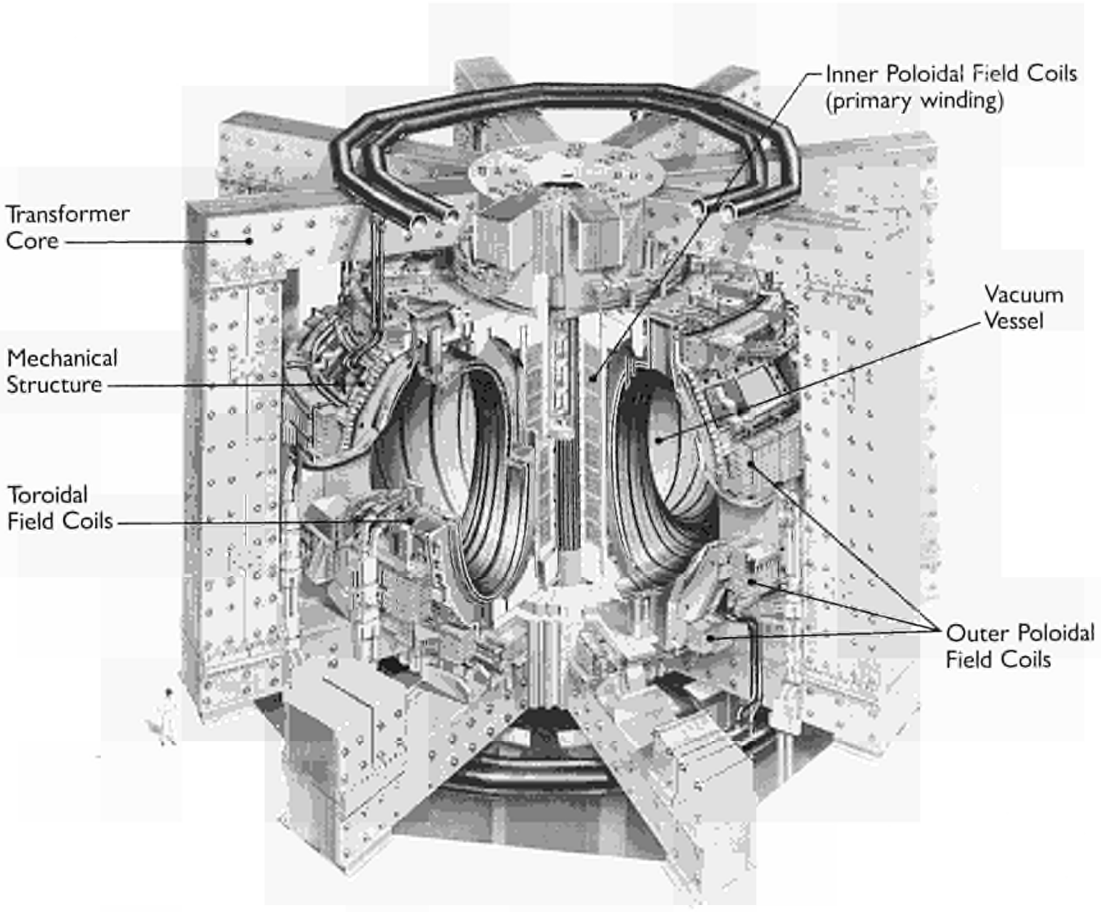

Fig.1 Diagram of the JET Tokamak.

Table I
Principal Parameters

Parameter	*Value*
Plasma minor radius (horizontally), a	1.25m
Plasma minor radius (vertically), b	2.10m
Plasma major radius, R_0	2.96m
Plasma aspect ratio, R_0/a	2.37
Plasma elongation ratio , ε=b/a	1.68
Flat top pulse length	25s
Toroidal magnetic field (plasma centre)	3.45T
Plasma current, D shaped plasma	7.0MA
Volt-seconds available	42Vs
Toroidal field peak power	380MW
Additional heating power (into torus)	~ 50MW
Weight of vacuum vessel	108t
Weight of toroidal field coils	364t
Weight of iron core	2800t

has already been modified to achieve 7MA. This current is produced by transformer action using the massive eight limbed magnetic circuit, which dominates the apparatus (see Fig.1). A set of coils around the centre limb of the magnetic circuit forms the primary winding of the transformer with the plasma acting as the single turn secondary. Additional heating of the plasma is provided by propagating and absorbing high power radio frequency waves in the plasma and by injection beams of energetic neutral atoms into the torus.

The plasma is confined away from the walls of the vacuum vessel by a complex system of magnetic fields, in which the main component, the toroidal field, is provided by 32 D shaped coils surrounding the vacuum vessel. This field, coupled with that produced by the current flowing through the plasma, forms the basic magnetic field for the

tokamak confinement system, which provides a full design field at the plasma centre of 3.45T. The poloidal coils, positioned around the outside of the vacuum vessel, shape and position the plasma in operation.

Initial experiments have been undertaken using hydrogen and deuterium plasmas, but in the later stages of the operation, it is planned to operate with deuterium tritium plasmas, so that fusion reactions can occur to produce significant a particle heating in the plasma.

In order to reach conditions close to those relevant to a fusion reactor, a plasma density of ~$10^{20}m^{-3}$ at a temperature of 10^{20}keV would be needed. Even with a current of up to 7MA in JET, this would be inadequate to provide the temperature rquired using ohmic heating alone. Consequently, additional heating is required and two main systems are being used at JET, as follows:

- Injection into the plasma of highly energetic neutral atoms (Neutral Injection Heating);
- Coupling of high power electromagnetic radiation to the plasma (Radio Frequency (RF) Heating).

The total power into the torus will increase in discrete steps up to ~50MW.

Project Team Structure

The Project structure adopted, for management purposes, is divided into four Departments (see Table II):

- Machine and Development Department;
- Experimental and Theory Department;
- Heating and Operations Department;
- Administration Department.

In addition, some scientific and technical duties are carried out within the Directorate and in the Coordinating Staff Unit.

The main duties of the Administration Department have been described in previous JET Annual Reports. This Report concentrates on progress made in the scientific and technical areas during 1990. To aid this description, the functions of these Departments are described below.

Machine and Development Department

The Machine and Development Department is responsible for the performance capacity of the machine as well as equipment for the active phase, together with enhancements directly related to it (excluding heating) and the integration of any new elements on to the machine. In addition, the

Table II
JET Departmental and Divisional Structure

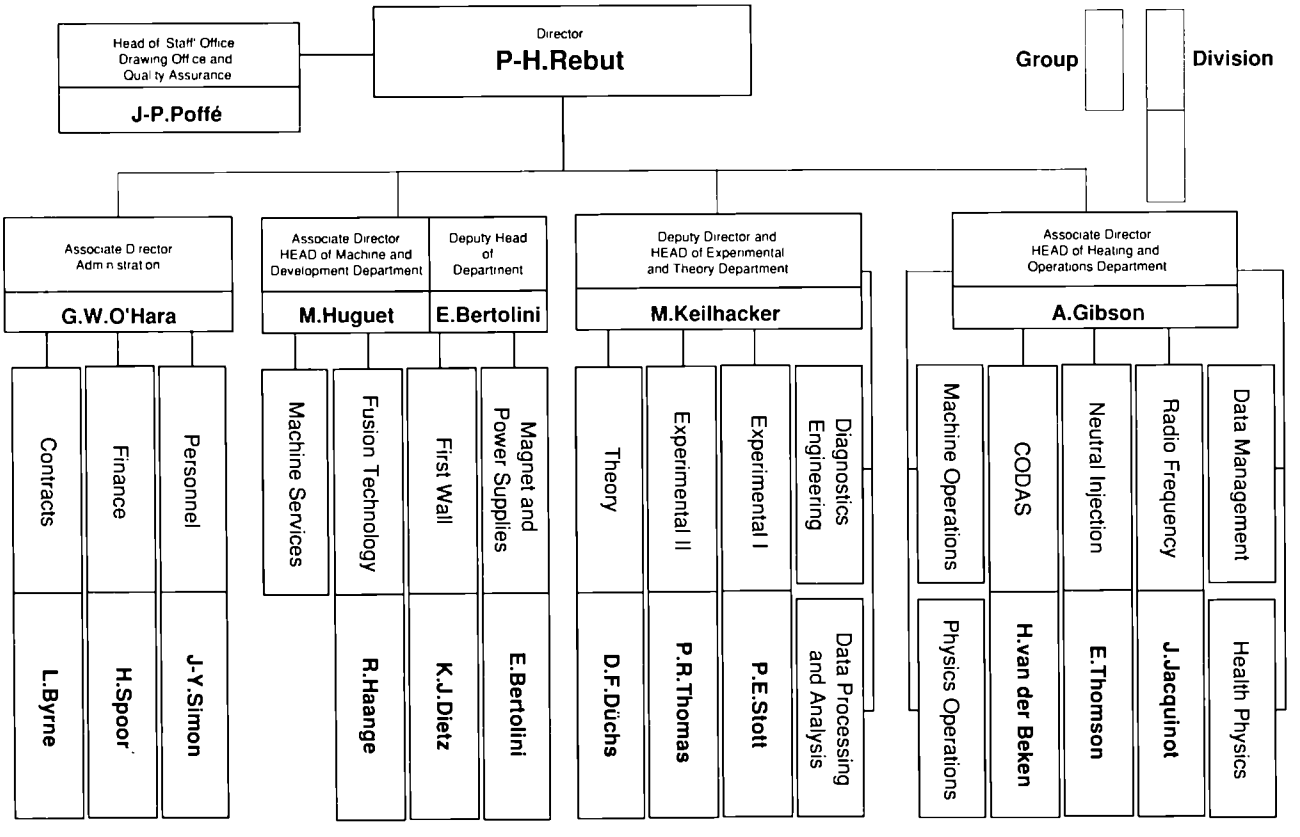

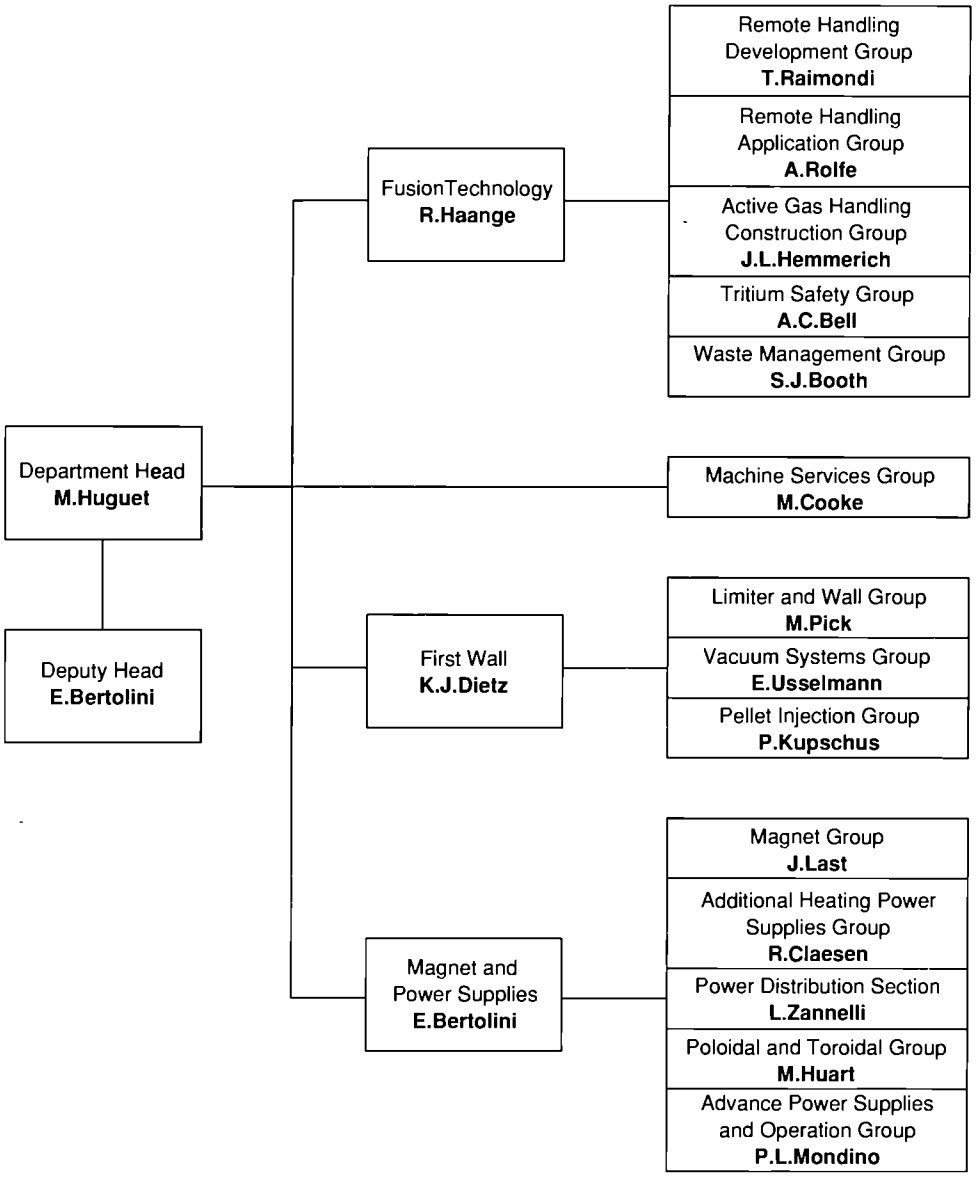

Fig.2: Machine and Development Department, Group Structure (December 1990)

Department is responsible for machine services. The Department contains three Divisions:

(a) Magnet and Power Supplies Division is responsible for the design, construction, installation, operation and maintenance of the tokamak electromagnetic system and of plasma control. The area of responsibility encompasses the toroidal, poloidal and divertor magnet, the mechanical structure, the methods for controlling plasma position and shape and all power supply equipment needed for magnets, plasma control, additional heating and auxiliaries;

(b) First Wall Division, which is responsible for the vital area of plasma wall interactions. Its main tasks include the provision and maintenance inside the vacuum vessel of conditions leading to high quality plasma discharges. The Division develops, designs, procures and installs first wall systems and components, such as limiters, wall protections and internal pumping devices. The area of responsibility encompasses the vacuum vessel as a whole, together with its associated systems, such as pumping, bakeout and gas introduction;

(c) Fusion Technology Division, which is responsible for the design and development of remote handling methods and tools to cope with the requirements of the JET device, and for maintenance, inspection and repairs. Tasks also include the design and construction of facilities for handling tritium.

MACHINE AND DEVELOPMENT DEPARTMENT
Head of Department: M. Huguet
Deputy Head of Department: E. Bertolini

D. Carre
Mrs. H. Marriott
S. McLaughlin
C. Sborchia

MAGNET AND POWER SUPPLIES DIVISION
Head: E. Bertolini

P. Bertoldi
T. Bonicelli
O. Buc
D. Chiron
C. Christodoulopoulos
R. Claesen
E. Daly
N. Dolgetta
P. Doyle
H.T. Fielding
C. Folco
M. Garriba
J. Goff
D. Halliwell
M. Huart
F. Jensen
J.R. Last
H. McBrian
J. McKivett
V. Marchese
G. Marcon
L. Mears
P. Mondino
G. Murphy
Mrs. J. Nolan
P. Noll
R. Ostrom
P. Presle
A. Santagiustina
G. Sannazzaro
S. Shaw
R. Suter
M. Tabellini
A. Tesini
S. Turley
J. van Veen
C.R. Wilson
G.C. Wilson
L. Zannelli

FUSION TECHNOLOGY DIVISION
Head: R. Haange

A.C. Bell
G. Benali
S.J. Booth
P. Brown
T. Businaro
C.J. Caldwell-Nichols
Mrs. J. Campbell
P. Chuilon
R. Cusack
F. Delvart
L. Galbiati
A. Galetsas
J. Gowman
J.L. Hemmerich
Mrs. M.E. Jones
L.P.D.F. Jones
J.F. Jaeger
J.G. Junger
A. Konstantellos
E. Küssel
R. Lässer
M. Laveyry
Miss J. Lech
A. Loving
J. Lupo
J. Mart
P. Milverton
G. Newbert
A. Nowak
T. Raimondi
K.D. Walker
M. Wykes

FIRST WALL DIVISION
Head: K.J. Dietz

W.P. Bailey
S. Bryan
H. Buttgereit
C. Celentano
Mrs. D. Cranmer
W. Daser
E. Deksnis
D. Flory
C. Froger
M. Gadeberg
D. Holland
Mrs. I. Hyde
G. Israel
H. Jensen
P. Kupschus
E. Martin
P. Macklin
A. Miller
J. Orchard
A. Peacock
M. Pick
L. Rossi
S. Scott
T. Szabo
R. Thomas
E. Usselmann
M. Watson
T. Winkel

Fig.3: Project Team Staff in Machine and Development Department (December 1990)

The Structure of the Machine and Development Department to Group Leader level is shown in Fig.2 and the list of staff within the Department is shown in Fig.3.

Experimental and Theory Department

The main functions of the Department relate to the measurement and validation of plasma parameters and to the theory of tokamak physics. The main tasks are:

- to conceive and define a set of coherent measurements;
- to be responsible for the construction of necessary diagnostics;
- to be responsible for the operation of the diagnostics

and the quality of measurements and the definition of the plasma parameters:

- to follow the theory of tokamak physics;
- to play a major role in interpretation of data.

The Department contains two Groups (Diagnostics Engineering Group and Data Processing and Analysis Group) and three Divisions:

(a) Experimental Division 1 (ED1), which is responsible for specification, procurement and operation of approximately half the JET diagnostic systems. ED1 undertakes electrical measurements, electron temperature measurements, surface and limiter physics and neutron diagnostics;

(b) Experimental Division 2 (ED2), which is responsible for specification, procurement and operation of the other half of the JET diagnostic systems.ED2 undertakes all spectroscopic diagnostics, bolometry, interferometry, the soft X ray array and neutral particle analysis;

(c) Theory Division, which is responsible for prediction by computer simulation of JET performance, interpretation of JET data and the application of analytic plasma theory to gain an understanding of JET physics.

The structure of the Experimental and Theory Department to Group Leader level is shown in Fig.4 and the list of staff in the Department is shown in Fig.5.

Heating and Operations Department

Heating and Operations Department is responsible for heating the plasma, the organisation of experimental data, and the day to day operation of the machine. The main functions of the Department are:

- heating the plasma and analysis of its effects;
- centralising the interpretation of experimental results and investigating their coherence;
- organising data acquisition and computers;
- preparing and co ordinating operation of the machine across the different Departments.

The Department is composed of four groups (Machine Operations Group, Physics Operation Group, Health Physics Group and Data Management Group) and three Divisions:

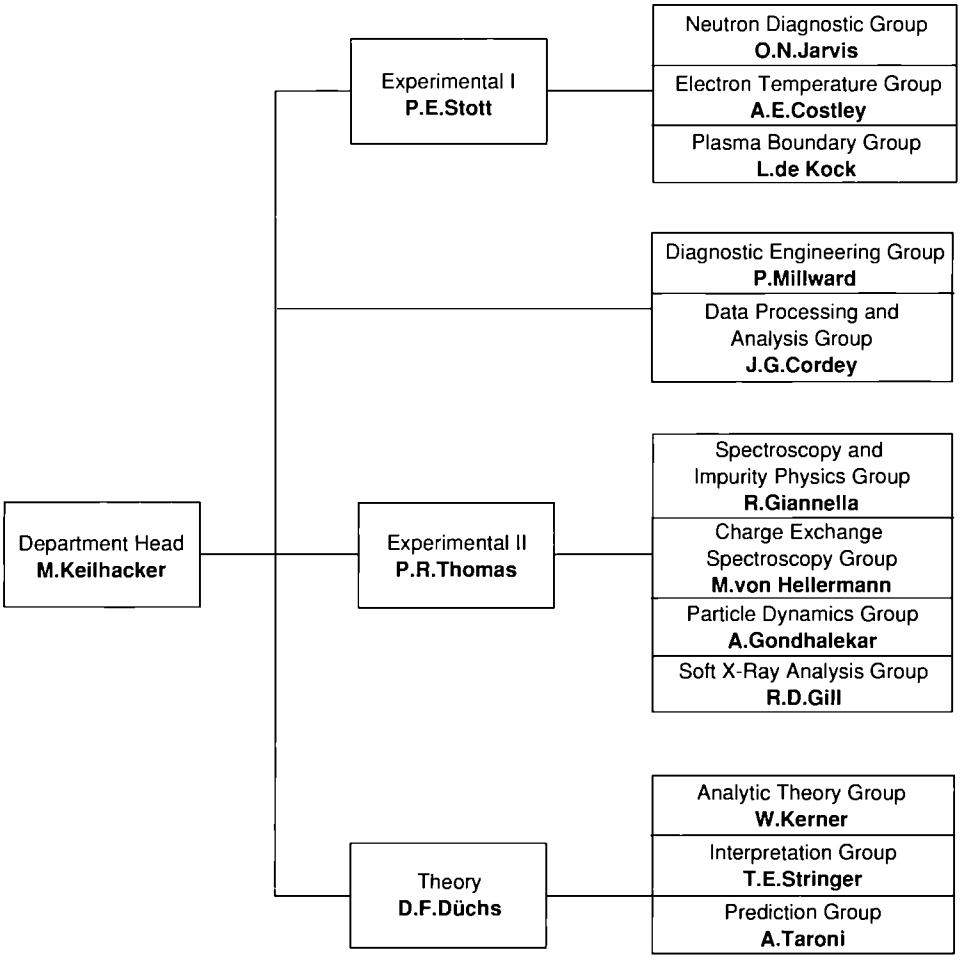

Fig.4: Experimental and Theory Department, Group Structure (December 1990)

EXPERIMENTAL AND THEORY DEPARTMENT

Head of Department: M. Keilhacker

B. Balet
M. Barnes
K. Blackler
J. Christiansen
J.G. Cordey
C.J. Hancock
J. Hoekzema
J.P. Jéral
P. Millward
M.E. Mynarends
D. O'Brien
R. Oord
J. Reid
P.J. Roberts
Miss K. Slavin
Mrs. P. Stubberfield
K. Thomsen
Mrs. R. Thormaehlen
A. Tiscornia
E. van der Goot
G. Vlases
D. Ward
J. Wesson
C.H. Wilson
D. Wilson

EXPERIMENTAL DIVISION I

Head: P.E. Stott

Miss N. Avery
D. Bartlett
B.W. Brown
D. Campbell
S. Clement
E. Clipsham
J.P. Coad
A.E. Costley
J. Ehrenberg
L. de Kock
J. Fessey
C. Gowers
Mrs. M. Harper
P.J. Harbour
M. Hone
I. Hurdle
O.N. Jarvis
B. Laundy
M. Loughlin
F. Marcus
G. Neill
C. Nicholson
P. Nielsen
H. Oosterbeek
R. Prentice
G. Sadler
G. Sips
A. Stevens
D. Summers
P. van Belle
J. Vince

EXPERIMENTAL DIVISION II

Head: P.R. Thomas

K. Bell
G. Braithwaite
J.L. Bonnerue
S. Corti
G.B. Denne-Hinnov
A. Edwards
Mrs. A. Flowers
R. Giannella
R. Gill
A. Gondhalekar
N. Gottardi
D. Halton
J. Holm
H. Jaeckel
G. Janeschitz
R. Konig
L. Lamb
G. Magyar
J.L. Martin
P. Morgan
H. Morsi
R. Reichle
J. O'Rourke
J. Ryan
D. Pasini
M. Stamp
M. von Hellermann
B. Viaccoz

THEORY DIVISION

Head: D.F. Düchs

W. Core
Mrs. S. Costar
L. Eriksson
A. Galway
Mrs. S. Hutchinson
B. Keegan
W. Kerner
F. Porcelli
H.C. Sack
R. Simonini
E. Springmann
T.E. Stringer
A. Taroni
F. Tibone
W. Zwingmann

Fig.5: Project Team Staff in Experimental and Theory Department (December 1990)

(a) Control and Data Acquisition System Division (CODAS), which is responsible for the implementation, upgrading and operation of computer based control and data acquisition systems for JET;

(b) Neutral Beam Heating Division, which is responsible for the construction, installation, commissioning and operation of the neutral injection system, including development towards full power operation of the device. The Division also participates in studies of the physics of neutral beam heating;

(c) Radio Frequency Heating Division, which is responsible for the design, construction, commissioning and operating

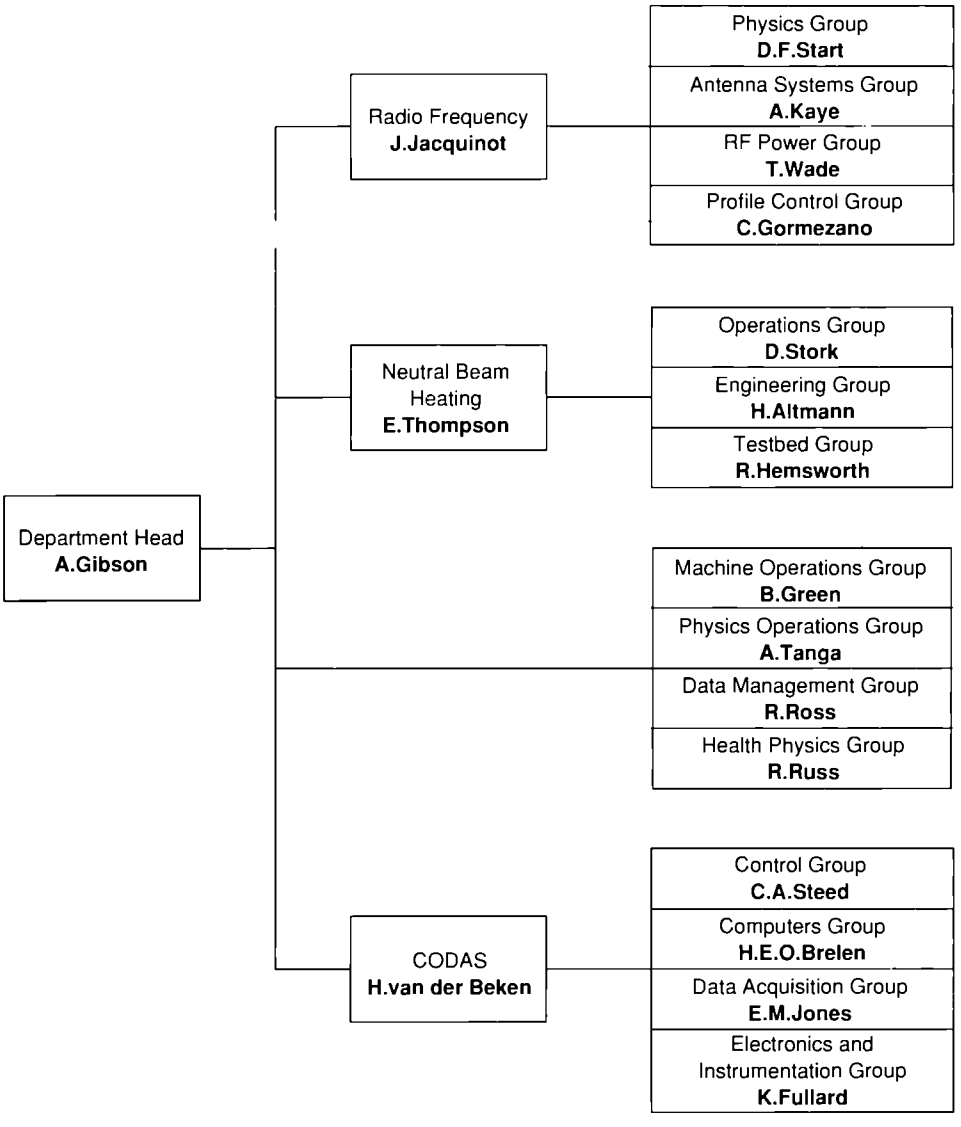

Fig.6: Plasma Heating and Operations Department, Group Structure (December 1990)

the RF heating system during the different stages of its development to full power. The Division also participates in studies of the physics of RF heating.

The structure of the Heating and Theory Department to Group Leader level is shown in Fig.6, and the list of staff in the Department is shown in Fig.7.

In addition, all Divisions are involved in:

- execution of the experimental programme;
- interpretation of results in collaboration with other appropriate Divisions and Departments;
- making proposals for future experiments.

Directorate

Within the Directorate are one scientific and one technical group, (Scientific Assistants to the Director and Technical Assistant to the Director (including Publications Group)), whose main tasks are as follows:

- Scientific Assistants to the Director, who assist and advise the Director on scientific aspects of JET operation and future development;
- Technical Assistant to the Director, who assists and advises the Director on organizational and technical matters related to JET operation. He also acts as JET Publications Officer, and is Leader of the Publications Group.

Coordinating Staff Unit

The Coordinating Staff Unit is responsible for the provision of engineering services to the Project and for the

PLASMA HEATING AND OPERATION DEPARTMENT

Head of Department: A. Gibson

K. Adams
A. Conway
D. Cook
S. Cooper
T. Dale
P. Gaze
B. Green
N. Green
R. Greenfield
C. Hookham
J. How
M. Hughes
M. Johnson
Mrs. J. Keene
P. Lomas
Mrs. P. Longworth
C. Lowry
M. Macrae
D. Pratt
R. Rigley
Mrs. J. Roberts
R.T. Ross
P. Rutter
G. Saibene
Miss D. Samuel
R. Sartori
P. Smeulders
W. Smith
A. Tanga
B. Tubbing
M. Walker
M. Wallwork
J.M. Watt
B. Workman

NEUTRAL BEAM HEATING DIVISION

Head: E. Thompson

H. Altmann
A. Bickley
A. Browne
C.D. Challis
D. Cooper
J.F. Davies
G. Deschamps
A. Dines
H.P.L. de Esch
D. Ewers
H. Falter
R. Hemsworth
Mrs. S. Humphreys
D. Hurford
J.Z. Jensen
T.T.C. Jones
F. Long
J.G. Lundqvist
D. Martin
P. Massmann
C. Mayaux
Mrs. D. Noyes
W. Obert
S. Papastergiou
A.J. Parfitt
D. Raisbeck
D. Stork
L. Svensson
J. Waterhouse

RADIO FREQUENCY HEATING DIVISION

Head: J. Jacquinot

V. Bhatnagar
S.C. Booth
G. Bosia
M. Brandon
H. Brinkschulte
M. Brusati
M. Bures
Miss M. Casson
G. Cottrell
P. Crawley
T. Dobbing
D.T. Edwards
A. Franklin
M. Gammelin
B. Glossop
C. Gormezano
R. Horn
G. Jessop
A. Kaye
M. Lennholm
P. Murray
M. Pain
J. Plancoulaine
F. Rimini
P. Schild
M. Schmid
Ms. V. Shaw
A. Sibley
D. Start
C. Steele
T. Wade
C. Walker

CONTROL AND DATA ACQUISITION SYSTEMS DIVISION

Head: H. van der Beken

M.B. Baronian
Mrs. A.M. Bellido
M.J.M. Botman
H.E.O. Brelen
W.J. Brewerton
Mrs. L. Brookes
T. Budd
P.J. Card
J.J. Davis
S. Dmitrenko
S.E. Dorling
K. Fullard
R.F. Herzog
Mrs. F. Herzog
E.M. Jones
F.J. Junique
G.J. Kelly
N.G. Kidd
J.G. Krom
D.S. Nassi
C. Perry
C.A. Steed
G. Wolfers
I.D. Young

Fig.7. Project Team Staff in Plasma Heating and Operation Department (December 1990)

implementation of specific coordinating tasks at the Project level.

It comprises four Groups:

- Technical Services Group;
- Planning Group;
- Drawing Office;
- Quality Assurance Group.

The structure of the Directorate and Coordinating Staff Unit to Group Leader level is shown in Fig.8 and the list of staff in these areas is shown in Fig.9.

Report Summary

The first section of this Report provides a brief introduction and background information relevant to the Report. The second and third sections set out an overview of progress on JET during 1990 and with a survey of scientific and technical achievements during 1990 sets these advances in their general context. This summary is specifically cross referenced to reports and articles prepared and presented by JET staff during 1990. The more important of these articles, which are

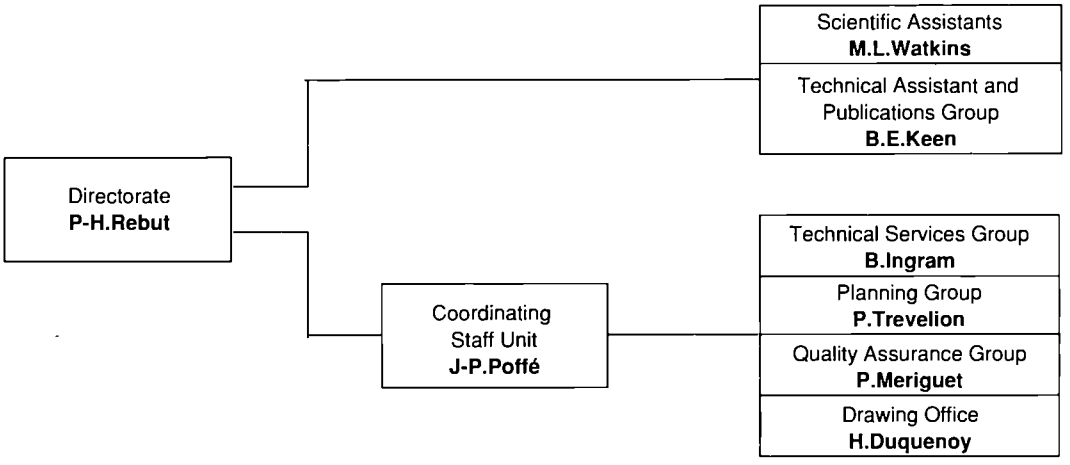

Fig.8: Directorate and Coordinating Staff Unit, Group Structure (December 1990)

DIRECTORATE AND COORDINATING STAFF UNIT
Director: Dr. P-H. Rebut

DIRECTORATE

Mrs. S-J. Ashwood	N.J. Hawkins	K. Musgrave
Mrs. G. Blackenback	M. Hugon	T. O'Hanlon
D. Boucher	Mrs. A. Kalmus	Mrs. C. Simmons
Mrs. R. Dietrich	B.E. Keen	Ms. M. Straub
M. Drew	J. McMahon	Mrs. J. Talbot
D. Gambier	J.H.C. Maple	M.L. Watkins
Miss C. Hampson	S. Morris	Miss C. Weaver

COORDINATING STAFF UNIT
Head: J-P. Poffè

Ms. L. Ashby	J.A. Green	P. Meriguet
P. Barker	M. Guillet	J. McDonald
G. Dalle-Carbonare	Mrs. E. Harries	H. Panissie
N. Davies	F. Hurd	Mrs. J. Reid
H. Duquenoy	B. Ingram	R. Smith
Ms. D. Field	H. Jones	P. Trevalion
A. Girard	Miss K. Luker	C. Woodward

Fig.9: Project Team Staff in Directorate and Coordinating Staff Unit (December 1990)

of general interest, are reproduced as appendices to this Report.

The fourth section is devoted to future plans and certain developments which might enable enhancements of the machine to further improve its overall performance. Some attention has been devoted to methods of surmounting certain limitations and these are detailed in this section.

The Appendices contain a list of work topics carried out under Task Agreements with various Association Laboratories, and selected articles prepared by JET authors are reproduced in detail, providing some details of the activities and achievements made on JET during 1990. In addition, a full list is included of all Articles, Reports and Conference papers published by JET authors in 1990.

Technical Achievements during 1990

Introduction

From October 1989 to May 1990, the machine was in a scheduled shutdown in order to carry out a number of main tasks as follows:

- removal of Octant No.3, replacement of a faulty toroidal field coil and reinstallation of Octant No.3 systems;
- modification of the toroidal field coil cooling loop and introduction of an organic fluid (freon) as a more effective coolant;
- lower X-point carbon dump plates changed to beryllium tiles to reduce carbon impurities during H-mode operation;
- installation of Beryllium ICRF antennae screens to eliminate nickel impurities in the plasma;
- installation of prototype Lower Hybrid Wave system to test effectiveness of current drive (LHCD);
- one Neutral Beam box was changed from 80kV to 140kV D operation to improve beam penetration and increase ion heating. Subsequently, one box converted to He operation (at 120kV) to reduce neutron production.

Machine operation took place from May to November with an interruption of four weeks in August due to an outage of the high voltage power grid for planned maintenance by the Generating Board. Operation was concluded by the end of November, as planned, and the machine again entered a shutdown period to install the dump plates for X-point operation. The dump plates will carry beryllium tiles in the vicinity of the bottom X-point and graphite (CFC) tiles at the top X-point. By the end of December 1990, the lower dump plates were installed and preparatory work started for fitting the upper dump plates.

The following sections detail the technical achievements made during this period.

Torus Systems

Introduction

Activities during 1990 were shared between carrying out maintenance and installation work during the earlier 1989-90 shut-down; provision of services for the subsequent machine operation (vacuum system, wall conditioning, gas introduction and pellet injection); activities related to the design and the procurement of components for the pumped divertor; procurement, test and installation of components for the high-speed pellet Prototype Launcher; and preparation work for the installation of upper and lower X-point dump plates during the later shut-down (started in November 1990).

In-vessel components

The new wall elements which were introduced into the vessel during the earlier shut-down were beryllium X-point target plates at the bottom of the vacuum vessel. Thirty two segments 200 mm wide and 800 mm long were installed (Fig. 10). Due to the narrow width of a few mm of the X-point strike points, their power handling capability was low (eg. 5MW for 1s) but it was anticipated that by tailoring the gas feed during discharges higher loads could be accommodated. However, during the experimental campaign, due to problems with inner wall protection, there did not remain sufficient time to evaluate this scenario

Problems experienced with the wall protection were related to vertical plasma movements during loss of position control. A fraction (up to 25%) of the total current was transformed into poloidal currents (halo currents) which upon wall contact were then transferred to the vessel wall including the wall protections. This is a new phenomenon which had not been observed earlier. The wall components were designed to withstand eddy current forces due to the decay of the poloidal magnetic field but they were not strong

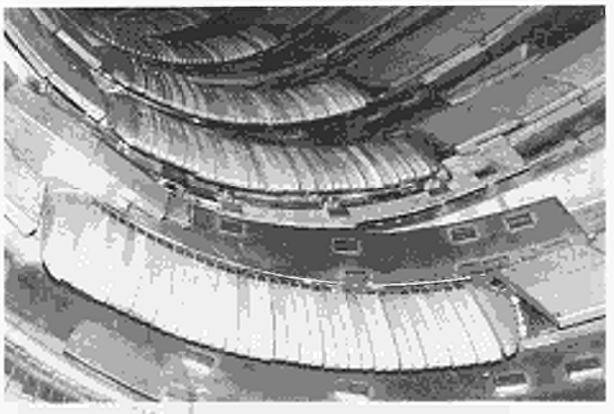

Fig.10 Discrete beryllium X-point target plates at the bottom of the vacuum vessel

enough to cope with the forces created by the interaction of wall transferred halo currents with the toroidal field. One example of the resulting damage is shown in Fig.11 for a section of the inner wall close to the midplane. Here, two tiles were lost by being pulled off their supports, and a third one is damaged and protrudes from the wall. The forces exerted on the tiles were calculated (and measured in a mechanical simulation) to be 500 - 700 dN for each tile. This is more than one order of magnitude higher than forces due to eddy currents. A poloidal current of 4 to 8 kA transferred to these tiles is sufficient to explain this behaviour.

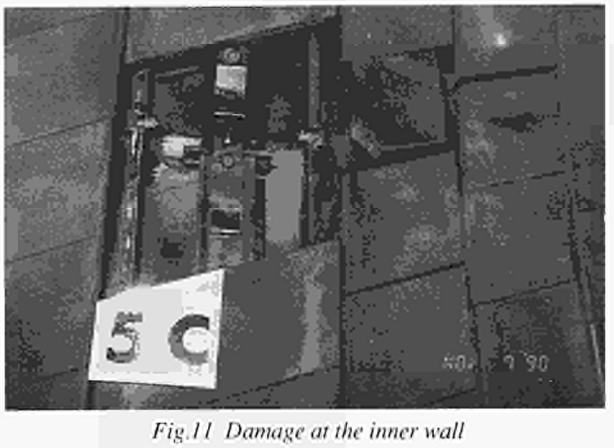

Fig.11 Damage at the inner wall

At the end of the experimental period, a total of 49 tiles out of 2300 were dislocated or damaged. This still represents only a small fraction of the total number installed but made plasma operation difficult as the plasma-wall distance had to be increased to values of up to 100 mm. For example, this made it impossible to systematically investigate high current operation (~7MA).

During the later shut-down, remedial action was taken to reinforce the wall protection in the affected areas: welds were strengthened, fasteners improved, weak mechanical supports were modified and cantilevered mountings were eliminated. The forthcoming operational period will show how far these modifications have been successful. If wall damage is still experienced, different recipes will have to be tested, such as, for example, mechanical decoupling between wall protection and vessel with spring loaded supports.

New wall elements being installed during the later shut-down are toroidally continuous X-point target plates at the top and bottom of the vacuum vessel. These replace the present target plates, which consisted of toroidally spaced energy dumps initially devised as wall protection. The power handling capability is anticipated to increase by a factor 2-3. It is expected that X-point discharges, compared with those before the change of target plates, can be run at higher powers or for longer times before incoming impurities degrade the plasma. Fig.12 shows the new X-point dump plates at the bottom of the machine during installation.

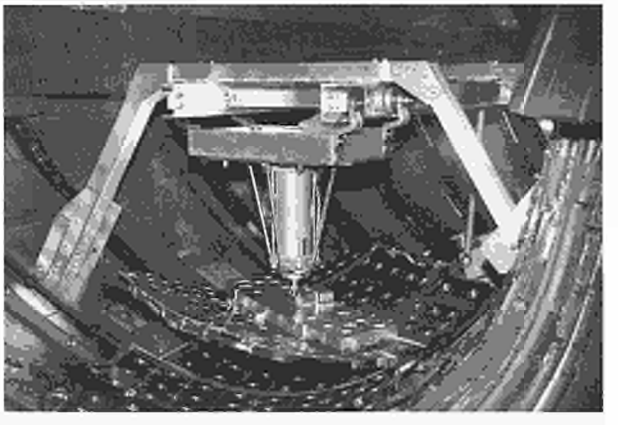

Fig.12 Continuous X-point dump plates during installation

The placing of contracts for components of the pumped divertor did not proceed as speedily as expected, mainly due a the change from one to four divertor coils. The design of all the main components is now completed and several contracts are placed.

Vacuum system

All components of the vacuum system worked well, without problems. Only normal maintenance was required to change oil, bearings or faulty gauge heads. Some electronic units had to be exchanged due to faults attributed to ageing of electronic components. Therefore, replacement units must be purchased. In this context, discussions will take place on whether the standard for vacuum measurement instruments, which served JET well for the last eight years, should be updated to take into account recent developments in this area.

Exchange of components directly connected to the vacuum vessel (eg. gauge heads) was more difficult, due to safety precautions taken to avoid Be-contamination in the Torus Hall, and, therefore, more time was required for exchange. However, contamination measurements indicated, that the safety precautions were more than adequate as airborne contamination was not detected. In future, for component exchanges on top of the vacuum vessel, a simplified procedure will be proposed using an efficient air flow into the vessel.

Leak testing of components and also of the torus, due to octant exchange and during tokamak operation were major activities during 1990. During 1988, a number of leaks were detected between the outer shell of the double-walled vacuum vessel, which forms the barrier between the interspace and the atmosphere. Four of the eight bellows connecting the gas baking loop to the U-joint interspace had developed leaks. No action had been taken at that time. A further leak from the interspace to the torus at one of the sixteen limiter feed pipes was found and repaired temporarily. In 1989, a leak from the interspace to the torus was detected in a U-joint cover plate behind the lower reinforcement ring in an inaccessible position and its repair was also postponed.

The earlier 1989-90 shut-down provided an opportunity to repair these leaks and to replace all eight connecting bellows with tubes, even those which were not yet leaking. The remedial work necessitated either the local removal of the lower reinforcement ring (Octant No.8) or cutting holes in the inner shell of the double walled vacuum vessel to gain access. All these repairs were successful and no further leaks, or reoccurrence of previous ones, were observed during 1990.

During machine operation in 1990, one of the most severe vacuum incidents occurred, that had been experienced so far. As a consequence of a disruption, a 32 mm flange weld fractured and the pressure in the torus rose to ~600 mbar with the vessel at 300°C, corresponding to a leak rate of about 10^{6} mbarℓs^{-1}. Cooling down was initiated immediately but due to the thermal inertia of the vacuum vessel, the temperature reduced only to values below 150°C after a few hours. This incident led to heavy oxidation of the torus walls. After leak repairs, satisfactory plasma operation was resumed following application of 24 hours of glow discharge cleaning in deuterium and subsequent beryllium evaporation, whereas attempts to restart with only employing beryllium evaporation were not successful. As a consequence, both methods will be used together in the future after major incidents or openings of the vessel.

The gas introduction system has been updated to cope with requirements for increased gas feed. Due to the high pumping efficiency of in-vessel components and the ability to operate at higher densities after the introduction of beryllium, the amount of gas required for a discharge increased by nearly one order of magnitude to a maximum of 1000 mbarℓ. Two more piezo-driven gas inlet systems were therefore installed and these worked satisfactorily. The related control system was modified to operate several valves in parallel. Experience with this approach was good and also proved the reliability of the valves, which are foreseen for use during the tritium phase.

Two more new systems of this new gas introduction module were designed and procured for installation in the 1990/1991 shut-down. The purpose is to feed gas between the strike zones of X-point discharges at the bottom of the machine. This is a simulation of high recycling operation and will serve to gain experience with gas flow requirements in the future divertor configuration.

Present vacuum instrumentation is not yet completely compatible with operation at radiation levels expected for the tritium phase, especially the residual gas analysis (RGA) and absolute pressure measurements require attention. The development of a radiation resistant RGA started in industry in 1989 and was successfully completed in 1990. The solid state pre-amplifier was replaced by electrometer tubes and the RF-generator which normally is mounted directly on the measuring head is now 100 m away. The first unit of the new RGA system to be operated from outside the Torus Hall was delivered and is in the process of installation in the torus for trial runs during the next operation period.

Pellet Injection

This section summarises matters concerning the present JET multi-pellet injector and its upgrading by implementation of higher pellet speed capability. A more detailed report on the status of injector development and future planning can be found in the later section on Developments and Future Plans of this Progress Report.

The collaborative effort under the Pellet Agreement with the United States Department of Energy (USDoE) continued, whereby the pellet team of JET and US members shared the development of the three-barrel, repetitive, pneumatic, single-stage gun launcher with pellets of 2.7, 4 and 6 mm diameter and speeds around 1.3 kms^{-1}, constructed by Oak Ridge National Laboratory (ORNL), U.S.A., and mounted on the pellet injector box (PIB) interface built by JET. The

U.S. team participated in the JET experimental programme. The attendance of US personnel during 1990 was somewhat lower than the four man-years per year foreseen under the Agreement.

The pellet injector was extensively used in experiments of all categories for various purposes of fuelling, and corresponding results can be found in the contributions in the sections of this report on Scientific Achievements. However, it should be noted that as in previous years, there was very little time to study long-pulse fuelling effects using strings of pellets. One of the reasons is that present attempts at continuous pellet feeding (high frequency, long pulse) easily lead to overfilling (density limit) and, if the plasma is not stationary, phenomena are difficult to interpret. Further fuelling experiments would best be accompanied by stronger and experimentally variable pumping from the plasma boundary as is foreseen in the future Divertor Phase of JET. During the next experimental campaign, this aspect of long-pulse fuelling will certainly gain in importance.

Long pulse fuelling during the New Phase of JET is not covered by the present collaborative agreement between JET and the USDoE. The ORNL Launcher now in operation is geometrically incompatible with future JET high-speed launchers and as well, is not compatible with the JET active phase, remote handling and tritium requirements (and was not intended to be). Negotiations with the USDoE have been initiated concerning continuation of the Pellet Agreement and a decision by the USDoE is expected soon. It is envisaged that the US would provide a similar pellet launcher to the existing one for the Divertor and Active Phase of JET. However, it would be slightly upgraded with regard to the length of pellet sequences. Meanwhile, in a joint effort JET and ORNL have technically defined this device, undertaken a conceptual design phase and concluded this by reviewing tritium and remote handling compatibility.

For a more central deposition of clean fuel by pellet injection - the only known method which is not accompanied by a simultaneous delivery of excessive power, pellet velocities higher than that presently available (1.5 kms^{-1}) are necessary to reach higher temperatures in the plasma. For this, and particularly important for the assessment of pellet fuelling potential for a reactor, reliable scaling of penetration depth with speed and experimental evidence on the behaviour of plasma following pellet injection is urgently required. As a first step towards an Advanced High-Velocity Multi-pellet Launcher, JET is preparing respective experiments by employing a 6 mm single-shot, two-stage gun prototype launcher of its own development with a pellet velocity of ~4 kms^{-1}.

The development work, forming the basis for the design of the prototype, had started in 1985 and culminated in 1989/90 in the demonstration of 4 kms^{-1} deuterium pellets being successfully formed, accelerated, separated from their supporting sabots and reproducibly delivered to a target in a teststand. (Sabots are plastic cartridges to support the pellet at velocities exceeding about 3 kms^{-1} because of erosion effects increasing with pellet speed). These trials were carried out with an experimental two-stage gun developed by JET, delivering the driver gas heated by adiabatic compression to increase its sound velocity, and an experimental cryostat as the pellet formation and loading unit, developed jointly with CEN Grenoble under an Article 14 Contract with CEA.

Such an experimental set-up is not suitable for implementation on the JET device, for reasons of remote control and maintenance requirements. Therefore, JET has carried out, in parallel, a two-stage gun and cryostat design fulfilling these needs, as well as a design for the necessary modifications to the existing Torus Hall pellet injector, where the prototype launcher will be installed alongside the ORNL Launcher. To make operation of the high-speed prototype launcher worthwhile (in view of the valuable experimental time on the JET device), it must be available for a session, with 10 successive JET pulses with an interval between pulses of about 20 minutes. This latter period is sufficiently long to re-initialise and re-arm a two-stage gun, but too short to permit thermal cycling at near liquid helium (LHe) temperatures. Therefore, provisions must be made to form pellets prior to a session and store them, accordingly; also it must be noted that the prototype launcher will not be manually accessible for typically a week at a time.

The development and design of the prototype launcher and the method and installation measures to implement it on the PIB interface have been described previously [2,3]. In the run-up to the 1990 JET experimental campaign, the prototype two-stage gun - a 3 m long pumptube with 60 mm ID with a ~1 kg titanium piston delivering the driver gas through a nozzle into a 6 mm ID barrel - was assembled and brought through its qualification tests (up to 5000 bar peak pressure) in the teststand. Modifications to the injectors - the main items being the strong support steelwork for the two-stage guns and the controls and specific pellet diagnostics - were nearly completed. However, the complexity of the cryostat, led to large delays in manufacture as well as in

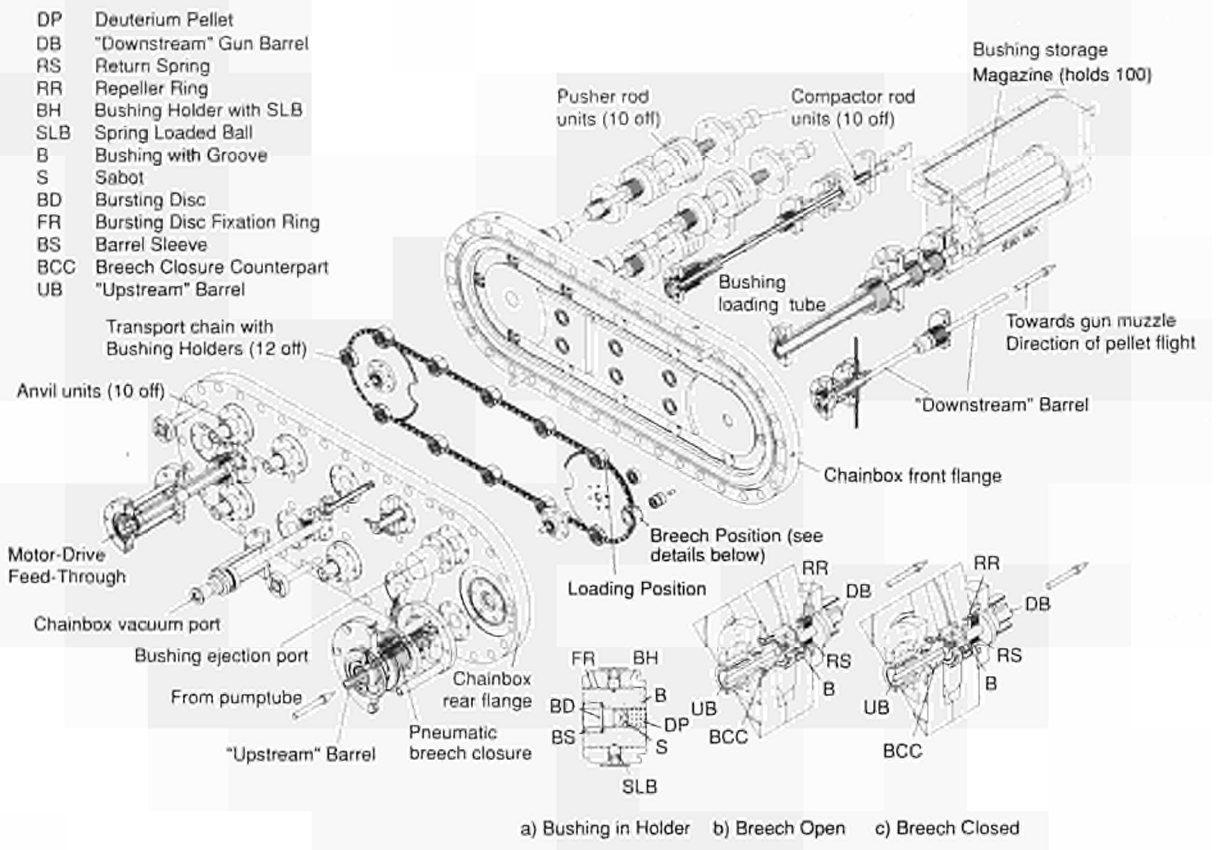

Fig.13 Schematics of Prototype Launcher cryostat

assembly and commissioning. As a consequence, the Prototype Launcher was not brought into operation during 1990.

A schematic of the essential parts of the cryostat is shown in exploded view in Fig.13. A chain with holders (see detail in Fig.13(a)) of disposable bushings, which are pre-loaded with sabot, bursting disc (to define the precise starting position of the pellet regarding the pressure wave), and deuterium pellet can be indexed to locate the bushings successively into the breech position for firing. The breech is pneumatically closed shortly before the shot (see details in Fig.13(b)) - with the upstream barrel being the movable part - and operation has shown that the breech tightness is sufficient. During the breech closure, the bushing is detached in the downstream direction from its groove - spring loaded ball fixture - and it snaps positively back into the safe position when pushed back by the return spring while the breech is being opened. The chain is enclosed in and guided by a chainbox (kept slightly above the condensation temperature of deuterium), which in turn is enclosed in thermal radiation shielding and guard vacuum vessel. From the magazine, which holds up to 100 bushings pre-loaded with sabot and bursting disc, warm bushings can be loaded one by one at the loading position into the bushing holders within the cold chainbox. Thereafter, the deuterium pellet formation by cryo-condensation can take place in parallel at each of the ten cold stations; each of these feature an anvil, the coldest part, against which the bushing is pressed by the pusher rod, the tip of which is slightly higher in temperature than the anvil and through the interior of which the deuterium gas is pre-cooled and guided to the bushing cylindrical volume in front of the sabot (see Fig.10(a)). A rod co-axial with the pusher rod can be used to compact the cryo-condensate. The pellets can be stored after formation for long times by lowering the temperature of the chainbox.

At present, the complete first prototype launcher is assembled in the teststand. Its two-stage gun is commissioned and sabot-only-shots have been fired in LHe cold conditions of the cryostat, proving that the the interface conditions regarding hot high-pressure gas versus high vacuum at the breech are met and that the in-flight separation of the sabot from the pellet trajectory is sufficient. The ice formation and storage commissioning is still continuing, although the basic LHe flow adjustments for the various temperature levels have been carried out. The deuterium pellet formation process is still being fine-tuned, but it is expected that the

launcher will be ready for operation in 1991. Provisions have been made that, once the gun is fully commissioned, its transfer to the Torus Hall and its re-commissioning on the machine can be accomplished within about 1 week. A second Prototype Launcher has been manufactured and is ready for assembly. The remaining site preparations have now been completed. Still under assembly are the modifications to the periscope to view the pellet plume in the plasma from a lower vertical port. These include enabling the periscope to home in on particular parts of the plume, magnifying it to the extent that the shielding cloud (~1 cm diam) can be spatially resolved, and freezing pictures of successive plume onto a single frame of a CCD camera by a pulsed image intensifier.

References

[1] B. Tubbing, et al., H-Mode Confinement in JET with Enhanced Performance by Pellet-Peaked Density Profiles, (1990), submitted to Nuclear Fusion.

[2] P.Kupschus, et al., Upgrading of the JET Pellet Injector by Employing a Two-Stage Light Gas Gun Prototype and Future Planning, in: Proc. 13th IEEE Symposium on Fusion Engineering, Knoxville, U.S.A., (1989), IEEE Cat No 89CH2820-9, Vol 2, pp 1293.

[3] P. Kupschus, et al., The JET High-Speed Launcher Prototype - Development, Implementation and Operational Experience, 16th Symposium on Fusion Technology, (SOFT-16), London, U.K., (1990), and this Progress Report.

Power Supplies and Magnet Systems

Introduction

The JET electromagnetic system is made up of the toroidal and poloidal coils with their mechanical structure, the purpose of which is to establish, maintain and control the tokamak magnetic configuration (Fig.14). It includes the toroidal coils, the poloidal coil P1, acting as primary winding of the tokamak transformer and the coils P2, P3 and P4, to control plasma radial position, vertical position and shape. To perform these functions, the coils must be energised by suitable DC power supplies, whose voltages and currents are controlled in real-time by the plasma position and current control system (PPCC). Additional DC power supplies

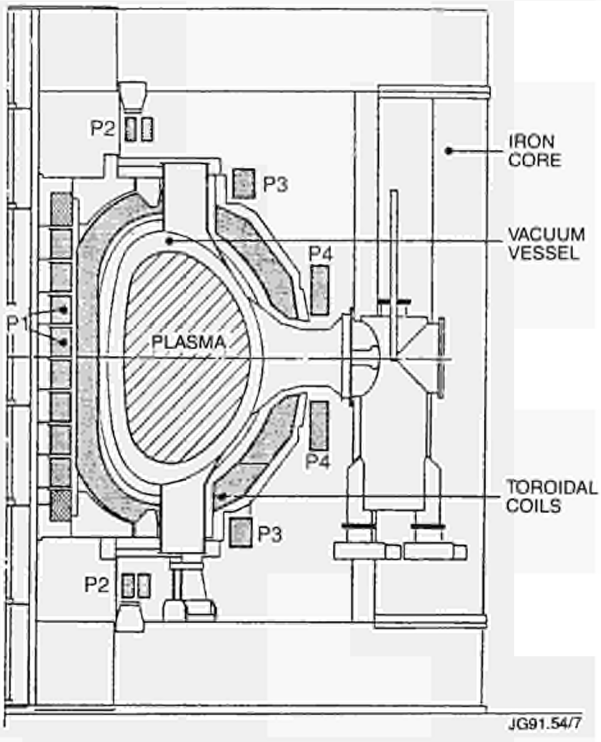

Fig.14 Cross section of JET showing toroidal and poloidal coils.

energize the neutral beam (NB) and radio frequency (RF) heating systems.

The total installed DC power required by JET is well in excess of 1500MVA with a delivered power peak above 1000MW and an energy content per pulse up to 10,000MJ. More than half of the power and of the energy is taken directly from the National Grid at 400kV and the rest is provided by two vertical shaft flywheel generators. Consequently, a major feature of the JET power supply scheme is the 400kV-33kV distribution system. Auxiliary power is supplied by the 20MVA, 11kV/3.3kV/415V distribution system.

The development programme to bring JET, first to its full design performance and subsequently well above, including new magnetic configurations, calls for continuous modification and upgrading of the electromagnetic system, of the plasma control and of the additional heating power supplies. The main objectives of 1990 were to bring forward the development underway in the tokamak and additional heating power supplies including the distribution system and to come to a full commitment in design and construction of the major components of the multi-coil divertor for the New Phase of JET, (i.e. the four poloidal coils and the associated power supplies), including extensive analytical and computer studies to confirm the feasibility and the stability of the required divertor configurations.

In addition, major repair and replacement work was undertaken on the faulty toroidal field Coil No.3.1, (Octant No.3, coil 1), discovered during the 1989 JET operation campaign.

Electromagnetic System

The electromagnetic system comprises the toroidal and poloidal coils with their associated mechanical structure, and the power supply to energise the coils.

The Magnet System

The magnetic system remained unchanged in its functions in 1990. However a major intervention on the machine was necessary to replace a faulty TF coil.

(i) Toroidal Coils

Changing TF Coil 3.1: A faulty TF coil was discovered in Octant No.3 during 1989 and at the end of 1989 the octant was removed from the machine and transferred to the Assembly Hall. The faulty coil was changed during January 1990. The operations for changing a coil had been defined previously but, as the interior of the vacuum vessel was now contaminated with beryllium, special precautions had to be taken to keep the vessel sealed and at the same time allow work to proceed inside the vessel. In February, the rebuilt octant was transferred to the Torus Hall and re-assembled into the machine. Again, this operation was similar to the original assembly with extra precautions to avoid beryllium contamination. Following octant replacement, it was possible to lower the upper poloidal coils (P3 and P4) and raise the lower poloidal coils to their normal positions and reassemble the rest of the machine.

Diagnosis of the Faulty Coils: With faulty coil in the machine, it was only possible to make measurements at the coil terminals and inspect parts of it externally using an endoscope. When the coil was removed from the machine, a series of tests were made to determine the cause of the fault.

a) Non-destructive test and inspections

Before further damaging the coil, as much information as possible was obtained as follows:

- When the coil was removed from the mechanical structure, water was found to be leaking from a crack in the coil ground insulation. The crack was at the end of a tapered copper section, which was part of a special pancake inter-connection plate. The tapered section was designed to relieve shear stresses but had caused a stress concentration at its (rather sharp) termination;
- Vacuum leak tests were made on each of the coil cooling circuits, which showed that the leak was in one turn near to the electrical and water connections of the coil;
- AC (50Hz) currents were passed through the coil and magnetic field measurements made using a simple coil and voltmeter, which enabled the faults to be located accurately. These measurements confirmed the location of the four interturn faults already shown by resistive measurements with the coil in the machine. The faults were all located at an opposite point on the coil circumference to the water leak (at the bottom of the straight nose in the collar tooth region), as shown in Fig.15.

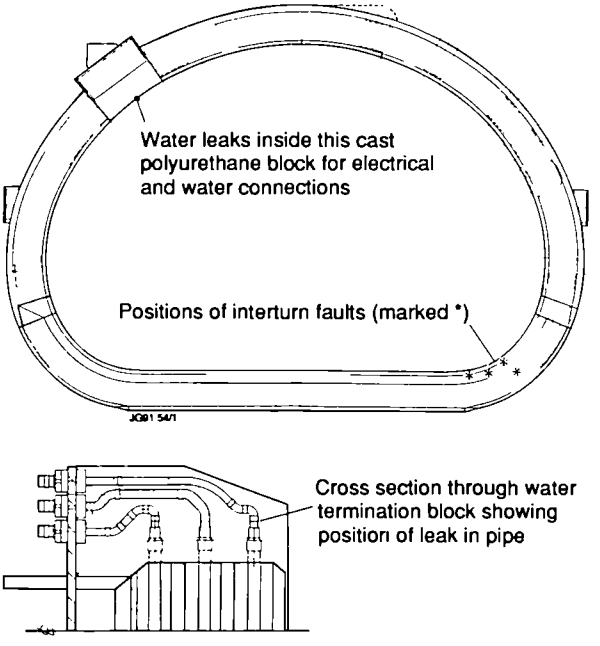

Fig.15 Location of water leak and inter-turn electrical faults in TF Coil No.3.1;

b) Destructive tests

Having confirmed the existence and location of the faulty regions, the coil was then partially dismantled, as follows:

- The epoxy glass ground insulation was removed first in the regions of the electrical faults and water leak, and later, over wider areas. Oxidation of the copper surface showed that water had penetrated between the coil conductors and ground insulation over practically the whole periphery of the coil. At the fault locations, the interturn insulation was carbonised. The source of the water leak was not found at this stage;

- The cooling water is fed into the coil via a system of copper pipes embedded in a matrix of polyurethane. The polyurethane was removed by burning in localised regions to reveal the water pipes. A repeat of the vacuum test then showed the leak was at a brazed joint in one of the pipes (Fig.15). The brazed joints were examined and found to be badly made. However, the leak appeared to be due to mechanical damage, which had caused a hole in the copper at the joint.

c) Cause of faults

The sequence of events leading to the electrical faults is believed to be, as follows:

- Water leaked from the pipe taking water to the coil pancakes. After the pipes were surrounded by polyurethane, the polyurethane would have retained water temporarily. If the leak developed after manufacture, then corrosion or erosion must be suspected, but visual inspection showed no evidence of this. The only evidence for corrosion was the location of the leak at the edge of a brazed joint;
- Water followed the path of the pipe through the polyurethane into the body of the coil. The pressure of water under the ground insulation caused progressive delamination until water had penetrated around most of the coil periphery;
- Fault currents flowed in the water between turns and eventually caused carbonisation of the epoxy glass insulation. The faults occurred at a particular location as the insulation was in some way inferior in this region. This inferior insulation could have been due to poor impregnation of the epoxy resin into the glass (this region on the coil was the most difficult to impregnate properly) or mechanical damage to the insulation during operation (this region is the most highly stressed part of the coil).

Change of Coolant: The coil fault was found to be due initially to a water leak at a pipe joint, which lead to electrical insulation failure in another part of the coil. To avoid future problems due to water leaks, it was decided to change from water to an insulating coolant.

As reported in the 1989 Progress Report, a fault was observed in Coil No.3.1 of the toroidal field coil at Octant No.3. The cause of the failure of the toroidal field coil was fully understood by the end of 1989 when the coil was removed from the octant. There was a leak at a brazed joint on one of the copper pipes between the external water connector piece and the main body of the coil. Since these pipes are enclosed in a rubber block, the water could not leak out. Instead the water found a path inside the coil outer insulation and travelled several metres along the coil circumference until it found a spot where the interturn insulation was not fully impregnated with epoxy resin. The interturn electrical faults were due to the relatively low electrical resistivity of the stagnant water.

It was realised that such a fault could occur in other coils if similar conditions existed. (Subsequently, a further fault was found in a coil at Octant No.4). By the end of 1989, (that is well before the discovery of the second coil fault), a decision was taken to replace water as a coolant with an organic dielectric fluid. The use of a fluid with intrinsically high dielectric properties would prevent the reoccurrence of this type of fault.

A survey of industrially available fluids was carried out.

Table III
Fluids for coil cooling

Fluid	*Compatibility with Coil and Cooling Components*	*Radiation Resistance*	*Cost (£/kg)*
perchloro-ethylene	effect on epoxy glass, damage to normal rubbers	not tested, chlorine products on break down	0.3
trichloro-trifluoroethane (Freon)	damage to normal rubbers	no effect at 25krad, chlorine products on breakdown	1.0
fluorinated hydrocarbon	no problems according to information	no effect at 25krad, florine products on breakdown	20.0

The main criteria for selection were non-flammability, compatibility with the epoxy used for the coil insulation and low toxicity (seeTable III). On non-flammability, most organic fluids would not be suitable, as these could easily ignite at a temperature lower than the vacuum vessel baking temperature. Fluid leaking at the top of the machine would reach the vessel, soak the vessel thermal insulation material and could leak to a potentially disastrous fire. Only chlorinated and fluorinated products were found to satisfy the criterion of non-flammability. Three products were pre-selected: Perchloroethylene, Trichlorotrifluoroethane and fluorinated fluids such as those used for the cooling supercomputers. The first option was incompatible with epoxy resin, and the third option was eliminated on financial grounds.

Chlorofluorocarbons are used for a wide range of industrial processes. They are non-toxic, but nevertheless, represent a potentialy safety hazard since the permissible concentration in air is typically 1000-2000 ppm. Chlorofluorocarbons (CFCs) are reported to be harmful to the earth's ozone layer when released to the atmosphere. For this reason, massive industrial use of CFC's is being progressively phased out. There is a wide range of CFC's, but the one selected for the cooling of the toroidal field coil, CFC-113, is a fluid with low viscosity which gives fairly good heat transfer properties. Organic fluids cannot match the heat transfer properties of water, but CFC-113 proved to be adequate for the purpose. Computer simulations of the complete cooling loop, including the coils and the heat exchangers, indicated that the cool-down time between full energy pulses would be in the range 25-35 minutes.

The use of Trichlorotrifluoroethane implied considerable modification of the cooling loop. The loop capacity was reduced to cutdown on the total volume and cost of the fluid. The large $10m^3$ mixing tank became a storage tank and basement pipework was simplified and shortened. Absolute leak tightness is essential when CFC is used. All non-essential flanged connections, valves and instrument flanges were systematically eliminated and welded connections were implemented wherever possible. Remaining flanges were tightly sealed by a special liquid- rubber compound. Pump seals were replaced with CFC compatible bellow seals. In the Torus Hall, all flexible rubber hoses (1536 in total) were replaced with new CFC compatible hoses and all hose connectors (remote handling Raffix connectors) were fitted with locking devices to ensure that these would not become loose. In view of the much higher density of CFC compared with water, stress analysis of pipework was carried out and additional supports installed, where required. New storage tanks were procured and new pipework for CFC-113 drainage and recovery of freon vapour were installed. Safety aspects were also most important and fixed CFC-113 detectors were fitted at various locations in the Torus Hall, access cell, basement and ventilation ducts.

In spite of the very short time available to carry out these major modifications, the new cooling system was ready by the end of March 1990 and filled with $65m^3$ (100 tonnes) of Trichlorotrifluoroethane. The system has operated fully satisfactorily throughout the 1990 experimental campaign.

During commissioning, a small quantity (less than $1m^3$) of CFC-113 was released due to a hose connector which became loose inspite of the special locking device. The event was never a safety hazard nor was it an environmental hazard in view of the small quantity of CFC-113 which was lost. However, there were inaccurate local press reports and the event was later reported in the national UK press, TV and some continental European newspapers. Even though reports were often grossly inaccurate, they emphasised the extreme sensitivity of the media and the public on environmental issues in relation to CFC's.

Following this event, a JET internal safety and engineering review was convened. It concluded that to guarantee that such an event would not recur could only be given, if the hose connectors were replaced with a more reliable type. By the end of 1990, a new hose connector had been selected and installation started during the 1990/91 shutdown.

Protection: The original coil protection system compared voltages between coils and worked satisfactorily. It was decided to fit extra instrumentation and protection so that any future faults could be monitored more closely. The voltage measurement system was therefore extended to all coils (the protection system already operates on all coils) and a new system for monitoring ampere-turns was installed.

A Rogowski coil was fitted to each toroidal coil. These of consisted of double layer helically wound cable, wrapped around the TF coil. These helical windings are connected to an integrator and should integrate the magnetic field around the coil, thus giving a measure of the enclosed current. The Rogowski coils give a satisfactory measure of ampere-turns and thus enable fault currents to be measured. Unfortunately, due to geometric imperfections, these also pick up other magnetic fields (due to poloidal currents, for example), which have to be removed, when post-processing the signals.

A Further Faulty Coil: When the machine was reassembled with the new coil Octant No.3, impedance measurements were made for all 32 coils. This showed a fault in another coil (Coil No.4.2, ie Octant No.4, coil No.2). This fault had not been noticed in previous measurements because it was masked by the much larger fault in the adjacent coil.

a) Inspection of Coil No.4.2.

Inspection of Coil No.4.2. with an endoscope and acoustic tests showed small cracks and evidence of delamination of the ground insulation near the coil connection region. To check whether the delamination was caused by a water leak and to prevent internal pressurisation by the leak, small holes were cut in the ground insulation of the coil. When the coil was filled with Freon, the existence of a leak, too small to be detected by vacuum tests was confirmed.

b) Development of fault in TF Coil No.4.2

The Rogowski coils installed on all TF coils were used to monitor fault ampere-turns in Coil No.4.2. A standardised TF coil pulse was needed and the daily power system test pulse (called a dry-run) was used. Fig.16 shows the peak fault current in dry runs, with fault current typically 3kA-turns. This compares with 30kA-turns for the fault in Coil No.3.1. and shows that the fault is less severe. During 1990, the TF current was reversed several times and the fault current increased after each polarity reversal but then settled down (Fig.16). Generally, the trend over the year has been for Coil No.4.2. to improve slightly.

c) Tests on other coils

Since the development of the second TF coil fault, the other TF coils have been examined carefully by on-line measurements during pulsing of out-of-balance ampere-turns and measurements during shutdowns at the coil electrical and water terminals. No evidence of other faults has been found. However, detection is difficult because:

- small differences in high field levels during pulsing have to be detected;
- damage to the coils by testing (eg at high voltage) must be avoided;
- the vacuum vessel, which is a single low resistance turn, couples inductively with the TF coils.

The most serious limitation of the coil testing methods used so far is that a loss of interturn insulation can only be detected when the insulation level has degraded by a factor of 10^4 or more: i.e. only interturn insulation less than 100mW can be detected. This is due to the very low copper turn resistance (~80μΩ). Better testing methods are being sought, aiming at detecting interturn insulation degradation at 1Ω and possibly at 10Ω level.

It should be noted that, an interturn insulation level of 0.1-1Ω may be more than adequate, since, due to the low copper turn resistance, the power dissipation in the fault is very limited (about 1kW) and does not cause further insulation deterioration (helped by the Freon coolant). This level of fault would have a negligible effect on the uniformity of the toroidal field. However, while the above consideration have allowed full performance operation during 1989, it is still planned to replace TF Coil No.4.2. during the 1991-92 shutdown.

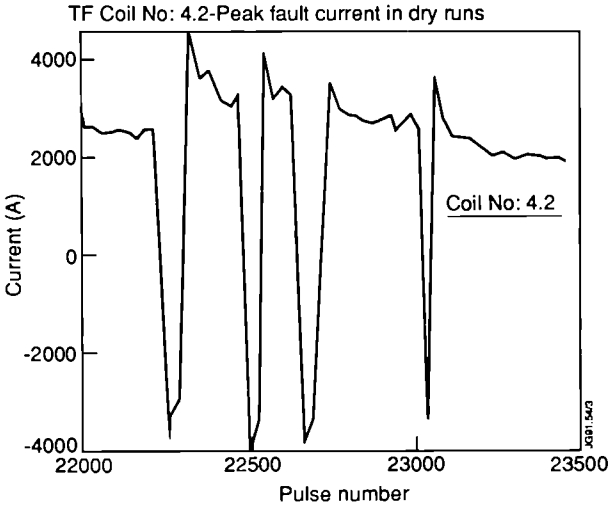

Fig.16 Peak fault current in TF Coil No.4.2 in "dry runs" during 1990;

(ii) Poloidal Coils

P1 Spare Coils: A set of six spare inner poloidal (P1) coils has been made and delivered to JET, with a similar specification as the original coils. The set have been machined together on their outer diameter so that they are ready to be assembled into the machine, in the event of failure of the central P1 coils.

The Magnet Power Supplies

The magnet power supplies are divided into two systems; the toroidal field power supplies for the establishment of the toroidal field confining the plasma column, and the poloidal field power supplies for the establishment and sustainment of plasma current iand for the control of the plasma column position.

The toroidal field power supplies consists of a flywheel-generator-diode rectifier, rated 67kA DC, 9.0kV no-load voltage, 2600MJ energy and two transformer-thyristor rectifiers supplied from the 33kV distribution.

The poloidal field power supplies consist of a flywheel-generator-diode rectifier, similar to toroidal field power supplies, a DC switching network and a transformer-thyristor rectifier PVFA 5-6, rated 2.8kV DC no-load voltage, 35kA DC, for the establishment of plasma currents, up to 7MA. In addition, the poloidal field power supplies includes amplifiers for the control of the plasma position: PRFA 1-2 + PRFA 3-4, rated + 5.2kV DC (no-load), +3kA DC, for the control of the vertical position; PVFA 3-4 + PVFB, rated 12kV at 1kA, 4.7kV at 6kA, 2.3kV at 25kA, for the control of radial position; and PVFA 1, rated 1.4kV DC (no-load), 40kA DC, for the control of plasma shape.

AC Plug Braking for the Flywheel Generators

The contract for the supply of two motor operated change-over/isolators, (11kV, 1250A), was placed in February 1990. The isolators consist of a six pole change-over, operated from a single motor drive, and provides the two required functions, i.e. to change-over the motor supply from 11kV (direct) for motoring to 5.5kV (reverse) for braking, and to isolate the 11/5.5kV step-down transformer when the braking mode is not used.

A prototype was built and subjected, to an extended mechanical endurance tests, and to necessary safety tests. The two isolators, isolator cubicles and control cabinets, where delivered in December 1990. Both have been installed and commissioning will start in early January 1991.

PVFA Conversion Four Quadrant Operation

This activity has been undertaken to conduct semi-continuous operation, in which the plasma current will be reversed during a JET pulse. This requires a four quadrant power supply for plasma radial position stabilisation. Each unit, PVFA 1 and PVFA 2, consists of two sub-units, (rated 1.4kV DC no-load voltage, 20kA DC load current), which can be configured in parallel (reference configuration) or in series. PVFA 1 normally supplies current to the shaping field circuit (single unit operation of PVFA 1-2 system).

A study of the modification of the control and protection system as well as the DC busbars was made to convert PVFA 1-2 into four quadrant operation (with current capability ±19kA and a no-load voltage ±2.4kV DC, with the sub-units series configured). The study of the control and protection systems were undertaken by the manufacturer, while the study and implementation of the DC busbar modifications, were undertaken by JET. Testing of the system on dummy load will be performed in January 1991.

Upgrading of the Radial Field Amplifier

During the 1989-1990 shutdown, the control loop of the radial field amplifiers was modified to improve the small signal frequency bandwidth (voltage loop) and to reduce the amplitude of the peak circulating current (current loop) during rapid voltage variations. The two amplifiers PRFA 1-2 and PRFA 3-4, in series, were tested on an inductive dummy load.

The tests showed:

- an improvement of the small signal 3dB frequency bandwidth from 90Hz to 300Hz (see Fig.17);
- increase of maximum voltage derivative from 1.1-1.8kV/ms.

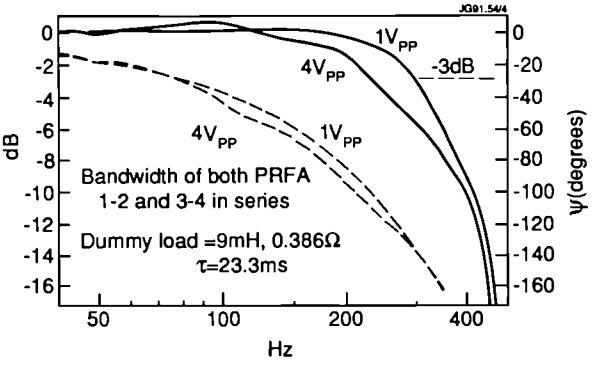

Fig.17 Upgrading of the Poloidal Radial Field Amplifiers PRFA 1,2,3,4;

Plasma Control

Automatic Control of the ICRF Coupling Resistance

The plasma position and current control system (PPCC) has been enhanced by the inclusion of a feedback control of the ICRF coupling resistance. The coupling resistance deviation from the desired reference value is evaluated within the ICRF system and transmitted to the PPCC. The feedback control of the radial plasma position includes a contribution by a proportional/integral controller for the coupling resistance error. This contribution overrules the original pre-programmed position within a selectable window. This system has been working satisfactorily for coupling resistances up to about 5W and permitted an effective and almost constant coupling of RF power.

Vertical Instabilities

The range of plasma configurations which can be stabilised is limited by the response time of the poloidal radial field amplifier (PRFA). For example, plasmas with double-null configuration become vertically unstable, if the distance of

during previous operation with carbon tiles as the plasma current quench was often delayed so that the vertical plasma displacement reached large amplitudes, while the current was still large. Fig.18 shows the disruption of a double-null 3MA plasma. The stabilisation system is saturated shortly after the onset of the disruption, as seen from the amplifier input voltage V_{Rin}; thereafter, the plasma displacement Z_p increases up to ~1m before the current quench. For these reasons, a new fast radial field amplifier (FRFA) has been specified which has an increased power (12 to 25MVA) and a reduced response time (2 to 0.3ms). This enhancement is also essential for future operation with a pumped divertor.

Further investigations have been carried out on the so-called halo currents, which play an important role during the later phase of a vertical instability. These currents flow outside the confined plasma and they are forced into the vessel wall at the location of intersection with the helical the X-points from the wall is too large, typically > 0.1 m. This represents an undesirable restriction on operation.

Another shortcoming of the present stabilisation system is apparent from the behaviour during disruptions. The system was often saturated shortly after the energy quench and the plasma then became vertically unstable. The resulting vertical forces and displacements at the vessel produced vacuum leaks at external vacuum pipes and damage to protection tiles. The forces were on average larger than

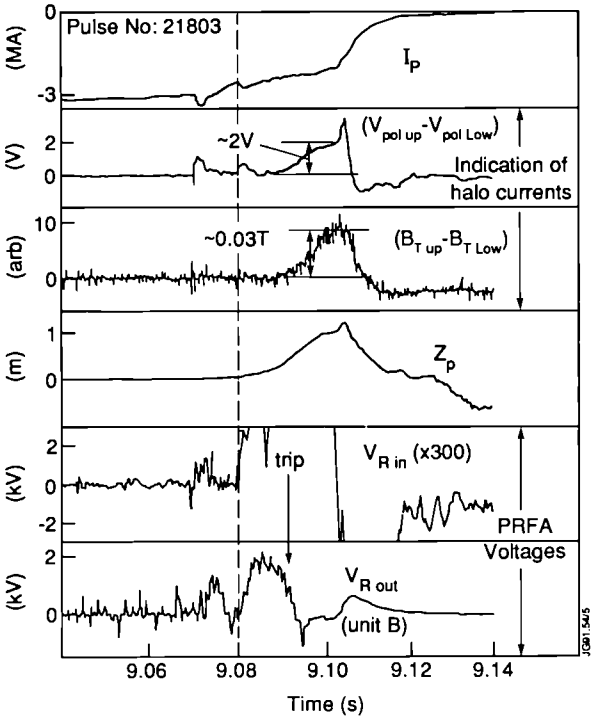

Fig.18 Vertical instability during a disruption;

lines of force. The observed damage of tiles and tile supports is to a large extent caused by these currents as they pass through these elements. An indication of the magnitude of the halo current is obtained from the toroidal field difference at the top and bottom inside the vessel, and also the difference of the poloidal voltage drop along the vessel at top and bottom. The total poloidal component of the halo current can reach about 20% of the instantaneous plasma current. However, the distribution of these currents has not been measured and requires further exploration.

During the 1990-91 shutdown, resistive shunts will be installed at selected vacuum vessel tile supports to measure halo currents in the vicinity of the upper and lower X-point dump plates, where some damage of tiles was seen. These measurements will be performed at two different toroidal locations to check whether the halo currents are non-uniform. This question is important because a local current concentration can produce particularly large magnetic forces at in-vessel elements.

The beneficial effects of the improved small signal bandwidth and of the increased maximum voltage derivative of the present poloidal radial field amplifier have not yet been fully assessed. This will be a goal of 1991 plasma commissioning programme. From experiments performed after the amplifier modification, the stabilisation range for elongated plasmas was improved, but there was no apparent effect on the frequency and the severity of vertical instabilities observed during disruptions.

Additional Heating Power Supplies

Radio Frequency Power Supplies for ICRF

This system is fully operational at its maximum design performance and no major problems were encountered with the supplies. Only routine maintenance was performed during the year. One of the design features of the power supply was that in case of arcing in the RF transmission line/antenna system, the high frequency power would be interrupted for not more than 5ms. On the power supply, this would reflect in the output current being interrupted for a maximum of 5ms. During the latter part of the operating period, it became apparent that these 5ms were not long enough to extinguish the arc and, in addition, it was better to reapply the power not as a step but as a ramp. Design changes to the power supplies are being undertaken to accommodate these changes. These will be tested during the present shutdown and if successful, the power supplies will be modified accordingly. In addition, a flexible pulse/pause

timing circuit is being tested. This will allow the pause time to be dependent only on the energy taken during the pulse. If the test is successful, this feature will also be implemented in the power supplies.

Lower Hybrid Power Supplies and Protections

During the year the installation of all the power supplies and the protective crowbars was completed. A schematic of the power supply is shown in Fig.19. The power supply is fed from the 33kV through one stepdown transformer with two secondaries to approximately 1kV. At this voltage level, off-load isolators are installed in order to be able to isolate one power supply/protective crowbar/klystron unit for maintenance and repair. The power supply itself is based on the star-point controller for regulation. At the output of the power supply the protective crowbar is connected, close to the klystrons. Each power supply/protective crowbar unit supplies four klystrons.

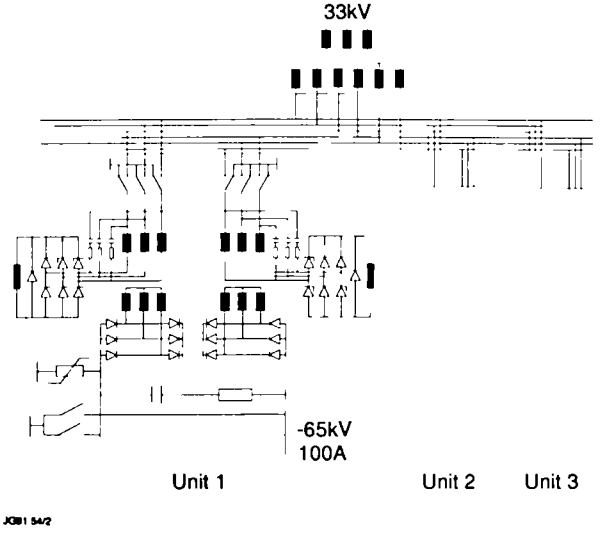

Fig.19 Schematic of the LHCD power supply.

One of the main design features of the overall system was to avoid any steps in power supply current. At the beginning of the pulse, the klystron works as a diode and the current is ramped up from zero to its required level during 100ms. If arcing occurs in the circuit downstream of the klystron, the high frequency power is interrupted. However, the klystron continues to draw the same current from the power supply and it operates again as a diode. In this way the design of the Power supply was much simpler and the output voltage could be kept within the required limits without a large filter or other additional requirements. One added advantage is that this design also avoids steps in active power on the 33kV network. The price to pay was an increase in heat loading on the collector of the klystron which required a larger cooling unit than normal. Commissioning of all the power supplies was carried out on dummy load as part of the contract. All the protective crowbars were functionally tested.

As the klystrons are connected to the power supplies, optimization of the feedback loop in the power supply is performed, as well as the final voltage test to the protecting crowbars. Part of these tests consist of connecting a wire in series with a sparkgap to the output of the crowbar instead of the klystron. By reducing the gap of the sparkgap, an arc is established; the crowbar must intervene before the wire melts.

Two power supplies have been operated with the eight klystrons as load on the machine. As a result of this early operation, several minor changes have been made to further improve the performance. During 1991, the remaining power supplies and the protecting crowbars will be tested with the klystrons.

Neutral Beam (NB) Power Supplies

During the year the remaining Octant No.4 power supply was converted for 160kV operation. The completed system was used for injection at 140kV during the 1990 operating campaign. On Octant No.8 power supplies, the maximum voltage was increased to 85kV in deuterium compared with the design value of 60A. Further changes were made both to the 140kV and the 85kV power supplies, to improve the reliability of the supply.

Neutral Beam (NB) Test Bed Power Supplies

During the year the Neutral Beam Test-bed was extensively used for testing components for the divertor coil. A new system beam modulation was added to the supplies to simulate the sweeping of the plasma over the divertor. This system was designed and manufactured in-house, and has been used extensively during testing.

During 1991, the Test-bed might be required to operate in continuous mode at reduced power instead of the present pulsed operation. A comprehensive study was undertaken to investigate what changes would be required to the supplies. Several components would have to be changed, some requiring more design work.

Design of the New Grid 2 Resistor

A new Grid 2 resistor has been designed. This new design uses forced air cooling instead of oil cooling. A prototype

was constructed and tested for a dielectric stand-off voltage of 260kV, cooling and operation. The first resistors were installed on module No.6 during August. After 2 weeks operation, the resistors were measured again, and several had changed value outside specifications. A few had increased their value substantially. An extensive program of testing is underway to find the cause of this problem.

The JET Power Distribution System

The 33kV Distribution System

A further extension of the 33kV switchgear compound has been implemented to provide for the three 33kV feeders on busbars 1, 2 and 3 for the three 50 MVAR Reactive Power Compensation System (RPCS) Units. In addition, the procurement of the 33kV/11kV feeder for the 30MVA bi-directional transformer is in progress. When operational this transformer will supply 33kV power to the RF and NB test-beds when the 400kV/33kV substation will be under maintenance or to supply 11kV to the 11kV/415V auxiliary system, when the 132kV/11kV substation is under maintenance.

Service, Construction and Installation Work

These activities comprise a variety of miscellaneous but important items, such as the completion of all building and experimental power supply distribution necessary for the Active Gas Handling System Building (at 415V), the installation of cable routing for the Disruption Feedback Amplifier System (DFAS), the auxiliary electrical supplies for the DFAS, LHCD, RPCS and for the extension of the Site Cryogenic system. Finally, the 415V Distribution System has required revision and extensions to suit the constantly expanding needs of the Experimental Divisions. The work has required considerable electromechanical design and the production of manufacturing drawings for the layout of the DAFS, the 30MVA bi-directional transformer, the Divertor Coil Power Supplier, the new arrangement for the power supplies of the KE4 Gyrotron Diagnostics.

Reactive Power Compensation System

The Contract for the Reactive Power Compensation was placed in May 1989; the design and the procurement of three identical 50 MVAR Units plus three Snubber Circuits were included in Stage 1; Stage 2 (two 50 MVAR Units) and Stage 3 (one 50 MVAR Unit), were to be placed at a later time. The design review meeting took place in December 1989: and the CODAS interface Specification was agreed both with the Manufacturer and with CODAS in January 1990.

All factory tests, on individual components, were completed successfully and installation started in June 1990. Before the end of 1990, the installation was completed, including personnel safety enclosures and fencing out earthing system. Due to the rearrangement of the experimental plans and of the 1990-91 shutdown activities, no specific commissioning time with JET operational pulses was allocated. It was therefore necessary to use the time allocated for maintenance and machine commissioning to test this new system.

The completion tests for Stage 1 (three 50 MVAR Units) were concluded successfully in November 1990, with the energisation of the third Unit connected to busbar 3. All identified minor problems have been listed and discussed with the manufacturers. Acceptance tests, with a standard JET pulse, will be performed during the commissioning period, at the end of the present Shutdown. The main purpose of these tests is to measure the harmonics produced by the standard JET Pulse and to compare with theory, with the Reactive Power Compensation System both connected and disconnected.

Supply of Electricity

The privatisation of Electricity Supply Industry in the UK, has caused a major disruption of the ten-year old Contracts for the supply of electricity to JET, and the situation would have been extremely difficult were it not for the excellent relationships developed over the years between JET and the CEGB (Central Electricity Generating Board) and the SEB (Southern Electricity Board).

The status of the renegotiated Contracts is, as follows:

a) The Contract with SEB for the supply of 11kV electricity to JET has been replaced by a new Contract placed with the privately owned Southern Electric Company. An annual saving of 15% - 20% has been achieved as a result of this new Contract;

b) CEGB has been split into two privately owned generating companies (National Power and Powergen), one state-owned nuclear power company (Nuclear Electric), and one grid company (National Grid). As a result, the former Contract with CEGB for supply of electricity at 400kV to JET on pulsed loads has been replaced by three new Contracts - one with National Power and two with National Grid.

National Power which owns all of the large non-nuclear power stations in England and Wales has made an attractive offer to JET and has accepted all pulse parameters previously

negotiated with CEGB. The relative lack of restrictions imposed on JET operation comes as a result of experience gained by JET and CEGB. The Contract is ready for signature pending clarification of some points of detail.

The consultancy contract with National Grid relating to system studies associated with aspects of JET operation in the future has now been signed, and the amount payable in any one year is limited to the cost of the studies requested by JET.

Of the above Contracts, the Agreement for connection to the 400kV transmission system is by far the most difficult as - in accordance with the Standard Site Conditions in the Host Agreement - the UKAEA is also involved. A draft Contract including only JET and National Grid has been prepared, and the relevant aspects of the Host Agreement are the subject of separate negotiations with UKAEA.

Neutral Beam Heating System

Introduction

The successful operation of both the Octant No.4 and Octant No.8 injection systems, achieved during 1989 experimental campaign, was maintained throughout 1990, with high levels of both reliability and availability. Prior to the start of the operations programme, the conversion of the Octant No.4 system to 140 kV was completed to give one injection system at 140 kV plus one at 80 kV. Although the change to 140 kV operation provided lower total power (7.8 MW compared with ~ 10.5 MW at 80 kV), this was offset by enhanced beam penetration and, hence, more efficient heating of the central plasma region. Furthermore, the voltage of the Octant No.8 system was progressively increased beyond its 80 kV design value to 85 kV, resulting in ~ 11.5 MW without decrease in reliability. These modifications resulted in record values for the plasma parameters achieved with NB heating in 1989 being marginally increased during the 1990 experimental campaign. The flexibility and usefulness of neutral injection in JET was further enhanced by the successful use of the Octant No.4 system to inject beams of ^{4}He and also of ^{3}He (at 120kV) into the plasma during the final weeks of operation.

The JET cryoplant has also maintained its high degree of availability and reliability throughout the year and work on upgrades necessary to supply future additional users of cryogens have been initiated.

Neutral Beam Operations

Performance of the Injectors in Deuterium

Throughout 1990, the general availability and reliability of the two beamlines on JET remained at the high levels achieved in the 1989 campaign. The reliability defined as the ratio of the total energy delivered to the plasma to that requested for a given pulse improved slightly from an average value of 82% for 1989 to 84% for the 1990 data set. System availability was also maintained at 90%, the same level as the 1989 campaign.

Both beamlines were upgraded in the 1990 period. The Octant No.4 system completed the commissioning of the final two PINIs of the 140 kV three-grid type. By the end of the campaign, all eight PINIs were operational at the full design voltage of 140 kV and a total power of 7.8 MW was delivered to the plasma with pulse lengths of up to two seconds. The Octant No.8 system remained in its original configuration throughout this period but the maximum operating voltage of the 80 kV four-grid PINIs was increased from 80 to 85 kV and operation at 83-84 kV was achieved routinely without any significant degradation in reliability. As a result, Octant No.8 system provided ~11.5 MW of neutrals to the plasma of duration up to three seconds. The pulse length was restricted only by power handling capabilities of the torus limiters and X-point tiles, and not by beamline considerations (the beamline components being capable of handling pulse lengths ~ 10 seconds). The maximum power injected into JET was 18.5-19.0 MW and more than 50 discharges were heated with NBI powers > 16 MW.

Conversion of the Octant No.8 system from 80 kV to 140 kV was started at the end of the 1990 operational period. This marked the end of the period during which this beamline was the only injector routinely capable of transmitting more than 10 MW to the plasma through a single injection port or drift duct. In addition, this beamline also transmitted the highest power densities through any drift duct with peak neutral power density > 200 MW m^{-2}.

The performance of the JET beam duct [1], while exceeding that of other systems in operation, is actually in excess of that required for a reactor in terms of transmitted power density and equivalent neutral current whilst simultaneously maintaining an acceptably low fraction of re-ionised power deposition in the duct.

During the total period of operation of the Octant No.8 80 kV beamline, from January 1986 to November 1990, a total of 2909 pulses were used to deliver heating power to the

plasma. The injected power spectrum of these pulses is shown in Fig.20. The peak at 3 MW reflects the use of this beamline to provide diagnostic beams for charge-exchange recombination spectroscopy. In addition, 10,000 pulses were fired in Asynchronous mode (i.e. independent of JET operation) into the beamline calorimeter. The majority of these were related to system and power supply commissioning. In the accumulated time of operation (> 10^5 seconds), no on-load failures of the water-cooled accelerator grids were encountered. The only failures during operation of other beamline components were of the original neutralisers which (as were the accelerator grids) fabricated using the electro-deposition of copper. No failures have been encountered since their replacement by a different design. In view of the high powers and complexity of these beamlines, this degree of reliability represents a remarkable achievement and can be used to provide statistical information on the reliability of beamline components and fabrication techniques for future beamline designs.

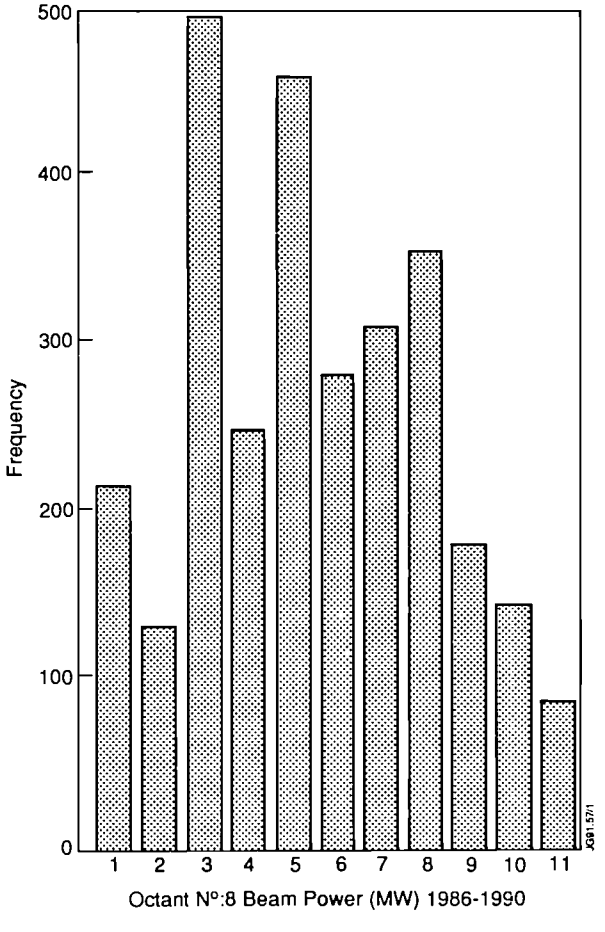

Fig.20: Power spectrum of all pulses from the Octant No.8 injector into the plasma;

Conversion of the Injectors to Helium Operation

The injection of beams of energetic helium (as opposed to deuterium) offers the possibility of carrying out various interesting experiments on JET, in addition to avoiding the production of beam plasma neutrons which both complicate the measurement of the thermonuclear neutron production and result in activation of the vacuum vessel. Following the successful tests of ^{4}He cryosorption pumping in the Neutral Beam Testbed (reported in the 1989 Progress Report, Vol 1, p 28), large scale pumping tests of helium cryosorption were performed on the Octant No.4 beamline using the total cryopumping capacity in an operational beamline. Measurements were made of the pumping characteristics for helium gas of a layer of argon 'frost' on the liquid helium cooled cryopanels. The argon gas for this frost was introduced via the gas neutralisers during the interpulse period between operation of the PINI gas introduction. The tests were successful and showed that adequate pumping speed was obtained by cryosorption for both helium isotopes in the full scale system. The apparent pumping speed was measured over a range of temperatures of the liquid helium cryopump panels and the results are shown in Fig.21. There is only a slight improvement in the pumping of ^{4}He for operation at temperatures below 4.2 K, whereas the pumping for ^{3}He shows a sudden improvement when the temperature is reduced to 4 K but no strong variation thereafter [2].

The results for the large scale pumps do not form a simple extrapolation based on the pumping speed per unit area of the small Testbed pump. In general, the pumping speed per unit area appears to be lower for the large scale pumps (see Fig.21). This probably stems, not only from the difficulty in achieving a uniform coverage of argon frost over the large area cryopumps due to the gas feed being at the neutraliser

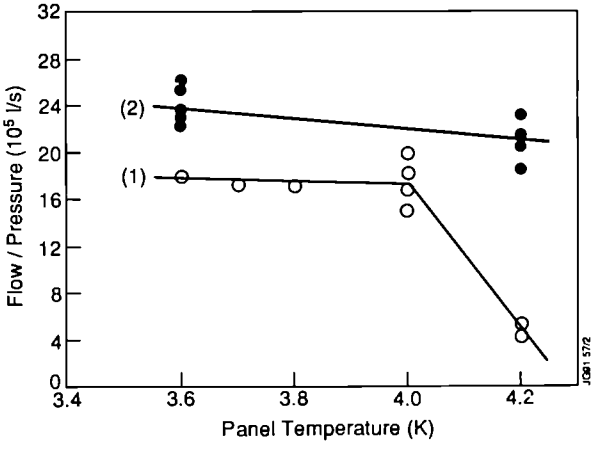

Fig.21: Measured apparent pumping speed for Helium gas;

end of the Neutral Injection Box (NIB), but also that of interpretation of the pressure measurement in a complex differentially pumped system. Nevertheless, for future upgrades consideration should be given to supplying a uniform gas feed of argon over the entire pump surface.

The Octant No.4 beamline was converted to ^{4}He beam operation in October 1990 and operation with eight 120 keV ^{4}He neutral beams was rapidly established. A limited experimental campaign was carried out using short pulses of injected ^{4}He to simulate a source of thermalised a-particles in the centre of the plasma and to measure their subsequent radial transport: During these experiments, a peak power of 6.8 MW of ^{4}He was injected into the plasma for 1.5 s, constituting a record power for helium injection. The cryosorption pumping by argon proved to be adequate in the presence of the high power beams and maintained the pressure in the torus injection duct at $\simeq$ 2-3 x 10^{-5} mbar during simultaneous operation of all eight beams. As a result, no problems were encountered with power loading in the duct from re-ionised beams.

It should also be noted that 120 kV ^{4}He operation confirmed the suitability of the beamline deflection magnet for the 160 kV operation in tritium which is foreseen for the final D-T phase of JET.

For the final week of operation in 1990, the ^{4}He beamline was used to inject beams of ^{3}He at energies up to 125 kV at a power level of 5.2 MW for pulse lengths of up to 3 s. This is the first time ^{3}He injection has ever been attempted in the world. Although the first experiments were limited to 125 kV by electrical breakdown in the accelerator, subsequent analysis indicates that minor adjustments of various timing circuits should enable the voltage to be increased to 155 kV.

Based upon the successful operation in ^{3}He and ^{4}He both beamlines will be converted to be capable of this mode of operation as required by the 1991 experimental programme. This should enable $\geq$ 13.5 MW of 120 kV ^{4}He or $\geq$ 15 MW of 155 kV ^{3}He to be available.

Neutral Beam Testbed

The work on the Neutral Beam Testbed in the past year can be divided into three major areas: support and development for the injection systems on the machine; development of high heat flux elements; and tests of beryllium-clad high heat flux elements for the pumped divertor for the proposed new phase of JET.

Neutral Beam Development and Supporting Activities

The characteristics of the beamline deflection magnet in conjunction with the upgraded full energy ion dumps to be installed in the injection systems have been measured over a range of beam energy for H, D and He operation. This was necessary, not only to confirm the power deposition profiles on the dumps, but also to confirm that the addition of extra iron to parts of the magnet yoke would enable safe operation using 160 kV beams of tritium. The results of an extensive series of detailed measurements confirmed that the upgraded system would indeed be suitable for long pulse (> 10 s) operation with beams of 140 kV(D) or 160 kV(T).

Six of the Positive Ion Neutral Injectors (PINIs) which are essentially the plasma source plus water-cooled beam formation and accelerator structures have been converted from the 80 kV to 160 kV configuration and conditioned to their full operating voltage and current in deuterium (140 kV and 30 A). Further developments of the PINI have included the successful testing of an alternative mode of operation, in which the first grid of the accelerator or beam forming electrode is permanently connected to the anode of the plasma source as opposed to being electrically floating. This modification can result in some simplification to both the mechanical design/construction and the electrical supply/transmission interface of the PINI.

During 1990, the Japanese JT60 team reported that beams of energetic helium contained a significant percentage of atoms in the metastable state (He^*_0). This can have serious consequences in terms of the beam having very much reduced penetration into the plasma and thereby damaging components adjacent to the injection port. A comprehensive study using cross-section data available in the literature was carried out to predict the yield of metastable atoms from electron capture on positive ions as a function of neutralization target thickness. As can be seen in Fig.22, the predicted percentage of He^*_0 is a maximum at very reduced values of target thickness and falls to $\leq$ 10% for values of target thickness closer to the equilibrium value which is more typical of injector operation. The first helium injection experiments on JET did not reveal any major effect which could be attributed to an excessive fraction of He^*_0.

Development of High Heat Flux Elements

Components capable of accepting heat fluxes ($\geq$)10MW m^{-2} will be an essential feature of not only the divertor for the proposed new phase of JET but also next generation fusion devices. The JET neutral beam systems have successfully

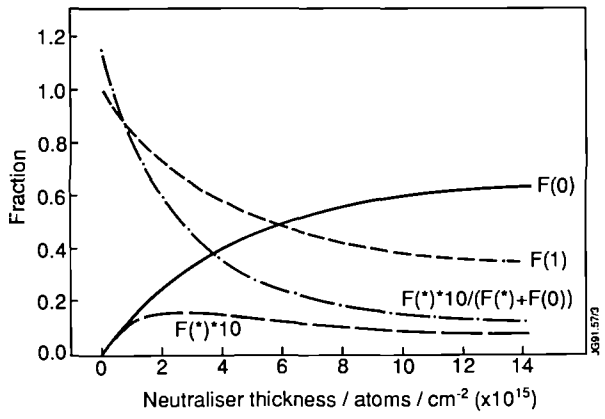

Fig.22: Calculated production of He^*_0 by electron capture as function of target thickness;

used the hypervapotron principle for high heat flux components and considerable improvements to their performance have been achieved in an experimental programme which has also led to a better understanding of their behaviour. A variety of designs of the internal cooling geometry were examined (Fig.23). From an analysis of the extensive set of measurements, it has been shown that the heat transfer mechanism is a function of the incident power density. For water flow velocities ~ 4 ms^{-1} and low values of incident flux ~ 5 MW m^{-2}, the mechanism is simply due to non-boiling turbulent heat transfer enhanced by the increased surface area of the internal fin geometry. In the range 5 to 12 MW m^{-2}, "quiet" boiling heat transfer dominates and at even higher values of heat flux the "quiet" stable boiling is replaced by more vigorous "noisy" stable boiling [3].

The extent of the various regimes is a function of the fin geometry, the velocity (as opposed to mass flow rate) of the cooling water and its degree of subcooling. Fig.24 illustrates

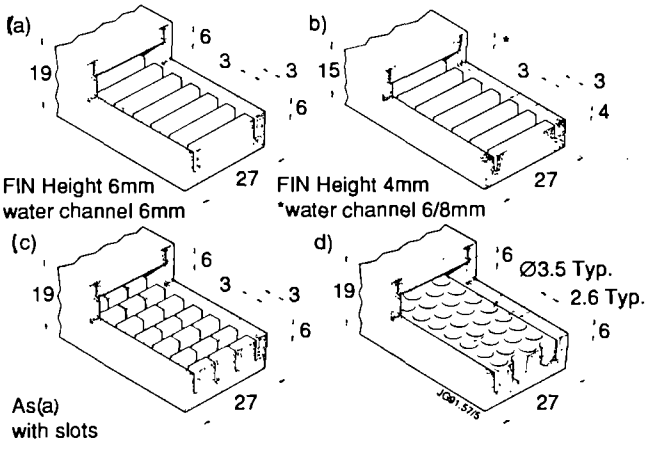

Fig.23: Schematic of various types of hypervapotron internal cooling geometry;

the significant improvement in power handling capability which has been achieved compared to that of the original design being utilized in the neutral injectors.

Comparative tests of a hypervapotron and swirl tube high heat flux elements have also been carried out for NET. Although both systems are virtually identical in their power handling capability the hypervapotron offers the significant advantages of making better utilization of the coolant and, even more importantly, of not exhibiting a very sharp limiting value of heat flux which leads to catastrophic failure (melting) of the structure. This confirms the choice of the optimized vapotron geometry for the JET Pumped Divertor.

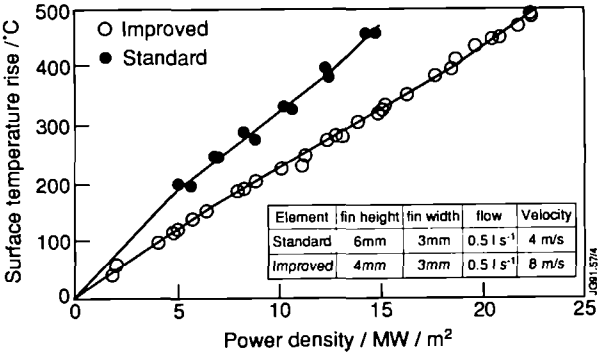

Fig.24: Measured performance of improved and original hypervapotron;

Tests of Beryllium Clad High Heat Flux Elements

An essential feature of the JET pumped divertor is that the plasma facing components are clad with beryllium in order to minimise the production of impurities with high atomic number. Methods are being developed of attaching beryllium to the surface of hypervapotrons using brazing or explosive bonding techniques. Progress in these areas is described in the Developments and Future Plans section of this report.

In view of the need to test the performance of beryllium clad elements, a new small dedicated test-stand has been built and brought into operation to avoid beryllium contamination of the main testbed facility. This new test-line is shown schematically in Fig.25 and uses a standard JET PINI. For reasons of speed and economy, this utilizes a reduced beam extraction area to minimise pumping requirements and shares the main Test-bed power systems, computer control and data acquisition system.

Cryosystem and Cryopumps

The cryosystem has continued to supply all users of cryogens on the JET site with an extremely high degree of reliability

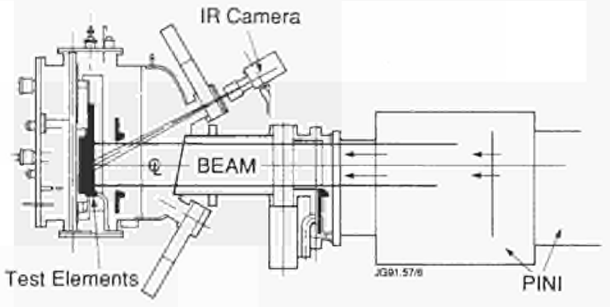

Fig.25: Schematic of new beam line for testing Be clad components;

and availability. Subcooled operation (< 4.2K) of the neutral injector cryopump was an essential feature which enabled the use of ^{3}He beams on JET.

In parallel with operation, preparations for upgrading the cryo plant and distribution system for new users (eg, Active Gas Handling System and Pumped Divertor) have proceeded. A new 10,000 ℓ liquid helium reservoir has been commissioned and a new (additional) cryogenic distribution valve box has been manufactured and installed (see Fig.26). This will enable liquid helium to be supplied to up to seven new users. It also incorporates the cold ejector for supplying the divertor cryopump with supercritical He plus a phase separator for the returning fluid. The connection and integration of this new valve box into the existing system is being carried out during the current 1990/1991 shutdown.

In addition, work has also been initiated to determine the potential tritium retention by the anodised black surfaces of the liquid nitrogen surfaces of the large injector cryopumps.

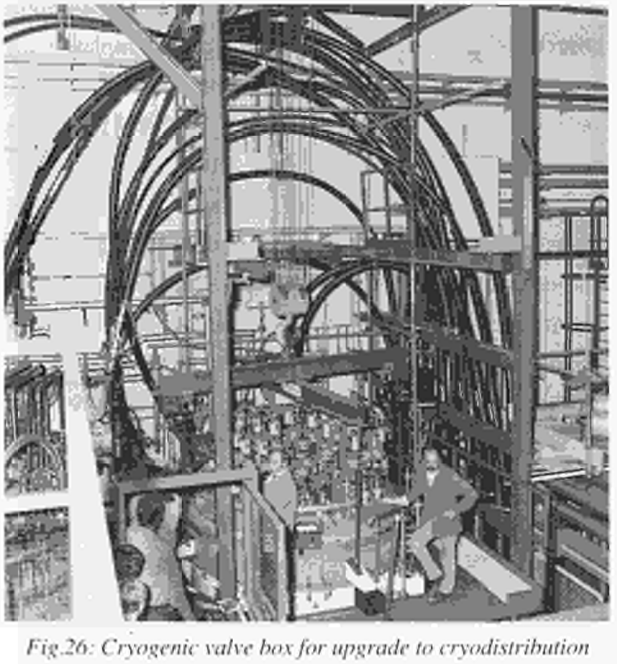

Fig.26: Cryogenic valve box for upgrade to cryodistribution system.

This is required in view of the plans to ultimately convert one neutral injector to tritium operation. Tests have been carried out using small samples of the surfaces with tritium at TSTA, Los Alamos, USA. The first results indicate that isotope exchange reactions do occur between tritium and the water which is trapped in the black anodised surfaces. Therefore, it has to be assumed that a certain amount of tritium will be trapped by this mechanism. Further tests are required in order to obtain reliable quantitative data which will enable the magnitude of tritium retention to be assessed.

Engineering and Development Work

Maintenance and Upgrading of Beamlines

No failures of mechanical components in the beamlines have occurred during 1990 and work on the planned upgrades - improved Full Energy Ion Dumps (FEIDs) and Duct Liner Assemblies - has continued. Although delays have been encountered in the FEID contract, the first four assemblies have been delivered and assembled ready for installation. Delivery of the final set is imminent. The cryopump manifolds in both injectors have been modified in preparation for installation of the upgraded dumps. Delivery of the Mark II Duct Scraper Assemblies is also scheduled early this year to allow preparation for installation in the 1992 shutdown and the manufacture of the upgraded Box Scrapers has been completed.

Beryllium-Related Topics

The large Beryllium controlled area has been constructed, commissioned and, following the development of procedures for routine working, has been in general use for the assembly of beryllium contaminated components. In addition, considerable effort was devoted to the construction of the dedicated Be testline which is now operational in the NB Testbed and to the development of isolators and procedures for the installation and transfer of components.

Developments for the Tritium Injector

All thin-walled bellows which form a vacuum to atmosphere interface will require replacement to ensure secondary containment in the event of catastrophic failure when tritium is used. A contract has been placed for the manufacture of double-walled units to replace the large bellows which connect the PINIs to the injector and enable the beam-axis to be correctly aligned. Installation of the first set is already underway. Double-walled insulated feedthroughs have also been designed, manufactured and delivered. A modification

to the PINIs compatible with remote handling requirements has been designed and successfully tested. This will allow potentially tritiated water to be drained out of the system should a water to vacuum leak occur during operation in tritium.

References

[1] D. Stork "Neutral Beam Heating and Current Drive Systems", 16th Symposium on Fusion Technology (SOFT) 1990, (Invited Paper to be published in Fusion Engineering and Design, and JET Report JET-P(90)63.

[2] P. Massmann, A.J. Bickley, J.F. Davies, G.H. Deschamps, H.P.L. de Esch, H.D. Falter, R.S. Hemsworth and T.T.C. Jones. Proceedings of 16th Symposium on Fusion Technology (SOFT) 1990, to be published, and JET Report JET-P(90)56.

[3] H.D. Falter, D. Martin, P. Massmann, H. Altmann, G. Deschamps, E.B. Deksnis, R.S. Hemsworth, R. Tivey and E. Thompson. Proceedings of 16th Symposium on Fusion Technology (SOFT) 1990, to be published and JET Report JET-P(90)56.

ICRF Heating and LH Current Drive Systems

The purpose of the powerful ion cyclotron resonance frequency (ICRF) heating and lower hybrid (LH) current drive systems (Fig.27) are quite different:

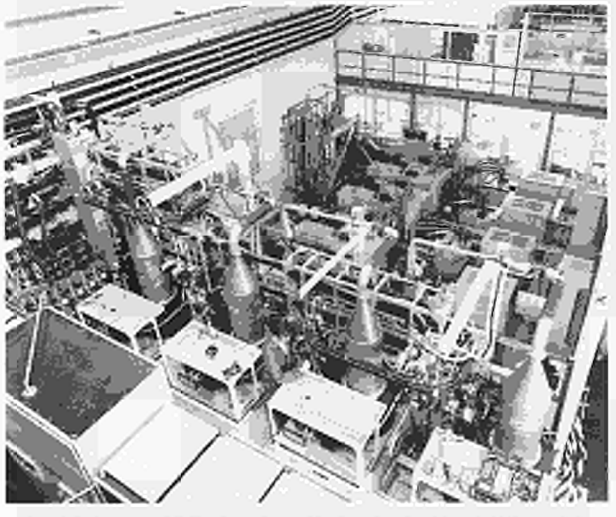

Fig.27: View of RF plant installation in the North Wing of the JET building where space is at a premium, showing four klystrons, part of the recently completed LHCD plant, installed above some of the existing ICRF generators.

- The ICRF heating system is used for highly localized heating of the JET plasma. The wide frequency band (23 to 57 MHz) allows variation in the position of heating as well as the ion species which is resonant with the wave (H or ^{3}He at present, D in the future D-T phase). The maximum design power is ~ 24 MW in the plasma. The system upgrade was recently completed and a power of 22 MW has been coupled to the plasma.
- The LHCD (Lower Hybrid Current Drive) system (12 MW at 3.7 GHz) is used to drive a significant fraction of the plasma current by direct acceleration of the plasma electrons, in order to stabilize sawtooth oscillations, thereby increasing the central electron temperature and improving the overall JET performance. This is the main tool for controlling the plasma current profile. A prototype system consisting of 2 launching units (LOC built by CEA Cadarache, France, and LOP built by JET) fed by a total klystron power of 4 MW was installed in 1990 and physics experiments have started (1.6 MW coupled to the plasma). The main results are discussed in a later section of this report (Profile Effects and Related Physics Issues). In this section, discussion is limited to technical achievements made during 1990.

Technical Achievements with the ICRF System

The original design power of the ICRF heating system was 15 MW for 20 s. However, the upgrade of each of the eight generators from 3 MW to 4 MW is now complete (two generators were finally upgraded at the beginning of 1990), and a maximum power of about 22 MW (21 MW for 1.75 s) has been coupled to the plasma. The maximum power achieved is within 5 % of the theoretical limit taking losses and reflection in the system into account. Pulse lengths were limited and longer times only possible at lower power level due to energy limitations on the vessel (excessive power loading on the plasma limiters). Table IV summarises the main characteristics of the RF system as used in 1990.

A number of enhancements to the power plant and antennae system were commissioned during the year. Most notable was the use of the antenna coupling resistance to automatically control the plasma position by feedback in order to maintain a constant loading resistance despite L-mode to H-mode transitions. This method is used in combination with the existing matching systems to produce

Table IV
Nominal Characteristics of the ICRF Plant in 1990

Frequency Range	23 to 57 MHz
8 Generators	4 MW output per generator module (20 s)
8 Antennae	• Beryllium bars (15° inclination) • Two adjacent loops operated with either Monopole phasing (0,0) or Dipole phasing (0,π), or a phased array. • Getter pumps on vacuum transmission lines
16 Transmission Lines (Generator to antenna)	Each line 84 m long rated at 50 kV peak (ϕ ~ 230 mm, 30 ohms)
Feedback loops for control of:	• Plasma position for constant coupling resistance • RF power level • Tetrode screen dissipation (acting on anode voltage) • Phase between the antennae • Frequency ($\Delta\nu$ ~ 1 MHz) for matching • Motorised tuning stub for matching

a constant match for the generators. These enhancements combined with the beneficial effects of the new beryllium screens have increased the availability of high RF power and have allowed important contributions to various aspects of the JET experimental programme [1].

Major new physics achievements include:

- The combination of two enhanced confinement regimes: the Pellet Enhanced Performance (PEP) and the H-mode using 10 MW of ICRF (central heating) heating and 2.5 MW NBI (diagnostics) with resulting high performance in the fusion product;
- A new record fusion yield - 140 kW obtained from ^{3}He-D reactions with ^{3}He minority accelerated by RF near the optimum of the fusion cross-section (0.5 MeV);
- Attainment of sawtooth-free periods of up to 8s (monsters) which proved an essential feature of high fusion yield discharges.

Enhancement of the ICRH Plant and Control System

A major difficulty for the ICRH plant is the rapid variation of the antenna load with plasma conditions. A good example of this is the change of the loading resistance (R_c) shown in Fig.28 during L- to H-mode transitions.

A new feedback circuit [2] has been added which complements the existing matching circuits. The plasma position is controlled by the desired RF coupling resistance and this is held constant throughout the pulse, see Fig.28. The existing frequency control makes (fast) orthogonal corrections for the plasma conductance (RF) and minor adjustments to the tuning stubs with the result that the RF generators tuning is held almost constant during the pulse.

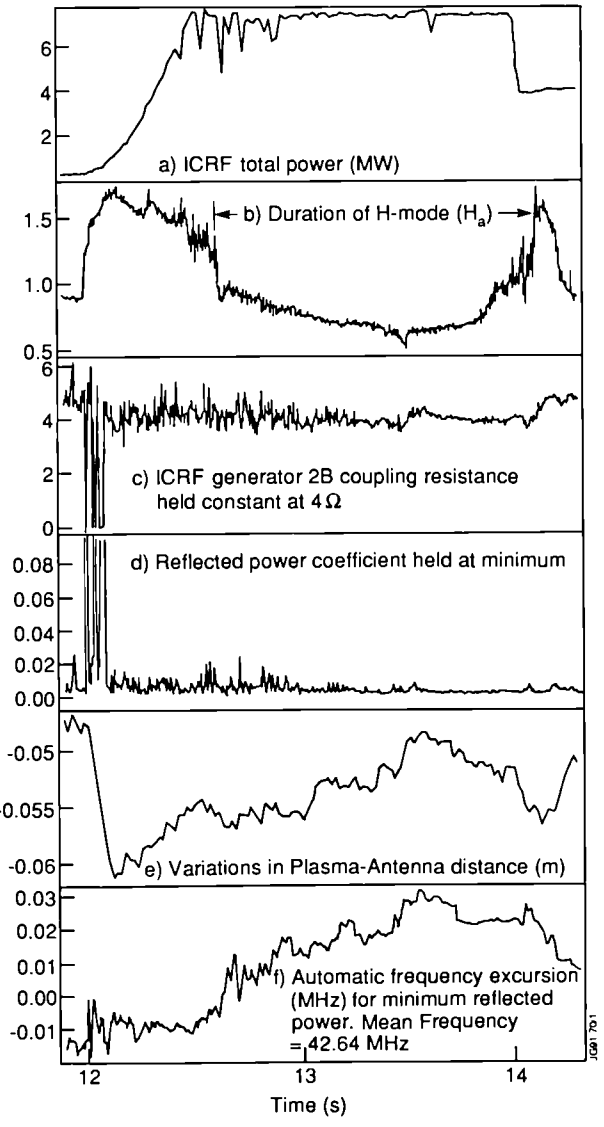

Fig.28: Antennae coupling resistive control of plasma position during H-mode transitions in Pulse No:21906. During the RF Power pulse (a), which contains an 'H' mode (b), the coupling resistance at the antenna (c) is held constant, and the reflected power kept at a minimum (d) by the automatic control of the plasma position (e) and incremental frequency.

It has also been found necessary to add further control circuits to cope with the transient high voltages occurring during antenna arcs. Some antenna arcs were inducing damaging "burn-outs" in the generators by referred high voltages to unprotected components. Tripping the RF power on detected arc-radiated light in the generator clears the fault so that power can be reapplied without final damage.

Fig.29 summarises the pattern of operation with the ICRF system in 1989 and 1990. It can be seen that the proportion of high power shots is larger in 1990 despite the short period of operation. This improvement is mainly due to the improved selectivity of the plant protection circuits. For clarity, low power tuning shots have been excluded from the statistics.

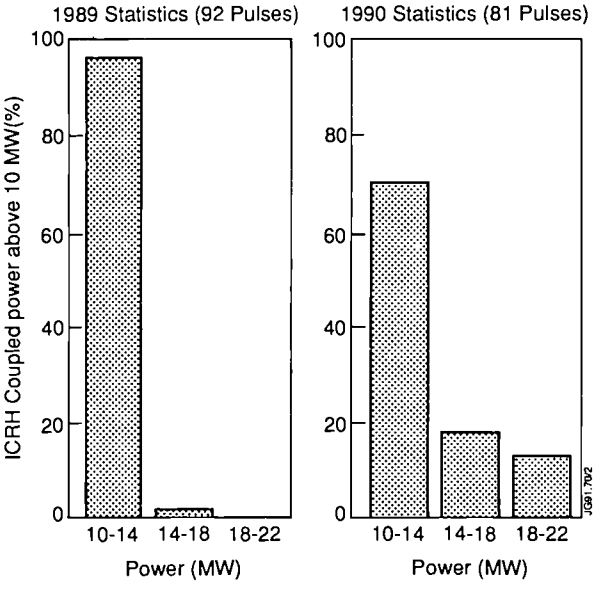

Fig.29: Histogram of the ICRF coupled power above 10 MW showing an increased proportion of higher power pulses. (Lower power tuning and commissioning shots have been excluded for clarity).

Beryllium Screens

JET has replaced the antenna screens made with nickel tubes by a new screen assembly made of solid beryllium rods (Fig.30).

The change was motivated both by impurity physics aspects and by certain technical reliability considerations as follows:

- Beryllium getters oxygen and has a very low self-sputtering coefficient which are dominant effects in impurity release due to RF sheath rectification on the screen [3,4]. Results obtained with beryllium screens have confirmed that impurity effects specific to ICRF heating have been reduced to negligible levels.
- The good electrical conductivity of beryllium together with the use of an open structure allowing the line-of-sight into the antenna, (see Fig.31) permits dispensing with circulating water inside the screen elements and eliminates the large number of welds between the elements and the water manifold. The heat can now be removed by radiation and by conduction from the end of the elements to water flowing in a manifold forming a "picture frame" around the antenna.

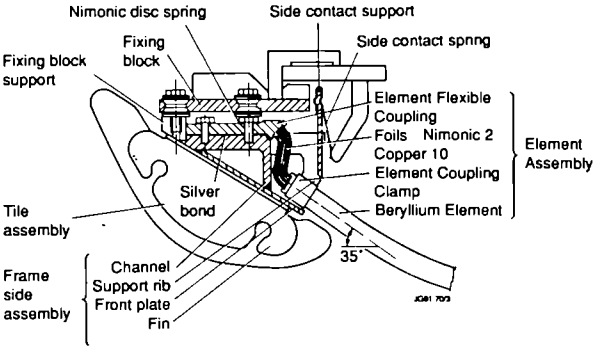

Fig.30: A section of the Be screen side manifold showing the attachment of the element to the water channel by a flexible pivot.

The construction and testing of the screens proceeded well. The 500 flexible couplings connecting the Be elements to the manifold (see Fig.30) were the critical components. These were fabricated by electron beam welding of copper chromium alloy foils to the mounting blocks, followed by precipation hardening. Fatigue testing of samples showed a lifetime in excess of 200,000 cycles for 3 mm displacement. Static load tests of 1000 kN radial load and 500 Nm torque about a vertical axis were also successfully applied to a test element mounted on two couplings.

The screen elements were produced by electro-erosion of curved elements from stock beryllium plates. These were subsequently machined on all surfaces and finally etched to remove surface damage. Load tests at room temperature and 400°C confirmed the mechanical design of the element.

The prototype screen was RF tested with aluminium elements up to 35 kV peak for 20s. The temperature rise in the screen was less than 20°C, and corresponded to a coupling resistance of ~0.01Ω. This is less than half the value used for thermal analysis, and confirm this validity of

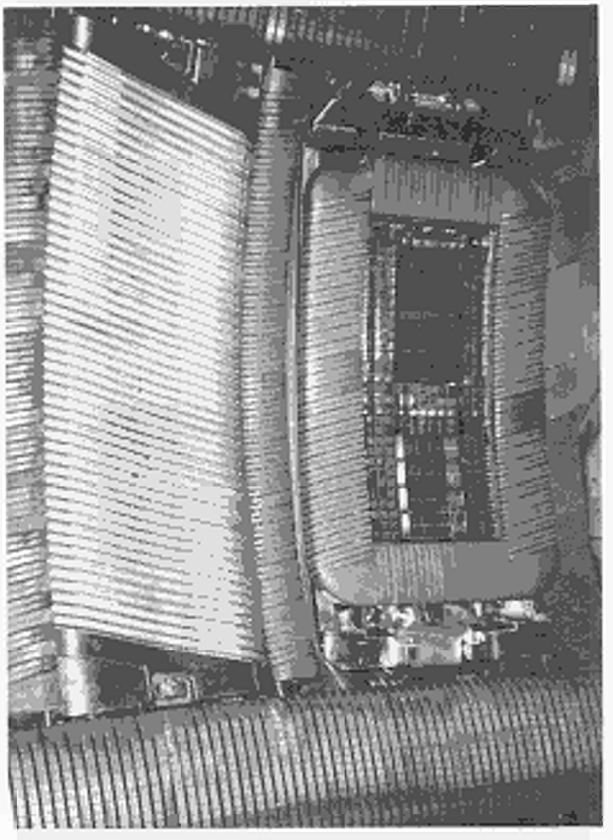

Fig.31: View of the LHCD launcher in the torus, adjacent to one of the existing eight ICRF antennae. The upper and lower prototype launchers together with the carbon side protection tiles (similar to ICRF) can clearly be seen. The ICRF antenna conductors are just visible through the beryllium bars of the new open ICRF screen.

the cooling system. In fact, during subsequent campaigns, the system will operate without cooling water in the antenna/belt limiter system.

Technical Achievement with the LHCD System

During 1990, the prototype launcher compromising one third of the number of waveguides of the full system was tested and installed on the torus. The corresponding eight klystrons and associated drive, phase control and power transmission system (Fig.32) have also been installed and commissioned, and the system used in operation during the experimental campaign [5].

The main achievements were:

- Up to 50% drop in loop voltage is observed which increases more than linearly with the power per particle parameter P_{LH}/n_e and has no apparent dependence on the plasma current;

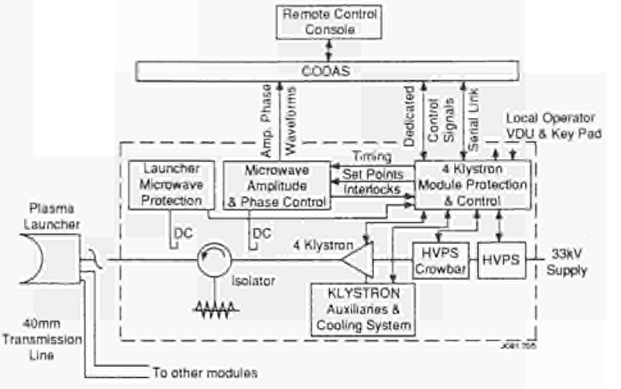

Fig.32: Block diagram of LHCD klystron amplifiers control and monitoring.

- Current Drive efficiency appears to increase substantially with the volume average electron temperature $< T_e >$;
- Non-inductive currents up to 1.2 MA are driven at $< T_e > = 1.9$ keV, with corresponding efficiencies $\eta = 0.3 - 0.4 \times 10^{20}$ m^{-2} A/W.

These results are in qualitative agreement with estimates based on the spectral gap model and quantitatively exceed the values originally predicted for the JET system.

In the limited experimental and commissioning period that was available, the prototype system has operated at 1.5 MW for 20s and 1.6 MW for 10s on JET, and these initial experiments were performed with phase control of the klystrons, at their output, and with ±180° phase modulation of the klystron output to assess relative phase at the grill mouth. Initial coupling studies in X-point plasmas have been performed (see Fig.33). The details of the LHCD final system are shown in Table V.

The assembly of the L0 launcher proceeded largely as planned, and provided valuable data for the impending assembly of the L1 launcher. Then the assembly and launcher were tested (under vacuum) by applying high power to each window in turn with a matched load at the grill mouth on some but not all channels. These tests showed that the required power (300 kW per window) could be reliably coupled after a short period of conditioning [6].

Installation of the launcher on JET was completed during the '89/'90 shutdown (Fig.31). In particular, this required precise positioning of the in-vessel hanger for supporting the grill mouth whilst enabling radial movement of the launcher. (This unit, which incorporates highly stressed inconel 718 flexure pivots, remains in good condition after the 1990 JET campaign). Subsequent installation included the system for controlling the radial position of the launcher. This is one of

Table V
LHCD System Parameters

Generator	*Final System*	*Prototype System*
Frequency	3.7 GHz	
Number of klystrons	24	(8)
Power (generator)		
10s pulse	15 MW	(5)
20s pulse	12 MW	(4)
Duty cycle	1/30	
Efficiency	42 %	
Phase control	10 degrees	
Maximum VSWR	1.8	
Length of transmission line	40m	
Estimated insertion losses	1dB	
Launcher		
Number of waveguides (48 multijunctions)	384	(128)
Waveguide material	stainless steel	
Coating	copper	(copper + carbon)
Maximum temperature	500°C	
Total weight	15 tons	(10)
Stroke	210 mm	
Response	12 mm/15 ms	
Pumping	100 000/s^{-1}	

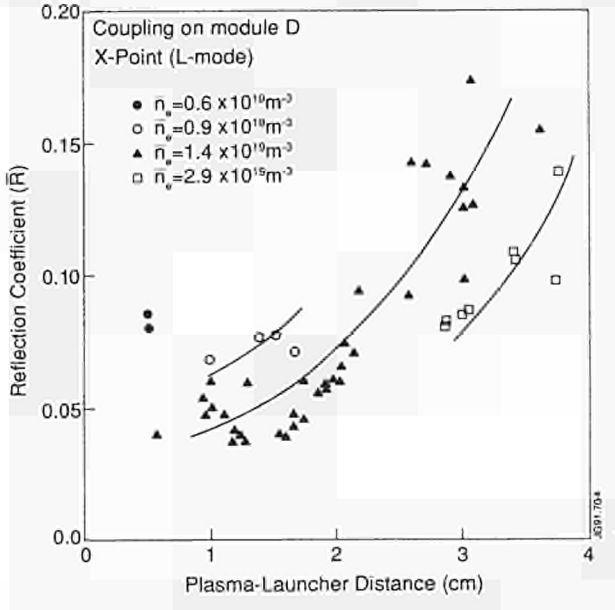

Fig.33: Reflection coefficient versus plasma-launcher distance for four different plasma densities.

the main tools for achieving the correct coupling between the RF waveguides and the plasma boundary.

The motion of the launcher is determined by hydraulic cylinders mounted between a reactive flange on the fixed torus port and thrust pads on the LHCD vacuum vessel (Fig.34). An electro-mechanical repro-valve is used to control two servo-cylinders connected in parallel, the launcher alignment being determined entirely by the two supporting hangers. The vacuum load of ~17 tonnes is supported by three offset cylinders, also connected in parallel and operating at near constant pressure. The feedback system on the servo-cylinders is designed to allow the position to be controlled within ±1 mm during the entire duration of the plasma pulse.

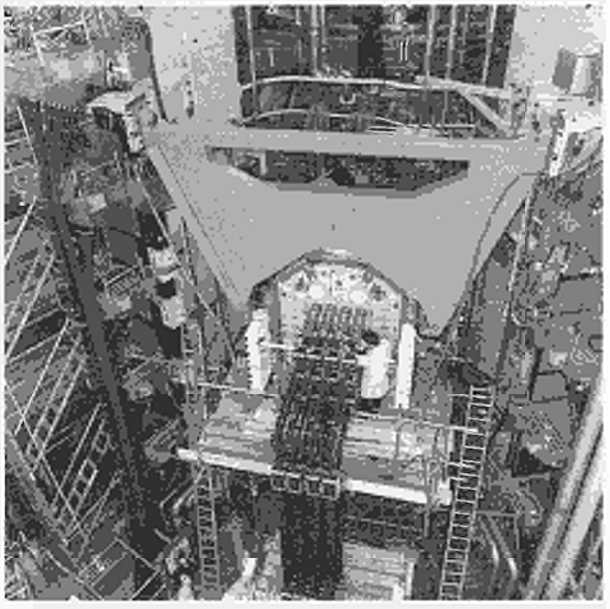

Fig.34: An external view of the Lower Hybrid Current Drive Launcher on JET. Its vessel is supported by the large frame. The prototype system has 16 waveguides connected to the RF vacuum windows at the point of entry to the vessel. The entire assembly can be moved with hydraulic actuators during the plasma pulse.

This system has operated for the first time on JET during the 1990 campaign. The launcher was maintained within ±2 mm for continuous periods up to ~100 hours during torus operation. Single sinusoidal waveforms have been applied during the pulse. The performance is presently hydraulically limited by failsafe components to a maximum velocity ~0.2m/s and an acceleration of 1m/s^2 in order to avoid any risk of damage to the launcher during commissioning. Residual problems with fluid contamination, magnetic interference and small oscillations will be resolved for the 1991 campaign. In-vessel inspection at the start of the present shutdown showed the launcher grill to still be in good condition.

Manufacture of the L1 launcher is in an advanced state. Following a review of the programme, it is now planned to

install this launcher with the pumped divertor in 1992. This has required some design changes to match the shape of the grill mouth to the larger plane profile, and has required some delay in manufacture pending completion of the design. The 48 multijunction units at the heart of the launcher are, however, complete apart from final internal machining to the revised design.

An Article 14 Contract with IPP Garching, F.R.G., to investigate coatings for suppression of multipactor arcs has also been completed. Many coating were investigated. Whilst none fully met the JET requirements, notably high temperature stability combined with low RF losses, two coatings show good potential and are being further assessed for possible application to the L1 launcher.

References

[1] "ICRF Heating in Reactor Grade Plasmas", The JET Team, 13th Conference on Plasma Physics and Controlled Nuclear Fusion Research (Washington, U.S.A.) (1990) IAEA-CN-53/E-2-1;

[2] "Automatic VSWR Control in JET ICRH Transmitters", G Bosia et al, JET Report JET-P(90)62, p 67;

[3] "ICRF Impurity and Antenna Studies", D. A. D'Ippolito, J. R. Myra, M. Bures, J. Jacquinot and M. Stamp, 13th Conference on Plasma Physics and Controlled Nuclear Fusion Research (Washington, U.S.A.) (1990), IAEA-CN-53/E-2-1;

[4] "A Model of Sheath-driven Impurity Production", D. A. D'Ippolito, J. Myra, M. Bures and J. Jacquinot, to be published in Plasma Physics and Controlled Fusion (1991);

[5] "Lower Hybrid and Current Drive Experiments in JET", 32nd Annual Meeting of the Division of Plasma Physics of the American Physical Society (APS), (Cincinatti, U.S.A.), (1990);

[6] "High Power Tests of the JET Prototype LHCD Launcher", H. Brinkschulte et al, JET Report JET-P(90)62, p91;

[7] "RF Heating and Current Drive Status and Prospects for the Next Step", C. Gormezano, to be published in Fusion Engineering and Design, Proceedings of the 16th Symposium on Fusion Technology (SOFT) (London, U.K.) (1990);

[8] "High Power Tests of the JET Prototype LHCD Launcher", to be published in Fusion Engineering and Design, Proceedings of the 16th Symposium on Fusion Technology (SOFT) (London, U.K.) (1990).

Remote Handling and Beryllium Handling

During 1990, remote handling development work was supported at a much lower level than planned due to the heavy involvement of manpower of the Remote Handling Groups in the major shutdowns. This involvement meant that the articulated boom was unavailable for mock-up work whilst installed on the torus and then also unavailable whilst being maintained and prepared for the next shutdown. In addition, the Beryllium Handling and Waste Management Groups were subjected to a heavy work load. Main progress in these areas is set out in the following paragraphs.

Remote Handling

Articulated Boom

During shutdowns, approximately 50 entries into the vessel were carried out under teach-repeat control. Substantial use was made of the new editing facilities to reverse or mirror image existing teach files. This resulted in considerable time savings, particularly in the difficult manoeuvre through the narrow entry port, and is a significant step towards true remote operation of the boom. The boom was used for the installation of the new LCHD antennae (side protection and hanger), a complicated operation which exploited to the full the articulations the boom provides and its precise control. In November/December, 32 dump plates were installed over a two week period.

Operational experience has enabled issues of reliability and operational safety to be addressed with increasing attention. Monitoring facilities have been introduced, including load detectors, monitoring of joint operating times for maintenance scheduling, joint current for setting of maximum values and monitoring and recording of operator commands to aid fault diagnosis.

A new boom extension structure was designed and verified with finite element analysis to check stress concentrations at the mechanical end stops during fault conditions. The new design allows an increase in the tilt angular range of motion so that vertical pick-up of components is safety achieved. This method has been used for both antennae and dump plate installation. A quick release mechanism has been designed to free the joints and retrieve the boom should the actuators seize in the vessel.

An overall safety assessment has been instigated and is now underway under a task agreement with the Ispra Research

Centre, Italy. It includes the aspects of operation, control and collision avoidance.

During 1990, a decision was made to build a new boom control system, to replace the existing PLC based design, which is ageing and difficult to enhance. The new hardware, based on Multibus II, has already been selected and procured, and the analysis and design of software is well under way. It is expected that the new system will be ready for operation by the next major shutdown in late 1991.

Telescopic Articulated Remote Mast (TARM)

Manufacture of mechanical parts and control was completed and the massive work of wiring was finished at JET. The TARM was delivered to JET and assembled on a stillage in the Assembly Hall, together with 80% of the service cubicles (see Fig.35). After careful mechanical testing and commissioning of the controls, a Mascot servomanipulator was installed on the terminal interface (docking) module and some turbomolecular pump maintenance scenarios were demonstrated. The TARM was subsequently hoisted onto the crane trolley to check its complex geometrical fit to the crane.

Commissioning and refinement of the robotics control system, a uniquely complex system controlling 32 degrees of freedom, is in progress. The main controls are already proving very satisfactory in both teach-repeat and resolved motion.

150T Crane

The cables of the reeling system had to be replaced with polyurethane sheathed cables, as the low smoke sheathing previously supplied proved unsuitable for the continual flexing movements. During this operation, about 50 optical fibres for the control of TARM were inserted. The problems encountered prompted the design and construction of a cable multiplexer. This will reduce the number of cables from about 120 (some heavy duty) to about 4 twisted pairs, with no discernible delay in response times. In addition, the multiplexer constitutes an ideal prototype controller for use in true remote conditions, and is easily enhanceable to add a variety of useful facilities, like automatic fault logging and control of special lifting equipment. Testing and installation of the multiplexer is planned for early 1991.

Mascot

Use of the two units has put in evidence the dexterity features of this manipulator. Using support staff seconded to JET by

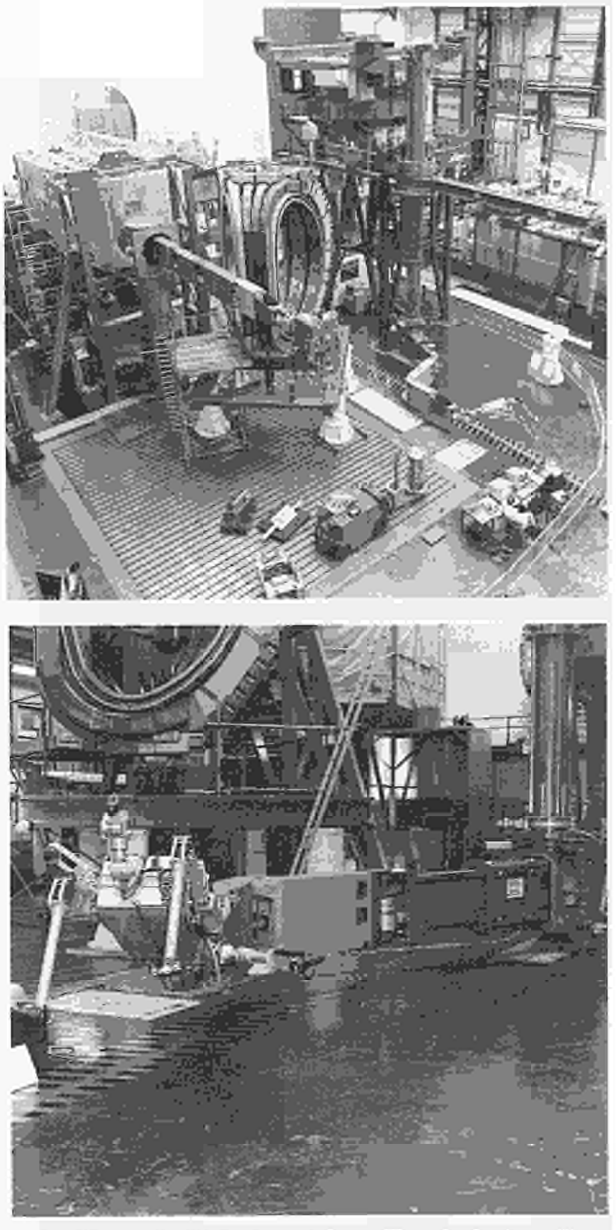

Fig.35: (a) The TARM installed on stillage in the Assembly Hall, shown with Mascot approaching a turbopump on a low level transporter for remote handling trials; (b) both TARM and Boom can reach the inside the spare Octant for in-vessel tests.

the Ecole Polytechnique de Lausanne (EPFL), Switzerland, the control algorithm has been reconfigured so that the control parameters are now decoupled and can be set independently from one another, with the help of a simplified computer model. Following this, an Article 14 Contract has been placed with EPFL to complete and refine the dynamic model of the servo to optimise aspects of the control, such as acceleration control and linearisation of motor characteristics. It is also intended to study the applicability of alternative motors with a view to trying to reduce the power losses. If successful, the practical result will be that the manipulator

can work for longer periods without overheating, a problem caused by the necessity of encasing the manipulator in gaitering to avoid contamination.

End Effectors

The lifting devices for the LHCD system side protections and hanger and for the beryllium antennae were successfully and intensively used in the vessel. Some details were improved to enhance safety and ease of control.

In-Vessel Inspection System (IVIS)

Inspections of the vessel after disruptions were requested with increasing frequency, and with IVIS, it was possible to point out where damage had occurred, so enabling the operational programme to be tailored accordingly. In view of the increasing importance of these inspections, improvements of the quality of the image and its interpretation are being implemented. An alternative camera unit prototype has been developed, including a zoom facility for better resolution. The prism was redesigned with a ray tracing programme developed for use on Silicon Graphics. A CCD camera is used because it is less affected by electrical noise and sensitivity can be enhanced by integrating with the existing Kristal image processor. A new interface system has been developed, to compose on the Silicon Graphics workstation a wide angle mosaic of the recorded images which are then easily retrieved and blown up.

The IVIS motors have been repositioned away from the magnetic field which was found to be intense enough to demagnetise the rotors. For the same reason, the motors driving the light guides and fans are being replaced with universal and AC types. The IVIS lights were also used as a convenient beryllium compatible lighting system during shutdown work.

The new probe, being developed by ENEA, Italy, under an Article 14 Contract, aims to eliminate optical aberrations by replacing the viewing cylinder with a flat sapphire window. It is now ready for hot tests in a temperature controlled oven under vacuum.

A preliminary study has been carried out on high resolution image acquisition by means of a vertical line scan camera with wide angle lens. A system of this type would give a 350 degrees panoramic picture and would not require a tilt motion. A more accurate and up to date analysis of the dynamic loading on the vertical IVIS entry ports during disruptions was made possible by new experimental data. This has led to the conclusion that the life of the material should be adequate without mechanical decoupling, unless future magnetic configurations change the situation.

Special Tools

The majority of work involving special tools has been concerned with the development and use of existing designs for hands-on work in the JET shutdowns. The new cutting and welding trolleys were used extensively during the Octant No.4 replacement work. These were used for a variety of lips but most notably were used to cut and weld the Octant 'U' joints. Further development to facilitate their application to slightly deformed lips is now being undertaken.

Other special tool work included:

- The new 20-27 mm diameter slitting saw and butt weld orbital welding tools were commissioned and used on the JET machine for the first time;
- The 91mm diameter circular port cutter has been improved by the modification of the swarf extraction system, the introduction of a facility to simply change and adjust the cutting tool bit, the introduction of a feed indication device and the remotisation of the power drill attachment mechanism;
- Various improvements have been made also to the 50 mm diameter slitting saws, the 50mm diameter bore cutter, the sleeve welders and the whole range of circular port welders;
- New design work has started on the range of tools which will be required for first installation of the pumped divertor system;
- Two additional cutting tool controllers have been built, bringing the total to four, all functionally identical. The latest software enhancements include the ability to drive the new hydraulic return punch on the cutting trolley, and the new 27 mm slitting saw with a variety of cut profiles.

Mock-Ups

The PINI mock-up which was started in 1989 was completed, reviewed and reported on during 1990. As a result of the mock-up work there were approximately 20 recommendations for changes to the PINI system components and 50 recommendations for modifications/enhancements to the remote handling equipment. The ex-vessel mock-up work has since ceased due to lack of available staff and will restart in 1991 with the intention to make full use of the TARM. A

program of bench testing various RH tools and handling devices has recently been started. This work is concentrating on the problems of handling in-vessel tiles.

RH Integrated Control System

It was decided during 1990, in line with the extensive CODAS modifications, to change the Remote Handling Man-Machine Interface to be based on UNIX workstations. This fitted well with previous development work, in conjunction with KfK Karlsruhe, F.R.G., in the area of real time 3-D image displays. As part of this the communication and control network for the RH equipment was also rationalised to be Ethernet based.

A new MMI concept was derived and an order placed for a prototype Hand Control Terminal. This HCT will facilitate control of any RH equipment both under "hand-on" or "local" control and fully remote from the RH Control Room.

The second phase of work with KfK was completed in 1990. This has resulted in the provision of a software facility installed on the JET Silicon Graphics UNIX workstation which enables the display of a computer generated 3-D image of the TARM operating within the Torus Hall, (see Fig.36). The model of the Torus Hall can be displayed at various levels of detail dependent on operator's choice. The models have been created using a CATIA system, downloaded to the Silicon Graphics and then displayed by the KfK "KISMET" modelling software. This facility is now being used to create a new in-vessel model showing the pumped divertor configuration. It is fully expected that the collaborative work with KfK will continue but with emphasis now on the application of the KISMET software package to the RH mock-up work.

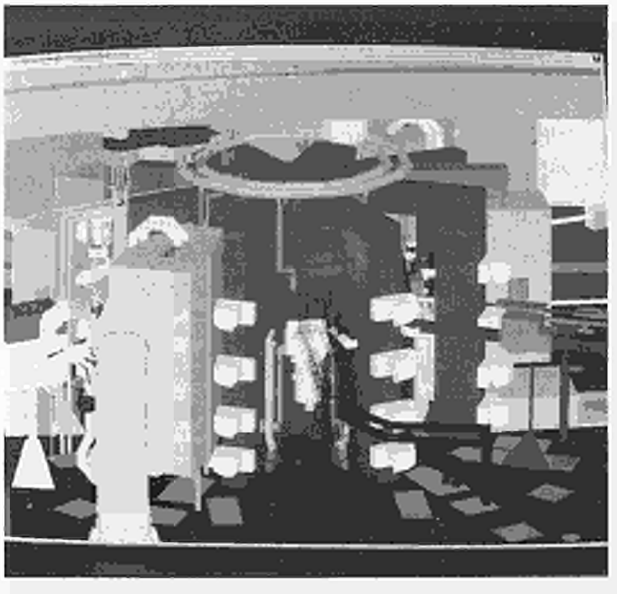

Fig.36: Display of computer generated 3-D image of the TARM operating in the Torus Hall.

RH Manual

The Remote Handling Manual has been reviewed and updates to existing chapters together with the generation of new chapters have been issued. This process will continue in 1991 as the work priorities allow.

Beryllium Handling and Waste Management

Beryllium Related Operations

There were about 27 weeks of in-vessel intervention work during 1990 in three shutdown periods. Respiratory protection and protective clothing were required throughout this period with most of the work being carried out in pressurised suits.

Further enhancements to the Torus Access Cabin (TAC) were carried out to improve the flow of personnel and materials. The most significant change was the attachment of the TAC to the Site Active Drain Line which, in combination with a new filtration system, allows the aqueous waste from the TAC to be disposed of without recourse to the mobile bowser.

The Beryllium Handling Facility (BHF) in the Assembly Hall has been in operation throughout the year on support operations for the in-vessel programme. These have included component decontamination and modification. Planned improvements in this area include new decontamination equipment and aqueous waste filtration. These will be installed in 1991 when the facility will also be linked to the Site Active Drain Line.

A dedicated facility for cleaning, inspection and repair of pressurised suits and respirators was commissioned in early 1990. Around 100 suits/week are handled during the shutdown periods. During the year, an $8m^3$ drain tank was commissioned for the wash water. This has also been connected to the Active Drain Line. The PVC workshop has been used to fabricate over 250 isolators during the year in addition to carrying out site work on isolator systems using mobile RF welding equipment.

Waste Management

Waste generated during in-vessel operations is classified initially as potentially active waste. A sampling facility has been commissioned in the Berylium Handling Facility and

the waste samples are analysed at AEA Harwell Laboratory for activity. A sniffing method is being used to detect tritium in potentially tritium contaminated solid waste. Results so far indicate significant levels of activity, and, assuming the surface tritium levels are also low, most of the arisings of in-vessel housekeeping wastes will be reclassified as non-active beryllium contaminated wastes.

During 1990, 100m^3 of beryllium waste were disposed of in 200 litre drums. Analysis of the waste indicated levels of beryllium significantly less than 1%. Consequently, following an agreement with the Local Authority, a disposal method using a lockable covered skip for the double bagged housekeeping waste has been introduced. About 100m^3 of waste were disposed of by this method during the year. The Q/A system covering the disposal of low level solid active waste will be finalised in early 1991. Transfer of the small amount of waste in this category via AEA Harwell Laboratory to the Drigg Site in the UK will follow.

A scheme for the storage and transport of tritiated aqueous waste from the Active Gas Handling Building has been devised and the equipment and facilities will be procured and installed during 1991.

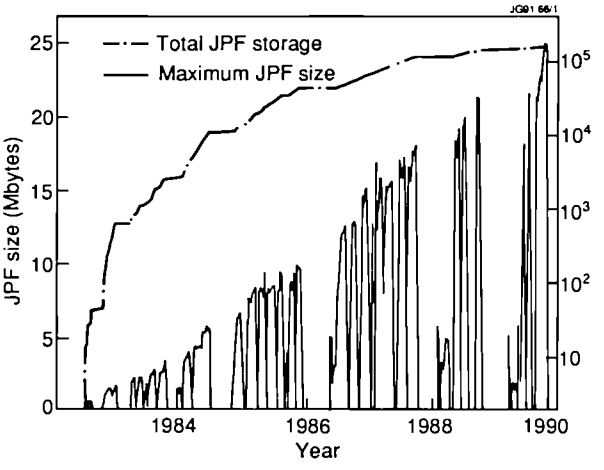

Fig.37: Evolution of JPF size and total JPF storage over the years.

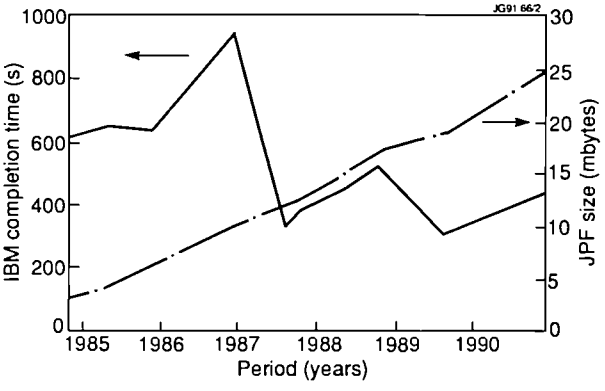

Fig.38: Evolution of JPF size and time to collect and transmit a JPF to the IBM mainframe computer.

Control and Data Acquisition (CODAS)

The JET COntrol and Data Acquisition System, CODAS, is based on a network of minicomputers. It is the only way to operate JET and it allows centralised control, monitoring and data acquisition. The various components of JET have been logically grouped into subsystems like Vacuum, Toroidal Field, Lower Hybrid additional heating, etc. Each subsystem is controlled and monitored by one dedicated computer interfaced to the machine and its diagnostics, through CAMAC instrumentation and EUROCARD-based signal conditioning. Embedded front-end intelligence is implemented through CAMAC-based microprocessors for real-time applications. The actions of the various computers are coordinated by a supervisory software running in the Machine Console computer. This supervisory function includes the countdown sequence for each plasma discharge. The present allocation and configuration of all CODAS computers is given in Table VI, while Tables VII and VIII provide other quantitative data. Figs.37 and 38 illustrate the evolution of the JET data acquisition over the years.

During 1990, CODAS Division has continued its role of expanding and improving its operational support to the operation of JET and has also laid the foundation to ensure that, if the project is extended beyond 1992, the availability and efficiency of its control and data acquisition system would be maintained in the best possible way. These points will be expanded within the sections on operational support and CODAS after 1992.

Operational Support

Electronic Interface

Expansion was moderate this year and a total of seven interface cubicles were designed, built, installed and tested for the Lower Hybrid system, for the precursors of the Pumped Diverter Diagnostics and for the Reactive Power Compensation systems. These installations required a corresponding software effort to incorporate those extensions into daily operation. In addition, a total of 263 fully documented improvements were made to existing systems. The

Table VI
CODAS Computer Configuration at the end of 1990

Sub-System	*Usage*	*Model (MByte)*	*Memory*	*Disks (MByte)*
AH*	NI Additional Heating (Oct 8)	ND110CX	3.5	1x70 1x450
AN*	Analysis and Storage	ND560	4.0	1x70 1x140 2x450
AS	Assembly Database	ND110CX	2.0	2x450
CB	Message Switcher B	ND110CX	4.0	1x70 2x140
CP	Cables Database	ND530	6.0	1x70 1x450
DA*	On-line diagnostic	ND520	4.0	1x70 1x140
DB*	On-line diagnostic	ND520	4.0	1x70 1x140
DC*	On-line diagnostic	ND520	4.0	1x70 1x140
DD*	On-line diagnostic	ND530	4.0	1x70 1x140
DE*	On-line diagnostic	ND520	4.0	1x70 1x140
DF*	On-line diagnostic	ND520	6.0	1x70 1x140
DG*	On-line diagnostic	ND520	4.0	1x70 1x140
DH	Diagnostic Commissioning	ND550	6.0	1x70 1x450
EC*	Experiment Console	ND570CX	6.0	1x70 1x140
EL	Electronics	ND110CX	2.0	1x70 1x140
GS*	General Services	ND110CX	2.5	1x70 1x140
XC*	Pellet Test Bed	ND110CX	4.0	2x70 1x140
LH	Lower Hybrid	ND110CX	3.5	1x70 1x140
MC*	Machine Console	ND110CX	2.5	1x70 1x140
PF*	Poloidal Field	ND110CX	3.0	1x70 1x140
PL*	Pellet Launcher	ND110CX	2.5	1x70 1x140
PM*	Pulse Management	ND550	7.0	1x70 1x140 1x450
RB*	Radio Frequency Test Bed	ND110CX	2.25	1x70 1x450
RF*	Radio Frequency	ND100	3.0	1x70 1x140
RH	Remote Handling	ND110CX	2.5	1x70 1x140
SA*	Message switching & JPFCollection	ND110CX	4.0	1x70 1x140
SB	Standby-System/Backup	ND110CX	4.0	2x70 1x450
XX	Built-in, Pool, Computer dB	ND110CX	2.5	2x45
SS*	Safety & Access	ND110CX	3.0	2x70 1x140
TB*	NI Test Bed	ND120CX	4.0	1x70 1x450
TF*	Toroidal Field	ND110CX	2.5	1x70 1x450
TR	Tritium	ND110CX	2.5	1x70 1x140
TR	Test	ND520	4.0	1x70 2x450
VC*	Vacuum	ND110CX	4.5	1x70 1x140
YB	Integration	ND530	6.0	1x70 1x450
YC*	NI Additional Heating (Oct 4)	ND110CX	3.5	1x70 1x450
YD	Sc Dpt Development	ND570CX	6.0	1x70 1x450
YE	CODAS System Development	ND520	6.0	1x70 1x450

* Indicates on-line computers used for operation and testbed

Quality Control facilities have been re-grouped and expanded to allow more in-house testing, leading to cost reductions.

Central Interlock and Safety System

This system provides the secondary line of protection for the JET device and is based on a network of Programmable Logic Controllers (PLCs). Some reorganization of the subsystem enable/disable key system was carried out. An almost complete recommissioning of the 1965 input/output signals was made together with a review of their fail-safe nature. Some of the subsystem logics were modified to include new equipment and the computerisation of the system's documentation has progressed significantly.

Services

The site-wide services like intercom, public address system, instrument pool and terminal network were modified to accommodate additional requirements. Of great significance, a new Local Area Network (LAN) was designed and

Table VII
Quantitative Information on CODAS Installation

Item	*End 1989*	*End 1990*
CODAS Interface Cubicle	159	157
CAMAC Crates	247	248
CAMAC Modules	3,382	3,289
Eurocard Modules (Signal Conditioning and Power Supplies)	7,346	7,951
CAMAC Serial Loop (Fibre Optic)	25	25
On-line Computers	24	
Off-line and Commissioning Computers	14	
Size of JPF	21MB	
Number of diagnostics on-line with CODAS	3	
Number of diagnostics under commissioning with CODAS	4	

implemented for the needs of CODAS. One of its servers is allocated for the storage and maintenance of computerised drawings (~4,000 using AutoCAD). The technology of this LAN, based on ETHERNET, has been selected at the project level to form the backbone of a JET site data network which may interconnect additional LANs and provide services like Electronic mail (E-mail).

The rationalisation of all of the CODAS hardware documentation and its integration into a single system, ELECTRA, has progressed well and should be completed in the coming year.

Feedback and Real-time Systems

Front-end feedback systems have continued to expand either by modifying existing control loops to adapt them to the operation or by providing additional facilities. The following are two typical examples:

- The plasma radial position feedback system has been modified to maintain the coupling resistance of the radio frequency (RF) antennae to a preset value during a specified time window. The coupling resistance is derived, in real time, from RF generator voltage measurements. This provides easier operation and a better control of the RF power coupled to the plasma;
- The changes in characteristics of the first wall have required substantial modification to the Plasma Density Feedback system which controls, in real-time, the setting of the gas introduction to obtain a pre-defined density. Although operating satisfactorily, the accuracy and dynamic performance of this system are still limited by the time lag between gas flow and density.

Table VIII
Review of CODAS Electronics Stock Holding
(installed, pre-procurement and spares)

	End 89	*End 90*
1. CAMAC system modules	918	911
2. CAMAC digital I/O modules	857	900
3. Timing system (CAMAC & Eurocard)	1,361	1,371
4. CAMAC analogue I/O Modules	1,224	1,389
5. CAMAC display modules	409	410
6. CAMAC auxiliary controllers	152	153
7. CAMAC powered crates	274	284
8. U-port adaptor	200	205
9. CISS modules	965	1,040
10. CCTV	698	694
11. Cubicle frames	345	345
12. Console devices (not CAMAC)	524	693
13. Power supply modules	1,848	2,071
14. Intercom, Public Address, Computer terminal network	635	651
15. Pool instruments	1,009	1,046
16. Analogue I/O in Eurocard	2,853	2,829
17. Digital I/O in Eurocard	4,909	4,901
18. Eurocard sub-racks	997	1,045
	20,178	20,938
Increase		3.8%

To improve the reliability of the operation of the JET device a new set of protective actions based on the real-time monitoring of the plasma behaviour has been devised and its implementation is underway. This new Plasma Fault Protection System has been devised and its implementation has been engineered by CODAS.

Expanded Facilities

The JET programme required changes to the Neutral Beam injection system. The CODAS hardware and software was enhanced to cope with the increase of the high voltage to 140kV and with the requirement to inject Helium as well as Deuterium or Hydrogen.

Future Work

During 1991, CODAS facilities will be expanded to provide the following services:

- Data link with the Active Gas Handling System;
- Interface with the Disruption Feedback Amplifier System;
- Interface to the Fast Radial Field Amplifier;

- New, or expanded, diagnostic systems;
- Initial preparation for the Pumped Diverter.

CODAS After 1992

Policy

After a comprehensive feasibility study and financial analysis of the possible means of maintaining the services of CODAS if the Project is extended beyond 1992, it was decided to port our existing system to a new platform. Practical considerations and timescale led to the conclusion that the present structure should be retained and that the existing facilities should be ported to a standard, i.e. non-proprietary, environment. The main characteristics of the new environment are:

- Computers using UNIX as operating system;
- Communication network based on ETHERNET (or FDDI if economical);
- CAMAC instrumentation to be retained;
- Computer interface to CAMAC to be based on Versa Module Eurocard (VME) standard;
- Man-machine interface to be based on workstations.

Considering the planning of JET and the time and effort required to port our control system, it was decided to make use of the JET 1992 shutdown to implement the change-over between the two systems. This approach, when compared to a gradual transition, has the advantage of reducing the effort which would have been requiredto have two co-operating systems which are of a different nature. At present, it is anticipated to run the Pellet Test Bed as a demonstration system by the end of 1991.

Current Status

A set of computers, a file server and two workstations were procured to start the development of the new system and about 11 man-years of effort have already been invested in this activity. A tool to facilitate the porting of low-level language to the C programming language is under acceptance procedures.

The first prototype of the VME board required to drive the CAMAC serial highway has been delivered (see Fig.39) and tests are underway. This required the implementation of a VME development system and usage of powerful software tools to exploit field-programmable integrated circuits. These tools will be used also for future development of advanced front-end intelligence. The cable scheduling service using the MIMER database management system has already been moved to a UNIX environment.

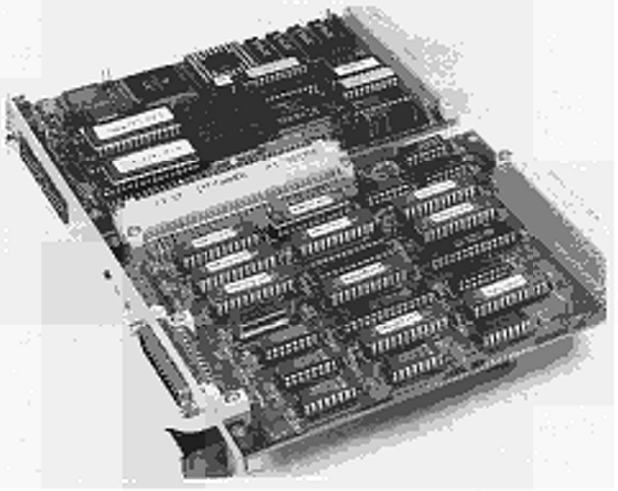

Fig.39: Prototype of the VME board.

The study mentioned earlier identified the need to carry out a complete review of all electronic modules in use at present, to ascertain their longer term adequacy. For assessment purposes, the modules were classified into four groups according to their importance. The groups were defined as

- Supported: These are essential types for which an assured source of new stock must exist. Maintenance spares stocks are held. New designs are built around these types;
- Maintained: Widely used types for which supported types could be substituted if all stocks were consumed or if maintenance became impossible;
- Tolerated: Non-essential types for which maintenance is not assured but which may remain in place;
- Abandoned: Nuisance types which are to be actively removed from systems.

The present stock has the profile shown in Table IX.

Table IX
Present Stock Profile

	CAMAC	EUROCARD
Supported Types	42	53
Supported Stock	4409	9738
Maintained Types	34	110
Maintained Stock	874	2369
Tolerated Types	3	45
Tolerated Stock	74	356
Abandoned Types	34	91
Abandoned Stock	120	87

Future Work

The design of the network required to link the new CODAS computers, the workstations and the computer terminals has started and should be completed in early 1991. The detailed

design of the new Man Machine Interface (MMI) is underway and should be completed in 1991. It will attempt to minimise costly retrofit in the existing application software. The tender action for the procurement of computers, workstations and X-terminals will be issued in the second half of 1991.

The main efforts of the Division will concentrate on the porting and testing of the CODAS software to its future UNIX environment. The effort required can be gauged by the fact that, at present there are more than 2,000,000 lines of FORTRAN source code and some 100,000 lines of lower level languages.

JET Data Management

The JET Data Management Group is responsible for the provision of a Mainframe Computing Service for scientific and engineering computing. This includes provision of appropriate software and hardware systems. The Group is also responsible for the management of JET data and for organisation and control of routine data processing.

The computing Service is based on an IBM 3090 three-way processor mainframe with two vector facilities. There are 70GBytes of disc storage and a further 240GBytes of IBM mass storage. The JET Mainframe Data Processing Centre is housed in a specially designed building at AEA Technology, Harwell Laboratory, and operated for JET under contract by a team from that Laboratory. The JET mainframe is also connected to the Harwell Laboratory CRAY2 computer.

The JET Computing Centre has been operating since June 1987 and the computing load has grown significantly since that date. In order to maintain good interactive response and also accommodate an increasing load of background batch work, the central computer was upgraded in February 1990 from an IBM 3090/200E with two processors, one vector facility and 64MBytes of memory to the IBM latest technology, 3090/300J with three processors, two vector facilities and 196 MBytes of memory (64MB central and 128MB expanded). This has almost double the processing capacity. Since the upgrade there has been a significant growth in all areas of the mainframe computing workload, most critically in the CAD work from the JET Drawing Office and interactive (TSO) work. The system software has also been upgraded during 1990, ensuring independence from the system on the Harwell IBM computer, leading to a simpler and more reliable system.

The Data Management Group provides the contact between the users, operators and system programmers, through the Help Desk Service, backed up by specialists in the Group. This ensures the smooth running of the system. The data communications between the JET site system and the Computer Centre are mainly the responsibility of CODAS Division and significant improvements in these areas are reported in that section.

The Group is also responsible for the storage of JET data and currently ~186GBytes of raw JET data (JPFs) are stored on the cached Mass Store in a compressed form, and a further 55GBytes of analysed data are stored on the PPF online database system. The Central Physics File (CPF), established during 1988 under the SAS environment, forms a complete higher level data selection and storage system. A subset of all data is extracted at time points of interest, determined by the Timeslice program and the interactive timeslice editor, TED, and stored in the SAS databases. These data are the basis for extended statistical analysis, and the source for other extracts such as the TRANSPORT bank. This complete system is a fully automated process, and is used by many physicists in the Project.

In addition to mainframe computing, the Group provides support for the increasing numbers of Personal Computers (PCs) on site which are used both as stand-alone workstations and terminals to the IBM and NORD computers, and for the Systems introduced for word processing.

Diagnostic Systems

The status of JET's operating diagnostic systems at the end of 1990 is summarized in Table X and their general layout in the machine is shown in Fig.40. The staged introduction of the diagnostic systems onto JET has proceeded from the start of JET operation in June 1983 and is nearing completion. The present status is that 41 systems are in routine operation. A further 27 systems are in preparation or in the design stage for operation in the New Phase of JET or in the active D-T Phase. This will be discussed further in the section on the New Phase of JET. Operational experience has been good and most of the systems are now operating automatically with minimal manual supervision. The resulting measurements are of a high quality in terms of accuracy and reliability, and provide essential information on plasma behaviour in JET. Further details on specific diagnostics systems are given below.

Table X
Status of the JET Diagnostic Systems, December 1990
Operational Diagnostics

System	Diagnostic	Purpose	Association	Automation
KB1	Bolometer array	Time and space resolved total radiated power	IPP Garching	A
KC1	Magnetic diagnostics	Plasma current, loop volts, plasma position, shape of flux surfaces, diamagnetic loop, fast MHD	JET	A
KE1	Single point Thomson scattering	T_e and n_e at one point several times	Risø	A
KE3	Lidar Thomson scattering	T_e and n_e profiles	JET and Stuttgart University	A
KG1	Multichannel far infrared interferometer	$\int n_e ds$ on six vertical chords and two horizontal chords	CEA Fontenay-aux-Roses	SA
KG2	Single channel microwave interferometer	$\int n_e ds$ on one vertical chord	JET and FOM Rijnhuizen	A
KG3	Microwave reflectometer	n_e profiles and fluctuations	JET and FOM Rijnhuizen	A
KG4	Polarimeter	$\int n_e B_p ds$ on six vertical chords	JET and CEA Fontenay-aux-Roses	SA
KH1	Hard X-ray monitors	Runaway electrons and disruptions	JET	A
KH2	X-ray pulse height spectrometer	Monitor of T_e, impurities, LH fast electrons	JET	SA
KJ1*	Soft X-ray diode arrays	MHD instabilities and location of rational surfaces	IPP Garching	SA
KJ2*	Toroidal soft X-ray arrays	Toroidal mode numbers	JET	SA
KK1	Electron cyclotron emission spatial scan	$T_e(r,t)$ with scan time of a few milliseconds	NPL, UKAEA Culham and JET	A
KK2	Electron cyclotron emission fast system	$T_e(r,t)$ on microsecond time scale	FOM Rijnhuizen	A
KK3	Electron cyclotron emission heterodyne	$T_e(r,t)$ with high spatial resolution	JET	SA
KL1*	Limiter viewing	Monitor hot spots on limiter, walls, RF antennae, divertor target tiles	JET	A
KM1	2.4MeV neutron spectrometer	Neutron spectra in D-D discharges, ion temperatures and energy distributions	UKAEA Harwell	SA
KM3	2.4MeV time-of-flight neutron spectrometer		NEBESD Studsvik	A
KM7	Time-resolved neutron yield monitor	Triton burning studies	JET and UKAEA Harwell	A
KN1	Time-resolved neutron yield monitor	Time resolved neutron flux	UKAEA Harwell	A
KN2	Neutron activation	Absolute fluxes of neutrons	UKAEA Harwell	SA
KN3*	Neutron yield profile measuring system	Space and time resolved profile of neutron flux	UKAEA Harwell	A
KN4	Delayed neutron activation	Absolute fluxes of neutrons	Mol	A
KR2	Active phase NPA	Ion distribution function, $T_i(r)$	ENEA Frascati	A
KS1	Active phase spectroscopy	Impurity behaviour in active conditions	IPP Garching	SA
KS2*	Spatial scan X-ray crystal spectroscopy	Space and time resolved impurity profiles	IPP Garching	SA
KS3	H-alpha and visible light monitors	Ionisation rate, Z_{eff}, impurity fluxes from wall and limiter	JET	SA
KS4	Charge exchange recombination spectroscopy (using heating beam)	Fully ionized light impurity concentration, $T_i(r)$, rotation velocities	JET	SA
KS5	Active Balmer α spectroscopy	T_D, n_D and $Z_{eff}(r)$	JET	SA
KT1*	VUV spectroscopy spatial scan	Time and space resolved impurity densities	CEA Fontenay-aux-Roses	A
KT2*	VUV broadband spectroscopy	Impurity survey	UKAEA Culham	A
KT3	Active phase CX spectrioscopy	Fully ionized light impurity concentration, $T_i(r)$, rotation velocities	JET	SA
KT4*	Grazing incidence + visible spectroscopy	Impurity survey	UKAEA Culham	A
KX1	High resolution X-ray crystal spectroscopy	Central ion temperature, rotation and Ni concentration	ENEA Frascati	A
KY1	Surface analysis station	Plasma wall and limiter interactions including release of hydrogen isotope recycling	IPP Garching	Automated, but not usually operated unattended
KY2	Surface probe fast transfer system		UKAEA Culham	
KY3*	Plasma boundary probes	Vertical probe drives for reciprocating Langmuir and surface collecting probes	JET, UKAEA Culham and IPP Garching	
KY4	Fixed Langmuir probes (X-point belt limiter)	Edge parameters	JET	SA
KY5	Fast pressure gauges	Neutral particle fluxes on target	IPP Garching	M
KZ3*	Laser injected trace elements	Particle transport, T_i, impurity behaviour	JET	M
$K_\gamma 1$	Gamma-rays	Fast ion distribution	JET	M

* Not compatible with tritium A=Automatic; SA=Semi-automatic; M=Manual

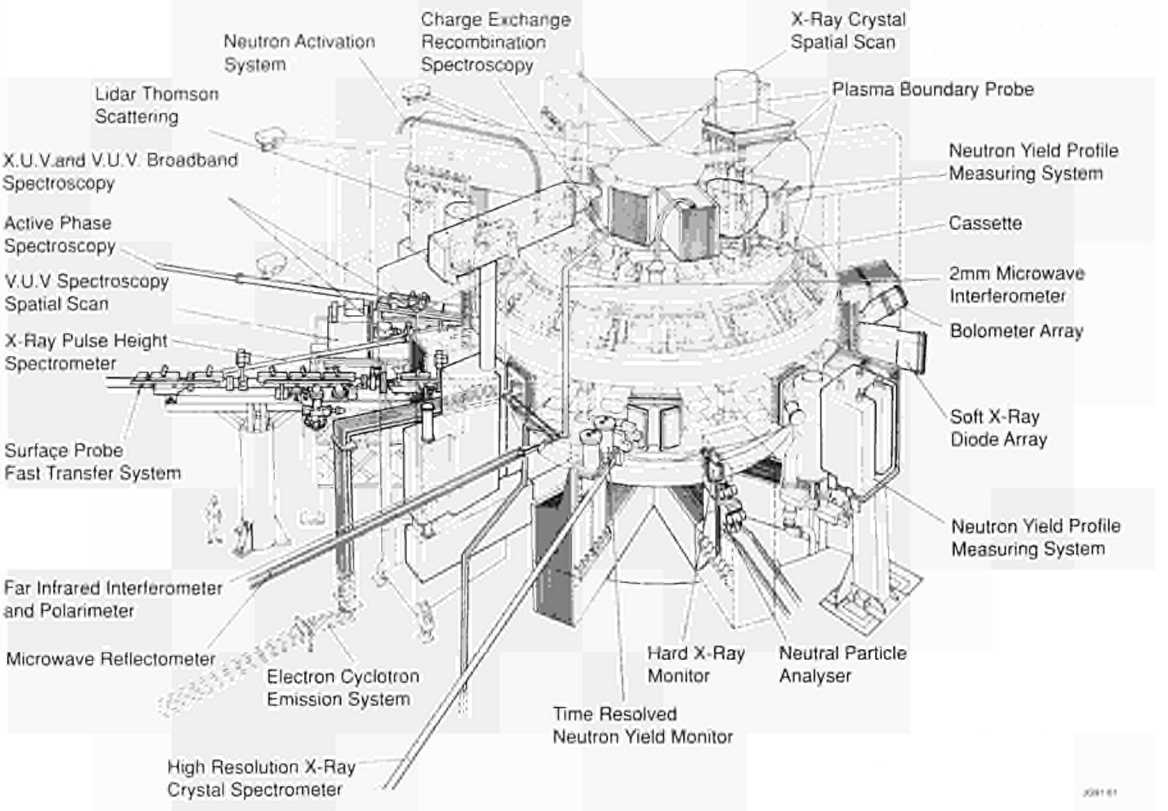

Fig.40: General layout of diagnostics in the JET machine.

Magnetics

The basic system of flux and field measurements has continued to work reliably. The occasional breakdown of input amplifiers has been substantially reduced by installing voltage limiting devices at the inputs. The removal of a number of short-circuits between the vacuum vessel and mechanical structure (leading to high common mode interference) may also have helped. The standard differential input isolation amplifier, which had a limited bandwidth (~ 10 kHz) has been redesigned to improve this aspect, specifically regarding the phase shift. The bandwidth now extends to 100 kHz. Manufacture of these units has now started.

Removal and reinstallation of Octant No.3 for the replacement of a TF coil made it necessary to remove the voltage loops which are routed in tubes running toroidally on the outer wall of the vessel. In the past, seven loops had been installed (out of eight possible) and after this operation only three voltage loops could be re-installed. These included the loops used to provide the main loop voltage.

Following identification of a fault in the torodial field coil to which the diamagnetic loop is attached a balancing circuit was set up for a second diamagnetic loop. The second loop is in Octant No.8, remote from the faulty coil in Octant No.4 and shows less variability from day to day, although it is more susceptible to direct coupling with the poloidal field. Data were taken from both loops simultaneously throughout the final 1500 shots of 1990 and the calculated energies agree well under most operating conditions. More experience of comparison of behaviour of the two loops is required before deciding to switch to the second loop as the main energy measurement. This decision must also take account of the reported reduction in the level of fault in the TF coil.

Hard wired plasma displacement signals based on the Shafranov moments of the current distribution have been successfully commissioned. These signals are particularly important for the measurement of vertical and horizontal displacements of small diameter plasmas and X-point plasmas, where more conventional methods break down. The hardwired signals were in perfect agreement with those calculated by software considerations. They have greatly assisted in the analysis of very fast vertical disruptions.

Work has also continued on the pick-up coils for the feedback stabilisation of m=2, n=1 modes. A full set of 4 pairs of coils have been installed and found to perform satisfactorily. A start has been made to build the circuits for the control of the gain and phase of the signals to be used in the feedback loop.

The standard differential input isolation amplifier, which had a limited bandwidth (~10kHz) has been redesigned to

improve this aspect specifically regarding the phase shift. The bandwidth now extends to 100kHz. The manufacture of these units has started.

Plasma Boundary Probes

Single element Langmuir probes in the carbon (upper) and beryllium (lower) divertor targets as well as in the belt limiters, RF and LH antenna protection have routinely provided measurements of the plasma parameters of the plasma edge scrape-off layer. Probes in the carbon divertor target plates have proven not to survive the extreme heat loads found near the strike point of the separatrix in pulses with full additional heating. A design study has started for a probe that would be retractable behind the limiter surface and could be extended for measurements only during a very short time (~50ms) (so called "pop-up probe"). Probes in the beryllium divertor target were severely affected by the melting of the target.

The fast moving reciprocating probe has been used regularly under remote control. The probe head had to be replaced several times due to unexpected plasma contact causing thermal shock damage. Therefore, new probe heads will be manufactured from 4D carbon fibre reinforced material offering improved protection against thermal shock.

A Retarding Field Analyser (RFA) was used for the first time on the Fast Transfer System Facility (FTS), mounted on the tip of the train, to measure the ion temperature in the Scrape-Off Layer (SOL). The entrance slit of this probe has proven to be too fragile for the power fluxes found in the SOL during heating and a new more rugged version is under construction.

The diagnosis of the divertor has been enhanced by fast in-vessel ion gauges mounted under the target protection plates. These gauges pose many new problems since the filament current is up to 30A and in-vessel routing and cable vacuum feedthrough are difficult. These problems have satisfactorily been resolved and the first measurements have shown good quality. The pressure measurement can be interpreted as a particle flux on the target and can therefore be compared with H_α measurements at the same location from CCD cameras. This is shown in Fig.41.

Plasma Wall Interactions

There is a continuing interest in the analysis of in-vessel components, particularly comparing beryllium first-wall with the all-carbon phase. First-wall components have been analysed by ion beam techniques in a specially equipped glove box for handling the Be-contaminated components by

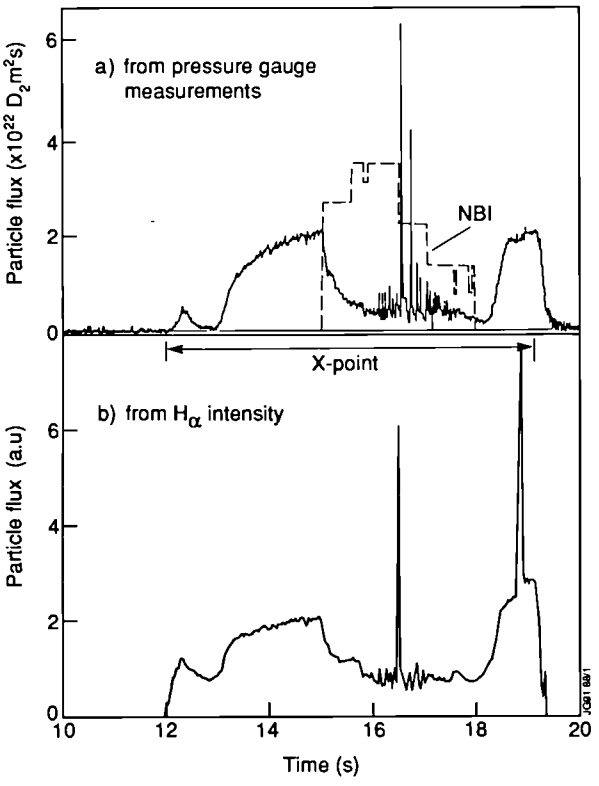

Fig.41: Neutral particle flux measurement in the carbon divertor target private region of the carbon divertor target measure by means of a pressure gauge and CCD camera. The peak in H_α at 19s is due to a UFO.

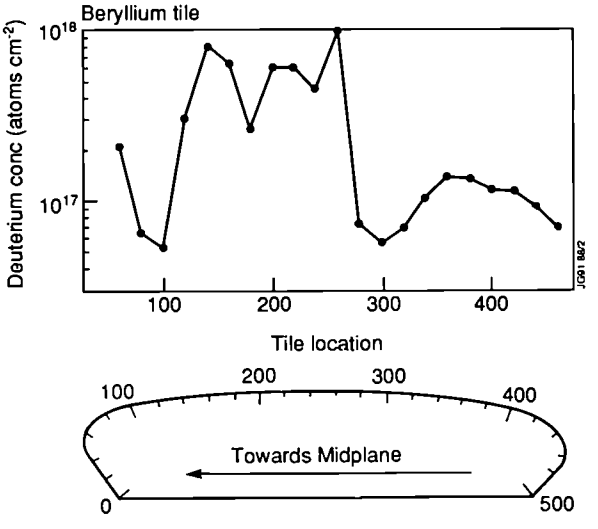

Fig.42: Surface deuterium concentration on a Beryllium belt limiter tile.

bringing the ion beam into the glove box through an ultra-thin window. First wall components are moved by computer controlled stepper motors so that the surface profile can be scanned automatically without the necessity to cut the material. Fig.42 shows the surface deuterium concentration on a Be-belt limiter tile.

The integral exposure/analysis facility for surface collector probes : Fast Transfer System (FTS) coupled to the

Surface Analysis Station (SAS) has suffered from technical limitations both in the transfer of probes and in the analysis facilities. Therefore a limited number of probes have been exposed and subsequently analysed mostly by means of ion beam techniques. Probes have been exposed in two different poloidal locations: near the outer midplane on the Fast Transfer System and at the top on the Plasma Boundary Probe System equipped with a cassette. Be evaporations were again successfully monitored and studies have been conducted on the ratios of the deposition of Beryllium and Carbon in the SOL. The evaluation has not been completed. On the FTS special probes have been exposed to measure the fluxes of fast helium ions as produced in ICRF heating experiments and with helium neutron beam injection heating.

From experiments at JET and other tokamaks, it is known that a substantial amount of the working gas is released when the vessel is vented before a machine opening. The study of this effect has continued by taking samples with the present beryllium walls and by trying to reduce the release by means of glow discharge cleaning before venting and flushing with nitrogen.

Limiter Observations

Several wide-angle views have been used for general operational use and routinely recorded. On carbon very high target temperatures are often observed during intense additional heating. Under these circumstances, disruptions often release UFO's that can clearly be followed. For detailed studies of limiters and targets, narrow-angle views have been used usually equipped with remotely controllable carousels with filters for H_α, BeI, II and CI, II, III. If the target temperature exceeds 1200°C, thermal radiation dominates line radiation and the surface temperature can be measured.

All this information is a recorded in standard professional video format and analysed afterwards on a PC-based system. This analysis system has further matured, so that saturated areas on the picture can be restored with a software procedure and so that also total deposited power deposited on a selected area can be obtained.

Electron Cyclotron Emission (ECE) System

The ECE measurement system has continued to provide detailed information on the spatial and temporal variations of the electron temperature on all JET discharges. The Michelson interferometers give a measurement of the whole ECE spectrum with modest spectral and temporal resolutions thus providing temperature profiles (with spatial resolution ~15 cm) under almost all plasma conditions. The twelve-channel grating polychromator, and the heterodyne radiometer (with corresponding typical spatial resolution ~ 6 cm and ~ 3 cm respectively) give detailed information about the time dependence of the electron temperature at a number of fixed points in the plasma. The real-time processing system analyses all data from one of the Michelson interferometers, allowing real-time calculation of interlock signals required for the Pellet Launcher Protection System and real-time display of electron temperature profiles in the control room.

During 1989, a cryogenic failure in the detector used for the Michelson interferometers necessitated the use of a temporary replacement detector from another system. The permanent replacement, installed before the start of 1990 operations, shows better cryogenic and detector performance than the original system. The complete Michelson interferometer system (including all the transmission waveguides, in-vessel components and the new detector) was again absolutely calibrated using a large area, high temperature black-body source located inside the vacuum vessel. A new source, with slightly improved radiation temperature and full remote control, was brought into service for use in the beryllium contaminated vacuum vessel. The source was subsequently de-contaminated and will be used for future calibrations. Comparisons of ECE data with that from other diagnostics (in particular the LIDAR Thomson scattering) indicate that the measured electron temperatures are within the normal level of accuracy (±10% in absolute level). The stability of the calibration appears to be as good as, or better than, that of the system before the 1989 detector problems.

The upgrade of the heterodyne radiometer to 44 channels, giving coverage of the frequency ranges 73-103 GHz and 115-127 GHz at ≈1 GHz intervals, has been completed. Different frequency bands in the system can simultaneously view the plasma in different polarizations (ordinary or extraordinary mode) allowing both exploitation of the first and second cyclotron harmonics. This, combined with the extended frequency coverage, allows useful measurements over almost the full operating range of the toroidal field. At some values of the toroidal field, there is almost complete coverage of the plasma minor radius. Fig.43 shows an example of data obtained. In this case, data from 25 radiometer channels each having a spatial resolution of ≈2 cm, spread over a range of ≈1 m, have been used. The signal-to-noise ratio of the measurements is typically >100, with a

signal bandwidth of 10 kHz. The improved measurement capability of the upgraded system has already been exploited in a variety of physics studies such as MHD phenomena in high β discharges, high-resolution studies of the sawtooth collapse, edge phenomena and edge temperature profiles.

Preparations for the exploitation of the non-thermal ECE spectra expected during lower hybrid wave experiments have been in progress for sometime. The first Lower Hybrid Current Drive (LHCD) experiments have shown the expected substantial effects on the ECE spectra measured with the Michelson interferomcter. As predicted, the perturbation of the thermal spectrum appears to be dominantly at low frequencies (ie. below the second harmonic, in the extraordinary mode), so that electron temperature measurements using the optically thick second harmonic are still possible. A quantitative investigation of the non-thermal emission, with the aim of obtaining information on the energy and space distribution of the non-thermal electrons, is in progress.

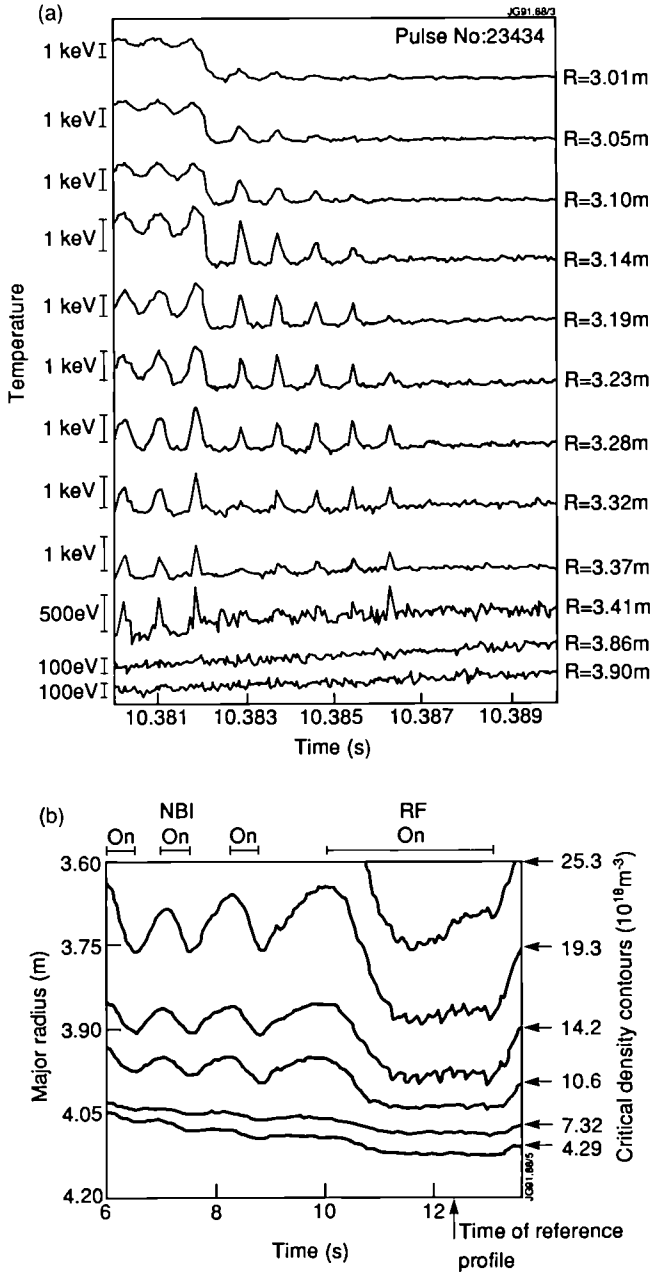

Fig.43: (a) the time evolution of the electron temperature around a sawtooth collapse, at a number of fixed radii. The signals shown are a subset of the 44 channels measured by the heterodyne radiometer. The existence of a localized MHD mode which persists through the sawtooth collapse is clearly visible;

(b) data from 25 radiometer channels spanning the outer half of the plasma have been used to obtain the time evolution of the temperature profile in the same time range as part (a).

Microwave Transmission Interferometry and Reflectometry

The microwave transmission interferometer has continued routine use for measurements of the line-of-sight electron density and for plasma control purposes. It has operated with high reliability and without modifications.

The work on reflectometry has three components: development and application of a multichannel instrument which operates with radiation in the ordinary mode ($\underline{E} \parallel \underline{B}$); development of correlation reflectometry, a technique specially devised for studying density fluctuations; and construction of a novel 'comb' reflectometer to estimate density in the X point region.

The multichannel instrument has 12 probing frequencies in the range 18 - 80 GHz and so probes electron densities in the range 0.4 - 8.0 x 10^{19} m^{-3}. It has two modes of operation: narrow band swept, for measuring the electron density profile; and fixed frequency, for measuring relatively fast movements of the different density layers.

The instrument was brought into initial operation at the end of 1989 and was used extensively during 1990. The principal operational difficulty that has been experienced, arose from density fluctuations which caused inaccuracies in the data given by the automatic fringe counting and period counting electronics. To overcome these difficulties, three modifications to the system were made. Narrow band filters were fitted to the IF stage of the heterodyne receivers, the gain of the IF amplifiers was increased, and cross-talk between the plasma and reference arms was reduced. In addition, a new mode of operation was developed, in which the probing frequencies were alternatively swept and held constant ('swept-dwell" mode) and the output from the fringe counters recorded. Data taken during the fixed frequency period was interpolated to provide a 'baseline' for the measurements taken during the frequency sweep. In this

way, an accurate measurement of delay time of the radiation in the plasma is obtained. Inverting the data from the different measurement channels provides the electron density profile.

These modifications have enabled useful measurements to be made for a range of plasma conditions. For example, Fig.44 shows movements of the different density layers measured during pulsing of the NBI and during ICRF heating. These measurements were obtained with the fixed frequency mode of operation. This gives the relative movements of the different density layers and these are put on an absolute scale by referencing against a profile measured with the far infrared transmission interferometer. Fig.45 shows some density profiles measured with the swept frequency mode of operation during oscillations of the gas feed to the torus. The profiles are compared with those measured with the interferometer.

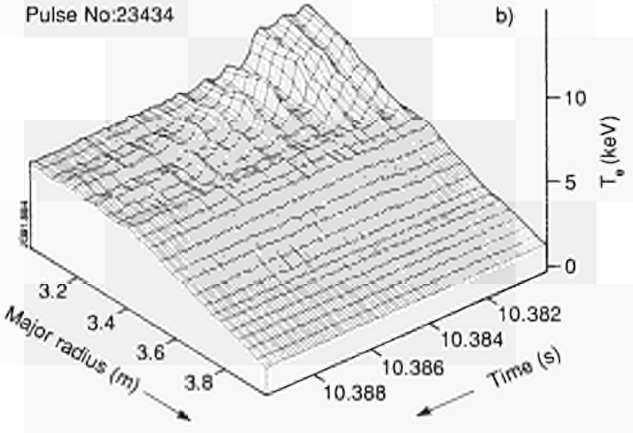

Fig.44: Reflectometer measurements of the movement of six density layers during pulsing of NBI (2.5 MW) and during ICRF heating (4 MW). The absolute location of the different density layers is determined by referencing against a profile measured with the far infrared transmission interferometer at 12.2 s.

Measurements made with the reflectometer have been used in a range of physics studies. In particular, they have been used to derive a particle diffusion coefficient by measuring the density perturbation following a sawtooth collapse and results have been combined with determinations of the heat pulse thermal diffusivity obtained from measurements of ECE. Profile measurements have been used in investigations of the plasma edge region especially under H-mode conditions.

The work on correlation reflectometry has been carried out with a four channel reflectometer which operates with radiation in the extraordinary mode ($\mathbf{E} \perp \mathbf{B}$). The probing frequencies are 75.5, 75.6, 75.75 and 76.15 GHz which give separation between the reflecting layers typically in the

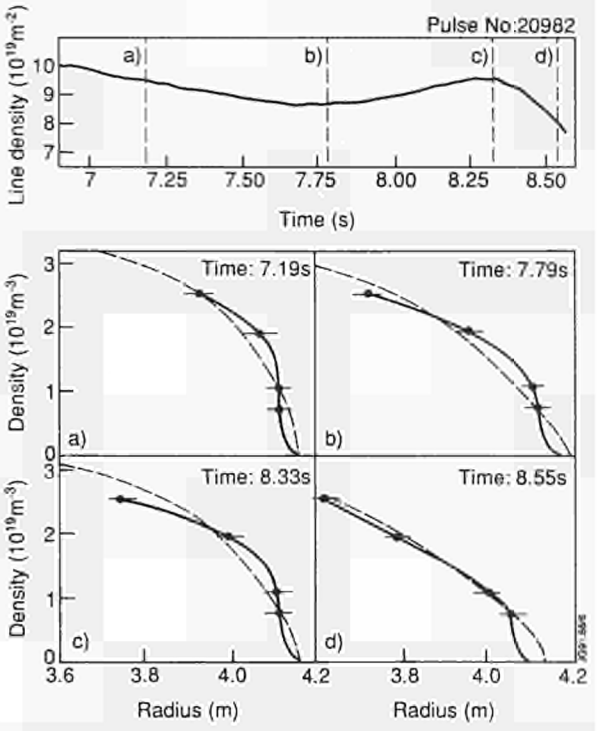

Fig.45: The upper trace shows the time evolution of the line integrated density (central channel) during pulsing of the gas feed to the torus. The edge density profile measured with the reflectometer at four times (a,b,c and d) is shown (solid line). Profiles measured with the transmission interferometer are also shown (dotted line).

range 3 - 20 mm. The fluctuating signal on each channel is recorded and the correlation level (γ) between the signals is calculated. The dependence of γ on the layer separation is determined by analysing results from the different channels. The data are interpreted in terms of fine-scale structures (ie. 'density cells'), which rotate toroidally under the influence of the additional heating. From the analysis, an estimate of the radial extent of the structures (L_c) and the effective toroidal wavenumber spectrum are obtained.

The level of correlation has been found to vary substantially with plasma conditions. Under ohmic conditions, the correlation between the channels is generally low, suggesting the radial extent of any structures is ($\geq$) 3 mm. Under additional heated L-mode conditions, correlation level depends on additional heating power. For power levels ($\geq$) 8 MW, correlation level is high and L_c ($\geq$) 1.5 cm. On the other hand, under H mode conditions the correlation level and L_c are much reduced and generally closer to ohmic values. In all cases, the effective toroidal wavenumber spectrum is broad-band in the range 0.2 - 6 m^{-1}. The significance of the results is not clear at this stage but could have important implications for energy and particle transport.

The comb reflectometer has four probing frequencies,

27, 40, 60 and 90 GHz, and operates in the ordinary mode. It will probe the upper X point region through a waveguide mounted in a top vertical port. The maximum frequency in reflection will be determined, by observing the level of fluctuations (these are expected to be relatively high for the channels in reflection), and thereby an estimate of the plasma density in the X point region will be obtained. The device is presently under construction and the first results should be obtained in the 1991 experimental campaign.

Thomson Scattering

During 1990, work on the LIDAR Thomson Scattering system has concentrated on maintaining routine operation and on the planned upgrade of the repetition rate. In addition, modifications are being prepared which will permit high spatial resolution measurements in the plasma edge region.

The system was operated routinely during the experimental campaigns in either the standard 0.5 Hz/9 pulse mode or the ~ 1 Hz/6 pulse mode for higher time resolution. During the year, an event occurred accidentally which enabled the robustness of the time-of-flight (LIDAR) technique to be demonstrated. The carbon tile used as a laser beam dump was dislodged from the inner wall exposing a bright metallic surface leading to a large increase (at least two orders of magnitude) in the stray laser light level. Despite this difficulty, it was possible to maintain operation, by the addition only of an extra polarizer in the collection optics path. Some data obtained under these conditions are shown in Fig.46. These results are also important because

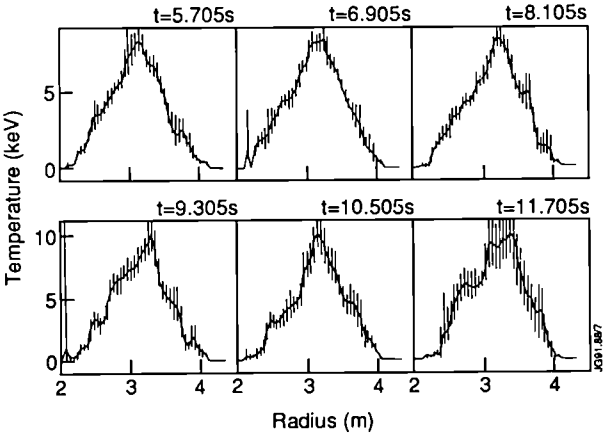

Fig.46: The electron temperature profile measured by LIDAR Thomson scattering in the presence of severe stray light. Note that the central temperature is >10 keV for a period > 4 s.

they demonstrate that the central electron temperature was > 10 keV for a period > 4 s. They were obtained during a sawtooth free period of an ICRF heated D - He^3 discharge.

The upgrade for higher repetition rate has three main components: the installation of high reflectivity (99%) broad band dielectric collection mirrors, the use of PCs for fast data read-out and storage between laser pulses; and the procurement of a high repetition rate (10 Hz) short pulse laser. The first two modifications were made during 1989 and were used successfully in 1990. Unfortunately, procurement of the 10 Hz laser has met with difficulty and the contract has been terminated. As an alternative, a new system based on a 4 Hz ruby laser is being considered, and tender action for such a laser has been initiated. Delivery is planned for the first half of 1992.

For the edge LIDAR diagnostic, one of the six parallel collection optical paths of the main LIDAR system has been redirected in the roof laboratory to provide an additional detection path. This path will include a new dispersion system suitable for lower temperature measurements and a new faster detection system based on a streak camera (Fig.47). This arrangement will provide LIDAR measurements with a considerably higher spatial resolution over a limited radial range in the outer region of the plasma. Preliminary stray and plasma light characterisation tests were successfully carried out towards the end of 1990 operations. A loaned streak camera and intensifier unit were used together with an existing CCD camera, suitably modified, as a digitizer. Delivery of the final optical and detection systems is expected early in 1991 and after testing, will be commissioned during 1991 operations.

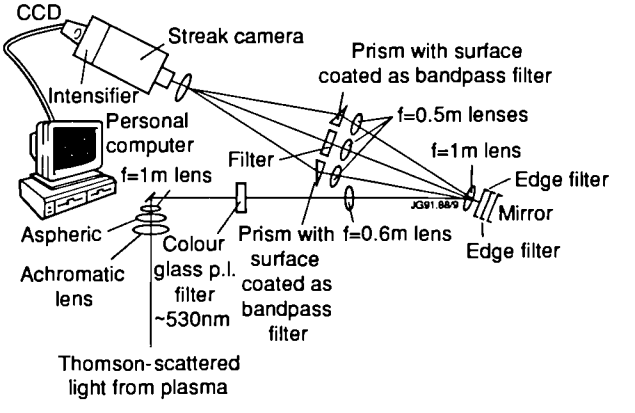

Fig.47: Schematic of the high resolution LIDAR Thomson scattering system under construction for edge measurements.

Use of the laser, laser beam-line and operating system of the original Single Point Thomson Scattering system has continued as a source for laser ablation experiments, and the results have been used in studies of impurity transport. In addition, the laser beam has been used as the source for

preliminary tests of the new q-profile Thomson scattering experiment designed to obtain an estimate of local internal magnetic field. The axicone collection optics for the system have been completed. The detection system including the pressure scanned Fabry-Perot etalon, the Peltier cooled CCD-camera and the data collection system was completed, delivered and installed by the AEA, Culham Laboratory, for this collaborative experiment.

Attempts at measurements were conducted in the latter half of the experimental campaign. To measure successfully the direction of magnetic field, the central electron cyclotron frequency must be resonant with the Fabry-Perot etalon. Although resonant conditions were not determined unambiguously in any of the relatively few high density discharges on which a measurement was attempted, measurements proved the ability of the system to discriminate against stray laser light and showed a significant number of photoelectron events from Thomson scattering. Serious attempts at local field measurements were abandoned, when a tile from the inner-wall fell and blocked the alignment beam.

Fast Ion and Alpha Particle Diagnostic

During 1990, the development of high power 140 GHz gyrotrons were sufficiently advanced to permit ta start of construction of the collective scattering system for measuring the spatial and velocity distributions of fast ions including alpha-particles. Design of the system was completed and contracts placed for all major components. The system will be implemented in two stages. There will be a preliminary stage aimed at validating the physics of the technique and making the first measurements of fast ions. This stage will also involve important tests of technical aspects of the system and will be undertaken in 1991. The system will then be upgraded for D-T operation and made compatible with the pumped divertor geometry of JET.

The principal system components are a gyrotron with power supplies and modulator, a mode convertor, oversized waveguide transmission systems for launch and detection, a multichannel heterodyne detector system, and signal conditioning and data acquisition electronics (Fig.48). The gyrotron is a high power (> 400 kW), long pulse (> 5 s) whispering gallery mode tube. For initial experiments, an existing prototype tube will be used. The anode modulator is under construction at JET and will permit modulation of the gyrotron output at frequencies up to 40 kHz. This is necessary to discriminate the scattered radiation from the background ECE. The output of the gyrotron will be in the $TE_{15,2}$ mode and this will be converted to a Gaussian beam by means of an improved efficiency Vlasov convertor. Power will be coupled to the HE_{11} mode in the oversized

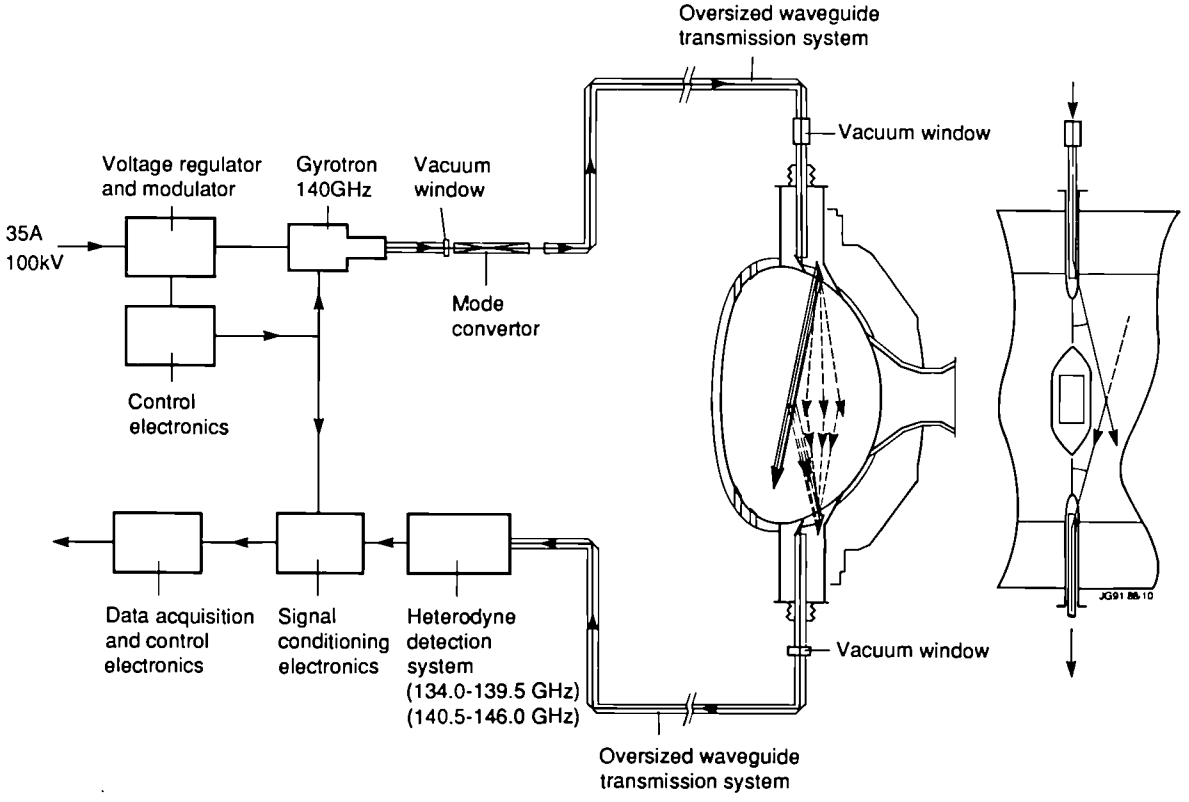

Fig.48: Schematic of the collective scattering system for measuring the spatial and velocity distributions of fast ions including alpha-particles in JET.

(diam. 88.9 mm) corrugated waveguide and transmitted to a main vertical port at the top of the JET vacuum vessel. The waveguide will include special resistive sections to absorb power in unwanted modes. These sections have been produced using the technique of plasma spraying of stainless steel. For initial operation, an inertially cooled sapphire disc will be used as the torus vacuum window. This will limit the gyrotron pulse length to a few seconds and so the design of a cyrogenic sapphire window has been initiated. Radiation will be launched into the torus via two mirrors, the last mirror being rotatable in two independent directions. The in-vessel components have been mocked-up and tested. An identical arrangement at the bottom of the vessel will be used to detect the scattered radiation. In addition, there will be two slave detection lines to collect (spectrally integrated) scattered radiation from volumes adjacent to the main scattering volume. Eventually, these will be used in a real-time feedback system to maintain optimum alignment between the launched and received beams. The scattered radiation will be transmitted to a heterodyne detection system using oversized (diam. 31.75 mm) corrugated waveguide and quasi-optical mitre bends. Initially, the spectrum will be resolved into 32 channels between 134 and 146 GHz. Ultimately, there will be 40 channels between 123 and 156 GHz. Both the fast ion and thermal ion features will be detected. Repetitive pulse addition techniques will be used to improve the signal-to-noise ratio and special signal conditioning electronics are being developed for this purpose. For the initial measurements, a simplified control system is being prepared which will give local control of the gyrotron and subsystems. The interface to CODAS and control from the diagnostic control room will be implemented at a later stage.

Theoretical work supporting the technical developments has continued. The work has been directed at assessing the effects of the dielectric properties of the plasma and at developing predictive and interpretation codes. The dielectric properties have now been analysed using cold, hot and relativistic models of the plasma. The cold plasma model has been found to be adequate for describing scattering with radiation polarized in the ordinary mode, but for scattering with radiation in the extraordinary mode hot plasma effects can be important. The scattered signal can be up to an order of magnitude larger with extraordinary mode scattering and so there is considerable advantage in using this mode but there is an upper density limit. This limit has been evaluated using the hot plasma theory and is found to be higher than that given by the cold plasma theory.

The predictive code will be used to determine the necessary antenna orientations and polarizer settings for the diagnostic. The code includes a modified ray tracing routine which can make use of real data on plasma density, magnetic field and electron temperature distributions from previous plasmas. Codes for interpreting the measured spectra are also being prepared.

Neutron Flux Measurements

The strength of the neutron emission from JET plasmas is routinely recorded with sets of Fission Chambers mounted near three of the main horizontal ports of the machine. These chambers are suitable for recording brief bursts of photoneutrons, produced by runaway electrons following major plasma disruptions. A study of photoneutron emission was carried out [1] at a time when all the plasma facing components were constructed from carbon. Although photoneutron yields are inherently erratic, the "standard" scaling of the average yield (Y) with plasma current (I_p) is $Y \approx 2 \times 10^{13} I_p^{2.6}$ photoneutrons per disruption (I_p in MA) was established. This study has been updated to investigate the effect of introducing beryllium in place of carbon in the machine. Pulse Nos: 19160 to 21959 were examined as this covers the period prior to introduction of beryllium, the use of beryllium evaporation and the subsequent installation and early use of beryllium belt limiters. The following preliminary conclusions can be drawn:

(i) for carbon limiter plasmas, the standard scaling still applies;

(ii) with carbon limiters and beryllium evaporation, the standard scaling applies up to 3MA, but for higher currents yields were lower than predicted by 1 to 2 orders of magnitude (but there were few occurrences);

(iii) for beryllium limiter plasmas, the yield at 1MA was the same as for carbon, but the yields fell with increasing current so that by 5MA they were 3 orders of magnitude lower than predicted (as illustrated in Fig.49);

(iv) for disruptions occurring in the X-point configuration (with carbon dump plates), there was no clear I_p dependence and the yields were 1 to 2 orders of magnitude lower than predicted with the standard scaling, irrespective of limiter material.

It is evident that the generation of runaway electrons during disruptions is strongly inhibited by the presence of beryllium at the plasma boundary. It is well known that the disruption characteristics with beryllium are quite different from those for carbon and are related to the formation of

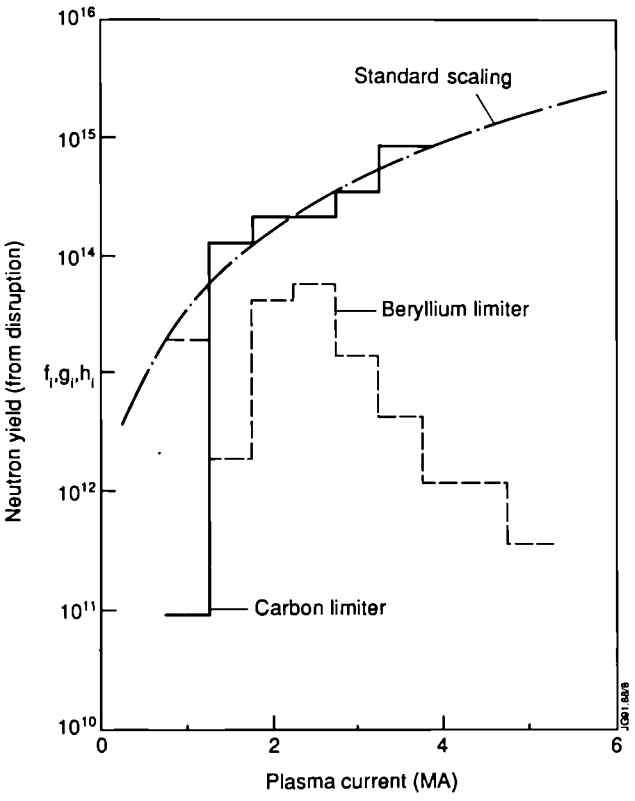

Fig.49: Neutron yields measured after major plasma disruptions; the results for beryllium limiters are in marked contrast with those for carbon limiters.

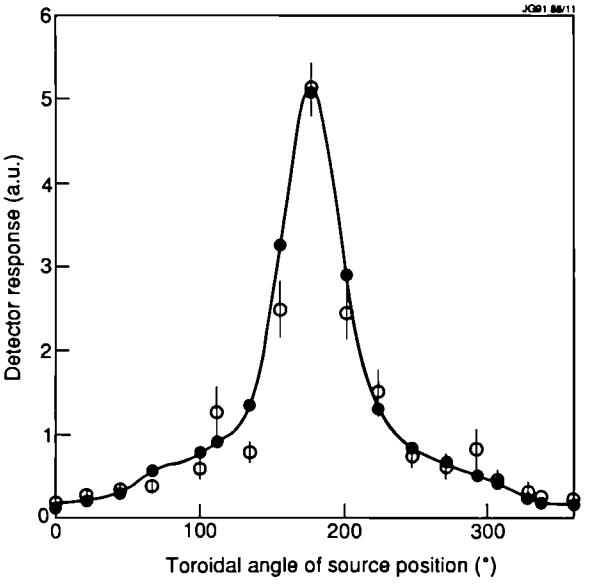

Fig.50: Comparison of experimental measurements with Monte Carlo neutron transport predictions for the variation of the neutron counter response with toroidal position of a Californium neutron source in the vacuum vessel. The good agreement obtained validates the computer model.

MARFEs. The above findings indicate that runaway electron formation is most favoured in the outer regions of the plasma and that the edge electron densities for the beryllium cases are higher than for carbon, possibly because of MARFE formation.

The use of the Fission Chambers for measuring the instantaneous neutron emission strength from well-behaved plasma discharges requires determination of absolute detection efficiencies to better than 10% accuracy. This is now achieved through the employment of foil activation techniques, using two new irradiation positions that have been established inside the vacuum vessel to minimize the problems of modelling structures surrounding the plasma. Although the Fission Chamber detection efficiencies are now well established, they sometimes alter between operating periods in a manner that is not expected from the nature of the changes made to nearby hardware. To assist in understanding these changes, a simplified computer model of the tokamak has been developed for use with neutron transport codes. This model has been validated by comparison with extensive in-vessel measurements made in 1985 with a ^{252}Cf neutron source [2]. Fig.50 shows that the model calculations reproduce very well the scan obtained by moving the source around the tokamak on the plasma axis. These calculations indicate that the detection efficiency is relatively insensitive to the equipment arrayed around the ports (but absolute calibration purely by direct calculation is not possible to better than ±30% accuracy). They also showed that the 15% change in efficiency that took place over the 1989/1990 shutdown is attributable to the change from water to freon as a toroidal field coil coolant.

Neutron Emission Profiles

The Neutron Profile Monitor provides a measure of the spatial variation of neutron emissivity throughout the plasma volume. A topic of particular interest is the change in emission profile during sawtooth crashes, which has been studied using tomographic inversion methods. Fig.51 gives an example of the dramatic change which takes place in the profile for a D° beam-heated discharge, whereas the change in total neutron emission strength recorded by the Fission Chambers is only 15%. Of course, if the sawtooth crash leads only to a displacement of the hot ions, conserving their energy and density, then no change in global emission would be expected. The change observed in Fig.51 is attributed mainly to the contribution to total emission from beam-beam interactions which is important on-axis when the beam ion density is high, but varies inversely with density and so becomes small after the redistribution.

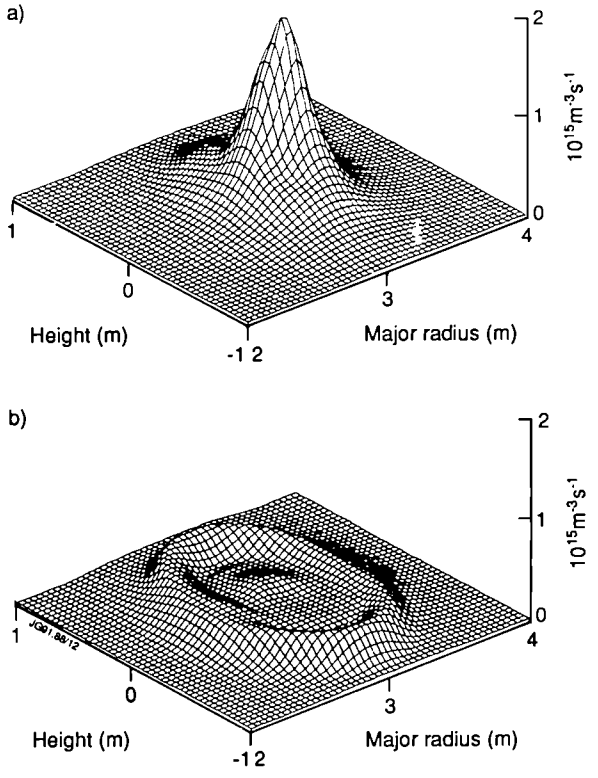

Fig.51: Tomographic presentation of the neutron emission profiles before and after a sawtooth crash for a discharge in which the central neutron emission before the crash is dominated by beam-beam reactions.

The interpretation of neutron emission profiles for ohmically-heated discharges is considerably easier than under D° neutral-beam heating conditions, since the measurements give a direct indication of the ion temperature profiles; by means of a simple local transport analysis, the ion thermal conductivity, κ_i, for r/a ≈0.4 calculated from the temperature profile is in the range 0.5 to 2.5m²/s and shows a tendency to increase with plasma current, contrary to the dependence expected from neoclassical calculations.

During 1990, the vertical camera of the Neutron Profile Monitor has been used on occasions for measurements of the X-ray emission from fast electrons driven by the Lower-Hybrid Current Drive system, to study the localization of the fast electron current. The X-ray energy range of interest is 50-500keV and is studied with CsI/silicon photodiode detectors. The horizontal camera will also be brought into use during 1991.

Concerted effort was devoted to the measurement of emission profiles for the 14MeV neutrons emitted from the t-d burnup reactions undergone by the 1MeV tritons emitted from d-d reactions. The birth profile for the tritons is given by the 2.5MeV neutron emission; the peak reaction cross-section for t-d reactions is ~180keV triton energy, so the 14MeV neutron emission profile gives information on the confinement and diffusion of the tritons as they slow down and thermalize. This experiment is of direct relevance to the study of plasma heating by 3.5MeV alpha-particles from D-T reactions. In practice, it has been found that the analogue pulse-processing systems used to distinguish neutrons from gamma-rays lack the dynamic range required to cater simultaneously for 2.5 and 14MeV neutrons. Some results were obtained under restricted conditions, sufficient to indicate that the tritons behave as expected. However, to obtain results for normal conditions, it will be necessary to duplicate the analogue signal processing equipment. This upgraded system should be operational during the 1991 campaign.

Neutron Spectrometry

Neutron Spectrometry has proven to be an indispensable diagnostic for the study of discharges in which high power ICRF heating is employed. This is due to the presence of beryllium as the major plasma impurity; ICRF heating generates a high energy tail of light ions (p, d, or ^{3}He), which undergo exothermic reactions with beryllium that release energetic neutrons and gamma-rays. The neutron yields from these reactions can be sufficiently strong as to compete with the d-d neutron yield. Under favourable conditions (low density and low impurity content), the application of RF power in addition to NBI leads to an enhanced D-D reaction rate due to second harmonic interaction with deuterium ions; Fig.52 illustrates the manner in which the interpretive code TRANSP (which does not simulate the second harmonic interaction) underestimates the neutron emission when the RF is applied.

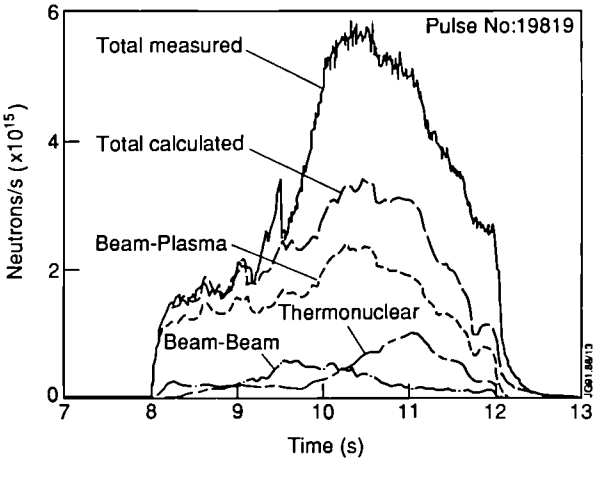

Fig.52: Comparison of a TRANSP simulation with the measured neutron yield, showing the enhancement due to second harmonic RF enhancement.

Experiments with ^{3}He neutral-beam injection provided an opportunity to exploit the Neutron Spectrometers for the measurement of ion temperatures up to 14keV, directly from the Doppler-broadening effect, without the added complication of neutron emission from beam-plasma interactions. This permitted direct comparison with temperatures obtained from the charge-exchange diagnostic, which has not previously been possible. Acceptable agreement is obtained.

The Associated-Particle Time-of-Flight Neutron Spectrometer, constructed for use with d-t plasmas [3], was delivered at the end of 1990. Rather than mothball this diagnostic until the start of the active phase, it was decided to use the new detectors and much of the electronics to upgrade the existing 2.5MeV Neutron Spectrometer. The improved instrument should retain its present energy resolution of about 120keV, but its efficiency should be enhanced six-fold, so that the time-resolution should approach 100ms. The upgraded diagnostic will be brought into service for the 1991 campaign.

Gamma-Radiation Spectrometry

Now that lower Z_{eff} values are routinely obtainable in the presence of the beryllium belt limiters, it was hoped that high power ICRF heating (^{3}He minority) would provide record ^{3}He-d reaction rates. The 16MeV gamma-emission from these reactions provide a reliable measure of the reaction rate. Although a new record of about 140kW of fusion power has been obtained, for a heating power of 16MW, the gamma spectra were significantly contaminated with high energy gamma-rays from ^{3}He-beryllium reactions, so that only a subset of the discharges run were analyzable (Fig.53). Attempts to exploit the beneficial effects of central fuelling with ^{3}He NBI were not successful due to the excessive background level of ^{3}He gas from outgassing of the inner wall components.

Studies of the gamma emission from ICRF-heated ions interacting with impurity ion species using a large volume high-purity germanium diode were not very rewarding because of the very low efficiency of such a detector. Despite the good energy resolution (10keV), the ratios of photopeak to Compton background signals were disappointingly small. A Compton suppression detector array would be a welcome addition to provide a better signal to background ratio, but would further reduce the signal level. This enhancement is being considered since the energy resolution of the HPGe detector is needed to identify unambiguously the gamma-ray lines that are observed, but it is considered unlikely that line-shape studies to determine fast ion energy distributions will be possible until machines providing very long discharge times (minutes, if not hours) become available.

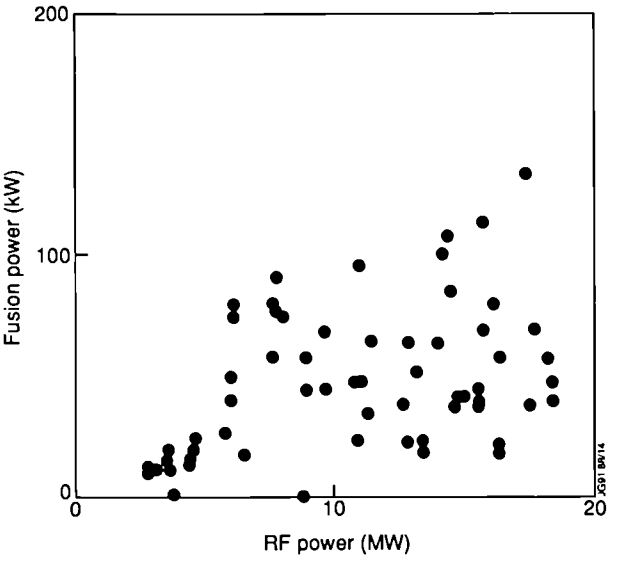

Fig.53: The ^{3}He-d fusion yield power deduced from gamma-ray measurements versus RF power for 1990 discharges.

Triton Burnup

The code used for modelling the burnup of 1MeV tritons in deuterium plasmas has been enhanced by the addition of a Monte-Carlo method for simulating triton diffusion. With this addition, it has bee possible to demonstrate that the need, in early analyses, for an anomalous slowing down rate and, in one special case, for an anomalous loss term can be removed by the introduction of a diffusion coefficient of 0.1m^2/s. This value is close to that obtained from classical predictions. Fig.54 shows an example of 14MeV emission

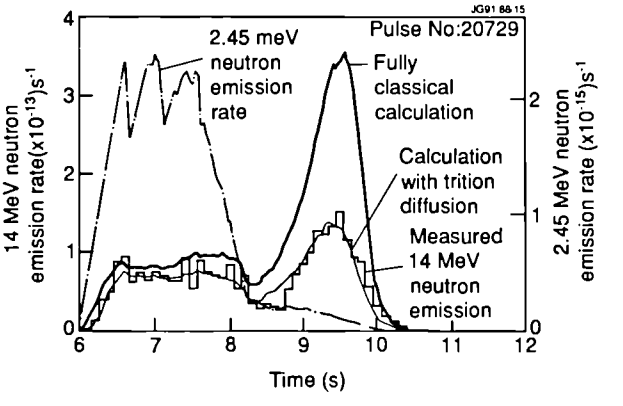

Fig.54: A discharge for which the triton slowing down time was exceptionally long; the 14MeV neutron emission, calculated from the observed 2.5MeV neutron emission, agrees well with the experimental measurements when the effect of triton diffusion are included.

from one exceptional discharge in which the plasma density fell to a low level but the electron temperature remained high, so that a very long slowing down time resulted. The calculation including particle diffusion fits the observed emission very well. However, this does not rule out the possibility of triton confinement losses (e.g. through charge exchange). The code is now being extended to compute line-integrated emissivities for 14MeV neutrons as observed with the Neutron Profile Monitor for a definitive investigation of triton diffusion and confinement losses.

Lost Alpha-Particle Diagnostic

A computer code has been developed to assist in the design of a detector for escaping alpha-particles from d-t reactions in the active phase of JET operations. The code uses the experimentally determined magnetic field configurations to calculate the flux of escaping fast particles reaching the vessel walls and permits the detailed geometries of proposed detectors to be modelled. Calculations made with this code show that the majority of the 15MeV protons recorded with a previous escaping particle detector [4] had their turning points inside the vertical port in which the detector was located. The code has also been used in the interpretation of ^{3}He depth profiles from nickel samples in the fast transfer system and for studying possible effects of toroidal field ripple.

Soft X-ray Measurements

The toroidal, vertical and horizontal cameras, containing 120 detectors have produced much new data in 1990, mainly due to the routine operation of the real-time trigger system. This allows the selection of events by a set of pre-programmed microprocessors in real time and also allows the imposition of logical relations between the trigger systems. With this system, a large amount of new data has been obtained on MHD effects, the snake and sawteeth. In particular, sawteeth with both pre- and post-cursors have been selected (Fig.55) and studied in detail. This should produce important new information about the sawtooth collapse mechanism.

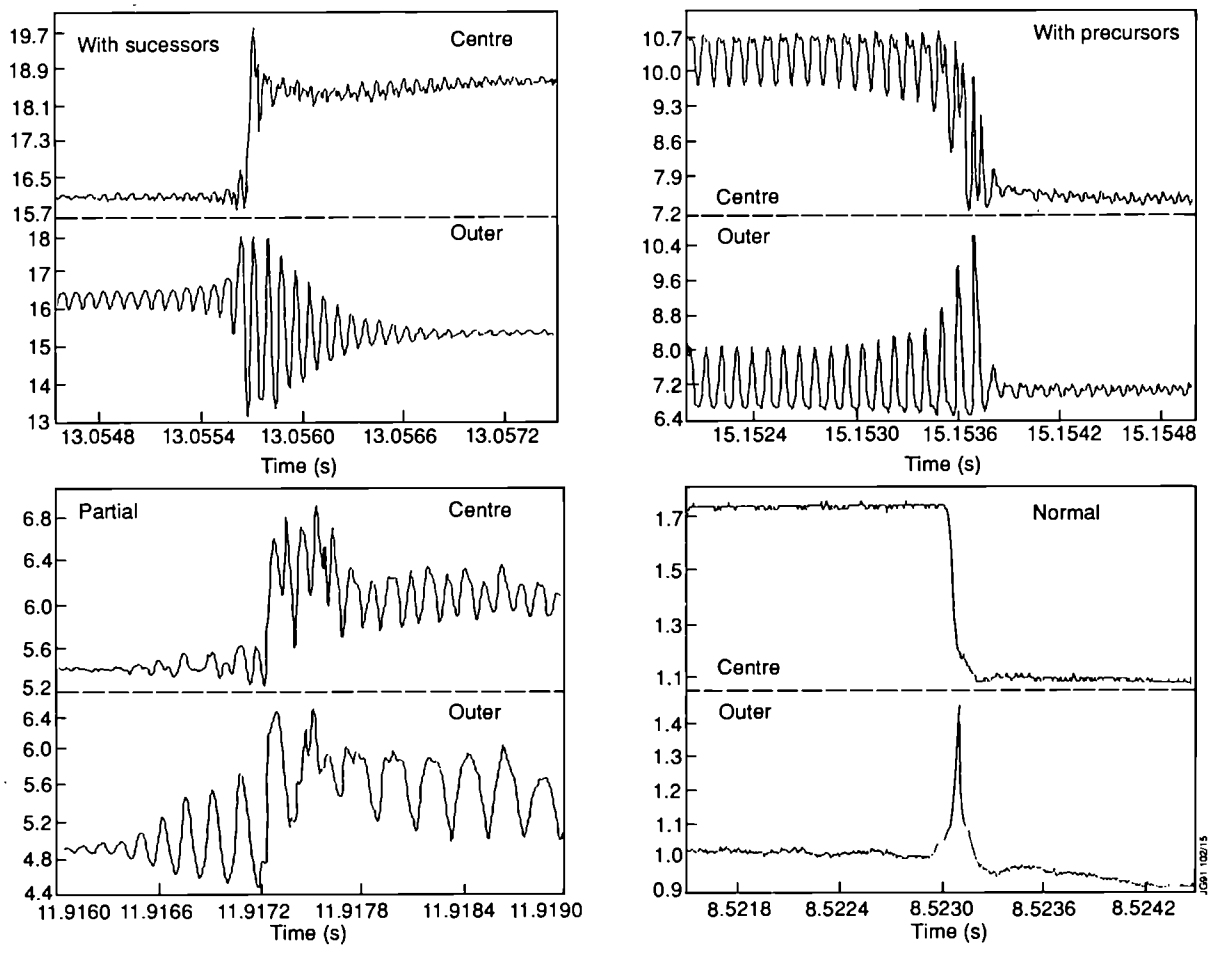

Fig.55 Sawteeth of different types some showing enhanced MHD activity selected by the new trigger system.

Data has also been taken using the two filter technique with alternate filters of different thicknesses in front of adjacent detectors. By tomographic inversion, this allows the determination, of two separate profiles of soft X-ray emission from which, with knowledge of the impurity species, the plasma temperature and density may be determined on a rapid timescale (5μs). This method works reliably and has been applied to the study of the pre-disruption phase and has shown that the electron temperature exhibits the same "erosion" behaviour as the soft X-rays and as the ECE, and that the electron density profiles become hollow. Analysis is continuing on the impurity influx phase of the disruption.

The real-time tomography system has been installed and successfully operated and should be in routine operation in 1991. Adequate inversion speeds have been obtained and typical results are shown in Fig.56.

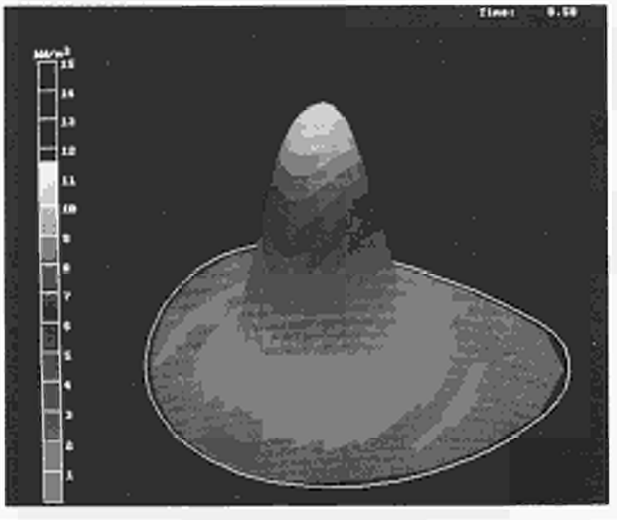

Fig.56 Typical output from the real-time tomography display taken during a plasma discharge.

Work has started on the design of compact soft X-ray cameras based on Silicon strip detectors which have 40 detectors on a 40 x 5 mm array. Modelling has established the correct location of these detectors in relation to existing cameras on Octant No.2 and tests have shown that detector/preamplifier assemblies inserted into one of the toroidal camera positions work well, with the expected noise level. It has also become clear that the detectors will operate in the JET radiation environment, with a reasonable signal to hard radiation noise level.

New methods of analysis of the soft X-ray data have been developed allowing the impurity density and Z_{eff} profile evolutions to be obtained automatically [5, 6]. Following introduction of beryllium in JET, the X-ray emission at energies above keV is dominated by Bremsstrahlung radiation from the background deuterium ions, and both Bremsstrahlung and recombination radiation from one or two light impurity species such as beryllium and carbon. Under these circumstances, local values of impurity densities and concentrations, or alternatively of the effective charge Z_{eff}, are derived from tomographic measurements of the local X-ray emissivity at energies above 1-3 keV, in conjunction with measurements of electron density and temperature profiles (Figs. 57 and 58). These calculations are performed using the intrinsic emissivities due to impurity ions. Typical uncertainties are ~25% and there is good agreement with measurements of impurity contamination using visible Bremsstralung. In addition, detailed impurity transport measurements have been made by following the evolution of the impurity density profile after injection of high-Z impurities by laser blow-off [7, 8].

The Pulse Height Analysis system has operated with a Ge detector, with a sensitivity of up to several 100 keV, in order to detect high energy electrons produced by the lower hybrid

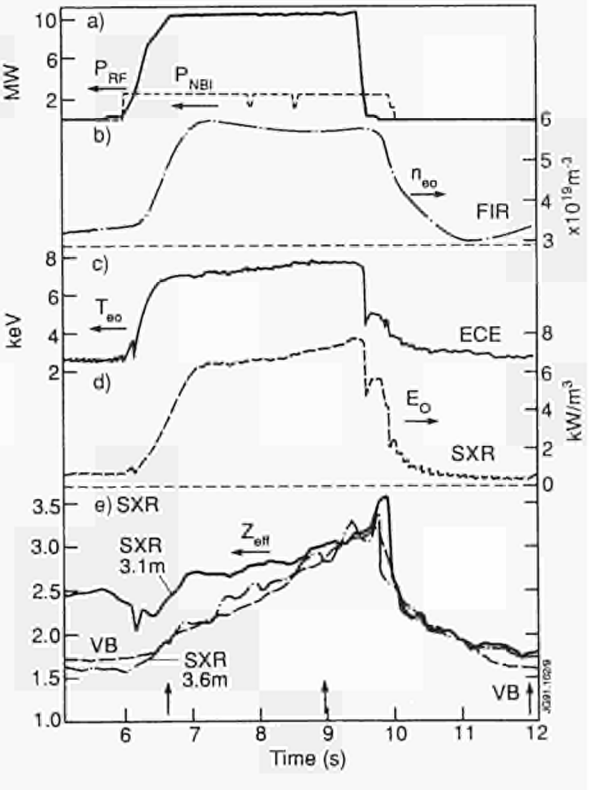

Fig.57 Evolution of radio-frequency heated discharge (Pulse No.20087); (a) radio-frequency (P_{rf}) and neutral beam (P_{NB}) power; (b) central electron density from far infrared interferometry; (c) central electron temperature from electron cyclotron emission (ECE); (d) central X-ray emissivity, using a Be filter of 250mm thickness; (e) inferred values of Z_{eff} in the plasma centre and at mid-radius).

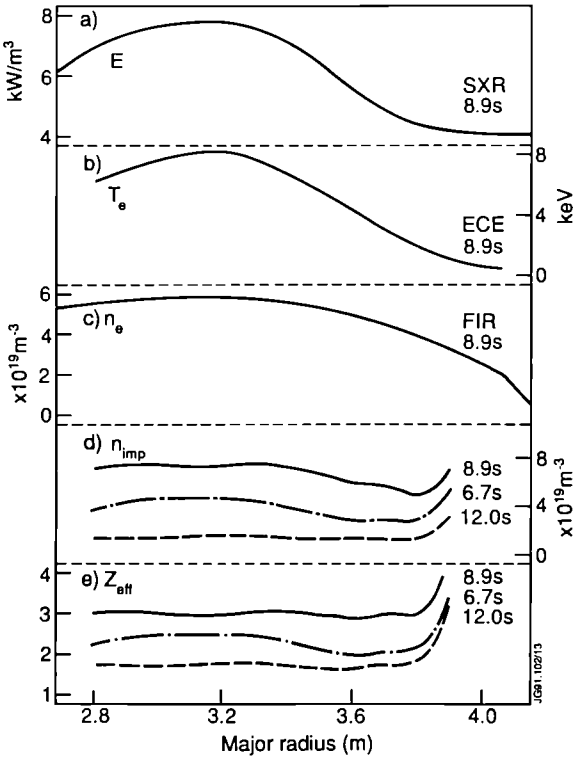

Fig.58 Radial profiles (Pulse No.20087); (a) soft X-ray emissivity; (b) electron temperature from electron cyclotron emission; (c) electron density from far infrared interferometry; (d) corresponding impurity density profile; (e) corresponding Z_{eff} profile.

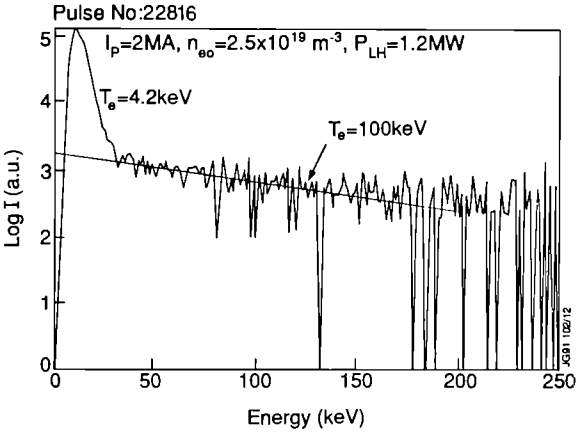

Fig.59 Pulse height analysis spectrum taken during lower hybrid heating showing the high energy tail.

heating system. Many spectra have clearly shown (Fig.59) the existence of high energy X-rays with a characteristic temperature of 100 keV.

Neutral Particle Analysis

A new time-of-flight (TOF) Neutral Particle Analyzer (NPA), was installed during 1990. The NPA is located at the bottom of Octant No.1, with a vertical line-of-sight crossing the torus mid-plane at major radius of 3.1m. The NPA is absolutely calibrated for the measurement of H+, D^+, T^+, $^3He^{++}$ and $^4He^{++}$ ions in the energy range 0.5-200 keV, although the analyzer is capable of measuring ≈ 300 keV singly charged and ≈ 600 keV doubly charged ions.

The NPA employs a cylindrical parallel plate electrostatic analyzer for energy selection. The subsequent mass analysis is performed using time-of-flight/coincidence measurement. The latter feature gives discrimination against noise in the neutral flux measurements induced by the high neutron and γ-ray environment of JET. The full energy range is covered by 15 energy channels with ΔE/E = 0.05-1, each equipped with three coincidence channels, enabling simultaneous measurement of a wide selection of particles. The two key features of the new system, discrimination against neutrons and high energy range, have been tested and successfully exploited in the last experimental campaign. High neutron and g-ray discrimination factors of 100-400 have been measured, which makes it possible to measure neutral particle spectra during pulses of $3x10^{18}$-10^{19} neutrons/s.

Routine measurements of neutral particle spectra to determine ion temperatures, relative concentrations of different plasma ions, and high energy tails have been performed [9]. By making use of specific features such as sawtooth modulation of detected neutral fluxes, spatially localized values of the plasma parameters have been obtained. Slowing down ion energy spectra during deuterium and helium NBI heating, and hydrogen and He^3 fast ion tails during minority ICRF heating schemes have been observed. Effects on the ion velocity distribution of toroidal field ripple, and the ∇B_T drift have been inferred. Minor upgrades of services are in hand to bring the NPA up to and beyond its specified energy range.

A new contract has been arranged with the A.F. Ioffe Physico-Technical Institute, Leningrad, U.S.S.R., for the manufacture and supply of an analyzer capable of measuring neutrals with energies up to 3.5 MeV. Used in conjunction with a helium atom injector to increase the neutral helium density in the plasma core, the instrument would be suitable for detection of α-particles arising from D-He^3 fusion reactions during He^3 minority ICRF heating experiments, and D-T fusion reactions during the active phase of JET operation.

Installation is planned in two stages. A provisional instrument, based on a design for the T14 tokamak, is being prepared for installation during early 1991 and exploitation for the rest of the year. The NPA will be located on top of

Octant No.4 with a vertical line of sight crossing the torus mid-plane at major radius ≈3.12m. This line-of-sight will intersect the Octant No.4 neutral injector beams. An improved instrument will be designed and manufactured to JET standards for D-T phase operation, for installation at the end of the 1992 shut-down.

Far-infrared Interferometer and Polarimeter

Both these instruments have performed routinely and the measurements widely used in the control of JET operation and interpretation of plasma performance. During 1990, preparations were started to modify the interferometer/ polarimeter system for the pumped-divertor phase. At least two of the six vertical chords will be lost. The loss will be made-up by increasing the number of lateral channels to four. These lines-of-sight require vessel mounted internal mirrors, whose mechanical displacements will be compensated by deploying a two-colour interferometer, as for the present lateral chords. The laser for the 0.118 mm compensating interferometer will be upgraded to higher power, whilst that for the plasma interferometer at 0.195 mm will remain unchanged.

For the Faraday rotation measurements, depolarization effects due to the plasma are estimated to be negligible. To reduce errors due to beam depolarization by optical components in the path, polarizing grids were installed in the probing beam immediately before entry into the torus, and on the reference beam immediately before recombination. This reduced signal power in the undesired polarization by a factor ≈5, removing most of the depolarization error. Six vertical and one lateral chords of the polari-interferometer were equipped with a depolarization monitor, greatly enhancing the capability analyzing the poloidal field structure of the plasma and the evolution of the safety factor on axis, q_0.

A study of changes in the q-profile at sawtooth collapse was performed using the improved polari-interferometer data [10]. At sawtooth collapse, $(\Delta q_0)^{collapse} < (1 - q_0)$ is measured, indicating that the associated reconnection within the q=1 surface is incomplete. Comparison of the measured rate of change of q_0 between sawteeth and that deduced from field diffusion calculations reinforces the interference that the reconnection is not complete. Fig. 60 shows a plot of $(\Delta q(0))^{collapse}$ against the preceding sawtooth period, t_s, for ohmic and ICRF heated plasmas. Also shown are the corresponding calculated changes in q_0 in a time t_s, assuming neo-

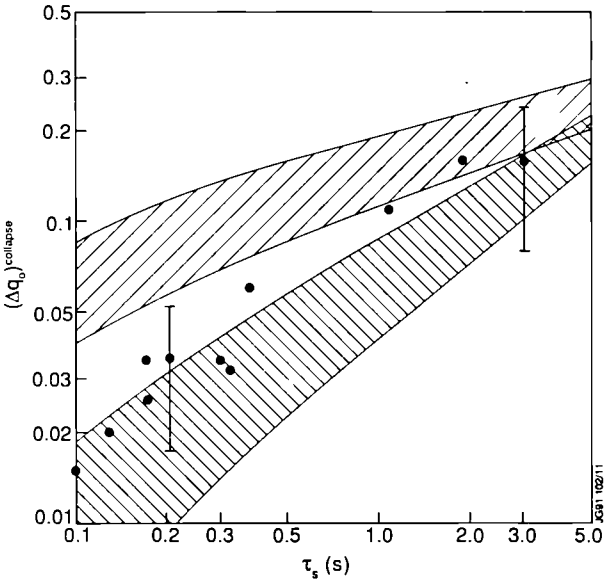

Fig.60 The change in the central safety factor qo during sawtooth collapse against the preceeding sawtooth period. The shaded bands cosrrespond to neoclassical calculations in which q_0 is reset to 1 (upper) and 0.75 (lower) at the crash.

classical resistivity. An assumption of complete reconnection after a sawtooth, equivalent to resetting q_0=1 at each sawtooth, gives values in the upper band shown, while resetting q_0=1 at each sawtooth, gives values in the upper band shown, while resetting q_0 = 0.75 gives the lower band of values for $(\Delta q_0)^{collapse}$. For shorter duration sawteeth, assuming that q_0=1 initially, the field diffusion calculations give values for $(\Delta q_0)^{collapse}$ which are 2-5 times larger than the measured ones, again suggesting that incomplete reconnection is effected by sawtooth collapse.

Alpha Particle Density and Transport Studies

The study of slowing-down and thermalised alpha-particles has been an important study at JET. Therefore, a comprehensive experimental and theoretical campaign has been undertaken for the assessment of atomic data required for a quantitative analysis. Particularly in the energy range below 50 keV/amu, different theoretical approaches and new input from experimental sources have led to a significant revision (up to factors of 3) of excitation cross-sections. The JET data-base - including multiple step processes for the neutral beam stopping in an impurity dominated plasma - were completed in 1990.

The injection of $^3He^0$ and $^4He^0$ beams (120 keV, 6 A neutral current) into JET plasmas has given a new boost to interest in the absolute measurement of helium densities and its radial distribution. The importance of high energy neutral

injection in contrast to gas fuelling, lies in a central deposition of helium atoms with a well defined source of particles and known radial deposition profile. Another scenario, where helium is the target plasma and its density diagnosed by a neutral deuterium beam, has enabled transport studies of hydrogen in helium plasmas.

In the first instance, with helium a minority in a deuterium plasma, the total number of alpha-particles derived from the C-X measurement of a radial helium density profile and its volume integration is compared to the number derived from the source rate. Results have shown that after an initial deposition phase recycling processes need to be taken into account during a subsequent steady state. Striking differences of central helium confinement were found in the case of injecting helium in L- or H-mode plasmas. In the L-mode case, the central helium density decays immediately after switching-off the fuelling He beam, whereas in the H-mode, it is usually found that helium accumulates in the plasma core. In both cases, however, the evolution of central density appears not to be correlated to recycling signals observed at the same time from HeI and HeII light emission at the boundary, and follows a significantly different time evolution.

In the case of helium being the main constituent, the CXRS derived helium density profile can be compared directly to an electron density profile measured by Thomson scattering (LIDAR). That is, the sum of electrons provided by the main low-Z impurities (carbon, beryllium, helium) and by the fuelling diagnostic hydrogen beam needs to add up to the electron density. A line averaged value of effective

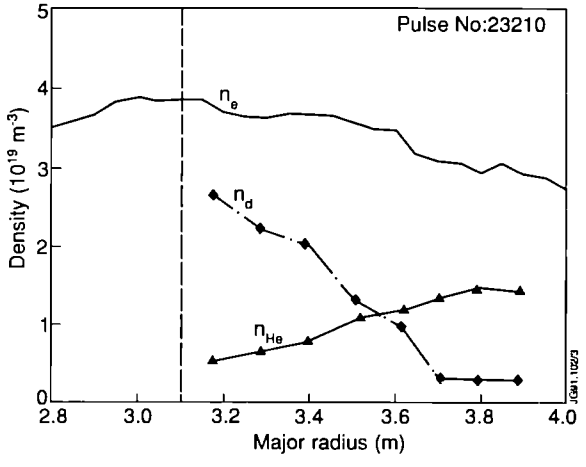

Fig.61 Radial density profiles of helium, electrons (LIDAR) and deduced deuteron profiles, in the case of a helium target plasma; the fuelling properties of the diagnosing deuterium beam leads to a distinctively hollow helium profile. The contributions of the other light impurities are n_C/n_e=0.3% and n_{Be}/n_e=0.8%.

ion charge can be deduced from the radial helium density profile shape and compared to $<Z_{eff}>$ from visible bremsstrahlung (Fig.61).

A somewhat unexpected result of the helium target test cases was the extent of hollowness of the observed helium profiles, the centre indicating clearly the fuelling role of a 'diagnostic' deuterium neutral beam, even at modest power levels. The implication of this observation is, that enhanced transport caused by a centrally deposited hydrogen beam and frictional forces may lead to a significant removal of alpha particles from the plasma centre.

Improved Analysis of Ion Temperature and Toroidal Rotation Data

A spin-off of the advances in the JET atomic data-base are comprehensive and much improved calculations of C-X cross-section effects on measured CXRS ion temperatures and toroidal rotation. As a result, it was possible to compare systematically results of central ion temperatures and toroidal rotation derived from the two independent JET diagnostics, CXRS and high resolution X-ray spectroscopy.

The correction factors due to C-X cross-sections effects apply in particular to the measurement of radial profiles of toroidal velocity. Depending on ion temperature and geometry, for example corrections of up to 10 krad/s arise at temperatures of 30 keV, if the CV I(8-7) transition is used for the C-X velocity measurement, for example. In hot-ion-mode plasmas, with central angular frequencies of the order 105 rad/sec, the effect may be relatively small, but in the case of high-density, low toroidal speed-plasmas, e.g. pellet-fuelled and RF-heated plasmas, the C-X correction factor may have the same order of magnitude as the measured central angular velocity.

For the active poloidal rotation measurements at JET, planned for 1991, the cross-section effects must be taken into account. Minute changes in poloidal rotation speed during L to H-mode transitions, observed in other tokamaks, may possibly be due to changes in the gradients of high ion temperatures near the edge, which may lead to apparent Doppler shifts in the observed C-X spectra.

The deduction of central ion temperature and rotation from line-averaged measurements of the Ni^{26+} X-ray resonance line has become increasingly difficult for JET plasmas with high electron temperatures (> 7 keV), broad electron density profiles and high toroidal rotation (100 krad/s). A novel analysis technique was recently completed and tested at JET which uses a synthetic line emission spectrum, which

is based on measured profiles of T_e and n_e (LIDAR) and a peaking factor for T_i and Ω_{tor} (CXRS). The synthetic spectrum is fitted to the observed X-ray spectrum and central values are derived.

A comparison of central ion temperature values, in a range 1-30 keV, has shown that corrections applied to the two diagnostics (5% in the case of CXRS and up to 40% for the X-ray spectrum), give agreement within the statistical errors (Fig.62(a)). The observed differences in experimentally deduced central rotation speeds can be explained by the predicted effects of cross-sections (C-X) and line averaging process (X-ray) (Fig.62(b)). Advances in understanding of emission processes for both CX and X-ray spectra, have therefore enabled significant progress in the measurement of low level toroidal rotation speeds.

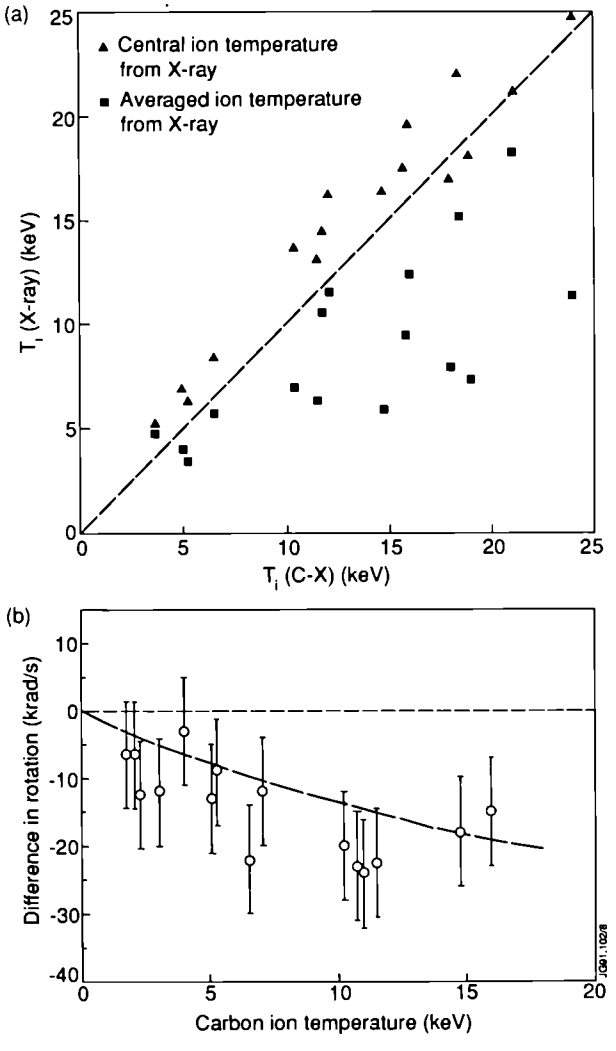

Fig.62 Effects of broad radial emission profiles on the line-of-sight integrated Ni^{26+} X-ray spectrum due to high electron temperatures and high toroidal rotation speeds.
(a) Comparison of central ion temperatures based on CXRS C^{6+} spectra with X-ray values, uncorrected for line-of-sight effects, and deduced central X-ray values based on a synthetic spectrum which is fitted to the observed X-ray spectrum;
(b) Predicted C-X cross-section effect on C-X rotation measurements (dashed line) versus ion temperature and experimentally observed differences between C-X values and results from the X-ray Doppler shift.

In addition to the measurement of central ion temperature and central rotation, the X-ray instrument has been absolutely calibrated enabling deduction of central nickel concentration from its line intensity and a line average value of Z_{eff} from its baseline. The latter result may be a significant asset in doubtful cases of high values of $\langle Z_{eff} \rangle$ derived from visible bremsstrahlung. A greatly enhanced level of apparent continuum radiation may be possibly attributed to blackbody radiation from the background wall and a simultaneous measurement in the X-ray range should give some useful information.

Combined Measurements of Local Magnetic Field Strength and Pitch Angle

Beam emission spectroscopy is making use of the D_α light emitted by neutral deuterium atoms in the JET heating beams. The Stark multiplet caused by the Lorentz field $\mathbf{E} = \mathbf{v}_b \times \mathbf{B}$ has given precise (<1%) values for the local total field strength. Poloidal field values derived from the Stark splitting and toroidal field values from the equilibrium code were consistent with the equilibrium code predictions. After discussions with DIII-D, it was decided not to follow the scheme pursued at DIII-D and PBX, which uses an active single channel modulated polariser technique to derive local pitch angles. It was decided to maintain the potentially stronger technique which measures spectrally and spatially resolved entire Stark multiplet, and combine it with an additional polarisation sensitive detection (Fig.63(a)). The optical head of the CXRS diagnostic has therefore been modified into a multiple purpose instrument for simultaneous measurement of temperature, rotation density and magnetic field at several radial points. During 1990, however, only three radial channels were used for magnetic field measurements. In principle, the diagnostic can provide accurate toroidal field profiles for both vacuum and plasma cases. Preliminary tests with beam injection into low-density neutral gas targets have confirmed this option, and will be pursued more systematically in 1991.

For both toroidal field directions (Fig.63(b)), resulting pitch angle profiles were in reasonable agreement with values predicted from the equilibrium code. Present error bars of the system are estimated to be ~10% for the pitch angle.

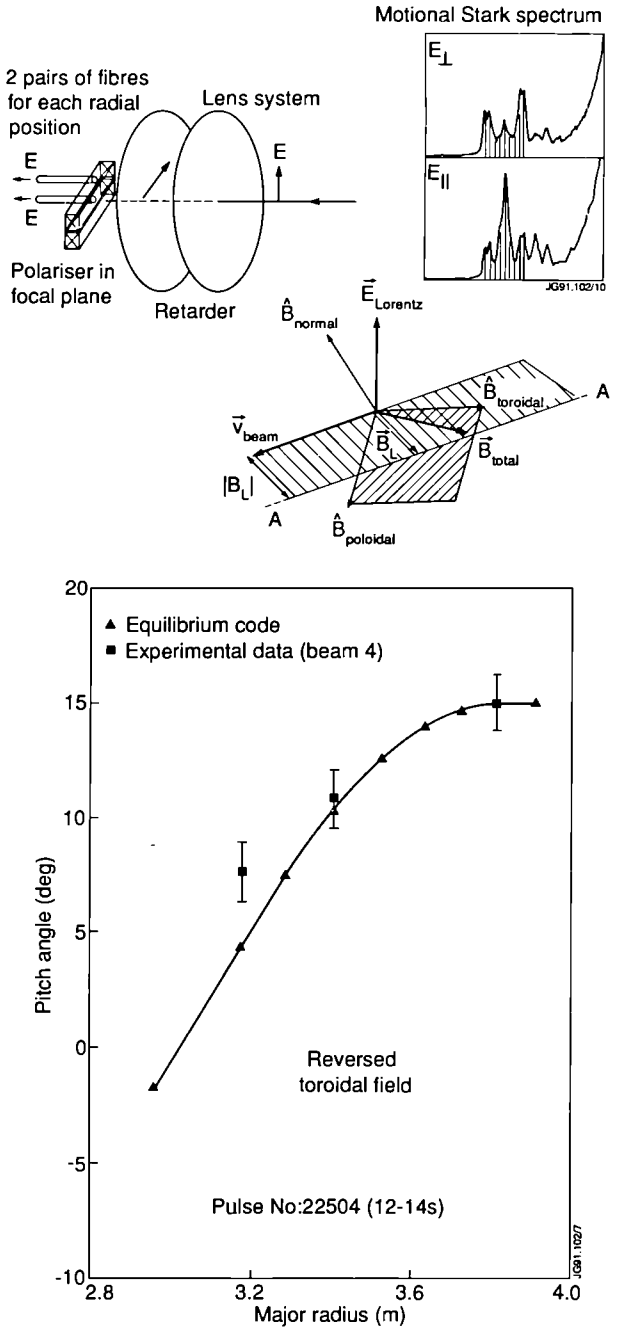

Fig.63 (a) Schematic showing the principle involved in the measurement of magnetic field using the Doppler Stark polarisation together with sample spectra for the two polarisations;
(b) comparison of the measured field line pitch angle with that determined from equilibrium analysis.

Direct Measurements of Deuteron Density Profiles

The density of deuterons in a plasma can be measured spectroscopically either directly from the C-X D_α spectrum or indirectly by measuring local impurity densities and subtracting contributions from an independently derived electron density.

Considerable effort was devoted to understanding the C-X excitation processes for the D_α spectrum and its absolute intensity. Competitive processes such as beam halo effects were taken into account. The present status is good agreement for (n_d/n_e) values derived either from local n_d or n_e measurements or even agreement between the first two techniques and values derived from visible Bremsstrahlung and C-X ratios of dominant impurities. A promising calibration technique for the relative sensitivity of the radial channels of the C-X multi-chord system was tested by comparing radial profiles of deuteron density measured by the same instrument either via C, Be or D C-X intensities.

However, there is still a puzzling inconsistency between experimentally observed intensities of the Doppler-shifted D_α beam emission spectrum and the intensities predicted by known excitation processes. In spite of a complex model for the excitation, including multiple step processes, the ratio between experimental and predicted intensities is still ~2. This observed discrepancy has direct implications for future operations in high-density plasmas, where beam emission spectroscopy will possibly provide the only tool for reliable data on fast neutral densities. The use of beam attenuation codes for the calculation of neutral power deposition profiles is obviously only applicable in the cases where the error propagation introduced by the exponential beam attenuation can be accepted. For example, at volume averaged densities of $5 \times 10^{19} m^{-3}$, the central beam attenuation is ~0.05, and the error in the calculated neutral beam density exceeds 30%.

High Boundary Ion Temperatures

A dedicated database on high edge ion temperatures was compiled in 1990 based on data from active C-X measurements (CVI) and passive line emission spectroscopy (CVI, BeIV, D_α etc.). Ion temperatures up to 10 keV and electron temperatures up to 5 keV have been obtained within 10 cm of the last closed flux surface (LCFS) in high-power hot-ion H-modes (Fig.64(a)). The results show that it is possible to bring the entire plasma volume to thermonuclear temperatures, with a considerable boost to the overall fusion performance. The high pedestal ion temperatures (defined as $T_i(0.9a)$) and high edge densities can contribute typically 30 to 40% of the entire stored plasma energy. Fig.64(b) shows a systematic survey of 'edge' ion temperatures as a function of deposited beam power per particle, sorted for different confinement phases.

The technical implications of the high T_i results for future operation of the CXRS diagnostic have clearly emphasised

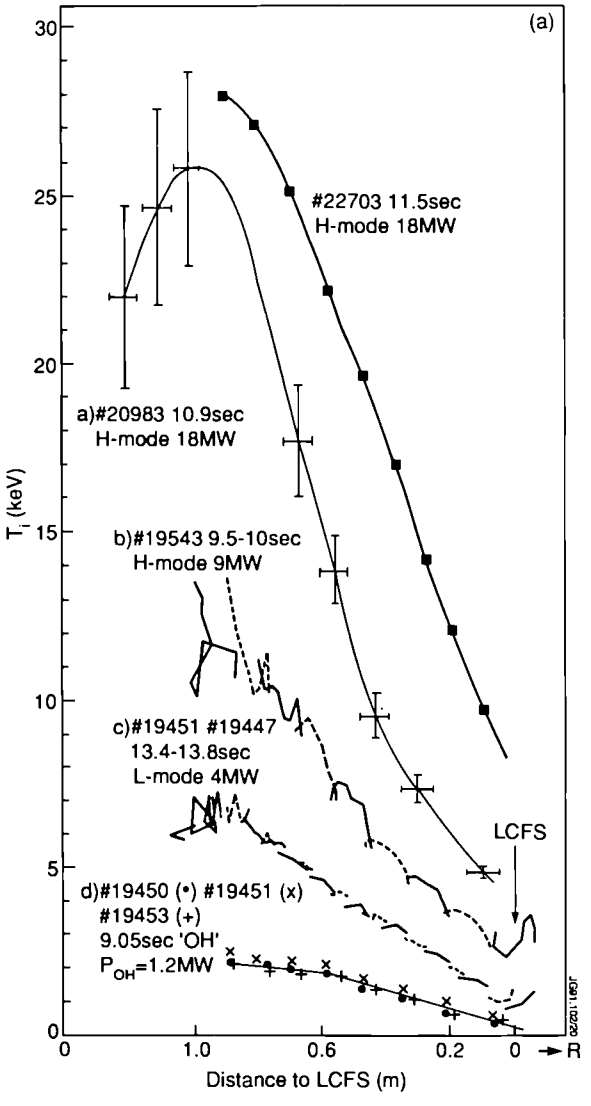

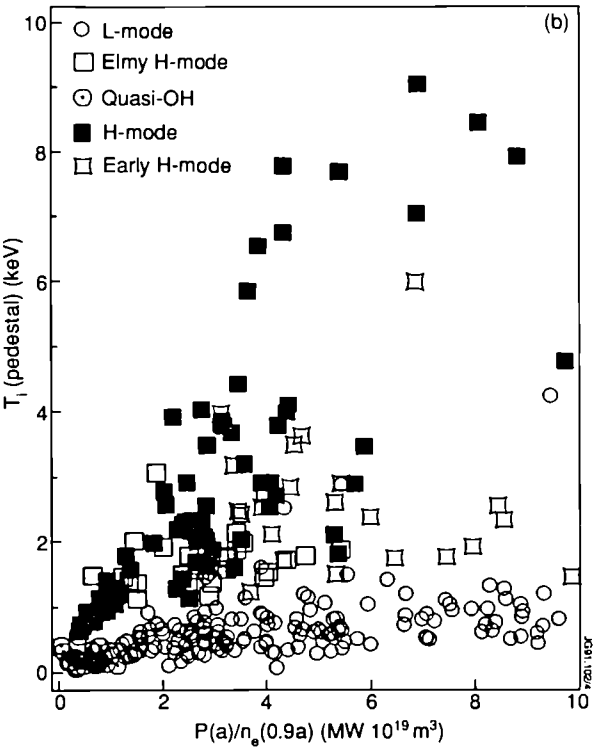

Fig.64 (a) Ion temperature profiles in Ohmic, L-mode and H-mode plasmas with different input power levels. The abscissa is the distance to the LCFS; in examples (b) and (c) the full time history is plotted for fixed radial positions, but varying positions of magnetic axis and distances to LCFS;
(b) A survey of a number of JET pulses shows the scaling of pedestal ion temperature with power per particle and the distinctive difference in pedestal level for L- and H-mode plasmas.

the need for an improved spatial resolution and active radial alignment system. The present alignment system is preset before operation starts but is affected by vessel baking and expansion process. For 1991, an active remote controlled stepper motor alignment facility will be installed.

Tritium-phase Active and Passive Spectroscopy in the UV and Visible Wavelength Range

A direct optical link between a vertical torus port and spectroscopic equipment in the Roof Laboratory was implemented and tested during 1990 operation. The link is based on several remote controlled mirrors and a penetration through the ceiling which minimises the neutron flux (Fig.65). First results have shown that spectral line emission can be observed down to a wavelength ~2500 Å. The final commissioning phase has not yet provided convincing C-X signatures in recorded signals. It is hoped that a more thorough alignment procedure may optimise the signals in 1991. The design of the UV link is such, that, in principle, any short quartz fibre cable from any port of the machine could be coupled at acceptable loss levels into the detection channel. For the future pumped divertor phase, it is planned to exchange the present linear detector arrays by two dimensional CCD cameras with the option of a spatial resolved observation of the divertor chamber. A fibrescope observation of the target area is linked into the optical channel to the Roof Laboratory and either analysed spectrally or viewed directly with a CCD camera.

Interpretation of Passive Line Emission Intensities from the Plasma Boundary

The spectroscopic instrumentation covers a large number of viewing liners directed at outer wall, limiter, inner wall, X-point target and IRCF antennae. Most collect light in a narrow wavelength bandwidth specified for selected impurity

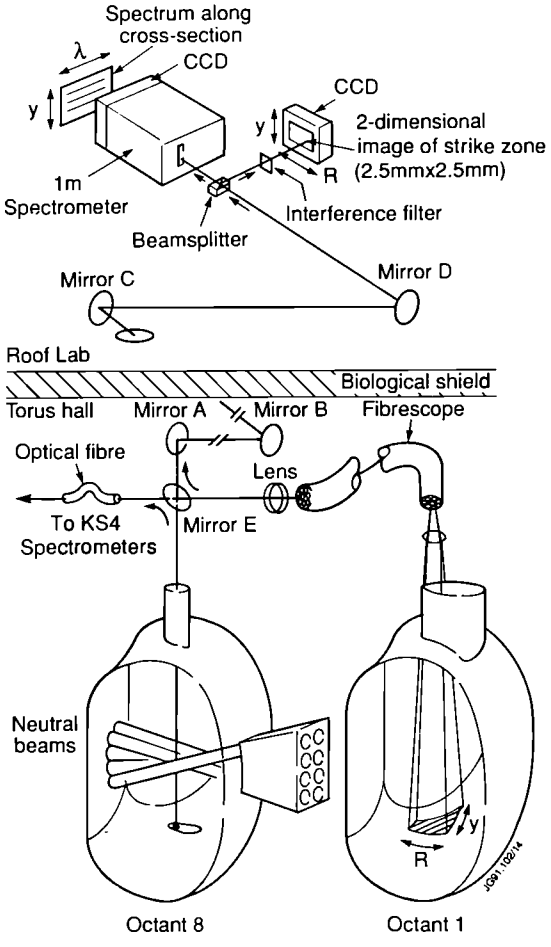

Fig.65 Schematic diagram of the active-phase optical link to the roof laboratory is zigzagging via relay mirrors, mounted on the transformer limbs, through an oblique penetration in the Torus-Hall ceiling, supressing direct neutron fluxes to the Roof Laboratory. The optical link is designed for multiple purpose applications. Direct view of the neutral beams in the plasma centre gives access to C-X lines in the UV wavelength range. A beam-splitter on top of Octant No.8 enables either the coupling of a coherent fibre bundle into the light path for spatially resolved observations of the X-point strike zone area in Octant No.1, or a fibre link to further C-X spectrometers.

lines and ionisation states. A single multi-channel instrument (OMA) provides high resolution spectra from one viewing line (usually limiter or X-point). In addition to these dedicated passive viewing lines, active viewing lines of the CXRS system can be used. In this case, the line emission spectra of 'cold' boundary lines are part of the complex C-X spectrum and may be used for interpretation. This aspect of a more efficient use of existing data appears to be particular important for a comprehensive understanding of the line emission at the edge and close to the last closed flux surface.

Many of the observed passive spectral lines are characterised by at least two populations. One representing a very cold (<50eV) electron impact excited emission layer, and the second, which is just inside the LCFS, is thought to be the result of interaction of a dense cold neutral hydrogen layer, with recycled deuterium from the wall or impurities in low ionisation states. The temperatures of this 'intermediate' layer can reach values up to several keV. Since the observed line intensity is a sensitive function of the parameters of the neutral layer (T_e, n_e, n_H, see Fig.66), its amplitude may change much more rapidly than, for example, active C-X line intensities well inside the separatrix.

Reversing the argument, if it were possible to combine all information on passive line emission (for example a comprehensive analysis of the spectrum around 4685 Å, which contains the spectra of several ionisation states of beryllium, carbon and helium), it appears feasible to infer some data on the edge neutral hydrogen layer. It is obvious that any progress in this field will be beneficial for the interpretation of divertor chamber results.

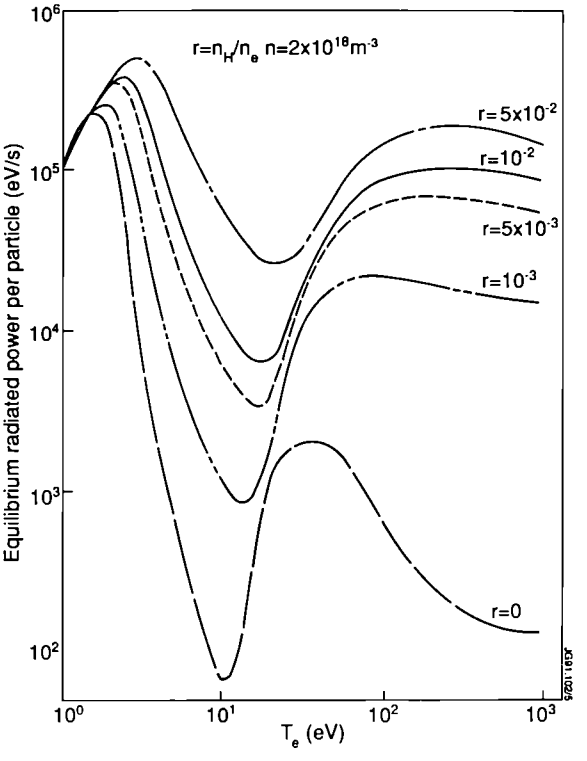

Fig.66 The line emission of Be I is a sensitive function of the balance between C-X and impact excitation processes. Small changes in the cold neutral hydrogen concentration (n_n/n_e) at the plasma boundary will therefore affect greatly the observed intensity.

Improvements in Reliability and Operation of Spectroscopic Diagnostics

(a) Active phase double crystal spectrometer

This is an instrument for broad band spectral survey of impurities and high resolution spectral analysis. After

substitution of the high precision real time angle encoder, the system reliability was much improved and it was on line for most 1990 pulses. Some of its data was integrated into the data set of line intensities obtained from the VUV spectrometers and used for the analysis of radiated power. Due to its comparatively high sensitivity at wavelengths below ~20Å, it gave useful information on the behaviour of oxygen (only present in traces in the discharge after the introduction of Be in the JET vacuum vessel) by monitoring the Lyman-α intensity of this element (Fig.67), usually too faint to be detected by the VUV instruments. In its high resolution mode, the instrument gave some preliminary results on the temperature of different ions located at various radii across the plasma discharge.

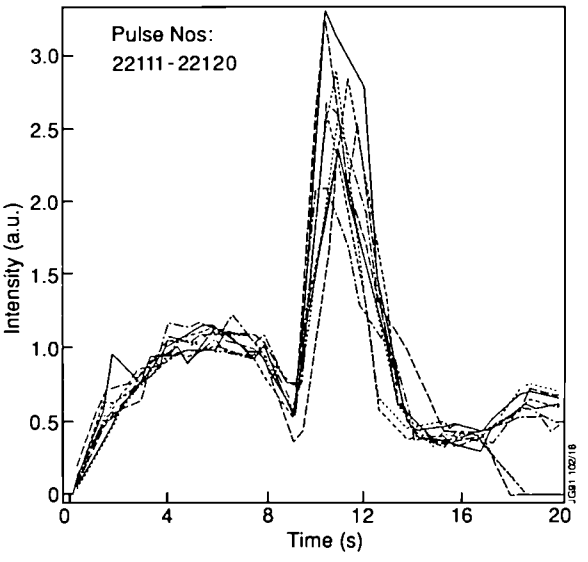

Fig.67 The time history for a series of pulses (Pulse Nos. 22111-20) of the Lyman-α line of oxygen, monitored with the active phase crystal spectroscopy system.

(b) Double-crystal spatially-scanning monochromator

This instrument was given a major upgrade in 1990 to improve its repeatability, sensitivity and signal-to-noise ratio. This has enable radial profiles of line radiation from the Nickel impurity to be recorded with better time resolution and increased dynamic range, compared to previous results. Fig.68 shows radial profiles of emission from He-like Ni XXVII, in the H- and L-mode phases after Ni injection. The profiles consist of several scans added together but without smoothing. The dynamic range is about 1000.

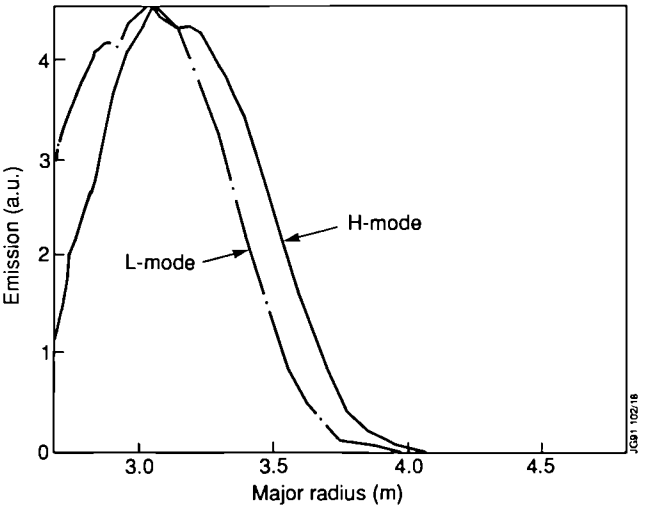

Fig.68 The emission profiles of helium-like nickel for L- and H-phases obtained using the spatial scan crystal spectrometer.

(c) Laser blow-off impurity injection system

This system had been quite unreliable during 1989 and only used on a few discharges. Careful realignment and focusing of the laser beam led to a substantial improvement in operation. Laser ablation of impurities was used in a number of experiments on a variety of discharges and proved to be the most effective tool for the study of the transport of metal impurites in the bulk of the plasma.

(d) Spatially Resolved VUV Spectroscopy

This diagnostic consists of two identical low spectral resolution (1Å), high throughput grazing-incidence spectrometers. A rotating mirror is mounted in front of each spectrometer to perform a scan through the plasma column. Due to many technical and design difficulties, this system did not work reliably over the past 7 years. To improve this, a major rebuild and upgrade was carried out and was successfully commissioned and brought into routine operation at the end of 1990. The biggest changes were to the detector and data acquisition system. Instead of the channeltrons used previously with analog amplifiers, 100 metre long transmission cables for the signals and ADC's at CAMAC station, a new detector system has been developed. A spectral resolving detector system (10 channels covering 3.5 Å) was developed. The new detectors, using micro-channel plates for the photo-electric conversion and charge muliplication and multi-anode arrays for charge collection, are operated in photon counting mode. The photon counts are coded into logic signals and relayed to the acquisition system via fibre optic transmission lines. The viewing range of the two spectrometers covers the upper half of the plasma

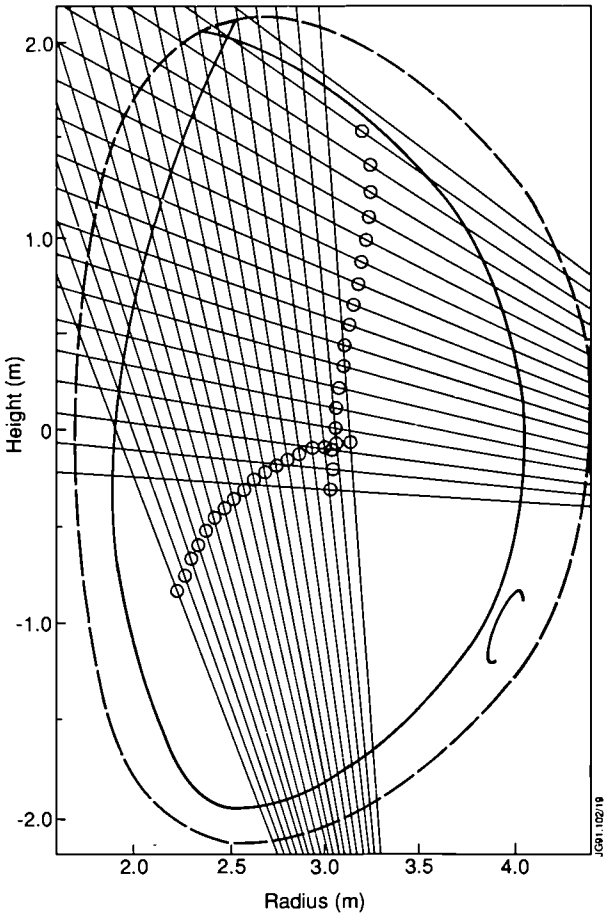

Fig.69 Lines-of-sight accessible to the spatial scan VUV spectrometer. The last closed flux surface of an X-point plasma is shown to demonstrate that this instrument gives good coverage of the target region.

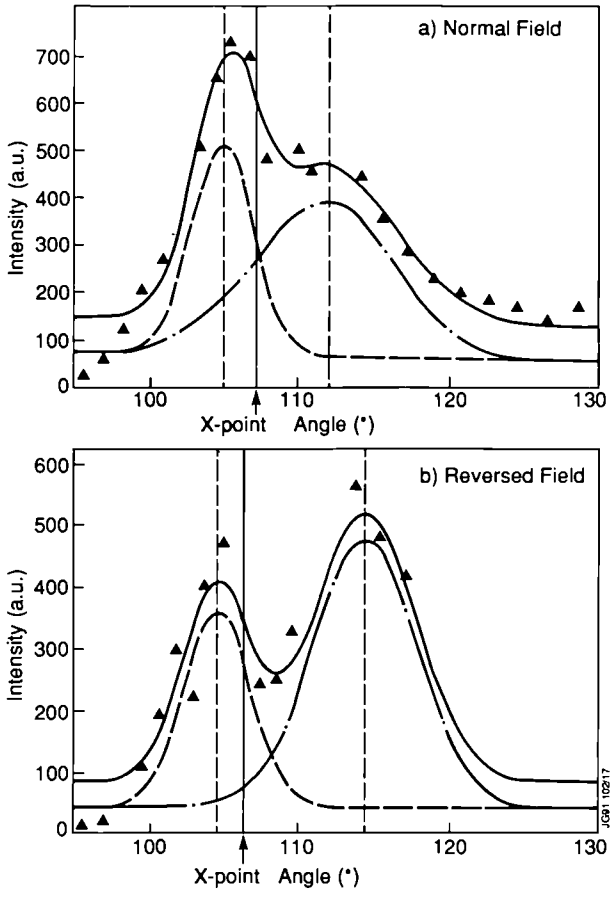

Fig.70 CII emission at 9025 Å versus poloidal angle from the X-point region obtained with the vertical camera of the spatial scan VUV system. The upper trace is for the normal toroidal field direction (Pulse No.22885 with ∇B upwards) and the lower for reversed toroidal field (Pulse No.22521 with ∇B downwards).

cross-section, including the upper X-point (Fig.69) looking between two of the discrete ribs of graphite target tiles.

Carbon and helium emission from the X-point region was mainly investigated. The emission was mainly investigated with CII and CIV lines, which show maxima on both sides of the X-point. The maxima of CII light are very close poloidally to the strike zones, those of CIV are about 10 to 20 cm from them. The relative intensities of the emission peaks were found to depend strongly on the discharge conditions and in particular upon the polarity of the magnetic field. In Fig.70 examples are given of CII emission for normal (ion ∇ B drift towards the X-point) and reverse field polarity.

Radiation power analysis

Improvement of instrumental calibration stability and operational procedure led to an extensive set of impurity data. The major impurites were Be and C, depending on the material of the limiting surface or X-point target plates.

As in 1989, Cl was found to be a significant contaminant (N(Cl)/Ne ~ 0.01 - 0.1%) limiting operational performance, particularly at high densities when Cl could radiate over 90% of the power. With reduced Cl level, higher gas fuelled density limits were achieved. Ni and Cr, whose source is the exposed inconel surfaces where also found to be present and at times were significant particularly towards the end of operations. In some cases, there was clear evidence of their concentration depending on plasma position.

Initital results of a statistical analysis of the impurity data suggests that the most important factors affecting the release of Cl into the bulk plasma are the vessel temperature, the presence of other impurities, such as F from SF_6 and a connection with T_e was found. High T_e tended to indicate the release of Cl. Factors such as magnetic configuration, additional heating type plasma position and other plasma parameters eg. current etc. were not found to be important.

In contrast to Cl for which a range of concentrations are found, there is a tendency for Be to radiate a certain proportion of the input power. For example during the ohmic limiter phase 2s. into the pulse, Be typically radiates 0.2 - 0.35 of the radiated power, whereas Cl radiated power ranges from 0.05 - 0.5 of this total input power.

Atomic Physics Studies and Data Compilation

Atomic physics properties of atoms and ions in plasmas, typically collisional reaction rates, radiation emission coefficients and wavelengths, are used in two distinct ways at JET, namely, as part of simulation of plasma behaviour (both present and future) and in the reduction of diagnostic measurements (mostly spectroscopic) to key physical quantities. The primary atomic physics developments and studies are in the latter area. This is a testing use, sets the standards of quality and precision and provides the guidance for global improvement of data for simulation.

It is generally the case in a plasma that a number or perhaps many atomic processes occur simultaneously so that it is the resultant or effective coefficients which must be identified and computed. The applied atomic physics studies at JET seek to provide and then exploit these coefficients. It is to be noted that JET provides a number of unique conditions for atomic processes not previously encountered in other experiments. Thus it has led to commissioning of concomitant new fundamental atomic investigations as well as the applied studies.

(a) Charge Exchange Resonance Spectroscopy (CXRS)

To exploit visible spectroscopic signals following charge transfer from neutral deuterium in the heating beams to fully ionised impurities in the plasma, there are certain atomic data requirements. To begin with, fundamental state selective charge transfer cross-sections to high principal quantum shells of the fully ionised receiving ion are required. New calculations, measurements and assessments of this data for helium, beryllium, carbon and oxygen have been assembled in an interpolable data-base. Extended ranges of collision energy are covered with special attention to helium for future α-particle analysis. Effective emission coefficients are derived by merging this data with complete reaction kinetic equations (collisional-radiative equations) describing the plasma environment. Data for all possible visible transitions of the above ions have been computed. The resulting derived data are used in all CXRS analysis and is of an accuracy sufficient to allow second order corrections to ion temperature, ion density and plasma rotation deduction in high temperature regimes.

Deduction of impurity density in the plasma by CXRS requires knowledge of beam attenuation in the observed volume. Fundamental data on all stopping cross-sections by plasma ions, impurity ions and electrons are used in calculating this attenuation. Enhancement of the stopping through excitation of beam atoms is preferably also taken into account although a small correction (<20%) of JET densities. At JET, a complete computational solution for deuterium beams has been implemented which not only describes the beam attenuation but also the beam emission itself, the CXRS emission of plasma deuterons and is in fact part of a consistent collisional radiative model for deuterium emission in all parts of the plasma including the scrape-off-layer. Commissioned calculations (charge transfer and excitation of deuterium in the n = 2 shell for deuteron impact, excitation of deuterium in the n = 1 shell by He^{+2} and Be^{+4} impact) and reassessments (electron impact excitation cross-sections of deuterium up to the n = 5 shell) have been performed to improve key fundamental cross-sections. The fundamental and derived effective coefficients form an extensive data collection. The spectral profiles of spectrum lines emitted by deuterium in the heating beams in JET are strongly perturbed by Lorentz electric fields. The resultant 'Stark features' have been modelled in detail and are the subject of intensive experimental investigation at JET.

(b) Influx Spectroscopy

Spectral observations along lines-of-sight directed at plasma/surface interaction regions are intensively studied for diagnostic information on impurity release and parameters of the edge and scrape-off-layer plasma. Neutral and near neutral ionisation stages of the principal impurities (Be^{0}, Be^{+1}, Be^{+2}, C^{+1}, C^{+2}, O^{+1}, O^{+2}, Cr^{0}, etc) are key indicators. They are excited and ionised by electron impact primarily (although charge transfer from co-located thermal neutral deuterium can have an influence) and calculations of their line radiating efficiency are required for reduction of observations to impurity fluxes, electron density and electron temperature. Computation of relevant derived quantities always involves a multi-level excited state population calculation in the collisional-radiative picture and the starting point for this is assembly of complete sets of energy levels, A-values and electron impact collisional rate coefficients for the ion. An

extensive data-base, organised by isoelectronic sequence, of this type has been prepared for many impurity ions. This has been by commissioned calculations (Be^{o}, C^{+2}, Cr^{o}), inhouse ab initio calculations and critical literature review. Computer codes operate on this data to obtain populations, emissivities, photon efficiencies and line ratio behaviours and have allowed preparation of a derived data base covering most relevant species. New methods which take account of metastable states in complex ions and departures from 'coronal' modelling have been developed to enhance the diagnostic scope in difficult regimes such as in the divertor. New comprehensive derived data has also been prepared for neutral deuterium.

(c) Ionisation, Recombination and Radiated Power

The familiar spectral radiation from the bulk high temperature plasma is at XUV or X-ray wavelengths and is from highly ionised states of atoms. Heavier species such as chlorine and nickel are prominent radiators if present in the bulk plasma. Location of ion emission shells is a central issue for reduction of spectral observations and so is closely linked to impurity transport models. For these models, effective ionisation and recombination coefficients are required as well as emission coefficients. Because of the range of possible elements and ionisation stages this has proved a major task for theoretical atomic physics. At JET, extensive computer look-up tables have been created for important elements spanning ionisation, recombination, total line power, recombination/bremsstrahlung power, specific line emission and charge exchange recombination. They are available both based on the approximations commonly used in fusion plasmas as well as on assessed astrophysical research sourced data. These approaches were defined some years ago and constrain the accuracy levels achievable. They are not sufficient for the future fusion programme, especially in divertors. Extensive new calculations and data set replacements are in progress at a more appropriate level of precision. The methods are those of generalised collisional-radiative theory which take account consistently of metastable states and finite density plasma similar to the detailed analysis data described in the previous section. External collaborations have been established to aid the merging of best available fundamental data into these calculations. The calculations are nearing completion.

(d) The Atomic Data and Analysis Structure

A computer package for the above manipulations of atomic data, calculation of radiating properties of atoms and ions and preparation of desired data for spectroscopic interpretation has been implemented on the JET IBM 3090. Four types of active use are supported, namely, fundamental data preparation, theoretical investigative studies, preparation of derived data and interfacing to application programmes. This is as well as interrogation and display of all fundamental and derived data sets in the database. Extensive data is stored in the centralised data base, but a user can create his own personal database for manipulation with ADAS.

References

[1] JET Progress Report, EUR11579 EN (EUR-JET-PR5) (1988);

[2] O.N. Jarvis, J. Källne, G. Sadler, P. van Belle, M. Hone, V. Merlo, E.W. Lees, M.T. Swinhoe, A.R. Talbot and B.H. Armitage. "Further Calibrations of the Time-Resolved Neutron Yield Monitor (KN1)", JET Report - JET-IR(85)06;

[3] G. Grosshoeg et al, "TANSY, a Neutron Spectrometer for Fusion Plasma Diagnostics", Chalmers University of Technology, Gothenburg, Sweden, CTH-RF-54 (1985);

[4] G.J. Sadler et al, "Investigations of Fast-Particle Behaviour in JET Plasmas using Nuclear Techniques", Fusion Technology **18** (1990) 556.

[5] Weisen H, Pasini D, Weller and Edwards A W, JET Report - JET-P(90)36. To be published in Rev. Sci. Instrum. (1991);

[6] Pasini D, Weisen H, Weller A, Edwards A W, 32nd Meeting of the Division of Plasma Physics of the American Physical Society (Cincinnati, USA, November) (1990);

[7] Pasini D, Mattioli M, Edwards A W, Giannella R, Gill R D, Hawkes N C, Magyar G, Saoutic B, Wang Z, Zasche D, Nucl. Fusion **30**(1990) 2049;

[8] Pasini D, Giannella R, Hawkes N, Lauro Taroni L, Magyar G, Mattioli M, von Hellermann M and Weisen H, 18th European Conference on Controlled Fusion and Plasma Physics (Berlin, F.R.G., 3-7 June 1991);

[9] G Bracco, *et al.*, 1990, to be published;

[10] J O'Rourke, JET Report - JET-P(90)43, (1990).

Summary of Machine Operation

During 1990, JET operations were essentially made up of three periods:

a) The first period (Weeks 12 to Week 24)

This period included the following activities:

- CODAS and Power Supplies commissioning (Weeks 12 to 23) in parallel with shutdown activities. Initially, this work was carried out in extended-day operation, but as plasma operation approached, shift operation started (Weeks 20 and 21);
- Installation of the lower X-point beryllium tiles in the vessel.
- Power supply commissioning culminating in plasma recommissioning (Week 23). This led to the start of the experimental programme in Week 24.

b) The second period (Week 24 to Week 30)

- Experimental operation (Week 25) was terminated to undertake remedial in-vessel work in Weeks 26 and 27. This work was required due to damage to the in-vessel protection tiles (some fallen and some out of position). The damage resulted from the high performance operation (involving some disruptions) in Week 25.
- After some power supplies recommissioning (Week 27), the experimental programme was continued in Week 28, but was halted in Week 29 for vacuum-leak testing and repairs. During a plasma disruption, a diagnostic vacuum connection had been ruptured. This resulted in the abrupt loss of torus vacuum. Remedial work was rapidly performed.
- Plasma operation was achieved late in Week 29 and continued in Week 30 until a 400/33kV power outage (Weeks 31 to 34) which had been agreed with the CEGB to allow for maintenance on the 400kV supply network. During this break, some in-vessel remedial work was carried out. In particular, protections were fitted between the lower X-point beryllium tiles and neighbouring graphite tiles to cover small gaps.

c) The third period (Week 35 to Week 45)

- Week 34 was devoted to commissioning as many systems as possible in the absence of the pulsed HV supply so that relatively little power commissioning was required before plasma operation and the experimental operation were successfully restarted in Week 35.
- The experimental programme proceeded to the end of Week 44, when the planned 1990/91 shutdown began. Remedial and maintenance work was kept to a minimum to allow as much as possible for the experimental programme. However, this phase of high-power operation was difficult, due to:

i) increasing in-vessel damage as a result of high performance operation (protection tiles and their supporting structures dislodged and either fallen or projecting into the vessel). This damage was regularly monitored with the in-vessel inspection system (IVIS).

ii) the constraint to restrict the neutron activation of the vessel (to limit the radiation dose for the in-vessel workers in the subsequent shutdown). During this period, one of the neutral beam injectors was converted from deuterium to helium operation. This permitted new and important experiments, while restricting neutron production.

- In Week 45, commissioning of the HV pulsed-power-supply reactive power compensation system was completed. This system will be operated in fully integrated fashion in 1991.

In 1990, the machine was operated for 86.5 days (i.e. for about the same period of time as in 1989). However, the relative amount of time for the experimental programme in 1990 was increased (69 double-shift days compared with 56.5 double-shift days in 1989). This was due to:

i) much of the recommissioning activities were carried out in parallel with the shutdown work;
ii) there were fewer maintenance and remedial days;
iii)regular six day-a-week working (Monday to Saturday) was used both for operation and commissioning;
iv)commissioning was carried out in double-shift-day operation.

These operation days were divided among the different heating programmes as follows:

3%	Ohmic (OH) heating only;
21%	Radio Frequency (RF) heating only;
18%	Neutral-Beam (NB) heating only;
58%	Combined (NB and RF) heating.

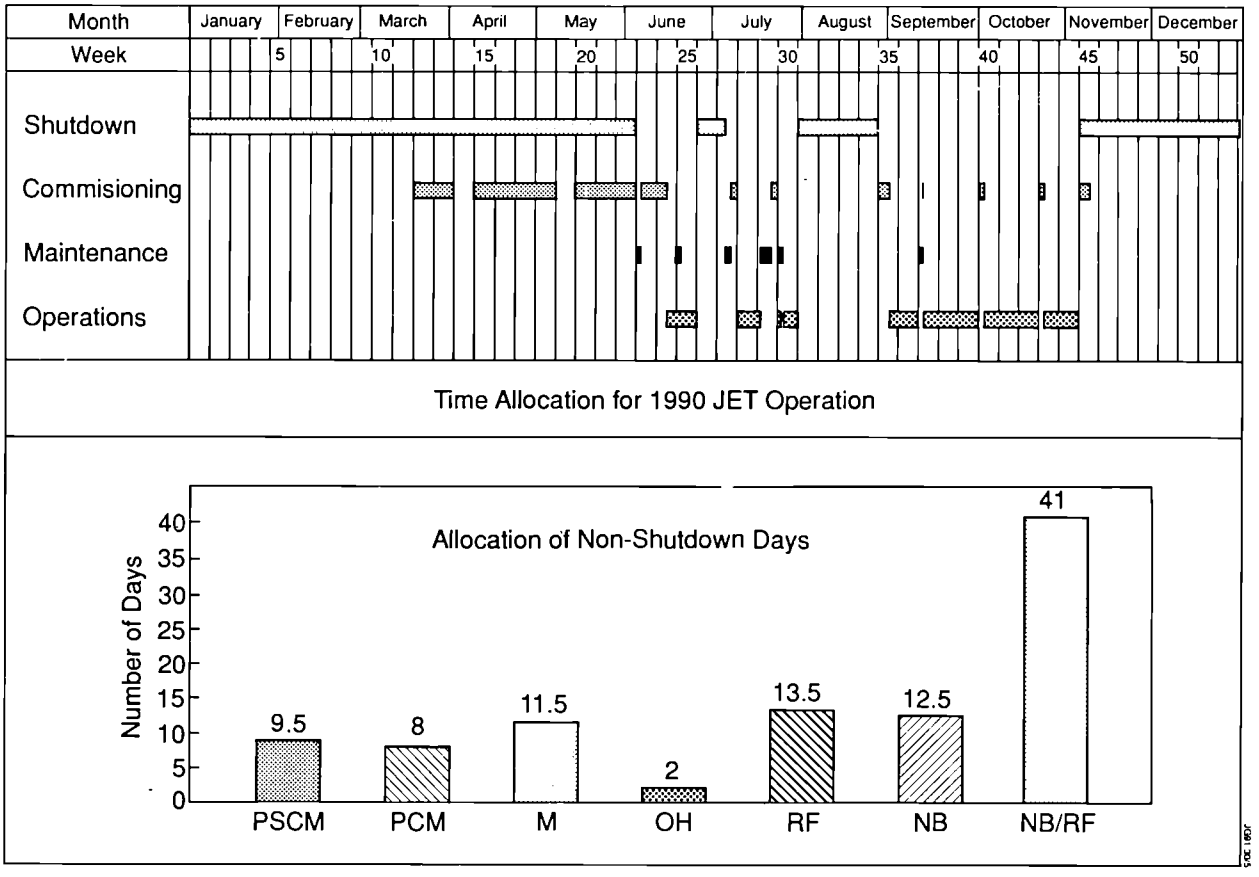

Fig.71: Allocation of days in which machine pulses were performed during 1990.
PSC = power supplies commissioning,
PCM = plasma recommissioning,
M = maintenance and remedial work,
OH = ohmic heating,
RF = radio-frequency heating,
NB = neutral beam heating,

Lower Hybrid Current Drive (LHCD), which involves some plasma heating and the prospect of profile control was brought into initial operation.

The allocation of time to different activities is shown in Fig.71. The experimental programme was carried out by three Task Forces, and the double-shift operation days in which these were involved were distributed as follows:

Task Force L	(Performance Optimisation in Limiter Plasmas)	36%
Task Force P	(Profile Effects and Related Physics Issues)	29%
Task Force X	(Performance Optimisation in X-Point Plasmas)	35%

The number of pulses in 1990 was 2500, bringing the total number of cumulative JET pulses to 23530. The relative number of commissioning pulses continued to decrease (Fig.72). 1990 operation clearly moved to higher plasma currents (>3MA) (Fig.73).

In spite of the limited time available for operation and the relatively small number of pulses, 1990 was a year in which high performance operation was repeatedly achieved and in which most systems performed satisfactorily. Of most concern are the in-vessel components which became damaged as a result of the large forces associated with disruptions during high performance plasma operation. Improvements in the fixing of such components will be carried out in 1991 and methods for improving the control of disruptions are being considered.

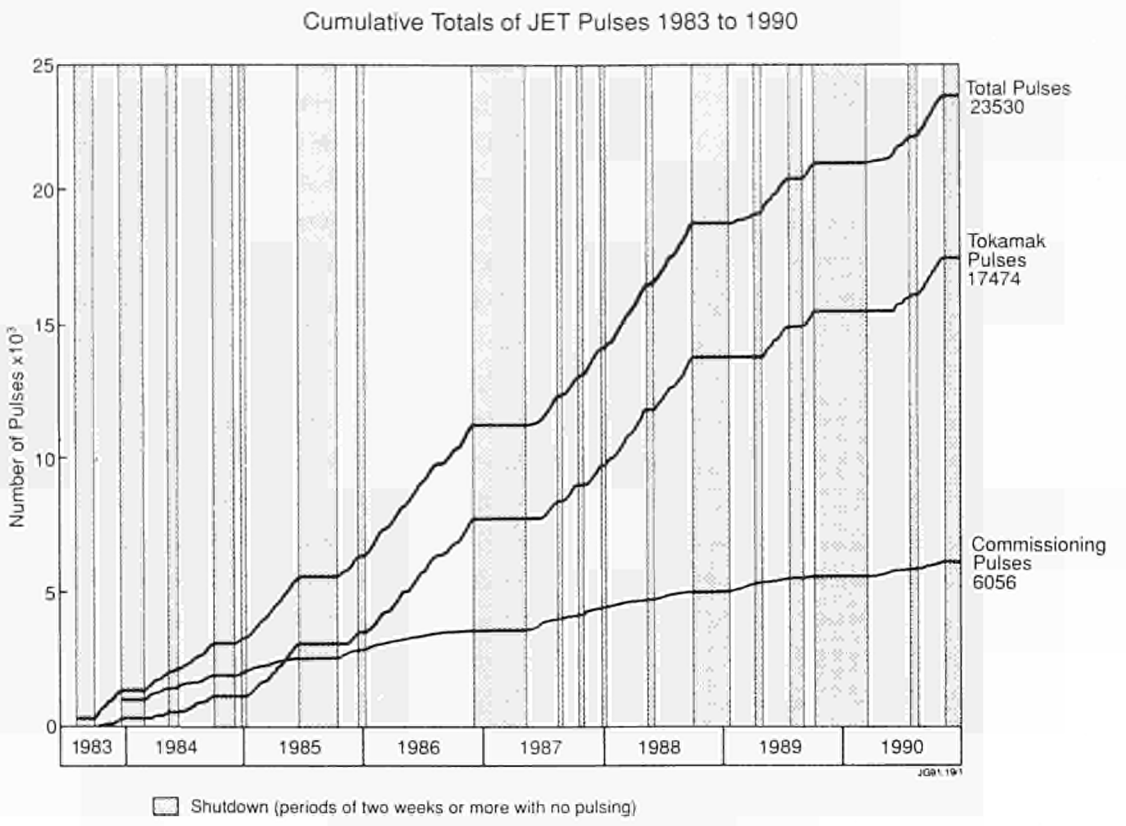

Fig.72: Cumulative totals of JET pulses.

JET Pulses 1989 to 1990

1989

Tokamak Pulses	1709	24.8%
Commissioning Pulses	535	17.0%
Total Pulses	2244	58.2%

1989 Plasma Current Distribution

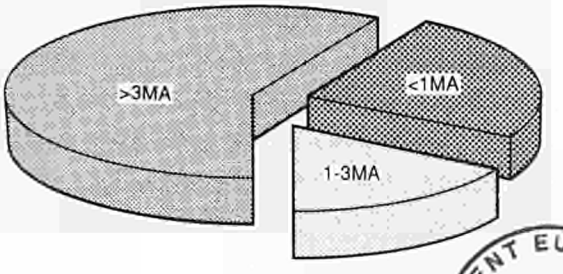

1990

Tokamak Pulses	1982	22.3%
Commissioning Pulses	518	12.2%
Total Pulses	2500	65.5%

1990 Plasma Current Distribution

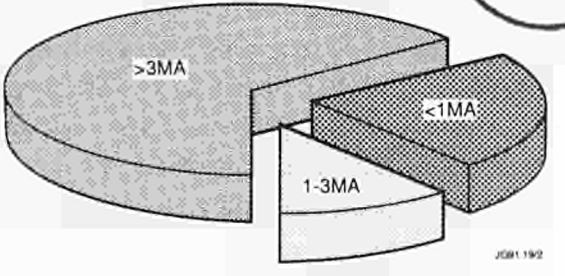

Fig.73: Comparison of numbers of pulses and distributions of plasma currents for 1989 and 1990. The 1989 plasma current distribution differs from that in the 1989 Report which was limited to technically successful pulses only. The present comparison is for ***all*** *tokamak pulses, both non-successful (mainly <1MA) and successful.*

Summary of Technical Achievements

From January to May 1990 the machine was in a scheduled shutdown period. The main tasks of the shutdown, which started in October 1989, were to replace a faulty toroidal field coil, install beryllium screens for the ICRH antennae and assemble the prototype Lower Hybrid launcher and waveguides.

Following the successful replacement of the faulty toroidal field coil with a spare one, the re-assembly of the machine proceeded smoothly. One particularly critical operation was the rewelding of the internal strengthening rings of the vacuum vessel. Due to excellent preparation work, no particular difficulty was experienced and mechanical surveys confirmed that the vessel octant had been reassembled within 1-2mm of its original location. It should be noted that advantage was taken of the shutdown to repair a number of small leaks between the main vessel volume and the interspace. Such small leaks do not pose any problem as long as the machine operates with deuterium, but would not be acceptable during tritium operation.

Early in 1990, a decision was taken to replace the graphite X-point protection tiles at the bottom of the vessel with beryllium tiles. The tiles used for this purpose were the ICRF antennae side protection tiles and therefore were not optimised for X-point operation. Due to the curvature of the tile profile and shadowing effects between adjacent tiles, the useful length in the toroidal direction (ie, the length intersected by magnetic field lines) is only one-tenth of the total toroidal circumference. Nevertheless, the use of such tiles was considered desirable to gain experience with beryllium target plates prior to the installation of the larger and better designed dump plates. The design of the supports and the installation of these X-point beryllium tiles extended somewhat the duration of the shutdown. The vacuum vessel was closed and evacuated by 4th June 1990.

The other main in-vessel activities of the shutdown were the installation of beryllium screens for the ICRF antennae and the assembly of the lower hybrid launcher. No particular difficulties were encountered during this work.

The shutdown from October 1989 to 1990 involved work in two shifts, six days per week for about seven months. A total of 8000 man-hours was spent inside the beryllium-contaminated vessel. There were no safety incidents involving beryllium. This must be considered as a major success and a consequence of the considerable effort made at JET in terms of organisation and the provision of support teams and facilities for beryllium handling and contamination control. It is important to note that between January and March 1990, in-vessel work was able to proceed without full protective suits. Face masks were found to be quite safe in view of the low residual beryllium contamination. The use of face masks allowed up to eight workers simultaneously inside the vessel, whereas this number was restricted to four when full-suits were used.

In February 1990, immediately after the reassembly of Octant No.3, which had contained the faulty toroidal field coil, electrical tests were carried out on the complete toroidal field magnet. These tests revealed that another coil, at Octant No.4, was also faulty. Of course, this was a major setback which lead to the concern that the fault in the toroidal field coils might be systematic and potentially could develop in other coils. The newly found fault was an order of magnitude smaller than the previous one and this explained why it had not been detected earlier. Detection methods rely on inductive measurements and due to the close proximity of the Octant No.3 coils, the strong magnetic coupling between the two faulty coils resulted in the smaller fault being masked by the adjacent large fault.

More electrical tests were systematically carried out on all toroidal field coils. These tests used improved comparative resistive measurements, inductive measurements, Rogowski coil techniques and, finally, high frequency resonance techniques. These tests clearly indicated that no other fault comparable to the first or even the second one existed on any other toroidal field coil. However, some of these detection techniques when used to the limit of their resolution, gave some indication of smaller faults in other coils. However, these indications were not consistent, different detection techniques pointed to different coils, and it was concluded that even though small faults may be present they were below the limit of detection.

By the end of 1989, and well before the discovery of the second electrical fault in a toroidal field coil, the decision had already been taken to use an organic dielectric fluid to cool the toroidal field coils. Since the electrical faults were caused by the presence of low conductivity water inside the coil insulation, the use of a fluid with intrinsically high dielectric properties would prevent the reoccurrence of such faults.

A survey of existing fluids restricted the choice of fluid to chlorinated or fluorinated products which combine the

desirable properties of non-flammability, adequate radiation resistance, low viscosity and low toxicity. The final choice, following chemical compatibility tests with the epoxy resin used for the coil insulation, was for Trichlorotrifluoroethane-113 (CFC-113). The use of this fluid implied considerable modifications of the cooling loop to ensure absolute tightness. The flexible rubber hoses which connect each turn of each coil (1536 hoses in total) had also to be replaced with a CFC-113 compatible type of hose. The conversion work had to be carried out within a very tight time schedule but was nevertheless completed in time for re-commissioning of the cooling loop in April. The system operated fully satisfactorily throughout the 1990 experimental campaign. During commissioning a small quantity of CFC-113 was lost due to a faulty hose connector. The event which caused some embarrassment due to inaccurate press reports, was neither a safety nor an environmental hazard.

Operation took place from May to November with an interruption of four weeks in August due to an outage of the high voltage power grid for planned maintenance. Operation was successful especially during the period from September to November. It is noteworthy that the toroidal field coil fault did not affect operation. In fact, no long term evolution of the fault was detected throughout the 1990 experimental campaign.

Heating systems achieved a very high degree of availability and both ICRH and neutral beams were able to inject in excess of 20 MW into the plasma. One of the two neutral beam systems operated with all ion sources at 140 kV (30A deuterium). The prototype Lower Hybrid system went smoothly into operation and with some 2 MW of RF power injected into the plasma, significant plasma current drive was observed.

During the second phase of operation, the experimental programme had to be somewhat limited due to damage to wall protection tiles. Some graphite tiles were fractured and some tile supports were bent or ripped from the walls. Such effects had been observed before but to a much lesser extent. The damage was attributed in most cases to large forces produced by currents flowing in the poloidal direction along the vessel walls or tile supports. The mechanisms which cause these poloidal currents are now better understood and the current value can be predicted. These currents appear during vertical instabilities and it has been estimated that the total intensity is abunt 0.2-0.25 of the total plasma current. The forces resulting from the interaction with the toroidal field are therefore considerable.

Monitoring the status of the wall protection tiles was essential during this period and was carried out every week by means of the In-Vessel Inspection System (IVIS). This system, which has been improved and extensively automated, proved invaluable and became an indispensable tool for the operation teams.

As planned, operation stopped by the end of November and the machine was again in a shutdown period to install the dump plates for X-point operation. The dump plates will carry beryllium tiles in the vicinity of the bottom X-point and graphite (CFC) tiles at the top X-point. By the end of December 1990, the lower dump plates were installed and preparatory work started for fitting the upper dump plates. Remedial work was also carried out to strengthen the tile supports and tile attachments in such a way that they could resist the large forces due to poloidal and eddy currents. A large part of this work was already underway at the end of 1990.

Scientific Achievements during 1990

Introduction

For 1990, the system of operation of the scientific programme was the same as that in 1989. The programme operated for a series of Campaign periods, the standard being of eight weeks duration (composed of six weeks tokamak operation and two weeks of maintenance/commissioning). Two Programme Leaders were nominated with responsibility for formulating near programme proposals (one campaign ahead) and outline plans (two campaign periods ahead). These proposals were within the broad outline of the JET Development Plan and subject to guidelines provided by the Experiments Committee. These proposals were presented to the JET Experiments Committee for discussion and approval before implementation.

Programme Leaders for 1990 were:

P.J. Lomas and P.E. Stott

Three Task Forces carried through the programme, as follows:

L) Performance Optimisation in Limiter Plasmas
(involving progression to full performance in material limiter configuration with currents up to 7MA, with high energy content; and including progression to the highest fusion product, long pulse operation Beryllium optimization, etc.) (Task Force Leader: A. Tanga)

X) Performance Optimisation in X-Point Plasmas
(involving progression to full performance in magnetic limiter (X-point) configurations at high currents (up to 6MA) to explore the H-mode regime of operation both in the single and double-null configurations; and including progression to higher NB and RF powers and towards quasi-steady-state operation)
(Task Force Leader: D.J. Campbell)

P) Profile Effects and Related Physics Issues
(involving a study of profile effects (using LHCD, RF, NB and high speed pellet injection, etc.); and including particle and energy transport studies in transient conditions, and disruption and sawtooth stabilisation)
(Task Force Leader: J. Jacquinot)

Task Force Leaders were appointed with responsibility for (i) interacting with and advising Programme Leaders on programme requirements within that task area; (ii) devising and setting out a detailed programme for allocated time within a campaign period; (iii) driving through that task programme (including acting as Control Room representative); (iv) analysing data (in conjunction with Topic Leaders, if appropriate); (v) disseminating information in the task area through internal meetings and publications (in conjunction with Topic Leaders, if appropriate).

In addition, Topic Groups were formed, as follows:

Topic Group	*Topic Leader*
(a) Energy and Particle Transport;	A. Taroni
(b) Plasma Edge Phenomena and Impurity Production (including fuelling and recycling);	P.R. Thomas
(c) MHD and Disruptions (including sawteeth);	P. Smeulders
(d) Physics Issues Relating to Next-Step Devices (including α-particle heating effects, etc.)	D. Stork

Topic Group subjects are of longer term interest than the immediate tasks undertaken by the Task Force Groups. The Topic Groups are responsible for analysis of results within many areas across the Task Force spectrum, but they also

have responsibility for advising Programme Leaders on programme requirements which are topical and relevant to the Groups areas of activity. In addition, the Groups disseminate information through internal meetings and in external publications.

Programme Objectives

JET operation during 1990 was mainly devoted to the introduction and exploitation of new facilities; on further improvements in plasma performance; and to the further assessment of beryllium as a first-wall material. Impurity control in JET, as for other long-pulse high power tokamaks, is of fundamental importance and therefore significant effort has been devoted to this area of study.

The main themes for the 1990 Experimental Programme were:

- introduction and exploitation of new facilities;
- further improvement in plasma performance;
- improvements in understanding in key areas of tokamak physics: such as: particle and impurity transport; physics of the H-mode; energy transport and confinement;
- experiments relevant to Next Step devices.

The scientific achievements for 1990 in these phases are described in the following sections, within the Task Force and Topic Group headings.

Performance Optimization in Limiter Plasmas

The superiority of beryllium limiters over those with graphite was already demonstrated during 1989 high performance discharges. Dilution of plasma fuel and radiative losses were observed at moderate levels of plasma current. The benefits of using beryllium were more evident at higher plasma density, where the density limit was increased. The aim of the 1990 high current experiments was to extend the range of operations at high plasma current, up to 7MA with high power additional heating. To further improve the plasma performance at high plasma current, a fast ramp-up of the plasma current was developed in which the onset of the sawtoothing activity was delayed until well into the flat-top of plasma current, assisted by ICRF current rise heating. With this new mode of operation, higher central values of plasma temperature, coupled with relatively good global energy confinement could be expected from the scaling with plasma current in a sawtooth-less L-mode discharge at high plasma current.

Experiments at high plasma current were performed to demonstrate a target discharge at 7MA with total input power of 20MW. However, the high current experiments had to be suspended because of extensive in-vessel damage caused by disruptions, thereafter the plasma current had to be limited to 5MA.

Experiments with plasma limited on the inner-wall were focussed on the extension of improved performance regimes (such as hot-ion and H-modes) to this configuration, which also has potential for high current operation. Some H-mode experiments with inner-wall limited plasmas were achieved with NB heating in a magnetic configuration with substantial edge shear, and hot-ion high performance pulses were obtained at 5MA. However, these experiments also had to be suspended because some of the inner-wall midplane graphite tiles were displaced and produced high levels of plasma contamination.

The later part of the experimental programme was devoted to the exploration of Helium neutral beam injection heating. One NB injector box was converted to monoenergetic He^4 injection at an energy of 120keV, and later to He^3 at 135keV. Particle transport studies, both in H and L-mode were carried out. The relaxation of the injected helium profile was measured as a function of the time by using charge-exchange (C-X) spectroscopy. Helium confinement time was found to be similar to the energy confinement time in the L-mode, a few times longer than the energy confinement time in ELM H-modes, and orders of magnitude longer than the energy confinement time in ELM-free H-modes. When compared to D injection, H injection produced similar heating efficiencies, while transport properties of the heated plasmas were similar, within errors. Improvements in central values of ion temperature, due to the higher average energy of the He beams, compared with D beams, were expected at relatively high plasma density and powers, which were not accessed.

In low density plasmas and with large values of ICRF power, high electron temperature regimes were produced, with central electron temperatures ~12keV. With increasing ICRF power, however, the electron temperature did not increase further. The saturation effect could be explained as reduced heating efficiency caused by the large D shaped orbits of the accelerated minority ions, extending in extreme cases, over half of the plasma minor radius.

The control of impurity influxes, especially the beryllium ions, originated by sputtering, and at high powers, by the onset of the melting of the surfaces, by heavy gas puffing was actively investigated. Preliminary analysis has been carried out.

Performance of High Current Belt Limiter Plasmas in JET

Beryllium belt limiter experiments have been performed for plasma currents 5-7MA with total input powers up to 30MW. This section describes experiments on sawtooth suppression, electron heating at low density, ion heating in sawtooth free discharges and the density limit.

Operation at 7MA has been demonstrated for the first time on the beryllium belt limiter. A fast 1MA/s current ramp at constant q_ψ was employed making a 3s flat-top at 7MA, as shown in Fig.74. By making D-shaped plasmas to fill the vacuum vessel, q_ψ was held above 3. In this discharge, sufficient inductive drive (V-s) remained that future extension to 10s duration should be possible. Initial heating experiments were performed with such plasmas up to 13MW of input power confirming the global confinement increases with plasma current in line with expectation. A steepening of the electron temperature gradient in the region r/a ≥0.3 was clearly observed as the plasma current was increased. For smaller minor radii, the gradients were small, consistent with an outward shift of the RF resonance as a result of a large paramagnetic effect.

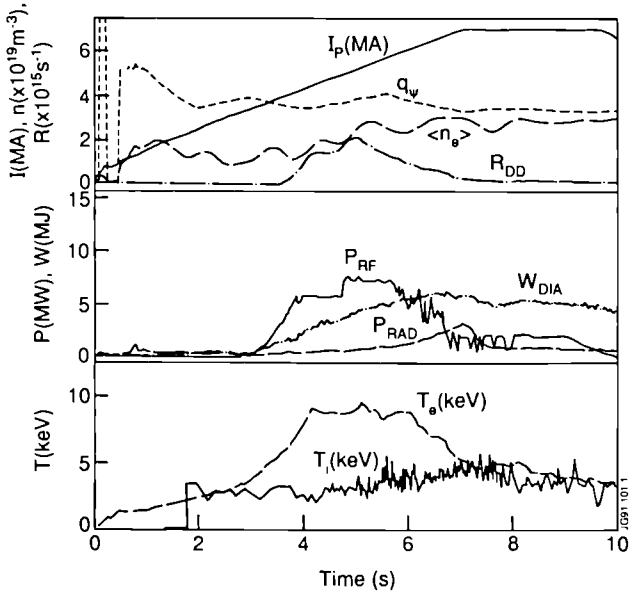

Fig.74: Operation at 7MW with beryllium limiter, showing 3s flat-top.

With ICRF applied during the current rise, sawteeth were suppressed until well after the flat-top of a 6.5MA discharge. At the first sawtooth crash, the inversion radius was r/a ~ 0.3, which is much smaller than the fully diffused case, where r/a ~0.6. In such sawtooth free plasmas at 5MA, the electron temperature increases approximately linearly with total power per particle, up to $P_t/n_{eo} \sim 3x10^{-19}MWm^3$, consistent with a simple prediction based on the Rebut-Lallia-Watkins model. For P_t/n_{eo} in the range $3\text{-}6x10^{-19}MWm^3$, T_{eo} remains in the range 10-12 keV.

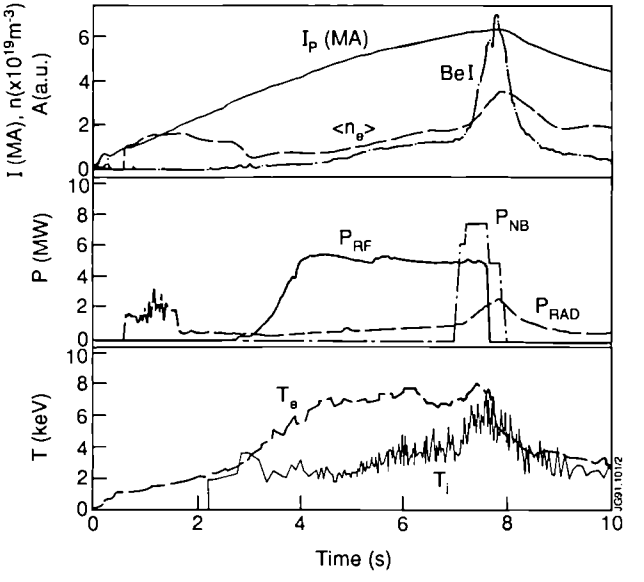

Fig.75: Operation at 6MA with 40MJ of additional heating.

Neutral beam heating has been applied to such sawtooth free discharges to heat the ions. As shown in Fig.75, at 6.5MA, 6MW of ICRF combined with 8MW of NB heating produced $T_{io} \sim 7.5$keV and $T_{eo} \sim 8.0$keV at $n_{eo} \sim 5x10^{19}m^{-3}$ with $\tau_E \sim 0.65$s. In this case, the central value of fuel concentration was high, $n_D/n_e \sim 0.88$, giving a fusion product $(n_{D0}\tau_E T_{io}) \sim 2.1x10^{20}m^{-3}$skeV. Higher ion temperatures in the range 10-13keV were obtained at lower density at 5MA as illustrated in Fig.76, but values of $(n_{D0}\tau_E T_{io})$ were lower due to poor fuel concentration.

The density limit has been explored at 5MA and, as a lower current, the maximum density reached with gas fuelling is set by the appearance of MARFEs. The highest density reached with 20MW of additional heating was $n_{eo} \sim 1.45x10^{20}m^{-3}$ with a flat profile. The maximum central density achieved scales as $n_{eo} = 3x10^{19}x[P_t(MW)]^{1/2}m^{-3}$, which is only 15% higher than previously found at 3MA.

Chlorine (Cl) impurity has been observed throughout 1989 and 1990 operation. Although its concentration, n(Cl)/

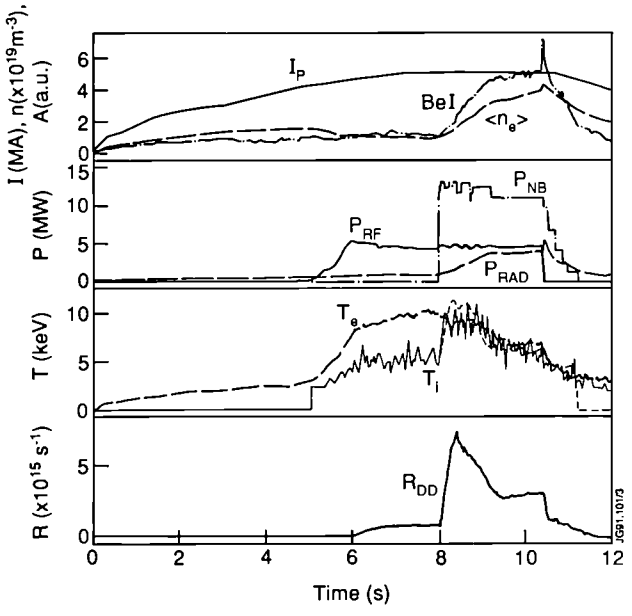

Fig.76: Operation at 5MA and lower density showing higher ion temperature achieved.

n_e, is small (~0.1% or less), it has a significant effect on the power balance. This is particularly evident during high density operation, when it can account for over 90% of the radiated power. In most cases, the Cl radiation effectively determines the density limit.

Analysis of the XUV spectrum enables radiated power components to be derived for the different impurity elements found in the plasma and this has allowed Cl contributions to be regularly monitored. An understanding of Cl behaviour and factors which affect Cl release have been gained from this study. Most notably, the presence of fluorine in the vessel significantly increases the plasma Cl content, whereas suppression of the Cl release is correlated with a reduction in vessel temperature. A difference in Cl behaviour is noted when the plasma limiting surfaces are either C or Be, the C limiting surfaces leading to a faster depletion of the Cl inventory. This is presumed to be due to the higher vapour pressure of C-Cl compounds compared to Be-Cl compounds.

During 1990, the conditioning of the vessel improved and a 5MA density limit programme was carried out in October 1990, when the Cl content of the plasma was low. Despite Cl levels increasing during the programme, a record line-averaged density of $4.3 \times 10^{20} m^{-2}$ was achieved in Pulse No:23301.

Hot-ion and H-mode Plasmas in Limiter Configuration

The inner-wall in JET is a shaped surface of $12m^2$ area protected by reinforced fibre-graphite tiles. Limiter plasmas were produced in contact with the inner wall up to 5MA currents. To avoid overheating of the graphite tiles with NB heating, with a consequent sharp increase of carbon impurities, it is essential that the plasma has the same shape as the contour of the inner wall. Fine tuning of the plasma shape feedback allows control within 1cm. In these optimized discharges, it was possible to apply 16.5MW of neutral beam heating for 2s, without a strong influx of carbon.

Overnight beryllium evaporation on the inner-wall graphite protection plates produced plasmas with good control of plasma density and a significant improvement in plasma purity, and allowed low beam target densities $n<0.7 \times 10^{19} m^{-3}$. With high NB heating on low density deuterium target plasmas, it was possible to achieve L-mode hot ion regimes at 5MA. Typical parameters were: $n=2.5 \times 10^{19} m^{-3}$, $T_e(0)=9.0$keV, $T_i(0)=22.0$keV, $n_D(0)/n_e=0.85$, $\tau_E=0.6$s. In these conditions, the best value of the fusion product $(n_D \tau_E T_i)$ for limiter discharges $3 \times 20^{20} m^{-3}$skeV was achieved, and, at the same time, the best value of Q_{DD} was 1.4×10^{-3}. Typical traces are shown in Fig.77.

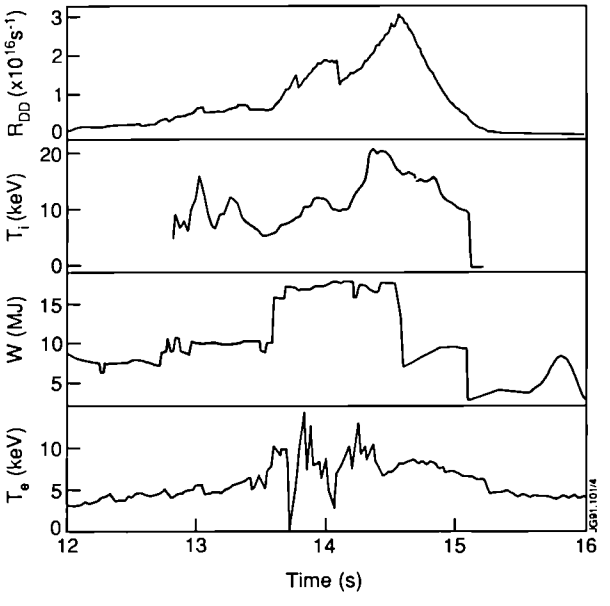

Fig.77: High performance inner-wall operation at 5MA.

At lower plasma currents and at low values of toroidal field, it has been possible to produce H-mode transitions at values of $q_\psi \sim 3$, (with $I_p \approx 2$ and 3MA). In these discharges, the H-mode transition had the typical signatures of the H-modes achieved in the X-point configuration, but the duration of the H-mode phase was, at most 0.8s. The H-mode phase appeared to be ELM free with a sharp increase both of the edge electron density and global confinement time, as

shown in Fig.78. The increase of plasma energy in the H-mode was also similar to that of similar discharges in the X-point configuration. The power threshold of the inner-wall H-modes scales linearly with the applied toroidal field at values about twice those in double-null X-point configuration, as shown in Fig.79.

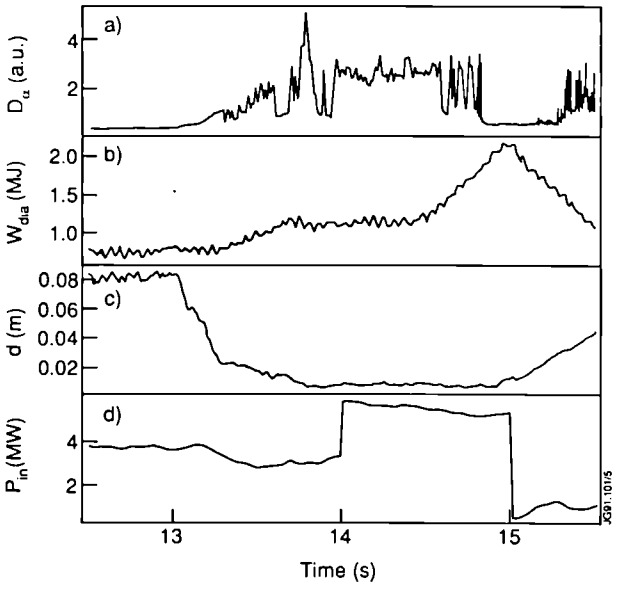

Fig.78: Inner wall H-mode at I_p=2MA; a) D_α emission; b) diamagnetic stored energy; c) distance between plasma and inner wall; d) total input power, as a function of time.

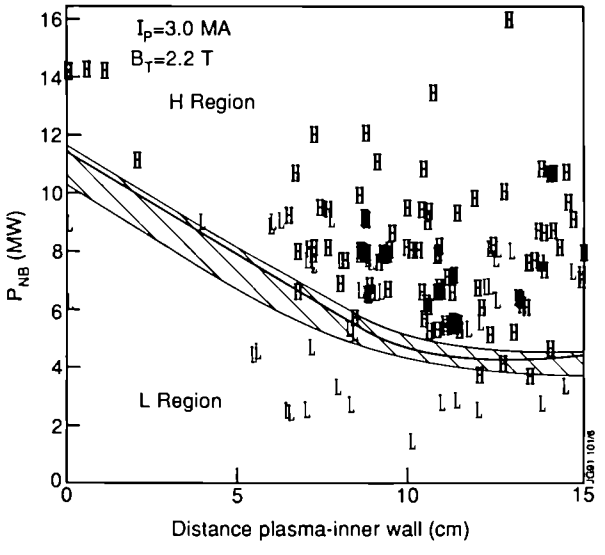

Fig.79: H-mode threshold power as a function of plasma-inner wall distance (I_p = 3.0MA, B_T = 2.2T).

Heating and Diagnostics with He NBI/ICRF

Initial experiments have been carried out by NB injection of 5MW of ^{3}He or 7MW of ^{4}He beams at 120keV for 3s from one beam box. This is the first use of ^{3}He NB heating in a tokamak, and as a record power of ^{4}He injected. ^{3}He and ^{4}He injection was expected to be advantageous for: eliminating beam-plasma neutrons in deuterium plasmas and enhancing neutron and CXRS diagnostic interpretation, providing a precise particle source for He transport studies and ^{3}He resonant ICRF heating, heating ions preferentially due to the high critical energy, enhancing D-^{3}He fusion reactions, and studying instabilities by varying fast ion distributions.

The use of He beams was found to be an efficient heating method, and high ion heating was clearly observed. At low electron temperatures, similar stored energy increases were observed with either 80keV D beams or 120keV ^{4}He beams, at the same power level, as shown in Fig.80, where Pulse Nos: 22975 and 22976 are compared. He beams are expected to give better deposition profiles than other species at high plasma density.

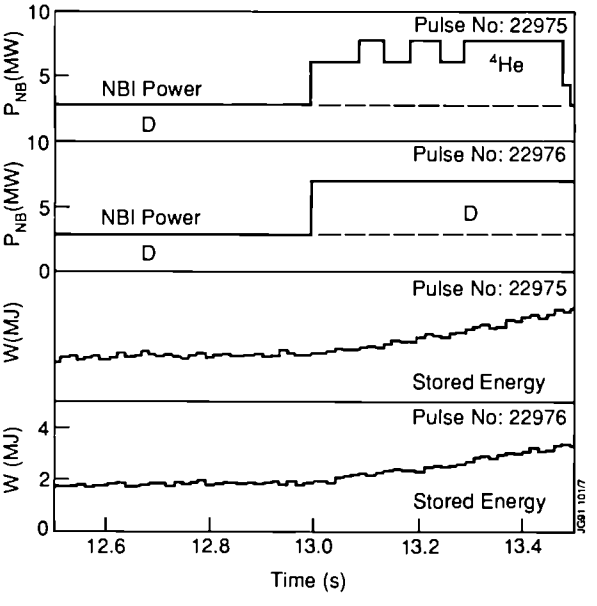

Fig.80: Stored energy increases as a function of time for similar NB power inputs (Pulse No: 22975: P_{NB} (He^4) = 8MW (120kV); and Pulse No: 22976: P_{NB}(D) = 8MW (80kV)).

^{3}He beams are able to produce an H-mode in double-null divertor plasmas. When 4.7MW of 120keV ^{3}He is combined with 10.5MW of 80keV deuterium NBI into a deuterium plasma, as shown in Fig.81 (for Pulse No:23275), a hot-ion H-mode with T_i up to 25keV is produced. This is comparable to the best results with deuterium injection only. The temperatures decrease after the peak due to impurity influx, as was seen in experiments with deuterium only. Increased ion temperatures are expected with higher power ^{3}He beams only.

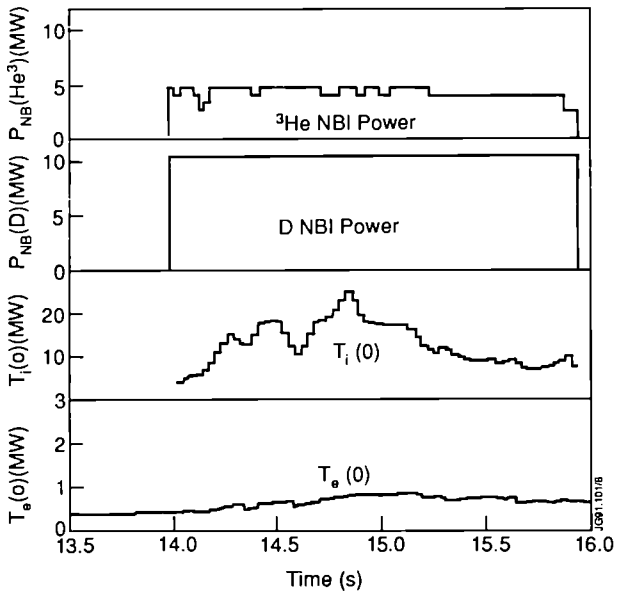

Fig.81: $P_{NB}(He^3)$ = 4.7MW (120kV) and $P_{NB}(D)$ = 10.5MW (80kV) into a DN plasma to produce H-mode with T_i = 25keV (Pulse No: 23275).

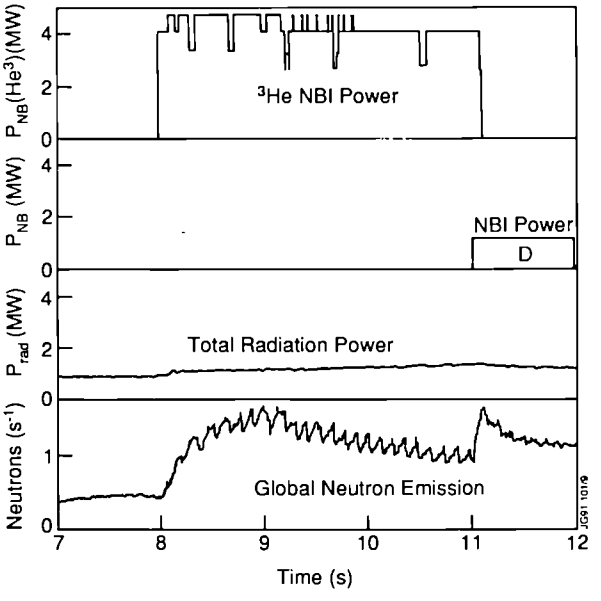

Fig.82: A He^3 neutral beam (4-5MW, 3s) into a 5MA plasma does not appreciably affect the total radiation power.

A particular concern with He injection is that metastables formed during beam neutralization would ionize at the plasma edge and cause localized limiter or dump plate heating. Most recent calculations indicated that about 10% or less of the beam would be metastables. Experimentally, He metastables in the neutralized beam do not seem to be a problem, as shown in Fig.82 (for Pulse No:23252). A He beam at 4-5MW of 3s duration in a 5MA limiter plasma does not produce a significant increase in impurity radiation power. Localized limiter heating from direct impact of metastables ionized in the edge is below the detectable level of cameras viewing the limiter. The global energy confinement time, τ_E~0.53s, is the same as for deuterium beam heating at the same power level.

By eliminating the beam-beam and beam-plasma neutron generation occuring with deuterium beams, He beam heating allows a reduction of total neutron generation, while still allowing efficient plasma heating, which is important for reducing vessel activation. The neutron rate shown in Fig.82 is comparable from 5MW of ^{3}He or 1.3MW of D injection. The elimination of beam-beam and beam-plasma reactions also allows a greatly improved measurement of the ion temperature directly with neutron spectrometers, since the broadening of the D-D neutron spectrum is due only to thermal ion motion. Measured temperatures agree with CXRS measurements taken by adding a deuterium beam at the end of the He heating pulse.

In Pulse No:23252, the ion temperature at the end of the ^{3}He NBI was ~3.6keV, and the axial neutron emissivity was 10^{13} neutrons/m^{3}s. Since local emissivity depends only on ion temperature and density, the axial deuteron density was calculated to be 2.6×10^{19}m^{-3}, which is consistent with Z_{eff} and electron density measurements. A combination of He and deuterium beams has been used to measure the particle transport of injected He, which provides a distinctive means of simulating alpha-particle transport with He beams deposited on axis. Complete radial profile and time dependent data have been obtained by this method.

D-^{3}He High Fusion Yield Experiments

To optimize the D-^{3}He fusion yield, a series of experiments has been performed using the ICRF heating system to generate a high energy ^{3}He minority tail. Both 5MA limiter discharges and 3.5MA discharges in the double-null configuration have been used, with the power loading to the plasma facing components being shared between the belt limiter and the upper and lower X-point dump plates.

RF power in excess of 15MW was coupled to the plasma in the ^{3}He minority regime. To counteract the relatively strong pumping of He by the gettering action of Be, the ^{3}He injection system was used to provide a central source of ^{3}He. Best results were obtained with 3.5MA discharges in the double-null configuration with most of the power being deposited on the upper carbon X-point tiles. The fusion power was increased to a record level of 140kW (corresponding to a reaction rate of 4.6×10^{16}s^{-1}). At the same time,

Q_{rf} ($=P_{fus}/P_{rf}$) was improved from just below 1% in the Be gettering phase to 1.25% in these conditions, but as observed previously, saturation seemed to occur at ~10MW of coupled RF power. The beneficial effect of central ^{3}He deposition by the NBI system could not be exploited to its full extent due to excessive ^{3}He concentrations in the plasma. Time resolved measurements show a clear correlation between fusion power and energy stored in the fast ^{3}He ions. First comparisons with simulations show reasonable agreement, although some experimental observations could not be fully reproduced.

Most experimental results were obtained in 3.5MA double-null discharges with the wall power loading shared between the upper (Carbon), the lower (Beryllium) X-point dump plates and the Be belt limiter. High current discharges ($I_p \geq 4.5$MA) can only be obtained in the limiter configuration and, therefore, are likely to have a higher Be contamination preventing a proper analysis of the γ-ray spectra and/or leading to a poorer performance.

Converting count rates into total γ-ray yields, taking into account line-of-sight and absorbers, give a good measure of generated fusion power. As shown in Fig.79, the highest yields achieved approach 140kW, and therefore lie substantially above the previous record of 100kW obtained during the Be gettering phase in 1989. At >10kW RF power, the yield seemed to saturate, possibly caused by excessive impurity generation and/or an acceleration of the minority ions above their optimal energy ($T_{tail} > 250$keV). The effect of this saturation can be seen clearly in Fig.83, where the fusion multiplication factor $Q_{rf}=P_{fus}/P_{rf}$ is shown as a function of coupled RF power. The maximum of Q_{rf} is reached at moderate values of the coupled power and clearly exceeds the previous best of 1% from the Be gettering phase.

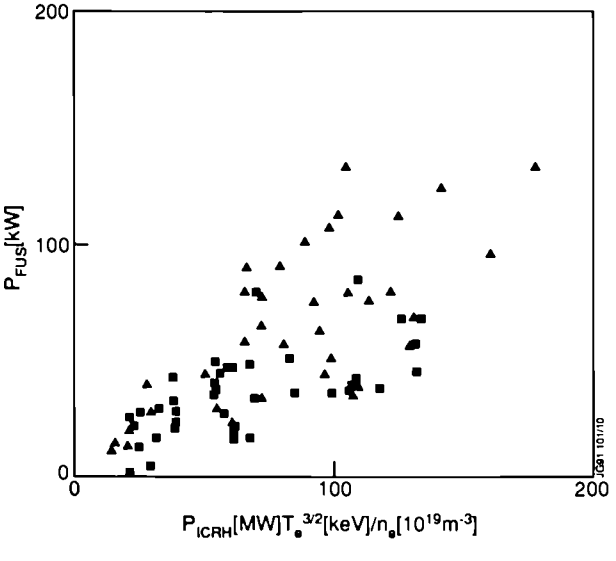

Fig.83: Fusion factor Q_{fus} ($=P_{fus}/P_{rf}$) as a function of $P_{rf}(MW)[T_e(keV)]^{3/2}/n_e(x10^{19}m^{-3})$.

A clear correlation between generated fusion power and energy stored in the minority ions has been observed. The g-ray detector count-rate and the energy stored in the fast ions obtained from the diamagnetic loop can be seen to rise steadily during the heating period. However, the electron temperature after an initial sharp rise, only rises by a very small amount during the main part of the heating phase.

Helium Transport Experiments

He neutral injection has been employed to provide a source of He ions in the plasma core, thus simulating the production of He ash. Recent theoretical and experimental efforts have led to the establishment of a comprehensive database of cross-sections for relevant beam-stopping and C-X processes, with a view to the eventual study of slowing-down and thermalised alpha-particles. These results have been applied to determine the density of thermalised He^{2-}, introduced by NB injection with a precisely known source profile. The He^{2+} density has been derived from measurements of the intensity of the HeII C-X line during simultaneous injection of deuterium diagnostic beams. The results demonstrate the capability of the C-X diagnostic to measure the temporal and spatial evolution of the radial He^{2+} density profiles (80ms and 10cm resolution), and hence the radial He^{2+} flux. The He^{2-} density measurements correspond closely to values expected from the He particle input, and results from discharges with He majority plasma confirm the absolute calibration; also the reconstructed Z_{eff} value obtained from simultaneous C-X measurements of He, Be and C densities gives good agreement with values derived from Bremsstrahlung measurements.

He transport behaviour has been investigated by measuring the relaxation of the He^{2+} profiles following short (≤0.5s) full-power He beam pulses into deuterium target plasmas. He recycling was measured from the intensity of edge HeI and HeII lines. The conventional particle flux model, $\Gamma_{He} = -D\nabla n_{He}+n_{He}v$ (diffusion plus inward pinch), has been used to interpret the profile evolution, applied at early times after the He beam pulse, before the onset of He recycling. For L-mode plasmas, a rapid (<0.5s) decay of the He^{2+} density was observed, accompanied by an onset of He recycling on a similar timescale to the central decline. An effective central He^{2+} diffusion coefficient D~0.4m^{2}s^{-1} has been derived for

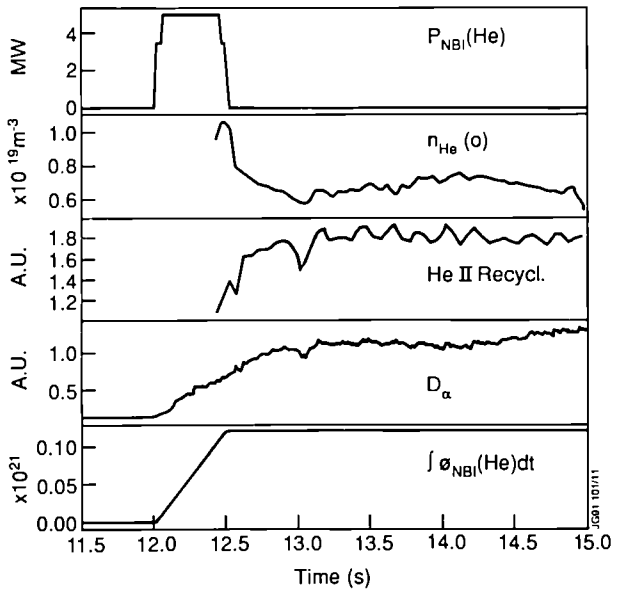

Fig.84: Evolution of central He^{2+} density following He NB injection, in a sawtoothing L-mode discharge. The HeII recycling signal is derived from the cold component of the HeII charge exchange line, viewed horizontally away from material limiter surfaces. The D_α signal is from a vertical line-of-sight, and increases due to formation of an X-point at 12s.

the L-mode transient phase in the presence of sawteeth (Fig.84). For H-mode plasmas the behaviour is more varied; the decline of central He^{2+} density was generally less marked, or absent in some ELM-free cases (Fig.85). In the approach to steady-state conditions, hollow He^{2+} density profiles often developed, implying additional driving terms not included in the model flux (see Fig.86). All the C-X data was taken

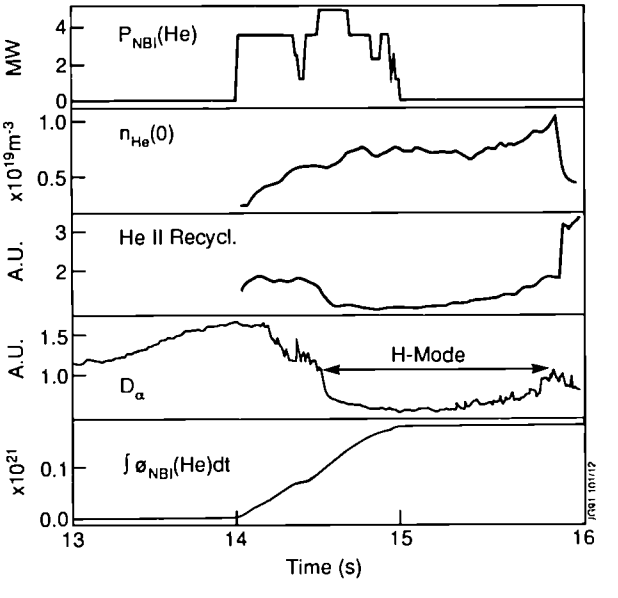

Fig.85: Evolution of central He^{2+} density following He NB injection in a sawtoothing H-mode discharge. The duration of the ELM-free H-mode phase is indicated.

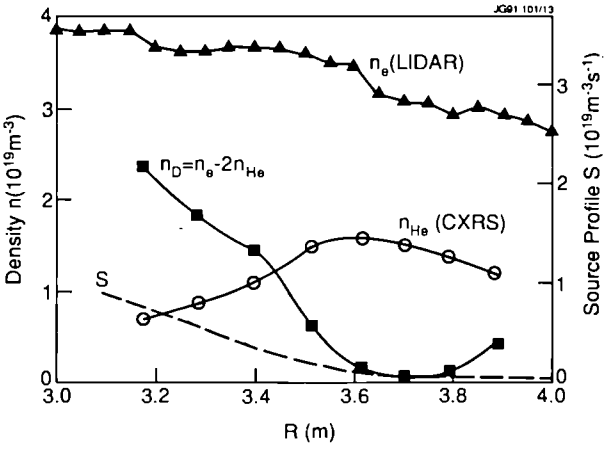

Fig.86: He^{2+} and electron density profiles measured about 0.5s after the start of D neutral injection into a He plasma. The particle source profile S of the D beams is also indicated. The plasma is in approximately steady state conditions; the main feature is the hollow He^{2+} density profile, which suggests an interaction between the outward D^+ flux and the He^{2+}.

in the presence of a significant deuterium outflow maintained by the deuterium diagnostic beams, which suggests an interdependence of the fluxes of the two species, eg. due to additional frictional forces.

Exploration of High Electron Temperature Regimes

In previous experiments of minority ICRF heating (using graphite limiting surfaces), studies of the central electron temperature increase (ΔT_{eo}) were made with values of the additional heating parameter $P_{rf}/n_{eo} < 2x10^{19}$MW m^3. In this operating regime, a linear dependence, $\Delta T_{eo} \propto P_{rf}/n_{eo}$, was found. With the first use of beryllium as a first-wall material in 1989, enhanced density control allowed the operating regime to be extended to $P_{rf}/n_{eo} < 5x10^{19}$MW m^3 in sawtooth free discharges. Results [1] showed an apparent saturation of T_{eo} at values of ~12keV, thus indicating a departure from linear scaling (Fig.87). Such behaviour could be caused by either a degradation in the electron energy confinement, a broadening of the RF deposition profile (effectively giving rise to a saturation in the electron heating rate from the minority ions in the discharge core), or by an increase in losses of the energetic minority ions. To investigate further the temperature saturation, a new set of experiments was conducted in 1990 with coupled RF power increased to 22MW in both the (H)D and (^{3}He)D minority heating regimes and with similar high values of P_{rf}/n_{eo}. The total anisotropic energy content of the fast ions was determined using magnetic diagnostics and showed values

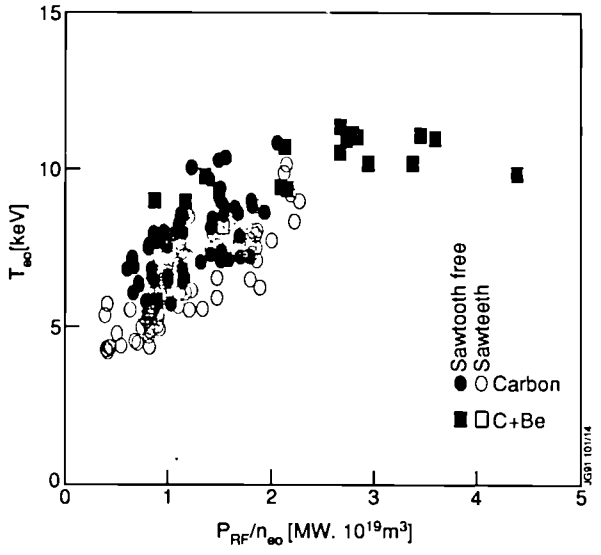

Fig.87: The axial temperature (ECE) in current rise ICRF heating experiments versus (P_{rf}/n_e).

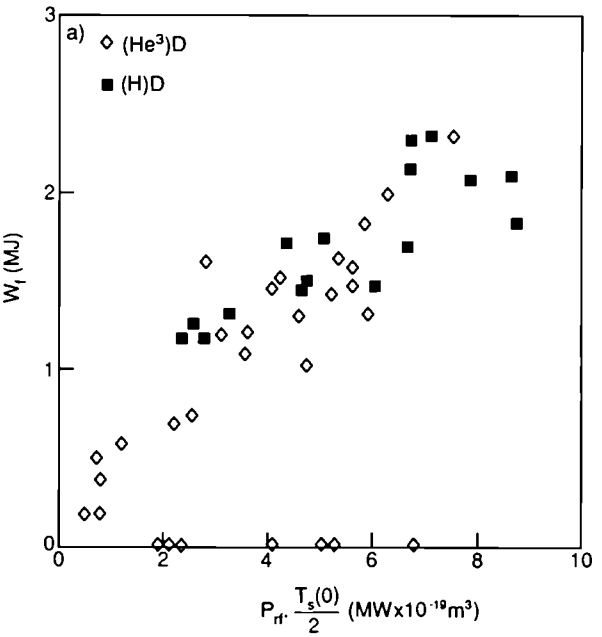

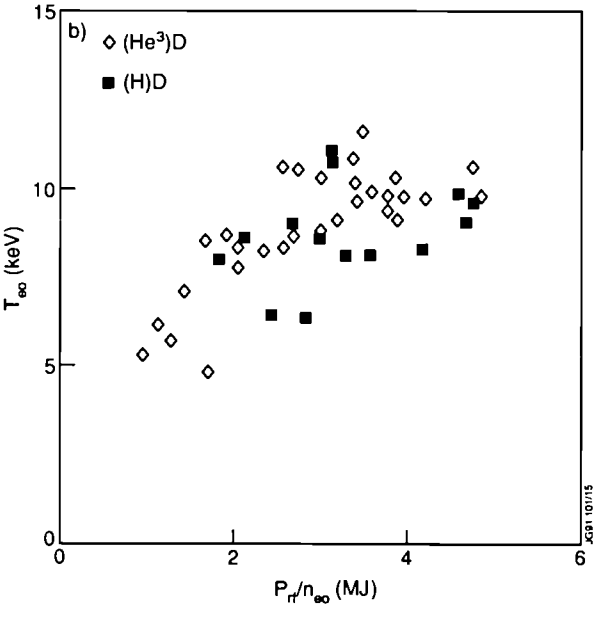

Fig.88: (a) Central electron temperature ($T_e(0)$) versus (P_{rf}/n_{e0}); and
(b) Fast ion energy versus $P_{rf}\tau_s(0)/2$, for both (He^3)D and (H)D cases.

of up to 2.5MJ for both H and ^{3}He minorities (Fig.88(a)). The fast ion energy scaled linearly with the theoretical central value: $P_{rf}\tau_s(0)/2$, where $\tau_s(0)$ is a central ion-electron slowing-down time. The differences in scales between the axes are a combination of profile and finite orbit effects. However, in the experimental parameter range, the central electron temperature, did not exceed 12keV (Fig.88(b)), confirming the earlier data.

For the parameter range of these experiments, and with typical minority concentrations of a few percent of the electron density, it is expected that the average energies of the fast ions will be about a few MeV. As such particles are deeply trapped in the field, they follow drift orbits having maximum radii which are a significant fraction of the radius of the discharge. These particles therefore explore the cooler outer plasma region in which the collisional drag is larger than in the core. Therefore, the finite orbital size not only lowers the effective slowing-down time experienced by the particles, but also results in broadening of the heat deposition profile to the plasma electrons. Preliminary calculations of these effects, based on a self-consistent 2D solution of the Fokker-Planck equation [2], indicate that reasonable quantitative agreement can be obtained between measured and calculated fast ion energy contents of these discharges. An extension of these calculations has been made to obtain the electron heating profile $p_e(r)$ shown in Fig.89, where the results are compared with a Monte-Carlo calculation [3]. In this 'benchmark' case, both models indicate a broadened electron heating profile which has a characteristic width of ~30-40cm, and that <40% of the RF input power is deposited inside the innermost 30cm of plasma.

To increase the electron power deposition in the plasma core from minority heating, it will be important, in future experiments, to constrain the orbital spreading by limiting the energy attained by the minority ions. This could be achieved in two possible ways. One method could be to simply increase the minority concentration; this would decrease the RF power per minority ion and therefore decrease

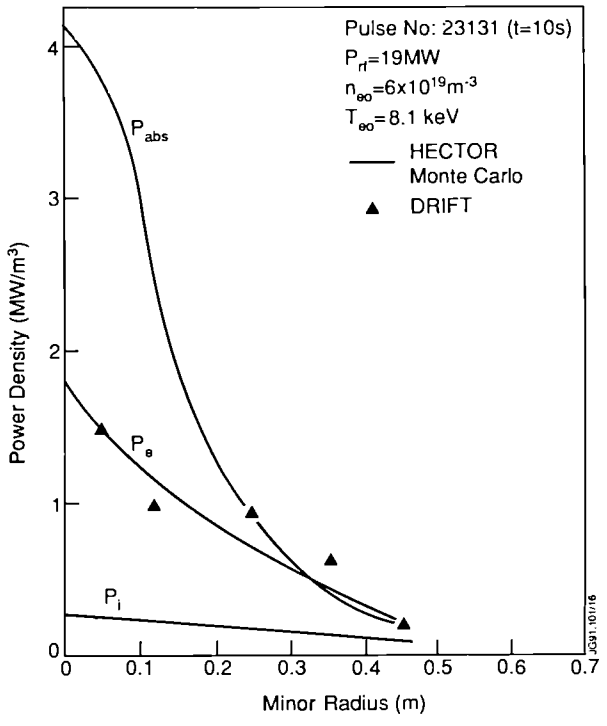

Fig.89: Calculated heating profile p(r) as a function of radius.

the average energy per particle. The limit on this procedure is the onset of mode conversion. A better scheme is to use the minority species with each density near the mode conversion limit. This effectively doubles the total input power for the same tail temperature and orbit spreading. Preliminary calculations confirm that it might be possible to double the electron heating power density to the electrons in the core using this technique.

References

[1] P.J. Lomas et al (1990) 17th EPS Conference on Controlled Fusion and Plasma Heating, Amsterdam, The Netherlands, (1990);

[2] G.A. Cottrell and D.F.H. Start, Nuclear Fusion **31** (1), 61-71 (1991);

[3] M. Kovanen and W.C. Core, private communication.

Optimization of Plasma Performance in X-Point Plasmas

Introduction

The main aims of the 1990 experimental campaign were: to extend the fusion performance of X-point plasmas at the highest currents and powers attainable; to characterize the parameters of the divertor plasma to provide a basis for prediction of performance in the Pumped Divertor phase; to investigate impurity retention in the divertor plasma; to exploit new facilities to improve H-mode performance with ICRF heating; to extend understanding of H-mode physics and to establish routine control of elm behaviour; and to investigate the use of beryllium as an X-point target material using a preliminary beryllium target.

A number of new facilities were available which were anticipated to have a significant impact on the X-point programme:

- a preliminary beryllium target was installed in the lower X-point region (graphite tiles were maintained in the upper region);
- the nickel Faraday screens of the ICRF antenna were replaced with beryllium screens;
- a new radial position control system, which utilized the RF antenna coupling resistance, was commissioned;
- the gas fuelling system was extended to permit gas puffing (both majority and impurity gases) into the 'private flux' region of the X-point plasma;
- improved magnetic analysis of the X-point geometry permitted a more accurate determination of the X-point position, which stimulated experiments on the influence of the X-point to target distance on plasma performance.

Unfortunately, as a result of damage to internal protection tiles and their supports, several diagnostic systems provided limited information for much of the campaign, and the lack of quantitative information, particularly on plasma purity, has restricted the interpretation of a number of experiments.

Investigation of the Beryllium Target

To obtain initial evidence of the influence of beryllium as a target material for X-point plasmas, a preliminary target was devised which used tiles of a non-optimum design, originally intended for use in the ICRF antenna protective frame. Fig. 90 shows the geometry of the interior of the JET vacuum vessel with the beryllium target. In this case, the plasma shown is a single null X-point plasma utilizing the upper (carbon fibre, or CFC) target tiles. For the beryllium target experiment, an identical configuration, but reflected about the vessel midplane, was used. To optimize the heat flux onto the tiles, which was known to exhibit a significant in-out asymmetry, the direction of the toroidal magnetic field

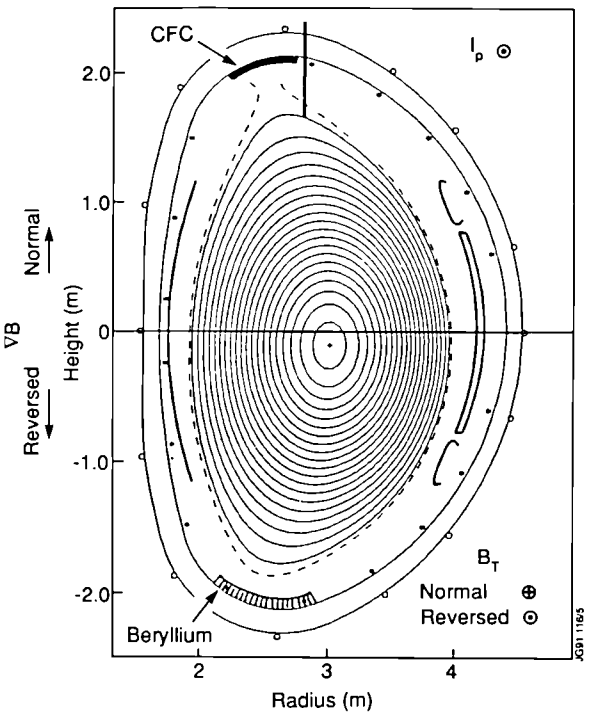

Fig. 90: Cross-section of the JET vacuum vessel with flux surfaces of an upper single-null X-point discharge. The locations of the upper graphite (CFC) and lower beryllium targets are shown.

was also reversed. This ensured that the direction of the drift of ions due to the magnetic field gradient (the so-called ion ∇B-drift) was towards the tiles. Nevertheless, calculations indicated that, for deposited powers of ~10MW, the time to raise the Be tiles to melting temperature (1278°C) would be ~100ms. It was, therefore, anticipated that experiments might be of limited duration, but that they would yield preliminary information on the effect of Be as a target material.

H-modes were initially achieved on the Be target at power levels ~50% higher than the power threshold for an equivalent configuration on the CFC target [1]. For example, at 3MA/2.2T, the H-mode threshold power on the carbon tiles was about 5MW NBI, whereas about 8MW was required using the Be target. However, after a few 100ms, local melting on the Be tiles was observed by a CCD camera viewing the target. Spikes of Be emission were observed and these were correlated with spikes in the radiated power. While these spikes were usually less than 50% of the input power, the exact radiated power fraction was unknown as the bolometer cameras cannot see the lower divertor region and, moreover, cannot detect an important BeII line which is responsible for radiation from regions with electron temperatures of ~10eV.

Fig 91 compares H-modes on (i) the Be target and (ii) the CFC target, under very similar conditions. In the Be case, the H-mode persisted for ~0.5s (the longest duration obtained) and termination coincided with a rapid increase in the Be radiation. On the CFC target, the H-mode lasted for 1.7s, although the decrease in the D-D reaction rate, R_{DD}, and the rise in the radiated power after 1.5s indicates that a carbon bloom occurred. Moreover, there was evidence of a gradual increase in the H-mode power threshold on the Be target and, ultimately, it proved impossible to obtain H-modes at the highest NBI power levels then available (11MW). The implication was that the performance of the target degraded as damage due to melting became more extensive, but it was not possible to identify the critical plasma parameter which prevented the H-mode transition.

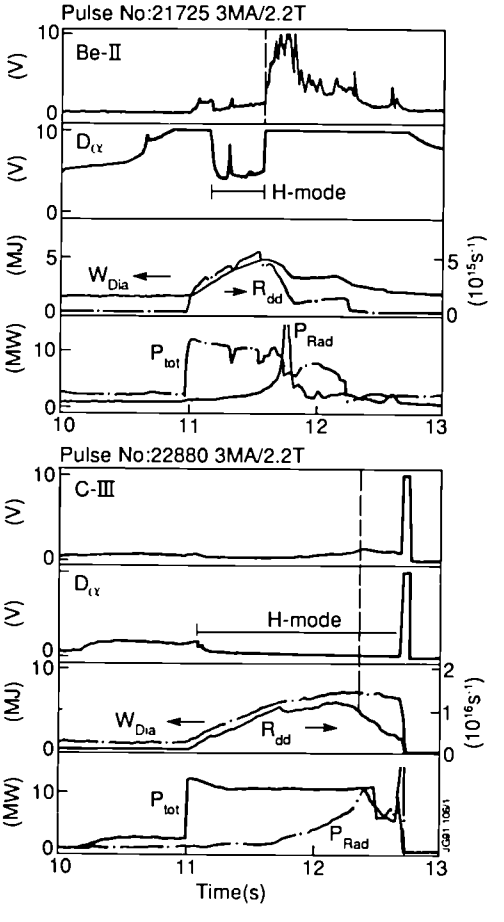

Fig. 91: A comparison of plasma parameters during 3MA 2.2T H-modes produced on:
(i) the Be target;
(ii) the CFC target.

Due to the short duration of these H-modes, it was not possible to perform a local transport analysis. In addition, the limitations of the bolometric observations made a full power balance impossible. However, by analyzing confinement

200ms after the H-mode transition, when, admittedly, the rate of change of stored energy was large, an initial comparison of the confinement properties of H-modes on the different targets was possible. As shown in Fig. 92, there is no significant difference in the global confinement properties between the two cases.

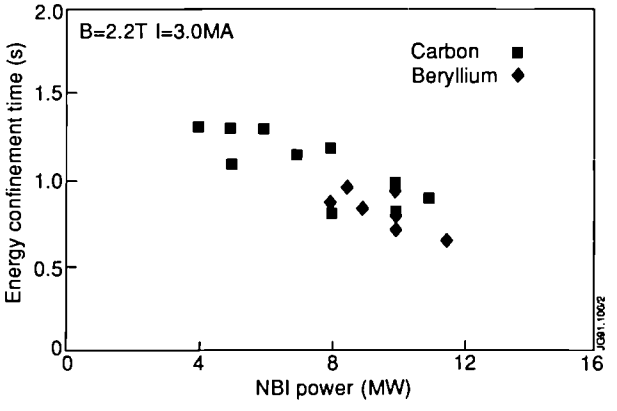

Fig. 92: This comparison of global energy confinement in 3MA/2.2T H-modes on the Be and CFC targets shows that confinement in the two cases is similar. The diamagnetic stored energy, W_{dia}, is plotted against the corrected input power, $[P_{in} - (dW/dt)]$.

Influence of Toroidal Field Direction

Evidence from experiments on several tokamaks has shown that significant changes occur in some aspects of H-mode behaviour when the direction of the toroidal field is reversed, so that the ion ∇B-drift is away from (-∇B) rather than towards (+∇B) the X-point. Specifically, the H-mode power threshold can double and the distribution of power on the inner and outer X-point strike zones can change substantially. A series of experiments was performed to investigate such differences in JET H-modes. The plasma configuration used for these experiments was a single-null X-point (SNX) plasma for which the plasma current was varied between 3 and 3.5MA for toroidal fields in the range $2.2<B_T<3.4$T. In addition, the X-point to target separation, ΔX, was varied over the range $3<\Delta X<-17$cm (where the convention is such that a positive value of ΔXindicates that the X-point lies *behind* the surface of the target tiles).

As in other tokamaks a significant increase, by approximately a factor of 2, was observed in the H-mode power threshold with the change in direction of the ∇B-drift. Fig. 93 illustrates the variation of H-mode threshold power, P_{th}, as a function of toroidal magnetic field, B_T, for SNX discharges with the ion ∇B-drift away from the X-point. A distinction is made between those plasmas which made the

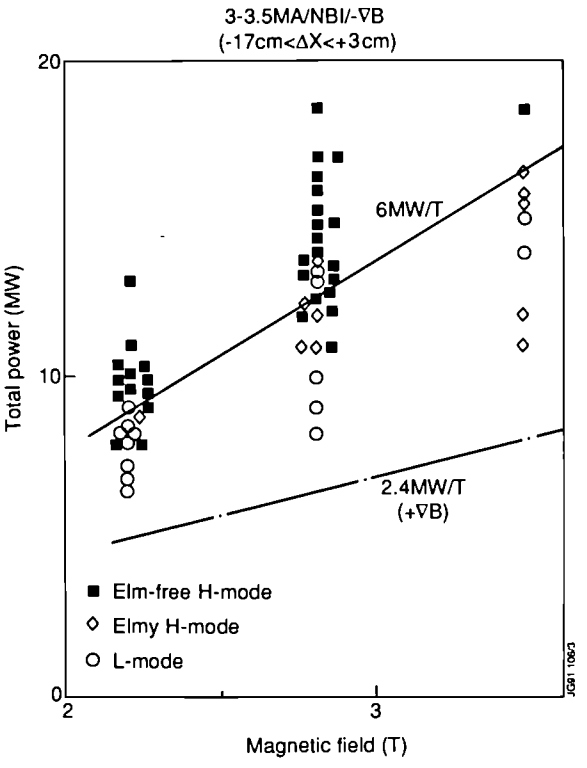

Fig. 93: Existence diagram showing input power, P_{tot}, during elm-free H-modes, elmy H-modes and L-modes as a function of toroidal magnetic field B_T. The data shown here are for plasmas with −∇B. The dashed line indicates that the threshold power for achieving an H-mode rises at $6MWT^{-1}$. For comparison, the H-mode power threshold in discharges with +∇B is shown ($2.4MWT^{-1}$).

transition to an elm-free H-mode and those which remained in the L-mode. Discharges which produced only an elmy H-mode are also indicated. The dashed line which separates those plasmas which made the transition to an elm-free H-mode from the remainder has a slope of $6MWT^{-1}$. For comparison, the power threshold for plasmas with the ion ∇B-drift towards the X-point is also shown [2]. Double-null X-point (DNX) plasmas in JET (which normally have a small displacement towards the X-point for which the ion ∇B-drift is positive) exhibit an intermediate behaviour.

A second striking difference between plasmas with opposite toroidal field directions was observed in the power deposition on the target tiles. Measurements were made of the time evolution of the temperature of the carbon X-point target tiles using a CCD camera with an infrared filter. These observations were used to determine the time variation of the power deposited on the targets and, in particular, to determine the distribution of power between the inner and outer strike zones. As is illustrated in Fig. 94, the ratio of the powers on the outer and inner strike zones changed from

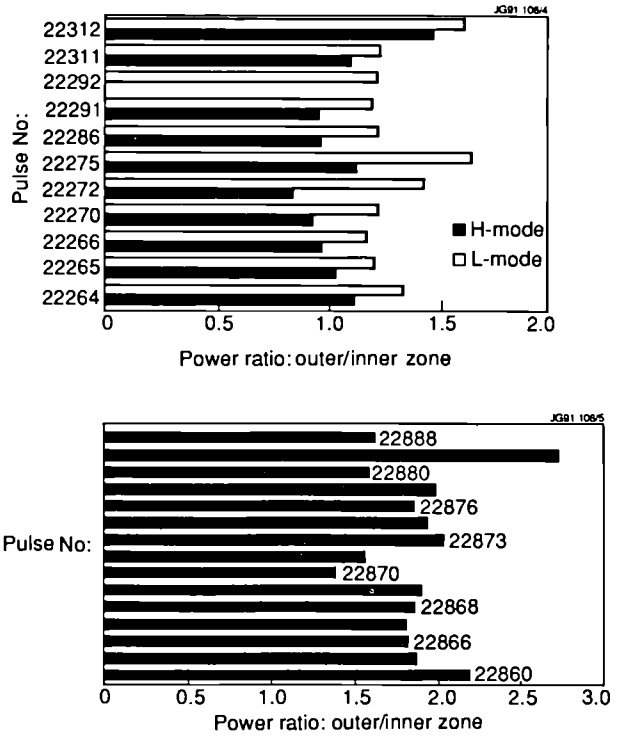

Fig. 94: The ratio of deposited power on the inner and outer strike zones for a series of discharges with (i) + ∇B and (ii) - ∇B ion drift directions. Note the striking change in the distribution of deposited power between the two cases. When geometric factors are taken into account, the change is even greater.

~1.7 for the +∇B-drift direction to ~1 (H-mode) or ~1.2 (L-mode) for the -∇B-drift direction. When corrections to the deposited power (to account for the geometry of the target tiles) are included, the asymmetry in the former case rises to ~2.5, while that in the latter case is 0.7 (H-mode) or 0.85 (L-mode). In addition, the asymmetry for the +∇B-drift direction increased with increased rates of recycling.

Similar asymmetries were observed in the ion saturation current to the target measured by Langmuir probes embedded in the tiles. On the other hand, the peak of the (impurity) radiation from the divertor plasma moved from the inner to the outer strike zone (i.e. the peak radiation was emitted from the ion drift side). In addition, the so-called third strike-zone [3] was observed to move from the inner to the outer side of the X-point when the field was reversed, a result which is consistent with the interpretation of this effect being due to a hot ion population close to the plasma boundary. This behaviour of particle and energy fluxes to the target and their dependence on the sign of ∇B is similar to that observed on other tokamaks.

The change in the distribution of power at the target has implications for the power-handling capabilities of the target and for plasma performance which are discussed in the following sections. H-mode global energy confinement was, however, found to be insensitive to the direction of the ion ∇B-drift. Fig 95 shows confinement data from the 1989 and 1990 operating periods for SNX plasmas. The total diamagnetic energy, including fast ions, is plotted against the input power (corrected for the rate of change of energy) for plasma currents in the range 3 to 4MA. The data broadly follows the behaviour of the ITER9OH-P H-mode scaling [4], but the best data at 3MA lies on the same line as the best at 4MA (the 3MA points correspond to an enhancement factor of 3 over Goldston L-mode scaling). These points correspond to the best hot-ion H-modes [5] and, in addition to peaked density and ion temperature profiles, have a substantial fast-ion component from neutral beam injection.

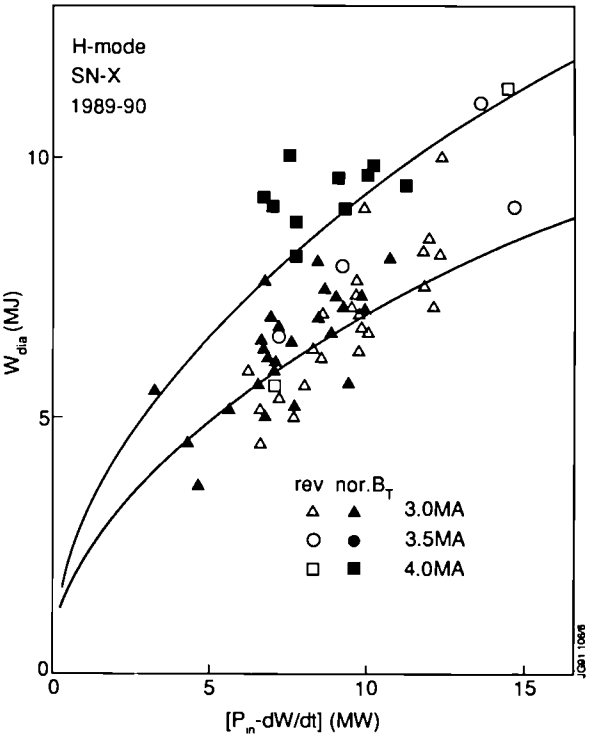

Fig. 95: Comparison of global energy confinement in terms of total stored energy, W_{dia}, versus corrected input power, [P_{in} - (dW dt)], for elm-free H-modes with + ∇B and - ∇B ion drift directions. There is essentially no difference between the two cases.

Carbon Bloom

The present X-point graphite target, which is of a preliminary nature and consists of 32 discrete poloidal rings of tiles, will be replaced by quasi-continuous targets (top and bottom) for 1991. Nevertheless, since neither of these targets incorporates active cooling, limitations on JET performance due to blooming (i.e. sublimation of carbon or melting of beryllium) of the target materials is expected to persist until

without the necessity of radial X-point sweeping. However, the precise advantage gained is still to be quantified inasmuch as several factors must be considered. In particular, the design of the present graphite target slightly favours the use of reversed field due to the toroidal inclination of the tiles. In addition, the tile edges themselves have a significant impact on the time required to produce a carbon bloom. Due to residual misalignments of the tiles, it is the edges which rise in temperature, and cause blooming, most rapidly. Therefore, the incidental location of the strike points may have an indeterminate influence on the carbon bloom. Moreover, this may also explain the experimental observation that, with the present target, it is difficult to combine advantageous factors (such as -∇B-drift and sweeping) due to irreproducibility in the occurrence of the bloom.

Fig 96 summarizes the results of analysis of the carbon bloom. The conducted energy, E_{cc},

$$E_{cc} = \int_0^{t(Bloom)} \left[P_{tot} - P_{rad} - \frac{dW_D}{dt} \right] dt \qquad (1)$$

(where P_{tot} is the total input power, P_{rad} the radiated power, (dW_D/dt) is the rate of change of plasma energy) is shown for different plasma configurations without X-point sweeping. The influence of the ∇B-drift direction and of the separation between the X-point and the target is unclear. In addition, there is no dependence on the toroidal field strength. It does appear, however, that by increasing the X-point to target separation, plasma dilution is reduced. Thus, although the carbon bloom may occur at similar levels of conducted the installation of the Pumped Divertor. Therefore, the study of techniques to delay the carbon bloom and to prevent the resultant impurity fluxes into the plasma has been a key aspect of the X-point programme.

Previous experiments in JET have shown that radial sweeping of the X-point strike zones across the targets, to increase the effective areas of the targets utilized, can increase the delay until the carbon bloom occurs to about 1s at the highest heating powers [6]. Furthermore, it was observed that heavy gas puffing could be used to produce long elm-free H-modes (>5s) with controlled Z_{eff} (~2.5) [7]. During 1990, further experiments investigated the use of vertical X-point sweeping (in which the X-point to target distance was varied), the exploitation of the more symmetric power distribution of the -∇B-drift direction and the role of the distance between the X-point and the target.

Operationally, the best results in 1990 were obtained with the -∇B-drift direction, which provided high fusion yield

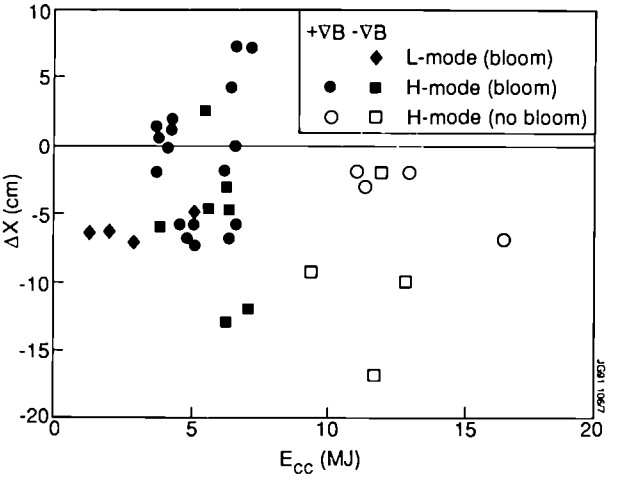

Fig. 96: Comparison of conducted energy, E_{cc} (defined in text), required to produce a carbon bloom as a function of the X-point to target separation, DX, and the direction of the ∇B-drift. Discharges which survived without a bloom are also shown. In this data set there appears to be no major quantitative difference between the two ion drift directions.

energy, the shielding of the plasma is increased by increasing ΔX.

It was also found that all plasmas which survived without a bloom had a high recycling divertor (i.e. a divertor plasma in which the ratio of particle flux at the target to that flowing across the separatrix is large). Operationally, high recycling can be set up by strong gas puffing before or during the H-mode, but the regime is more stable if gas-puffing is started well before additional heating. Furthermore, high recycling is more readily established with the X-point well inside the vessel. On the other hand, the regime seems to be more difficult to achieve in hydrogen plasmas and this may be related to the increased likelihood of elms in these discharges.

Impurity Retention

Retention of impurities in the divertor plasma to shield the main plasma is a critical aspect of divertor performance. This includes impurities generated at the target plates, which must flow back out of the divertor plasma, and those generated at the wall, which need only cross the separatrix. Experiments were performed to investigate the retention of the divertor for recycling (helium and argon) and non-recycling (silicon) impurities. These impurities were injected as gases into either the divertor plasma or the vessel midplane and the time evolution of the impurity content of the main plasma was followed by VUV spectroscopy of impurity emission lines.

For silicon, which was injected in a continuous bleed of silane (SiH_4), it was found that the divertor provided a very efficient trap for silicon injected into the divertor, but was ineffective when the impurity was injected at the midplane. Thus, in the former case, it was found that silicon penetrated the main plasma during the limiter phase of the discharge, but, as soon as the X-point was formed, the level of silicon emission from the main plasma dropped dramatically, as silicon was retained in the divertor.

The recycling gases, helium and argon, were injected only from the plasma midplane in a single puff during the X-point phase, but several seconds before heating was applied. To obtain the characteristic retention time of the divertor, t_D the impurity emission was modelled using measured plasma temperature and density profiles. Fig 97 compares the measured behaviour of the HeII emission line for two plasmas with the same X-point to target distance (the X-point was 3cm *behind* the target tiles). The two discharges had opposite toroidal fields (and hence ∇B-drift) directions, but this was not found to play a significant role. The overshoot following the injection of helium (at 13s in both cases) is a good measure of τ_D. As discussed below, the increased value of the τ_D for curve (ii) is associated with xenon contamination.

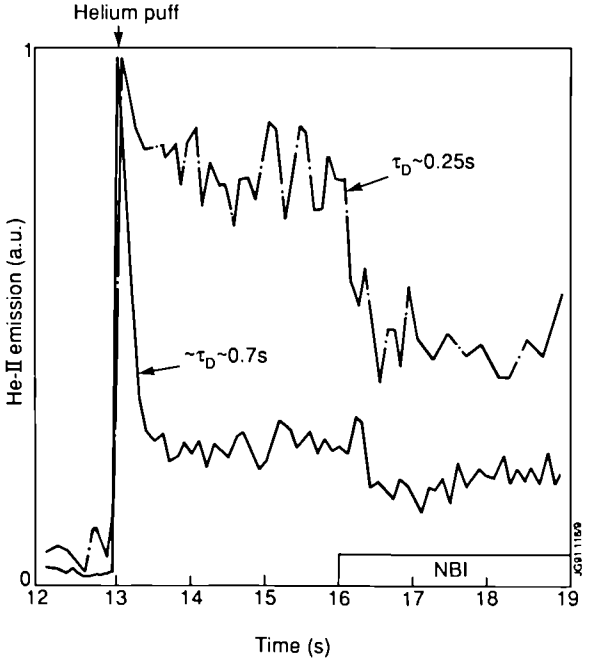

Fig. 97: Helium-II line emission from the bulk plasma following injection of a puff of helium into the vessel midplane at 13s. The indicated divertor retention times, τ_D, are obtained from simulations of the emission using measured plasma profiles. The plasma with higher divertor retention times was accidentally contaminated with xenon, which resulted in radiative cooling of the divertor.

The retention of the recycling gases in the divertor plasma did not depend on the X-point to target separation as long as the X-point was behind the vessel. However, discharges with an X-point inside the tiles displayed better retention and this might be associated with the discrete design of the X-point target, which contains substantial trapped volumes between the individual poloidal rings. In addition, τ_D increased significantly to values ~0.7s, in discharges which were accidentally contaminated with xenon (Fig.97). These plasmas exhibited a higher level of radiation from the X-point region and, as a result, a lower divertor temperature due to this high-Z contamination. The improved retention of the divertor can then be understood as the result of increased collisionality in the divertor plasma.

High Performance Plasmas

The development of the hot-ion H-mode [5,6] has allowed the attainment in JET of plasma conditions close to those required for breakeven. However, these conditions have, to date, been transient and, as explained above, the regime has been limited by the occurrence of the carbon bloom. A major effort, therefore, was made during the present campaign to extend this regime in duration and to improve the plasma parameters obtained. The major advance achieved was in the exploitation of the more uniform deposition of power on the X-point target when operating with the ∇B-drift away from the X-point. The duration of the regime has been extended up to 1.2s without X-point sweeping and up to 1.5s when combined with vertical sweeping of the X-point to target distance. Since shielding appeared to be improved at larger X-point to target distances, ΔX, high current ($3 < \Delta X < 4$MA), SNX plasmas were used in preference to the DNX configuration (since the JET poloidal field and shaping circuit permits SNX plasmas with substantially larger values of DX than can be obtained in DNX plasmas).

Fig 98 illustrates the time evolution of the pulse with the highest neutron production (both peak and integrated) and best value of the thermonuclear triple product, $n_D(0)T_i(0)\tau_E$. This discharge was a 3.5MA/2.8T discharge with 18MW of neutral beam injection (10MW of 80keV D^0 and 8MW of 140keV D^0). A peak neutron yield of $3.8 \times 10^{16} ns^{-1}$ was achieved, corresponding to a Q_{DD} of 2.5×10^{-3}. In addition, $Q_{DD} > 2 \times 10^{-3}$ was maintained for over 0.5s. The parameters of this discharge were $T_i(0) = 28$keV, $n_D(0) = 4 \times 10^{19}$ m^{-3} and $\tau_E = 0.85$s, corresponding to a triple fusion product $n_D(0)T_i(0)\tau_E = 9 \times 10^{20}$ m^{-3}skeV.

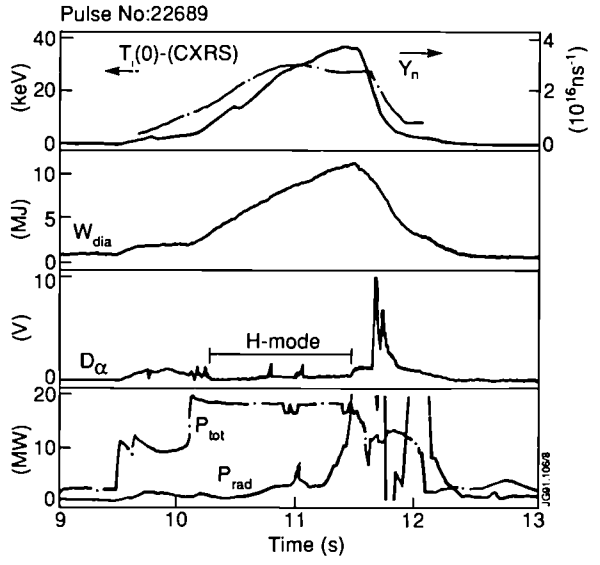

Fig. 98: Overview of the hot-ion H-mode which has the best neutron yield. This was a 3.5MA/2.8T plasma with -∇B ion drift.

TRANSP analysis of these discharges has been limited by diagnostic limitations. However, it has been possible to perform a detailed analysis on a similar Pulse No:22701 (4MA/2.8T), which yielded a fusion reaction rate close to that of Pulse No:22689. As shown in Fig 99, while these discharges are initially dominated by beam-thermal and beam-beam contributions, when the peak fusion reactivity is reached thermal reactions account for ~50% of the fusion power.

Hot-ion H-modes are characterized by a significant population of fast beam injected ions, which contribute not only to the reaction rate, but also to the plasma energy. In addition, both density and ion temperature profiles are highly peaked. As a result, confinement of these discharges is very good and can reach values ~$3\tau_G$, as shown in Fig 95. At lower plasma parameters, H-mode energy confinement generally follows a $P^{-0.5}$ power dependence [4] with a linear dependence on the plasma current, but only a weak dependence on the toroidal magnetic field. Experiments in this campaign have yielded a dependence on toroidal field of B_T^{α} with $\alpha<3$.

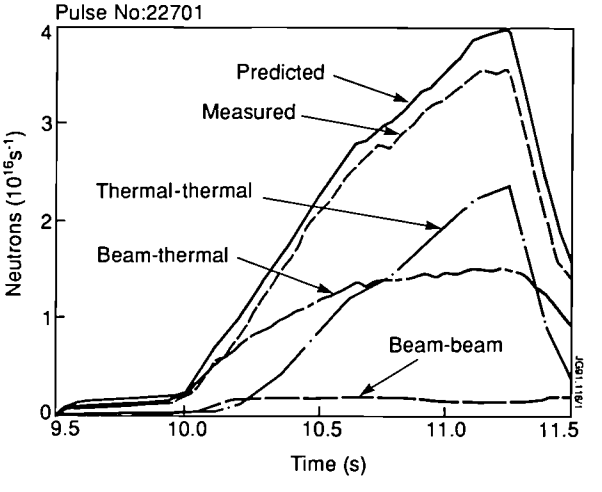

Fig. 99: TRANSP analysis of a hot-ion H-mode with plasma parameters and neutron yield close to to that of Pulse No:22689. Pulse No:22701 was a 4MA/2.8T plasma with -∇B ion drift. At the peak of the neutron yield, thermal reactions account for ~50% of the neutron emission.

Edge Ion Temperatures

Recently, it has been realized that ion temperatures of up to 10keV can exist within 10cm of the separatrix in hot-ion H-modes [8]. Fig. 100 shows ion temperature profiles from several types of X-point discharge: (a) a quasi-ohmic X-point discharge (just after the start of NBI); (b) an L-mode with 4MW of NBI; (c) a moderate density H-mode with 9MW of NBI; (d) a hot-ion H-mode with 18MW of NBI (1989); (e) a hot-ion H-mode with 18MW of NBI (1990).

In two of these discharges, (b) and (c), the plasma was swept radially across the line of sight of the CXRS diagnostic system to improve the effective radial sampling of the diagnostic. Careful analysis has confirmed that, in the moderate density H-mode, ion temperatures of several keV exist to within a few cm of the separatrix. Although such detailed measurements are not available for the two hot-ion H-modes illustrated, the high values of ion temperature observed at the final measurement point indicate that substantial gradients must exist in the last 10cm, possibly with large pedestals. While pedestals in the electron density and temperature profiles have been recognized as a characteristic feature of the H-mode since its discovery, significant ion temperature pedestals have not previously been reported. Their existence may have significant implications for an understanding of the H-mode since the observed scale-length of <10cm for the edge ion temperature decay lies in the range of banana widths, $2\rho_p$, for the ion energies observed ($4 < 2\rho_p < 14$cm for $1 < E < 10$keV).

As is shown in Fig 101, edge ion temperatures in the best H-modes scale with the power conducted to the edge divided by the edge electron density. Edge temperatures in these H-modes lie within a boundary $T_i(a) < 1.3P_c(a)/n_e(0.9a)$[keV, MW, $10^{19}m^{-3}$], while temperatures in L-modes follow a much weaker scaling which saturates below 1keV. A range of H-mode plasmas, including high density and elmy H-modes, populates the region between these two boundaries.

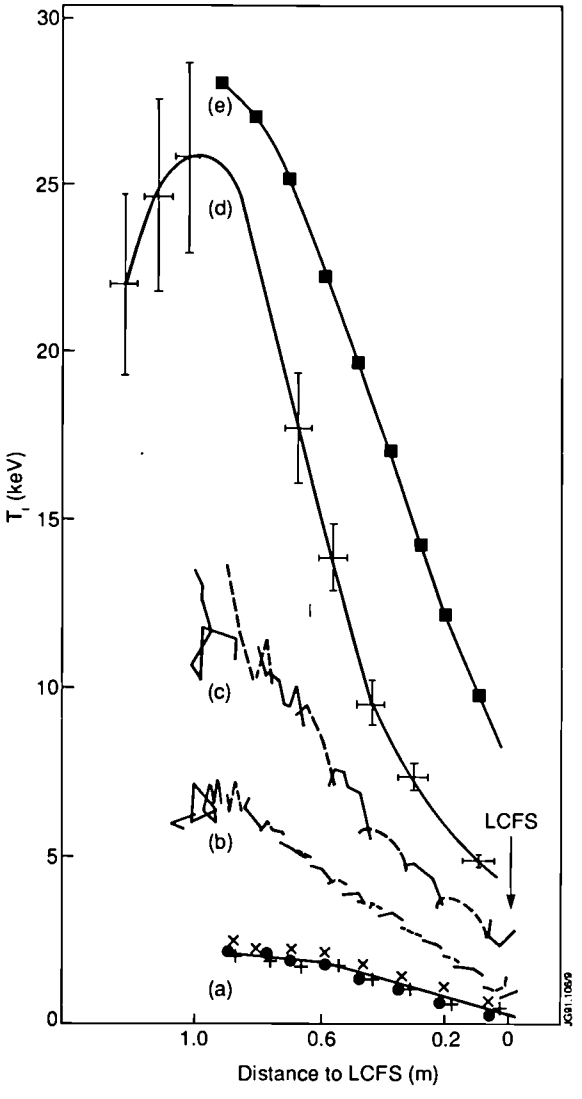

Fig. 100: Ion temperature profiles, measured by active charge exchange resonance spectroscopy, for a range of X-point discharges:
(a) quasi-ohmic discharge (just after start of NB1);
(b) L-mode plasma with P_{NB} = 4MW;
(c) H-mode plasma with P_{NB} = 9MW;
(d) hot-ion H-mode with P_{NB} = 18MW (1989);
(e) hot-ion H-mode with P_{NB} = 18MW (1990);
In cases (b) and (c), the plasma was swept radially to obtain a quasi-continuous profile.

The observed behaviour of T_i in the edge of H-modes raises several issues concerning edge transport and confinement in these plasmas. For example, such high ion temperature pedestals can contribute significantly to the thermal energy of the plasmas, amounting to as much as 50% of the stored energy. In addition, it is found that decoupling of ions and electrons is a prerequisite for the existence of high edge ion temperatures. In particular, the equipartition power calculated from the measured density and temperature profiles is always less than the available input power to the ion channel.

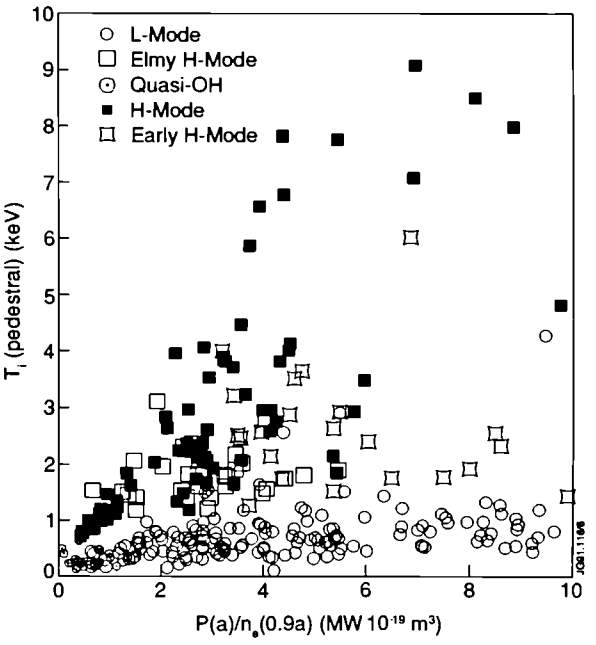

Fig. 101: Variation of edge ion temperature, T_i(Pedestal), with power per particle into the plasma edge, P(a)/n_e(0.9a), for various X-point plasma regimes.

The major difference between the hot-ion H-modes of 1989 and 1990, which underlies the higher edge temperatures in the latter campaign, was a substantial difference between the density profiles. In 1989, fairly flat density profiles with slight peaking in the plasma centre, but high edge densities (~$3x10^{19}m^{-3}$), were obtained, while the hot ion H-modes produced in 1990 had significantly more peaked profiles with lower edge densities (~$1x10^{19}m^{-3}$). The reason for this remarkable difference is not yet understood. Nonetheless, the edge ion pressures are very similar for the two cases.

Perhaps the most significant conclusion of this analysis is that the effective thermal conductivity in the plasma edge region can decrease by an order of magnitude in the H-mode. Fig. 102 shows the total heat flux, $[n_e dT_e/dr + n_i dT_i/dr]$, determined 10-20cm inside the last closed flux surface, plotted against the effective conducted power, $[P_{in} - (dW/dt)]$. As indicated, the thermal conductivity, χ_{eff}, of L-mode plasmas averages ~$3m^2s^{-1}$, but this falls as low as $0.3m^2s^{-1}$ in the best H-modes.

H-modes with Elms

The majority of JET H-modes are free of elms. As a result, the density rises throughout and the H-mode is usually terminated by a high level of radiation (or, at the highest powers, by a carbon bloom). It has been shown that impurity influxes can be reduced, and the H-mode duration extended, by heavy gas puffing [7]. However, in these cases, the

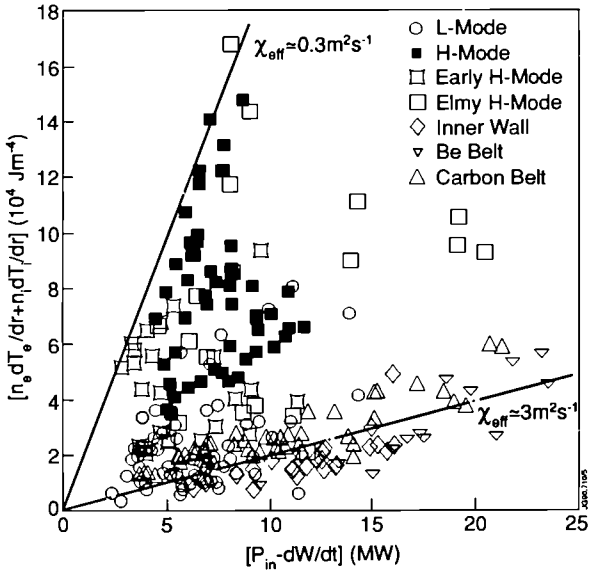

Fig. 102: Effective thermal conductivity in the plasma edge (10-20cm inside the last closed flux surface) for different plasma regimes. The effective conductivity, χ_{eff}, can decrease by an order of magnitude in the H-mode, from ~3m²s⁻¹ to ~0.3m²s⁻¹.

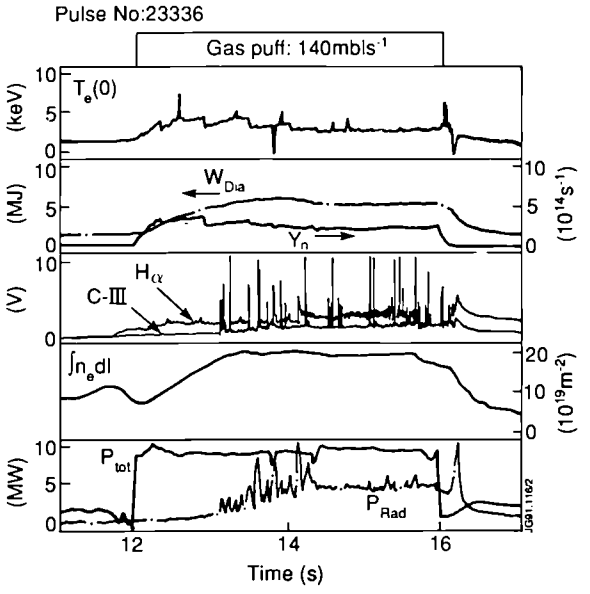

Fig. 103: Overview of an elmy H-mode, at moderate NBI power (~9MW), in which plasma parameters were held constant for 2-3s by the elms. This regime was established by gas puffing into the midplane of a hydrogen target plasma heated by deuterium NBI.

density continues to rise and the regime never achieves stationary conditions. Experiments in both D-IIID [9] and ASDEX [10] have shown that, under certain conditions, a steady-state H-mode can be achieved in which the particle and impurity influxes are controlled by regular elms.

In JET, elms are observed rather irregularly. They are routinely observed for input powers close to the H-mode threshold power, but disappear as the power is raised. In addition, they are observed in irreproducible bursts during hot-ion H-modes. More regular elm behaviour has been observed in discharges in which deuterium beams are injected into hydrogen target plasmas, both at moderate plasma parameters and at high β. Although a number of detailed investigations of elm behaviour have been performed (e.g. [11,12]), there is, at present, no systematic characterization of elms in JET. Nevertheless, a short series of experiments was performed in this campaign to investigate the possibility of establishing a steady-state H-mode with elms.

Fig. 103 illustrates the most promising result obtained. This discharge was a 3MA/2.2T SNX plasma with +∇B-drift in which deuterium beams were injected into hydrogen. The use of hydrogen as a target gas was dictated in this case by the need to minimize neutron production, rather than specifically to increase the probability of elms. In the course of these experiments it emerged that elms could be produced reliably by gas puffing (with hydrogen) from the midplane. Lack of experimental time prevented similar studies with deuterium as a target and fuelling gas. As shown, after an initial phase lasting ~1s, elms appeared and plasma parameters were held constant under the influence of the elms. In particular, in spite of continuous gas puffing, plasma density, radiated power, impurity content, stored energy, and neutron production were maintained at a constant level for almost 3s. Furthermore, the elms appear to have been instrumental in preventing a carbon bloom during the 4s heating period.

The range of plasma parameters investigated during this study does not permit an analysis of confinement scaling in this elmy regime. However, the data does shed some insight into the influence of elms on global plasma confinement. In Fig. 104, the stored energy for three discharges with very similar magnetic configurations (3MA SNX plasmas with ΔX~8cm) is compared. There are several differences between the discharges, but which, in the light of experimental results obtained in this campaign, are not crucial in relation to the issue of global confinement.

The figure shows an elm-free H-mode (Pulse No:22526), an L-mode (Pulse No:23331) and an elmy H-mode (Pulse No:23336) together with lines corresponding to the Goldston scaling prediction for deuterium with enhancement factors of 1 (L-mode) or 2 (H-mode). The stored energy of the L-mode plasma lies very close to the Goldston scaling line, while that of the elm-free H-mode discharge has an enhancement factor of ~2.2. It is clear that the degradation due to

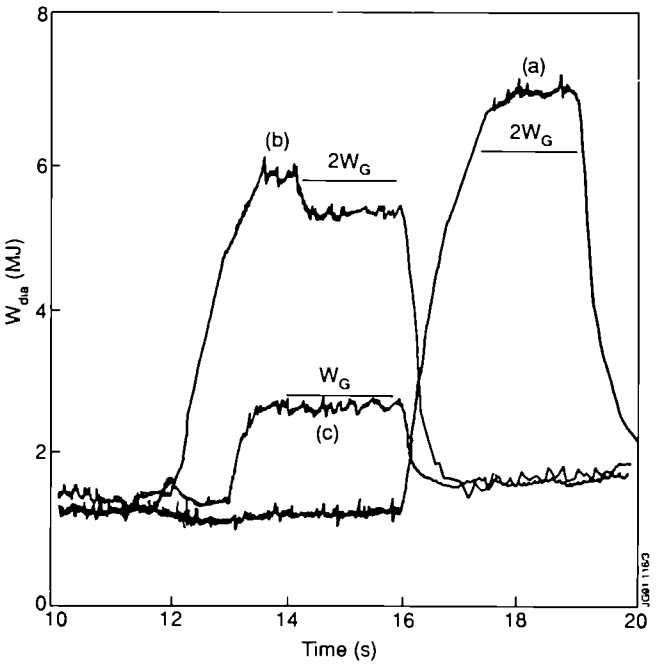

Fig. 104: Plasma stored energy in three similar discharges, which attained different regimes:
(a) Pulse No:22526 - 3MA/2.2T elm-free H-mode, P_{NB} = 10MW, $D^0 \rightarrow D$, $-\nabla B$;
(b) Pulse No:23336 - 3MA/2.2T elmy H-mode, P_{NB} = 9MW, $D^0 \rightarrow H$, $+\nabla B$;
(c) Pulse No:23331 - 3MA/2.8T, L-mode, P_{NB} = 8MW, $D^0 \rightarrow H$, $+\nabla B$;
The predicted stored energy from Goldston, W_G, and 2xGoldston scaling is indicated for each discharge (assuming a deuterium plasma).

regular elms in the elmy H-mode is not great, since the enhancement factor obtained is 1.8. Of course, more extensive studies must be performed to investigate the parametric dependence of the confinement of elmy H-modes.

H-modes with ICRF Heating

The first H-modes in JET with ICRF heating alone were obtained during 1989, primarily as a result of the use of beryllium gettering to reduce impurity generation from the ICRF antennae shields [13,14]. A major limitation encountered during these experiments was the change in coupling resistance of the RF antennas which occurred at the H-mode transition. This caused difficulties in maintaining the RF power during the H-mode. To eliminate this problem, a new position control system was installed and commissioned during 1990. This system used the RF antenna coupling resistance, via a feedback loop, to control the position of the plasma to maintain constant coupling resistance during changes in the plasma edge (e.g. the L-to-H transition). In addition, to further reduce RF specific impurity generation, the nickel screens were replaced by beryllium screens.

Fig.105 shows an overview of an ICRF-only H-mode which utilized the new position control system to maintain the coupling resistance. This discharge was a 3MA/2.8T DNX deuterium plasma using hydrogen minority heating with the RF antenna in the dipole configuration ($k_{//} = 7m^{-1}$). Note the movement of the plasma edge under control of this system and the fact that the coupling resistance is kept almost constant during the L-to-H and H-to-L transitions. The power threshold for the H-mode transition in such plasmas is ~5MW, slightly lower than the threshold for similar NBI-heated plasmas. The confinement is similar to that in NBI-heated plasmas with an enhancement factor ~2 relative to Goldston scaling.

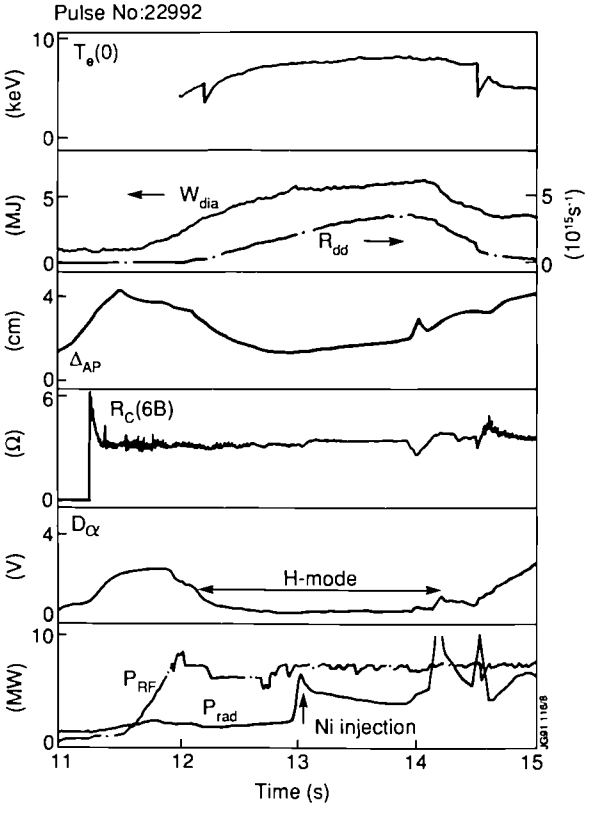

Fig. 105: Overview of an ICRF H-mode (hydrogen minority, dipole coupling) in a 3MA/2.8T DNX plasma. Note the slow change in the plasma to antenna distance, D_{AP}, as the new position feedback control system maintains a constant coupling resistance, R_c.

A significant advance made in this campaign, which can be ascribed to the new facilities, was the attainment of an H-mode with the RF antennae in the monopole configuration ($k_{//} = 0$). However, the power threshold for conditions similar to those outlined above was ~8MW, which is close

to the NBI power threshold for these conditions. In addition, the global energy confinement of these plasmas is slightly lower than in the dipole case. Nevertheless, by using beryllium screens, RF-specific impurity problems have been eliminated and there is no significant difference in the impurity behaviour of dipole and monopole heated H-modes.

Significant progress was made in the parameters of ICRF-heated H-modes during this campaign. H-modes lasting up to 2.8s, with both gas and pellet fuelling have been obtained. Monster sawteeth were routinely observed in these discharges. Global energy confinement times of up to 1.2s and deuterium reaction rates of up to $5.5 \times 10^{16} s^{-1}$ were achieved, with a thermonuclear fusion product $n_D(0)T_i(0)\tau_E < 2.2 \times 10^{20}$ m^{-3}skeV. Fig.106 summarizes the confinement properties of ICRF-heated H-modes. Note that the confinement of (edge ablated) pellet-fuelled plasmas is systematically slightly lower than that of gas-fuelled plasmas, although this result may not be statistically significant.

ICRF-produced H-modes are generally elm-free, though combined heating H-modes may have elms. This is, in itself, an interesting observation. However, it raises the question of whether elms can be stimulated, or whether other techniques for degrading particle and impurity confinement (without significantly degrading energy confinement) can be developed. Such a phenomenon was, indeed, observed in a number of discharges. Fig. 107 illustrates a plasma in which gas puffing into the X-point was employed with the aims of cooling the divertor plasma (to suppress the carbon bloom) and extending the H-mode. After ~ 1.5s of H-mode, during which the density and radiated power increased, a transition occurred which significantly changed the particle confinement, leading to a substantial fall in the density and radiated power (with Z_{eff} approximately constant). However, the energy confinement characteristics of the H-mode were little affected, the stored energy falling by ~10%. The cause of this transition is not understood, but a similar phenomenon was observed during laser ablation experiments in which metallic impurities were injected into the plasma causing a substantial increase in the edge radiation.

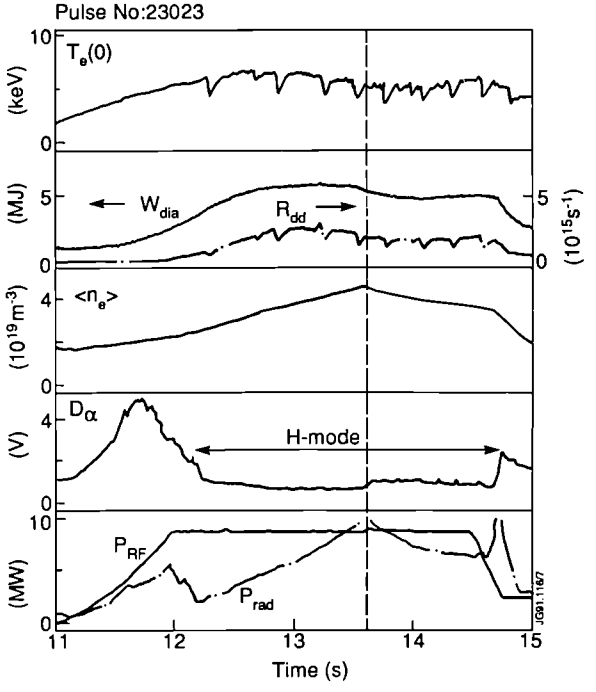

Fig. 106: Summary of global energy confinement in ICRH-only H-modes. The energy confinement times are of the same order as in equivalent NBI H-modes. However, H-modes with dipole antenna configuration have systematically better confinement than H-modes with the monopole antenna configuration (though only a few of the latter have been obtained). In addition, it appears that gas-fuelled discharges have slightly better confinement than (edge ablated) pellet-fuelled discharges, though, once again, the number of discharges involved is small.

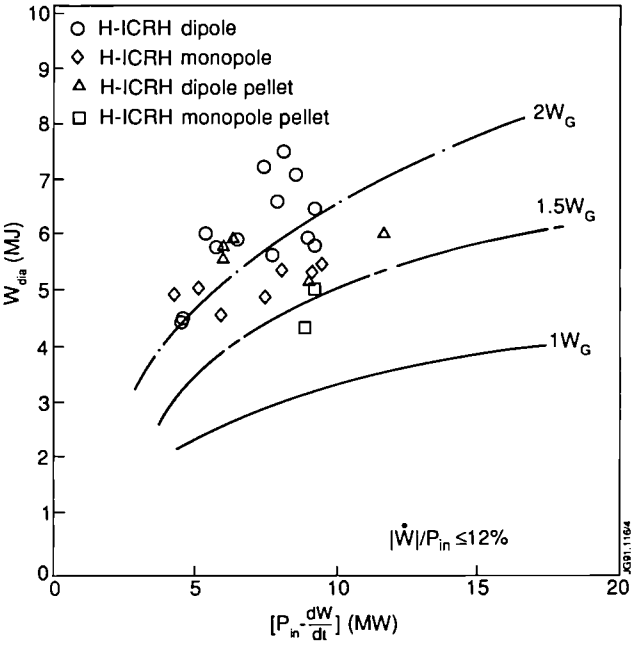

Fig. 107: An ICRH-only H-mode with gas-puffing into the X-point region. Note the sudden change of conditions at 13.5s at which the density and radiated power starts to fall, indicating a dramatic change in particle confinement properties, while the energy confinement is little degraded. Insofar as can be ascertained, there are no elms.

Summary

Progress has been made in several areas of H-mode physics in this campaign. First experiments using beryllium as a target material were limited by the low power handling capabilities of the preliminary target and definitive experiments must await the installation of the X-point dump plates

for the 1991 campaign. An extensive series of experiments was performed to investigate the influence of the ion ∇B-drift direction on the H-mode. The changes in power threshold and on in-out asymmetries in the divertor plasma observed in other tokamaks were confirmed. However, due to the limitations set by carbon blooms in X-point experiments in JET, the more symmetric power distribution of the -∇B-drift direction proved to be a significant advantage in optimizing high performance plasmas. This enabled the fusion yield of the best discharges to be extended to $Q_{DD}=2.5\times10^{16}s^{-1}$, with a thermonuclear fusion product $n_D(0)T_i(0)\tau_E=9\times10^{20}m^{-3}$ skeV.

Studies of the impurity retention capabilities of the divertor plasma showed that non-recycling impurities, such as silicon, were retained in the divertor plasma if injected into the X-point region. The retention efficiency for recycling impurities such as helium and argon could be increased by radiative cooling of the divertor plasma. Although, in these experiments, the X-point to target separation appeared to have little influence on the retention time of the divertor, analysis of the effects of the carbon bloom provided evidence of improved shielding of the bulk plasma against carbon when the separation was increased.

Recent analysis of edge ion temperatures yielded evidence of very high temperatures (of up to 10keV) in H-modes within 10cm of the plasma edge. On the other hand, edge ion temperatures in L-mode discharges appear to saturate at about 1keV. These pedestals are indicative of very low transport (perhaps an order of magnitude lower than in the L-mode) near the plasma edge in the H-mode. Little further progress has been made in understanding the nature of elms in JET, but, by use of heavy gas puffing in hydrogen plasmas, it has been possible to produce an elmy H-mode at moderate power (~9MW) in which plasma parameters were maintained in a stationary condition for 2-3s. Finally, several new facilities in the ICRF heating system have been exploited to improve performance in ICRF H-modes. In addition, H-modes using the monopole plasma configuration have been obtained for the first time in JET and a regime has been observed, apparently without elms, in which particle confinement is significantly degraded at minimal cost to energy confinement.

References

[1] C G Lowry et al, 32nd Annual Meeting of the Plasma Physics Division of the American Physical Society, (Cincinnati, USA) 1990.

[2] C Nardone et al, JET Internal Report - JET-IR(90)06, 1990.

[3] D O'Brien et al, Proc 17th European Conference on Controlled Fusion and Plasma Physics (Amsterdam, The Netherlands, 1990) **1** 251.

[4] ITER Report ITER-IL-PH-4-1-1.

[5] B Balet et al, Nucl. Fus. **30** 2029 (1990).

[6] A Tanga et al, 31st Annual Meeting of the Plasma Physics Division of the American Physical Society, Anaheim, USA, 1989.

[7] D Stork et al, 31st Annual Meeting of the Plasma Physics Division of the American Physical Society, Anaheim, USA, 1989.

[8] H Weisen et al, 32nd Annual Meeting of the Plasma Physics Division of the American Physical Society, Cincinnati, USA, 1990.

[9] R D Stambaugh et al, Proc 13th International Conference on Plasma Physics and Controlled Fusion (Washington, U S A, 1990) Paper IAEA-CN-53/A-1-4.

[10] F Wagner et al, Proc 13th International Conference on Plasma Physics and Controlled Fusion (Washington, U S A, 1990) Paper IAEA-CN-53/A-4-2.

[11] A Hubbard et al, Proc 15th European Conference on Controlled Fusion and Plasma Physics (Dubrovnik, Yugoslavia, 1988) **2** 651.

[12] E Joffrin et al, Proc 16th European Conference on Controlled Fusion and Plasma Physics (Venice, Italy, 1989) **1** 225.

[13] B J D Tubbing et al, Nucl. Fus. **29** 1953 (1989).

[14] V P Bhatnagar et al, JET Preprint- JET-P(90)44 (submitted to Plasma Phys. and Contr. Fus.).

Profile Effects and Related Physics Issues

The objective of the Task Force was to study plasma performance improvements and underlying physics issues related to profile control of heating, current and density. During the course of this work, several important developments in plasma engineering were made. These included X-point formation during the current rise which requires low voltage plasma breakdown (Mode-B discharges), long pulse ICRF and LHCD operation and an RF plasma position feedback control system to maintain constant coupling resistance during L-mode to H-mode transitions.

The physics programme concentrated on four main areas:

a) peaked density profile experiments using pellet injection;
b) current profile control by neutral beam and lower hybrid current drive;
c) electron heating by ICRF power at high values of power per electron, for which the heating profile is broadened by orbit effects and possibly MHD and micro instabilities;
d) impurity confinement studies using laser blow-off techniques.

In addition the new beryllium ICRF antenna screens were assessed for reduced impurity release.

The most significant achievements of these experiments were as follows:

1) The pellet injection experiments succeeded in combining the pellet enhanced performance (PEP) regime with the H-mode regime which, with 9MW of ICRF power and 2.5MW of NBI, achieved central ion and electron temperatures of 10keV, a central deuterium density of $8x10^{19}m^{-3}$ and a neutron production rate of $10^{16}s^{-1}$ which was predominantly thermonuclear. The fusion triple product reached a thermal value, $n_d T_i \tau_E \approx 7x10^{20}$ m^{-3} s keV;
2) Injection of 3.5MW of 133keV tangential D∞ beams produced 300kA of current drive at a density of $10^{19}m^{-3}$ which corresponds to an efficiency $\gamma=0.04x10^{20}m^{-2}$MA/MW, which is twice that obtained in previous experiments. Current drive with lower hybrid waves reached 1MA for P_{lh}=1.6MW at a density of $3x10^{19}m^{-3}$ and an average electron temperature of 1.9keV. The efficiency increased with increasing $<T_e>$ up to a value $\gamma=0.4x10^{20}$ m^{-2}MA/MW;
3) The central electron temperature during ICRF heating tends to saturate at about 13keV as the launched power per electron is increased. Fast ion energy content measurements indicate that this is due to a broadening of the electron heating profile, which is consistent with a model which takes account of fast ion orbit effects;
4) Heat and particle diffusivity measurements have been made using mainly sawtooth heat pulse propagation and gas puff methods. The incremental heat diffusivity is independent of applied heating power and is typically $3m^2/s$ for 3MA discharges. The incremental particle diffusivity lies in the range 0.35-0.6m^2/s for $0.5<r/a<1$ in similar plasmas;
5) Laser blow-off experiments have shown that the diffusion coefficient in the plasma centre is only 0.03-0.1m^2/s compared with 1-3m^2/s on the outside. In L-mode plasmas, the global impurity confinement time is of the same order at τ_E, whereas in H-mode plasmas $\tau_{imp} >> \tau_E$ due to improved confinement in the outer half of the plasma;
6) The beryllium antenna screens have reduced the ICRF specific impurity influx to negligible amount with $\Delta Z_{eff} \approx 0.005 P_{rf}(MW)$;
7) 22MW of ICRF power has been coupled into a limiter discharge which has an energy confinement time, τ_E, approximately 1.3 times the Goldston L-mode value.

Detailed results of these experiments are described in the following sections.

Plasma Engineering

Mode-B Operation

In the pellet enhanced performance [1] discharges of 1988 and 1989, a long-lived peaked density profile was achieved most easily by pellet injection before sawteeth occurred. To repeat this for the combined PEP + H mode experiments required the X-point configuration to be formed close to the beginning of the current flat-top. In JET, the production of a double-null X-point configuration, with sufficient triangularity to match the curvature of the ICRF antennae, relies partly on the stray field from the central solenoid. Control of the shaping is obtained by driving the mid-section of this solenoid by a separate power supply, which can only be used in the early part of the discharge, if the plasma start-up is performed without premagnetisation. This mode of operation (mode-B) is uncommon in JET but was commissioned successfully and achieved plasma breakdown with an electric field of 0.15V/m. A typical field configuration obtained in this way is shown in Fig.108(a) along with that used for previous PEP experiments in limiter discharges. In addition to facilitating the PEP+H-mode scenario, model-B has been used in other ICRF experiments which obtained monster sawteeth of 8s duration and 140kW of fusion power from the ^{3}He-D reaction. The D-D fusion reactivities obtained with 3MA and 4MA mode-B discharges are shown in Fig.108(b). These are by far the highest thermal reactivities observed in JET.

Long Pulse Operation

Current drive studies on JET using NBI and Lower Hybrid waves require long pulses to achieve substantial profile modification since the current diffusion time is of the order

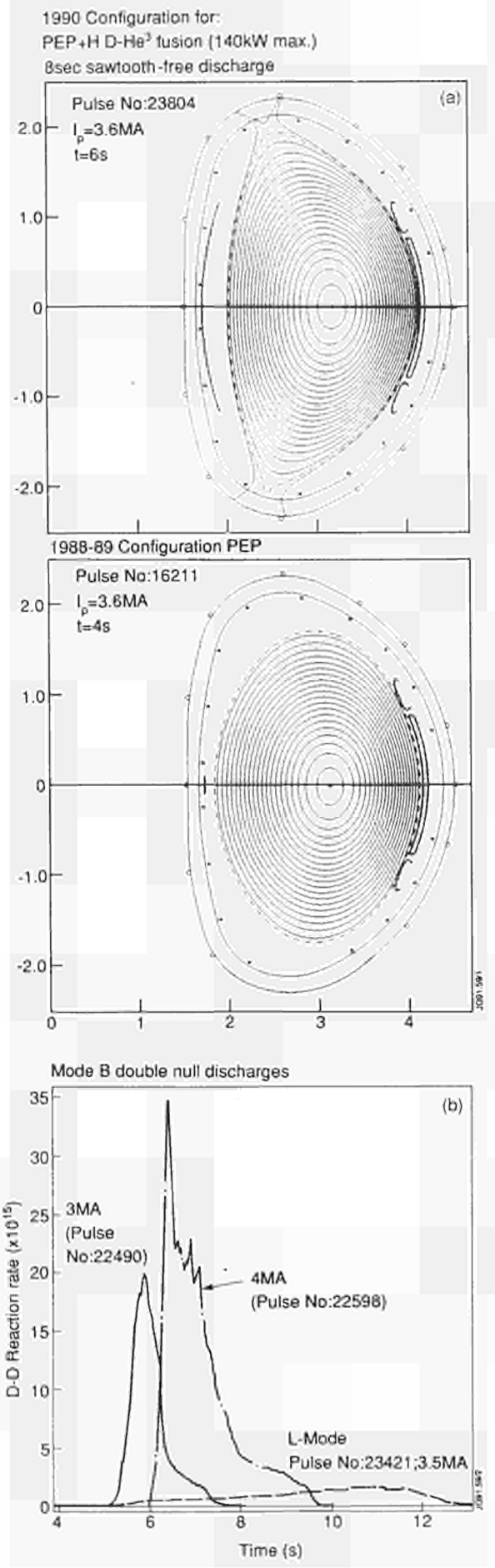

Fig.108 (a) Magnetic configurations close to the start of the current flat-top for PEP discharges in limiter and double null X-point plasmas.
(b) D-D reaction rate during high performance mode-B discharges (PEP + H-mode and record D-^{3}He fusion yield).

of 10s. With NBI, pulse lengths of 7s have been obtained for 4MW of 135keV tangential beams. The lower hybrid launcher has provided 1.3MW for 20s which has enabled current profile modification during monster sawteeth to be observed as shown in Fig.109. With low LHCD power, 4MW of ICRF power is able to create only short monsters

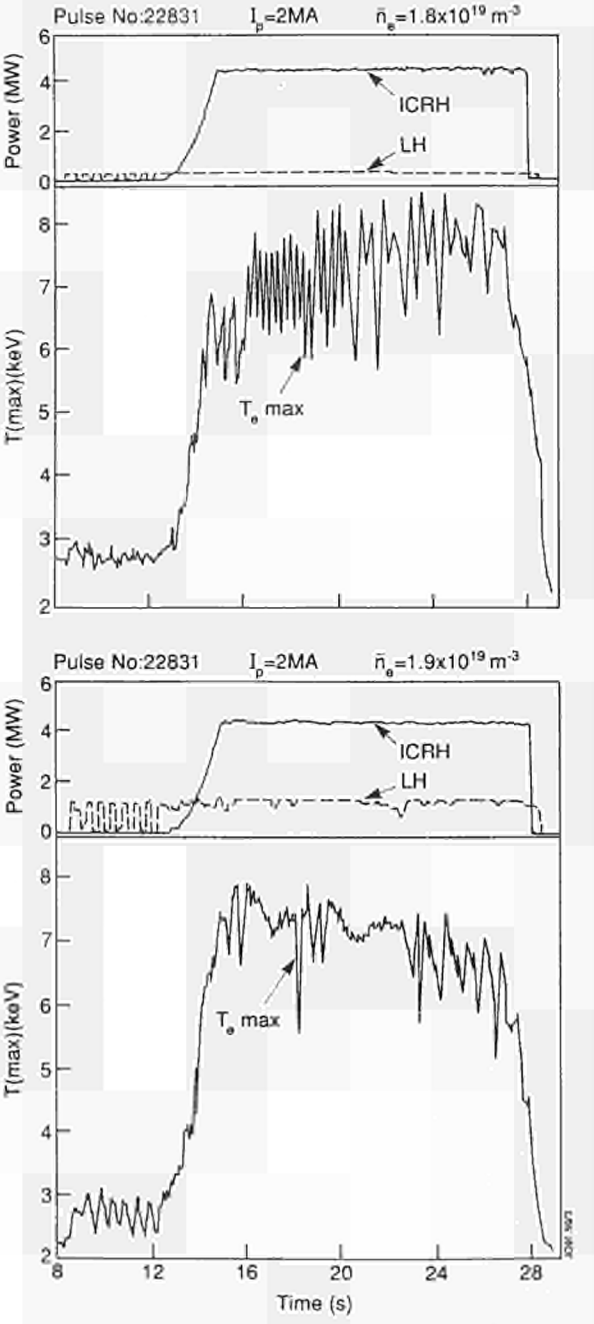

Fig.109: Long pulse LHCD and ICRF heating showing enhanced monster sawtooth duration as the non-inductive current drive is increased.

towards the end of the pulse. The addition of 1.3MW of LHCD power increases the duration of the monsters by a factor of two and they appear early in the heating pulse.

ICRF Feedback Position Control

The formation of an H-mode is accompanied by a reduction of the thickness of the scrape-off layer, which can reduce the ICRF coupling resistance by typically a factor of two. Such changes can cause generator trips which sometimes lead to the loss of the H-mode. Recently, a novel system has been commissioned which moves the plasma radial position under feedback control to maintain a constant RF coupling resistance. The effect of this system can be seen in Fig.110, which compares a discharge without feedback to one with feedback. In the former case, there is a twofold decrease in resistance at the L-H transition resulting in power loss through generator trips. With feedback on, the plasma moves by a few cms to keep R_c constant and continuous heating of the H-mode is accomplished.

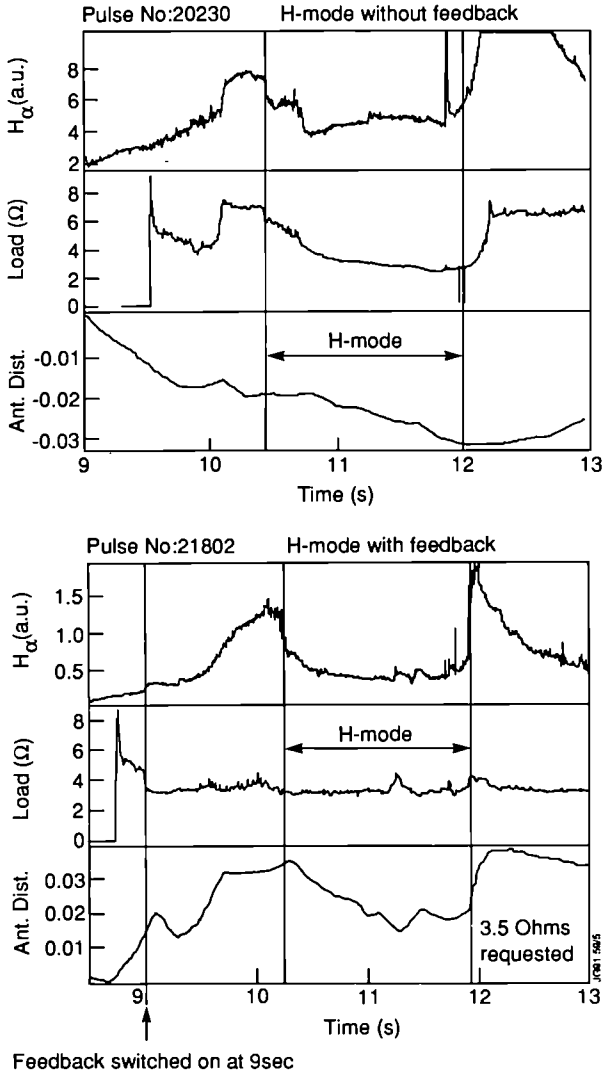

Fig.110: Comparison of the effect of the L to H-mode transition on RF coupling resistance both with and without position feedback control.

Physics Results

Combined PEP and H-Mode Scenarios

Two regimes of enhanced performance, namely the H-mode and the pellet-enhanced performance (PEP) mode, have been combined in JET [2] to take advantage of the improved edge confinement in the former and the better central confinement of the latter. The evolution of plasma parameters is shown in Fig.111(a) for Pulse No:22490. The X-point is formed at t=4s (causing the D_α signal to rise), the pellet is injected at t=5s and the PEP + H-mode exists between t=5.5s and 6.2s. The plasma is heated by 9MW of ICRF and 2.5MW of NBI which produces almost equal ion and electron temperatures of ~10keV. The evolution of the soft X-ray emissivity during the various phases of the

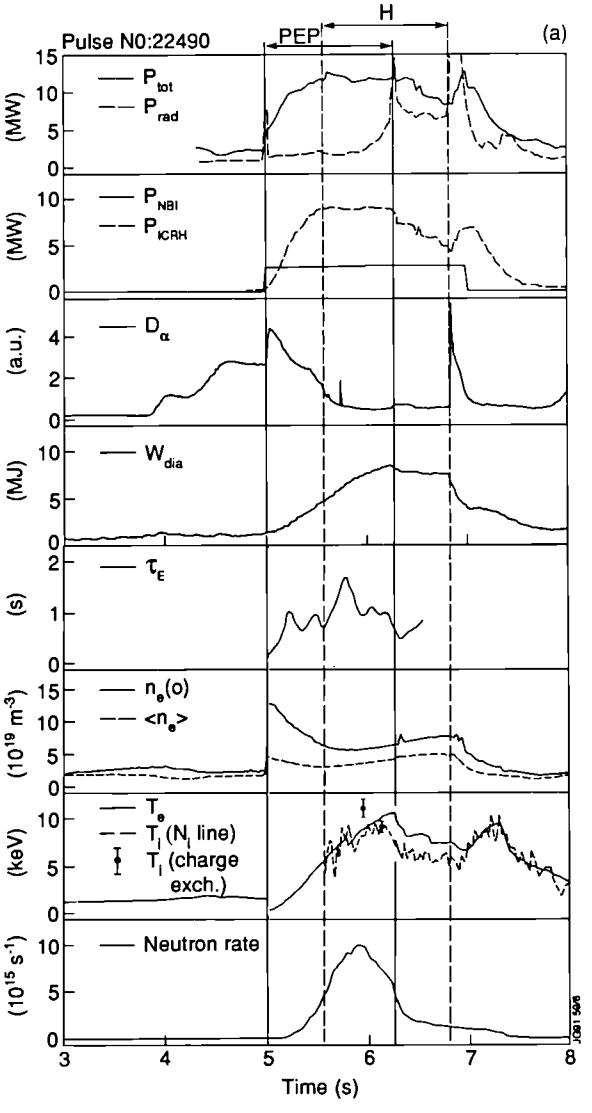

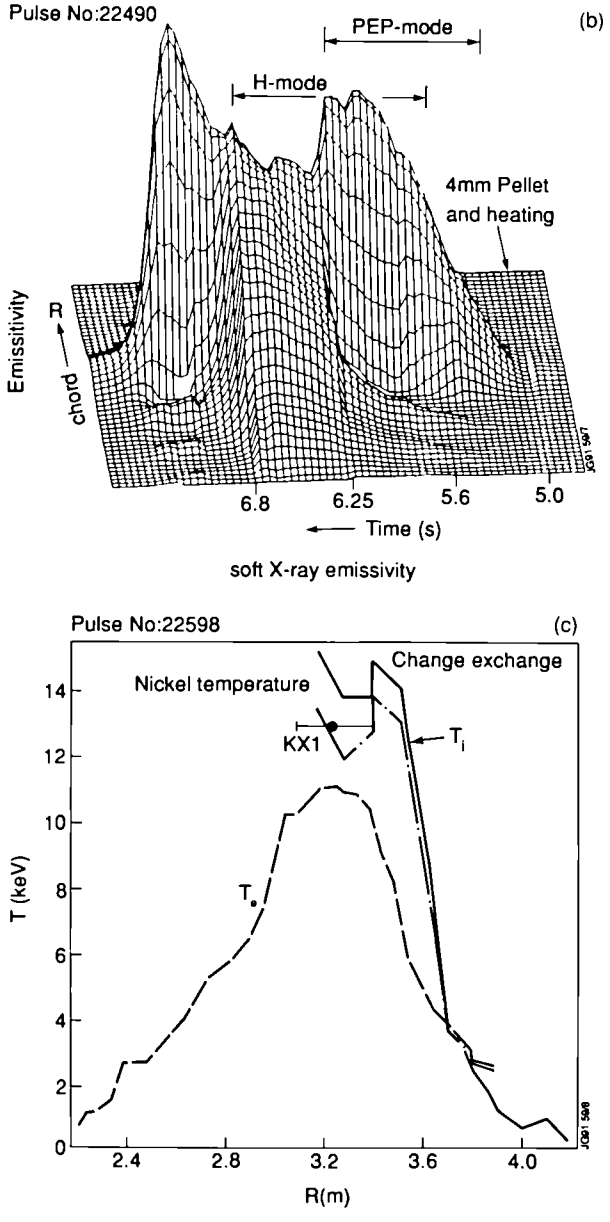

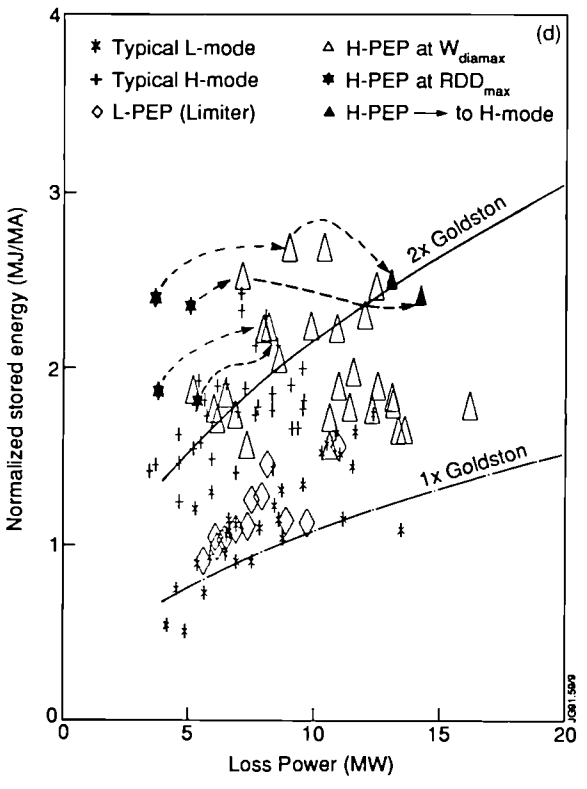

Fig.111 (a) Evolution of plasma parameters during a PEP + H-mode discharge in a 3MA double null X-point configuration; (b) Soft X-ray emissivity during a PEP + H-mode, illustrating the evolution of the profiles during various phases of the experiment;(c) Electron and ion temperature profiles during a PEP + H-mode experiment (10MW of ICRH + 2MW of NBI, I_p=4MA);(d) Global confinement during the PEP + H-mode experiments. The stored energy is normalized to the plasma current.

experiment is shown in Fig.111(b). The ion and electron temperature profiles are shown in Fig.111(c) and the global confinement aspects are illustrated in Fig.111(d). The neutron production rate reached $10^{16}s^{-1}$ (see Fig.108(b), which, according to both TRANSP calculations and neutron spectroscopy measurements, is predominantly (80%) thermonuclear in origin. The fusion triple product ($n_dT_i\tau_e$) is ~ $7x10^{20}m^{-3}$skeV, as shown in Fig.112. The ICRF power input used hydrogen minority ions with a relative concentration of approximately 13%. Detailed analysis of the heating progress using full wave and Fokker-Planck codes [3] shows that the minority ions transfer 50% of their energy to the bulk ions and 50% to the electrons as shown in Fig.113. To a large extent, this models the 30% minority (D)T ICRF scheme which has been proposed [4] to provide bulk ion heating for ITER. With this scenario, a smaller power is required to reach ignition than with a pure electron heating scheme.

Current Drive with NBI and Lower Hybrid Waves

NBI current drive studies have been carried out with 133keV deuterium beams. For optimum efficiency, only the tangential beams were used and these provided 3.5MW of power which was injected into a 3MA limiter discharge. At a density of $10^{19}m^{-3}$, the beam drive current was 300kA. The higher energy of the beams and the lower Z_{eff} achieved in these experiments resulted in a twofold improvement in efficiency compared with earlier experiments using 80keV D° beams, as shown in Fig.114. The maximum efficiency (γ) achieved is $\gamma(10^{20}A/Wm^2)=0.04$. Also shown in Fig.114 is the scaling with electron density which fits the theoretical

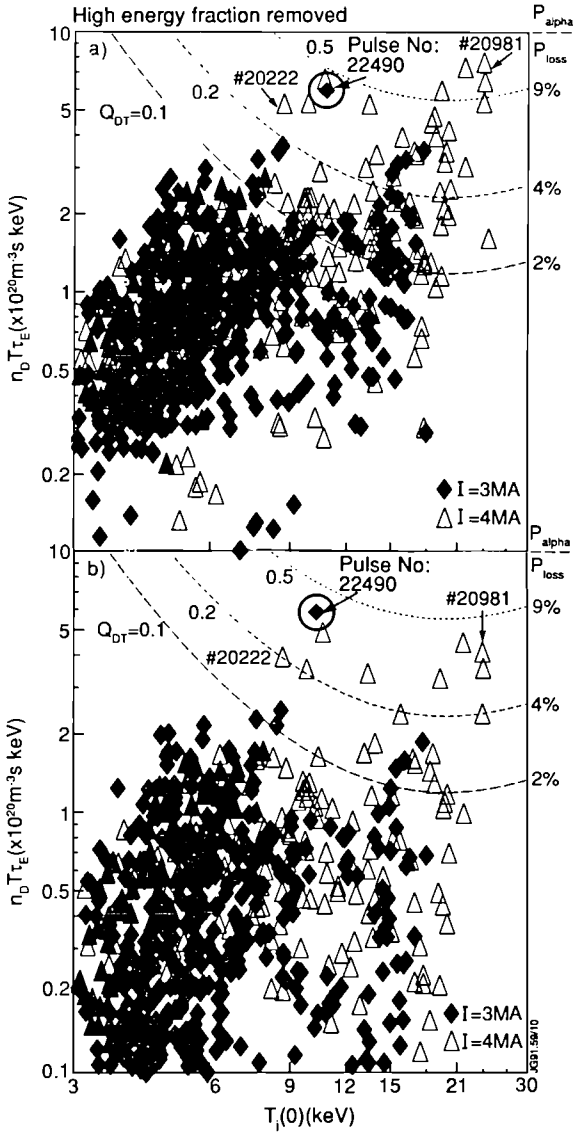

Fig.112: Fusion triple product ($n_d T_i \tau_E$) versus T_i showing the relation of the PEP + H-mode values to those obtained in other high performance JET discharges.

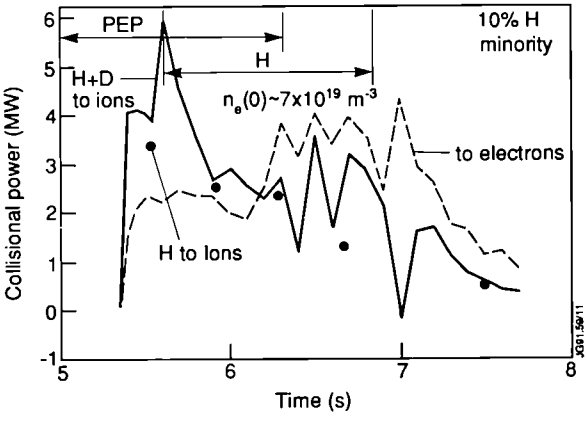

Fig.113: Bulk ion and electron heating due to ICRF during the PEP + H-mode (Pulse No:22490).

predictions and the expected improvement, by a factor of two, for injection with beams tangential to the magnetic axis (R_t = 3.1m).

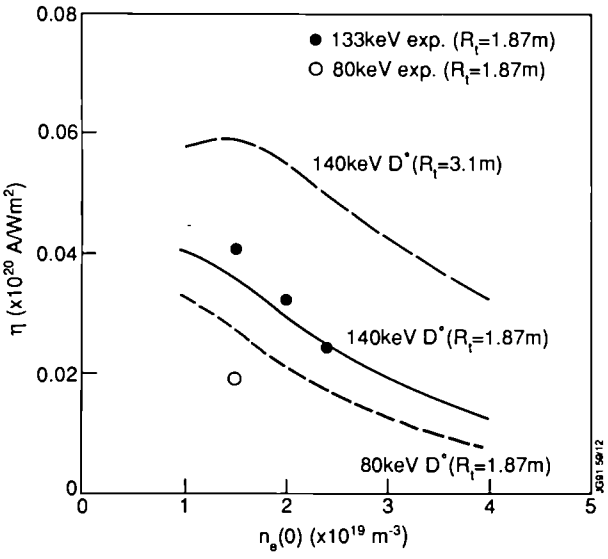

Fig.114: NBI current drive efficiency as a function of plasma density. The curves are theoretical predictions assuming the plasma energy and profiles are invariant. The efficiency decrease with increasing density is primarily due to the reduced beam penetration and the implicit decrease in plasma temperature.

The prototype Lower Hybrid system was commissioned during this period of operation and achieved 1.6MW of power coupled to the plasma and pulse lengths of up to 20s. This power level allowed 12MA of LHCD at a density of $3x10^{19}m^{-3}$ and an average electron temperature of 1.9keV. Using a combination of Lower Hybrid Current Drive (LHCD) and ICRF heating, a measurement of the scaling of the current drive efficiency parameter, $\gamma = I_p R n_e/P$, with average electron temperature $<T_e>$ was obtained and is shown in Fig.115. The efficiency increase with increasing $<T_e>$ is similar to that obtained in JT-60 [5] and reaches a maximum value [6], $\gamma(10^{20}MA/MWm^2) = 0.4$, which is slightly higher than the value expected from the theory of Fisch [7] and is the highest value achieved by any non-inductive current drive method. Clearly, it is important to establish whether this improvement is sustained at higher values of $<T_e>$ or

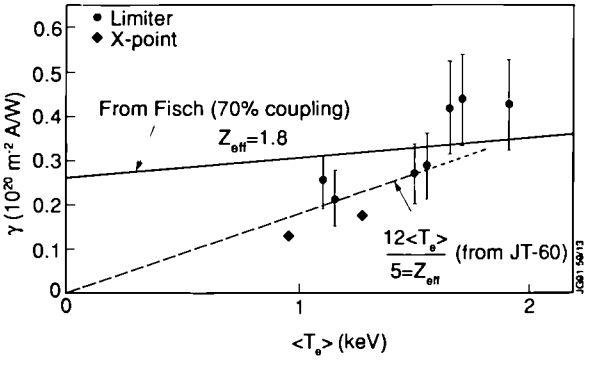

Fig.115: Lower Hybrid Current Drive efficiency versus average electron temperature.

whether saturation occurs. These experiments will be attempted in the next period of operation.

Broadening of the current profile has been observed during LHCD from changes in the sawtooth inversion radius and this is probably the reason for the extension of the monster sawteeth shown in Fig.109. So far, the LHCD system has been able to save up to 3V-s of inductive flux.

$T_e(0)$ *versus* $P_{rf}/n_e(0)$ during ICRF Heating

For monster sawtooth discharges, the scaling of the central electron temperature with the coupled RF power per electron is typified by the data shown in Fig.116. The central electron temperature, $T_e(0)$, increases with increasing P_{rf}/n up to $P_{rf}/n(MW/10^{19}/m^3) \approx 3$ but then appears to saturate for higher values. The maximum central temperature achieved is ~ 13keV. In these experiments, the electron heating arises predominantly from the slowing down of the minority ions, with very little (<10%) being provided by direct damping of the fast wave. Also, the fast ion energy content, relative to that expected for central confinement of these ions, decreases as P_{rf}/n increases as showing Fig.117. Thus, it appears that the fast ion profile is broadening as P_{rf}/n increases and this leads to a broadening of the electron heating profile. A candidate explanation of this broadening is the effect of the large orbits that these fast ions can achieve. For example, ^{3}He ions, which are accelerated to 5MeV in the plasma centre, can follow D-shaped trapped ion orbits which allow them to access cooler plasma ~ 40cm in minor radius, where they deposit most of their energy. A model which takes account of these orbit effects has been developed and reproduces the fast ion energy content and $T_e(0)$ scaling reasonably well as shown in Fig.116 and Fig.117.

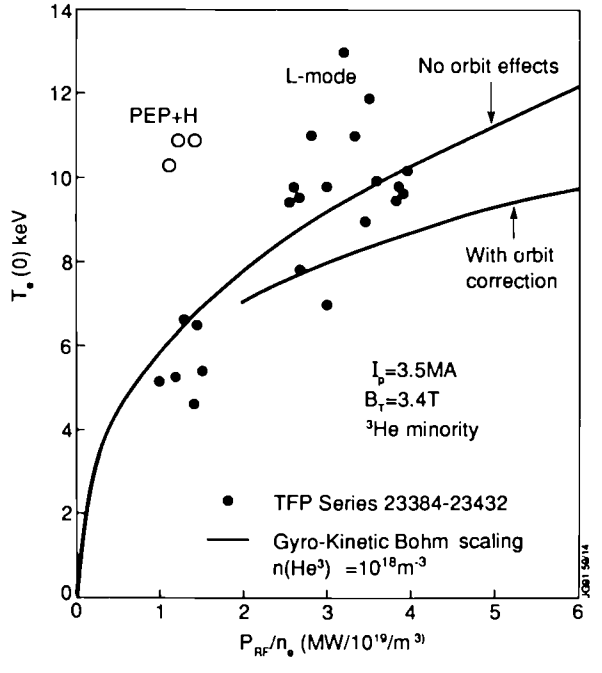

Fig.116: Central electron temperature produced by ICRF power versus $P_{rf}/n_e(0)$. The curves are model calculations for gyro-Bohm diffusion and show the reduction in $T_e(0)$ due to the effect of the fast ion orbits broadening the heating profile.

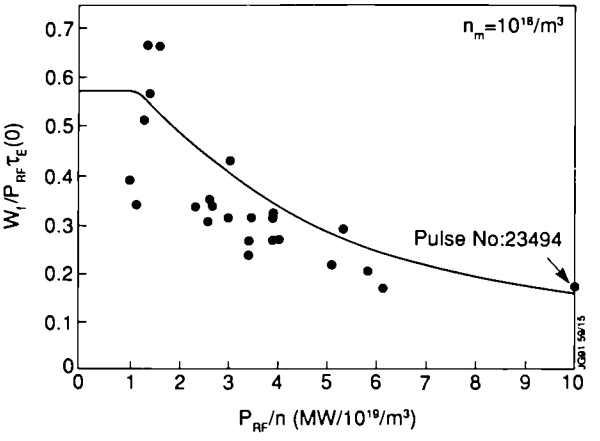

Fig.117: Normalised fast ion energy content versus $P_{rf}/n_e(0)$. The curve is a model calculation with orbit effects included.

Heat and Particle Diffusivity Measurements

Measurements of the incremental heat diffusivity have been carried out by studies of the temperature perturbation following the collapse of a sawtooth. The evolution of T_e is simulated with a transport code which takes account of possible coupling with density changes. Examples of the data and theoretical predictions are shown in Fig.118 for both ohmic heating and 9.5MW of ICRF in 3MA discharges. In each case, the code fits the data for $\chi^{inc} \approx 3.2m^2/s$ compared with values $\chi \approx 1m^2/s$ and $\chi \approx 2m^2/s$ given by power balance calculations for the ohmic and ICRF heating, respectively. Thus, χ^{inc} does not depend on the heating power applied to the plasma.

Measurements of the particle diffusivity D^{inc} have been obtained from studies of sawtooth induced density pulses, nitrogen puffs and an accidental influx of a piece of nickel into the plasma. The transport coefficients were obtained by:

a) using the coupled transport code referred to above; and
b) using the FIR-interferometer to measure the density gradient changes and to evaluate the perturbed particle flux.

Values of D^{inc} obtained in the region 0.5<r/a<1 by these various experimental methods and analysis techniques are reasonably consistent, shown in Table XI.

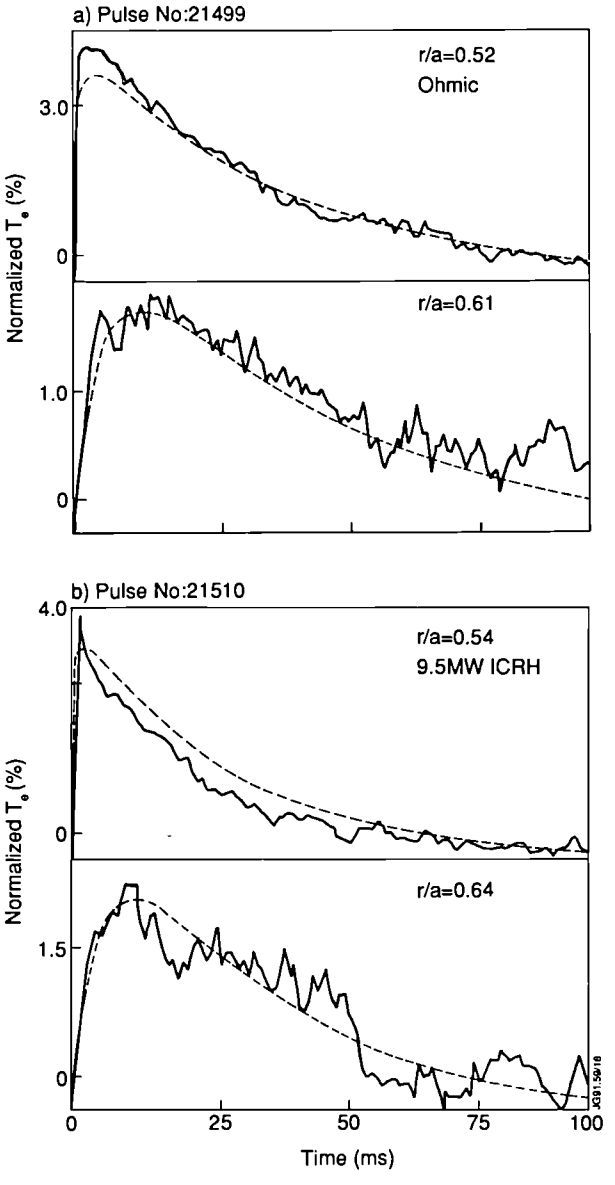

Fig.118: Evolution of T_e after a sawtooth collapse for: (a) an ohmically heated plasma and (b) a plasma with 9.5MW of ICRH. The data are normalised to the central electron temperature before the collapse. The dash curves are model calculations for $\chi_{inc}=3.2m^2/s$.

Impurity Transport

Impurity transport has been studied in laser blow-off experiments using Al, Fe, Ni and Ge material as well as gas-puff experiments with N_2, SiH_4 and Ar. There is no noticeable difference in transport with the Z value of the impurity or with the Z_{eff} of the background plasma. With Ni injection, comparisons have been made between ohmic, L-mode and H-mode plasmas. The results for the global impurity confinement are shown in Fig.119. In L-mode discharges, the confinement is somewhat less than in ohmic, which in turn is much less than in H-mode plasmas, where τ_{imp} can be several seconds. Detailed studies of the evolution of the impurity radial profile show that the central confinement in all types of discharge is close to neoclassical. The central diffusion coefficient lies in the range $0.03<D(m^2/s)<0.1$, in

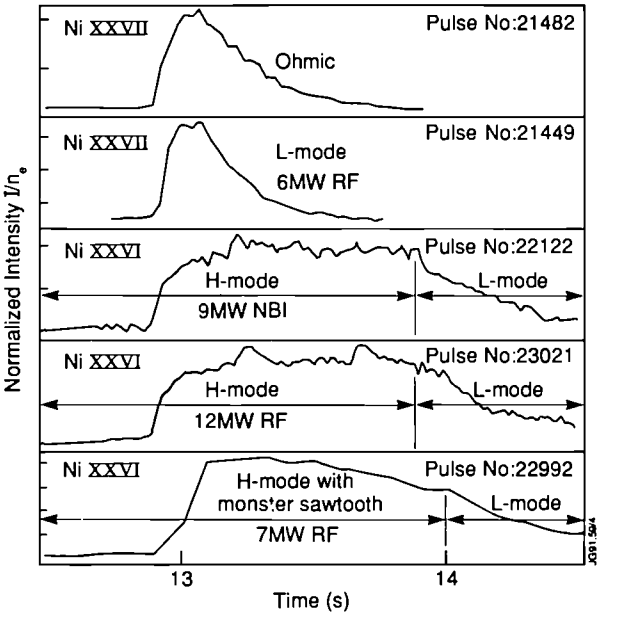

• τ_{imp}(Ohmic) > τ_{imp} (L-mode) • τ_{imp} ~ several seconds in H-mode

Fig.119: Nickel line intensity versus time for laser blow-off experiments in ohmic, L-mode and H-mode plasmas.

Table XI:
Particle Diffusion Coefficient (D^{inc}) for Various Experiments

Method	*Analysis*	*Diagnostic*	*D^{inc} (m^2/s) technique*
Sawtooth	Numerical code	Reflectometer	0.35 ± 0.1
Nitrogen puff	Numerical code	Reflectometer	0.50 ± 0.1
Nitrogen puff	Flux/Gradient	Interferometer	0.60 ± 0.2
Nickel Piece	Flux/Gradient	Interferometer	0.50 ± 0.1

Note: These are determined for JET, 3MA/2.8T ohmic plasmas. Indicated is the experimental method used to induce changes in the electron density profile, the analysis technique used to determine D^{inc}, and the diagnostic used to measure the changes in the density profile.

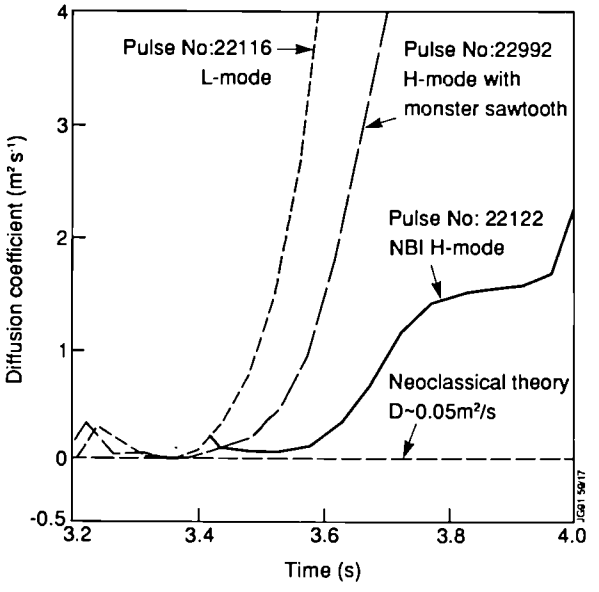

Fig.120: Impurity diffusion coefficient for L-mode and H-mode discharges.

the absence of sawteeth. Beyond half radius, D is about 50 times neoclassical and lies in the range $1<D(m^2/s)<3$. The better global confinement in H-modes is partly due to a reduction of the diffusion coefficient in the outer half of the plasma (see Fig.120) and partly due to an increase in inward convection at the edge.

Energy Confinement Issues

The attainment of 22MW of ICRF power coupled to a 3MA limiter plasma has demonstrated that the L-mode confinement remains somewhat higher than the Goldston value ($\tau_E \approx 1.3\tau_{Eg}$) at high ICRF power levels, as shown in Fig.121. Note that the similarity between the diamagnetic and MHD measurements shows that the fast ion energy contents are small in these experiments which were performed at high density.

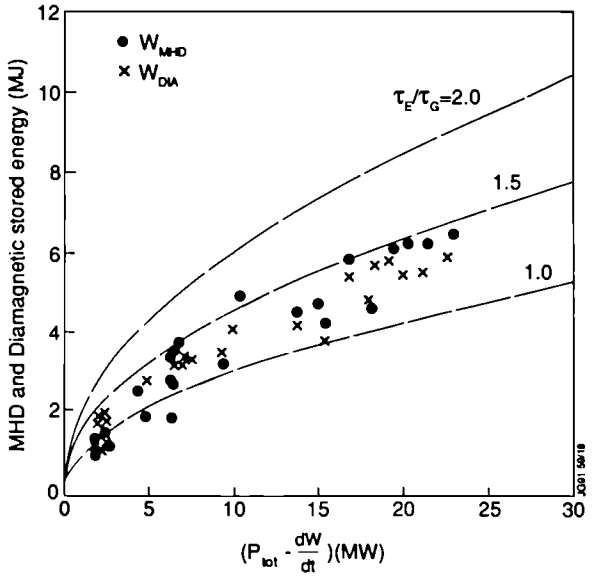

Fig.121: Plasma energy content versus power loss for 3MA plasmas heated by ICRF. The curves are Goldston scaling enhanced by the factors shown.

Plasma current ramp-up and ramp-down experiments on TFTR [8] have shown an improvement in energy confinement, relative to the appropriate L-mode value, with increasing central plasma current density. Initial attempts to reproduce this result have not succeeded so far, probably because the ramp rates and the changes in λ_i were much smaller than on TFTR. However, in ^{3}He-D non-thermal fusion studies, λ_i was observed to increase steadily throughout an 8s monster sawtooth with a corresponding improvement of confinement. These experiments will be pursued in the next campaign when faster current ramp rates will be available.

Beryllium Antenna Screen Assessments

It has been known for some time that impurities are released from the screens of powered ICRF antennas. The flux depends on antenna voltage, the plasma density near the screen, the angle of the screen bars to the magnetic field, the phasing and the screen material. By replacing the nickel screens with beryllium, it was expected to reduce the impurity influx by virtue of the low self-sputtering coefficient of Be. Some results of applying a modulated power to an antenna are presented in Fig.122, which shows the sensitivity to voltage and phasing. Note that the threefold reduction

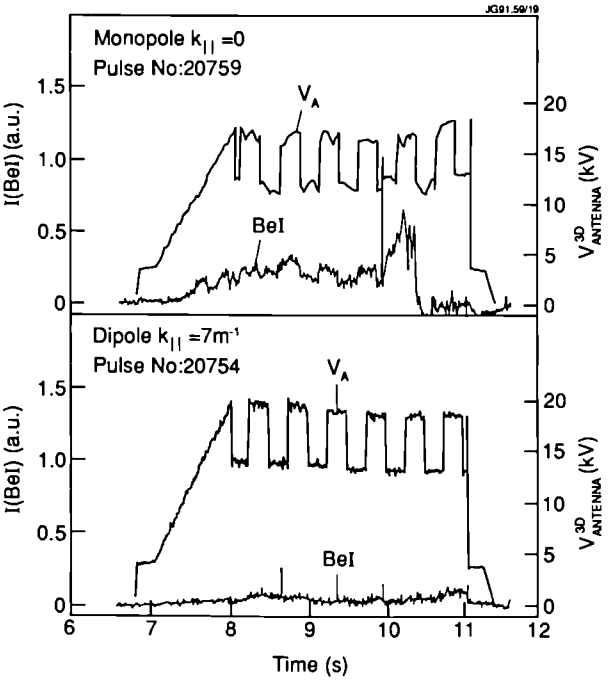

Fig.122: Beryllium influx sensitivity to antenna voltage and phasing.

in impurity production when dipole phasing is used as opposed to monopole. The behaviour can largely be understood [9] in terms of sputtering due to RF field rectification in the sheaths formed where the magnetic field intercepts the screen bars. With the present antennas, the magnetic field lines can connect: (a) adjacent bars; and (b) different points on the front face of the same bar by virtue of its V-shape. The latter effect is sensitive to phasing and disappears for dipole phasing. The combined effects of dipole operation, the low sputtering coefficient of beryllium and the alignment of the bars to the magnetic field have rendered negligible the impurity influx contribution to Z_{eff} ($\Delta Z_{eff}/P_{rf} \approx 0.005$/MW) [10].

References

[1] G.L. Schmidt and the JET Team, in Plasma Physics and Controlled Nuclear Fusion Research 1988 (Proc. 12th Int. Conf., Nice, 1988), IAEA, Vienna (1989) p215;

[2] B.J.D. Tubbing et al, H-Mode Confinement in JET with Enhanced Performance by Pellet-Peaked Density Profiles, accepted for publication in Nuclear Fusion;

[3] L-G. Eriksson and T. Hellsten, JET Report-JET-P(89)65;

[4] J. Jacquinot et al, ITER Ion Cyclotron Systems - Interim Report, ITER-IL-HD-7-9-5, 1989; also J. Jacquinot et al, A Fast Wave Heating and Current Drive System for NET/ITER, Proc. of Int. Conf. on Plasma Physics and Controlled Nuclear Fusion, Washington, U.S.A. (1990), IAEA-CN-53/E-2-1;

[5] T. Nagashima and the JT-60 Team, Applications of Radio Frequency Power to Plasmas (Proc. of the 7th Topical Conf., Kissimmee, U.S.A., 1987) American Institute of Physics, New York (1987), 94;

[6] C. Gormezano et al, Lower Hybrid Current Drive Experiments in JET, 32nd Meeting of the Division of Plasma Physics of the American Physical Society (APS) (Cincinatti, U.S.A.) (1990);

[7] N.J. Fisch and C.F.F. Karney, Phys. Fluids, **28** (1985) 116;

[8] M.C. Zarnstorff et al, Proc. 13th IAEA Int. Conf. on Plasma Physics and Controlled Nuclear Fusion Research, Washington, U.S.A. (1990), IAEA-CN-53/A-II-2;

[9] D D'Ippolito and J. Myra, Proceedings of the IAEA Technical Committee Meeting on Fusion Engineering and Design, Garching, F.R.G. (1990), p209;

[10] The JET Team, Performance of ICRH in JET Plasmas. Presented by D.F.H. Start, Proc. of Int. Conf. on Plasma Physics and Controlled Nuclear Fusion, Washington. U.S.A. (1990), IAEA-CN-53/E-2-1.

Energy and Particle Transport

During the year, progress has been made in consolidating knowledge of transport phenomena in the following areas:

- *Global energy confinement* : The approach followed has been based on a systematic use of rigorous statistical methods and aimed to determine the physics basis of energy confinement;
- *Electron and ion energy local transport analysis:* The main emphasis has been in attempting to determine similarities and differences in these two loss channels and in validating existing transport models;
- *Local particle transport models, including impurities:* The aim has been to identify the most important features to be explained, pointing out the relationship with energy transport and the relevance of neoclassical impurity transport.

Global Energy Confinement

Much of the work in this field has been performed in collaboration with the ITER team and is baed on the analysis of data not only from JET but also from other devices. These data refer to both L and H-regimes and are included in the so-called ITER databases.

A rigorous application of standard techniques of statistical analysis has led to proper treatment of the problems of correlation among data and scarcity of data in some directions of the space of the variables used in the regression analysis. Data have been selected in order to derive scaling laws as representative as possible of the basic mechanisms that determine the plasma transport properties. This has been achieved by excluding from the analysis discharges that appear to be strongly influenced by radiation losses, sawtooth activity and power deposition profile effects. Both power law scaling and offset-linear scaling have been considered, to take into account the observed degradation of τ_E with input power. Results with both representations are comparable.

The contribution of the energy of fast particles, W_f, has been assessed both for L and H-regimes by subtracting it from the total energy content W_{tot}. The energy confinement time τ_E derived in this way takes into account only the thermal energy and is the appropriate one for the prediction of performance of next step devices aimed at ignition. Work is still in progress in this field. Indications so far [1] are for

a stronger dependence of τ_E on density and input power than found when W_{tot} is used in the analysis ($\tau_E \propto n^{0.3\text{-}0.4}\ p^{-(0.7\text{-}0.8)}$, when τ_E is expressed in power law form). The dependence of τ_E on geometrical quantities, as well as the dependence on toroidal field B_T and density, are questions requiring further investigation. Further investigation is also needed to assess the effect of the so-called ELMs (edge localised modes), and more generally of boundary phenomena, on the scaling properties of the H-mode. It has been demonstrated that most "working" scaling laws produced so far in terms of the so-called engineering variables (such as plasma current I, plasma radius a, etc.) can be written in terms of non-dimensional variables, subject to minor changes and practically without losing accuracy. Even more interestingly, the extent to which the so-called Connor-Taylor constraints [2] can be imposed has been investigated [3-4]. This shows that most of the scaling laws satisfy the constraint imposed by the high β-Fokker-Planck equation. Attempting to go further in establishing the physics basis of energy confinement scaling laws, results are much more difficult to obtain. It appears that short wavelength turbulence might be dominant in H-mode discharges (leading to gyro-reduced Bohm scaling), because the related constraint is satisfied within the required accuracy. On the other hand, the long wave turbulence (leading to Bohm type scaling) might be dominant in L-mode discharges [1]. Figs.123 and 124 show the accuracy of the fits obtained for H-mode data in cases with high-b collisional constraint and both this constraint and the short wavelength one. These results are preliminary and appear to be rather sensitive to the influence of phenomena such as the dependence on density of the NBI heating profile.

Further work aims to establish to what extent similarity techniques can be confidently used for the prediction of the performance of next step devices as previously suggested [3,5].

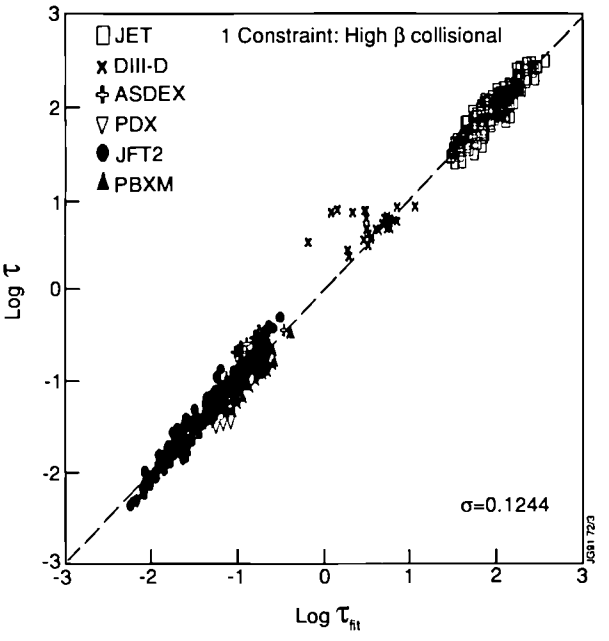

Fig.123: ITER data base H-mode: τ_{th} as a function of theoretical scaling with one constraint imposed.

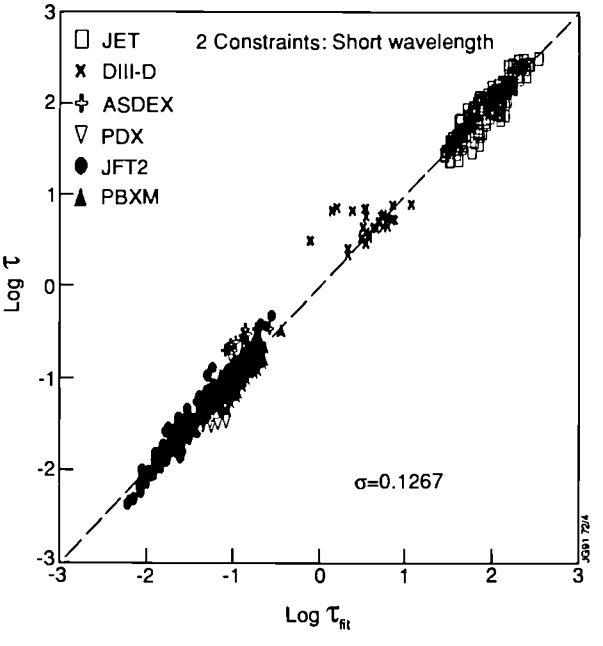

Fig.124: ITER data base H-mode data: Fit of τ_{th} to theoretical scaling with two constraints imposed.

Interpretive Approach to Local Electron and Ion Energy Transport Analysis

A selection of pulses representative of the variety of plasma regimes that are observed in JET have been analysed [6]. They include standard L-mode discharges; H-mode discharges (with various possible combinations of auxiliary heating) including hot-ion and high performance cases; monster sawtooth discharges; and pellet-fuelled ICRF heated discharges.

In cases with neutral beam injection, when T_i profiles are available from charge-exchange recombination spectroscopy, it has been possible to determine separately the values of the thermal diffusion coefficients χ_e^{pb} and χ_i^{pb}. In the other cases, an overall coefficient χ^{pb} has been determined. These experimental values of χ have been compared with the "theoretical" values obtained by using experimental values of local temperatures, etc, in the formulae provided by various theoretical models for the same quantities. Within experimental uncertainties, the ion heat conductivity χ_i^{pb} is lower than the electron heat conductivity, χ_e, near the centre, for hot ion H-modes and monster

sawtooth discharges. For other discharges, the value of the ratio χ_i^{pb}/χ_e^{pb} is more uncertain and might be anywhere between 0.2 and 3. χ_i^{pb} is equal to or larger than χ_e^{pb} in the outer part of the plasma for all discharges except for the hot-ion H-mode discharge where the ratio χ_i^{pb}/χ_e^{pb} may be between 0.3 and 1.8. In any case, χ_i^{pb} is larger than its neoclassical value throughout the profile but approaches it in the plasma centre when peaked density or ion temperature profiles are established. The H-mode discharges all exhibit lower values of thermal conductivities near the plasma edge than L-mode cases. The improvement in confinement from the L- to H-phase appears in both ion and electron thermal conductivities and does not depend on heating scheme.

Comparisons with theoretical models given in Refs [7-12] show that they fail to reproduce the anomalous transport. The neoclassical pressure-gradient-driven turbulence model

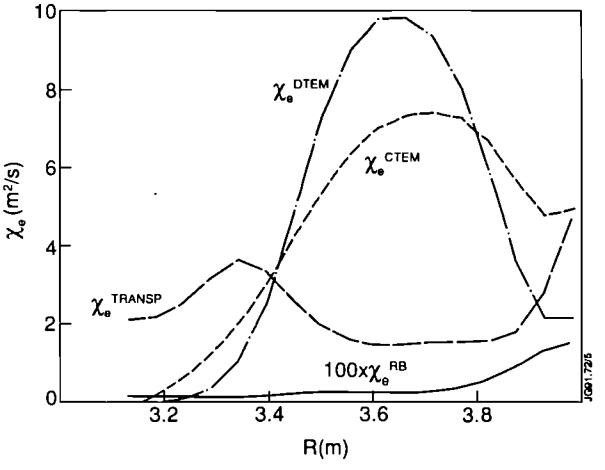

Fig.125: Comparison of the electron thermal conductivities χ_e simulated by TRANSP and predicted by the trapped electron drift mode theory (DTEM for the dissipative regime, CTEM for the collisionless regime) and by the resistive ballooning mode theory (RB) for the monster sawtooth discharge.

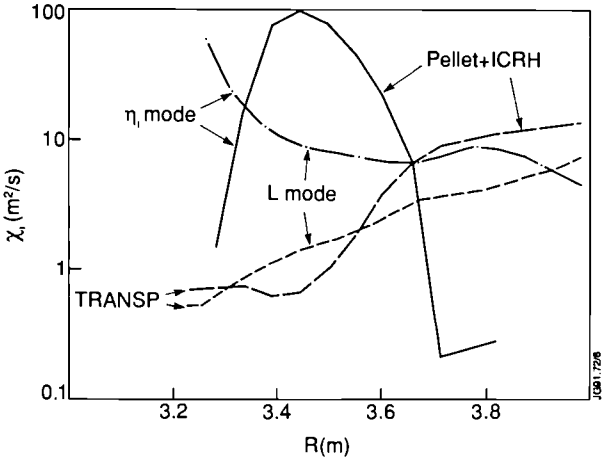

Fig.126: Comparison of the ion thermal conductivities χ_i simulated by TRANSP and predicted by the η_i-mode theory for the pellet fuelled ICRH discharge and the L-mode discharge with P_{NB} = 9.2MW.

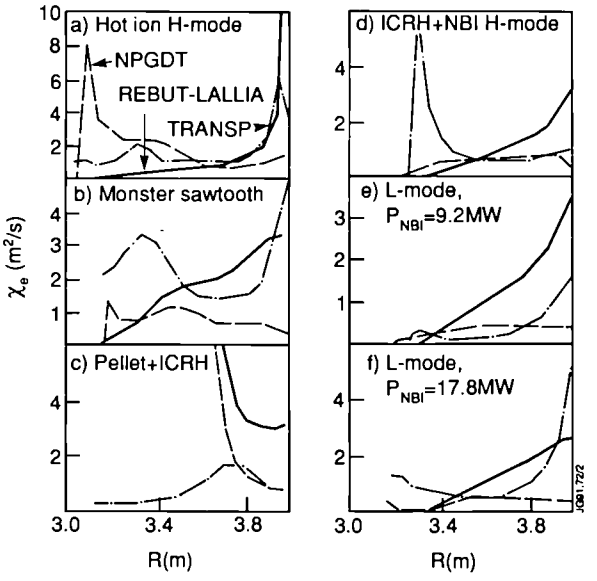

Fig.127: Comparison of the electron thermal conductivities χ_e simulated by TRANSP and predicted by the neoclassical pressure-gradient-driven-turbulence (NPGDT) and the Rebut-Lallia models for six discharges.

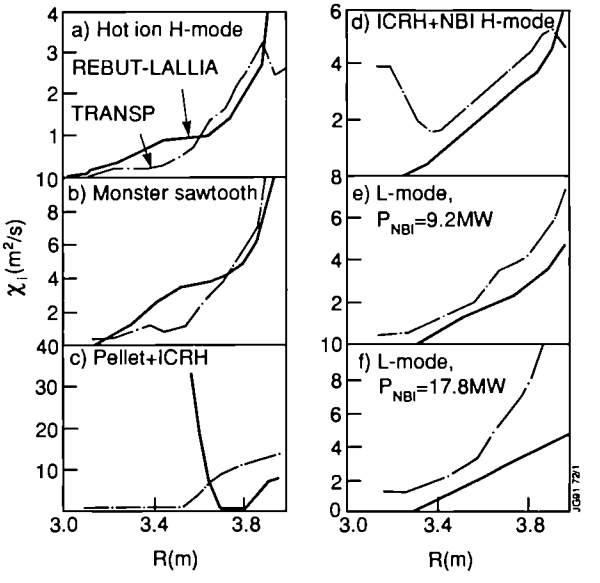

Fig.128: Comparison of the ion thermal conductivities χ_i simulated by TRANSP and predicted by the Rebut-Lallia model for the six discharges.

of χ_e [13] and the Rebut et al critical temperature gradient [14] model of χ_e and χ_i give generally reasonable agreement. It must be noted that in the case of pellet shots, it is practically impossible to determine from experimental data the "theoretical" value of χ_e^{pb} predicted by the Rebut model et al in the plasma core, given its theoretical dependence on the sign of Vq (which is essentially unknown in the case of pellet fuelled discharges). Thus, the model cannot be properly tested by means of the interpretive approach in this case. Results of the comparison with "theoretical" coefficients are shown in Figs.125-128.

The possibility of relating the anomalous ion energy transport to models derived from the theory of ion temperature-gradient-driven turbulence [9-12] has extensively also been tested in Ref.[15]. This analysis shows that while there is qualitative agreement (e.g. in pellet fuelled auxiliary heated discharges [16]) between theoretical predictions and experimental findings, there is a serious quantitative disagreement, namely (see Fig.129):

- all models predicted ion energy transport which is too low in the region $\rho \geq 0.7$ (ρ is the normalised radius) even when fully developed turbulence is taken into account;

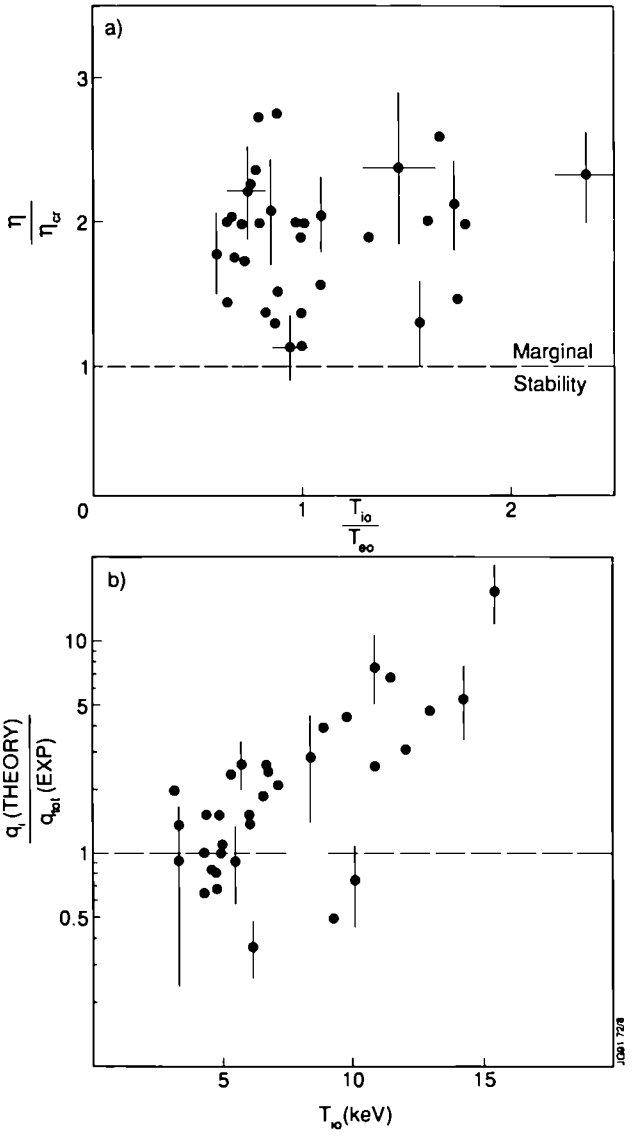

Fig.129: JET data (referring to sawtooth-free, L-mode, 3MA pulses) compared with the predictions of one of the published versions of η_i-mode theory [11]: (a) ratio of the measured $\eta = L_n / L_T$ to the theoretical threshold value as a function of T_{io}/T_{eo}; (b) ratio of the predicted ion heat flux to the total measured heat flux at $\rho = 0.4$, as a function of peak ion temperature.

- all models predict a large χ_i in the central and intermediate plasma region. Hence, T_i is expected to be determined by $\eta_i = n_i \nabla T_i / T_i \nabla n_i$ close to the instability threshold η_i^{cr}. Thus, to reconcile theory with JET results, a substantial increase of η_i^{cr} would be required.

The lack of observation of hot electron regimes has been the subject of intense debate at JET. The apparent saturation of the electron temperature at about 12keV may be explained by the standard degradation of transport with power and the widening of the power deposition profile with ICRF at high power and low density due to various effects (finite amplitude orbits, MHD, etc.). However, it remains unclear and to be investigated experimentally whether it will be possible to produce hot electron regimes. These regimes require that very low values of χ_e^{pb}, comparable to χ_i^{pb} in hot ion regimes, are obtained at high electron temperature.

Predictive Simulations of Energy and Particle Transport

An extensive campaign of simulations with predictive codes (both 1-D and $1^1/_2$-D) has been carried out to assess various transport models. Particular attention has been given to standard ohmic and L-mode discharges but, as in the case of the interpretive approach, representative shots of all of the most relevant plasma regimes observed in JET were considered. The propagation of heat and density pulses following a sawtooth crash were also simulated. Only relatively complete transport models, claimed to be valid from the core to the plasma boundary, have been considered. Among these, models based on the explicit introduction of a "profile consistency" constraint have been shown to be completely empirical tools of limited validity, being applicable only to standard ohmic and L-mode discharges in quasi-steady state situations [17]. The Rebut model [14] has been shown to be much more satisfactory. It has been extended to include particle transport, and its theoretical basis, while being still largely incomplete, has been extended by studying two mechanisms of self-sustainment of the magnetic field configuration, believed to be responsible for anomalous transport [18,19]. The first one is based on the different behaviour of electrons and ions in the presence of islands as a result of their different Larmor radii. This effect leads to a difference in their drift velocities and hence to a current which maintains the islands. This mechanism could maintain magnetic turbulence resulting from a mixture between islands of the size of the ion Larmor radius and chaotic regions. The second mechanism is a pseudo-gravity, used as a simple

analogue for pressure gradient/field curvature modes. The electron and ion drift velocities, associated with the pseudo-gravity, combine to produce the current sustaining islands much larger than the ion Larmor radius.

Fig.130 shows the experimental and simulated profiles of electron temperature and density for two discharges, one with ICRF heating, the other with NBI, which illustrate how the Rebut model can cope with rather different situations [20]. Referring to particle transport, case (a) is representative of those cases where no inward pinch term in the diffusion equation of deuterium ions is required. They are found in high density discharges with NBI (both L- and H-modes) but also in relatively high density ohmic discharges and discharges with pellet injection. Case (b) is representative of those cases where an inward pinch term was required, in the present version of the model, in the region r/a ≥ 0.3-0.4. Such cases are commonly found among relatively high Z_{eff}, RF heated discharges. However, it must be noted that the required anomalous inward pinch term might simply be a manifestation of the incompleteness of the presently available model with respect to impurity transport. The model has been successfully applied in a 1-D code to simulate the propagation of the temperature and density perturbations following a sawtooth crash. The model indeed predicts different values of χ_i^{pb} and χ_e related to the heat pulse propagation, as well as a relatively high values of χ_e/D, (D being the particle diffusion coefficient) as observed in experiments (see next Section).

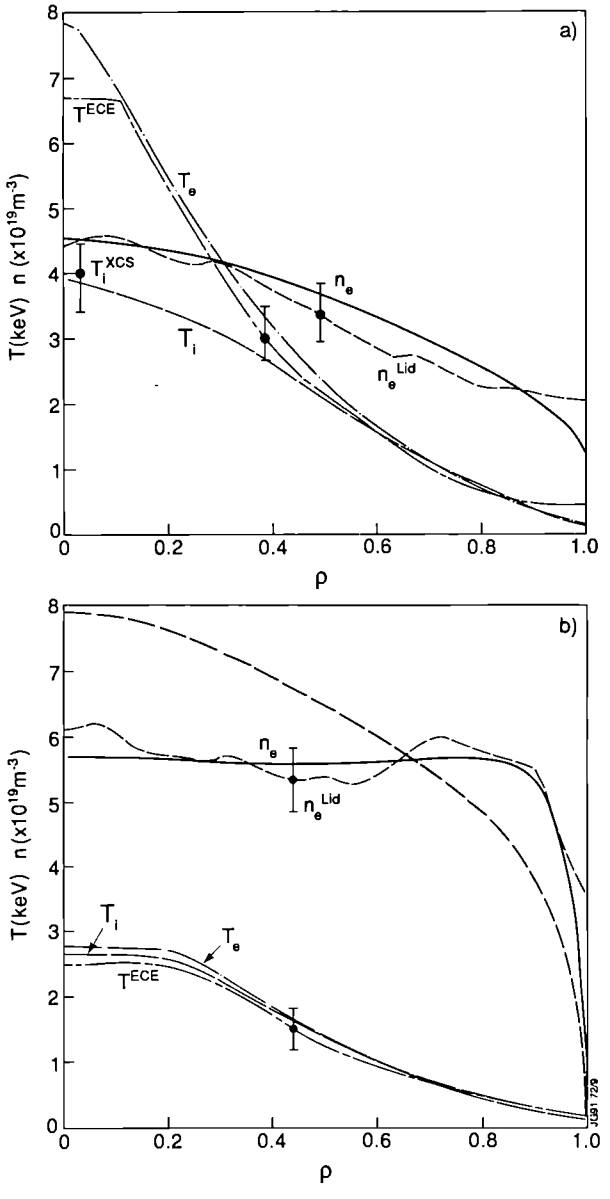

Fig.130: Comparison of computed and experimental T_e and n_e profiles for a sawtoothing RF discharge ((a) Pulse No.19617. B_T = 3.1T, I = 3MA, P_{RF} = 8MW) and a sawtoothing NBI discharge ((b) Pulse No.20334, B_T = 3.1T, I = 3MA, P_{NBI} = 8MW). In (b), the peaked density profile was computed with the same v_{an} as in (a), the flat one was computed with v_{an} = 0.

The main deficiencies with the model have been found in the outer region of the plasma, where $|\nabla T_e''|$ (the absolute value of the critical electron temperature below which transport is predicted not to be anomalous) tends to exceed the observed $|\nabla T_e|$ in L-modes at low boundary density. It is expected that the model, based on a single phenomenon has to be augmented by, for example, atomic physics processes and phenomena related to MHD instabilities which might be important in the boundary region. An empirical solution to this problem, adopted in the predictive $1^1/_2$-D code JETTO, is to reduce the anomalous transport gradually when $|\nabla T_e|$ approaches and becomes smaller than $|\nabla T_e''|$. We also remark that a quantitative validation of the Rebut model in the central region of the plasma is subject to large uncertainties owing to the dependence of χ_e^{RLW} on the local shear and the practical difficulty of measuring ∇q in this region.

Analysis of Heat and Density Pulse Propagation Measurements

The analysis of fast transients provides a method for determining a linearised matrix of transport coefficients from measured data and complements interpretive and predictive studies. Recent work at JET has been based on an analysis of the heat and density pulses following sawtooth crashes (see Fig.131), which takes into account the coupling between heat and particle transport [21, 22]. The main result of the analysis is the determination of the 2 x 2 diffusion matrix in a system of linearised diffusion/convection equations simulating temperature and density perturbations

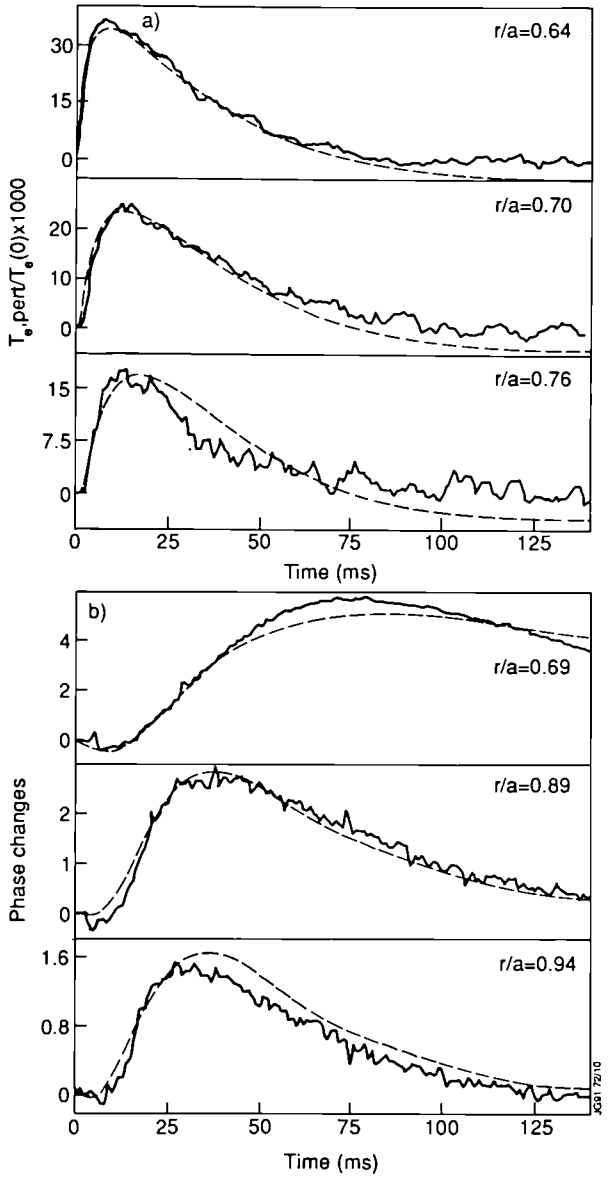

Fig.131: Measurements and simulations of the propagating perturbation of T_e (case (a)) and n_e (case (b)); ΔT_e is normalised to the central temperature before the sawtooth crash, Δn_e is given by the phase changes of the reflectometer.

evolving at various radii in a typical case. Values of the linearised particle and thermal diffusion coefficients D^p and χ_e^p with $D^p / \chi^p \leq 0.1$ are derived in the outer plasma region $r \geq 0.6$ from this kind of analysis. These values are consistent with the values of D and χ_e found in the simulation of the same pulse with the Rebut model (see previous Section). The pulse propagation analysis shows that there is a linear coupling between the particle inward pinch and negative temperature gradient. This recalls the effect of the thermo-electric force in parallel classical transport (which in the Rebut model is related to impurities).

Recent work has shown that the same method of analysis can be applied consistently to data from other tokamaks (TEXT and TFTR). However, further investigation is required to establish whether this interpretation of the pulse propagation following a sawtooth crash is unique or other interpretations, such as the "ballistic" one proposed by the TFTR team, may be equally valid and general.

Impurity Transport Studies

A coherent picture of impurity transport, applicable to the various experimental situations which are found in JET, is starting to emerge. Data for impurity transport studies have been obtained mainly from ad-hoc experiments where impurities were injected into the plasma either by gas puffing or laser blow-off. Useful data, currently being analysed, have been obtained for He transport from discharges with He neutral injection.

The global impurity confinement time, τ_{imp}, has been determined in various experimental conditions and for different impurity species. It has been found that τ_{imp} is the same when injecting T_i (Z=22), Fe (Z=26) or Mo (Z=42). This probably indicates that the mechanisms which are responsible for the anomalous transport affect all particles in a similar way. Similarly, τ_{imp} is independent of Z_{eff} as verified for Z_{eff} values ranging from 1.4 to 5. Values of τ_{imp} are 0.35s and 0.2s in ohmic and L-mode plasmas, respectively. The experimental data presently available are too limited to determine quantitatively the dependence of τ_{imp} on input power or plasma parameters. This should be an objective of the next experimental campaign. In H-modes, the confinement time is longer than in L-modes. Confinement times of the order of seconds have been observed in pure H-modes without ELMs. Fig.132 illustrates the difference between impurity confinement in L- and H-regimes.

Local impurity transport analysis of the predictive type [23] for ohmic and L-mode discharges shows that between sawtooth crashes the experimental data can be properly simulated assuming three different regions. A central region where the impurity diffusion coefficient D~0.03 - 0.15m^2/s, an outside region where D~1.3m^2/s, the largest value being for L-mode plasmas in both cases, and a transition region around the sawtooth inversion radius where the value of D is taken to smoothly join the two regions. The central values of D are in agreement with neoclassical predictions and a factor 20 to 60 larger on the outside. The value of V is more uncertain, but it is also small in the central region with a value of ~0.025ms^{-1} and 0.15ms^{-1} at r=a/4 for ohmic and L-mode plasmas respectively. At the plasma edge, V~2ms^{-1} in the ohmic case and V~6ms^{-1} for L-mode plasmas.

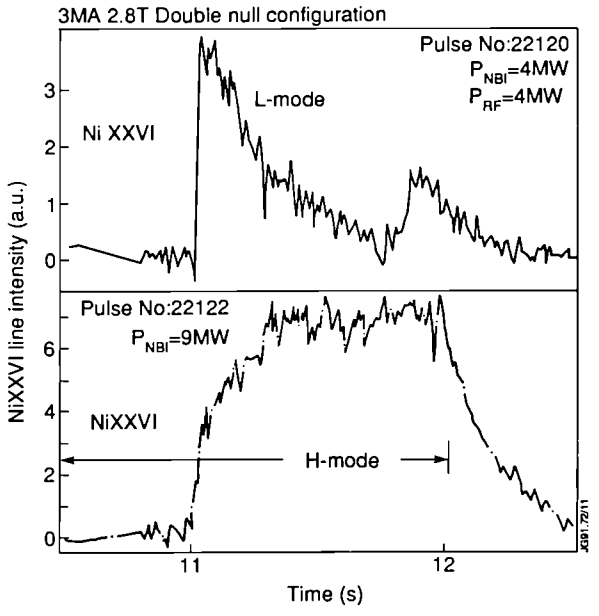

Fig.132: Comparison of the time evolution of line intensity following Ni injection into L-mode and H-mode plasmas.

A similar analysis of H-mode discharges derives a rather low diffusion coefficient D≈0.1m^2/s across most of the discharge, and a spatial variation of V which depends on the plasma temperature and density profiles [24, 25]. Fig.133 shows the empirically determined spatial profile of V during the H-phase of a high density pulse. Before density steady state, in a phase lasting ~3.5s, the velocity V must be outward in the region r≤0.8 in order to explain the nickel emissivity lines and radiated power; the empirical convective velocity V is consistent, within the large uncertainties of the analysis, with neoclassical theory. These results are confirmed both for L- and H-modes by the interpretive approach whose application in the case of an L-mode is illustrated by Figs. 134 and 135 [23].

The decay of soft X-ray emission after laser ablation of Ni allows the measurements of Ni profiles and fluxes (Fig.134). Fig.135 shows a plot of the normalised particle fluxes and normalised density gradient at different radii calculated from the time evolution of the Ni density profile. It shows that fluxes and gradients are linearly related. Therefore, for each curve which corresponds to different plasma radii, the slope represents the diffusion coefficient and the intercept is

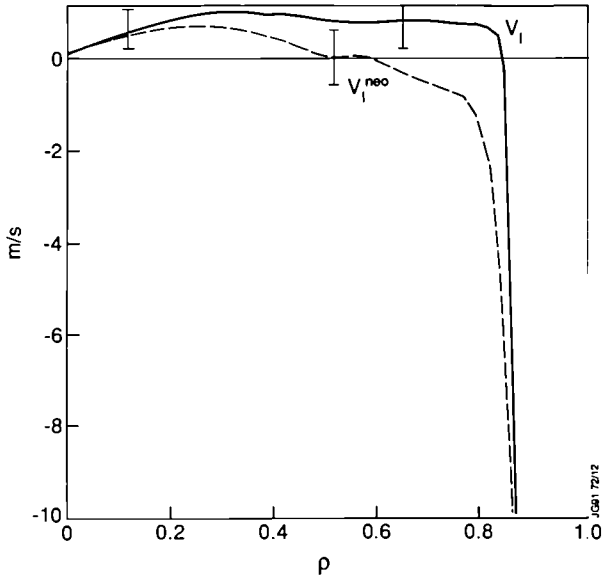

Fig.133: Radial dependence of the empirical and neoclassical velocity v_I found by simulating the impurity behaviour in an H-mode with a hollow density profile (Pulse No.21022).

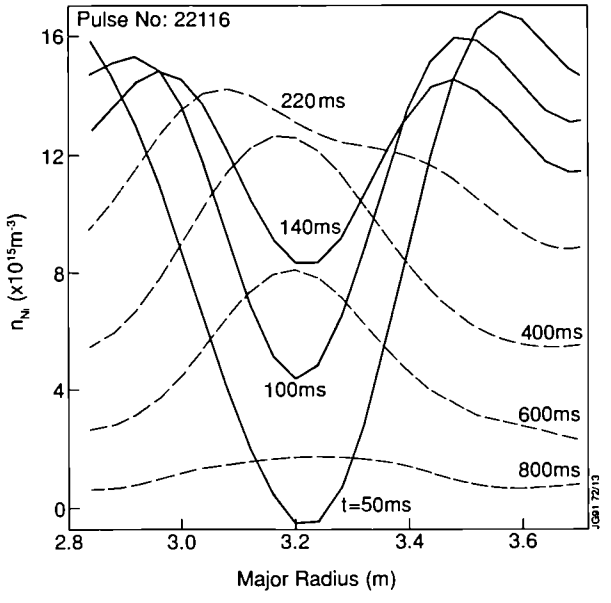

Fig.134: Time evolution of Ni density profile, as inferred from SXR tomography following Ni-injection into a L-mode plasma.

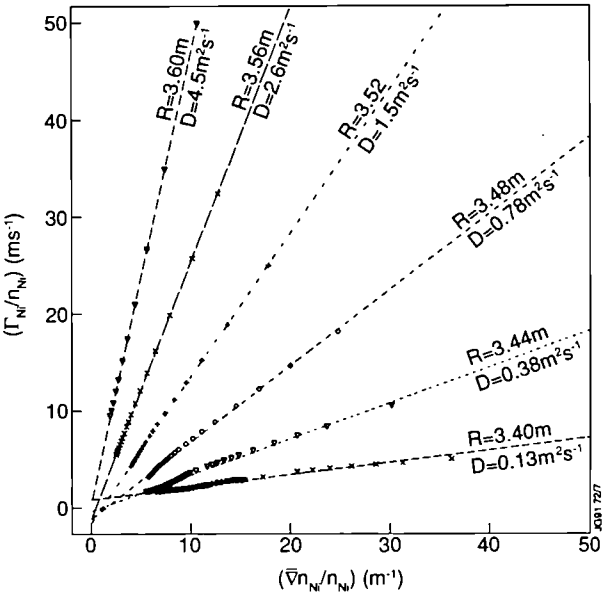

Fig.135: Plot of normalised Ni fluxes and normalised density gradients at different radii calculated from the time evolution of the Ni density profile.

the convection velocity. Clearly in the central region of the plasma, small values of the diffusion and the pinch term are required, while both values increase with radius.

All of these findings indicate that neoclassical transport must be an important ingredient of a complete transport model of impurities.

References

[1] K. Thomsen et al., 32nd Meeting of the Division of Plasma Physics of the American Physical Society (APS) (Cincinnati, U.S.A.) (1990);

[2] J.W. Connor and J.B. Taylor, Nucl. Fus. **17** (1977) 1047;

[3] J.P. Christiansen, J.G. Cordey and K. Thomsen, Nucl. Fus. **30** (1990) 1183;

[4] J.G. Cordey et al., Proc. of 13th International Conference on Plasma Physics and Controlled Nuclear Fusion Research (Washington, U.S.A.) (1990). Paper IAEA-CN-53/F-3-19;

[5] R.E. Waltz, J.C. DeBoo and M.N. Rosenbluth, Proc. of 13th International Conference on Plasma Physics and Controlled Nuclear Fusion Research (Washington, U.S.A.) (1990). Paper IAEA-CN-53/D-4-7;

[6] B. Balet, J.G. Cordey and P.M. Stubberfield, Report JET-P(90)51, to be published in Nuclear Fusion;

[7] B.A. Carreras et al., Phys. Rev. Lett. **50** (1983) 503;

[8] F.W. Perkins et al., Proc. 4th International Symposium on Heating in Toroidal Plasmas, Rome, Italy (1984), **2** 977;

[9] G.S. Lee and P.H. Diamond, Phys. Fluids **29** (1986) 3291;

[10] N. Mattor, Culham Laboratory Report - CLM-P872(1990);

[11] F. Romanelli, Phys. Fluids B **1** (1989) 1018;

[12] S. Hamaguchi et al., Fluctuation Spectrum and Transport from Ion Temperature Gradient Driven Modes in Sheared Magnetic Field.s DOE/ET-53088-388, ISFR #383;

[13] J.D. Callen et al., Plasma Physics and Controlled Nuclear Fusion Research (1988), (IAEA, Vienna, 1989) Vol II, p53;

[14] P.H. Rebut, P. Lallia and M.L. Watkins, Plasma Physics and Controlled Nuclear Fusion Research (1988), (IAEA, Vienna, 1989) Vol II, p191;

[15] F. Tibone, G. Corrigan and T.E. Stringer, Proc. of the 17th EPS Conference on Controlled Fusion and Plasma Heating, Amsterdam, 1990, Vol 1, p162;

[16] G.L. Schmidt et al., Proc. of the 17th EPS Conference on Controlled Fusion and Plasma Heating, Amsterdam, 1990, Vol 1 p215;

[17] Ch. Sack et al., Proc. of the 17th EPS Conference on Controlled Fusion and Plasma Heating, Amsterdam, 1990, Vol II, 801;

[18] M. Hugon and P.H. Rebut, Proc. of 13th International Conference on Plasma Physics and Controlled Nuclear Fusion Research (Washington, U.S.A.) (1990). Paper IAEA-CN-53/D-1-4;

[19] P.H. Rebut and M. Hugon, JET Report JET-P(90)58, submitted to Plasma Physics and Controlled Fusion;

[20] A. Taroni et al, Proc. of 13th International Conference on Plasma Physics and Controlled Nuclear Fusion Research (Washington, U.S.A.) (1990). Paper IAEA-CN-53/A-2-1;

[21] J.C.M. de Haas, J. O'Rourke, A.C.C. Sips and N.J. Lopes Cardozo, JET Report JET-R(90)04;

[22] G.M.D. Hogeweij, J. O'Rourke and A.C.C. Sips, JET Report JET-P(90)4, submitted for publication in Plasma Physics and Controlled Fusion;

[23] D. Pasini et al., Nucl Fusion **30** (1990) 2049;

[24] L. Lauro-Taroni et al., Proc. of the 17th EPS Conference on Controlled Fusion and Plasma Heating, Amsterdam, 1990, Vol I, p247;

[25] R. Giannella et al., Proc. of the 16th EPS Conference on Controlled Fusion and Plasma Heating (Venice, Italy) (1989), Vol I, p209;

[26] D. Pasini and H. Weisen, Private Communication.

Plasma Edge Phenomena and Impurity Production

Effort has been devoted to coordinating the physics understanding of essential phenomena of plasma-wall interactions and providing necessary diagnostics. The use of beryllium as a getter and limiter material has lead to a greater involvement in the experimental progamme and has focussed attention on processes taking place in the scrape-off layer such as: recycling of hydrogen isotopes, plasma parameters and their scaling with global plasma parameters, mechanisms of the impurity release and transport, and damage to limiter surfaces.

Details are set out in the following paragraphs.

Langmuir Probe Measurements of the Edge Plasma Parameters

During the period September 1989 - November 1990, JET operated with beryllium toroidal belt limiters, a carbon upper target plate and a beryllium lower target plate. Extensive measurements of the edge plasma parameters both in limiter and divertor configuration have been made over a wide range of plasma conditions. Several types of Langmuir probes have been used to measure the edge parameters i.e. ion saturation current (I_{sat}), electron temperature (T_e), electron density (n_e), deposited power (P_d) and plasma potential (V_p).

Many probes were installed into different plasma facing components (belt limiter tiles, divertor target plates, ICRF antennae and LHCD launcher side protection tiles and in the ICRF Faraday screen) at various positions inside the vessel. The general layout of these probes is shown in Fig. 136. Although these probes are in a fixed position they are radially separated allowing rough estimates of the scrape-off layer (SOL) profiles. Hence a database of the edge parameters as a function of main plasma parameters has been created for the different plasma configurations. This is similar to the database already obtained with discrete graphite limiters and carbonised walls [1].

A second type of probe is the fast reciprocating probe, containing two Langmuir elements facing ion and electron drift directions. This probe can make up to three radial movements, from an adjustable rest position, of 100 mm in 200 ms at any time during a discharge. Data have been taken up to 20 mm inside the last closed magnetic flux surface (LCFS) and the detailed SOL profiles measured have agreed with extrapolated data from the fixed probes in the radial direction up to the LCFS. However, profiles have been measured for only a limited number of plasma conditions.

An adjustable set of Langmuir probes has also been inserted on the front of the Fast Transfer System (FTS) train, also used for exposure of time resolving collector probes (near the outer midplane). The FTS train contains also a Retarding Field Analyzer (RFA), mainly to measure the edge ion temperature, and a grazing incidence probe to study the effect of the angle of incidence of the field lines on the power flux measured by the probe.

The study of SOL parameters as a function of the main core parameters aims at describing the physics of the energy and particle transport from the core to the SOL where the contact with plasma facing materials is responsible for impurity release. Control of the impurity release and subsequent transport depends on the details of the behaviour of the

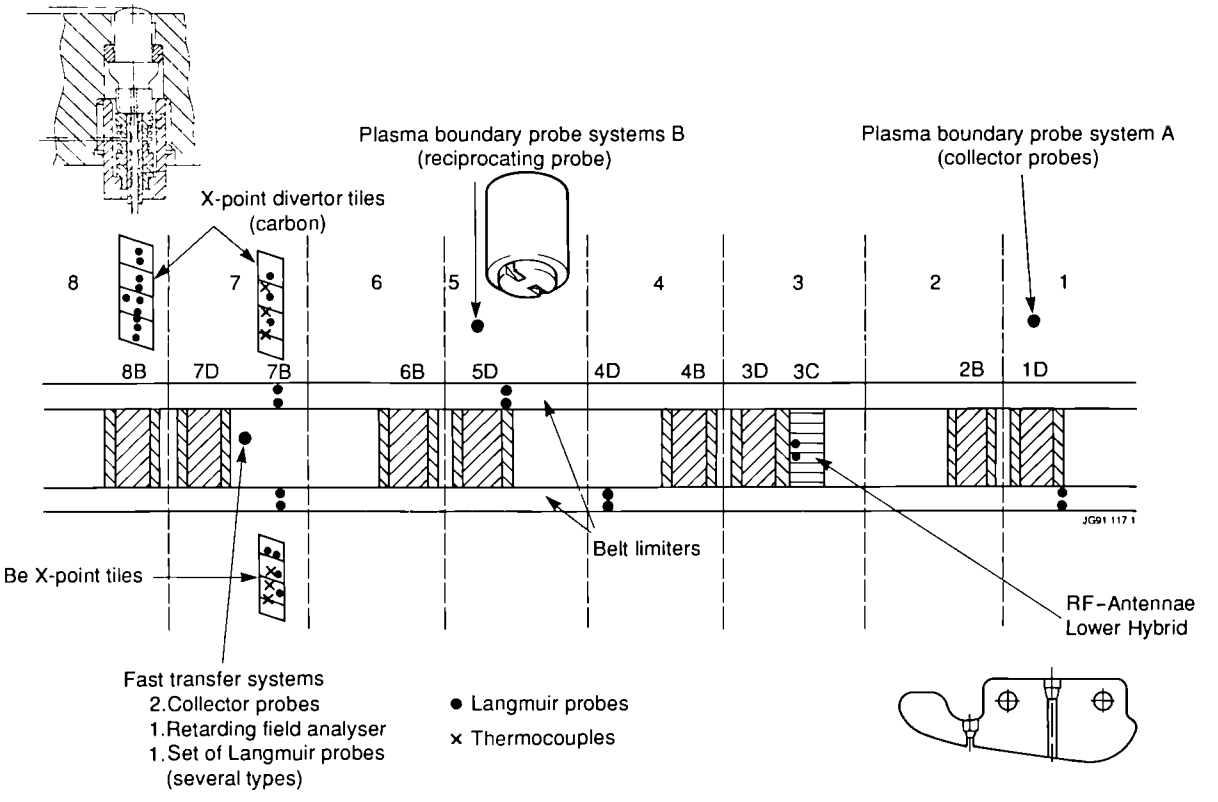

Fig. 136 General layout of plasma boundary diagnostics during 1990. Insert is a detailed sketch of Langmuir Probes on X-point target plates and belt limiter tiles.

SOL and this aspect is extensively studied in the gas puffing/ pellet injection experiments. In addition, SOL parameters and those in the outer layers of the core plasma are essential for the successful interpretation of spectroscopic signals, while the results of those affect the detailed interpretation of the Langmuir probe measurements.

Limiter Plasmas: Edge Parameter Scaling and Impurity Production

The database of ohmic and heated discharges now extends to I_p=7MA with volume averaged electron densitites ranging from 0.3 to 5.0 x $10^{19}m^{-3}$ with carbon and beryllium limiters. The behaviour of the edge electron temperature and density with beryllium limiters found at low plasma densities is $T_e(a) \propto n_e(a)^{-1/2}$ and becomes steeper at higher densities ($T_e(a) \propto n_e(a)^{-1}$) as is shown in Fig.137 [2]. The same dependence occurs for heated discharges up to 30MW (NBI and ICRF combined heating), and is also found in Fig.137,

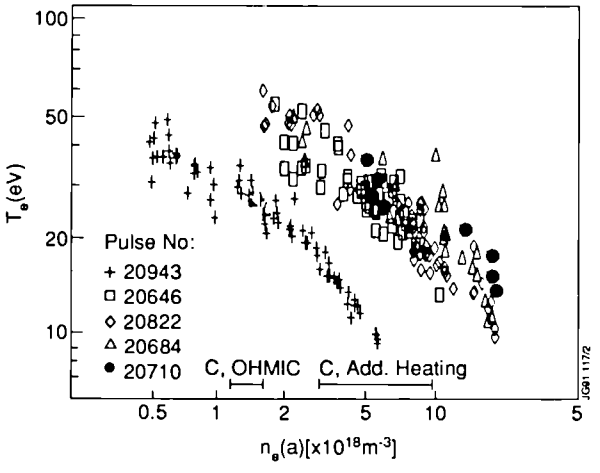

Fig.137 Edge electron temperature against edge density for beryllium limiter plasmas. The lower set of data is for ohmic discharges and the higher for additionally heated discharges (NBI /CRF). The density range for similar discharges with carbon limiters is indicated.

but in this case the wide variation in the relative fraction of radiated power is so important that a bigger scatter is introduced in the data. The shift in the value of $T_e(a)$ at fixed density $n_e(a)$ is due to the higher power conducted to the SOL. In comparison with scaling obtained for the graphite limiters [1], the maximum edge electron temperatures are lower for the beryllium case, and seem to be clamped at lower densities. The heat flux to the belt limiters estimated from Langmuir probe measurements (assuming $T_i = T_e$ in the SOL), is much lower than that given by the power balance, and that derived from calorimetric estimates of the power deposition. This effect is more noticeable at lower plasma densities (higher power per particle at the edge). An attempt has been made to explain this by assuming $T_i \sim 5\text{-}10$ T_e in the plasma boundary [3,4,5]. This power may be under-estimated by bolometry, in part for geometrical reasons and in part due to the bolometer sensitivity decreasing at low energies typical of some of the radiation from beryllium. The radiation from recycled hydrogen and traces of carbon is also being investigated, especially near the density limit. There are measurements from spectroscopic diagnostics which corroborate this inference i.e. that $T_i > T_e$ in the plasma boundary (see the later section on line profile measurements). The role that the radiated power from the beryllium limiters plays in this power discrepancy is under investigation.

With beryllium limiters, the scaling of the edge parameters with main plasma parameters was frequently very difficult due to temporal variation of plasma parameters. Higher levels of deuterium fuelling are required to maintain the central density than for carbon limiters. However, for ohmically heated discharges (see Fig.138), the dependence of the edge electron density and temperature as a function of global plasma parameters is presented. From Fig.138(a), there is a dependence of n(a) on $\langle n_e \rangle^{1.4}$, which lies in between other scalings with volume-averaged density, either linear [6,7] or square [7,8]. The decay lengths for the electron density (λ_{ne}) and temperature (λ_{Te}) remain relatively independent of density at low densities for a given input power, and both decrease with input power (higher plasma currents). However, λ_{ne} decreases and λ_{Te} increases rapidly as the density rises to high values for fixed input power. In Fig.139 we present the scaling of the power SOL thickness for the same discharges. As with previous scaling with carbon limiters, the dependence on volume-averaged density is weak but it is now becoming clear that the dependence on q is stronger than on I_p. The dependence of T_e (a) on I_p could still have a significant impact on future machines (i.e. $I_p \approx 30$MA).

Limiter Plasmas: Edge Parameters under Forced Fuelling Conditions

The strong pumping of hydrogen isotopes (and helium) by beryllium covered walls necessitated fuelling the discharges at a high rate even in low density discharges. Depending on the starting density and the fuelling rate, the steady state relation between average core density and edge density was

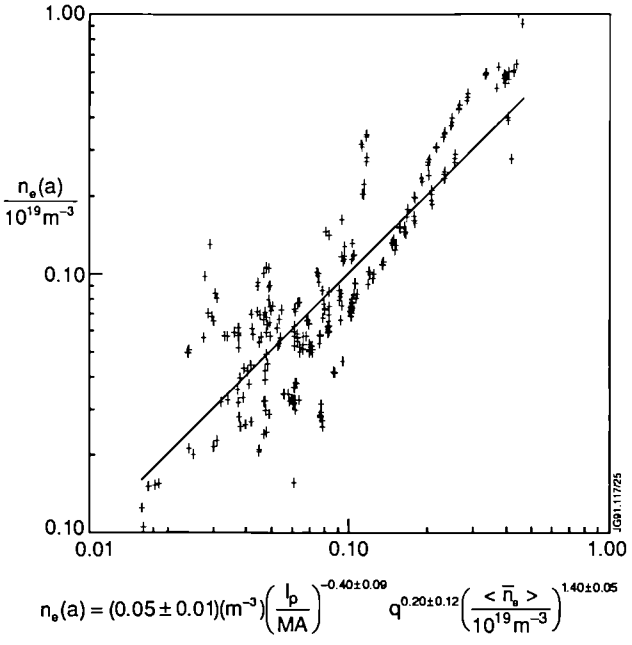

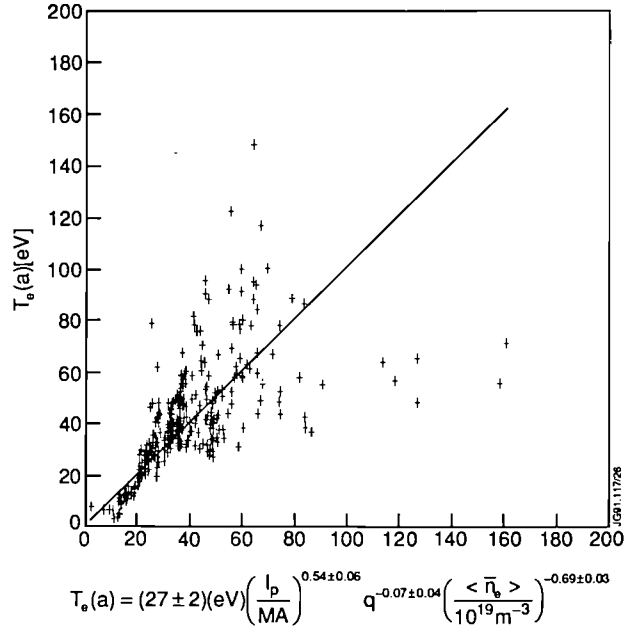

Fig.138 The scaling for (a) edge density and (b) edge temperature for ohmically heated beryllium limiter plasmas.

frequently broken. Therefore, it is sensible to relate edge temperature to edge density and not to core density.

By making the edge density transiently higher without affecting core density, the edge temperature and sputtering are reduced while the total edge radiation might increase. In principle, this effect has opened up a much larger accessible range of edge densities, although at high density, transient effects dominate with a relaxation time of about 0.5 s. Heavy fuelling and pellet injection have proven to be a powerful means to control impurity influx.

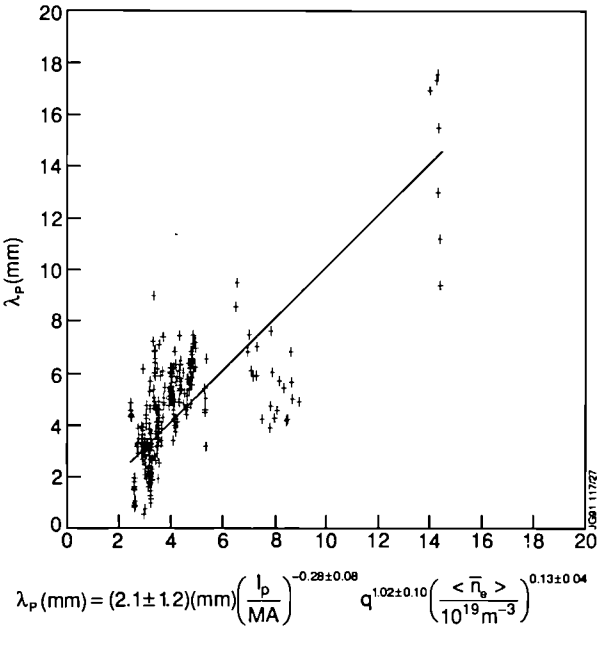

Fig.139 The scaling of power SOL thickness for ohmic beryllium limiter plasmas.

The effectiveness of the different fuelling scenarios for impurity control are shown in Fig. 140 where the electron temperature, as a measure for impurity sputtering, is shown as function of the power conducted to the edge per particle. Low edge temperatures at high power per particle are only achieved by heavy gas puffing [9]. Similar conditions were obtained with carbon limiters but then it was necessary to use a combination of pellet and gas fuelling to maintain low edge temperatures and reasonably peaked profiles.

In the end, high gas fuelling rates lead to very high edge densities and low edge temperatures. This leads to the loss

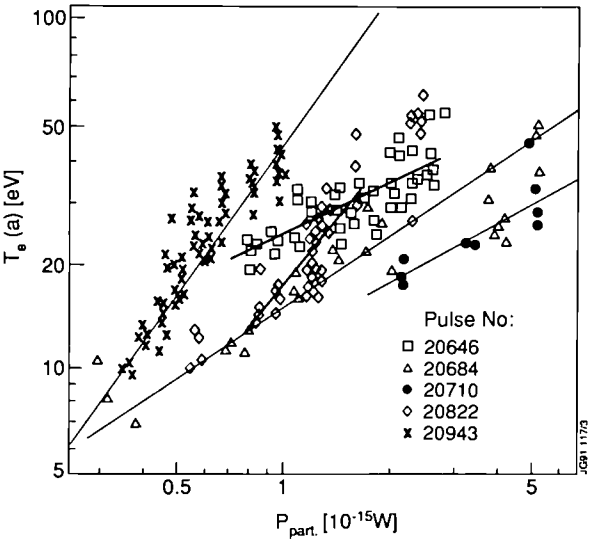

Fig.140 The edge temperature versus power per particle for a number of discharges. The further the trajectories are to the right, the higher is the fuelling rate.

of thermal stability in the edge region which manifests itself as a MARFE or edge fuelling limit depending on the dominant impurity. In Fig. 141, the behaviour of the edge parameters for an ohmically heated plasma (I_p=4MA) with fast edge cooling by rapid fuelling, is presented, which was taken in the presence of MARFE's. Similar results were attained in heated discharges. The MARFE leads to a reduction in density with a return to quiescent operation and the process can be repeated several times [9]. Two such MARFEs are shown in Fig. 141. Prior to the peak in radiation, T_e is ≈ 10eV and the ion-saturation current and H_α intensity at the limiter are maximum; these both decrease rapidly as the radiation increases [10].

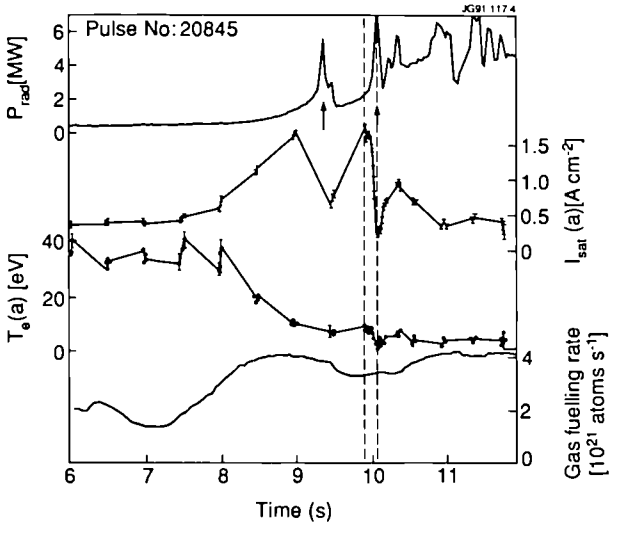

Fig.141 Several boundary parameters versus time for a plasma with repetitive MARFEs. Lines for T_e(a) and n_e(a) connect sparse data points.

value, (ie., linearly dependent on edge temperature [11]). In a simple model, the central impurity content has an inverse dependence on the cross-field diffusion coefficient, so, in principle the faster the increase of $D_\perp^{SOL}$ with edge temperature improved values of Z_{eff} could be obtained. This is shown in Fig.142, where $D_\perp^{SOL}$ as a function of T_e(a) is calculated for different fuelling scenarios both in the beryllium coated carbon limiters and beryllium limiter (Fig.140). $D_\perp^{SOL}$ has been calculated assuming $T_i = T_e$ in the SOL, and appears to be lower for beryllium than for the carbon limiter case, but within measurement uncertainties, $D_\perp^{SOL} \propto T_e(a)^\alpha$ with $1 \le \alpha \le 3$ [2].

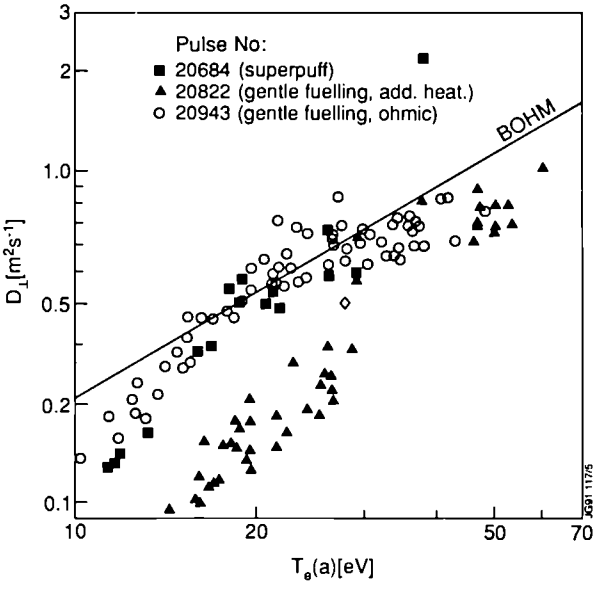

Fig.142 The SOL diffusion coefficient versus edge temperature for three discharges. The solid line is the Bohm value.

Limiter Plasmas: Edge Parameters and Radial Transport

Transport coefficients in the SOL (particle diffusion coefficient $D_\perp^{SOL}$ and heat diffusivity $\chi_\perp^{SOL}$) and their variation with plasma conditions are important parameters for the scaling and design of the next generation of Tokamaks.

If diffusive transport is assumed, then from simple theory, ignoring sources, the edge value of $D_\perp^{SOL}$ and $\chi_\perp^{SOL}$ can be deduced from Langmuir probe measurements of density, temperature and deposited power scrape-off layer thickness. For operation with carbon limiters the scaling of D^{SOL} was Bohm-like: $D^{B} = 0.06(T_e^{SOL}/B)m^2 s^{-1}$ [1]. A similar conclusion has been drawn for beryllium limiters. For 3.0 MA, 2.3 T ohmically heated discharges, the D^{SOL} values are also in fairly close agreement with the Bohm

From measurements of floating potential and of temperature profiles, the radial electric field has been deduced and has been related to the increase of radial transport occuring in limiter discharges during ICRF heating [12]. During ICRF heating, a DC poloidal electric field is alsogenerated producing a radial drift, comparable to diffusive drifts [12]. As a consequence, a strong local outflow occurs and ion sputtering and impurity production are enhanced.

Limiter Plasmas: The Retarding Field Analyser

The Retarding Field Analyser (RFA) can be used to measure the velocity distribution of ions moving parallel to the total magnetic field in the scrape-off layer. Ions are extracted through a small aperture of width comparable to the local Debye length and are analysed using retarding potentials

applied to internal grids. An analyser has been exposed to JET plasmas using the Fast Transfer System (FTS). Experiments have demonstrated the potential of the FTS for more complex probe techniques other than the standard collector probe methods. Due to the high heat loads experienced by the delicate probe during high power, high current discharges, preliminary data are available only for the low current, ohmic plasmas. In this case, the parallel ion velocity distribution is consistent with a one-dimensional Maxwellian distribution shifted in velocity space by an amount due to ion acceleration in the sheath electric field spanning the RFA entrance slit. Values of $T_{i\|}$ deduced during the plasma current flat-top were ~ $3T_e$ a few cm behind the limiter leading edge, whilst the sheath potential at $V_s \approx 2T_e$ was consistent with simple theoretical expectations. Future work, using a more robust design will build on this early experience in attempting to provide scalings of T_i and V_s under a much wider range of operating conditions.

X-point Plasmas

Edge parameters profiles in the SOL and along the divertor target plates have been measured during internal magnetic separatrix discharges (X-point) using a reciprocating probe entering the plasma at a position between X-point and the midplane and by using an array of 11 fixed Langmuir probes in the divertor target plates. While the measurements with the reciprocating probe were made for a limited number of discharges and at one time per discharge, the poloidal array at the target plates produced up to eighty local edge parameters per pulse for almost every discharge. However, due to high heat loads at the target plates, many of these probes did not survive to the end of the campaign. Edge parameters were measured during single and double-null operation, and particular attention was devoted to the L to H-mode transition. Fig.143(a) shows profiles of the local flux density (I_{sat}) and electron temperature (T_e) for a double-null discharge at three different times: ohmic, L-mode and H-mode phase. Clearly identifiable are two peaks associated with the inner and outer strike zone, where the separatrix intersects the target plates.

In the outer SOL, the profiles always broaden when the plasma goes through an ohmic to L-mode transition and steepen in a region close to the separatrix during the H-mode phase [1]. The steepening of the SOL density profile is shown in Fig.143(b) for a NB heated plasma with 11 MW power, after the transition to the H-mode. These profile changes have not been observed in the inner SOL of double-

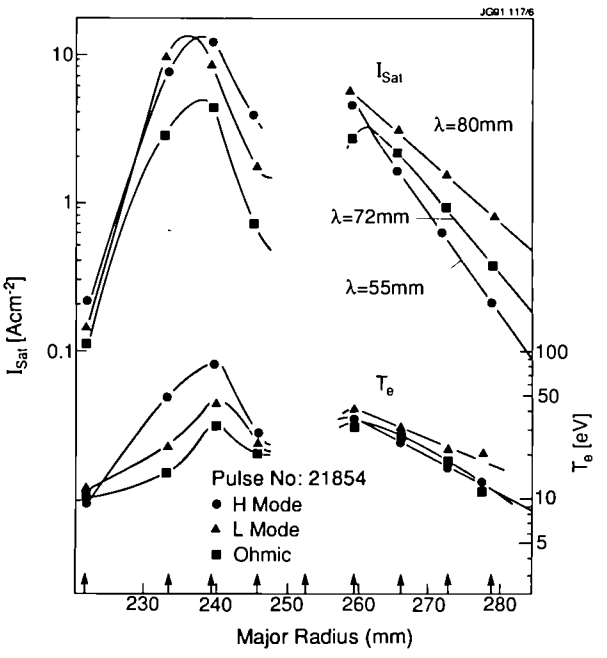

Fig.143(a) The ion saturation current and electron temperature obtained with an array of Langmuir probes built into the X-point target for ohmic, L-mode and H-mode phases of a double-null discharge. The scale-lengths l are measured at the target.

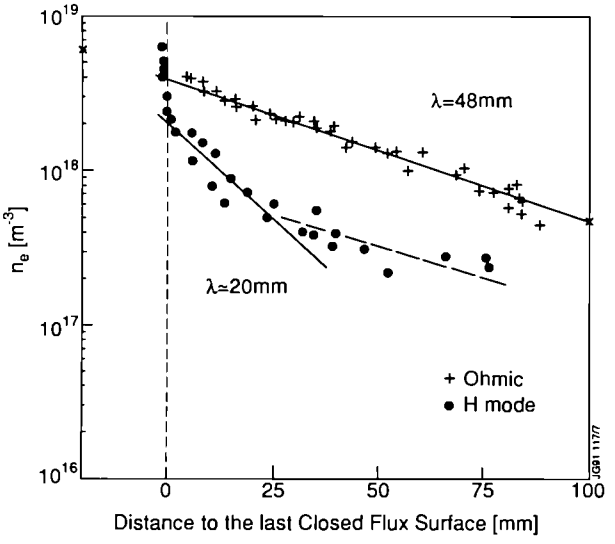

Fig.143(b) The SOL density profile for the ohmic and H-mode phases of a discharge measured with the reciprocating probe. The scale-lengths, λ, are measured at the probe location.

null discharges (see Fig.143(a)) and are independent of the limiter/wall material used (full carbon, beryllium coated carbon, or full beryllium).

The influence of beryllium gettering and the use of beryllium target tiles has been investigated for X-point discharges in JET. Unfortunately, in 1990 the probes in the lower beryllium target sustained damage due to the increased power in the SOL and so probe measurements for single-null discharges with solid beryllium target tiles are not available for the 1990 campaign. However, with beryl-

lium evaporation, an increase in power flow into the SOL was observed, as with the solid beryllium target, and there were other improvements, including reduction of oxygen to insignificant proportions, leading, in turn, to a reduction in the sputtering of carbon. Improved density control by gettering of deuterium as been described [13], the pumping speed due to gettering decreasing after evaporation, and spectroscopic evidence shows that the beryllium layer on the target is eroded in about 10 pulses. Carbon emission from hot tiles increases strongly ($\sim x10^2$) with temperature (1500°C < T < 2600°C) and is independent of the amount of beryllium on the tile, as expected. Discharges with beryllium are tolerant to strong gas puffing, which allows radiation in the divertor region to increase (up to ~ 70% of input power), and reduces edge electron temperatures and also the temperature of the target tiles. This in turn reduces the sputtering and the carbon influx due to heating the target, and the Z_{eff} then decreases.

Measurements were made with forward toroidal field direction (ion ∇B drift towards the target) and the maximum heat load appeared at the outer strike zone. From Langmuir probes in the target, assuming $T_e = T_i$, the ratio of power fluxes (P_{out}/P_{in}) was up to 6:1 during the H-mode. For reverse field direction (∇B drift away from the target), the relative amplitude of the peaks reversed and the load was more equally distributed on each strike zone. In single null divertor discharges with forward field, the particle fluxes and temperatures on the target increased during the L to H transition, while with reverse field, a decrease of these parameters was observed.

The edge parameters were also monitored during H-modes obtained with ion cyclotron heating (ICRF) only. In contrast to the NBI H-modes, the power flux density at the separatrix extrapolated from SOL measurements is higher by up to a factor 5 . A preliminary observation shows that monopole antenna phasing gave a higher power flux density at the edge than dipole phasing, while the quality of the H-mode was only slightly degraded and no difference in impurity behaviour was evident.

Using the simplest non-collisional uniform SOL model, radial profiles have been used to derive the relative variation of transport coefficients. Absolute values are model dependent, but it is generally seen that the cross-field diffusion coefficient $D_\perp$ ($\approx 0.5\ m^2s^{-1}$) increases by $\approx 50\%$ at the transition from ohmic to L-mode and decreases by $\approx 60\%$ at the transition from L to H-mode; similar behaviour is found for the heat diffusivity, $\chi_\perp$ ~2-7 m^2s^{-1}.

Database for Modelling the Edge Plasma

The design of the impurity control system and plasma facing components for the next generation of large Tokamaks (ITER, etc.,) must be guided by predictable modelling of the edge plasma and its plasma surface interactions. Therefore, knowledge of prediction accuracy from existing edge modelling codes requires the creation of a reliable plasma edge data-base. The first step to create this data-base of JET data has been completed for a few discharges. The edge plasma model is a multi-fluid one linked to a Monte Carlo method for the neutral deuterium and impurity species. A relatively complete set of the edge data has now been evaluated for a discharge with a short H-mode phase and the X-point very close to the target plates. [14].

The aim of the study was to establish the assumptions needed to obtain consistency between experiment and model, as the first step towards validation of the model by comparison with experiment. Together with the geometry of the discharge the input for the model required a set of plasma parameters at the target plates and in the SOL. The edge parameters profiles were measured at the divertor target plates by the poloidal array of fixed Langmuir probes, and also in the SOL with the fast reciprocating probe located at the major radius, R = 3.25m. The profiles are shown in Fig.144 plotted as a function of mid-plane major radius using the mapping of the drift magnetic flux surfaces from the equilibrium code. The edge measurements were also matched with the D_α light from the target plates as, in order to locate the separatrix. The values of Fig.144 together with power balance and impurity concentration were used as an input to the model [14]. The results of the multi-fluid model of the X-point SOL show good agreement with the main experimental parameters. However, an additional rather large flow was invoked in the model (in a qualitative way) to permit radiation and impurity density distributions to be well represented by the model. A more complete set of edge data is being assembled including discharges with a systematic variation of the main plasma parameters and variation of the separation of the X-point to the target plate.

CCD Camera Observations at X-Point Targets

Improvements in manipulation of CCD camera data have permitted more refined interpretation of the spatial distribution of power deposition and impurity recycling of the X point targets.

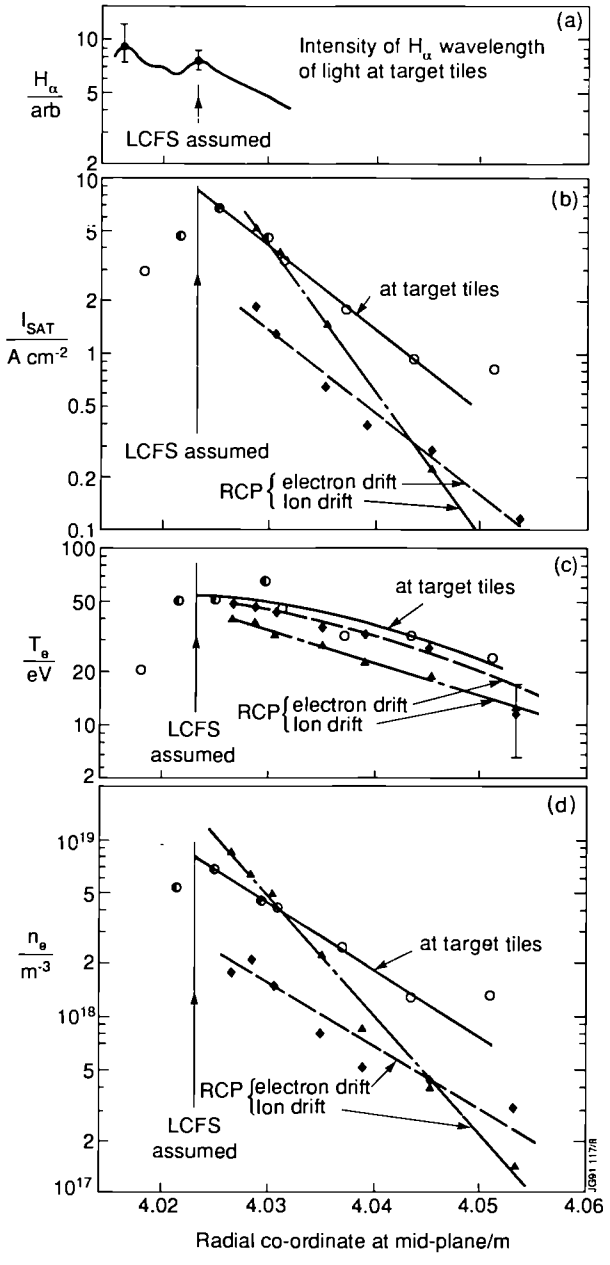

Fig.144 Profiles in the SOL versus radius (mapped to the mid-plane). (a) D_α on the target tiles, (b), (c), and (d) I_{sat}, T_e, and n_e, from Langmuir probes.

Measurements at the Beryllium Target

At the lower beryllium X point target, small eruptions of molten beryllium were observed, and these occurred at progressively earlier times during sequences of similar discharges. This was interpreted as shot-by-shot degradation of the target surface, not only at the point of observation, but at all of the 32 bands of target tiles. Despite these effects, estimates of peak values of power deposition were made of ~0.1 kW/m^2 per MW of NB heating power. Since the ion ∇B drift was in the direction of the lower target, the power was deposited almost exclusively on the outer strike zone. Subsequent in-vessel examination showed large toroidal variations in melt damage at these targets. The eruptions often preceded the formation of MARFEs or disruptions during which beryllium spectral intensities were dominant.

Measurements at the Carbon Target

Systematic studies were performed of the interaction at the upper target of simultaneous temperature and spectral measurements. The power deposition profiles with forward (ion ∇B drift towards the target) and reversed field (ion ∇B drift away from the target) were significantly different and varied with recycling rates. The ratio, P_{out}/P_{in}, of the power deposition at the outer strike zone to that at the inner strike on the band of tiles varied for H-modes in forward field from 1.4 to 1.7 with an average value of 1.7 (see Fig 145(a)). Comparable discharges in reversed field configuration showed a

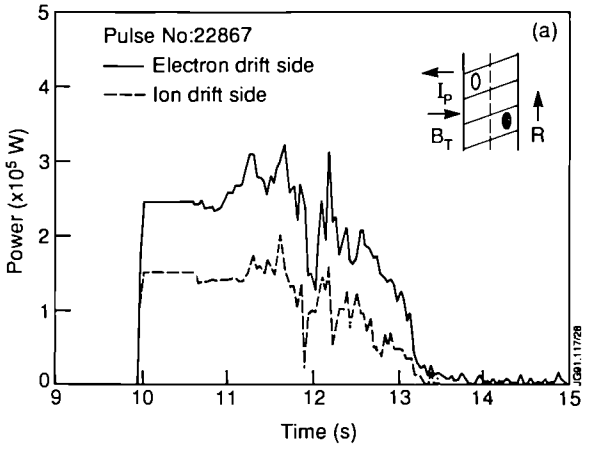

Fig 145(a) Total power deposited on each of the two strike zones in a forward field discharge (Pulse No: 22867) with B_T=2.2T and I_p=3MA. The loading on the inner (ion drift side) strike zone is significantly smaller than on the outer strike zone (electron drift side).

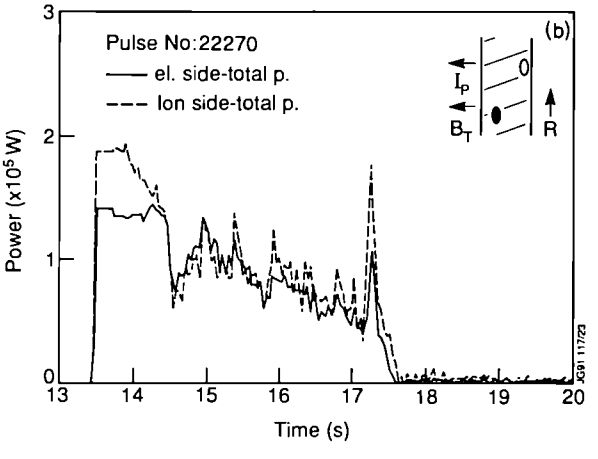

Fig 145(b) Total power deposited on each of the two strike zones in a reversed field discharge (Pulse No: 22270) with B_T=2.2T and I_p=3MA. During H-mode (starting at 14.5 s), the loading on inner and (electron drift side) outer strike zone are almost equal.

variation of P_{out}/P_{in} from 0.8 to 1.5 with an average value of 1.0 (see Fig 145(b)). The recycling taken from the D_α intensity in the private flux region was well correlated with a pressure gauge data, and absolute flux values agreed well during H-modes and the initial phase of L-modes when an ionisation to excitation ratio of 20 was used. However, during later phases of L-modes the pressure gauge often showed significantly higher values. High recycling values corresponded in both field directions with high P_{out}/P_{in} ratios and low recycling values corresponded to low P_{out}/P_{in} values (Fig.146). For both field directions, heavy gas puffing showed a reduction of loading, especially on the inner strike zone, which is similar to the effect of high recycling.

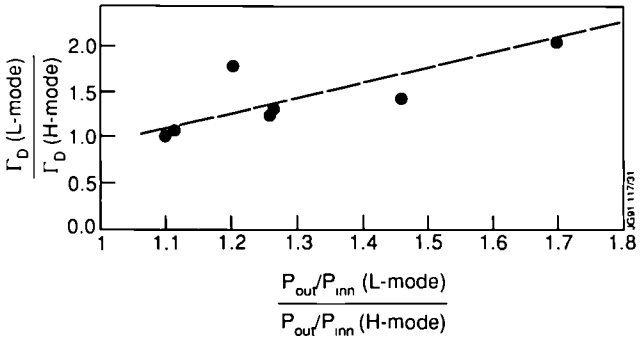

Fig 146 Correlation of the change of recycled deuterium flux, G_D, at the L-to H-transition with the change of the ratio of P_{out}/P_{in} for reversed field discharges.

In the toroidal direction, the targets plates are not entirely equidistant toroidally due to the mechanical substructure of the vessel. If all other alignments were perfect a correction of the observed results for a toroidally equidistant distribution could be made by multiplying the results of P_{out}/P_{in} from forward field by a factor 1.4, and, in reversed field by a factor of 1/1.4, which would enlarge the difference between the forward and reversed field even more. However, it would still leave the reversed field as the more even balanced case. This ratio of P_{out}/P_{in} reflects the powers carried by the plasma in the outer and inner divertor. The observation of the total deposited power, however, shows stronger effects probably due to misalignment of whole bands of tiles, which may supersede this idealised argument to some degree.

The difference of total input power and total radiated power plus change of diamagnetic energy, which is the power available to be deposited on the target (if the effect of radiated power re-deposited onto the target is ignored) was compared with power to the target. Three times more power was deposited on the band of tiles than the calculated available power, assuming equal distribution to the 32 discrete targets. The interpretation of this higher than average loading is, that the band of tiles under observation protrudes deeper than intended into the vessel. This is in agreement with photographic evidence that this band of tiles showed more than average erosion. With large separation, δ_x, between the X-point and the target, the deposition profiles were narrower, but the relative overloading was smaller, consistent with a large angle of incidence of field lines on the target. For these reasons, the preferred separation was 7-10cm.

H-mode Studies

During H-modes, the target temperature often reached values above 2500°C. Substantial increases in carbon flux were measured when the temperature exceeded 2300°C, due to thermal sublimation. Carbon blooms occurred within several 100ms, and often the peak target temperature had reached ~3000°C by this time. At this temperature, the energy lost from the target by sublimation and radiation was calculated to be up to 20% of the measured total plasma radiation. The transition from L to H-mode produced a number of effects at the target. Probably due to the changes in plasma β values, the X point position moved closer to the target (up to 3cm). This movement gave rise to substantial changes in deposition, if δ_x was already small.

At constant power input, the transition caused a temporary decrease in total power deposition at the target, due to changes in energy confinement. Up to 30% reduction was observed in the reversed field case (Fig 147). The ratio of P_{out}/P_{in} in L-mode was significantly larger than in H-mode. This was observed regularly with reversed field, but in cases where the L-phase in forward field was long enough to be investigated, this effect was also observed. In the reversed field case, the drop in D_α light intensity in the private flux region (used as an indicator of recycling rate), showed a strong correlation (almost proportional) to the drop in P_{out}/P_{in} ratio (Fig 148).

Another effect resulting from the transition is the additional power flow at the ion drift side of the target. The original strike zone, from which substantial carbon fluxes were measured, remained substantially unchanged. A rapid temperature increase occurred at a position closer to the X-point radius than the original strike zone. No carbon flux was observed from this region until sublimation temperatures were reached. From this, it was concluded than only higher energy ions strike this zone and this is reinforced by probe

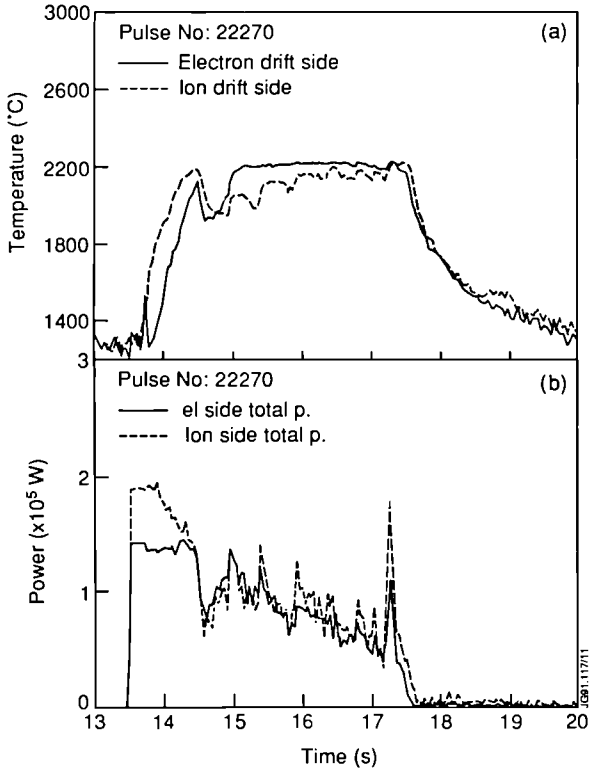

Fig 147(a) The time development of the maximum temperature of the inner and outer strike zones with reversed toroidal field.

Fig 147(b) The total power on the strike zones for Pulse No: 22270. Note the deposition of the plasma energy at the end of the heating pulse.

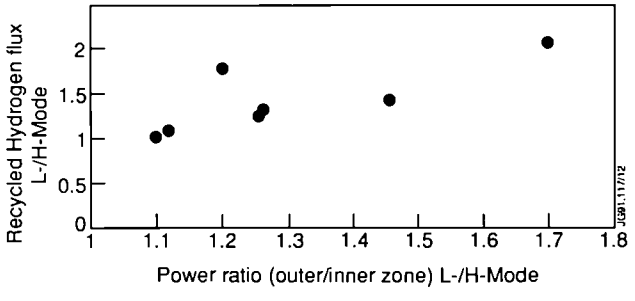

Fig 148 The change in hydrogen flux versus the change to the outer/inner power ratio at the L- to H-mode transition.

measurements of low ion saturation currents and relatively low T_e values.

Fig 149 shows a typical case with reversed toroidal field, in which radial scans of CII light intensity across the ion drift side of the target are plotted. The first scan, prior to NB injection, shows the distribution in the ohmic phase. The second scan, (400 ms later), shows the situation just after the H-mode transition. The small additional peak at R≈2.55m shows that the spectral intensity from this region is smaller than that at the original strike zone. The third scan (400 ms later) shows the distribution when the temperature at the new

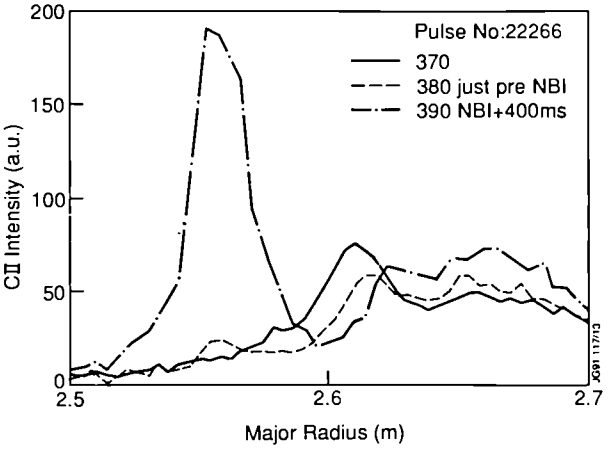

Fig 149 Radial scans of CII intensity on the ion drift side of the target at various times during Pulse No: 22266.

zone has increased substantially, so that the intensity is much greater than that at the original strike zone. Similar data were obtained at different wavelengths, including CI, CIII and BeI.

This observation may be explained in terms of the energy dependence of ion drift orbits. Simulations show that the two normal strike zones are due to flows of plasma with low-energy ions (<200eV) in the boundary outside the LCFS. Particles with energies of a few keV can also reach the target from regions a few centimetres inside the midplane LCFS. Those arriving at the electron drift side, strike a position close to the original strike zone. For small δ_x values (<10cm), those energetic particles reaching the ion drift side, arrive at a position closer to the X-point than the original strike zone. This interpretation is consistent with camera observations and with T_i measurements in the outer plasma regions. It suggests a direct flow of energy from the plasma to the X-point target when T_i near the LCFS is in the keV range.

Beryllium Spatial Distributions near the Limiter

The radial distribution of beryllium atoms from the top belt limiter has been studied as a function of density. The 2D distribution is viewed from the top of Octant No: 3 using a CCD camera and filter (825.4nm). The penetration of neutrals decreases and the distribution narrows as the density is increased, as expected. Although there is some density and temperature dependence of the photon efficiency for the atoms, the radial distribution in principle, gives a measure of the ionisation source function. Detailed calculations are in progress of the expected distributions using the LIM Monte Carlo code and measured density and

temperature profiles. Results agree in qualitative trend but experimental profiles are much broader than code predictions.

Poloidal and toroidal distributions have been viewed at the bottom belt limiter. Individual tiles are clearly resolved in many cases (Fig.150), and hot spots developing on the tiles during high power heating can be seen in real time. The scale length of the tiles shows clearly in the radiation, suggesting that the mean-free-path of the BeI atoms is ~ 1mm, but depends on density. The poloidal distribution shows the typical double-humped structure, determined by the tile shape and plasma e-folding lengths in the SOL. Comparison of experimental data with LIM Monte Carlo calculations shows good agreement over a range of densities (Fig. 151).

At high power, hot spots occur due to localized melting at the tile edge, where the field lines strike the surface at normal incidence. Molten metal is occasionally detached and redeposited on other tile faces, where it causes new hot spots to form.

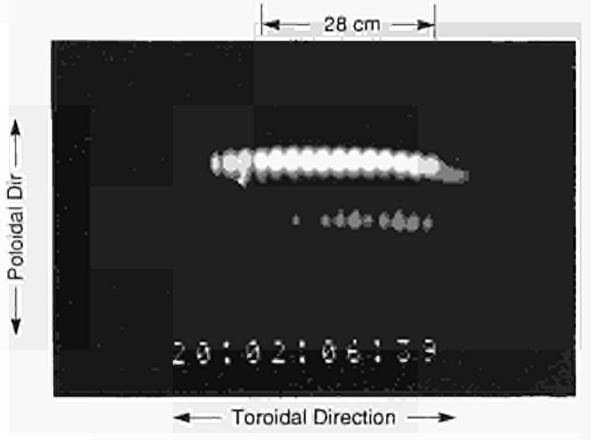

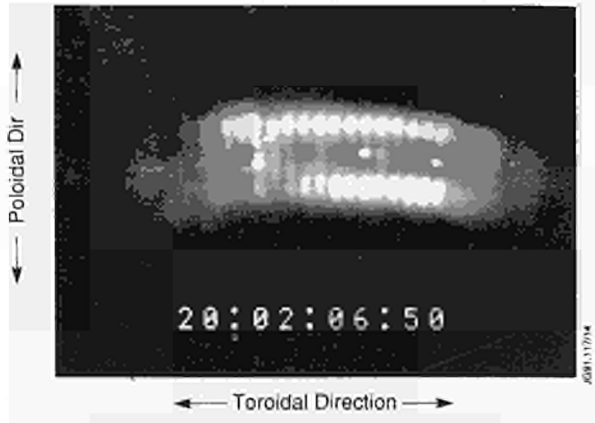

Fig 150(a) CCD image of the lower belt limiter tiles, viewed through a BeI optical interference filter, showing typical footprints for a 3MA ohmic discharge.

Fig 150(b) CCD image of the lower belt limiter tiles for an additionally heated plasma (about 10 MW total input power), showing several bright spots in addition to the regular footprints.

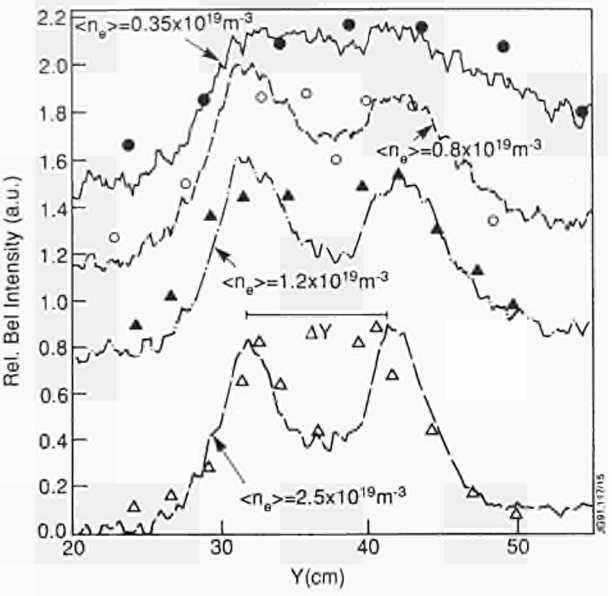

Fig 151 CCD recording of the lower belt limiter poloidal profiles of the BeI intensified at various volume average plasma densities, and the corresponding computed LIM results

Impurity Influxes and Screening

Impurity Influxes and Screening Impurity Influxes

Impurity influxes are generated when outflowing particles (deuterium and impurities) strike the limiter, the wall, or the X-point target plates. At low input powers, the impurity generation mechanism is physical sputtering. This is illustrated in Fig.152, where spectroscopically measured effective sputtering yields (Y_{eff}) are plotted as a function of line average electron density, $<n_e>$, for two different limiter materials and two power levels.

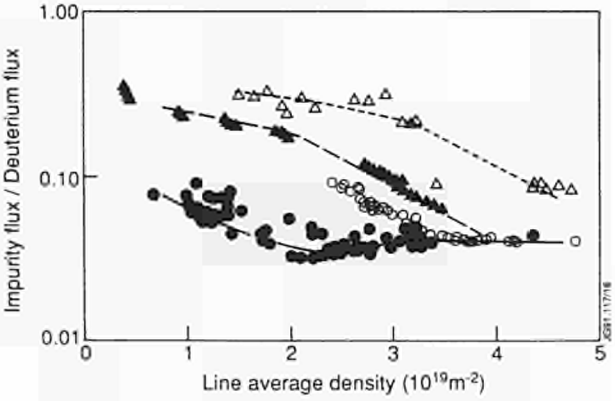

Fig 152 The spectroscopically measured impurity yield for beryllium and carbon (circles) limiters with ohmic (open symbols) and 10 MW of additional heating (shaded).

For constant input power, an increase in $<n_e>$ produces higher edge electron density, and lower edge T_e. Therefore, the energy of ions striking the limiter, and hence the impurity physical sputtering yield is also lower. The monotonic decrease of Y_{eff} with increasing $<n>$ is therefore characteristic of physical sputtering, although the exact shape depends on the detailed behaviour of Y_{DI}, Y_{II}, since - $Y_{eff} = Y_{DI}/(1 - Y_{II})$, where Y_{DI} = Sputtering yield of deuterium on impurity I (eg. Be or C), Y_{II} = Impurity and, I, self-sputter yield.

At high input powers, when parts of the limiter or X-point tiles show strong heating, impurity fluxes increase strongly due to thermal sublimation and radiation enhanced sublimation, for carbon, and due to melting for beryllium. Impurity influxes can increase by two orders of magnitude in such cases, leading to contamination of the plasma core, and a reduction in the plasma reactivity. Some (usually small) fraction of the impurity influx is shielded from the plasma core, by processes in the plasma edge.

However, the shielding factor can be large in both limiter and X-point configurations when strong gas puffing is applied. In such cases, the edge electron density increases while the central electron and impurity densities show little change. This operational regime is only accessible when the walls, etc, are acting as a strong pump, and this suggests that the flow of particles (from the gas value inlet to the pumping surfaces) is trapping the impurity influxes, and exhausting it from the plasma. This process is predicted and is necessary for the projected operation of the JET pumped divertor.

Line Profile Measurements

Multi-Gaussian line fitting routines have been applied to spectrally resolved emission from deuterium and beryllium. Ion temperatures have been measured from the Doppler widths (Fig. 153), and suitable line intensity ratios have been used to measure the edge electron density.

The deuterium spectrum has been resolved into two Gaussian components, giving a "cold" population (5eV) of Frank-Condon atoms, and a "warm" (40 - 200 eV) population of charge-exchange (C-X) atoms. These C-X atoms were previously D^+ ions in the plasma edge, and therefore represent the edge ion temperature, $T_i(a)$. The BeI, and II ion temperatures are lower than $T_i(a)$ because the plasma edge is strongly ionising: these low charge-state ions do not survive long enough to reach equilibrium with the local ion temperature. Line intensity ratios (normally D_α/D_γ and BeI 8254A/Be I 4407A) have been used to measure the edge

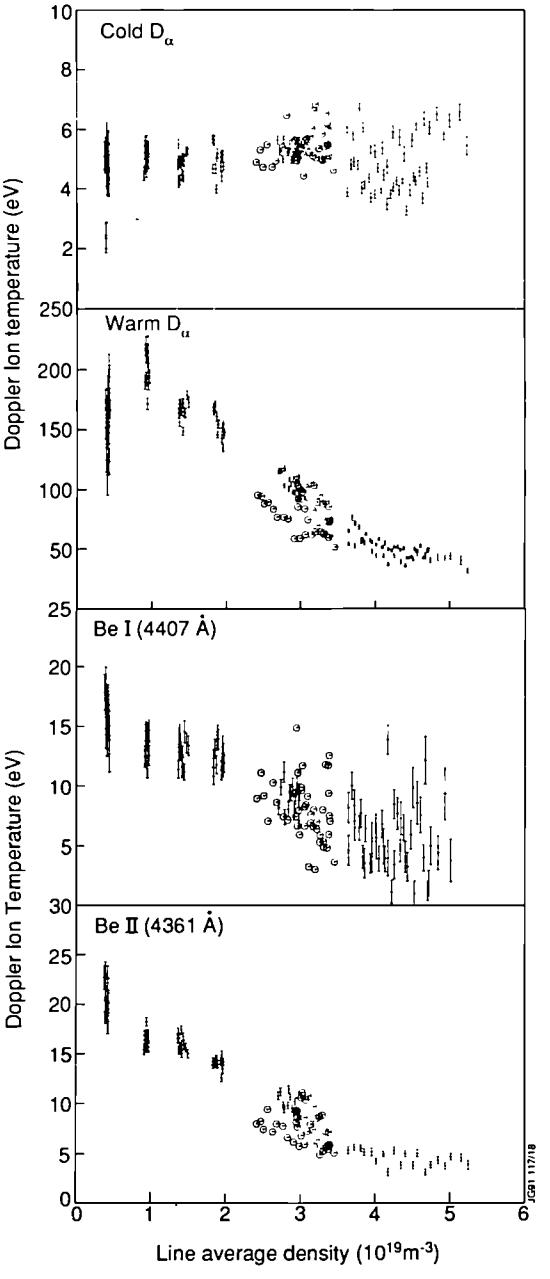

Fig 153 The boundary ion temperature for ohmic heating density scans derived from the Doppler broadening of D_α/D_γ (upper) and BeI (8254 Å)/BeI (4407 Å) (lower) against line average density.

electron density, $n_e(a)$ (Fig. 154) and the results agree with probe measurements.

Correlations of $n_e(a)$, $<n_e>$, $T_i(a)$, Γ_{imp} (impurity influxes) have proved that the impurity and fuel influxes and the edge ion temperature are functions of the edge electron density, rather than the line or volume averaged density (Fig. 155(a) and (b)). This would explain the different scalings observed in different tokamaks, in the deuterium flux, $\Gamma_D \propto <n_e>^x$, where $1 \leq x \leq 3$ depending on the change in the density profile with $<n_e>$.

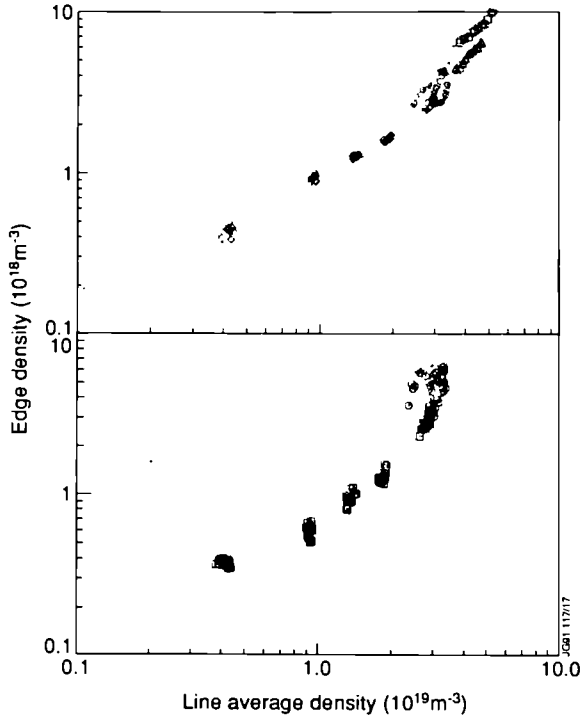

Fig 154 Electron densities deduced from line-intensity ratios, D_α/D_γ and Be I 8254A/Be I 4407A.

The strong pumping of beryllium surfaces in JET has given a degree of density profile control that has still to be fully utilised, but by decoupling the core and edge plasmas, and controlling the impurities in the edge, the potential for increased fusion performance is considerably increased.

Particle Balance Analysis and Pressure Measurement in the Divertor Region

Particle Balance Studies

Analysis of deuterium or helium particle balance in JET discharges serves two main purposes. First, it reveals the distribution of the fuel gas between the plasma and the material structures surrounding it, as not all neutral particles admitted reappear as ions in the plasma. Secondly, it provides information on the amount of gas needed to set up specific densities under different conditions, such as plasma configuration (limiter or X-point discharges) or wall materials (carbon or beryllium). It also elucidates the physical

Fig 155 The D_α ion temperature, D_α intensity and BeII intensity against (a) line average density and (b) edge density.

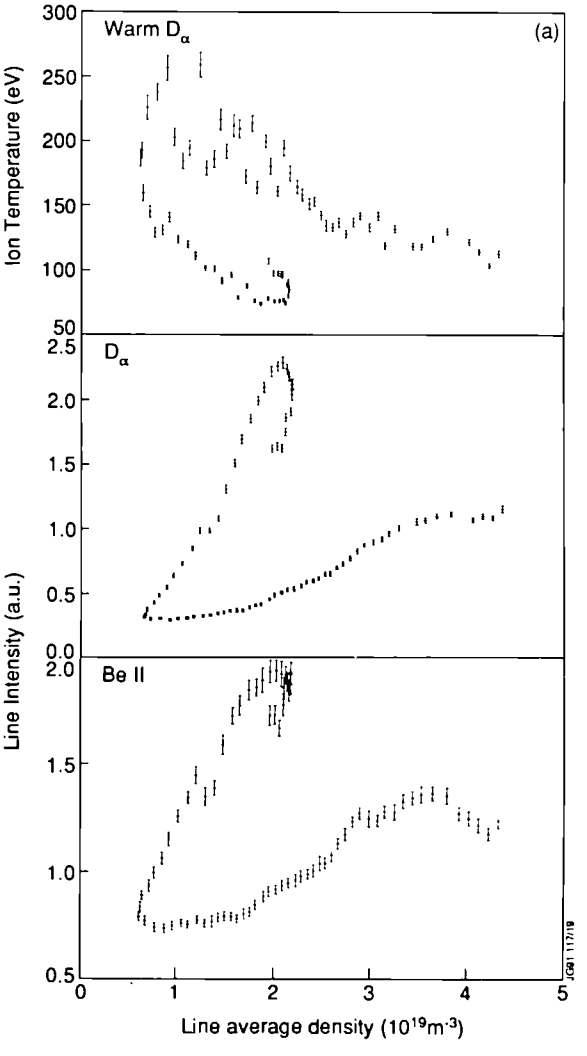

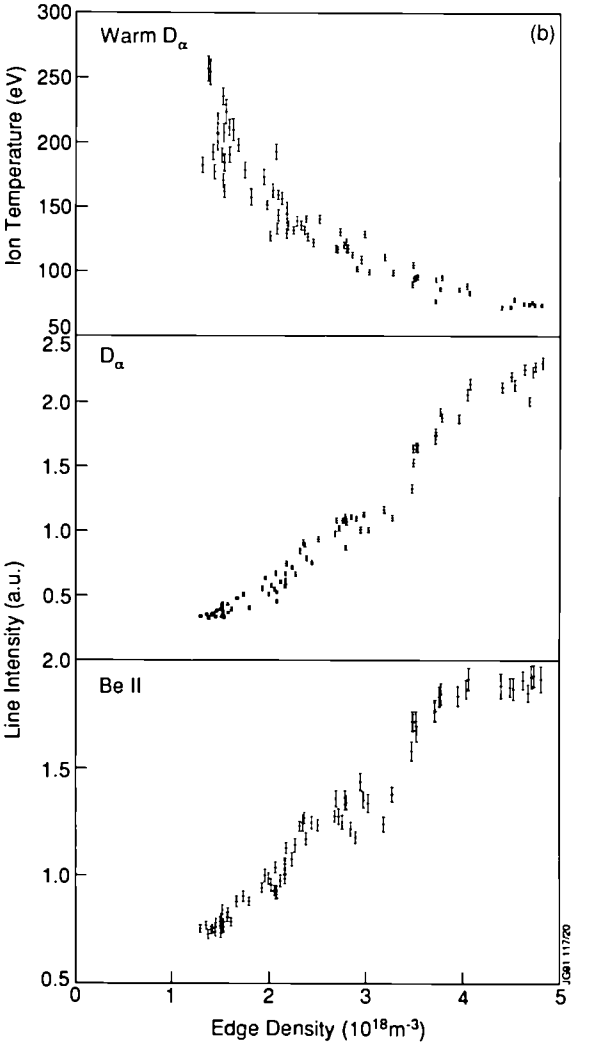

mechanisms which govern particle retention in and release from these structures, which, in turn, affects the fuel (deuterium) contents and, of importance in future D-T experiments, the ash (helium) contents of the plasma. Knowledge of these effects is of particular importance for making estimates of the plasma particle composition in long duration (>1000 s) discharges anticipated in next step fusion machines. Most investigations were performed in ohmic discharges as they provided the most reproducible results.

Before the introduction of beryllium, JET limiters and X-point target plates were made of graphite and the remainder of the vacuum vessel interior was covered by micron thick layers of carbon due to earlier carbonisations and to deposition of carbon eroded from graphite surfaces. From mid-1989, the limiters were beryllium. The carbon surfaces were all covered with beryllium primarily due to evaporation of beryllium in the torus, but also due to erosion from the beryllium limiter and subsequent plasma induced deposition. In 1990, the lower X-point carbon target plates were exchanged for beryllium plates. Even so, locally (particularly at the wall), beryllium surfaces still contain a large proportion (>50%) of carbon.

The beryllium usage has altered the particle balance during discharges. For deuterium discharges, the amount of gas needed to set up a limiter discharge with a certain density has increased by more than a factor of four. There are two reasons: first, the ratio (η_D/η_e) has increased by about a factor of two (dilution reduced from 0.5 to 0.2). Second, limiters and walls pumped larger amounts of deuterium under beryllium conditions than for carbon. [In ohmic discharges at constant current, the pump rate increased from $\approx 10^{20}$ particles/s for a conditioned carbon limiter/wall, to $\approx 10^{21}$ particle/s for beryllium conditions]. The fraction of deuterium admitted appearing as plasma deuterons was typically 0.1 under beryllium conditions, whereas it varied between 0.1 and above 1 for carbon (indicating uncontrolled deuterium release from surfaces into the plasma). These large fluctuations of wall conditions due to varying experimental history and typical for carbon surfaces has been reduced after beryllium use. Most of this also applies to X-point discharges. However, the transition from the limiter phase of deuterium fuelled discharges to the X-point phase causes pumping, which is independent of type of material used in JET for target plates. An example of this is given in Fig. 156(a) and (b). Here, the measured effective time τ_p^* for the deuteron content is indicated for two similar discharges, one with carbon and the other with beryllium. τ_p^* is quite

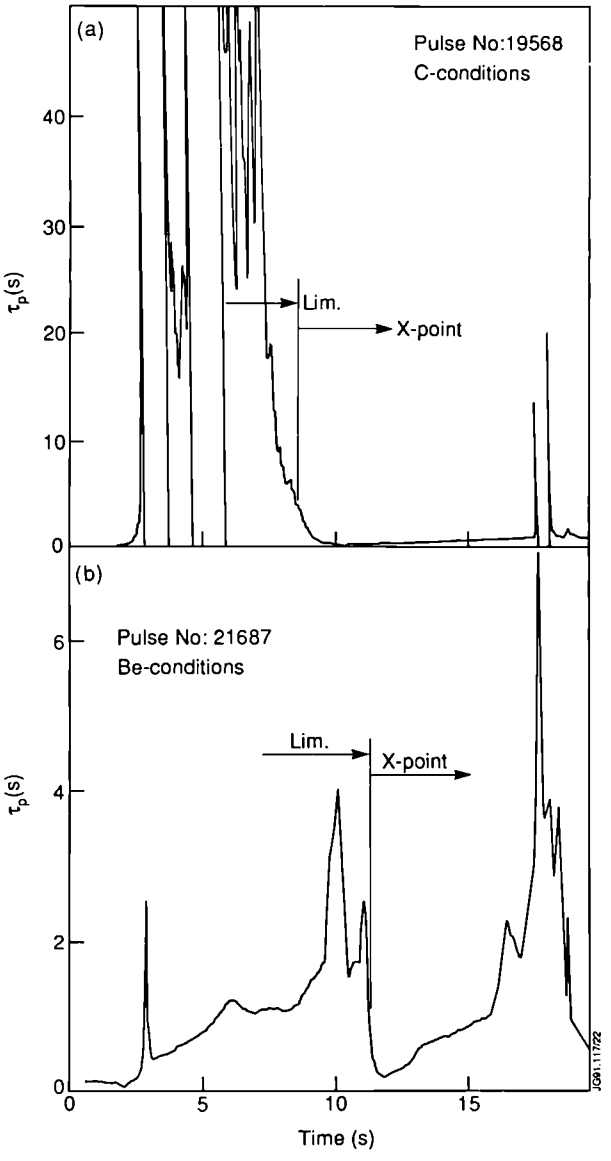

Fig 156 The time history of the effective deuterium delay time for (a) carbon and (b) beryllium conditions.

different during the respective limiter phases. The larger values for carbon indicate larger recycling coefficients or lower pumping rate compared with beryllium. However, after the transition to X-point configuration, the differences disappear and the values for τ_p^* in both cases are as low as they were for the limiter discharge under beryllium conditions. These results are consistent with the onset of increased screening of neutral particles recycling in the divertor region (flux amplification and this flux dominates the external gas supply). For pumping, particles must be retained in the material surfaces and although this is different for C and Be, these differences become less important if the screening effect is large enough. Net particle removal rates from the plasma during X-point discharges $\sim 10^{21}$ particle/s, is slightly lower with carbon, but in both cases were sustained

for several seconds. The gradual increase of τ_p* with time suggests a gradual onset of saturation of the material surfaces with deuterium.

The use of beryllium has also altered the recycling behaviour of He-plasmas. During the carbon phase, all the admitted helium appeared in the plasma. There was no helium pumping which commonly led to a disruption during the plasma current ramp-down. Under beryllium conditions, however, helium was pumped, although somewhat less than deuterium.

Results consistent with these observations are obtained from studies of outgassing of deuterium and helium after the discharges. They indicate that apart from the case of helium discharges under carbon conditions, there is a rather slow outgassing process lasting hundreds of seconds. For deuterium, the fraction of particles put into the discharge and recovered in 1000s is about twice as large (50-70%) with beryllium compared with carbon.

The temporal dependence of the deuterium outgassing rate ($\propto \tau^{-0.7}$) is, within uncertainties, the same for carbon and for beryllium. The total outgassing and the temporal dependence give indications of the possible release mechanisms. Under the assumption of limiters and walls with semi-infinite geometry, (i.e. a bulk material with surface facing the plasma), the deuterium release cannot be well described, regardless of which model for the transport of deuterium within the material is assumed. Much better agreement with experiment is found if it is assumed that a surface layer exists in which hydrogen is dynamically retained (i.e. able to diffuse out) and which prevents deuterium losses to the bulk material. However, no conclusive result can be obtained on the physical mechanisms (diffusion, recombination, detrapping) responsible for deuterium release. Comparison of the initial release rate after the discharge with the final release rate during the discharge indicates that the release processes are likely to be independent of the presence of a plasma, provided a steady state has been reached during the discharge (power flux to the limiter nearly constant).

The existence of a surface layer on walls and limiter has been shown by surface analysis. It is believed to be the result of continuous erosion and depositon processes occurring during discharges. Apart from dynamic retention, these layers also contribute to pumping by trapping deuterium (and helium for the case of beryllium), which is a permanent removal of particles from the plasma not followed by outgassing after the discharge. In combination with the layer build up, this process leads with increasing number of discharges to an increasing deuterium inventory in and at the limiters and walls and means must be found to limit the process in order to limit the retention of tritium in future D-T machines.

Pressure Measurements

An important task is to test and study means of reducing impurity production at the X-point plates and to minimize impurity transport from the X-point plasma into the plasma core during these discharges. Theoretically, this can be achieved by creating a high density, high recycling plasma close to the dump plates. In 1990, three ionisation gauges capable of operating in high magnetic fields (>3 T) were installed forming a linear array close to the X-point target plates. The gauges measure the local neutral particle flux (or pressure) which establishes due to particle recycling and atomic processes between the recycling particles and the local X-point plasma. Results have been obtained with the gauge positioned in the private region between the strike zones of the plasma with the dump plates. The discharge was heated by neutral beams and made a transition from L to H-mode. This has been compared with results from D_α intensity measurements at an equivalent position on the target plates. In general, both signals behaved similarly, and the transition from L to H-mode was followed by a decrease of both signals. However, there were detailed differences which allow conclusions to be drawn about particle and power situation in the X-point plasma. Measured pressures in JET divertor discharges tend to be at least a factor three larger than those found for similar plasmas in other machines, such as D III-D or ASDEX.

Results from a series of discharges revealed, that for plasmas with otherwise identical parameters, the divertor pressure increased with pulse number up to a factor five. This effect was attributed to a memory effect of the carbon target plates due to particle loading in previous discharges causing increased particle desorption and higher recycling.

Estimates from locally measured flux density ($>10^{22}/m^2s$) on the total particle flux striking material surfaces suggest that, even during ohmic divertor discharges, the target fluxes must be $>>10^{22}/m^2s$ and, therefore, higher than the particle fluxes estimated to leave the plasma core. That is, flux amplification at the X-point plates takes place after an X-point plasma is formed, in agreement with results from probe measurements.

Analysis of In-Vessel Components

First-wall components (inner-wall tiles, X-point protection tiles and belt limiter tiles) have been analysed using the ion beam from a 1.6 MeV Tandem accelerator. To allow safe handling of these large beryllium-contaminated samples (up to 400 mm long), analysis has taken place in a glove box fitted with remote handling facilities. This requires that the ion beam passes through a normally used high vacuum analysis chamber and out through a small orifice containing a 6 μm aluminium window into the glove box (which contains helium gas at atmospheric pressure). Helium is used to avoid spurious analysis peaks due to the oxygen,etc, present in air. The facility has been used to continue assessments of the deuterium inventory in the JET vessel, and to examine beryllium belt limiter tiles after operations.

Since beryllium was introduced into JET, much larger amounts of gas (usually deuterium) are needed to fuel the plasma due to a much stronger pumping action. However, at the end of the discharge a much larger percentage of the fuelling gas is emitted from the torus than in the all-carbon machine (pre-June 1989). Gas balance measurements suggest that the long-term retention of deuterium in the vacuum vessel could be similar (as an average per discharge) to that during operations in the carbon phase, but this value is the difference between two large numbers and so is not very accurate. Since the current deuterium retention is very important to the planning of future operations involving tritium (when up to half of the deuterium will be replaced with tritium), a direct estimate of the retention of deuterium has been made from the analysis of first-wall components after use in JET. The results confirm the gas balance measurements that the rate of accumulation of deuterium in stable deposits in the vessel since the introduction of beryllium is similar to that previously observed (a global average for hundreds of pulses of ~ 4 x 10^{20} detuterium atoms per pulse). Another observation of concern for tritium-phase operations is the release of a small fraction of the hydrogen isotopes trapped at the walls when the vessel is vented to air. For the carbon-phase, the number of deuterons released was ≈10^{23} atoms, if venting was carried out without adopting any measures which could reduce this emission. Measurements following beryllium operations show that the release was approximately twice as large as in the carbon phase.

Much of the deuterium retention occurs at the belt limiters, which although they include the areas of most erosion in the torus, also include the areas of maximum redeposition. The results of ion beam analysis of a beryllium tile from the upper belt limiter have shown in that the depth of analysis for deuterium is ≈ 1 μm would be proportionally greater. The general pattern for deuterium includes a maximum near the point of contact with the plasma, minima to either side and a broad subsidiary maximum towards the end of the tile away from the vessel midplane, and is similar to patterns observed previously on carbon belt limiter tiles. The maximum near the tangency point (which in principle is the region of maximum **erosion** on the belts) occurs because most erosion takes place at the **edges** of the tiles, and much of this eroded material is rapidly re-deposited further along the field lines. The situation with beryllium tiles is complicated by the common observation of melting at the tile edges which on resolidification causes a rim to form along the tile edge, which both shadows the surfaces of the tile behind this rim (making it a prime site for redeposition) and makes the edge more liable to melting in subsequent discharges. Thus the analysis of this region is a rather random mixture of raised, resolidified areas (with relatively low levels of incorporated deuterium) and "pools" of redeposited material with large deuterium contents. The beryllium content of the surface region (which is also limited to ~ 1 μm, approximately) decreased towards the edge of the tile nearest the midplane, which indicated an increasing dilution of the bulk material by other elements, principally by the deuterium and by carbon (much of which originates from the RF antenna protection tiles). The similarities between carbon and beryllium-phase results are particularly significant since the beryllium tiles were not expected to retain hydrogen isotopes after high temperature cycling to anywhere near the same extent as graphite tiles (based on laboratory measurements on pure bulk materials).

Exposure of Collector Probes in the Plasma Boundary

Time-and spatially-resolved collector probes have been exposed during 1990 using the Fast Transfer System (near the outer midplane) and the Plasma Boundary Probe System near the top of the machine. Probes have been exposed to over 60 discharges, since the beryllium phase commenced. The results are being collated to show the effects on impurity levels in the boundary of parameters such as different phases of the discharge (eg. profile broadening during the rampdown), auxiliary heating (eg.changing C:Be ratios and profile broadening during RF heating) and position in the torus.

The Fast Ion Collector Probe

Measurements have been made of the helium ion energy distribution near the limiter radius, using of the fast ion collector probe, to study the slowing down of energetic helium ions a and to develop a technique for measuring escaping a-particles in the D-T phase. The technique uses nickel collector probes mounted in an array on the Fast Transfer System as shown in Fig.157. Ions with small Larmor radius, travelling along the field, can only be collected in slot O. Ions with Larmor radius comparable with the probe diameter (50 mm) can enter slots 1 or 2. Both carbon and nickel collector probes have been used in slots 0, $^{+}1$, $^{+}2$.

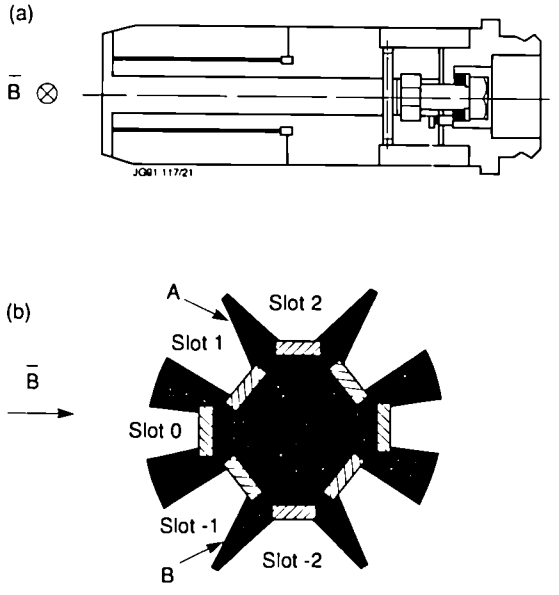

Fig 157 The fast ion collector probe.

The nickel samples have a high trapping efficiency for helium. By sputter eroding these samples and measuring the release rate, helium depth profiles have been obtained. From known range-energy relationships the energy distribution of the incident helium ions can be inferred. Samples have been exposed to a variety of discharges including 120 keV ^{3}He neutral beam injection and ^{3}He minority ICRF heating. In the RF discharges, the mean energy varies with angle between the sample and B_T, from 3 keV parallel to B_T to 8 keV perpendicular to B_T. This is considerably less than the initial energy of the ICRF heated ions (~1MeV) indicating the the $^{3}He^{+}$ ions normally thermalize before escaping from the plasma. However the ratio of the perpendicular to parallel flux is anomalous indicating that there may be a significant fraction of ions with high transverse energy.

References

[1] L de Kock, et al, 12th Int. Con. on Plasma Physics and Controlled Nuclear Fusion Research, (Nice, France, 1988) [in JET-P(88) 78, p89]

[2] S Clement et al, J. Nucl. Mat **176** and **177** (1990) [see also JET-P(90)41 p.155].

[3] S K Erents et al, Proc. 17th Eur. Conf. on Contr. Fusion and Plasma Physics, (Amsterdam, Netherlands, 1990). Europhysics Conference Abstracts Vol. 14B, Part III (1990) 1385 [see also JET-P(90)14 p.177].

[4] H Weissen et al, 32nd APS Annual Meeting, (Cinncinati, USA, 1990). Bulletin of APS vol. 35(1990)1991.

[5] P R Thomas and the JET Team, J Nucl. Mat **176** and **177** (1990) [see also JET-P(90)41, p.1].

[6] C Lowry P J Harbour and J A Tagle, Contributions to Plasma Physics Vol. 28, 1988 no. 4/5 pp 349-354

[7] S K Erents, et al, Nucl. Fusion **28** (1988) 1209

[8] K F Alexander et al, Nucl. Fusion **26** (1986) 1575

[9] C G Lowry et al, 17th EPS Conference on Controlled Fusion and Plasma Heating, (Amsterdam, Netherlands 1990). Europhysics Conf. Abstract vol. 14B, Part I (1990) 339 [see also JET-P(90)14, p.125].

[10] S Clement et alProc. 17th Europ. Conf. on Controlled Fusion and Plasma Physics, (Amsterdam, Netherlands, 1990). Europhysics Conference Abstracts vol 14B, Part III (1990) 1373 [see also JET-P(40)14, p.109.

[11] P C Stangeby, S K Erents, L de Kock and J A Tagle, Plasma Physics and Controlled Fusion **32** (1990)475

[12] J A Tagle et alFusion Engineering and Design **12**(1990) 217.

[13] P J Harbour et al, 31st APS Annual Meeting, (Anaheim, USA, 1990) **11**, 89 (in JET - P(89)80)

[14] P J Harbour, et al, J Nuclear Materials - **176** and **177** (1990) 739 [see also JET-P(90) 41 p.283].

MHD Phenomena

In 1990, studies of magneto-hydrodynamic (MHD) phenomena were undertaken in the following areas:

- m=1 instabilities;
- mode topology;
- simulation of a major current disruption;
- simulation of MARFE's;
- high-β discharges;
- locked modes;

- SVD mode analysis;
- vertical instabilities.

The main advances are described in the following paragraphs.

m=1 Instabilities

Topology of the m=1 Instability during the Sawtooth Crash

Possible limitations of the SXR tomographic analysis in relation to its poloidal resolution have been studied for full-reconnection (Kadomstev) and quasi-interchange (convection) models [1]. If the orientation of the structure is either in the vertical or horizontal plane the two cases can be clearly distinguished. Previously published data was orientated in this way and shows a distinct quasi-interchange pattern that accurately reproduces the emission profiles.

Sudden Onset of Sawtooth Collapse

The displacement of the plasma core is measured from Soft X-Ray (SXR) profile measurements derived using two-dimensional tomography [2]. The onset of the instability was seen to be sudden with a growth rate $\gamma=(25\text{ms})^{-1}$, as shown in Fig.158. Present sawtooth theory cannot account for this. However, by including electron inertia terms into Ohm's law, connection times close to these experimental values have been obtained [3] and is described in more detail in later paragraphs of this section.

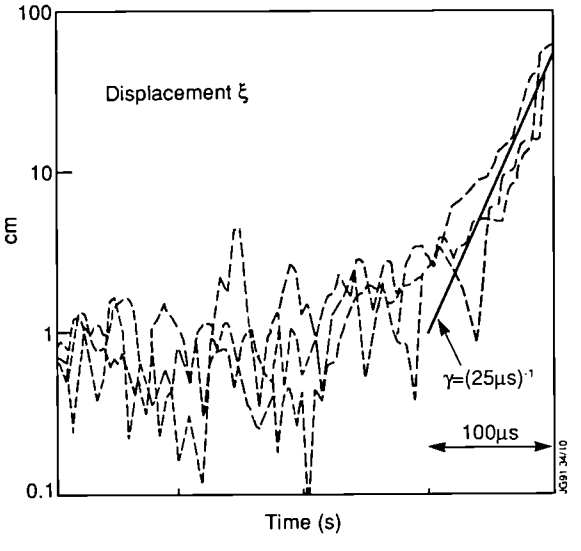

Fig.158: Displacement of the peak of the SXR emission during the fast sawtooth collapse, derived from two-dimensional tomography. Three cases are depicted showing that a constant growth rate of $(25\text{ms})^{-1}$ is maintained up to the collapse phase.

Sawtooth Parameters, Growth Rates and Displacement Times

The displacement of the hot plasma core was measured from the raw data directly [4] to overcome objections to the tomographic technique. A large number of ordinary and so-called monster sawteeth were studied. In all cases, the collapse is characterised by exponential displacements of the central plasma from its equilibrium position to a final position which is 80% (±20%) of the sawtooth inversion radius, on a time scale of $t_{disp}\approx$100-300ms. The growth rate is found to be related to this by $\gamma_{exp}^{-1} \sim 1/3\,\tau_{disp}$. For monster sawteeth, the displacement time is seen to saturate at $t_{disp}\approx$100ms, in good agreement with the predicted growth rate [3].

Sawtooth Parameter Scalings in JET

Several sawtooth scalings have been established from JET results [5]. The inversion radius in ohmic discharges was found to scale strongly with q_{cyl} *and* λ_i, but not with any other global plasma parameter. The scaling with q is supported by polarimetric measurements of the q-profile and is consistent with the assumption that the inversion radius is related to the q=1 position. The sawtooth period was not found to scale with any global plasma parameter. The inversion radius during H-mode discharges decreases in time, typically at a rate of 2cms^{-1} on a resistive time scale. This is expected to be due to respectable bootstrap currents present in the discharge and eventually, in case of even longer H-modes, may result in sawtooth free discharges. Similar effects have been observed previously in the ASDEX tokamak.

ICRF-heated plasmas show an increased inversion radius and sawtooth period. In the case of monster sawteeth, the inversion radius can be 50% larger than in the ohmic case. It is seen that $r_{inv}=r_{q=1}$, within the error-bars on the q-profile. The stabilisation of sawteeth is believed to be due to the fast-ion population leading to an extended sawtooth period in which q=1 radius expands until a threshold in the stability is reached. Indeed, there exists a linear relation between the relative increase in the sawtooth period and the relative expansion of the inversion radius.

Fast Event Trigger

This system was fully commissioned during 1990, and has given a vast amount of information on all kinds of MHD-phenomena occurring during a discharge [4]. Data, on a fast timescale (up to 200 kHz sampling rate), has been obtained

with the SXR, magnetic and ECE diagnostics. Pre- and post-cursors of normal, monster and partial-sawteeth and other MHD modes (like fishbones) have been registered systematically. An example is shown in Fig.159, where several time windows are shown that are obtained by the selective trigger-system in a Pellet-Enhanced-Performance (PEP) discharge, during which various MHD-modes occur.

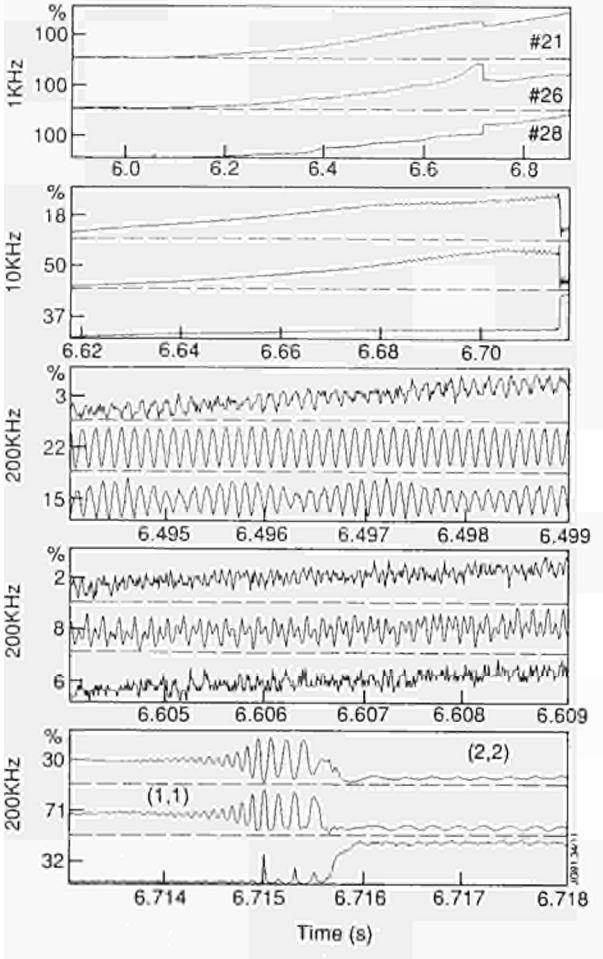

Fig.159: Results from the fast event trigger system. A nearly complete set of data is obtained showing the evolution of the MHD activity in course of a discharge (Pulse No.23079). In the last 200kHz block, the PEP crash linked to (1,1) mode can be seen on diode Nos.21, 26 and 28 located at R=3.14, 3.51 and 3.66m, respectively. The crash is followed by a growing (2,2) mode leading to substantial rearrangements in radial profiles.

Spontaneous Snakes

An example of MHD activity found with the new trigger system, which allows selection of particular events of interest, is the spontaneous snake. Snakes were originally discovered in JET following pellet injection and were shown to be regions of high plasma density in the q=1 surface with m=n=1 topology.

Recently, snakes have been observed immediately after the onset of the sawtooth oscillation and following neutral beam injection. It would appear that these "spontaneous" snakes are a more general feature of MHD behaviour in a tokamak than had been previously realized. These are formed following a period of m=1 activity which was probably associated with the central q value falling below unity. These latter snakes have many similarities with the pellet induced snakes, except that their density perturbation is very much smaller and their main characteristic is that they are small regions of very much increased impurity density. There is also some evidence that spontaneous snakes were observed but not recognised, as long ago as 1984. An example of a spontaneous snake observed during neutral beam injection is shown in Fig.160. The spontaneous snake survives many sawtooth crashes and can be be used to monitor the position of the q=1 surface immediately after the onset of sawtoothing (Fig.161).

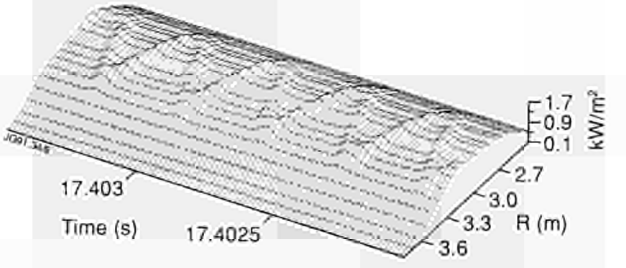

Fig.160: The spontaneous snake seen by the SXR vertical camera as a function of time for Pulse No.22334.

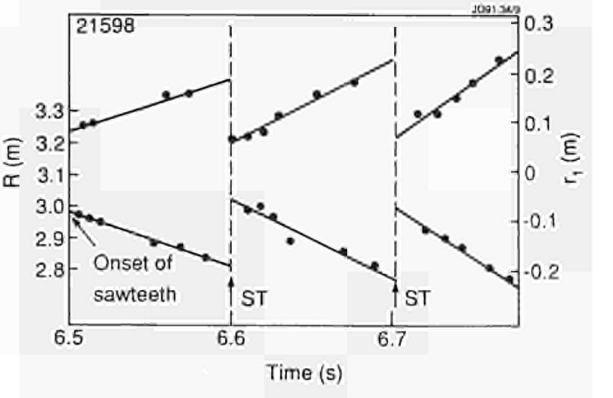

Fig.161: The evolution of the radial position of the snake during a sawtoothing discharge (Pulse No.21598). The expansion of the q=1 radius (2.5ms^{-1}) in between the sawtooth crashes can be seen and is a factor of one hundred faster than the expansion of the inversion radius in an H-mode discharge, indicating a low shear region near the q=1 surface.

Sawtooth Reconnection

Under the usual conditions of sawtooth reconnection in a tokamak, the electric field resulting from the flux reconnec-

tion becomes very large [3]. This leads to an acceleration of the electrons in the reconnecting layer, such that the reconnection times are determined by the electron inertia rather than by electron collisions. Reconnection times are decreased by an order of magnitude compared to Kadomstev reconnection times. Inertial reconnection times are typically around 300ms for a full flux reconnection within the q=1 surface in JET plasmas. If q(0) is not restored to unity, these times become even shorter. Other effects such as finite Larmor radius, possible anomalous electron viscosity and velocity space instabilities of the runaway electrons in the layer may also play a significant role in the process, but these have not been included in this study.

Electron Inertia, Ion Larmor Radius and Magnetic Reconnection

In high temperature JET discharges, electron inertia replaces the collisional resistivity in causing reconnection at the q=1 surface [6]. If a fluid ion equation of motion is assumed, the reconnection takes place in a layer whose width, δ, is of the order of the plasma skin depth, d. However, for realistic plasma parameters, the ion Larmor radius, ρ_i is significantly larger than the plasma skin depth. A linear kinetic theory, which treats the ion dynamics correctly has been developed. Growth rates $\gamma/\omega_A \approx (\delta/r_s)(\rho_i/d)^{2/3}$ and layer width $\Delta \approx \rho_i$ have been found, where ω_A is the Alfvén frequency and r_s is the q=1 radius. For typical JET parameters, $\gamma \approx 50\text{-}100\mu s$. Interestingly, for $\rho_i < d$, the linear theory yields a growth time $\gamma^{-1} \approx \tau_A(r_s/d)$ and a linear reconnection layer $\delta \approx d$, which are comparable to the non-linear ones. This suggests that the linear theory remains relevant up to relatively large mode amplitudes, as also hinted by the experimental observation of a continuing exponential growth rate up to displacements comparable with the sawtooth inversion radius (Fig.158).

Magnetic Topology

This theme has been investigated by measuring the MHD activity with several diagnostics sampled at high frequencies (10-200kHz) at the same instance in time. The diagnostics involved are the magnetic pick-up coils, the polychromator and the heterodyne radiometer for the electron temperature, and the reflectometer for the electron density and the soft X-ray cameras. Simultaneous measurements of the MHD activity have been made in 1990 during the current rise, the PEP (pellet enhanced performance) mode and the monster sawtooth. Some of the results are presented below.

the low-field side of the mid-plane at toroidal angles 180° apart. This coupling corresponds to a maximum in the mutual energy between helical wires of toroidal mode number n=1 having a constant current in the same direction. In Pulse No:20209, several MHD modes are excited and a snake is formed on the q=1 surface after pellet injection. The dominant modes have n=1 and n=2 components. After a few hundreds milli-seconds, these modes couple together before the rotation slows down and the modes lock. Fig.162 shows a tomographic reconstruction of the soft X-ray emission in a poloidal plane just before locking. The snake (at the position of the "O-point" of the (1,1) island) can be seen to be aligned with the "X-points" of the (3,2) and (2,1) islands on the low-field side of the mid-plane. The position of the corresponding rational surfaces is in reasonable agreement with the computed q-profile. The observed coupling between the "O-point" of the (1,1) island and the "X-points" of the (3,2) and (2,1) islands suggests that there could be a current excess in the snake. However, this seems to be in conflict with a lower electron temperature initially (20% up to 100ms) seen in the pellet induced snake, that itself last up to 2s, and the higher impurity concentration in the spontaneous snake, which suggest a higher resistivity and therefore

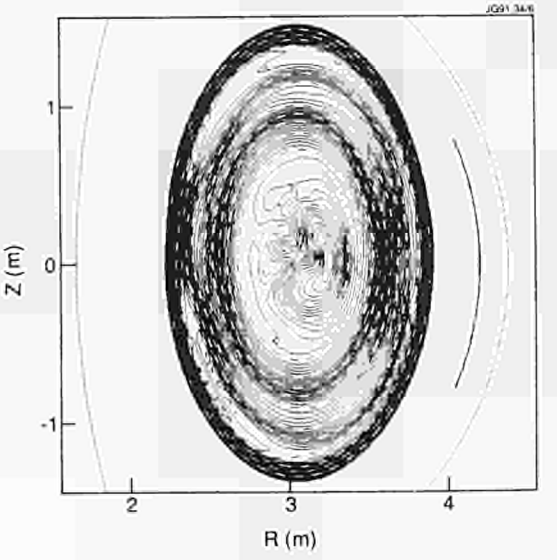

Fig.162: Cross-section of plasma, as seen by the SXR cameras, during a pellet injuced snake with MHD activity. The snake is phase coupled to a (3,2) mode and a large (2,1) resistive mode, with the X-point of these modes orientated in this cross-section in the outer toroidal mid-plane. The contours have a logarithmic scale in 70 equally spaced steps from 15 to 0.1kW/m^3.

Application of Coupling between Islands to determine the direction of Perturbed Current in the Snake

Experiment shows that, when the m=1, n=1 and m=2, n=1 islands are coupled, their "X-" and "O-points" are aligned at

a current deficit in the snake. Clearly, further study is required.

Current Rise Studies

Current rises with a ramp rate of ~1MAs^{-1} have been made in 1990 in preparation for a 7MA limiter discharge campaign. Magnetic modes are observed to be destabilized, when the field line safety factor, q_φ, at the plasma edge decreases and before it reaches an integer or half-integer value. This is an indication that these modes are resistive, since their resonant surfaces are located inside the plasma. Most of the study has been focused on the crossing of the q_φ=4 surface at the plasma boundary. From an operational point of view, two cases can be distinguished:

- at low inductance, with high central electron temperature and low density, the radiation is low and current penetration is slow. The axial safety factor q(0) computed with a magnetic equilibrium code is larger than 1.5. The magnetic diagnostic measurements indicate the presence of a dominant m=4, n=1 mode at the plasma edge and give a radial width around 10cm for a magnetic island on the q_φ=4 surface. When q(0) is larger than 2, hardly any mode can be detected from the soft X-ray emission in the plasma centre and the current rise is successful. In the opposite case, a dominant m=2, n=1 mode is measured by the soft X-ray cameras at the plasma centre and there is a persistent locked mode, which can terminate the discharge by a disruption;
- at moderate inductance, with low central electron temperature and high density, the radiation is high and current penetration is fast. q(0) becomes smaller than unity early in the discharge. A dominant m=2, n=1 mode is measured by the magnetic pick-up coils. A tomographic reconstruction (Fig.163) of the soft X-ray emission shows an m=2, n=1 island, which is 8-10cm wide radially. The island width and the position of the q=2 surface agree with the magnetic measurements and calculated q=profile.

PEP Mode

During the PEP (Pellet Enhanced Performance) mode, the neutron yield reaches a maximum a few hundred ms after injection of a pellet and application of additional heating before decaying in approximately the same time during the additional heating phase. There is experimental evidence

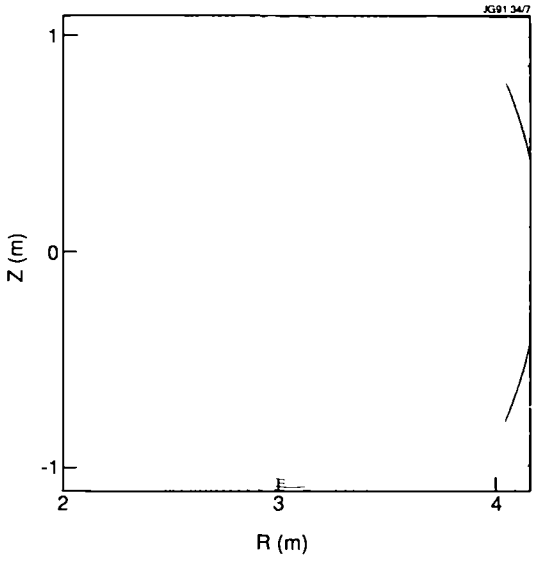

Fig.163: Contours of equal X-ray emission on logarithmic scales in 35 equally spaced steps from 3.5kW/m^3 to 3.5mW/m^3 during a current-rise experiment for Pulse No.21604 at t=1.4636-1.4658s, showing a resistive (2,1) MHD mode at the calculated q=2 position.

that the collapse of the neutron yield is triggered by a fast MHD event. This event causes a moderate increase of the impurity influx at the plasma boundary.

Before the event, the discharge is now sawtoothing, the safety factor on-axis calculated from a magnetic equilibrium code is above unity and MHD modes are observed with a main toroidal mode number n=2, 3 or 4. The MHD event occurs in the central region of the plasma and has a dominant toroidal number n=1 (from the magnetic and soft X-ray emission measurements). After this event, the postcursor oscillations generally have a dominant m=2, n=2 mode in the central zone of the plasma. In some cases, the precursor and postcursor oscillations measured on the electron temperature are non-sinusoidal, having a narrower maximum than the minimum. A careful and thorough analysis of the experimental data is underway to confirm these preliminary observations and to determine more accurately the nature of the MHD event and the magnetic topology.

Simulation of Density Limit Disruptions

The Article 14 Contract on "Numerical Simulation of Disruption on JET using a Cylindrical Resistive 3-D Reduced MHD Code" with CRPP Lausanne, Switzerland, was completed in December 1990.

MHD activity during density limit disruptions is numerically modelled by a three-dimensional resistive reduced MHD code with a simple transport model and radiation losses. The simulations reproduce the following sequence

of experimental events: destabilization of MHD modes near the plasma edge during the early contraction phase; growth of the m=2, n=1 mode to large amplitude; several minor disruptions; and the major disruption. The main results is a new theoretical description of the major disruption, which agrees with the experimental observations in JET. The major disruption takes place in two phases: flattening of the temperature in the central region by an internal relaxation has a mainly m=1, n=1 displacement, consistent with the observation of "profile erosion" in JET. During the "erosion", the (1,1) mode has a strong convective character as can be seen from the kinetic energy of the various modes shown in Fig.164, at t=2800τ_A. The magnetic perturbation has also a strong m=3, n=2 component because of non-linear

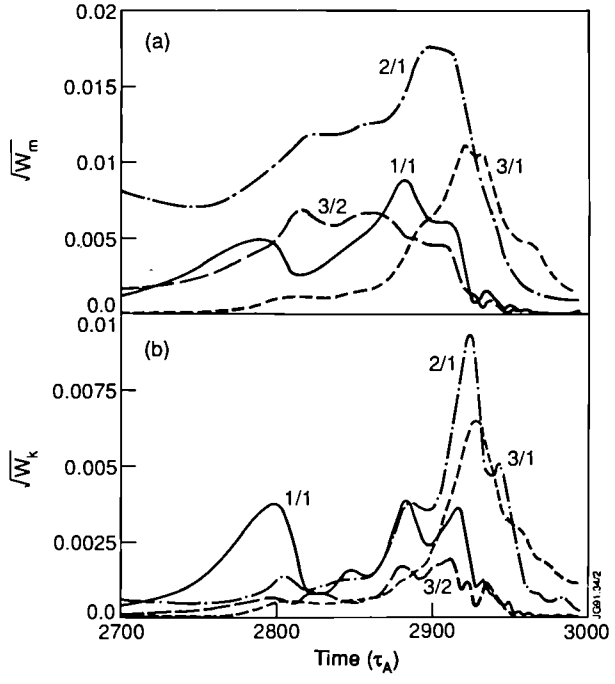

Fig.164: The calculated magnetic (top) and kinetic (bottom) energy of the various modes occuring inside the plasma during a major disruption (energy quench phase).

coupling with the large m=2, n=1 mode. The large amplitude (2,1) (1,1) and (3,2) modes give rise to stochastic magnetic fields first in the q=1 region and then inside q=2 at the end of the internal relaxation. During the second phase, ~t=2900τ_A, MHD turbulence develops in the stochastic field, which results in a filamentation and a broadening of the current density, first starting in the central region. This leads to a rapid growth of the m≥2, n=1 modes, resulting in a full magnetic field stochastisation and current profile broadening across the entire plasma at the end of the disruption.

Simulation of MARFE Behaviour at the Density Limit

A new linear theory has been developed for the MARFE. Also a 2-D transport code has been developed and used to study the MARFE, an example of such a simulation is shown in Fig.165. The results show how the radiated power fraction to trigger a MARFE increases with the parallel thermal conductivity. Since parallel thermal conductivity ($\chi_{\parallel}$) is a strong function of temperature, ($\chi_{\parallel} \propto T_e^{5/2}$), MARFE's will form at lower radiated power fractions as the edge temperature is reduced. This suggests that the differences between beryllium (MARFE's form at P_{rad}/P_{in}≈40%) and carbon (formation at 100%) limiters, may be that discharges with beryllium limiters have impurities which radiate at lower temperatures; this is currently under investigation. Other theoretically predicted dependencies of the MARFE threshold on input power are found to be in good agreement with experiment.

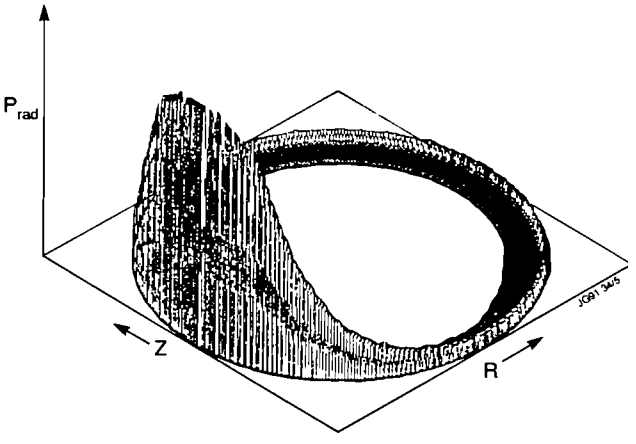

Fig.165: Simulation of a MARFE showing radiated power P_{rad} in a constant toroidal angle plane (R,z).

High-Beta Discharges

Experimental Programme

No specific high-beta programme has been carried out in 1990. However, some low-q inner wall discharges came close to the Troyon limit, with beta values ~5%. The most interesting work on beta-limits was carried out in PEP (Pellet-Enhanced Performance) and H-mode combinations, where very steep pressure gradients were produced in the plasma core. It is possible that the collapse of the very peaked profiles is related to local beta effects, although globally the plasma is well below the toroidal beta limit. Discharges, such as Pulse No.22490, are being analysed for their stability limits [8].

Computational Studies

Analysis of the high-β shots in the range of Pulse Nos:20200 to 20900 was completed. Most discharges near the Troyon

limit have a triangular pressure profile, which within error bars on the equilibrium reconstruction is found to be marginally stable to n=∞ ballooning modes. In some cases (particularly those which have a very peaked pressure profile due to pellet injection), the core is unstable to n=∞ ballooning modes and cannot be stabilised by credible adjustments to the q-profile. For such cases, the effects of hot trapped particles, on the ballooning stability has been studied. Using the Pencil model to assess the hot particle population ($\omega_D > \omega_{*_i}$) from the neutral beams (≈10MW), it is found that the trapped particles should be sufficient to stabilize the ballooning modes in the core (which is otherwise ideally unstable) [9].

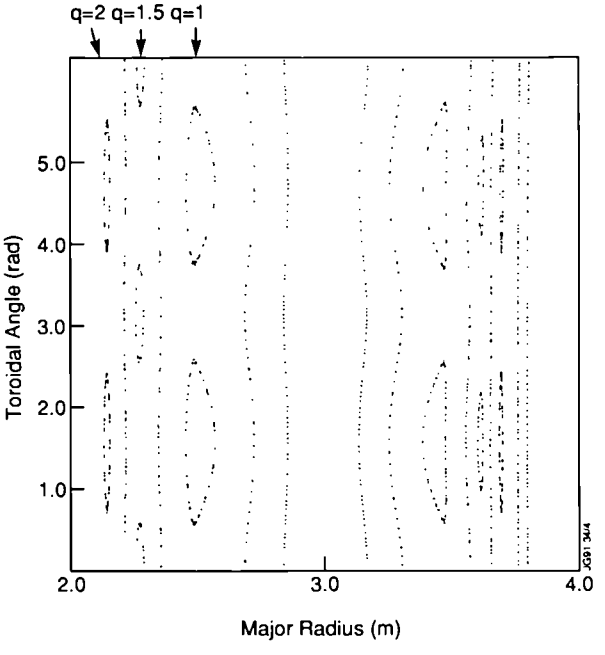

Fig.166: Flux surfaces in the horizontal midplane showing n=2 high β instabilities at the various rational q surfaces.

In 30-40% of the discharges with $\beta > 0.7\beta_{Troyon}$, there is a 'rapid' collapse of β. This is almost always associated with large n=2 activity. Studies with the toroidal resistive MHD code, FAR, show that the most likely candidates for the n=2 activity are the pressure driven infernal modes occuring in the low shear core region. Soft X-Ray (SXR) chord measurements reconstructed from the theory calculations give a reasonable match to the observed SXR signals during n=2 β-collapse activity. Fig.166 shows this calculated mode activity at the various rational surfaces in the toroidal horizontal midplane.

Large Amplitude Modes

Large amplitude modes can exist in various plasma conditions as seen in previous sections. Magnetic perturbations can be as large as $\delta B_r/B_T \approx 1\%$ at the plasma edge and typical growth rates are 10^2 to $10^3 s^{-1}$. Usually, these modes are initially rotating and hence are visible as oscillations on electron temperature, density, soft X-ray and magnetic diagnostics. As the modes grow in amplitude, their rotation (and the plasma rotation, also) slows down and comes to a complete standstill. The modes are then referred to as locked modes. Once the perturbations are locked, it is difficult to analyze them using the standard technique used on rotating modes. However, using the radial magnetic field or saddle coils, it is possible, by careful removal of n=0 fields (e.g. shaping fields), to study the evolution of these long-lived modes. This has revealed that a so-called locked mode which can persist under certain conditions over most of the discharge changes its structure in time. For instance, the structure changes from a dominant m=4, n=1 mode to a m=2, n=1 mode when the inductance increases as a function of time (Fig.167).

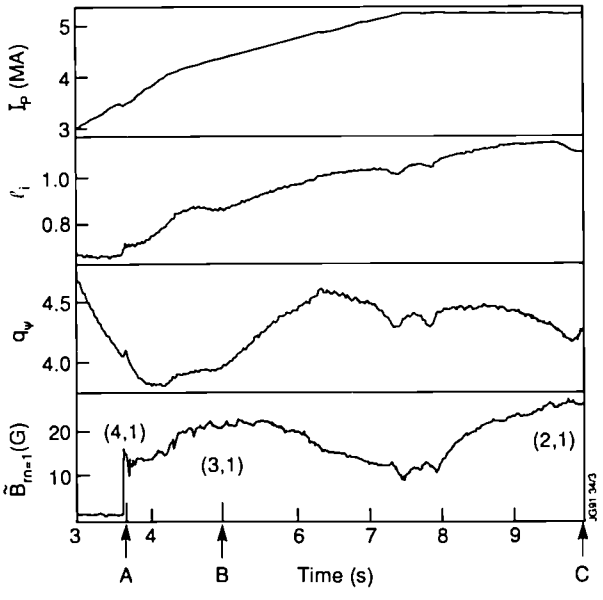

Fig.167: Time history of a 5MA discharge (Pulse No.22442) with a long lived locked mode. The mode starts at 3.6s, when the q=4 is reached and lasts up to the end of the discharge. At the time A, the mode has a dominant (4,1) character but changes in time. At time B, it has a mainly (3,1) and it becomes a dominant (2,1) at time C.

A different type of locked mode has also been studied in some detail. This mode has no rotating phase, in contrast with the above. The development of this perturbation (dominant m=2, n=1 as seen on the saddle coils) was first observed in low density X-point configuration discharges, but has also been found in low density inner wall discharges and high plasma current pulses. All these discharges have a high degree of shaping in common.

Singular Value Decomposition (SVD) Mode Analysis

A new method has been devised to analyse the Mirnov coil signals, in order to detect the MHD modes spatial distribution and temporal evolution. It can be used on any set of oscillating signals coming from many channels distributed in space. The technique relies on the Singular Value Decomposition (SVD) of a rectangular matrix X. The SVD of a square matrix reduces to the well-known diagonalisation. The columns of X are the sampled time series of a particular channel, i, while the rows given the configuration vector at a given instant, t, in time. The SVD generates two set of orthogonal eigen-vectors which, respectively, give the spatial distribution and the time evolution of the amplitude of the modes detected, without the necessity of additional assumptions. This is particularly useful in the case of the dependence on the poloidal angle. In the case of a sum of pure sinusoidal modes in the space variable, pairs of degenerate singular values are obtained from the SVD, which correspond to the sines and cosines components of the mode with a given m number. these singular or eigen-values are proportional to the amplitude of the mode itself. An example is given in Fig.168, which refers to PEP discharge (Pulse No.23081). It shows the amplitude of the m=4, n=1 mode, around the poloidal plane for the cosine and sine components. The asymmetry around the poloidal angle can be seen.

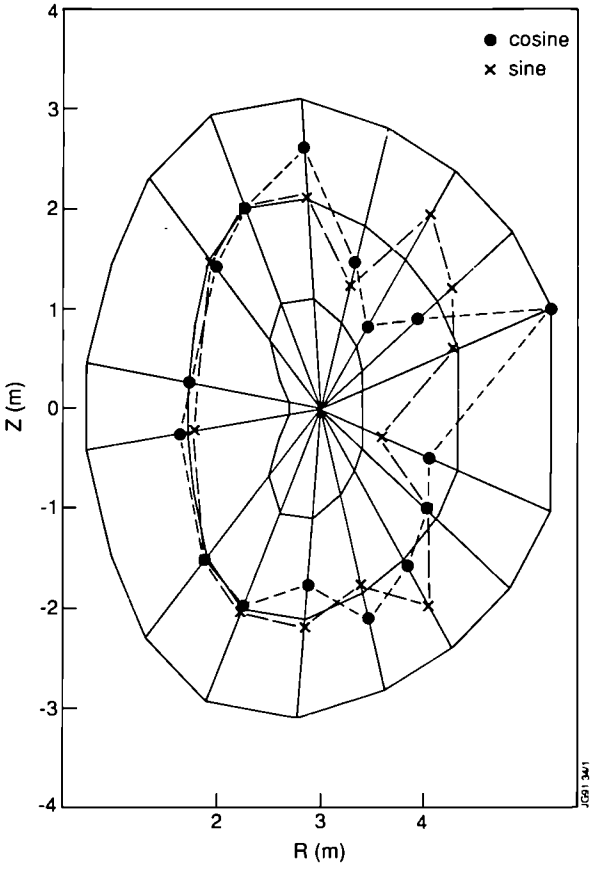

Fig.168: Amplitude of the cosine and sine component of the MDH mode analysed with the SVD method shown in the poloidal plane at 5.8s in a PEP discharge (Pulse No.23081). The mode has (4,1) feature, determined by the poloidal and toroidal pick-up coils used in the analysis. The m=4 character can be seen. Note the strong in/outside asymmetry of the mode.

The Evolution of Disruptive Plasmas in JET with Beryllium

The dynamics of plasma disruptions is strongly affected by the material of the limiter and inner wall. The disruptive plasma is further contaminated by the wall particles which are produced during the strong plasma wall interactions that already took place at the onset of the disruption. The current decay time is determined by the plasma resistivity which in turn also depends on the radiative losses caused by the first wall material entering the plasma. In JET discharges with graphite limiters, large amounts of power can be lost through radiation, resulting in relatively short plasma current decay-times. With beryllium, the plasma current decay is much longer, up to ~1s. With beryllium, the plasma energy quench is followed by a series of minor disruptions of increasing frequency. The power lost through these relaxations is between 20 and 40MW and can be the main power loss, much larger than the radiated power.

In the case of fairly elongated discharges, with b/a>1.65 at the onset of the first energy quench, the control of the vertical plasma position can be lost (20% of the cases) and the plasma abruptly moves vertically. However, the vertical movement slows down after an exponential growth. There is experimental evidence from toroidal field pick-up coils that strong poloidal currents of up to 1MA flow from the plasma into the vessel components and wall which steady the plasma motion and at the same time transfer the destabilising forces to the vacuum vessel. A model of the poloidal currents in the plasma and vessel due to these kind of disruptions in JET explains the forces on the vessel components [10]. The calculated vertical force on the vacuum vessel is in good agreement with that measured on the vessel supports of up to 300 tonnes.

References

[1] Wolfe, S. et al. Proc. 17th European Conference on Controlled Fusion and Plasma Physics (Amsterdam, the Netherlands) (1990);

[2] Wesson J., Edwards A., Granetz R., Nuclear Fusion, Vol.31, No.1, 111-116 (1991);
[3] Wesson J., 13th International Conference on Plasma Physics and Controlled Nuclear Fusion Research (Washington, U.S.A.) (1990) and JET Report-JET-P(90)62;
[4] Edwards A., et al, to be published;
[5] Pearson D., Ph.D. Thesis in preparation;
[6] Porcelli F., JET Report -JET-P(90)23, to be published in Phys. Review Letters (1991);
[7] Bondeson A., Parker R. and Hugon M., JET Report-JET-P(90)73;
[8] Huysmans G., et al, Plasma Physics and Controlled Fusion, **31** (1989)2101;
[9] Hender T., et al, Proc. 17th European Conference on Controlled Fusion and Plasma Physics (Amsterdam, the Netherlands) (1990);
[10] Marcus F.B., et al, Nuclear Fusion **30** (1990)1511.

Physics Issues Relating to Next Step Devices

The objective of this Topic Group was to consider physics issues relating to Next Step devices, which were relevant to JET. These are described in the following.

Simulation of Helium Ash Production and Transport

The successful operation of one NI Box with ^{3}He and ^{4}He beams at 120kV has provided the possibility of simulating production of He ash in the core of the plasma. This has been achieved by virtue of the excellent penetration and central deposition of the He beams. The use of NBI as a He particle source for transport experiments is intrinsically more satisfactory than gas modulation, since the deposition profile of the He beams is precisely known, and the radial flux of He^{2+} can then be determined accurately from the temporal and spatial evolution of the He^{2+} density profile. Such profile measurements have been obtained from the intensity of the He II charge-exchange (CX) line observed via a multi-chord array, in the presence of Deuterium diagnostic beams. The results represent the first experimental test in JET of this CX technique applied to He^{2+} ions, for which the method was developed to diagnose fast and thermalised α-particles during future D-T operation.

Preliminary results on He transport have been obtained. The 80ms time resolution of the present He^{2+} profile data makes it difficult to relate the He^{2+} radial flux Γ_{He} to the density gradient ∇n_{He} in all cases, due to the presence of sawteeth which occur between successive measurements. Nevertheless, initial conclusions can be drawn on the relative behaviour in L and H-mode plasmas. In a sawtoothing L-mode discharge, the characteristic time for He removal from the plasma core is ~ τ_E, which is favourable for a steady-state reactor. This is illustrated in Fig.169, where the redistribution of the centrally deposited He is seen in the central decline of He^{2+} density and in the simultaneous increase of He I edge recycling light. In H-mode plasmas, the behaviour is more varied; in some cases, there is evidence of He retention in the plasma core, in contrast to the L-mode cases. The results point to the importance of confinement regime, sawteeth, and ELMs in determining the efficiency of He removal/exhaust. Preliminary evidence has also been obtained for the existence of a frictional interaction between

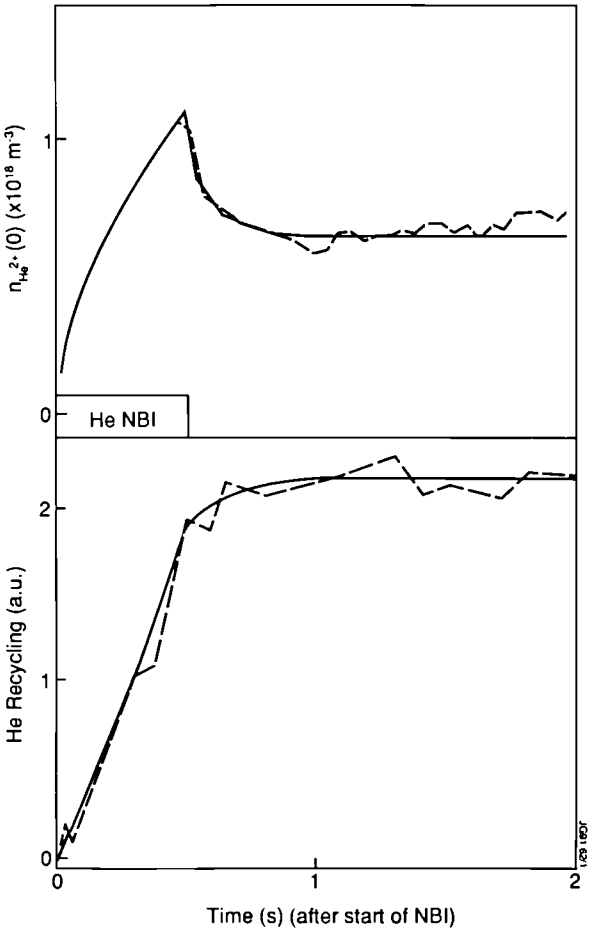

Fig.169: Measured (dotted line) and simulated (solid line) central He^{2+} density and edge recycling following (0.5s, 5MW, 120kV, ^{4}He) NBI pulse, in sawtoothing L-mode discharge (Pulse No:22977). The simulation assumes an effective diffusion coefficient $D_{eff}(r) = 0.4(1+2r^2/a^2)m^2s^{-1}$.

radial flows of D^+ and He^{2+} ions. This is expected on the basis of a model [1] of tokamak transport in which the anomalous terms arise from parallel transport along chaotic lines of force, projected onto the radial direction. The basic physics of this effect is identical to impurity control by forced plasma flow in a divertor. The present result, if confirmed, could have significant implications for a steady-state reactor, since hydrogenic species, necessarily deposited close to the edge in a reactor plasma, must flow inwards against the outflux of He ash in order to refuel the plasma core. The consequences are presently being investigated in simulations.

It is planned to perform further experimental He transport studies in 1991. Additional technical developments to both the CX diagnostic and NB systems (eg. 100% beam modulation) will permit a large improvement in signal/noise ratio and time resolution of the He^{2+} profile measurements, enabling further elucidation of all these phenomena.

Beam Driven and Bootstrap Current Studies

Neutral Beam Current Drive (NBCD) studies have been undertaken for NET/ITER geometries at the request of the NET team. Using the usual theory of NBCD, which was again validated for the 140keV D^0 system on JET in 1990, extrapolations were performed for the results of large machines using the NET/ITER geometry and equilibria. The extrapolation involves the NBCD dependence on injection angle; and dependence on beam deposition profiles (principally through dependence on density and beam energy) as validated on current machines and dependence on T_e. The NBCD efficiency $\eta(=R_o \langle n_e \rangle I_{NBI}/P_{NBI})$ depends roughly linearly on T_e when beam slowing down is primarily on the electrons (as in the case of ITER). This dependence on T_e, though well understood, makes it extremely difficult to give precise current drive efficiency figures for ITER. The PENCIL code predictions have been run for many ITER cases and compared with analysis performed elsewhere. Figs.170(a) and (b) show the variability of η achieved for two density profiles. The profile comparison is made for two plasma scenarios; (i) the steady state ITER case with $\langle T_e \rangle$ = 20keV; and (ii) the ITER hybrid case with $\langle T_e \rangle$ = 11keV.

The central values of T_e and n_e are obtained by preserving total β. One noticeable feature of the graphs is the relatively slow variation of η with beam energy (E_b) around the standard ITER value of E_b = 1.3MeV. The current drive

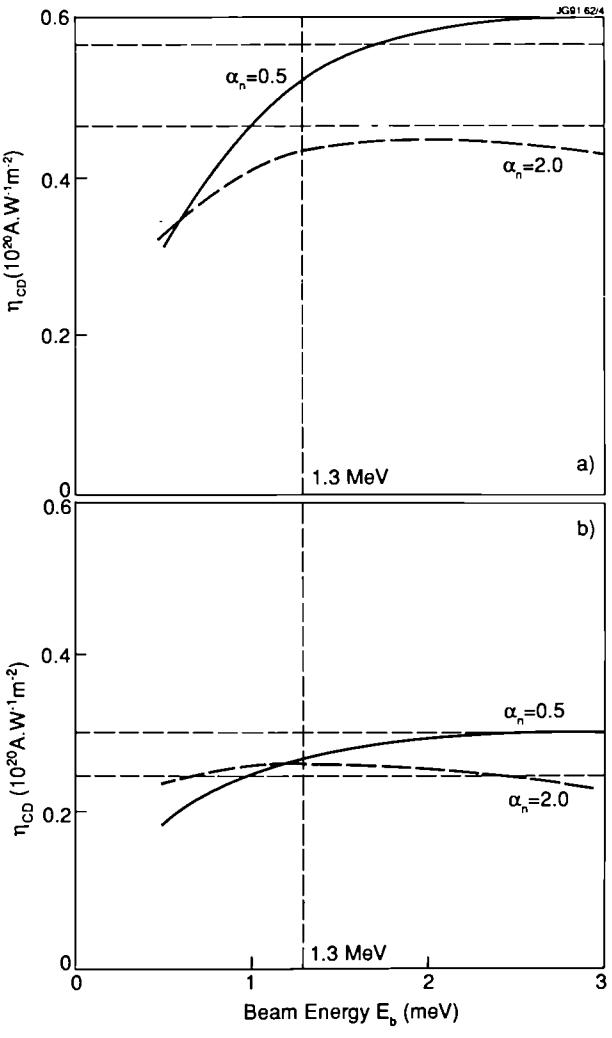

Fig.170: Predicted NB current drive efficiency (using the PENCIL code) for different density profile peaking factors (a_n) as a function of beam energy (E_b) for two standard ITER plasma scenarios: (a) the full non-inductive steady-state ITER plasma with $\langle T_e \rangle$ = 20keV; (b) the ITER hybrid case with $\langle T_e \rangle$ = 11keV. The horizontal bands indicate the ± 10% limits on the central value of η_{CD} obtained for the ITER reference beams which have E_b = 1.3MeV. Note that the central value of density ($n_e(0)$) is obtained by keeping β constant separately for each ITER case.

efficiency varies by < ± 10% between E_b = 1.0MeV and E_b = 2.0MeV for the flatter density profiles.

Studies have also been undertaken on the current profile to be expected from the ITER beams, in the case where beams are positioned off-axis in the vertical direction and aimed parallel to the mid-plane. It is foreseen that the ITER NBI system would have vertically steerable beams to build a profile control capability for non-inductively driven current. An example of the variable profiles of non-inductive beam current obtainable from such a system is shown in Fig.171.

Bootstrap Current Studies have also been performed on

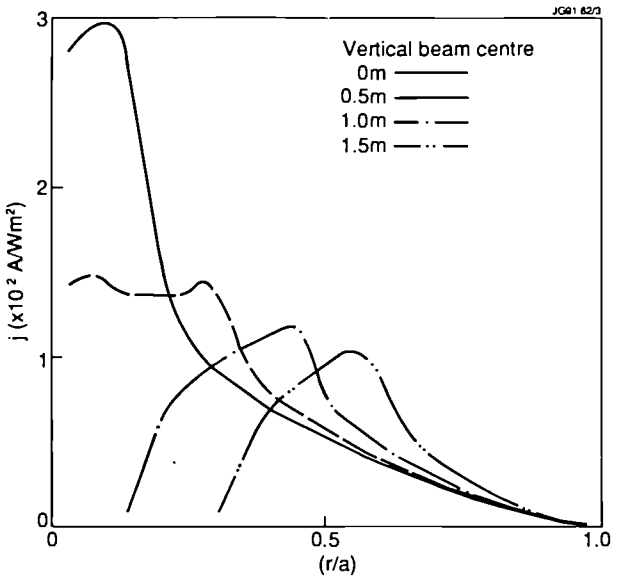

Fig.171: Current profiles obtained for different vertical steering values of the ITER reference beams. Predictions using the PENCIL code. Conditions $n_e(0) = 1.2x10^{20}m^{-3}$; $a_n = 0.5$; $T_e(0) = 35keV$; $\alpha_T = 1.0$; Beam width 0.35m; Beam height 1.0m.

JET which can be extrapolated to the Next Step machines [2]. Earlier bootstrap current studies of JET H-modes [3] have shown the necessity for invoking a large bootstrap current (~0.8-0.9MA in a 3MA plasma) to explain the behaviour of the loop voltage (V_L) and the second Shafranov moment (Y_S^2) during the H-phase.

The Bootstrap current for H-modes is predominantly at the outer edge of the plasma (r/a>0.8). Simulations have also been made of the Bootstrap current profiles in peaked profile, (pellet fuelled) L-mode plasmas with RF heating and in the peaked-profile H-mode plasmas such as the 'PEP+H-mode' (Pulse No:22490). In such peaked-profile shots the predicted bootstrap current peaks in the region r/a ~0 .25 and can reach quite high values (~ 0.55MA m^{-2}) in the pellet L-mode case discharges.

JET results are consistent with the Hirschmann formalism for bootstrap current [4] and the extrapolation to the larger machines has also been performed using this model. An important part of this formalism is the strong inverse aspect ratio ($\varepsilon^{-1} = r/R_0$) dependence of density and temperature gradient coefficients (L_{n_e}, L_{T_e} and L_{T_i}) in the bootstrap expression for pure hydrogenic plasma:

$$J_{boot} = -\frac{\varepsilon^{\frac{1}{2}}}{B_{pol}}\left[L_{n_e}(T_e + T_i)\frac{dn_e}{dr} + L_{T_e}n_e\frac{dT_e}{dr} + L_{T_i}n_e\frac{dT_i}{dr}\right]$$

The predictions for future machines are still heavily dependent on the temperature peaking parameter α_T and, to a lesser extent, the density peaking parameter α_n. Fig.172 shows the variation of the fraction of current which might be driven by the bootstrap mechanism (I_{boot}/I_P) in a Tokamak with aspect ratio of 3 (the remaining plasma current is assumed to be Ohmic). This shows the importance of a flat temperature profile.

The importance to a peaked density profile is also seen from Fig.172, especially in the more normal peaked T_e plasmas. However, prospects for peaked density profiles on Next Step machines remain poor. It is unlikely that pellets will be able to penetrate to the core of a reactor plasma. For NBI, the energies ~ 1MeV foreseen for current drive lead to small fluxes into the plasma. The effect of 100MW at E_b = 1.3MeV beam density profile of an ITER sized plasma assuming particle diffusion coefficients similar to those measured on JET leads to an increase in bootstrap current of <5%. As the 'natural' density profiles of H-modes (need to ignite ITER) are generally flat ($\alpha_n < 0.25$), it is probable that the bootstrap current will not be a substantial fraction of the plasma current.

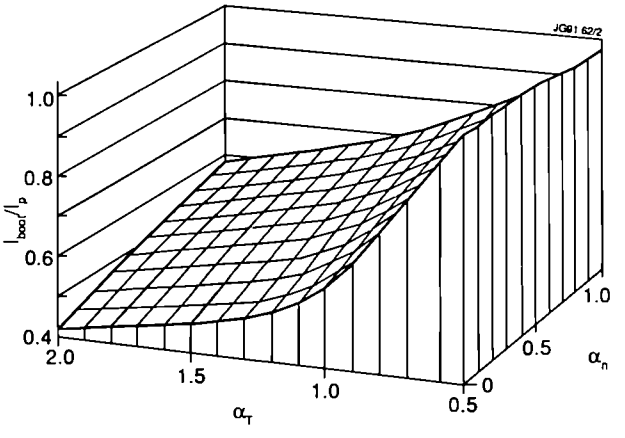

Fig.172: Profile dependence of the fraction of plasma current driven by the bootstrap mechanism (I_{boot}/I_p). The dependence on the density (α_n) and temperature (α_T) profile peaking factors is shown. The calculations are for a tokamak with aspect ratio = 3 and β_{pol} = 1.5.

H-Mode Scaling Studies For ITER

Throughout 1990, work proceeded on an H-mode database for global confinement scaling as requested by ITER. The work was performed as a combined effort from JET and from several other tokamaks (DIIID, ASDEX, JFT2M, PBXM and PDX). A database consisting of measurement from NBI-heated H-mode phases during shots on these tokamaks was assembled. The main criteria for inclusion of the data in the H-mode part of the database were that the H-phase showed a clear transition in the divertor H_α/D_α light;

the H-phase duration was at least 1-2 times the L-mode energy confinement time for the discharge; the radiated power was relatively low ($P_{rad}/P_{in} < 0.6$); the fast particle energy content of the discharge was relatively low ($W_{fast}/W_{tot} < 0.4$); the discharge had approached a fairly steady state ($W_{tot}/P_{in} < 0.35$) and the safety factor q was above 3.

An extensive statistical exercise on the quality of the data showed that there were large variations in all the 'independent' variables of the dataset ***except*** for q and toroidal field (B_T). The overall 'standard H-mode' dataset contained 1239 observations and separate datasets were formed for H-modes with and without so-called Edge Localised Modes (ELM's). The ELM and ELM-free datasets were found to scale differently.

Two different scaling law models were fitted to the ELM-free data and these, and other results, were presented at the major IAEA Conference in Washington, U.S.A. [3]. The power law scaling (ITER 90 H-P) is given by:

$$\tau_E = 0.082\, I_p^{1.02}\, B_T^{0.15}\, P^{-0.47}\, A^{0.5}\, R^{1.6}\, \kappa^{-0.19} \qquad (2)$$

This fit to the ELM-free dataset also describes the overall standard data set selection. The dependence on A and B_T was fixed (a dependence being established from smaller machines). Dependence on electron density (n_e) and inverse aspect ratio ($^a/_R$) was described by a zero exponent within the errors. The difference in H-mode confinement between the closed divertor Tokamaks (eg: ASDEX) and the open divertor Tokamaks (eg: JET) could not be distinguished from the effects of elongation (κ).

An alternative scaling law involved an offset linear law of the type ($W = W_o + \tau_{inc} P$) with an 'incremental' confinement time (τ_{inc}) given by:

$$\tau_{inc} = 2.9\ 10^{-8}\, I_P^{1.0}\, R^{0.87}\, A^{0.5} \qquad (3)$$

$$\text{and } W_o = 0.046\, I_P^{1.1}\, R^{1.9}\, B_T^{0.91}\, A^{0.5} \qquad (4)$$

Once again the A dependence was fixed ***a priori*** whilst the I_P and B_T dependences were established from the JFT2M results.

In addition to these 'free' parameter fits, the H-mode standard dataset was tested against four of the existing L-mode scaling laws (Goldston, Kaye-Big, ITER-P and Rebut-Lallia) to find the value of the confinement enhancement factor (H) of the H-mode confinement over L-mode. The best value of H for L-mode scaling law 'LS' was found by:

$$\tau_E^{\text{H mode}} = H_{fit}^S\, \tau_F^{LS} \qquad (5)$$

$$\text{where } H_{fit}^S = \text{mean}\left\{\frac{\tau_E^{\text{H mode}}}{\tau_F^{LS}}\right\}$$

The mean is calculated over the full set of observations. Fitted values of H_{fit}^S ranged from 1.65 (for Goldston scaling) to 2.35 (for Rebut-Lallia scaling). In general the statistical quality of the fits obtained by Eq.(5) were significantly worse than the fit obtained in Eq.(2).

The compiled H-mode database for ITER was made available to all parties in November 1990.

References

[1] P H Rebut, M L Watkins, D J Gambier and D Boucher, to be published in Phys. Fluids;

[2] C Challis, private communication;

[3] P M Stubberfield, B Balet, D Campbell, C D Challis, J G Cordey, G Hammett, J O'Rourke and G L Schmidt, Proceedings of 16th European Conf. of Fusion and Plasma Physics (Venice, 1989), Europhysics Conf. Abstracts 13B, IV, 1255.

[4] Hirshmann, Phys. Fluids **31** (1988), 3150.

[5] J G Cordey, J P Christiansen, K Thomsen, A Tanga, et al., Proceedings of 13th Int. Conf. on Plasma Physics and Contr. Fus. Research, (IAEA, Washington 1990) (IAEA-CN-53/F-3-19).

Theory

The purpose of theoretical work at JET is twofold; it aims to increase physical under-standing of the plasma behaviour in JET and hence predict theoretically the performance of future experiments; and it assists experimentalists and engineers with present problems.

Typical of the latter category has been the collaboration in the design of the pumped divertor. Existing codes were used to evaluate the magnetic geometry produced by different coil configurations. This was combined with numerical modelling of the scrape-off layer to estimate the effect of plasma flows on the impurity flux, and hence to optimise the overall design.

Reliable evaluation of the magnetic surfaces and current profiles within the plasma is essential for inverting line integrated diamagnetic signals or predicting MHD stability. This is difficult due to the insensitivity of the external magnetic signals to the current profile deep in the plasma. Improving the accuracy of this evaluation, partly by including diagnostic signals originating from the central plasma, is an ongoing problem. A new extended version of the equilibrium identification code was successfully implemented during the year.

Theory has been relatively successful in explaining and predicting the effect on the plasma of ICRF heating, and agreement has been further improved. Equally important has been the development of a more approximate RF energy deposition code, which is fast enough for routine use and inclusion in transport codes.

Analysis of the energy balance in JET plasmas serves both the above purposes. Rapid evaluation of the different loss mechanisms provides guidance for experimentalists when new operating regimes are entered. Of more long term significance is the assembly of an extensive data base of analysed pulses, and the comparison of the derived energy loss with different theoretical predictions.

Predictive transport codes have been used to predict both the behaviour of JET in planned operating conditions and the performance of next step devices such as ITER. These also provided an important tool for testing different transport models, by comparing predictions for JET with measurements.

An important task is to keep informed on all current theoretical work which may help explain plasma behaviour in JET. Work is also carried out to advance theory in areas particularly relevant to JET. Effort on MHD theory has increased over the past year, with particular attention to b-limits and H-mode stability. This work has been greatly assisted by collaboration with the Associated Laboratories, through contracts and Task Agreements, and by short term visits to JET.

Interpretation Codes and Data Banks

Local Transport Analysis

Heat and particle fluxes have been evaluated for more than 1600 time slices from 600 JET pulses, using the FALCON energy analysis code [1]. The resulting data-base is now one of the main sources for data analysis in the Project, allowing detailed and extensive comparison between experimental and theoretically predicted energy fluxes, as well as the characterisation of individual discharges. A careful quantitative assessment of several models has led to the conclusion that existing predictions of the anomalous transport induced by ∇T_i-driven instabilities are inconsistent with observations in JET [2]. Severe limitations associated with semi-empirical versions of other theories of transport based on drift waves have also been highlighted [3].

An attempt is being made to determine the dependence of the observed local transport on major physics parameters, using for the first time a large set of complete and internally consistent profile data. This investigation is still in progress. For example,there are indications of a systematic favourable dependence of L-mode transport on the plasma particle content, and of stronger electron than ion heat losses near the plasma centre, while ion transport tends to dominate near the plasma edge [4].

The FALCON system now plays a key role in ongoing experimental campaigns. Its data handling techniques and checks on internal consistency of measured data have largely inspired the new design of routine data processing programs for JET. At the same time, JET has provided a reliable fast evaluation of local confinement properties of newly accessed plasma regimes, notably the H-mode with peaked density profiles [6].

Equilibrium Identification

The existing code for routine evaluation of the magnetic surfaces and current profile within JET (IDENTC), uses mainly magnetic data from coils and loops outside the plasma. So far 655 shots have been analysed and stored in the data-base. A new code, IDENTD, with improved performance is now operational and used for analysing recent discharges, which were difficult to analyse with IDENTC. IDENTD is based on quadratic finite elements, which yield higher numerical accuracy, in particular for X-point equilibria. It also uses additional data from the plasma interior, e.g. the pressure profile from LIDAR or ECE, and the magnetic field from Faraday rotation. The current profile can be represented by global (polynomials) or local expansion functions (finite elements) giving enhanced flexibility. The code has been shown to yield higher numerical accuracy and to be more robust than IDENTC, especially when analysing discharges with strong gradients in the plasma, as in H-mode shots with pellet injection.

An application to a Pellet Enhanced Performance (PEP) discharge (Pulse No:22567, t = 6.25s) is shown in Fig. 173.

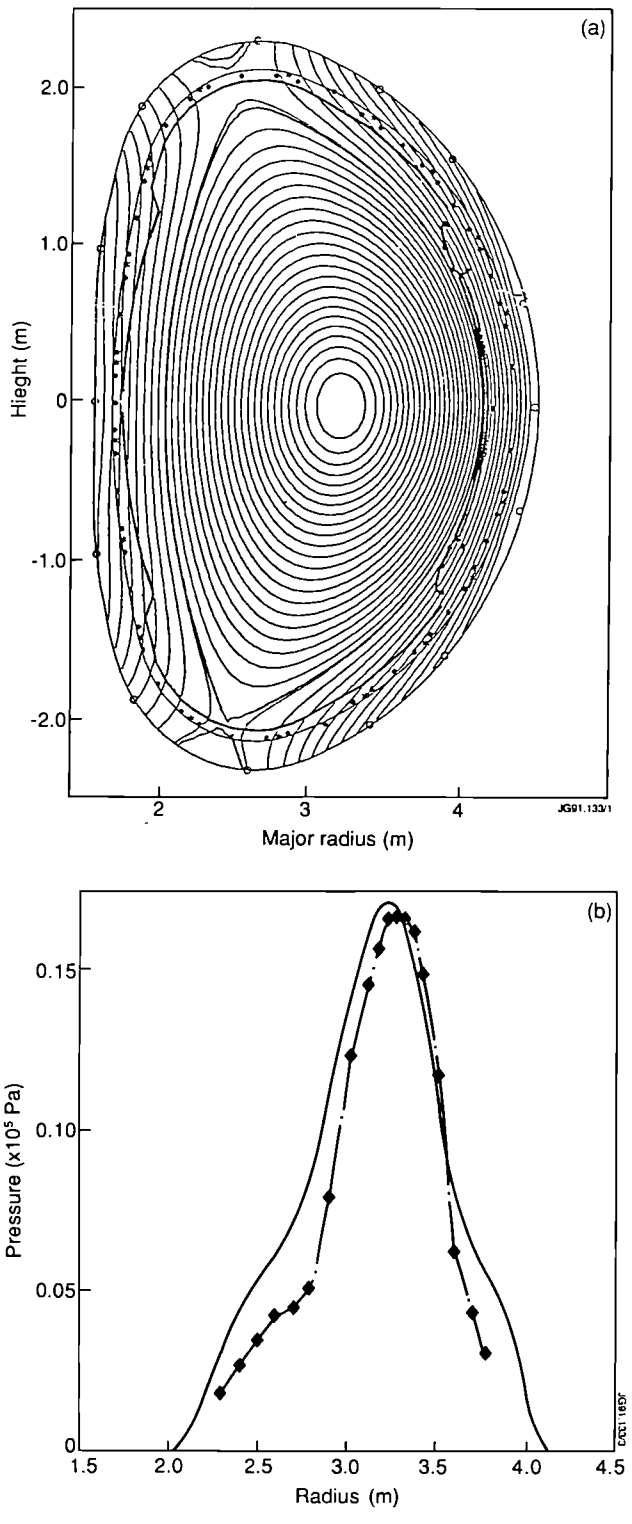

Fig.173(a) Equilibrium magnetic surfaces; (b) LIDAR pressure profile (dashed line) and that reconstructed from the equilibrium (solid line).

The computation used the LIDAR measured pressure profile. To check the accuracy, this is compared in Fig.173(b) with the pressure corresponding to the computed equilibrium. The deviation is acceptable bearing in mind the uncertainty in the LIDAR profile. It is emphasised that the value of the safety factor on axis q(0) is below unity (q(0) ≈ 0.8), whereas when utilising magnetic data alone a value above unity was found (q(0) ≈ 1.2). The good agreement (typically within a few percent) of measured and computed magnetic boundary data remains when using additional internal data. The resolution is good at the X-point as well as around the axis.

To further increase the resolution near the plasma centre, more accurate data will be included. A recently developed diagnostic, based on the motional Stark effect, provides local information on the magnetic field. The code IDENTD has already been adapted to include this. First tests show that the equilibrium reacts sensitively to the additional information. The effect on the computed current profile of including one additional value of B_p inside the plasma is shown in Fig. 174 for the same plasma as in Fig. 173.

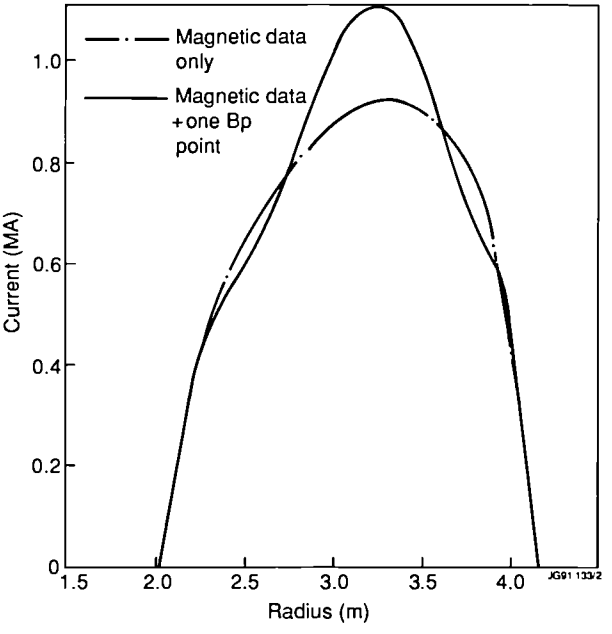

Fig. 174 Two evaluations of the current profile. The dashed curve is derived from magnetic data alone whereas the solid curve uses B_p at one interior point in addition (R = 3.55m, Z = 0.07m).

RF Modelling Codes

The PION code [7], for rapid evaluation of the steady state ICRF power deposition and ion velocity distribution, has been extended to include time dependence [8]. It uses a simplified model, based on the more exact, but very time consuming, global wave code. Since the fast ion slowing down time is comparable to the RF pulse length in JET, time dependence can be important. A model for calculating current drive by electron Landau damping and transit time magnetic pumping in the ICRF-regime has been introduced

in the global wave code LION [9]. Frequencies near the fourth harmonic of deuterium have been found to be suitable for demonstrating current drive in JET, a current to power ratio of ≈ 0.4 A W^{-1} might be obtained [10].

A weakness in existing RF power deposition codes is the neglect of the finite orbit width. Since the resonant minority species may acquire energies of several MeV, their trapped orbits are a significant fraction of the radius, thus broadening the power deposition profile. This broadening has been evaluated using the Monte-Carlo code HECTOR [11]. Studies of high power minority heating with peaked RF profiles show a reduction in the power absorbed and transferred to the background plasma at the discharge centre. Furthermore a significant reduction occurs in fast ion energy content and total thermonuclear yield [12]. Simulations of JET high power shots show improved agreement over that obtained using Fokker-Planck modelling. As Monte-Carlo computations are time-consuming, an improved Fokker-Planck treatment is being developed, which should be fast enough for routine use in the PION codes.

A code has been developed to evaluate the mode conversion of the fast wave used for ICRF heating [13]. This conversion could explain the observed partial absorption of RF power at the plasma edge, instead of at the resonant layer. WKB type solutions, used previously, are inaccurate in the edge region, as the gradients are usually large. A finite element method has been used to solve the ICRF wave equation in a one-dimensional inhomogeneous plasma, which gives faster convergence than finite difference methods.

Theoretical Models

A review of the correlation between observed energy and particle transport and the measured fluctuation level has been completed [14]. This correlation is not strong enough to establish beyond doubt that the fluctuations are solely responsible for the transport. Other possible transport mechanisms, particularly neoclassical, have been re-examined [15].

The separation of the energy flux into convective and conductive components, about which there has been recent controversy, has been studied. It is concluded that to evaluate only the kinetic energy flux is misleading. The periodic exchange between kinetic and potential energy in the gyrating motion produces a spurious component, which is balanced by a potential energy flux. The total energy flux (kinetic and potential), which is more physically meaningful, has a convective contribution $(3/2)\Gamma T$, where Γ is the particle flux.

In some ICRF scenarios, the RF wave, after traversing the plasma, may be converted to an Alfvén wave on the high field side. This occurs where the cyclotron frequency of the majority species exceeds the wave frequency. This process has been studied analytically, and results checked against numerical evaluation [16]. In resonant heating of tritium in a JET D-T plasma, nearly complete absorption of the power reaching the conversion layer is predicted.

Observations of the JET X-point target plates show the formation of discrete impact zones or hot spots. These observations are at variance with the usual fluid description of plasma flows in the SOL and X-point regions, according to which plasma flow in the SOL is subsonic along field lines connected to the target plates. This gives rise to a bifurcation of the flow in the X-point region with heat maxima on or near the intersection of the separatrix with the plates. While this description is appropriate for the electron flow, it is clearly inadequate for the ion component for which the ∇b drifts are important. Analytic [17] and computational [18] studies of the effect of finite orbit drift on power and particle flow into the X-point region have been made. The results are in good qualitative agreement with observations.

MHD Stability

With finite resistivity, the magnetic field is no longer frozen into the fluid and tearing instabilities can cause changes in magnetic topology. JET discharges are in the high temperature regime, where the electron-ion collision time, τ_{ei}, is comparable to, and sometimes exceeds, the duration of sawtooth relaxations. In this regime, the rate at which magnetic reconnection can occur is determined by electron inertia and by the ion gyroradius, rather than by collisional effects. The collisionless m = 1 tearing mode was analysed by adopting a kinetic treatment for the ions and a fluid treatment for electrons. The relevant linearised Ohm's law included the electron inertia $(m_e/n_e e^2)\,\partial J/\partial t$, which greatly exceeds the usual ηJ term near the collisionless limit. By this linear analysis, growth rates $\gamma/\omega_A \sim d/r_s\,(r_i/d)^{2/3}$ were found [19], with ω_A the Alfvén frequency, r_s the radius of the reconnecting surface, and the ion gyroradius r_i replacing the skin depth d as the width of the mode boundary layer. For JET parameters, a typical timescale is $\tau=\gamma^{-1}=50$-100 ms. This compares favourably with the observed growth time of the displacement of the magnetic axis, which defines the first phase of sawtooth relaxation. As the temperature is in-

creased, diamagnetic effects eventually become important. However, the condition for diamagnetic stabilisation of the m = 1 mode is more stringent in the collisionless regime than predicted by the two-fluid model. The main conclusion from the present analysis is that the m = 1 tearing instability can remain virulent at high temperatures, contrary to expectations based on collisional models. However, it must be kept in mind, that the nonlinear convective inertial term $v_e \cdot \nabla j$, (with v_e the electron velocity) becomes the dominant term in the generalised Ohm's law for large displacements. Nevertheless, this linear analysis reveals the important role played by electron inertia in magnetic reconnection for the plasma regimes attained in recent IDENTD experiments.

The ideal ballooning stability properties of high-beta discharges produced in JET have been analysed with the HBT code [20]. A broad pressure profile (Pulse No: 19970) with b = 4.2%, (i.e. 90% of the Troyon limit), is completely ballooning stable. Changing the pressure profile until marginal stability is reached on each flux surface allows beta values up to 7.3%. However, such very broad profiles may lead to external kink instabilities. Peaked pressure profiles (e.g. Pulse No: 20272 and Pulse No: 20303) yield pressure gradients in the central plasma which exceed the critical value by a factor 1.5 to 2. This raises interesting questions concerning the accuracy of the measured gradients and the validity of the theoretical model. Even taking into account large errors in the data, the ballooning beta limit must be exceeded for a monotonic q profile. However, it is not clear whether hollow q-profiles, which would yield complete stability, are possibly consistent with the data.

MHD spectroscopy, i.e. the identification of ideal and dissipative MHD modes for the purpose of diagnosing tokamaks and optimising their stability properties, requires a numerical tool which accurately calculates the dissipative MHD spectrum for observed equilibria. The new spectral code CASTOR (Complex Alfvén Spectrum for Toroidal Plasmas), in conjunction with the equilibrium solver HELENA which yields the mapping into a non-orthogonal flux coordinate system with straight field lines, provides such a tool. The equilibrium solver is interfaced with the identification code IDENTD to facilitate analysis of JET discharges. In CASTOR, the perturbed density, velocity, temperature and magnetic field are discretised by high order finite elements in the radial direction and by a Fourier expansion in the toroidal and poloidal angles. The temporal dependence is given by $e^{\lambda t}$. The resulting generalised non-symmetric eigenvalue problem is solved by means of the QR algorithm, the Lanczos scheme and inverse iteration yielding the entire spectrum, branches of the spectrum in the complex eigenvalue plane, or single eigenvalues, respectively. The importance of the MHD spectrum for providing the underlying structure of the different temporal and spatial scales of the different macroscopic normal modes (continuum modes, gap modes, quasi-modes, kinks) is well established. The modifications caused by dissipation are much less understood. The finite-element techniques employed in CASTOR permit spatial resolution of the resistive modes in tokamak conditions down to values of 10^{-11} for the inverse magnetic Reynolds number. The structure of the code allows extension to other dissipative terms, such as thermal conductivity, a generalised Ohm's law and eventually energetic particle effects. This work was carried out collaboration with IPP Garching, FRG, and FOM Nieuwegein, The Netherlands.

Global Alfvén waves, which are closely related to the ideal Alfvén continua, were studied. A circular cross-section equilibrium with aspect ratio 2.5 and safety factor increasing from $q_0 = 0.95$ on axis to $q_s = 2.3$ at the edge has been analysed. The toroidal coupling of the m = 1 and m = 2 modes produces a gap in the Alfvén continuum around Im l = 0.5, as shown from Fig. 175. The spectrum has been

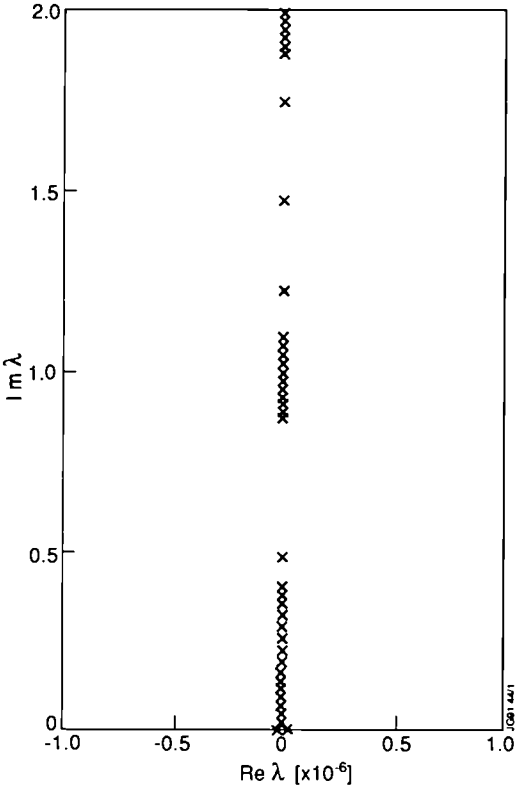

Fig. 175 The spectrum of eigenvalues λ of a circular cross-section tokamak in ideal MHD, (i.e. no damping and Re λ ≡ 0). The gaps in the Alfvén continuum are pronounced.

computed with five poloidal Fourier components m = 1 to 5 and the toroidal wave number n = -1. Inside this gap a discrete mode, the toroidicity induced Alfvén mode (TAE), was found. A similar gap exists at Im $\lambda \approx 1.5$ due to higher order coupling. Owing to their global nature the global Alfvén waves can be destabilised by energetic particles such as fusion born a-particles [21]. On the other hand, these modes are expected to experience Landau damping by coupling to continuum modes. This damping is especially pronounced for non-uniform density profiles. The dominant Fourier components of the radial velocity are displayed in Fig. 176. The m = 3 and 4 components yield the coupling to the continua and hence the damping. The singular component of the discrete mode with Im $\lambda \approx 1.5$ is much more pronounced and, therefore, these modes should not be dangerous. In general, mode coupling is more pronounced for JET equilibria due to elongation and increased shear. This enhances the probability that a-particles will be damped before destabilising Alfvén modes.

The effect on MHD instabilities of the large orbit widths of minority ions, accelerated to MeV energies by ICRF heating, has been studied. An analytic description of trapped orbits that encompasses both the standard banana limit and the non-standard D-shaped limit has been developed. This formulation has been used to rederive the fast ion response to m = 1 perturbations. The influence of energetic particles on these modes tends to be reduced because of the large D-shaped orbits. The reduction is modest for typical JET parameters, but can become significant in smaller tokamaks.

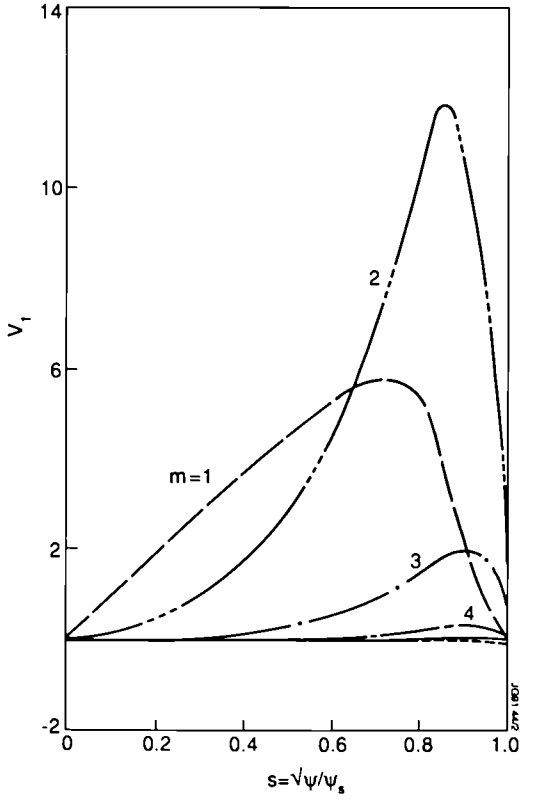

Fig. 176 The dominant Fourier harmonics of the perturbed velocity for the eigenvalue $\lambda = i\,0.49$. The radial component v_r, defined by $v_r \propto \nabla v_\perp$, has a step-function type dependence on the radius.

Predictive Computations

Models of the SOL and Predictions for the JET Pumped Divertor

In connection with the planned pumped divertor, magnetic field calculations have been performed. Two codes INVERSX and PROTEUS, based on different methods and different finite-element discretisations, produced the same configurations within error bars of ~ 1% on integral quantities (e.g. plasma volume). The difference for the connection length between plasma and divertor plate >10%. The connection length for a 6 MA plasma current equilibrium was ≈ 7 m for a 'slim' configuration, with a plasma volume of 79 m^3 and ≈ 3.5 m for a 'fat' configuration with a volume of 93 m^3. These magnetic field configurations were subsequently used to model the scrape-off layer.

Modelling impurity control requires, in general, a 2-D model, since the boundary plasma in tokamaks, including the scrape-off layer, is at least two dimensional (2-D). A number of 2-D codes have been developed but none contains all the elements needed to model impurity retention. In particular, no 2-D code for the edge plasma contains all the following elements: Monte-Carlo treatment of neutrals; ability to handle arbitrarily high impurity concentrations; parallel current flows; and solutions obtained from one target plate to the other without imposing a plane of symmetry. A versatile 1-1/2-D model has been developed which contains all these features. This model is complementary to existing 2-D codes.

It is based on a plasma model [22] and an impurity model [23]. The two dimensional structure of the code EDGE2D [22] has been retained for the magnetic field geometry, the metric coefficients needed for the transport equations, and the transport of neutral deuterons and impurities computed by the 2-D Monte Carlo code NIMBUS [24]. Fluid equations for the conservation of particles, momentum and energy along the magnetic field are solved for electrons, deuterons and impurity ions. Transport coefficients are classical and allow for arbitrarily high impurity concentrations. The full non-coronal distribution of impurity charge

states and the corresponding radiated energy losses are evaluated. A single impurity temperature, set equal to the deuteron temperature, is assumed. The temperature and density profiles transverse to the magnetic field are assumed to decay exponentially, with decay lengths based on experimental values.

This model has been used to simulate JET experimental results [25] and to predict the retention of impurities by the pumped divertor planned for JET [26,27]. While much remains to be done for a satisfactory validation of the model, results obtained so far show an overall consistency of the model with experimental results. In particular, agreement has been observed between the prediction that T_i can be significantly larger than T_e at the separatrix and the values of T_e and T_i derived experimentally from probe and power balance measurements. There is also agreement between the predicted retention of impurities and radiated power in the X-point region of JET and the experimental observations. The elimination of the so-called carbon catastrophe by means of the flow induced by a strong gas puffs also predicted.

Computations for the performance of a pumped divertor show that impurity control may indeed be achieved. However, a rather high boundary density seems necessary ($n \approx 10^{20} m^{-3}$). A benefit of operating at high density is that particle fluxes due to recycling at the divertor targets are very large, and the related friction can be sufficient to retain target produced impurities, minimising or even eliminating the requirement for pumping or recirculating particles.

Assessment of Transport Models

Transport codes for predicting the performance of next step tokamaks require "complete" transport models. This means that such models must represent the local plasma properties from core to boundary in ignition relevant regimes. However, most transport models derived from theory are known to be invalid in the edge region and in many cases also in the plasma core, where sawtooth activity often masks local transport effects.

For this reason, the existing models have to be completed by adding empirical prescriptions, and need to be tested against experimental results. In particular, it is important to clarify the role and relative importance of theoretical and empirical assumptions in a model. This kind of analysis has been carried out [28,29] for various models and, in particular, for those models that claim to be based on the assumption of a "profile consistency" constraint [30-32] and for the Rebut model [33].

It has been shown that energy transport coefficients based on the assumption of "profile consistency" are simply a convenient way to translate in terms of local coefficients some general empirical observations on the global energy confinement scaling and the shape of temperature profiles in quasi-steady state ohmic and L-mode discharges. This, of course, limits their range of applicability to this kind of discharge. Using the Rebut model [12] it has been found that H-mode cases can also be simulated, provided an appropriate confinement barrier is introduced at the plasma boundary. Moreover, the evolution of temperature profiles following pellet injection in ohmic cases may be well represented by the model that predicts a strongly reduced confinement when $\nabla q < 0$.

Predictions For Proposed Next Step Devices

An extensive campaign of simulations of the IGNITOR device was carried out using the 1-1/2-D transport code JETTO with transport models validated against JET results. This was carried out at the request of the EEC panel appointed to assess the possible performance and interest in this device for the European fusion programme. The results of these simulations have clearly shown that IGNITOR would require an energy confinement time of at least 0.4 s at 35-40 MW power level to reach ignition. This confinement capability is 30 - 40% larger than predicted by most transport models for L-mode plasmas. The same computations also showed that the following requirements are important: low impurity level ($Z_{eff} \leq 1.3$): relatively peaked density profile ($n_o/\langle n \rangle \geq 2$ with $n_o \approx 1.2 \times 10^{21} m^{-3}$; and practical elimination of sawteeth.

A similar analysis has been initiated for the ITER device, showing that in this case also the margin for ignition might be too narrow and sensitively dependent on sawteeth, impurity control and the not well understood boundary phenomena that determine the H-mode edge transport barrier.

References

[1] H Hamnén et al., JET Report JET-IR(90)06.

[2] F Tibone et al., Proc. 17th EPS Conf. (Amsterdam, The Netherlands, 1990), Vol. 14B, Part II, p. 805.

[3] T E Stringer and F Tibone, JET Report - JET-IR(90)03.

[4] A Taroni et al., Proc. 13th IAEA Conf. (Washington, USA, 1990), paper IAEA-CN-53/A-2-1.

[5] J P Christiansen et al., Nucl. Fusion **29** (1989) 1505.

[6] B J Tubbing et al., "H-Mode Confinements in JET with Enhanced Performance by Pellet-Peaked Density Profiles", submitted to Nucl. Fusion (Nov. 1990).
[7] L-G Eriksson and T Hellsten, JET Report - JET-P(89)65.
[8] L-G Eriksson, U Willén and T Hellsten, JET Report - JET-P(90)42.
[9] L Villard et al., J. Computer Phys. Reports **4** (1986) 95.
[10] L-G Eriksson and T Hellsten, JET Report - JET-P(90)50.
[11] M Kovanen, W G Core, hector: A Code for the Study of Charged Particles in Axisymmetric Tokamak Plasmas, JET Report JET-P(90)40, (submitted to J. Comput. Phys.)
[12] M Kovanen, W G Core, T Hellsten, Finite Orbit Effects in ICRF Heated Tokamak Plasmas, JET Report - JET-P(90)68, (submitted to Nuclear Fusion).
[13] M J Alava, J A Heikkinen, JET Report - JET-IR(90)04.
[14] T E Stringer, JET Report - JET-P(90)15
[15] T E Stringer, JET Report - JET-P(90)29, to be published in Phys. Fluids B.
[16] J A Heikkinen, T Hellsten, M J. Alava, JET Report - JET-P(90)28.
[17] W G Core, E Lazzaro, Orbit Effects in the Power and Particle Flow in the X-Point Region of a Tokamak Plasma, (Varenna, Italy, 1990).
[18] M Kovanen, et al., Particle and Heat Deposition in the X-Point Region at JET, (submitted to Plasma Phys. and Contr. Fusion).
[19] F Porcelli, The Collisionless m = 1 Tearing Mode, JET Report - JET-P(90)23.
[20] G T A Huysmans, R M O Galvão and J P Goedbloed, High-Beta Stability Studies of JET Discharges with the Numerical Program HBT. Rijnhuizen Report 90-193.
[21] G Y Fu and J W van Dam, Phys. Fluids B, **1**, (1989), 1949.
[22] R. Simonini, W. Feneberg, A. Taroni, 12th EPS Conf. on Controlled Fusion and Plasma Physics, 1985, Vol. II, p. 484.
[23] Yu.L. Igitkhanov, Contrib. to Plasma Phys. **28** (1988) 477.
[24] E. Cupini, A. DeMatteis, R. Simonini, NET Report EUR XII-324/9 (1984).
[25] P.J. Harbour, et al., 9th Int. Conf. on Plasma Surface Interactions (Bournemouth, UK, 1990).
[26] R. Simonini, M. Keilhacker, A. Taroni, M.L. Watkins, 17th EPS Conf. on Controlled Fusion and Plasma Heating, Amsterdam, The Netherlands, 1990, Vol. III, p. 1369.
[27] M. Keilhacker, et al., 13th Int. Conf. on Plasma Physics and Controlled Nuclear Fusion Research, Washington, USA, 1-6 October 1990, Paper IAEA-CN-53/A-5-1.
[28] Ch. Sack, et al., 17th EPS Conf. on Controlled Fusion and Plasma Heating, Amsterdam, The Netherlands, 1990, Vol. II, p. 801.
[29] A. Taroni, et al., 13th Int. Conf. on Plasma Physics and Controlled Nuclear Fusion Research, Washington, USA, 1-6 October 1990, Paper IAEA-CN-53/A-5-1.
[30] B. Coppi and E. Mazzucato, Phys. Lett. **71A** (1979) 337.
[31] M.H. Redi, et al., Nucl. Fusion **27** (1987) 2001.
[32] R.C. Englade, Nucl. Fusion **29** (1989) 999.
[33] P.H. Rebut, et al., Proc. 12th Int. Conf., Nice, France 1988. Paper IAEA-CN-50/D-4-1.

Summary of Scientific Progress

As mentioned previously, the 1990 experimental programme concentrated on three main themes:

(i) the introduction and exploitation of new facilities;
(ii) improving the understanding of tokamak physics (including detailed studies of thermal, particle and impurity transport and various aspects of H-mode physics);
(iii) improving plasma performance.

A summary overview of the main achievements is given in the following sections.

Exploitation of New Machine Facilities

Plasma Purity

During the first few years of JET's operation, extensive areas of the inconel torus walls, including the belt limiters, inner wall and X-point interaction regions, were covered with carbon tiles, and other surfaces were carbonized. Beryllium was introduced in 1989, first as a thin layer evaporated onto the carbon surfaces from four sources equally spaced around the torus mid-plane, and later with solid beryllium tiles on the belt limiters. Oxygen and carbon impurity concentrations in the plasma were strongly reduced, leading to lower Z_{eff} and higher fuel concentrations, n_D/n_e. Density control was previously a problem with all-carbon surfaces, but beryllium was found to pump both hydrogen and helium, giving better density control and the

possibility of using strong gas puffing to maintain a low edge temperature with reduced beryllium influx.

Nickel screens on the ICRF antennae were previously the source of a serious influx of impurity during ICRF heating, which prevented the plasma entering the H-mode with ICRF alone. H-modes heated by ICRF power were obtained in 1989 when these nickel surface were covered with a thin evaporated beryllium film. For the 1990 experimental programme, the nickel screens were replaced by beryllium screens and the operational range of H-modes with ICRF was extended. Further improvement to ICRF heating in the X-point configuration was obtained with a new position feedback system that maintained a constant plasma coupling impedance. This was effective in allowing high ICRF power (up to 10MW) to be maintained throughout the transition from L to H-mode. H-modes with ICRF heating have confinement properties comparable to those with neutral beam heating.

Beryllium X-point Tiles

The lower X-point protection tiles were changed from carbon to beryllium, although the beryllium tiles were intended for a different purpose and consequently their shape was not optimized for the power flux at the X-point. H-mode discharges were obtained with similar power thresholds and comparable confinement properties to discharges on the upper set of carbon tiles. As with carbon, H-modes on the beryllium tiles were terminated by "blooms" due to the formation of localized "hot-spots" on the tiles. Various techniques to delay the onset of the blooms were explored including sweeping the X-point strike point radially in order to distribute the power more uniformly over a wider tile area. Carbon blooms were effectively suppressed in conditions of high recycling at the upper divertor tiles. The high recycling regime can be established by gas puffing either before or during the H-mode, but was more stable when the gas puffing started before the high power neutral beam heating. The high recycling regime was improved when the X-point was well inside the vacuum vessel, but otherwise there appeared to be no clear systematic dependence of the H-mode duration on the position of the X-point.

A quantitative comparison between H-modes with carbon and beryllium tiles is inconclusive at present, since the beryllium tiles were badly melted during the first series of experiments (these beryllium tiles were not optimized for the X-point power flux) and subsequently, it was not possible to establish an H-mode on the damaged tiles. These experiments will be continued during 1991 using new carbon and beryllium tiles specifically designed for the X-point region.

Lower Hybrid Current Drive

A lower hybrid current drive (LHCD) system capable of launching 10MW at 3.7MHz is being prepared for JET. Preliminary experiments have coupled up to 1.6MW to the plasma for up to 20s. A significant drop in the loop voltage corresponding to a non-inductive current of about 1MA was achieved at plasma densities up to $3 \times 10^{19} m^{-3}$. Adding LHCD to a 2MA discharge with 4MW ICRH extended the monster sawtooth period from 0.5s (without LHCD) to 2.9s (with LHCD).

High Current Discharges

Plasma currents of 7MA were achieved in 1988 using simultaneous ramps of toroidal field and plasma current to maintain $q_\phi \approx 2.5$. The variation of toroidal field prevented heating during the current rise. A faster current ramp at constant $q_\phi \approx 3.5$ has been developed and extended to 7MA discharges. These discharges have longer flat-tops (3s compared to 2s for the earlier 7MA discharges) and adequate flux remains in the core to extend the flat-top further. Valuable experience of operating tokamaks at high currents near to stability limits was gained.

Helium Neutral Beam Injection

Helium neutral beam injection has been demonstrated. Up to 5MW of ^{3}He and 7MW of ^{4}He at 120keV have been injected into 5MA limiter and 3.5MA double-null plasmas for up to 3s. Although a low level of localized heating was observed on the lower belt limiter, there were no indications of serious problems such as increased impurities or limiter heating due to the ionization of metastable neutrals in the beam. Beam penetration at these energies was excellent over the typical range of JET plasma densities. Preliminary results show that stored plasma energy and global energy confinement with He beams are comparable to those with D beams. The elimination of beam-beam and beam-plasma reactions resulted in significant reductions in neutron yield, which was advantageous in reducing vessel activation and in permitting a more direct interpretation of neutron diagnostic measurements of thermal neutrons. He injection also provided a precise particle source for alpha-particle transport studies and for ion cyclotron minority heating.

Improved Understanding of Tokamak Physics

Sawtooth Oscillations

Sawteeth determine the central plasma parameters and thus the fusion performance. Neutron emission profiles showed a dramatic change following sawtooth collapse. In discharges where the neutron emission was mainly thermal, there was a correspondingly large change in the total neutron yield consistent with the loss of thermal ions from the core. In discharges where there was a significant non-thermal contribution from beam-plasma and beam-beam reactions, the neutron emission profile also showed a dramatic change, though there was a much smaller drop (typically <20%) in the total neutron yield. Careful examination of the neutron profiles revealed that after the collapse, the fast ions appeared to be redistributed but not completely expelled from the core.

Sawteeth have been suppressed for up to 5s following pellet injection, both during the current rise phase and during the flat-top. Polarimetric measurements indicate that the current profile is broadened by the change in electron temperature due to the pellet ablation so that $q_o>1$. Long sawtooth-free periods up to 5s have also been obtained in discharges where q_o is significantly less than unity ($0.6<q_o<0.8\pm0.15$). These "monster sawteeth" are produced most efficiently when the ICRF power is applied at the magnetic axis. Monster sawteeth are not stabilized when the heating is moved outside the q=1 surface. The stabilization mechanism is not fully understood but there is strong evidence that fast ions play an important role. Sawtooth stabilization is an important factor in optimizing fusion performance.

Particle and Energy Transport

Simultaneous localized measurements have been made of electron density and temperature perturbations propagating in the plasma following sawteeth crashes and during sawteeth free ("monster sawteeth") periods. The data have been analyzed in terms of a linearized electron transport matrix. The diagonal terms correspond to the incremental particle and heat diffusivities, D_e^{inc} and χ_e^{inc}. The off-diagonal terms are a a measure of the coupling between heat and particle transport and indicate that pure temperature perturbations are not eigenmodes. Thus if a pure temperature perturbation is launched, it will generate a density perturbation that will be transported at the same rate as the temperature perturbation even though D_e^{inc} and χ_e^{inc} have different values.

Impurity Transport

The transport of various elements including Si, Ar, Xe, Kr, He and several high Z elements, has been studied using gas injection and laser ablation. Impurities injected into the private flux region of X-point plasmas show impurity retention in the divertor whereas impurities injected at the mid plane penetrate and accumulate in the core. An interesting discovery during these experiments was that the noble gases are strongly pumped by beryllium surfaces. In particular, helium is pumped as strongly as deuterium. The pumping mechanism is not fully understood, but probably involves co-deposition of beryllium.

Alpha-Particle Transport

He beam injection has been used as an axial particle source to simulate alpha-particle diffusion in L- and H-modes. The time and space resolved profiles of helium densities showing the evolution of the injected helium and the subsequent recycling are measured with charge exchange spectroscopy. In L-mode discharges, the central helium density decays promptly after the He source is switched-off. In H-mode discharges the He concentration decreases more slowly and in some cases is seen to accumulate in the plasma core.

Improvement of Fusion Performance

Limiter Discharges

Previously, the energy confinement in high current, low-q limiter discharges in JET was close to L-mode values. Enhancement of the fusion yield requires strongly peaked temperature and density profiles. Sawtooth stabilization using ICRF power during the current rise of 5MA discharges has now been extended well into the flat-top by using a faster current ramp at constant $q_y \approx 3.5$ and exploiting the density control provided by beryllium. Strongly peaked electron temperature profiles with $T_e(0)\approx12$keV were obtained, though with modest ion temperature, $T_i(0) \approx 5$keV. A comparison of 3 and 5MA sawtooth-free discharges with similar input power and density shows that the temperature gradient is steeper in the 5MA discharge indicating a lower value of χ_e.

Gas fuelled discharges with beryllium limiters have flat density profiles even with beam refuelling. Refuelling with deeply penetrating pellets is required to produce peaked density profiles and careful timing of the pellets and heating is needed to obtain good penetration. Central electron densities $n_e(0)\approx2.3\times10^{20}m^{-3}$ have been obtained by injecting a string of 4mm diameter pellets into a 5MA discharge.

When heating (6MW of ICRF and 2MW of NBI) is applied, the central density decayed rapidly to $n_e(0) \approx 6 \times 10^{19} m^{-3}$ with $T_e(0) \approx T_i(0) \approx 5$keV and a transient peak $Q_{DD} \approx 5 \times 10^{-4}$. The global energy confinement time was enhanced transiently by ~30% compared to gas fuelled discharges. Higher ion temperatures with $T_i(0) \approx 18$keV have been obtained with beam heating and pellet refuelling in 3MA limiter plasmas. The profiles were strongly peaked; ($T_i(0)/\langle T_i \rangle \approx 7$ and $n_e(0)/\langle n_e \rangle \approx 4$) and the fusion yield was enhanced by a factor ≈3 compared to an L-mode discharge with flat profiles, even though the global confinement was not enhanced significantly.

Further development of higher current limiter discharges has continued with the aim of combining peaked profiles with the favourable scaling of global confinement time with current. Sawteeth were suppressed well into the flat-top of a 6MA discharge and during the current rise of a 7MA discharge. A central electron temperature $T_e(0) \approx 9$keV was obtained in both cases. The ions are heated by neutral beams in a 6.5MA discharge, giving $T_i \approx T_e \approx 7$keV at $n_e(0) \approx 5 \times 10^{19} m^{-3}$, with a confinement time of 0.65s. This resulted in a fusion product $n_D \tau_E T_i \approx 2.3 \times 20^{20} m^{-3}$skeV. This phase of high fusion performance was terminated by a sawtooth crash with a subsequent strong density rise and influx of beryllium.

Inner Wall Discharges

The inner wall of JET is protected by approximately $12m^2$ of carbon tiles. The plasma shape must be carefully matched to the shape of the inner wall in order to avoid carbon blooms due to localized overheating of the tiles. In optimized conditions, neutral beam heating powers up to 16.5MW have been applied for up to 2s without a strong carbon influx. Evaporation of beryllium onto the carbon tiles gave a significant improvement in plasma purity and density control. Neutral beam injection into low density target plasmas provides hot-ion L-mode discharges with $I_p = 4.7$MA, $n_e(0) \approx 3.0 \times 10^{19} m^{-3}$, $T_e(0) \approx 9$keV, $T_i(0) \approx 20$keV and $\tau_E \approx 0.55$s. These discharges have the best fusion performance ($n_D \tau_E T_i \approx 3.3 \times 10^{20} m^{-3}$skeV and $Q_{DD} \approx 1.4 \times 10^{-3}$) obtained in JET limiter discharges.

At lower plasma currents ($I_p < 3$MA) and low toroidal fields, H-mode transitions were obtained in inner wall plasmas. The characteristics of the transition are similar to those at the H-mode transition in X-point discharges. The power threshold of inner wall H-modes is approximately twice that of an X-point H-mode and scales linearly with the toroidal field. The inner wall H-mode appears to be ELM free but the maximum duration is 0.8s

X-point Discharges

The distribution of radiated power at the X-point and the power and particle fluxes to the tile surface depend on the direction of the toroidal field. When the toroidal field direction is such that the ∇B drift of the ions is towards the X-point, the temperature rise at the outer strike point is larger than at the inner strike point. When the toroidal field is reversed, so that the ion drift is away from the X-point, the tile temperatures at both strike points are lower and nearly equal. The carbon bloom is delayed significantly. The radiated power is greater at the inner strike zone when ∇B is towards the X-point and at the outer strike zone when ∇B is away from the X-point. The confinement properties and impurity behaviour appear to be independent of the field direction. The power threshold for the H-mode is lower when the ∇B drift is towards the X-point (as observed in other tokamaks) and increases more slowly with B_T, but in practice this is unimportant when the emphasis is on high power discharges that are well above the power threshold.

Global energy confinement times in H-mode discharges are 2-3 times longer than in the L-mode. An H-mode database has been compiled with data from JET and five other machines world-wide of different sizes. The preliminary analysis of these data gives an H-mode scaling law with τ_E increasing linearly with I_p.

Two routes have been explored to optimize fusion yield in JET H-modes. The first seeks to combine the good global confinement properties of the H-mode with peaked profiles produced by pellet fuelling and central heating. A peaked density profile produced by injecting a string of pellets is heated by a mixture of beams (2.5MW) and ICRF power (9MW) to produce peaked temperature profiles with $T_e(0) \approx T_i(0) \approx 12$keV which, although transient, persist into the H-mode phase. The fusion reaction rate peaks at $R_{DD} \approx 2 \times 10^{16} s^{-1}$ corresponding to $Q_{DD} \approx 9.5 \times 10^{-4}$ and is estimated to be about 90% thermal during the period when the peaked profiles and H-mode phases overlap. The enhancement in fusion yield due to peaked profiles is shown in Fig.177.

The second route to high fusion yield is the hot ion H-mode where powerful neutral beams are injected into a low density target plasma. Typically, a single null, 3.5MA discharge, heated by 18MW of D° (10MW at 80keV and 8MW at 140keV), produces a central ion temperature $T_i(0) \approx 28$keV and plasma energy $W \approx 12$MJ. These discharges

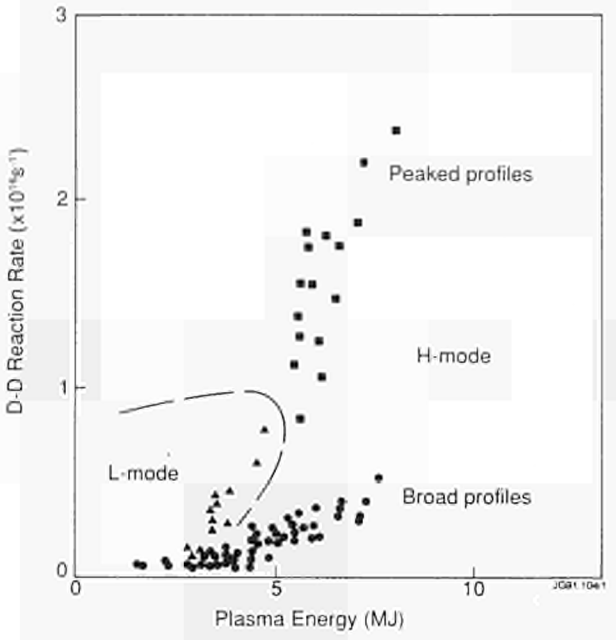

Fig.177 Enhancement of the fusion reaction rate for peaked profiles compared to broad profiles with the same plasma stored energy.

have obtained the best fusion performance with Q_{DD} = 2.4×10^{-3} and $n_D\tau_E T_i = 9\times10^{20}m^{-3}skeV$.

D(^{3}He) Fusion Experiments

Fusion powers ≈ 140kW were measured from the D^{3}He fusion reaction. These experiments used ion cyclotron heating of the ^{3}He minority and best results were obtained with low ^{3}He concentrations admitted by gas puffing. Centrally deposited ^{3}He from beam injection actually decreased the reaction rate, indicating that the optimum minority concentration is low (<1%) so that the fast particle energy is maximised.

Progress Towards a Reactor

During 1990, substantial progress was made towards reaching reactor conditions, in that very high values of the fusion

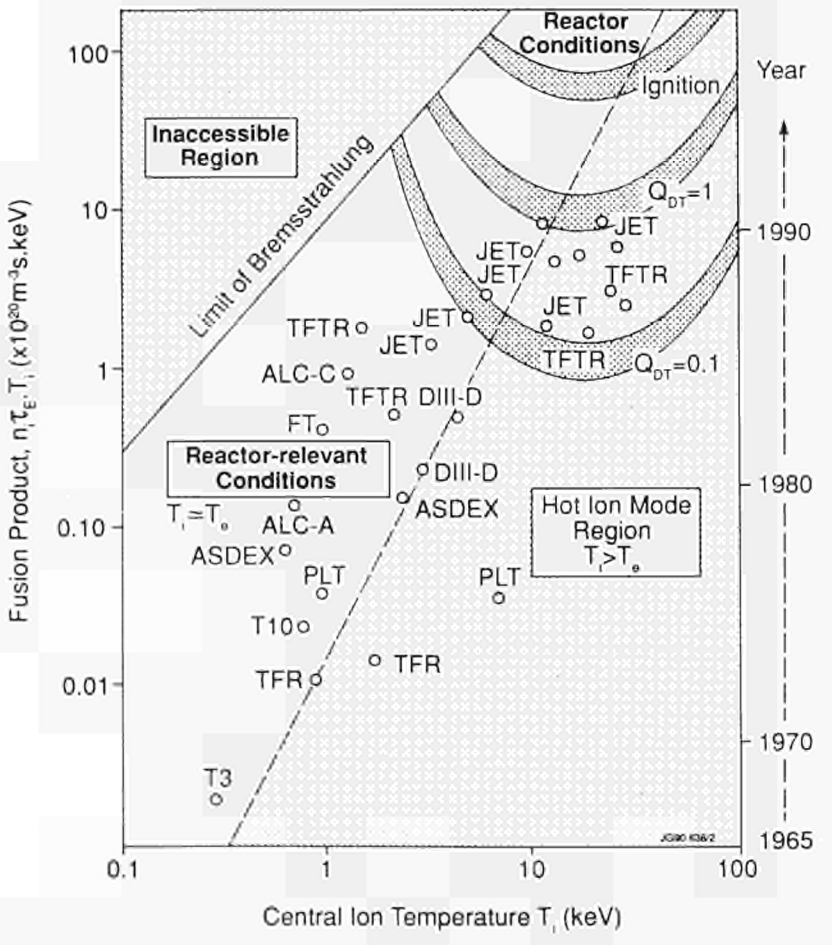

Fig.178 The triple fusion product as a function of central ion temperature for various fusion devices. The mode of operation relevant for a reactor is where the electron and ion temperatures are nearly equal at values between 15 and 50keV. The high density/low temperature region is forbidden due to radiation losses.

product ($n_i(0)\ \tau_E\ T_i(0)$) of ~$9x10^{20}m^{-3}keVs$ were achieved (see Fig.178). These high values were obtained within an H-mode X-point configuration; both with a hot-ion H-mode and with a Pellet Enhanced Performance (PEP) H-mode.

The neutron yield for this hot-ion discharge was the highest ever achieved on JET at $3.8x10^{16}ns^{-1}$, producing 50kW of fusion power with a $Q_{DD} = 2.5x10^{-3}$. A full D-T simulation of this pulse showed that ~13MW of fusion power could have been obtained transiently with the 18MW of injected NB power, giving a fusion product value ($n_i\tau_E T_i$), which was within a factor of 5-8 of that required in a D-T reactor.

The range of values of Q_{DD} that have been covered by JET during 1990 is shown in Fig.179. The marked points indicate the best values that have been obtained in the four different operating regimes of hot ion H-modes, H-mode with peaked density and temperature profiles, belt limiter and inner wall limiter discharges. Simulations of Q_{DT} have been made using the transport code TRANSP with the assumption that the plasma conditions remain the same as presently achieved in deuterium discharges. The results indicate that it will be necessary to inject both D and T beams in order to ensure an optimum mixture of fuel throughout the plasma cross-section. Several simulations where mixed D and T neutral beams are injected into a D + T target plasma give $0.8 < Q_{DT} < 0.9$.

Significant improvements were also achieved in the limiter configuration due to the improved pumping with beryllium tiles. Higher ion temperatures (>20keV) and higher values of the fusion product $(n_i\tau T_i)=3.3x10^{20}m^{-3}keVs$ were obtained. The highest achieved values of the fusion product in the various configurations are listed in Table XII.

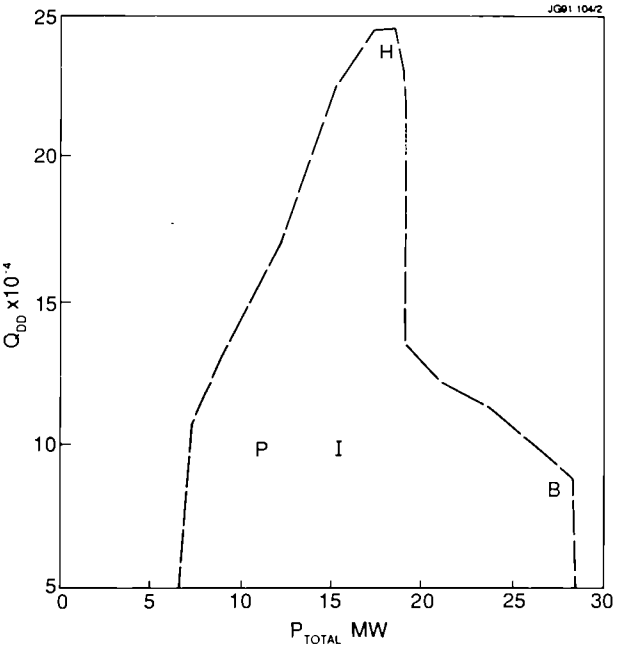

Fig.179 Q_{DD} as a function of total heating power. The shaded area indicates the range covered by JET experiments and four typical points are marked:
H - a hot ion H-mode
P - H-mode with peaked profiles following pellet injection and central ICRF (PEP-mode)
B - 5MA limiter discharge
I - Inner wall discharge.

Table XII
Maximum Values of $<n_i(0)\tau_E T_i(0)>$

Experimental Programme	Peak Densiy $n_i(0)$ ($x10^{19}m^{-3}$)	Energy Confinement τ_E (s)	Ion Temperature $T_i(0)$ (keV)	Fusion Product $<n_i(0)\tau_E T_i(0)>$ ($x10^{20}m^{-3}$.skeV)	Q_{DT} Equivalent	Plasma Current I_p (MA)
Ohmic (4.6MW)	4.0	1.0	3.1	1.2	0.010	5
ICRF (16MW)	3.8	0.4	8.0	1.2	0.025	3
NBI (16.5MW) Low n:	3.0	0.55	20	3.3	0.35*	4.7
Combined NBI+RF (22MW)	4.5	0.5	8.1	2.0	0.30*	3.5
X-point NB-(18MW)	4.6	1.0	19	8.7	0.8*	4.2
X-Point (PEP) Pellet + ICRF (9MW)	8.0	1.0	8.5-10.5	7-8.6	~0.4	3

(* Beam Plasma reactions are dominant)

Developments and Future Plans

In 1978, the original objectives of JET were set out in the JET Design Proposal, EUR-JET-R5, as follows:

> *'The essential objective of JET is to obtain and study a plasma in conditions and dimensions approaching those needed in a thermo-nuclear reactor. These studies will be aimed at defining the parameters, the size and the working conditions of a Tokamak reactor. The realisation of this objective involves four main areas of work:*
>
> *i) the scaling of plasma behaviour as parameters approach the reactor range;*
>
> *ii) the plasma-wall interaction in these conditions;*
>
> *iii) the study of plasma heating; and*
>
> *iv) the study of α-particle production, confinement and consequent plasma heating.*
>
> *The problems of plasma-wall interaction and of heating the plasma must, in any case, be solved in order to approach the conditions of interest.*
>
> *An important part of the experimental programme will be to use JET to extend to a reactor-like plasma, results obtained and innovations made in smaller apparatus as a part of the general tokamak programme. These would include: various additional heating methods, first wall materials, the control of the plasma profiles and plasma formation.'*

At the start of 1990, the JET Project was midway through its planned Phase III - Full Power Optimization Studies. The original design specifications of JET had been achieved and in many cases exceeded. Two of the main programme objectives of the JET programme - the study of plasma heating and of the confinement of plasma - had to a large extent been met, in that the results from JET have made it possible to define with confidence the main parameters of a Next Step device. Some aspects of α-particle heating had also been studied in simulation experiments.

During 1990, emphasis within the programme was further directed towards the fourth area of study, that of plasma-wall interactions, particularly the control of impurities in high performance plasmas. The Project has now demonstrated clearly the benefits to be derived (albeit transiently) from passive impurity control by the use of beryllium as a first-wall material for plasma-facing components.

The most recent experiments on JET achieved plasma parameters approaching breakeven values for about a second, resulting in a large burst of neutrons. These neutrons indicate that fusion D-D reactions are taking place. However, in spite of the plasma pulse continuing for many seconds after reaching peak plasma values, the neutron count fell away rapidly as impurities entered the plasma and lowered its performance. This limitation on the time for which the near-breakeven conditions could be maintained is due to the poisoning of the plasma by impurities. This has further emphasised the need to provide a scheme of impurity control suitable for a Next Step device.

The JET aims clearly state that JET is an experimental device and that, to achieve its objectives, the latest developments in Tokamak physics must be allowed to influence its programme. However, within a JET programme to 1992, it would not be possible to tackle thoroughly problems associated with impurities. In view of the central importance of impurity control for the success of a Next Step device, the JET Council unanimously supported in 1989 a proposal to add a new phase to the JET programme, the objective of which would be to establish effective control of impurities in operating conditions close to those of the Next Step. This involves providing JET with a new magnetic configuration, including principally the installation of a pumped divertor. A prolongation of four years from the current end date of 31 December 1992 is needed to carry out the changes and then

to allow sufficient experimental time to demonstrate the effectiveness of the new configuration in controlling impurities. This would provide for deuterium operation up to the end of 1994, followed by tritium operations in 1995 and 1996.

The JET Council has agreed the proposed prolongation of the Project. In addition, a recent European Fusion Programme Evaluation Board (under the Chairmanship of Prof. U. Colombo) has recommended that fusion should be maintained as a priority in the Community's energy research strategy and supported the proposal to prolong JET's lifetime. The Project extension has been incorporated into the Euratom Fusion Programme proposal and a decision by the Council of Ministers is awaited.

During 1990, much of JET's efforts have been directed to preparations for the future, in particular to pursuing in parallel the two programme paths;

- preparations for the new pumped divertor phase in the frame of a proposed programme to 1996;
- completion of a JET programme by the end of 1992 with the final phase of D-T operations.

In the context of preparing for D-T operations, the Active Gas Handling Building was completed. Installation of the main sub-systems of the active gas handling system has proceeded as the components have been delivered and subsystem commissioning has started. Some important components have suffered delays and this has put back the date at which overall plant process commissioning can start. At present, it is still considered possible to undertake a limited campaign of D-T operations before the end of 1992.

At the same time, the Project has pressed ahead strenuously with design and procurements for the new pumped divertor phase. The design of the main components - the divertor elements and the internal coils - evolved during the course of the year.

The Project has thus been able to maintain the dual programme stance required pending the decision of the Council of Ministers on a revised Fusion Programme and in particular on the proposed prolongation of the JET Programme. However, this position cannot be maintained during 1991 for both programmatic and resource reasons.

Present achievements show that the main objectives of JET are being actively addressed and substantial progress is being made. The overall aim for JET can be summarised as a strategy "to optimise the fusion product ($n_i T_i \tau_E$)". For the energy confinement time, τ_E, this involves maintaining, with full additional heating, the values that have already been reached with ohmic heating and in the H-mode with the X-point configuration. For the density and ion temperature, it means increasing their central values $n_i(0)$ and $T_i(0)$ to such an extent that D-T operation would produce α-particles in sufficient quantity to be able to analyse their effects on the plasma.

The enhancements to JET aim to build up a high density and high temperature plasma in the centre of the discharge (with minimum impurity levels) where α-particles could be observed, while maintaining an acceptably high global energy confinement time, τ_E. The mechanisms involved are to decouple the temperature profile from the current density profile through the use of lower hybrid current drive and neutral beam injection to ensure that, at higher central temperatures, the current density in the centre does not reach the critical value that causes sawteeth oscillations.

This will involve the following:

a) Increasing the Central Deuterium Density $n_D(0)$ by:
   - injecting high speed deuterium pellets and higher energy deuterium neutral beams to fuel the plasma centre and dilute impurities;
   - injecting pellets to control the influx of edge material;
   - stabilising the m=2, n=1 magnetic oscillations present at the onset of a disruption with magnetic perturbations produced from a set of internal saddle coils which will be feedback controlled;

b) Increasing the Central Ion Temperature, $T_i(0)$ by:
   - trying to lengthen the sawtooth period;
   - controlling the current profile (by lower hybrid current drive in the other region, and by counter neutral beam injection near the centre) to flatten the profile;
   - on-axis heating using the full NB and ICRF additional heating power (24MW, ICRH, and 20MW, NB)

c) Increasing the Energy Confinement Time τ_E by:
   - increasing up to 7MA the plasma current in L-mode operation;
   - increasing up to 6MA the plasma current in the full power, H-mode operation in the X-point configuration.

d) Reducing the impurity content, by:
   - using beryllium as a first-wall material to decrease the impurity content;
   - Controlling new edge material by using the pumped divertor configuration.

In parallel, preparations for D-T operation are proceeding at full speed to ensure that the necessary systems for gas processing, remote handling, radiological protection, active

handling and operational waste management are fully commissioned and operating satisfactorily in good time before the introduction of trtium into the JET device. In addition, the tritium neutral injection system at 160kV and α-particle diagnostics are being developed for this phase.

The following sections describe various developments which are underway on JET to implement these systems.

Current Drive and Profile Control

The main objectives of current drive and profile control remain:

- to suppress sawtooth activity and to benefit from higher core reactivity by sustaining peaked profiles of both density and temperature;
- to modify local values of the current gradient and improve energy confinement in the plasma centre;
- to assess the efficiency required for non-inductive operation of large tokamaks.

The main tool which is being prepared to control the plasma current profile in JET is the generation of non-inductive current by means of Lower Hybrid Waves. First results with a prototype system (LO) have already been obtained. The full system (L1) will be installed during the 1992 shutdown. A high directivity ICRF antenna array is also being manufactured. Its main function is to provide plasma heating but it will also be capable of driving non-inductive currents by means of Transit Time Magnetic Pumping (TTMP). These antennae (A2) will also be installed during the 1992 shutdown. A substantial amount of non-inductive current drive can also be produced by means of the 140keV neutral beams (NB) and the bootstrap current. The present status of the efficiency in various non inductive current drive methods [1] is shown in Fig.180. The required efficiency for Next Step devices is very high, especially for high density operation. However, current profile control can be achieved with lower efficiencies.

Table XIII
The JET LHCD System

Frequency	3.7GHz
Power (launched)	10MW
Launcher	Multijunction type
Fixed phasing in the multijunction	90 degrees
Central $N_{\|}$	1.8
Range of $N_{\|}$	1.4 to 2.4
No. of waveguides in a horizontal row	32
Phase accuracy	10 degrees
Width of the $N_{\|\|}$ spectrum	0.2
Directivity	80%
Density limit	$8x10^{20}m^{-3}$
Power handling	4-5kW cm^{-3}
Estimated drive current	
at $n_e = 2x10^{19}m^{-3}$	3-5MA
at $n_e = 5x10^{19}m^{-3}$	1.2MA

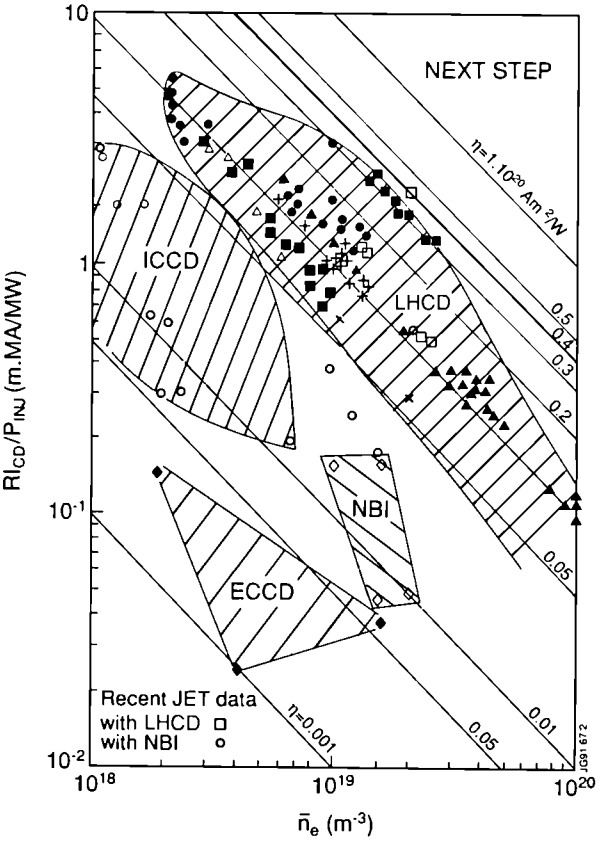

Fig.180 Efficiency in various non inductive current drive methods

Lower Hybrid Current Drive

The main characteristics of the JET LHCD system are shown in Table XIII. The programme is organised in two stages. The first stage consists of a prototype launcher installed during the 1989/1990 shutdown [2]. This prototype has the main technical features of the complete system which will be installed during the 1992 shutdown. Slight modifications of the geometry of the multijunctions arrangement is required in order to fit the new magnetic geometry of the pump divertor phase. The technical aspects

of the LHCD system and the initial results with the prototype launcher are presented in the section of this report on Technical achievements.

The initial main results [3] are the following:

- up to 1.6 MW of Lower Hybrid wave power has been launched for time duration of up to 20 s;
- significant loop voltage drop has been achieved for densities up to $n_{eo}=3 \times 10^{19} m^{-3}$, corresponding to Lower Hybrid non inductive current up to 1 MA;
- current drive efficiency (defined as $\gamma=nIR/P\ m^{-2}\ A/W$) appears to increase with the volume averaged electron temperature at a rate of $d\gamma/d<T_e> \sim 0.15 \times 10^{20}\ m^{-2}\ A/(WkV)$ up to $\gamma \sim 0.4 \times 10^{20}\ m^{-2}\ A/W$ at $<T_e> \sim 1.9$ keV
- increase of the central electron temperature is observed in excess of 1 keV per coupled MW of LH power;
- significant broadening of the current profile is observed which increased with plasma density;
- sawtooth free period up to 2.9 s have been achieved in ICRF heated plasmas.

These results are quite encouraging in particular for the application of LHCD to large plasmas with high electron temperature. Effiency achieved on JET with the prototype LHCD launcher is indicated in Fig.180 together with current drive efficiencies achieved with the JET 140 kV neutral beams. LHCD current drive efficiencies achieved so far are already within the range considered as necessary for the Next Step at low and medium densities.

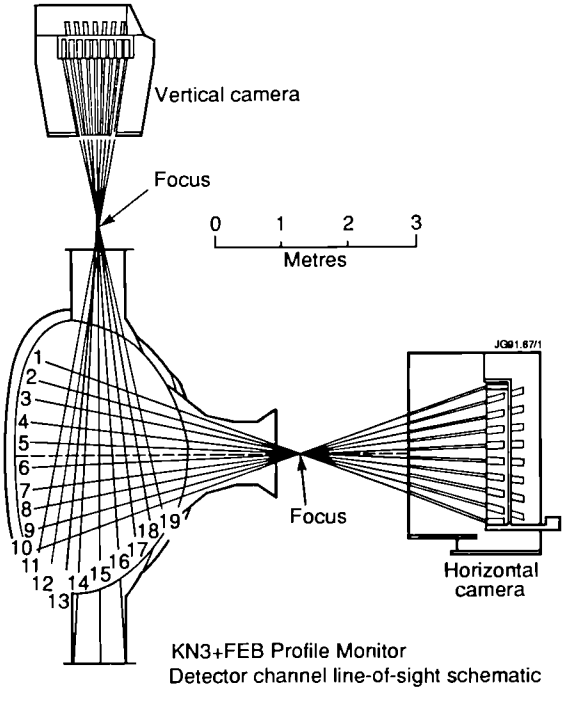

Fig.181 General set-up of the neutron tomography system

In order to assess the radial profile of the LH induced fast electrons and to study the radial transport of the fast electrons, tomography of the fast electron bremsstrahlung emission is being implemented using the general set-up of the neutron tomography system as shown in Fig.181. Initial results with the vertical camera confirms a broadening of the radial profile of the fast electrons when the density increases. The horizontal camera will be installed during the 1990/1991 shutdown.

Ion Cyclotron Current Drive

Ion cyclotron waves can induce non-inductive current drive either by asymmetric heating of minority ions or by direct interaction between the fast wave and electrons. The latter scheme appears to be a promising current drive method for a reactor grade plasma mostly due to its ability to drive central current independently of the density value.

The interaction between the fast wave and electrons is a coherent combination of two forces parallel to the direction of the electric field:

- electron Landau damping similar to LHCD;
- transit time magnetic pumping (TTMP) where the driving force is a product of the magnetic moment and of the magnetic field gradient.

Electron Landau damping and TTMP produce currents in the opposite direction. However, the TTMP component is dominant when the electron beta of the plasma is large or at low frequency and TTMP current drive will take place at the plasma centre where the beta is maximum. The advantage of TTMP current drive compared to other schemes such as LHCD is the absence of density limit. Profile control in a reactor can therefore be obtained with TTMP current drive at the centre and LH current drive at the plasma periphery.

Operation of JET at high beta values, where more than 20% of the input power was directly absorbed by the bulk electron population, has allowed the theoretical background for such a scheme to be confirmed [4]. However, the present ICRF antennae system, where the two central conductors are strongly coupled and cannot be arbitraily phased, does not allow high directivity to be obtained, high directivity being essential for effective current drive.

The new antennae array (A2), which is being developed for the pumped divertor geometry of the JET new phase, will allow the directivity to be significantly improved due to a septum (isolating screen) so that the antennae can be phased essentially arbitrarily for TTMP current drive experiments. However, the presence of a septum changes the excited $k_{\parallel}$

Table XIV
Antenna Parameters

		JET (A1)	JET (A2)	ITER (NET)
Antenna conductor to limiter distance	a(m)	0.06	0.12	0.2
Antenna conductor to backwall distance	d(m)	0.1	0.25	0.3
Antenna conductor to screen distance	χ_{sc}(m)	0.012	0.012	0.05
Length of one antenna element	ω_y(m)	0.8	0.8	1
Half-width of the antenna element	ω_z(m)	0.055	0.105	0.125
Current propagation constant in y	$\beta(m^{-1})$	2	2	1.57
Number of boxes energized	N_{box}	8	4	30
Number of antenna per box	N_yN_z	2.2	2.4	2.1
Mid-line distance between two conductors	L_z(m)	0.31	0.4	0.55

spectrum due to the current induced in them. Reduction of this effect is achieved by inserting slots whose optimum depth is based on testbed measurements [5].

The A2 antennae have four central conductors equally spaced in an integrated structure of two antenna boxes. A comparison between directivity for the A1 and the A2 antennae as a function of the toroidal mode number is shown in Fig.182, showing that a 75% directivity can be expected with the new antennae. The corresponding antenna parameters are in Table XIV. These antennae are very similar in their design to the antennae which can be envisaged for the Next Step device whose parameters are also given in Table XIV.

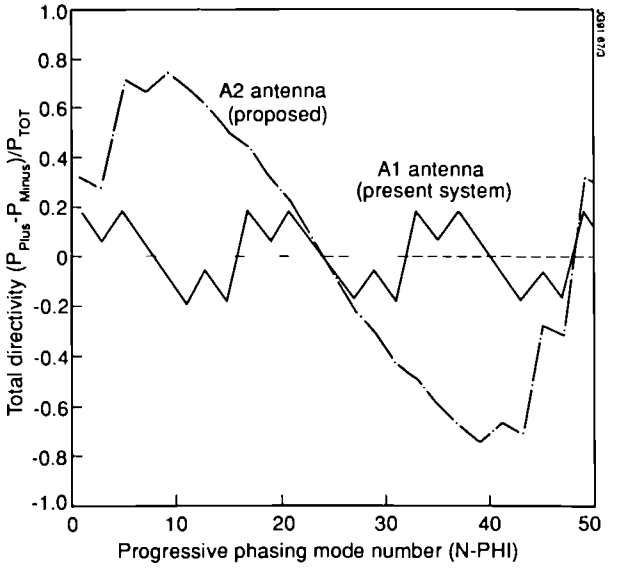

Fig.182 Comparison between directivity of the A1 and the A2 antennae as a function of the toroidal mode number

Theoretical computation using the combined ray tracing and Fokker-Planck calculations has been employed to calculate current drive efficiencies. Ray tracing has been carried out in full toroidal geometry for a non circular plasma including the poloidal field. A plot of the current drive efficiency factor $\gamma=n_eRI/P$ for A1 and A2 antenna arrays as a function of the toroidal mode number is shown in Fig.183 predicting a substantial improvement with the new antennae. A maximum value of 0.11 is found for a T_e = 10keV plasma, corresponding to a driven current of 1 MA at a density of 3 x 10^{19} m^{-3} with 5 MW of ICRH power.

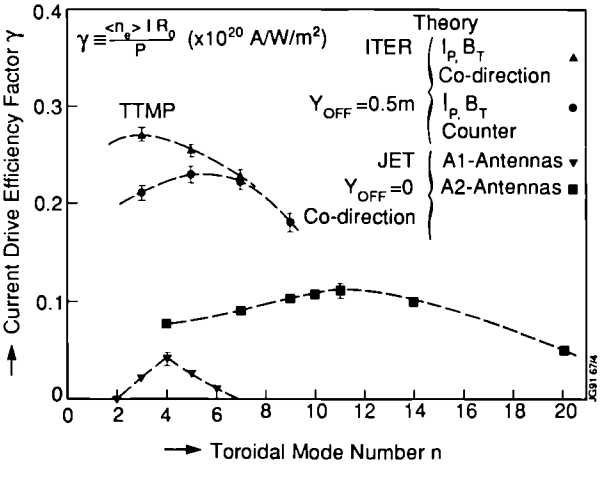

Fig.183 Current drive efficiency factor $\gamma=n_eRI/P$ for A1 and A2 antennae arrays as a function of the toroidal mode number

The same technique has been used to optimise the proposed ICRH system for NET/ITER like devices, in which JET has taken a leading role [6]. During the course of that study, it has been found that the Tokamak poloidal field can significantly change the $k_{//}$ spectrum and reduce the current drive efficiency, if antennae are located off the midplane. As shown in Fig.182, an efficiency factor of 0.28 can be obtained for an array of 30 antennae located in the midplane of the torus for a plasma central temperature T_e=30keV. Such an efficiency is comparable to LHCD and NB current drive techniques and make TTMP quite attractive for NET/ITER like devices.

References

[1] C.Gormezano, Radio frequency heating and current drive; Status and prospects for the Next Step. 16th Symposium on Fusion Technology (London, U.K.) (1990) and to be published in Fusion Energy and Design (1991);

[2] H.Brinkshulte et al, High power tests of the JET prototype LHCD launcher. 16th Symposium on Fusion Technology (London, U.K.) (1990);

[3] C.Gormezano et al, Lower Hybrid Current Drive Experiments in JET. 32nd Annual Meeting of the Division of Plasma Physics of the American Physical Society (APS), (Cincinnati, U.S.A.) (1990);

[4] F.Rimini et al, 17th EPS Conference on Controlled Fusion and Plasma Heating (Amsterdam, Netherlands) (1990), Vol.III p1150;

[5] V.Bhatnagar et al, Fast Wave Current Drive in the Ion Cyclotron Range of Frequencies. Joint Varenna-Lausanne International Workshop (Varenna, Italy) (1990);

[6] J.Jacquinot et al, ITER FWCD Specialists Final Report (1990)

Pellet Injection

This section summarises developments relating to the advanced multi-pellet injection system which will be installed during the 1992 shut-down and brought into operation in the 1993 operational period. The system presently comprises a high-speed multi-pellet Advanced Pellet Launcher (APL) incorporating two-stage gun technology; a new slightly upgraded version of the ORNL Launcher for medium-speed pellets (the repetitive pneumatic single-stage launcher JPL II, compatible with the geometry of the new APL and the tritium, radiation, and remote handling requirements for the Active Phase of JET); and a pellet centrifuge for low-speed pellets at a high rate suitable for the requirement of the pumped divertor programme. The report deals with the relevant planning and design activities, including the preparatory developments on the pellet testbed. Details of the high-speed Prototype Launcher have already been covered in the section on Torus Systems.

The envisaged spatial arrangement of the three pellet sources is shown in Fig.184. The APL and the JPL II are attached to the Pellet Injector Box (PIB), which acts as a differential pumping system to remove the driver gas of the pneumatic guns. The centrifuge bypasses the Pellet Injector Box PIB, but connects into the same main horizontal port of Octant No.2. Fig.185 shows an elevation view, seen in the direction of the arrow indicated in Fig.184.

The Advanced Pellet Launcher (APL)

Measures for the implementation of the existing ORNL Launcher and the Prototype Launcher have always been guided by the principle that the interface to the torus (the PIB and its cryopump) should cope with the final requirements of an advanced launcher system. Thus, only modest up-

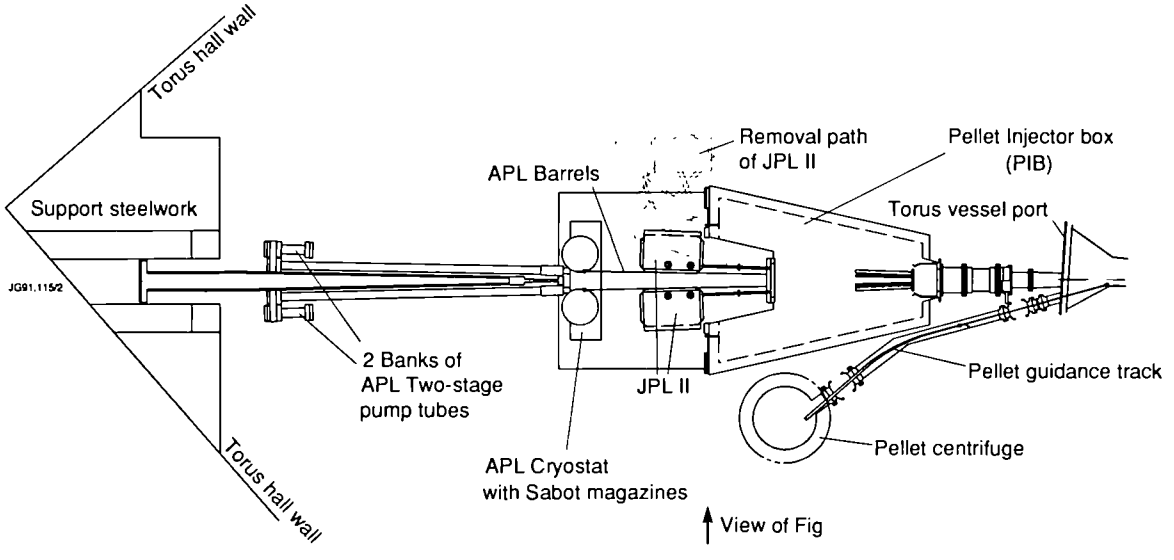

Fig.184 Conceptual sketch of future JET Pellet Injection (plan view);

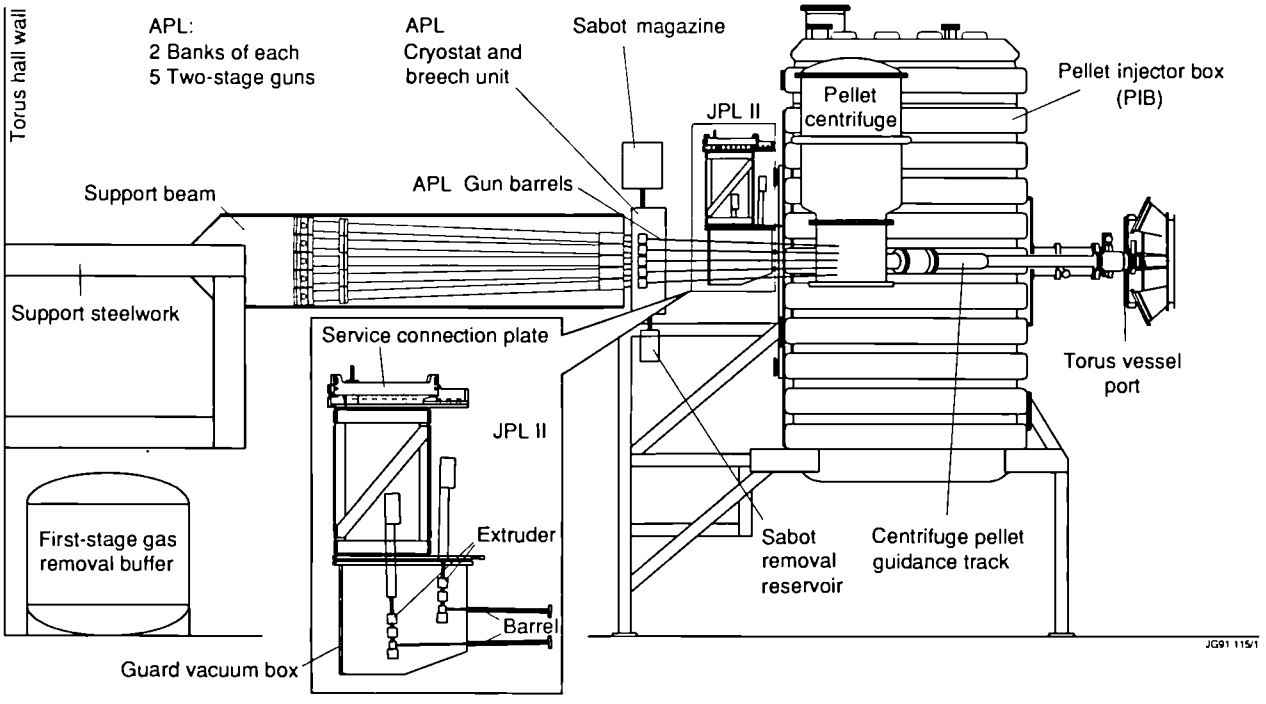

Fig.185 Conceptual sketch of future JET Pellet Injection (elevation);

grades can be expected, especially on the pellet characterising diagnostics. When the extent became apparent to which the two-stage gun principle might be expandable towards the goal of achieving higher pellet speeds, the support steelwork for the proto-type was designed to take peak APL loads. This may approach 4 MN (400 tonnes) at the time of reversal of a 60 mm diameter piston at 15 kbar.

Since the results of the high-speed pellet experiments are not yet available it is hard to settle on a firm specification for the APL. Desirable features now aimed for consist of: pellets in the 3 - 6 mm range; pellet velocities exceeding 5 kms^{-1}; availability of ~ 10 pellets per tokamak pulse, some as close in time as a fraction of a second; and pellet material of deuterium, but tritium should not be ruled out.

The conceptual design of the APL, which is still being carried out, is based on experience acquired during the construction and commissioning of the Prototype Launcher and on the JET Pellet Testbed. In addition, several R & D elements resulted from collaborative work with the CEA Centre d'Études Nucléaires de Grenoble (CENG), France, under a JET contract. Despite considerable efforts on both sides, there was no fully experimentally proven conceptual design available at the end of 1990, which would fulfill the desired specifications. Since the APL must start operation in 1993, a modular approach seemed sensible. The design would permit implementation in a flexible way of up to ten two-stage guns (fall-back solution with a single shot per gun per tokamak pulse). Alternatively, fewer repetitive guns in combination with a pellet formation cryostat unit, was an option which could easily be adapted to the respective gun solution as well as the number of guns. This ensures that the system can be commissioned at least partially on time and can be expanded during operation. The design must also call for easy exchange and upgrading of components not yet proven experimentally to lower the risk of operational failure.

The two-stage gun would look very similar to the prototype launcher but upgraded in several respects. To achieve higher pellet speeds, the second-stage driver gas temperature and pressure will have to be increased, requiring a higher compression ratio and hence larger pump-tube length (in the Torus Hall, the limit is 5.5 m). The high compression section of the pump-tube as well as the actual barrel must be lined with a high-strength high-temperature material. These measures are now being investigated on the testbed. To achieve a launcher repetitivity of ~$1s^{-1}$, the valve assembly at the rear of the pump-tube must be complemented to permit the fast release of first stage driver gas after the shot, and stoppage of the piston in the start position for the next pulse. CENG have successfully demonstrated the principle with a three-shot sequence (with closed barrel, no pellets) at 0.6 s^{-1} on a prototype-like gun. A buffer vessel to store the first-

stage gas needs to cope with ~ 10 shots during a tokamak pulse with up to 1000 barℓ each; such a vessel (~ 12 m^{-3}) will be procured soon and located beneath the launcher steelwork in the Torus Hall. It will be evacuated between pulses by a vacuum pump in the West Wing.

Two designs of the pellet formation cryostat and the gun breech were experimentally investigated during development work. The JET prototype cryostat used a transport chain and a parallel design at CENG uses a linear rod system. Both transport systems operate at near LHe temperature for the storage of pre-formed cryo-condensed deuterium pellets and the breeches use slightly different sealing techniques. These designs are being reviewed and revised, taking into account experience gained in the commissioning and operation of both systems. JET has concluded that the principle of using bushings, (short (≈ 2 cm) sections of the barrel which already contain the bursting disc to ensure the correct pellet starting pressure and the sabot to support the pellet during the acceleration) is still considered very sound. These bushings can be loaded into a magazine (which in its final form will have to be mounted and exchanged by remote handling), filled with ice, placed into the breech where they connect and seal to the two barrel sections, and can then be discharged into a collector vessel with the remainder of the bursting disc still trapped in them. However, the used space per breech or gun of the present systems is incompatible with the ten gun arrangement, restricted in space by the acceptance angle of the torus port. Both transport systems are hindered with respect to the fast re-loading of the breech by the need to move a bulky transport system, and, in addition, the stored number of bushings. The hot second-stage driver gas leaking through the breech seal during the pressure surge of several thousand bar during the shot is jeopardising the stored pellets in waiting, as well as the low temperature of essential cryostat parts. The transport system of both designs is interlinked with the breech frame in a very complicated way preventing modular design. The shear mass of the cold box environment which has to be temperature cycled near LHe conditions in the cryo-condensation process is too large, leading to large cycle times and difficult operational scenarios.

The revised design attempts to avoid these disadvantages in the following way: the breech unit is a module at room temperature in which the bushing is injected within ~ 10^{-2} s, from a LHe cryopump environment keeping the pre-loaded bushings at say 5°K for the day of operation. The injection of the bushing (~ 30 g) is performed by a shuttle with very small mass (~ 60 g) loaded from a gravity fed conveyor belt system, which permits the sorting of bushings with different pellet sizes (by choice of sabot) and moderately fast transport to the shuttle within the protective environment of a large (several x 10^5 ℓs^{-1}) cryopump (this also takes care of an instantaneous pumping of breach leakage). Pellets are being extruded into pre-cooled bushings by one extruder unit and these bushings are then handed over to the belt system. Thermal cycling is therefore restricted to the bushing pre- and final-cooling grabbers. It is hoped that this design will stand up to the modularity requirements and avoid most of the undesirable features encountered in previous developments. A first test of a warm breech and shuttle for a higher performance gun is planned for mid-1991, with deuterium pellet tests starting towards the end of the year. Procurement on long lead items will commence in parallel, with an initial APL system starting commissioning in second half of 1992.

The Intermediate-Speed JPL II

The conceptual design of the JPL II was carried out in a joint effort between JET and US Department of Energy (USDoE), Oak Ridge National Laboratory (ORNL), U.S.A., whereby JET contributed the interface elements leading to the compatibility of the launcher with the JET environment conditions. The JPL II was first split into two guard vacuum boxes each comprising two single-stage guns, each with their pellet trajectories either side of the two vertical banks of the APL. This made optimum use of the horizontal port / PIB acceptance angle (see Fig.184, where the difficult remote handling removal path is also indicated).

The two guns of each box are staggered, such that their extruders have sufficient clearance and that the respective actuators can be conveniently brought through the top flange (see insert in Fig.185). All services, cabling and piping apart from a few vacuum connections, have been designed to connect at a top plate, easily reached by remote handling tools. The gas handling valve assemblies and a high-pressure helium driven compensator (to provide constancy of the hydrogen propellant pressure for long pellet sequences) combined with a lower (and therefore safer) hydrogen reservoir are integrated in the frame space between the guard vacuum box and the top plate.

Each gun of nominally 3, 4, 5 and 6 mm inner barrel (i.e. pellet diameter) is essentially of the same proven design as that one of the present ORNL Launchers delivering pellets at speeds in the range 1.2 - 1.5 kms^{-1}. However, a major upgrade in LHe economy (to keep the consumption per gun

to < 10 ℓh^{-1}), the doubling of the volume of the deuterium ice reservoir (for extended length of pellet sequences of 160, 80, 40 and 20, respectively), an attempt to increase the repetition frequency (10, 6, 2 and 1 s^{-1}, respectively) and a careful revision of sealing and joining technology towards even higher reliability and nuclear compatibility (particularly in view of the use of tritium contaminated deuterium as the pellet fuel) were all elements of this conceptual design.

It is hoped that a positive decision concerning continuation of USDoE collaboration can be made in early 1991 and that the JPL II will then be delivered by the US under the Pellet Agreement ready for implementation for the 1993 experimental campaign.

The Pellet Centrifuge

A pellet centrifuge for JET should be capable of providing deuterium particles into the plasma beyond its recycling layer. This is to provide a minimum recycling flow into the divertor, which is sufficiently strong to sweep plasma impurities towards the divertor and to retain impurities from the dump plates in the divertor. The order of magnitude for the gas flow equivalent should approach 1000 mbarℓs^{-1}, a value which has been used in probing X-point plasma experiments. It is intended that up to this amount can be produced by the injection of 1.5 to 3 mm pellets in the plasma midplane at repetition frequencies up to 40 s^{-1} and relatively slow speeds of 50 to 500 ms^{-1}. Moreover, the centrifuge should be capable of maintaining these high gas flows for long pulses (~ 60 s).

A model for such a centrifuge is currently under construction for ASDEX Upgrade, a successor of the one used on ASDEX for several years. As far as mechanics are concerned, JET has decided to use the ASDEX Upgrade centrifuge design with minor modifications (including slightly downgrading the pellet speed, which lowers the centrifuge stresses) and has placed a contract with the IPP Garching, FRG., to transfer the design and experience and to obtain advice on the systems expansion necessary to cope with the specifications for JET. The two elements which are of main concern (and will become even more severe in the larger fusion experiments) are:

- The large amount of deuterium ice extrudate needed to produce these pellets for JET. (e.g., for 1000mbarℓs^{-1}, the extrusion speed for 3 mm pellets is about 150 mms^{-1}, which for 1 minute would correspond to an ice column of about 9 m). Therefore, the ice must be extruded from the large to the small cross-section and cooled to the state, in which it is to be accelerated, in a semi-continuous manner, which is different for the IPP centrifuge. (For JET, it is sufficient for a tokamak pulse to have an extruder ice supply of about 100 barl which can be handled in one batch, for future experiments even the condensation process will have to be included in the dynamics).
- The large gas losses of the pellet during acceleration (as much as 30 %) and during guidance on its way to the tokamak (another ~ 20 %). This means that as little as 50 % of the initial extrudate will arrive at the plasma boundary. With the now considerably increased amount of gas emanating from the pellets and the long duration injection, the usual technique of providing the centrifuge guard vacuum by the turbopump, on which the accelerator rod is mounted, breaks down and an additional large pump with speed of several x 10^5 ℓs^{-1} is required.

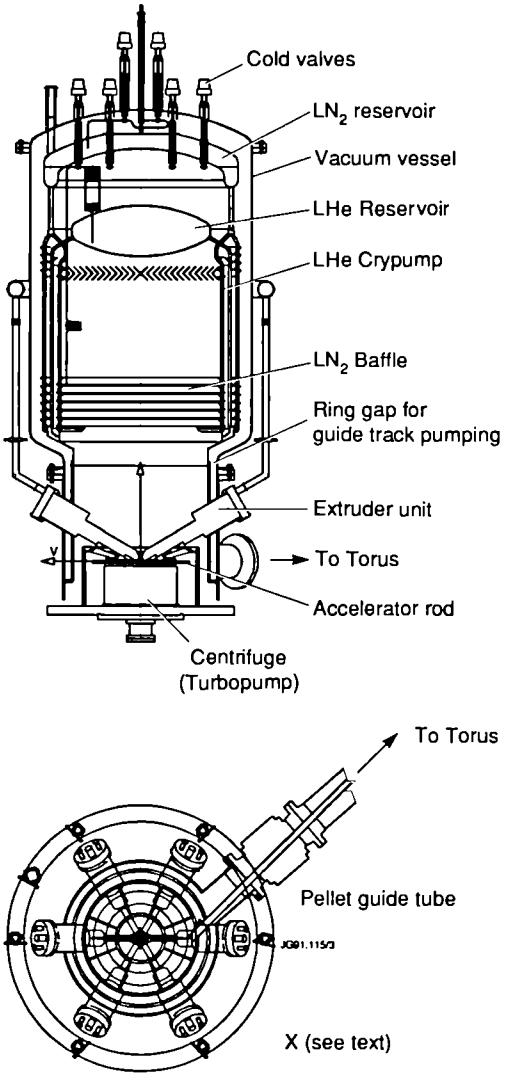

Fig.186 Sketch of pellet centrifuge, vertical cut and plan view.

So far, a conceptual design has been carried out (shown in Fig.186). The centrifuge rod can be fed with pellets near its hub by any one of the extruder units (up to 6 are possible), each one with the option of a specific pellet size. The pellets will then be oriented on the rod hub to suit the accelerator track and will leave the tip of the rod at full speed to enter the guide system towards the tokamak. The large LHe cryo-condensation pump on top of the centrifuge system will provide a guard vacuum of better than 10^{-3} mbar for the accelerator/extruder during the most severe conditions and will also cope with the gas from the guide system by the outer cryopump evacuating the ring gap in the centrifuge vessel.

The most difficult task is the design of the semi-continuous extruder, which is now being undertaken, while the centrifuge re-design and the design of the vessel (requiring particular attention due to the large amount of deuterium stored, i.e. up to 2500 barℓ) are almost completed. The design of the cryopump is not expected to cause problems, in view of the wide experience JET has acquired over many years with similar and even larger sized units. If a final decision is taken in the near future, implementation of the pellet centrifuge system is envisaged for the 1993 experimental campaign.

Tritium Handling

Introduction

On original planning, the Active Gas Handling System (AGHS) is still required to be functional for the D-T phase of JET planned for May 1992. As a result of additional workload in the Project related to beryllium activities and extensive design and procurement efforts for the pumped divertor, progress on the upgrading of components for a full D-T phase has been slower than planned during the previous year. It is now unlikely that it will be possible that the original programme of D-T shots will be carried out and a limited programme of up to 100 shots is currently envisaged. Nevertheless, before tritium injection into the torus can start, it will be necessary to demonstrate that the AGHS and safety systems essential for tritium operation have been fully commissioned with tritium and that sufficient operational experience has been accumulated. Several months of active commissioning/operation of the AGHS in isolation will be required plus a period with the AGHS providing exhaust and gas introduction for D-D operation to satisfactorily demonstrate torus interfaces. To meet this programme, the planning of tritium procurement and obtaining of official authorisations is based on the introduction of tritium into the AGHS in September 1991.

Preliminary investigation of the modifications required for a reduced D-T phase in 1992 have shown that:

a) The expected required modifications to the torus and subsystems are minor provided the tritium inventory in the machine can be kept very low;
b) The AGHS must be fully operational, although processing (of impurities) may not be required on a daily basis and the cryodistillation system would only be required for clean-up of discharged protium.

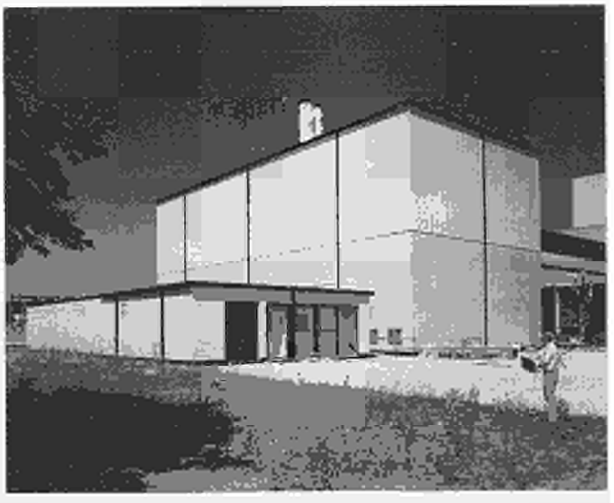

Fig.187: The AGHS Building in Summer 1990;

Active Gas Handling System Building

The AGHS Building (see Fig.187) was officially handed over in May 1990 and required some minor modifications, which were outside the building contract. With some dust still prevalent in the building due to some minor building modifications and installation of cable trays and other mountings into the concrete, designated clean areas have been established in a number of areas of the building. This will permit continual and timely progress of the interconnection of the various subsystem packages as they are available without contamination of the process with further dust.

A preliminary seismic "walkdown" has been undertaken on the AGHS building to determine whether there were any seismically vulnerable design details. Apart from minor modifications, such as extra stops to prevent the Cryodistillation modules swinging, the building is satisfactory.

Delays have occurred in the assembly of the Active Gas

Handling System (AGHS) due to the late completion of the building and due to serious delivery delays of a few key components. Plant design activities were nearly completed at the end of 1990. Only some interconnecting piping design was still underway. The overall status at the end of 1990 was as follows.

Mechanical Forevacuum System

The scroll-blower type dry mechanical pumps (600 m^3/hr and 150 m^3/hr) were delivered and placed in position. Installation of pipework and valves is nearing completion. One item - a water condenser necessary for pumping of air saturated with humidity - will be delivered and installed early in 1991.

Cryogenic Forevacuum System

Buffer tanks and cryogenic distribution systems for liquid nitrogen and liquid helium were delivered, installed and wired to local connection boxes. The delivery of the CF modules, ie cryopumps, cold traps, transfer pumps and reservoirs is delayed to February - April 1991, but all connections have been prepared for quick installation. Fig.188 shows the buffer tanks and partly installed cryodistribution system.

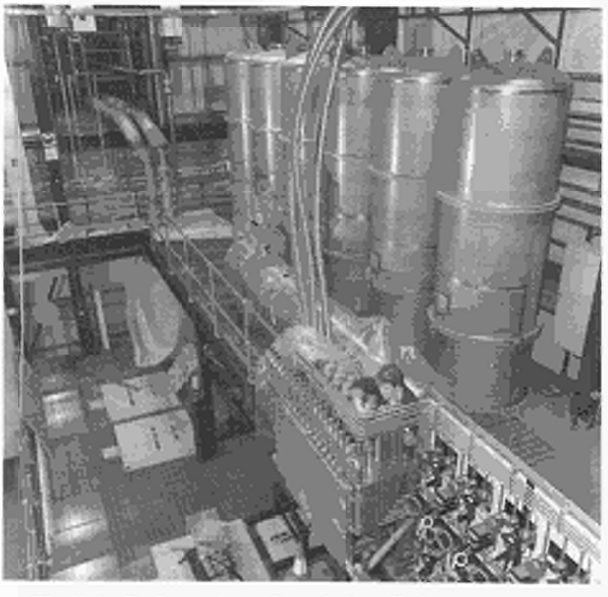

Fig.188: Buffer tanks and partly installed cryodistribution system;

Impurity Processing Loop, Intermediate Storage

Valve Box, Buffer tank, two Normetex pumps, Leak Test and Vacuum Box have been delivered and installed. Welding of interconnecting pipework is in progress. The delivery of Impurity Processing Modules is expected March 1991.

Isotope Separation System

Cryodistillation

The cryodistillation system was delivered and installed in 1990. Interconnecting pipework between components (ie process cold box, valve box, instrument box, instrumentation panel and helium refrigerator) is installed and leak and pressure-tested. Plant commissioning by the supplier will start in January 1991. Fig.189 shows the upper part of the process cold box and Fig.190 shows the instrument box with the outer containment withdrawn.

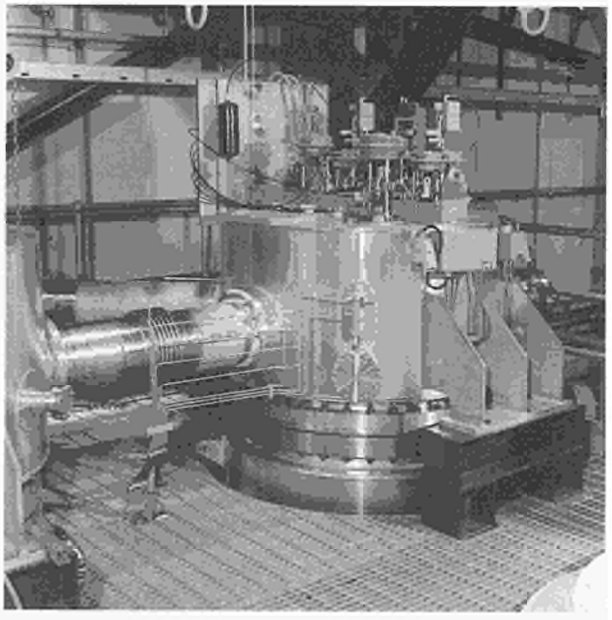

Fig.189: The upper part of the process cold box of the Cryodistillation system;

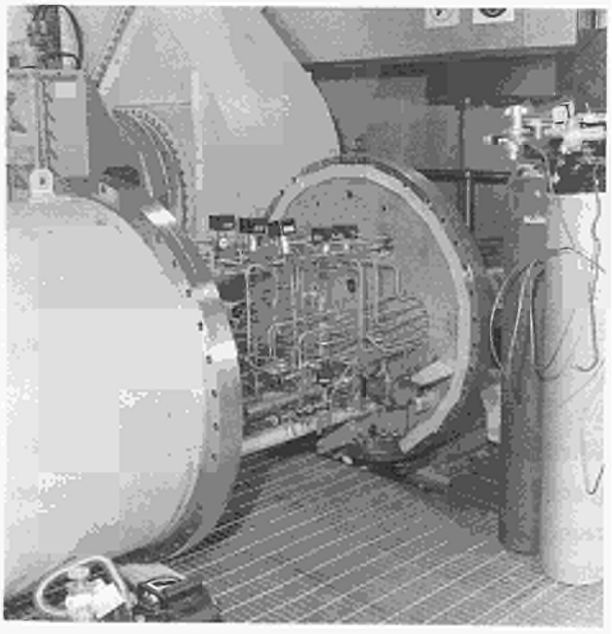

Fig.190: The instrument box of the Cryodistillation system with the outer containment withdrawn ;

Gas Chromatography

Most components were completed, delivered and installed in 1990, including the process box with four separation columns (see Fig.191), column packing, valve box, heating and cooling unit. Pipework connection is in progress.

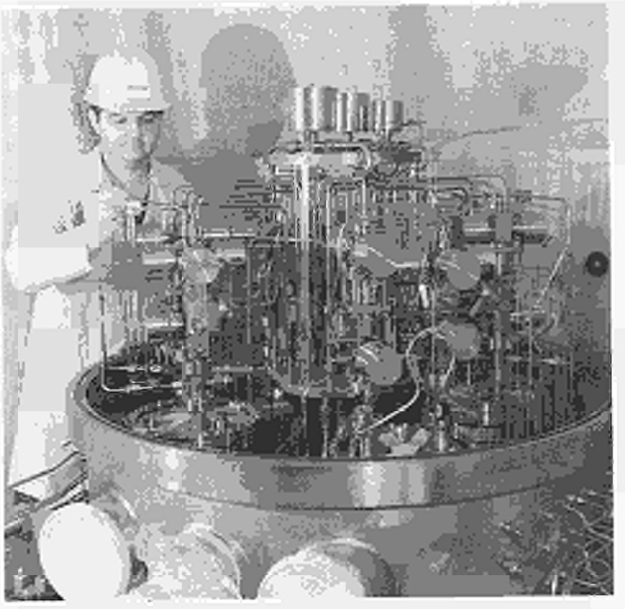

Fig.191: Column Heads of the Gas Chromatography System;

Product Storage

Two valve boxes for D_2 and T_2 storage and the dedicated leak test and vacuum box were delivered at the end of 1990 and installed. Interconnecting pipework installation is in progress.

Gas Introduction

Design was completed and contracts placed for a valve box, gas transfer lines to the Torus Hall basement together with a front-end connection box. Delivery is expected during the first half of 1991, followed by installation.

Exhaust Detritiation

The Exhaust Detritiation System was designed for detritiation of all AGHS exhaust gas streams and for maintaining positive flow into the torus during maintenance operations when the tritium contaminated vacuum vessel will be opened to ambient atmosphere. This plant consists of one recombiner rack and three molecular sieve adsorber racks which can be alternately used for adsorption and regeneration to provide continuous duty. The system was delivered, installed and tested in 1990. Some outstanding work on the plant control system is expected to be completed in January 1991.

Analytical Glovebox, Tritium Makeup

A Glovebox containing equipment for the analysis of gas samples was designed and a contract was placed for construction. The box will contain valve manifolds connecting to various gas sampling lines. Analysis will be done by a selection of two mass spectrometers (Omegatron for the H_2, HD, D_2, HT, DT, T_2, ^{3}He and ^{4}He species and a Quadrupole for the various impurity gases) and a multi-column GC system for quantitative analysis of hydrogen and impurity species. On-line purity monitoring for cryodistillation H_2 and D_2 products will be undertaken by specially designed ionisation chambers and thermal conductivity detectors.

Valve manifold and handling equipment for T_2 introduction from transport-Uranium-beds are located in a separate compartment of this box. Delivery for the glove box is foreseen in the first half of 1991. Some of the analytical equipment (Omegatron, Quadrupole RGA) is already on site. The delivery of the GC system is imminent.

AGHS Control System

The Active Gas Handling Plant Distributed Control System (DCS) was installed in the AGHS Building during summer 1990. Before delivery to JET the system underwent a three months' hardware and system acceptance testing at the manufacturers site. The DCS includes 15 front end Distributed Control Units (DCU's) covering most of the AGH subsystems. Two long delivery process subsystems (Exhaust Detritiation and Cryogenic Distillation) were equipped with PLC's. An additional DCU was ordered at a later time to be installed in the Building J1S area and be used for data acquisition of the AGHS Gas Distribution to the JET machine.

There is a dedicated Control Room in the AGHS building where a number of operators stations are installed in a modular L-shaped desk (see Fig.192), which gives the operators freedom to create working clusters of screens as required during commissioning of the plant and offer good ergonomic design. All control room equipment was successfully powered up in September 1990.

The DCU's (installed either in the AGH plant area, or in the control equipment room), and the computer and console units are all linked together via a dual/redundant Ethernet communications highway system for increased availability. The same LAN is extended to DCU#16 via dual fibre optic repeaters. By the end of 1990, approximately 80% of the cabling (between field terminations and control units) was

completed and the site acceptance test is scheduled for the first quarter 1991.

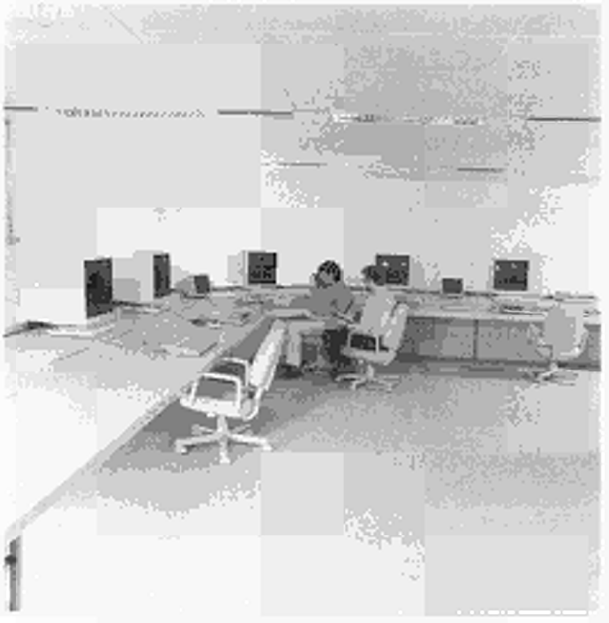

Fig.192: Active Gas Handling System Control Room;

The AGHS Control system has provisions for data links to CODAS, PLC's, PC's and Intelligent Analytical Instrumentation (Residual Gas Analysers, Analytical Gas Chromatographs and various mass spectrometers). The detailed Software Requirements Specifications have been prepared by JET in parallel with the process design in order to achieve a high degree of consistency and also minimise the time required for revisions and debugging. One third of the software has been generated and tested with simulated inputs and outputs or is in the process of configuration. About half of the required customised mimics/graphics/tables have been generated and tested. The availability of the mimics and the application software (sequences, control loops) at an early stage of the project will enable preparation of realistic commissioning and operating plans and evaluate the control system performance in advance of tritium operations.

In addition to the AGHS Distributed Control System all the field instrumentation (eg electronic amplifier, signal conditioning units and power supplies) are installed in a number of subsystems. Approximately 70% of these cubicles are completed and delivery to JET will be early 1991. The design of the Hardwired Interlock and Safety System as well as the Control room annunciator panel is subject to internal reviews before procurement.

Plant completion and Commissioning

The AGHS plant is expected to be completely installed in Summer 1991. This will be immediately followed by a commissioning phase without tritium to demonstrate plant performance. This performance will be critically analysed with respect to tritium safety prior to introduction of tritium at the end of 1991.

Radiation Protection Instrumentation (RPI)

The RPI procurement contract with AEA Technology, Harwell, U.K., has continued throughout the year though completion is somewhat delayed. The contract is in two basic sections, the on-line electronic systems and the sampling systems.

On-line equipment

The delivery of the on-line equipment has been considerably delayed. The first four area monitors have been delivered and are on pre-commissioning trials. The link to CODAS works well, but difficulties with local printers have been experienced. The delivery of the remaining units will be held back until after the problem is solved, probably early February 1991.

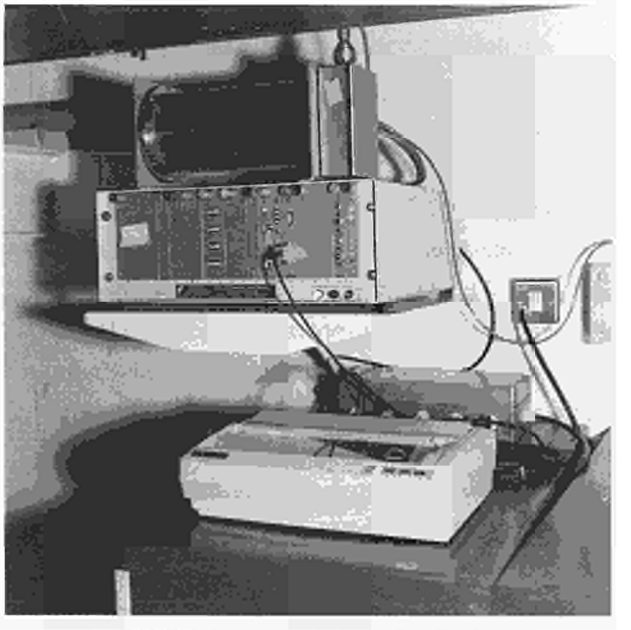

Fig.193: Environmental Monitoring Equipment.

Sampling systems

All equipment for the sampling systems was delivered on time to JET. This equipment includes devices for environmental monitoring, stack and working area monitoring

shown in Fig.193. The devices consist of columns through which air is drawn by a pump. The first column contains silica gel and removes all water vapour including any tritium in oxide form. The second and third columns consist of a catalytic system which oxidises any hydrogen including any elemental tritium which is subsequently collected on a final silica gel column. The environmental monitors were installed and commissioned during June/July, and in August, a contract was placed to start the routine monthly analysis of the deployed samplers, both active and passive, around the site boundary.

The stack samplers have not been installed as on-line equipment is awaited. The working area samplers haves also not been installed as the cabling has not been completed, though a few are to be installed in Building J1 in February 1991 for precommissioning tests.

Environmental Monitoring Programmes

The programmes are:-

- Sampling and analysis of air, rain, soil, and ground water from the Culham site and river water from the Thames for beta, including, tritium, and gamma radioactivity;
- Gamma and neutron dosimetry at points around the Culham site boundary;
- Tritium-in-air using both HTO and HT/HTO discriminating samplers at the Culham site boundary;
- Grass, crop and standing water sampling on the Culham site.

The first two have been in operation for several years and the latter two are being introduced and due to be fully commissioned before the first tritium is brought on to the JET site. The grouping of the various programmes is determined by various factors, notably the methods used for analysis and the frequency of analysis.

Beta and gamma analysis on samples from Culham site has been undertaken by AEA Technology, Harwell, UK for several years to determine the background levels of radioactive materials and to determine the effect of JET operations on these levels. There are four sampling point on the Culham site with airborne sampling at a height of 1 m. The mass of air sampled is about 75 tonnes per month. Rainwater is collected in a 40 cm diameter funnel and borehole samples are taken from a depth of several metres. River samples are taken from above and below the Culham discharge point. Essentially samples are taken quarterly, analysed and the full results presented annually. The operation of this programme is being reviewed and updated in view of organisational changes both at JET and Harwell, but the work itself will continue as before with possible enhancements to include grass, crop and standing water sampling on the Culham site.

Gamma and neutron dosimetry at the site boundary is carried out at 40 positions around the site boundary fence. At each location are two TLD dosimetry badges, one optimised for the detection of gamma radiation and the other for neutrons. These are identical to the TLD badges used for personal dosimetry at JET and are analysed using the same badge reader. These are changed and analysed monthly. These badges provide the integrated gamma and neutron dose from all sources, as opposed to the levels of radioactive nuclides determined by the beta and gamma analysis described above. To date they have provided information on the baseline levels over the past few years at the site boundary. This programme will continue throughout the JET D-T Phase.

A set of sampling devices for tritium-in-air monitoring has been installed around the Culham site boundary to determine the time integrated levels of tritium in air at these locations, as distinct from the tritium in liquid water levels described above. There are two types of device, the passive HTO samplers and the active HT/HTO discriminating samplers. Both were developed under contract to JET by AEA Technology, Harwell, UK. There are 20 passive HTO samplers located around the boundary fence. These devices essentially consist of a container with silica gel and a device to allow the controlled diffusion of atmospheric air into the container where the silica gel absorbs all the moisture, including any HTO. At monthly intervals these will be bulked in four batches by compass quadrant and analysed for tritium content. This involves extracting all the water for silica gel and determining the tritium content by liquid scintillation counting.

The active HT/HTO samplers are more complex devices as described above but also based on silica gel and will be analysed by identical techniques. Four devices are deployed at the same four sampling stations as the beta/gamma sampling programme. These are changed and analysed monthly. These will be the primary devices for determining the total tritium-in-air levels at the site boundary.

Other RPI Related Work

Contracts have been placed for the statutory annual testing of all JET's portable radiological protection instruments. A

call-for-tender is in preparation for the analysis of the stack and working area discriminating samplers. This analysis is similar to that for the environmental monitors but will be undertaken by contractors on site, due to the fact that there will be more samplers, they will be analysed more frequently and tritium levels are expected to be higher.

Progress in Obtaining Official Approvals for Tritium Operation

JET is required under the Host Agreement to satisfy the United Kingdom Atomic Energy Authority (UKAEA) in advance that the arrangements for tritium operation conform to the standards in the UKAEA. As certain UKAEA sites are licensed by the NII under the Nuclear Installations Act 1965, JET has decided to adopt comparable standards. Formal permission is also needed from Her Majesty's Inspectorate of Pollution (HMIP) and JET must comply with various statutory requirements monitored by the UK Health and Safety Executive (HSE). Progress is detailed below.

AEA Requirements

As part of JET's intent to comply with the general intent of the NII model licence, a Fusion Safety Committee has been established and will replace its predecessor the Tritium Safety Advisory Panel. The new committee has a much broader based membership for the review of not only the design of the AGHS but its operation, as well as for the whole of the JET site. The Safety and Reliability Directorate (SRD) of the UKAEA has granted JET permission to introduce up to 5 grams of tritium into the AGHS provided that this Safety Committee is satisfied that JET is ready to do so and that various agreed actions are carried out.

HMIP Requirements

JET must obtain the permission of the UK Department of the Environment, through Her Majesty's Inspectorate of Pollution (HMIP) before tritium may be brought onto site and before any discharges of radioactive material may be made. JET is already authorised to discharge the small amounts of radioactivity generated in the D-D phase and has been negotiating with HMIP on the conditions under which the increase authorisations for the D-T phase would be granted. These include the discharge monitoring arrangements; environmental monitoring; and demonstrating that "best practicable means' that are economically achievable have been used to limit the releases from the plant. An example of the latter is the facility to hold back and monitor discharges from the most significant routes so that recovery is possible if the discharge would breach any limit. In the AGHS, this is achieved by monitoring all process, service gas and secondary containment discharges and being able to delay discharge by means of a buffer tank. For liquid radioactive discharges, it is proposed to install holding tanks sufficient for at least one week's arisings. HMIP have indicated that these arrangements will be acceptable and formal application for the use of tritium will be made early in 1991.

In connection with the application for revised discharge authorisations, a re-appraisal of the routine releases is underway. This has taken into account the additional sources of tritium discharge, for example from permeation through the LHCD bellows and from protium discharge from the cryodistillation system. In view of the importance of the oxide layer on steel or inconel surfaces in reducing permeation of tritium, a contract has been placed with JRC Ispra, Italy to carry out tests on heated bellows under cyclic conditions.

HSE Requirements

The HSE have confirmed that the accountancy arrangements for tritium at JET will be acceptable.

Active Gas Handling System Safety Analysis

This has continued in parallel with the plant design to ensure that proposed designs are capable of meeting safety criteria and requirements equivalent to those of a licensed site. To meet these standards, the AGHS has been designed to incorporate a series of engineered "barriers" to contain primary and secondary containment overpressures, recover releases from secondary containments and reduce tritium concentration of exhausted gases.

Previous safety assessments had shown that identified failures within a subsystem would meet the design targets adopted by JET. A review of interconnections between subsystems, which is part of the final AGHS submission to SRD, has highlighted a number of areas which, although not directly breaching these design targets, could lead to certain releases in the event of multiple or certain common cause failures. To avoid these occurrences, and to provide additional safeguards against operator error, extra hardwired protection and interlocking has been introduced.

Also completed was a detailed assessment of the interconnecting duct which provides the double contained inter-

connection between the various subsystems within the AGHS. This system, which contains all-welded piping, was found to be acceptable. However, it highlighted the problem of using the standard nuclear plant failure data acceptable to the safety authorities for assessment of high quality process systems operating close to atmospheric pressure.

The twelve nitrogen-filled valve and glove boxes used as secondary containment have over/underpressure protection system and use the AGHS control system to maintain a slight underpressure. The safety review of design and operation led to a requirements for slight modifications. With these having been made, the system permits timely detection and recovery of tritium should it be released into the secondary containment as well as detection of loss of integrity of secondary containment.

The Gas Introduction System consists of a valve box in the AGHS Building, which contains a matrix of valves which permit supply of deuterium or tritium to the individual torus users; a triply contained transfer line; and a distribution box in the torus basement. The valves are interlocked to ensure that the correct gas of high purity is supplied to the torus systems at the correct time. The system has been reviewed and found to meet design targets. The total impact of the interface with the torus will be addressed in the torus Preliminary Safety Assessment Report (PSAR).

In the course of their assessment of the Design Safety Review of the Intermediate Storage sub-system, SRD had expressed some concern over the possibility of air entering a U-bed during maintenance operations. To provide experimental support for the calculations carried out by JET which showed that the containment design temperature would not be exceeded, SRD requested JET to carry out a test in which air was admitted to a fully conditioned U-bed. A controlled experiment has been carried out which, in addition to verifying the value of adiabatic heat capacity, has shown that the reaction resulting from the admission of air at room temperature self-extinguishes at a relatively low temperature.

The hardwired safety interlocks are nearing their final design. These interlocks were reviewed for compliance with safety criteria and for consistency with a view to permit practical implementation, operation and recovery. When completed the design will be subject to a thorough reliability study. Its impact on total plant safety will be assessed in the Final Safety Assessment Report (FSAR).

The final reliability assessment of the Exhaust Detritiation System was completed. Its contribution is important in meeting the design targets for the AGHS as well as the torus safety case [1]. Formal documentation of the impact of its reliability will be completed in the Final Safety Assessment Report (FSAR) for the AGHS and the torus.

Torus Safety Assessment

A Preliminary Safety Analysis Report (PSAR) is being prepared for an optional 100 D-T shot operational phase envisaged for the second half of 1992. In view of the reduced time at risk and throughput of tritium associated with a 100 D-T shot phase of six months' duration, it is anticipated that some of the modifications to the torus which would be necessary to achieve tritium compatibility for the full active phase (10^4 D-T shots over two years) will not be required for such a truncated D-T programme. Moreover, the accumulated tritium inventories within the torus and ancilliary systems (chiefly the various cryopumps) will be maintained at the minimum practicable levels by frequent regenerations and, in the case of tritium retained within the first wall, through periodic detritiation by glow discharge cleaning and possibly controlled venting to the AGHS [2]. It is planned to reduce the number of high risk components such as diagnostic optical windows to the absolute minimum necessary for the efficacy of the scientific programme.

A numerical analysis has been performed of the potential for oxidation of radiatively cooled graphite tiles under accidental air inleakage conditions [3]. The results of this study indicated that under the most onerous conditions of tile plasma heating and graphite oxidation rates relevant to JET, the power radiated from the oxidising tiles would always exceed the power imparted to such tiles by the oxidation. A study of potential steam/graphite reactions, which might occur following water leaks inside the torus is in hand.

References

[1] A C Bell et al, "Risk assessment methodology for the JET Active Gas Handling System (AGHS) and the significance of the exhaust detritiation system in meeting design targets", Proceedings of the 16th Symposium on Fusion Technology (SOFT), London, U.K., (1990).

[2] J P Coad, "Gas release on venting the JET Torus", JET-R(89)15.

[3] M E P Wykes, "Safety analysis of potential graphite oxidation effects in JET", Proceedings of the 16th Symposium on Fusion Technology (SOFT), London, U.K. (1990).

The New Phase of JET: Pumped Divertor

Plasma dilution is a major threat to a reactor. The entrainment of impurities in a forced flow of plasma towards the divertor target plates is a candidate concept for impurity control in Next Step tokamaks. This form of active impurity control is the focus of the New Phase of JET: Pumped Divertor planned to start in JET in 1992 [1]. First results should become available in 1993 and the Project should continue to the end of 1996. The aim of the New Phase is to demonstrate, prior to the introduction of tritium, effective methods of impurity control in operating conditions close to those of a Next Step tokamak, with a stationary plasma (10s-1minute) of 'thermonuclear grade' in an axisymmetric pumped divertor configuration. Specifically, the New Phase should demonstrate:

- the control of impurities generated at the divertor target plates;
- a decrease of the heat load on the target plates;
- the control of plasma density;
- the exhaust capability;
- a realistic model of particle transport.

The New Phase of JET should demonstrate a concept of impurity control; determine the size and geometry needed to realise this concept in a Next-Step tokamak; allow a choice of suitable plasma facing components; and demonstrate the operational domain for such a device.

Impurity Control Concept

Impurities which are produced at the divertor target plates tend to migrate along the magnetic field, out of the divertor region and into the scrape-off layer (SOL) plasma, due to thermo-electric forces. This migration is opposed by friction with plasma flowing towards the divertor. The plasma flow increases rapidly on approaching the target plates, due to the ionisation there of target-produced neutrals, but the flow can be extended further from the target plates by reflection from the side targets and transmission through the private flux region (Fig.194). Friction can then be effective over a greater range. It is also possible, in principle, to extend the effectiveness of the "natural" recycling by extracting some of the target-produced neutrals and directly "recirculating" them, e.g. by baffles, into the X-point region. Finally, it may be necessary to induce a moderate flow in the SOL, in excess of the natural flow from the main plasma, by strong gas puffing or shallow pellet injection. This imposed flow would then require pumping of an equivalent neutral flux from the divertor chamber to maintain a steady state.

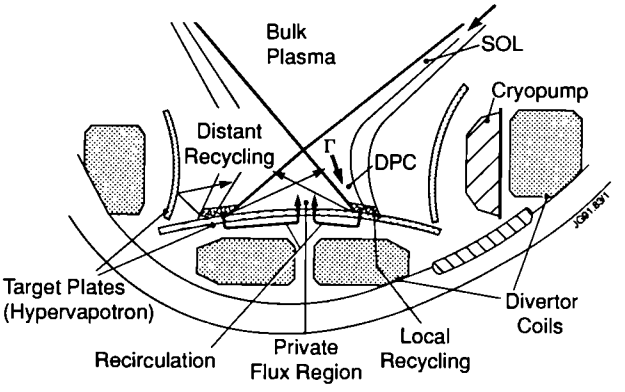

Fig.194: Schematic diagram of the JET Pumped Divertor.

Impurity Retention by Plasma Flows

Impurity retention in the divertor is determined from the steady state momentum equation for impurity ions along the magnetic field direction, x:

$$m_z n_z v_z \frac{dv_z}{dx} = -\frac{dp_z}{dx} + Zen_z E + \frac{m_z n_z (v_i - v_z)}{\tau_{zi}} + n_z \alpha_z \frac{dT_e}{dx} + n_z \beta_z \frac{dT_i}{dx}$$

A single impurity species of charge state Z, mass m_z, density n_z, temperature T_z, pressure p_z, and flow speed v_z is considered. The subscripts e and i refer to the electrons and the hydrogenic ions, and τ_{zi} is the hydrogenic ion-impurity collision time. The forces on the right hand side are due to the impurity pressure gradient (where $p_z = n_z T_z$) the electric field E, friction, and thermal forces with coefficients α_z for electrons and β_z for ions.

The simplest, realistic approximation to this equation gives:

$$\frac{1}{n_z}\frac{dn_z}{dx} = \frac{m_z v_i}{T\tau_{zi}} - (1 + Z\alpha_e - \alpha_z - \beta_z)\frac{1}{T}\frac{dT}{dx}$$

The impurity density decays exponentially with distance from the target on a scale length, λ_z:

$$n_z(x) = n_z(0)e^{\int dx/\lambda_z}$$

where: $\lambda_z^{-1} = \lambda_F^{-1} - \lambda_T^{-1}$

The frictional force is represented by:

$$\lambda_f^{\ 1} = \frac{m_z \nu_z}{T \tau_{zi}} \approx \frac{Z^2 \Gamma(x)}{T_i^{5/2}(x)}$$

and the thermal force by:

$$\lambda_t^{\ 1} = (1 + Z\alpha_e - \alpha_z - \beta_z)\frac{1}{T}\frac{dT}{dx}$$

To ensure impurity control, the frictional force must exceed the thermal force. The friction force is dependent on the plasma flow, $\Gamma(x)$ (and hence on the distribution of recirculated neutrals) and on the ion temperature, T_i. The thermal force is dependent on the ion temperature gradient scale length, and hence on the ion heat transport and ion input power, since the electron heat conductivity parallel to the magnetic field is dominant. For a large enough $\Gamma(x)$, $n_z(x)$ decreases towards the X-point until $\Gamma(x)$ becomes so small that thermal forces dominate. Beyond that point, $n_z(x)$ begins to increase. At fixed power into the divertor and very high plasma density, n_b at the position of flow stagnation at the separatrix, the plasma flow at the target, Γ_t can be sufficient for "natural" recycling to provide effective impurity retention. As n_b is decreased at fixed power, Γ_t decreases, the temperature in the SOL increases and the effectiveness of the friction force in overcoming the ion thermal force is strongly reduced. In order to retain impurities, $\Gamma(x)$ must then be "extended" further along the magnetic field, either by recirculation, e.g. at the X-point, or by injection of particles uniformly into the SOL. A simple analysis [2], assuming constant $\Gamma(x)$, predicts that for the case of recirculation at the X-point, the required plasma flow depends primarily on the ion heat flow, P_i and somewhat less strongly on the connection length, s_x and scales as:

$$P_i^{5/7} \cdot s_x^{-2/7}$$

This analysis does not include the contribution of the local high recycling region near the target, which, at high density and low temperature, leads to effective impurity control, reduced erosion and extended lifetime of the target plates.

Detailed Modelling of Impurity Retention

Impurity control in the flux surface geometries of present JET X-point and future JET pumped divertor configurations has been studied in more detail [2-4] using the 1-$^1/_2$D model (EDGE1D) of the scrape-off layer (SOL) plasma [4]. The model is based on the plasma model [5] of the 2-D boundary code EDGE2D [6] and the impurity model of Ref. [7] and includes: classical transport along the magnetic field with fluid equations for conservation of particles, momentum and energy (electrons, deuterons, impurities of arbitrary high concentration); impurity radiation with full non-coronal model (multi-ion impurity species); Bohm boundary conditions; temperature and density profiles specified transverse to the magnetic field; 2-D Monte Carlo methods (NIMBUS [8]) for neutral deuterium and impurities (Be/C); and erosion at target plates (calculated self-consistently, including cascades [9] and validated against JET experimental data [10]).

Present JET X-point Configurations

First steps towards validating these complex SOL models have been taken by establishing consistency with edge data in JET X-point operation [11]. In particular, the predicted edge conditions of T_i significantly larger than T_e and divertor temperatures in the range of 10-20eV at high SOL density have been observed. $T_i > T_e$ is also required to reconcile probe and power balance measurements [12], while high values of T_i are consistently confirmed using high resolution visible spectroscopy of neutrals and low charge state ions to measure Doppler ion temperatures near the plasma boundary [13]. In addition, the calculations of Ref. [11] show that plasma flows can provide sufficient impurity retention to reproduce the measured impurity radiation near targets. The arrest of the carbon catastrophe by strong gas puffing and the subsequent low carbon ingress, despite the outer SOL strike zone temperature remaining above 2000°C, provides further experimental support for impurity retention by plasma flows [14].

The Pumped Divertor Configuration

For the "slim" plasma in the pumped divertor configuration and a total input power of 40MW (shared equally between the ions and electrons and input uniformly along the separatrix into the SOL), calculated profiles of the deuterium and total impurity densities, the ion and electron temperatures, and the principal forces acting on the impurity ions are shown in Fig.195 as functions of the distance along the magnetic field from the outside target. A fraction, f_R of the target flux is extracted and reinjected uniformly along the separatrix from the main plasma into the SOL. Impurity retention is seen to be poor for f_R=0 (Case (a)) and good for f_R=10% (Case (b)). The relatively low level of external recirculation makes a major change in the retention. The ion temperature in the

SOL is higher than the electron temperature, in agreement with experimental observations in JET. The temperatures near the target plates are in the 10-20eV range at higher edge densities and correspondingly larger hydrogen fluxes to the targets. The force balance shows that for $f_R = 0$, the integrated friction force is insufficient to retain impurities, which accumulate near the point of maximum temperature until the impurity pressure gradient force balances the ion thermal force. For $f_R = 0.1$, the external recirculation extends the range of the friction force sufficiently to enable the integrated value to exceed that of the thermal force, and impurities are effectively retained in the divertor region.

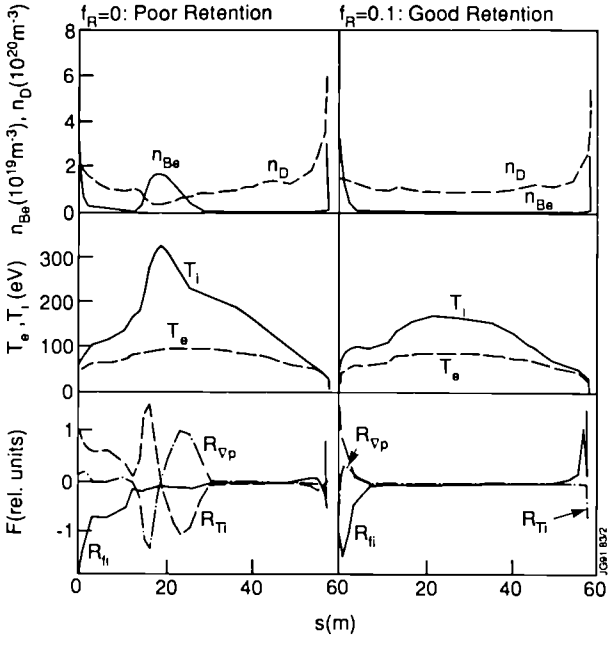

Fig.195: Behaviour of various plasma parameters versus s, for a case of poor impurity retention (left) and good impurity retention (right). f_R is the fraction of target flux which is externally recirculated.

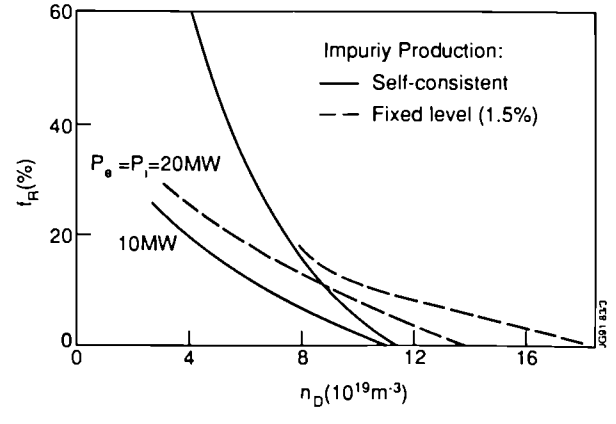

Fig.196: The external recirculation fraction required for 90% retention versus SOL density, for two values of ion power flow in the SOL.

Fig.196 summarises the results of an extensive series of calculations in which the SOL density, n_b, and the ion heat flow, P_i were varied. The fraction, f_R, of the target flux, Γ_t which must be externally recirculated in order to retain 90% of the impurities in the divertor region is plotted against n_b for P_i=20, 10 and 5MW. At high densities ($n_b > 10^{20}m^{-3}$, corresponding to divertor target densities approaching $10^{21}m^{-3}$), Γ_t is very large, friction with "natural recycling" is sufficient to retain target produced impurities and f_R=0. At moderate and low densities ($n_b < 10^{20}m^{-3}$, corresponding to divertor target densities $\sim 10^{20}m^{-3}$), Γ_t decreases, the "natural recycling" flux is insufficient and an increasingly large flow fraction, f_R must be recirculated externally. The plasma flow needed for adequate impurity retention is relatively independent of density for low and medium n_b, is fairly large (typically $\sim 2 \times 10^{23}s^{-1}$ near the X-point) and is probably not compatible with achievable steady state pumping rates. The situation improves somewhat at lower power levels, with lower values of f_R being required for a given n_b.

Operation with clean plasmas is likely, therefore, only at high densities. Furthermore, the concept could be developed towards even higher density and lower temperature (eg. a cold radiating plasma or gas target). This would have to be proven further before incorporation into a Next Step tokamak.

Evolution of engineering aspects

Although basic designs and engineering principles are similar to the 1989 design, significant changes have occurred in certain areas, principally the magnetic configuration and the divertor coils, the design of target plates and certain features of ICRF antennae and limiters.

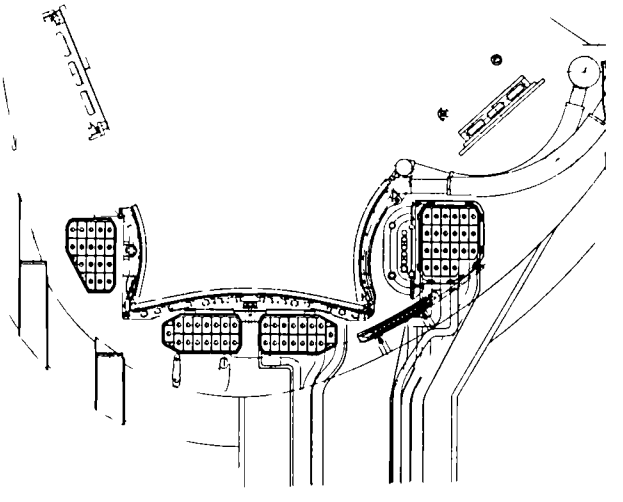

Fig.197: Details of four divertor coil arrangement;

The main modification was the move to a four divertor coils configuration (Fig.197). The initial motivation for this change was the need to increase the connection length (length of field lines) between the X-point region and the target plates in order to provide better impurity confinement. The new multicoil configuration has proven to be much more flexible and versatile than the original single coil design, and will allow investigation of a range of plasma and divertor configurations. The range of configurations is illustrated by the two typical cases, the so called, fat and slim plasmas (Figs.198 and 199). This much needed experimental flexibility fully warrants and justifies the design change. Details of the magnetic configuration are given in the following section.

The new layout of target plates features three target elements in a U-configuration to accommodate the new plasma and divertor contours. Installation of the target plates will proceed in two steps. During 1993, Step 1 will use solid radiatively cooled beryllium blocks as target plates. In 1994, Step 2 will use water cooled beryllium clad hypervapotrons. This approach was motivated by the desire to start pumped divertor operation with a robust and simple design. The development of beryllium clad hypervapotrons has also proven to be more difficult than anticipated and additional time was required for the full qualification of manufacturing processes. Details are given in the following section.

One difficulty of the ICRF antennae design was the large force generated by eddy currents flowing in the antennae structure during plasma disruptions. To minimise these currents, the antennae structures and conductors use thin metal sheets and stiffness is provided by corrugations on double walls. Resistive elements offering high resistance to eddy currents but low resistance to RF currents have also been incorporated.

The "slim" plasma configuration requires that the ICRF antennae should be moved radially and tilted to match the plasma profile and achieve good RF coupling. The new design features spacer blocks for the antenna support structures and extension pieces for the RF conductors which allow this radial displacement. The toroidal layout of the antennae has also been modified to allow neutral injection in all possible plasma configurations.

Nevertheless, in the divertor configuration, a limiter is required for plasma start-up and also as a protection for the ICRF antennae. The initial design used two fixed belt limiters located above and below the antennae. In the new configuration, the wide range of plasma shapes makes it impossible to use belt limiters which are at a fixed radial location. The new limiter design comprises six discrete poloidal limiters which extend from the top to the bottom saddle coils. These limiters will carry beryllium or graphite tiles and can be adjusted radially and tilted to provide adequate protection for the ICRF antennae.

The Magnetic Configuration

The original magnetic configuration with a single divertor coil at the bottom of the vacuum vessel had to be abandoned because it resulted in connection lengths between the X-point and the target plates of only ~3m. Such a short distance did not give sufficient safety margin and, indeed, entailed a considerable risk that impurities would not be adequately confined in the X-point region. Moreover, the original configuration also lacked flexibility and basically allowed only one type of plasma divertor configuration. In view of the exploratory nature of the JET pumped divertor experiment it was undesirable to restrict the experiments to a very narrow band of plasma types.

The new four-coil configuration, although more difficult to build, provides flexibility and versatility that is essential for the type of experiment which is planned during the divertor operation. The configuration features four coils and it should be noted that contrary to conventional divertor systems, all four coils carry currents in the same direction. The two bottom central coils produce the X-point and have been lowered and flattened as much as possible to maximise the vessel volume available to the plasma. Two coils are used instead of one to facilitate sweeping and provide better access to the X-point region for gas injection.

The two side coils allow a reduction of poloidal magnetic field in the region between the X-point and the target plates, thus changing the pitch of the field lines and consequently increasing the connection length. These side coils also contribute to sweeping the field lines.

Since all four coils will have independent power supplies, great operational flexibility can be achieved. Figs.198 and 199 illustrate the range of configurations from the so called "fat" to the "slim" plasmas, as follows:

- A "fat" plasma can be made using only the central bottom coils. This has a large volume, moderate elongation but short connection lengths;
- A "slim" plasma can be produced by adding currents in the side coils. Longer connection lengths are achieved at the expense of a smaller plasma volume.

In addition, the elongation is larger and the vertical stability margin is reduced.

Typical plasma parameters for these two typical configurations are given in Table XV. Intermediate configuration between these two extreme cases can also be obtained. It can be seen that there is a possibility to study the effect of the connection length on the confinement of impurities and select the optimum configuration. Moreover, the side coils allow the connection lengths to be adjusted independently of the plasma current, and separately on the inboard and outboard sides of the X-point.

The strike zone of the separatrix and scrape-off layer can be swept across the target plates to reduce the power deposition profile to an acceptable time averaged value. This sweeping action is easily achieved by shifting radially the centre of gravity of the divertor coil currents, while keeping the total current about constant. In the "fat" configuration, only the two central coils are used and the strike zone is swept 20 cm radially. In the "slim" configuration the side coils contribute to sweeping and also control the connection length at about 7m while the strike is swept zone 20 cm radially.

Table XV
Reference Plasma Parameters for the Divertor

Description	*"fat"*	*"slim"*
Plasma current (MA)	6	6
Plasma volume (m^3)	93	78
Connection length (m)	3	7
Safety factor q_{95}	2.3	2.1
Growth rate ψ (s^{-1})	270	800
Sum of divertor currents (MAt)	0.74	1.8

Target Plates

The layout of target plates has been modified to take into account the new magnetic configuration. The target plates are made up of three parts (see Fig.200). Horizontal plates at the bottom intersect the heat flux conducted along field lines. Therefore, these bottom plates are subjected to a severe power deposition. Vertical plates on either sides intersect the power radiated from the divertor plasma, and receive only a modest heat load. The horizontal and vertical plates are split into 384 radial elements grouped into 48 modules of eight elements each.

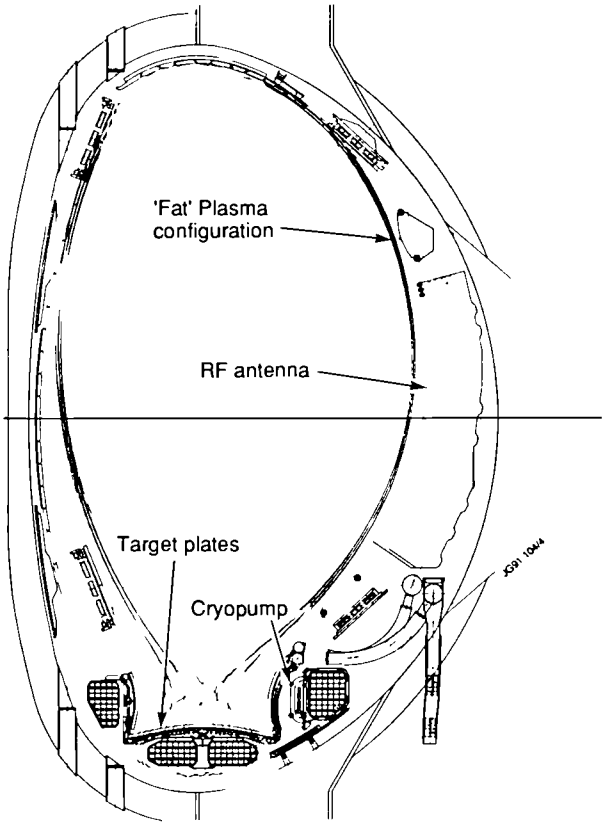

Fig.198: Configuration with so-called 'fat' plasma;

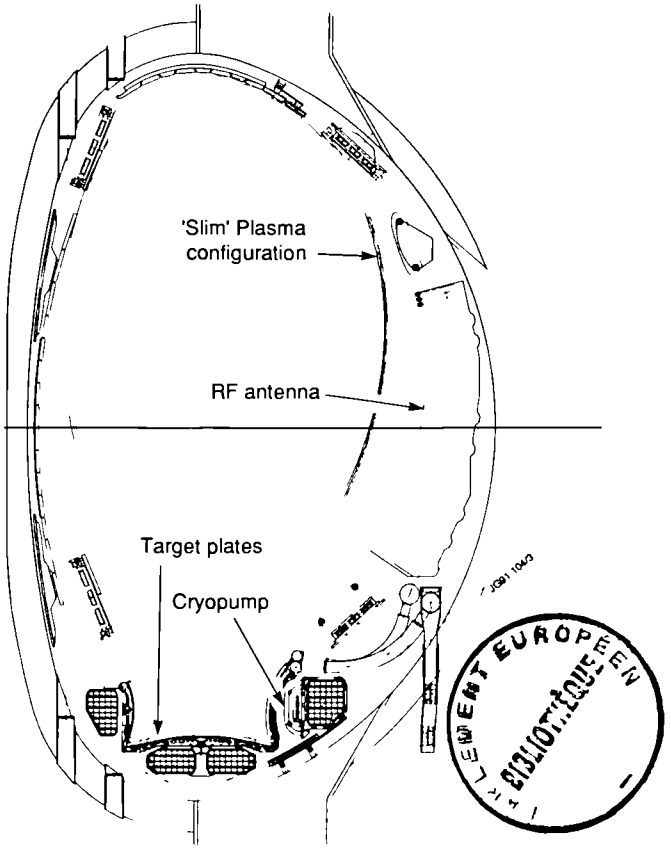

Fig.199: Configuration with so-called 'slim' plasma;

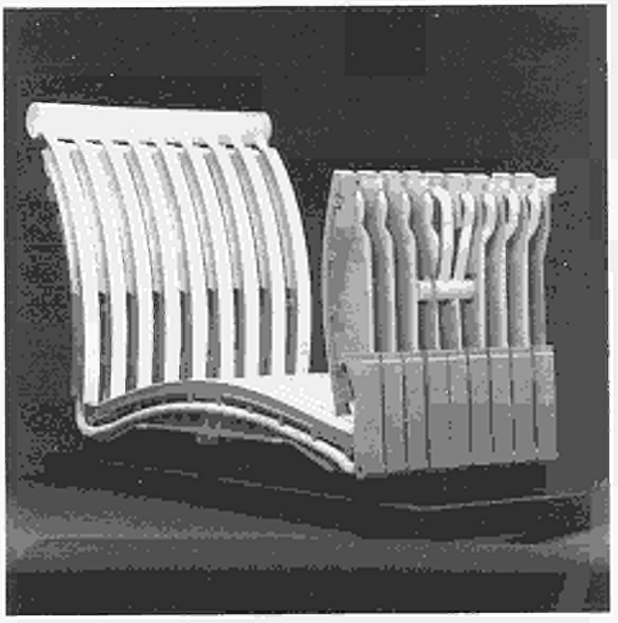

Fig.200: Layout of target plates:

If it is assumed that the full plasma power of 40 MW is conducted to the target plates. In other words, the radiation in the main and divertor plasmas is negligible. Then, the peak power density on the bottom target plates would reach 60MW/m^2 with stationary field lines. Since such a power density is unacceptably high even for the most advanced heat sinks, sweeping the field lines is mandatory. A 20 cm wide radial sweep reduces the time averaged power density to 10-12MW/m^2, which can be accommodated by hypervapotrons of the type used on the JET neutral beam systems. In contrast to the bottom elements, the side elements receive only modest radiative heat load from the divertor plasma. Assuming that all 40 MW are radiated in the divertor plasma, then the power density on the side elements should not exceed 3MW/m^2.

The surface of the hypervapotrons facing the plasma must be clad with a low Z-material. The choice of beryllium is natural in view of the results achieved on JET, although it is recognised that beryllium impurities generated in the divertor plasma will radiate only a negligible fraction of the incident power. However, the choice of material other than beryllium would entail the risk of impurities migrating back to the plasma and jeopardising the benefits of a beryllium first wall.

The most critical aspect of the development of the target plates is the bonding process between the 2-3mm thick beryllium layer and the copper-chromium alloy of the hypervapotron. This development proved to be more difficult than anticipated and there was a general concern about the long term reliability of a large number of beryllium clad elements subjected to severe heat cycles. Therefore, a more cautious approach involving two steps in the development of the target plates was decided.

In the first step, solid beryllium blocks about 40mm thick will be used as target plates. These blocks will be radiatively cooled by means of a water-cooled stainless steel structure. The mechanical arrangement similar to the one used for the belt limiter allows easy replacement of individual blocks without having to remove any water-cooled structure. The energy handling capability of these blocks is limited and restricts the power and pulse duration. However, the arrangement is robust, does not rely on any development and should guarantee trouble free operation during the initial phase of divertor work during which much of the exploratory research will be carried out at reduced power and pulse duration.

In the second step, beryllium clad hypervapotrons will be used for the bottom elements, while solid beryllium blocks will be retained for the side elements. Therefore, the beryllium clad hypervapotrons will be required only by the end of 1993. This will allow time for the full development of the beryllium/copper bonding process and of a pre-assembly testing method for the finished elements.

Mechanical Design of Target Plates

The forces acting on the target plates are due to eddy currents and "halo" poloidal currents. These currents can flow in the target plates during plasma disruptions and vertical instabilities. Eddy currents have been carefully minimised by providing electrical paths which are as axisymmetric as possible, thus avoiding the circulation of currents in a direction perpendicular to the toroidal magnetic field. Halo currents flowing along target plate elements may be minimised by providing short circuiting parallel paths to the vacuum vessel at each extremity of the elements. However, the design assumes conservatively that halo currents up to about 7 kA can circulate in each of the 384 target elements. This results in forces of about 2 tonnes per metre on each element. The forces are expected to push the elements away from the plasma but again the design assumes conservatively that these forces can act in either direction. This conservative approach is dictated by the lack of detailed knowledge on "halo" currents.

The mechanical arrangements for the two versions of the target plates must be the same to allow an easy replacement when the second version is ready. In both cases rigid

stainless steel beams provide mechanical supports. In the first version, the beams are water cooled and acts as a radiator as well as a structure. In the second version, the beams are only a mechanical support.

The bottom target elements are firmly clamped to the bottom divertor coils. The top ends of the side elements are firmly clamped to the side divertor coils. Thermal expansion of the elements, and relative displacements between elements and divertor coils are made possible by hinges and elongated holes which allow sliding. The replacement of a module will involve the removal of a small number of well accessible bolts and the cutting of the inlet and outlet water pipes to the module manifold.

Design and Evaluation of Target Plates: Mark I (Solid Beryllium Blocks)

In the first step, solid beryllium blocks approximately 50 mm thick will be installed in all three parts of the target plates, horizontally as well as vertically. These solid blocks are held in place by a water-cooled stainless-steel structure, which at the same time absorbs heat from the irradiated blocks. The method of heat removal is blackbody radiation between beryllium and steel parts; tests will be made to assess the degree of thermal contact that is intrinsic to this design. Individual blocks approximately 80 mm long, held in pairs in a manner similar to that used on the JET belt limiters, will be positively located so that plasma strikes a well-defined smooth surface. The energy handling capability of this design is limited due to the lack of active cooling of the tiles. However, using realistic figures for emissivity of blackened beryllium and steel, it has been calculated that a pulse of up to 5s with 20 MW uniformly conducted to the blocks could be sustained once every 45 minutes. During such a pulse, the tiles would undergo a temperature excursion from 400°C (standby) to peak values < 900°C. Preliminary thermo-mechanical analyses indicate that, provided the plasma facing surface of the blocks is castellated to 18 x 18 mm square and to a depth of 10-15 mm, the solid beryllium tiles could sustain 5s of half-power operation or 1s of full power illumination with a localised plastic thermal strain of < 1% in the bulk of the material. Testing is necessary and is planned for early 1991 to assess the fatigue life of this design under repeated cycling.

Table XVI
Brazed Joint Tensile Strengths - N/mm2

	Temperature		
Braze	250 C	350°C	450°C
BAg-18	90-165	75-165	40-140
Incusil ABA	200	203	180

Be Brazing Development for Target Plates: Mark 2 (Clad Hypervapotrons)

In 1984, an initial development contract studied the brazing of beryllium (Be) onto copper-chrome-zirconium (CuCrZr) substrates. The study resulted in a recommended brazing procedure of BAg-18 braze at 650°C for 30 minutes. This temperature lies below the braze liquidus temperature (723°C) to minimise adverse effects on the precipitation hardening of the CuCrZr and the growth of brittle inter-metallics between Cu and Be. During 1990, this study was extended to assess (a) the effect of pressure on the joint during brazing; (b) higher brazing temperature up to 690°C; and, (c) silver sputter coating of the CuCrZr but no consistent improvement was achieved. The tensile strengths of the joint were measured at elevated temperatures and the results are summarised in Table XVI where the wide scatter in results can be seen.

Following discussion with one of the suppliers of brazing materials, an active braze Incusil ABA (Ag-Cu-In-Ti) was tried with the results also shown in Table XVI. These look very promising and a second set of prototype target plates is being manufactured using this braze.

To assess the performance of the braze under operational conditions using a dedicated Neutral Injection Test Beamline, two prototype Target Plates were prepared with four different designs of Be tiles brazed on to the surface using BAg-18. These designs consisted of both plain and segmented tiles, which were slit both partially and fully through to the substrate in order to reduce thermal stress. The results of these tests were as follows:

- One section of a tile lost the thermal contact to the cooled base plate at a power density of ~ 10 MW m^{-2} and subsequently melted at higher power densities. It is assumed that a fault in the braze initiated this local failure.
- The brazed joints of all the other tiles remained intact until the power density during the beam-on period reached 16 MW m^{-2}. Fig.201 shows a photograph of the tiles after the test programme. The faults are marked in the sequence of their occurrence. All faults, with the exception of the first one, occurred at exactly the same power level.

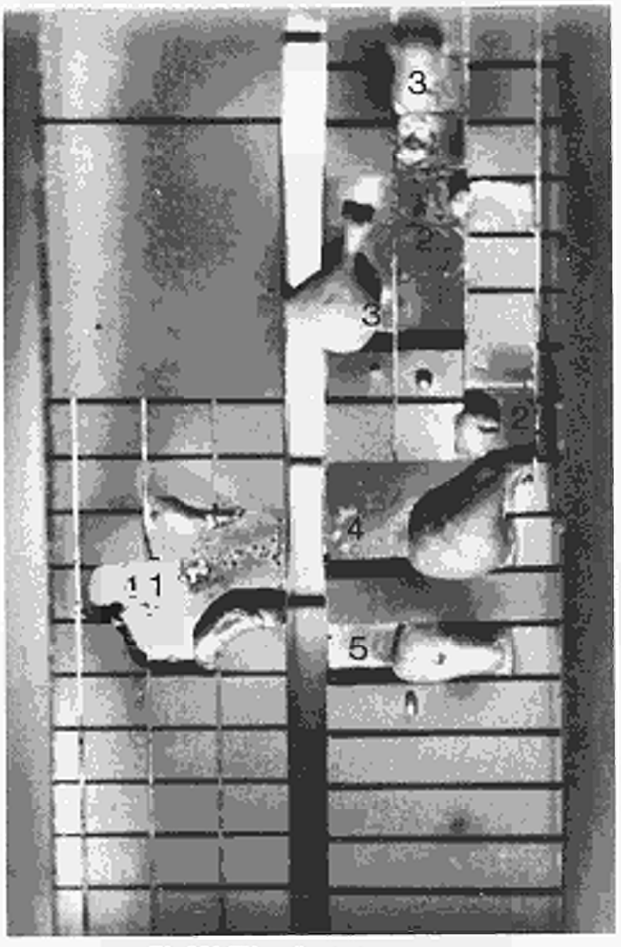

Fig.201:Tiles after test programme;

The larger tiles, which can be seen in Fig.201, were exposed to a slightly lower power density and were not detached during the first test. However, in a second test, these tiles also started to detach at exactly the same power density as the other tiles. So far, there is no indication of fatigue failure and no apparent influence from the tile size. This is a somewhat surprising result in view of the large scatter in the measured strength of the brazed joint and the computations of thermal stress in the tiles which predict failure of the larger tiles before that of the segmented versions. Micrographs of the joint which were obtained after the tests show that contrary to original expectations the failures appear to be due to failure at the Beryllium-braze interface and/or an intermetallic layer close to this interface and do not occur at the braze-CuCrZr interface. It should be noted that the temperature of the brazed joint was ~ 370°C when the tiles detached. This corresponds to the upper limit of the expected operating temperature in the divertor and shows that the present braze is almost capable of withstanding the expected power density but the safety margin must be extended considerably.

Explosive bonding of Beryllium to CuCrZr is being investigated as a possible alternative to brazing. The results of the first test of this process are being analysed and appear to be sufficiently promising to warrant continued development.

Pumped Divertor Cryopump

An integral part of the pumped divertor is a large cryocondensation pump with a nominal pumping speed of $5 \times 10^5 \ell s^{-1}$. The pump shown schematically in Fig.202 extends over the full toroidal length of the outermost divertor coil which also acts as the mechanical support. The design is somewhat conventional utilizing a liquid nitrogen cooled chevron baffle to protect the liquid helium condensing surface, which consists of corrugated stainless steel pipes, from high temperature gas molecules and thermal radiation. A water cooled chevron baffle ensures that the liquid nitrogen chevron is protected from direct line of sight to the high temperature of the JET vacuum vessel. The design is compatible with the extreme conditions of up to 10^{23} particles per second and, in the D-T phase, a neutron flux of 10^{19} ns^{-1} for a 10s pulse. The manufacturing contracts have been placed with European industry and provision of the cryosupplies is underway.

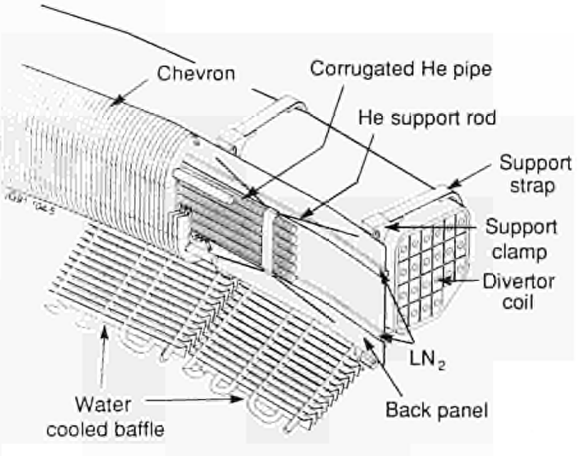

Fig.202: Divertor cryopump.

Coils

The arrangement of the coils in the vacuum vessel is shown in Fig.197.

Technical Design

The required coil currents (ampere-turns) are determined by plasma equilibria but the coils also have to withstand forces

Table XVII
Coil Currents, Forces and Technical Data

Coil number		1	2	3	4
Max. current in equilibrium (MAt)		0.34	0.56	0.56	0.65
Max. force in equilibrium (tonnes)	Rad.	220	160	-300	-870
	Vert.	-10	110	260	290
Max. force in vertical instability (tonnes)	Rad.	300	170	-330	-980
	Vert.	-100	140	320	350
Number of turns		16	15	15	21
Mean radius (m)		2.1	2.5	2.85	3.4
Weight of copper (tonnes)		3.1	3.4	3.9	6.4

due to the vertical instabilities occur with loss of plasma current. Forces and currents for equilibria and instabilities were calculated using the PROTEUS code to give the parameters in Table XVII.

The coils will be mounted inside the vacuum vessel, which will be at 350°C during operation. Therefore, they will be enclosed in vacuum tight inconel cases and will be cooled continuously. The coils are of conventional construction (water cooled copper, epoxy glass insulation) and are supported from the vacuum vessel by links, which are hinged to allow vacuum vessel movements. The links are connected to the coil by clamps and to the vacuum vessel by welded blocks. The coil water cooling system will recirculate warm water through the coil to avoid thermal stress problems.

Calculations based on the forces given in Table XVII give a maximum von Mises stress in the coil copper of about 40 MPa. The large inward force on Coil No.4 caused a tendency to elastic instability. This possibility was prevented by increasing the coil cross-section. The maximum net force transmitted to the vacuum vessel by the coils is about 1000 tonnes.

Manufacture Method

Final assembly of coils will take place in the vacuum vessel. The two basic manufacturing methods are:

- winding the coil in the vacuum vessel using a temporary winding table; or,
- pre-forming the conductor sections into half or third turns at the factory and brazing the conductors together in the vacuum vessel.

Both methods are feasible but the second has been chosen in conjunction with the coil manufacturer. In this method the sequence of operations is:

- bend the conductors to the correct radius to make half or third turns;
- assemble into a coil in the factory to check dimensions and fit;
- disassemble and apply dry glass and Kapton insulation to conductors;
- deliver coil components and tools to the JET site;
- assembly winding table and install other tools in the vacuum vessel;
- assemble conductors on winding table in the vacuum vessel, and braze together to form coil, insulate joints after brazing;
- apply dry glass tape and Kapton ground insulation to assembled coil;
- assembly coil in coil case and weld two halves of case together;
- evacuate case, vacuum impregnate coil with epoxy resin and heat to cure;
- lower coil to final position at bottom of vacuum vessel.

Progress of Contract

The Manufacturing Contract was placed in August 1990, design and documentation is almost complete and the main materials have been ordered. The coil parts will be ready for delivery to JET in early 1992 and in-vessel assembly is expected to take about four months.

Forces Acting on the Vacuum Vessel

The vertical forces acting on the four divertor coils will be transmitted to the vacuum vessel through 32 supports located at the octant rigid sectors: hinged connections allow, relative radial displacement between the coil system and the vessel during bake-out.

A total vertical load of 650 tonnes is expected for the

Table XVIII
Max. Vertical Forces on the Vessel (tonnes)
(Effect of local "halo" currents not included)

	Static configuration		*Disruption/Vert Instability Upw.*	*Disruption/Vert Instability Dwn.*	
	"Slim"	*"Fat"*	*"Slim"*	*"Slim"*	*"Fat"*
Inner Coil (Left)	-10	-	-100	10	-20
Central Coil (Left)	110	70	60	140	100
Central Coil (Right)	260	125	180	320	150
Outer Coil (Right)	290	-	120	350	-160
Eddy Currents in the vessel	-	-	700	-340	-250
Net force on the vessel	650	195	960	480	-180

design magnetic configuration at 6 MA, as shown in Table XVIII. This force will produce the reactions and stresses in the vessel, as follows:

- Reaction at octant joint sector = 11 tonnes
- Reaction at limiter sector = 30 tonnes
- Maximum stress (at the bottom wall) =180 MPa

During plasma disruptions and vertical instabilities, forces due to eddy current, induced in the vacuum vessel will act together with the forces transmitted through the divertor coils. Different cases have been simulated with the PROTEUS code for "fat" and "slim" plasmas: the worst load condition corresponds to an upward vertical instability, when the vessel should withstand a net vertical force of about 1000 tonnes (Table XVIII), with 700 tonnes due to toroidal eddy currents.

The effect of local poloidal ("halo") currents during a vertical instability should also be taken into account. Estimates show that a total current up to 1 MA can flow in the first wall components when the plasma approaches the vessel wall. Up to 300 tonnes of additional load can be transmitted to the vessel, but the timescale and the distribution of such a force is not yet clear. Further investigations will be carried out and experimental measurements will be attempted.

The disruption loads on the vessel can produce up to 10 mm displacement of the main vertical port even after the introduction of the new damper system and reduction in weight of the attached diagnostic systems. A maximum plastic strain of 0.5% has been estimated from a dynamical analysis of the port, which corresponds to a life of 1000 cycles as shown by fatigue tests performed on the vessel material. It has been estimated that five years of operation should produce up to 20% of total fatigue damage at the port base, which represents a good safety margin for the vessel performance.

Divertor Power Supplies

The magnetic configuration (X-point) for the new pumped divertor will be achieved by circulation of DC currents in four discrete coils to be installed inside the vacuum vessel. The accurate control of the magnetic configuration (X-point position) and the sweeping requirements will be achieved by supplying the divertor coils from individual thyristor controlled power supplies (PDFA). Following the mechanical design of the coils, the electrical characteristics were determined. Computer simulations were set-up to determine:

- the voltage/current range of the power supplies under normal operation, in various configurations;
- the voltage/currents induced in the power supplies during the plasma vertical instabilities and disruptions.

A basic configuration and rating of the power supplies, including the control and protection system was derived, which formed the basis of a reference design (Table XIX). A technical specification for the complete Poloidal Divertor Field Amplifier system, including the reference design, was written and a Call for Tender was issued in November 1990.

Plasma Control

Various simulations have been carried out with the PROTEUS code. These include scenarios for the plasma build-up, for sweeping the divertor strike zone across the target plates, and simulations of vertical instabilities and disruptions. These studies are performed to assess voltage and current requirements for the divertor and shaping coils, forces on the divertor elements and at the vessel arising from eddy currents, and to provide basic information on the magnetic configurations needed for the assessment of heat loads and divertor performance.

The requirements for the vertical stabilisation were of

Table XIX
PDFA: Technical Data

Nominal pulsed current repeated every 10 mins	40kA for 15 s, with linear rise and decay,
I^2t of Nominal Current Pulse	$32x10^9$ A^2s
Nominal Continuous Current	8kA DC
Maximum positive output voltage at nominal pulsed current and minimum supply voltage (28kV rms)	+ 500 VDC [+ 650 VDC (option No.1)]
Maximum negative output voltage at nominal pulsed current and minimum supply voltage (28kV rms)	-200 VDC [-250 VDC (option No.1)]
Maximum value of the peak instantaneous short circuit current at the output (connection point)	165kA

particular interest. The simulations indicate that the expected growth rate of a vertical instability can be as high as 800s-1 for a "slim" plasma configuration (see Table XV). It has been concluded that this plasma can be stabilised with the external radial field coil and the new fast radial field amplifier. There was some concern that deviations from the assumed plasma parameters such as the current profile of the stabilisation system and could even cause an MHD instability within an Alfven time. Further studies which include a better modelling of the mechanical shell are foreseen to establish more firmly the limits of vertical stabilisation system, as it is presently conceived.

Another matter of concern are the "halo" currents which are expected to flow across various components inside the vessel as a consequence of disruption and vertical instabilities. Preliminary estimates have been made of the magnitude of these currents and some studies were performed on the likely distribution of the currents and on the resulting forces on components. It is considered to incorporate a model of the "halo" currents in the PROTEUS code in order to improve the design basis for supports for in-vessel elements.

Fast Radial Field Amplifiers

Although a more powerful and faster plasma vertical control system was a requirement of the present elongated magnetic configurations such an amplifier is essential to establish and control the plasma magnetic configuration in the divertor operating mode. A modular system has been conceived, based on an H-bridge in which each arm consists of two Gate Turn Off (GTO) Thyristors, connected in parallel.

Each Module has the ratings: Voltage - 2.5kV; Current - 2.5kA; Rise Time - 0.5ms. The Fast Radial Field Amplifier (FRFA) will consist of two identical units each supplied by a circuit breaker. The two units will be connected in series so that each can be by-passed by a bipolar thyristor; each unit is made up of two modules that can be connected either in series or in parallel.

The main elements of the Fast Radial Field Amplifier are: A rectifier transformer with two secondaries reduces the voltage from 36kV to approximately 1kV, to supply two Thyristor Converter Units; filters are foreseen in front of each Module, which is a DC-AC power converter, capable of four quadrant operation (invertor).

Following the tender procedure in March-April 1990, the JET-Executive Committee (EC) approved the contract to a limit of 2 MECU and established a panel of experts to review the design before full contract approval. The panel fully supported the JET design and the JET-EC subsequently released the funds for the full contract.

ICRF Antennae Development

The ion cyclotron resonance frequency (ICRF) antennae require close proximity to the plasma to achieve adequate coupling. With decreasing coupling, the voltage required to couple the full generator power is increased beyond that sustainable by the antennae. In the pump divertor phase, both the 'flat' and 'slim' plasmas would be too far from the existing (A1) antennae to couple significant power. However, the much increased clearance available between the plasma and the wall allows the design of new antennae with improved coupling. A new set of antennae (to so-called A2 antennae) optimised to the new plasma configuration is therefore being produced. Initially, these will be set-up to

match the 'fat' plasma; operation with the slim plasma will require the antenna to be moved to a new position in the torus (requiring hands-on intervention in the torus).

Thermal Analysis

The duty cycle for design of the A2 antennae is 20 second pulse duration at 20 minutes intervals. With improved coupling, a reduced peak design voltage of 40kV is used. A screen design similar to the open structure of the A1 beryllium screen, and which also uses solid beryllium elements, gives very low RF losses in the elements. These factors enable the antenna to be designed without active cooling. Only radiation cooling is used, much simplifying the design and increasing reliability. With the high temperature of operation, nickel coating will be used instead of silver, the increase in RF losses being balanced by the increased emissivity of nickel.

Mechanical Design

The dominant factor in the mechanical design is the minimisation of the loads following a disruption. With the antenna projecting up to 0.7m from the torus wall, it is very exposed to changes in magnetic field, particularly radial flux changes during vertical disruptions. Furthermore, the pumped divertor configuration is anticipated to have a faster vertical movement at the onset of a disruption. These factors combine to produce forces not readily supported by the torus unless careful precautions are taken. The A2 antennae rely heavily on the use of the thinnest feasible material for fabrication of the antenna, much of this is only 0.8mm thick. Differential expansion and flexing of the torus then require a highly convoluted design to avoid stress concentrations. The resultant antenna (Fig.203) is a flexible structure which relies on connections to the torus by many articulated rods for mechanical support.

The antennae also relies on the use of resistors in series with each pair of screen elements to limit eddy currents. These resistors, which must approximate to a short-circuit to the RF currents, are manufactured by nickel plating metallised ceramics. Prototype units are currently under test. Graphite tiles will be used to protect all sides of the antenna from the plasma. These will be mounted 15mm behind the poloidal limiters.

RF Design

The A2 antenna incorporates a septum between the two central conductors (Fig.204). This decouples the conductors and allows operation with arbitrary phase differences. Both the septum and the side walls are slotted to a distance ~100mm from the plasma to minimise induced currents on these items, which also degrade the $k_{\parallel}$ spectrum. The positions of the antenna in the torus will be rearranged to give two groups of four adjacent antennae, which also improves the spectrum.

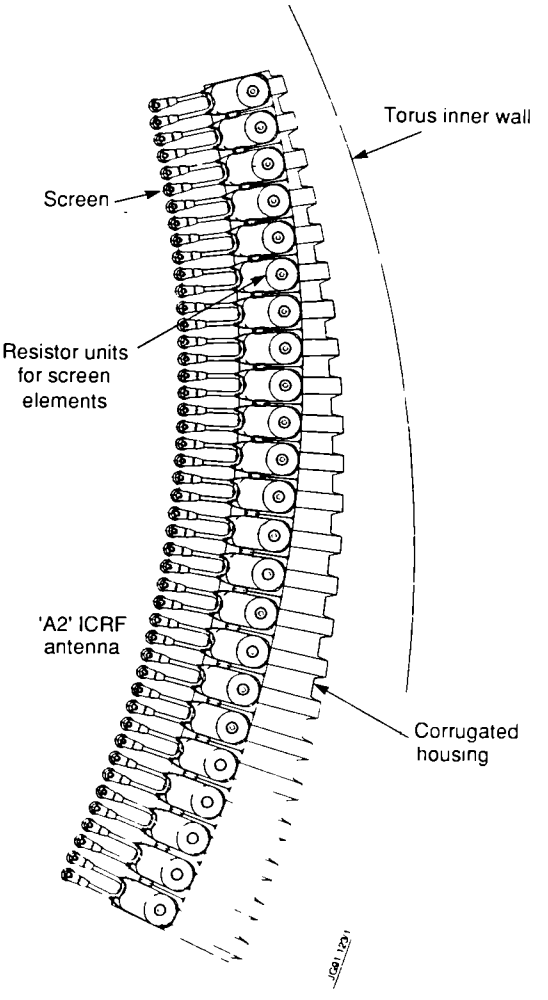

Fig.203 A simplified side view of the A2 antenna, showing the screen and its resistive attachments to the flexible housing. Attachments of the housing to the torus are not shown.

A full scale simplified model of the antenna has been constructed for low power RF tests which are presently nearing completion. These tests are used to define the optimum shape of the central conductors; as the antennae are no longer symmetrical top to bottom or left to right, this model is proving particularly beneficial for this optimisation.

The main limitations on the voltage of the existing A1 antennae have been breakdown of the conical ceramic where the vacuum transmission line enters the torus. This ceramic

is being removed from the A2 lines, which will now be all metal coaxial lines from the RF window to the antennae. The mechanical support of the lines is now made by a cylindrical ceramic inside the antennae housing. These changes are accomplished by modifying the existing hardware, which is largely re-used.

A full scale model of one quadrant of the antenna has been constructed (Fig.205), and is presently being prepared for high power RF testing under vacuum. This model includes all critical features of the antenna and can be tested in open and short-circuit configurations to fully evaluate the design. These tests will commence shortly and are a critical element in the programme for completion of the prototype antenna by the end of 1991.

LHCD Launcher Developments

The LHCD launcher must be located close to the plasma to achieve good matching. The pumped divertor plasma presents two problems in this respect. The grill mouth must be re-shaped to suit either the large or small plasmas, and the launcher structure must be modified to enable the launcher to be moved sufficiently into the torus.

The L1 launcher is being modified to suit the larger pumped divertor plasma, and will now be installed for the first time in the pumped divertor phase. The launcher will not couple to the 'slim' plasma; an alternative approach to the construction of the launcher is being explored for the slim plasma campaign.

The revised L1 launcher will re-use from the existing launcher the side protection, disruption supports and hangers for allowing movement of the launcher. Some modification of these items is required to support the additional disruption loads in the new configuration. With the reduced duty cycle, no active cooling is being incorporated apart from the RF window, as in the existing launcher. Some minor external machining of the L1 multijunctions is required, together with detailed changes in the connection of these to the incoming waveguides. The alternative approach, for which a feasibility study is presently underway, utilises quasi-optical transmission between the 48 input waveguides and the 384 reduced section output waveguides. This would enable matching to the small plasma by the rebuilding of a much simplified waveguide mouth.

Diagnostics

Definition of plasma diagnostics for the divertor, and engineering design and integration into the divertor have contin-

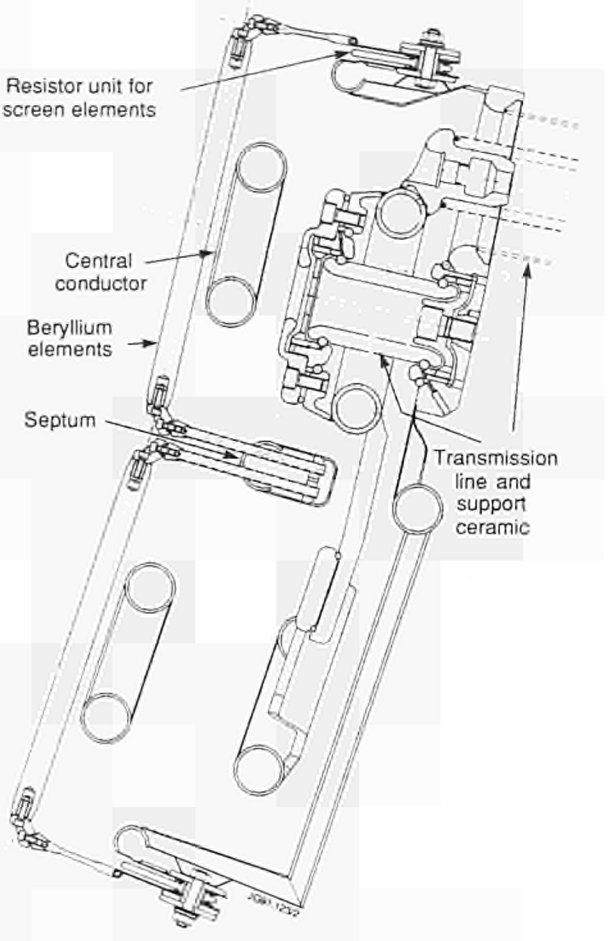

Fig.204 A horizontal cross-section through an A2 antenna at the level of a transmission line connection. The slotted septum and sidewalls, the screen resistors and the ceramic support inside the antenna are important changes compared to the A1 antennae.

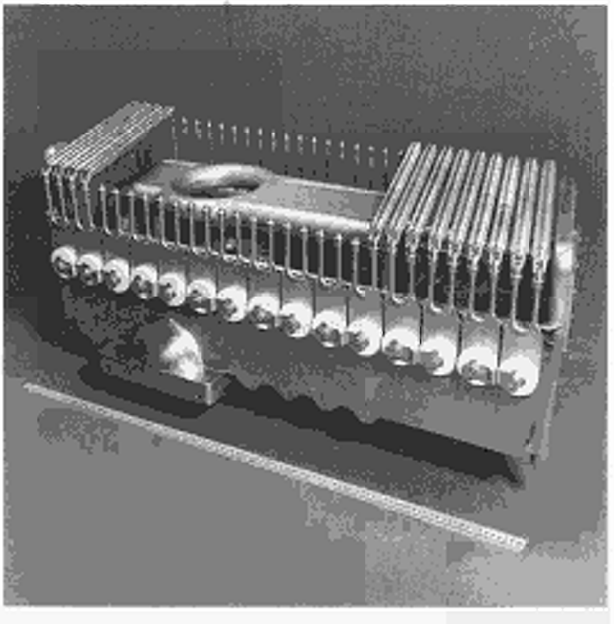

Fig.205 The full scale model of one quadrant of the A2 antenna to be used for high power RF tests.

Table XX
Diagnostics for the New Phase of JET

System	Diagnostic	Purpose	Association	Status
KB2X	X-point bolometer	Time and space radiated power from X-point region	JET and IPP Garching	Commissioning
KB3D	Divertor bolometer	Time and space resolved radiated power from divertor region	JET	Design
KC1D	Magnetic diagnostic for divertor	Identification of flux surface geometry	JET	Design
KD1D	Calorimetry for divertor	Poloidal temperature distribution on target	JET	Design
KE4	Fast ion and alpha-particle diagnostic	Space and time resolved velocity distribution	JET	Under construction
KE5	q-profile Thomson scattering	Measurement of q-profile	JET	Under development
KE7	Lidar Thomson scattering	Higher spatial resolution, n_e and T_e in plasma edge	JET	Design
KE9D	Lidar Thomson scattering	T_e and n_e profile in divertor region	JET	Design
KF1	High energy neutral particle analyser	Ion energy distribution up to 3.5MeV	Purchased from Ioffe Leningrad	Under construction
KG5X	X-point reflectometer	Peak n_e in X-point	JET	Under development
KG6D	Microwave interferometer	$\int n_e ds$ in divertor region	JET	Design
KG7D	Microwave reflectometer	Peak n_e in divertor region	JET	Design
KJ3	Compact soft X-ray cameras	MHD instabilities, plasma shape	JET	Design
KJ4	Compact soft X-ray camera	Toroidal mode number determination	JET	Design
KK4D	Electron cyclotron absorption	$n_e T_e$ profile in divertor region	JET	Design
KL3	Surface temperature	Surface temperature of target tiles	JET	Commissioning
KM2	14MeV neutron spectrometer	Neutron spectra in D-T discharges, ion temperatures and energy distributions	UKAEA Harwell	Under construction
KM5	14MeV time-of-flight neutron spectrometer		SERC Gothenberg	Awaiting installation
KS6	Bragg rotor X-ray spectrometer	Monitor of low and medium Z impurity radiation	UKAEA Culham	Design
KS7	Poloidal rotation	Multichannel spectroscopic measurement of poloidal rotation	UKAEA Culham	Design
KT3X	X-point target spectroscopy	Impurity and H spectra spatially resolved	JET	In preparation
KT5D	Toroidal view	Flow velocity	JET	Design
KT6D	Periscopes	Impurity density in divertor	JET	Design
KT7D	VUV and XUV spectroscopy	Impurity survey in the divertor region	JET	Design
KY4D	Fixed Langmuir probes for divertor	Plasma parameters at target	JET	Design
KY5D	Fast pressure gauges for divertor	Neutral particle fluxes on target	JET	Design
Kα1	Escaping alpha-particle detector	D-T alpha-particle confinement	JET	Design

ued during the year. Detailed engineering is underway for the diagnostic systems described below and the present status is detailed in Table XX. Magnetic geometry, electron density and temperature of the divertor plasma, radiative and conductive heat loading of the targets, and dynamics of impurity and hydrogen ions in the divertor plasma are the main measurement goals.

Magnetic Geometry and Plasma-Target Interaction

An important diagnostic task is to measure gradients of plasma parameters along the flux tubes in the divertor region, since these are manifestations of the active physical processes. For this, the magnetic geometry of the plasma needs to be determined accurately. This will be carried out with a combination of an array of magnetic flux and field

probes the divertor region poloidally encircling, and Langmuir probes located in the divertor targets. A coarse distribution of such combined measurements is sufficient since radial sweeping of the X-point and the plasma-target impact regions will give intermediate measurements needed to compute the spatial details of the target plasma parameters. Technical realization of the magnetic diagnostics, saddle loops and normal and tangential field coils, will follow closely the approach already used in JET. Since conventional Langmuir probes are susceptible to destruction in the divertor environment, new probes able to 'pop-up' into the plasma for a short exposure, employing **jxB** devices or pressurized bellows assemblies, are under development.

Thermographic observation of the target using CCD cameras with infra-red (IR) filters and a 32x32 pixel cooled IR array, is in preparation for determination of surface temperature. While the IR array gives good sensitivity and wide dynamic range with coarse spatial resolution, the CCD camera has a small dynamic range, good sensitivity and excellent spatial resolution. Absolute calibration depends directly on the emissivity of the beryllium surfaces. Since the emissivity of beryllium under heat and particle load is an uncertain quantity, an in-situ calibration using thermocouples is foreseen. Indeed calorimetry using thermocouples is envisaged as the main measurement of heat flux to the targets. At two toroidal locations, the inner, outer and centre target areas will be probed with fourteen thermocouples. The inlet and outlet cooling water temperature for all forty eight target modules will be measured, from which time-averaged toroidal heat load distribution would be deduced.

Miniaturized tetrode type pressure gauges similar to those employed in ASDEX and DIII-D are being developed to measure the neutral gas pressure and particle flux at the targets, and at the cryopump entrance. The short tubes required to couple the target area with the gauges will restrict the time resolution to 10ms. Three poloidal arrays are planned, 90° and 180° apart toroidally, to monitor asymmetries.

Electron Temperature and Density in the Divertor Plasma

Thomson scattering for the measurement of T_e and n_e is planned using the LIDAR technique. Coupled laser beam injection and scattered light receiving optics will be located in a main port at the midplane. Local measurements of $T_e \geq$ 10eV and $n_e \geq 3 \times 10^{19} m^{-3}$, with ≈4cm resolution along the laser beam, look feasible, using a 430nm, 1J, 200ps, Nd-YAG laser. Alternatively, a Ruby laser beam at 694nm shared with the existing LIDAR system may be used, in which case the resolution becomes 5-6cm. This will enable measurements of T_e and n_e to be made along the field lines from the inner target plate region region to well beyond the X-point. In addition, the beam can be moved transversely, which provides profiles perpendicular to the field lines.

Three inter-related microwave systems are under consideration for measurements of T_e and n_e. These would share the same waveguides and antennae, and thus measure on the same sightlines across the plasma. The three systems are: (i) a two-colour interferometer, at ≈130GHz and ≈170GHz, giving the line-integrated electron density; (ii) a multiple channel fixed frequency reflectometer operating in the frequency range 60-90GHz, to give peak density $\hat{n}_e$; and (iii) an electron cyclotron absorption measurement giving a profile of $n_e T_e$. From these three measurements profiles of n_e and T_e along the line-of-sight would be deduced. Such combined measurements would be repeated at up to three poloidal locations in the divertor region (three outside or two outside and one inside), giving information on the variation of n_e and T_e along the separatrix in the poloidal direction.

Dynamics of Impurity and Hydrogen Ions in the Divertor Plasma

A bolometer array, consisting of 32 detectors in 7 miniature cameras with good space and time resolution and large dynamic range, based on IPP/Tore Supra development, has been designed for determination of plasma radiation emissivity profiles. Tests are in progress of solutions to the main technical problems, miniaturization of detector heads an associated cabling, and the requirement that the whole assembly withstand high temperature baking of JET, without active cooling. A prototype detector has been built and tested.

Preparations for combined visible and VUV spectroscopic measurements are underway. Since $T_e \approx$ 10-150eV in the divertor plasma, the most important spectroscopic region will be the VUV range of wavelengths from 8-120nm. The intrinsically poor spatial resolution of the appropriate VUV instruments will be compensated by complementary close coupled visible spectroscopy measurements in the range 375-700nm.

A new VUV instrument will combine a double flat-field toroidal grating spectrometer covering the region 20-150nm, with a 2m concave-grating grazing incidence spectrometer

for the region 2-30nm. These instruments will observe the divertor plasma from a top vertical port, with facility for radial scan of the divertor plasma. In addition, the vertical camera of the existing rotating mirror VUV system (KT1) will be relocated to the top port, permitting rapid (25ms) spatial scanning of the SOL-divertor plasma. Spatially resolved determination of impurity densities, ionization states, and constitution of the total radiation are amongst the measurement objectives using this instrumentation.

Visible spectroscopy, using fibre-optic transmission, will be exploited for wide spatial coverage and good spectral resolution. A periscope coupled to a fibre-optic imaging system will be installed at the bottom of the torus for a close view of the divertor plasma and target surfaces. The light will be transmitted ≈100m to spectrometers in the Diagnostic Hall for analysis. In addition, a new midplane-mounted system looking obliquely into the divertor in two directions is being developed. Absolute line intensities for deduction of impurity influxes and densities, intensity ratios of lines from a species for electron density determination, Doppler broadening and line shifts for ion temperature and drift velocity measurements, continuum measurements for Z_{eff}, and observation of lines from low ionization stages for identification of charge-state distribution are amongst the objectives.

References

[1] Workshop on the New Phase of JET, JET Report-JET-R(89)16;

[2] Keilhacker, M., et al., Proc. 13th Int. Conf. on Plasma Physics and Controlled Nuclear Fusion Research (Washington, USA, 1990), Paper IAEA-CN-53/A-5-1;

[3] Simonini, R., Keilhacker, M., Taroni, A. and Watkins, M.L., 17th EPS Conf. on Contr. Fusion and Plasma Heating, Amsterdam, 1990, 14B(III), EPS (1990) 1369;

[4] Keilhacker, M., Simonini, R., Taroni, A. and Watkins, M.L., Nucl. Fus. (to be published) and JET Preprint-JET P(90)37;

[5] Braginskii, S.I., Review of Plasma Physics **1**, Consultants Bureau, New York (1965) 205;

[6] Simonini, R., Feneberg, W., Taroni, A., Proc. 12th European Conference on Controlled Fusion and Plasma Physics, (Budapest, Hungary, 1985), Vol.9FII, (1985) p484;

[7] Igitkhanov, Yu.L., Contributions to Plasma Physics **28** (1988) 477;

[8] Cupini, E., DeMatteis, A., Simonini, R., NET Report EUR XII-324/9 (1984);

[9] Hugon, M., Lallia, P.P. and Rebut, P.H., JET Report JET-R(89)14;

[10]Summers, D. D. R., et al., J. Nuclear Mater., to be published (1990);

[11]Harbour, P.J., Simonini, R., Tagle, J.A., Gottardi, N., von Hellermann, M., et al., 9th Int. Conf. on Plasma Surface Interactions in Contr. Fusion Devices, Bournemouth, UK, 21-25 May 1990 (to be published in J. Nucl. Mat.) and JET Preprint JET-P(90) 41(II), 283;

[12]Erents, S. K., et al., Proc. 17th European Conference on Controlled Fusion and Plasma Heating, Amsterdam, 1990, **14B(III)**, EPS (1990) 1385;

[13]Stamp, M. and Summers, H. P., Proc. 17th European Conference on Controlled Fusion and Plasma Heating, Amsterdam, 1990, **14B(III)**, EPS (1990) 1377;

[14]Stork, D., et al., 9th Int. Conf. on Plasma Surface Interactions and Controlled Fusion Devices, Bournemouth, UK, JET Preprint JET-P(90) **41(I)**, 135;

Future Plans

The JET programme was divided into phases governed by the availability of new equipment and fitting within the accepted lifetime of the Project. At the beginning of 1990, the planned programme was as set out in Table XXI. Taking account of the adjustments to the shutdown schedule and the need to allow for sensible periods of operation to establish high reliability in preparation for the active phase of operation, the period remaining for D-T operation was no more than eight months. However, with the advent of the proposal for a New Phase for JET until the end of 1996, the planned programme is now as set out in Table XXII.

On the JET programme, Phase I, the Ohmic Heating Phase, was completed in September 1984, and Phase II (Additional Heating Studies) was completed in October 1988. The present Phase III (Full Power Optimization Studies) is underway, with Phase IIIA completed and Phase IIIB just started. Future phases are set out in the following paragraphs.

Full Power Optimisation Studies - Second Part - Phase IIIB (Oct. 1990 - Dec. 1991)

After the shutdown at the start of this phase, the following are planned to be operational:

Table XXI
JET Development Programme to 1996

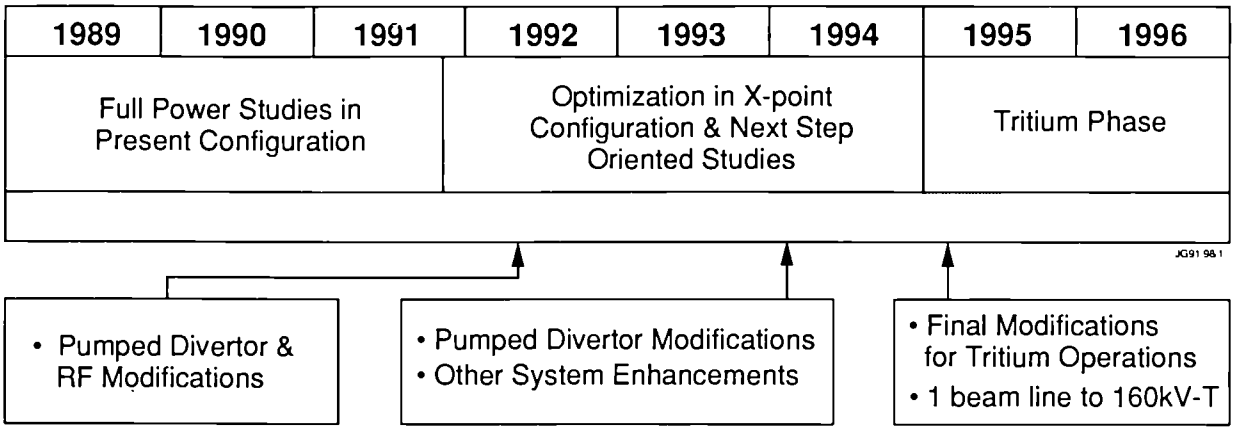

- uncooled separatrix dump plates (with beryllium protection at the bottom, and graphite at the top);
- gas injectors in the X-points regions;
- prototype high-speed pellet launcher;
- second neutral injector box converted to 140kV operation;
- in-vessel preparation for the fast ion and α-particle diagnostic.

The scientific aims of the operational period in this configuration will be to exploit these new additions in order to complete and obtain maximum performance in limiter configuration (current up to 7 MA) and to optimise X-point operation (current up to 6 MA), including a comparison of H-modes in X-point configuration using beryllium or carbon dump plates.

Preparations for D-T operations will also continue during this period, including commissioning of the Active Gas Handling System (AGHS) with tritium gas (subject to consent by the approving bodies).

Table XXII
JET Programme to 1992

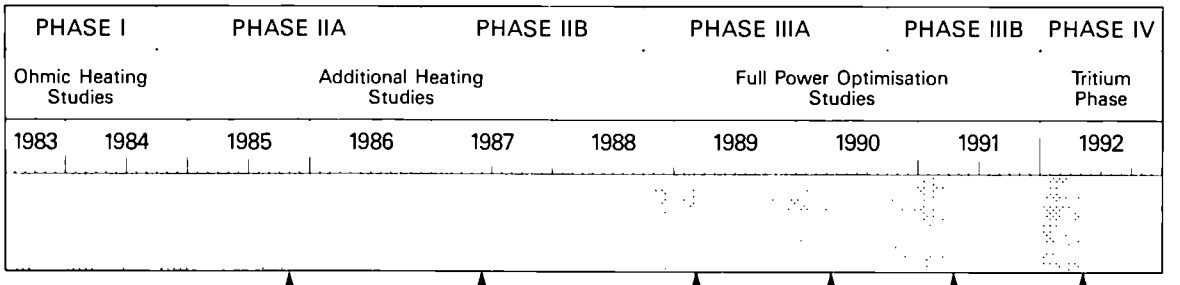

Ohmic Systems	5MA	Vessel restraints and improved volt-seconds for 7MA operation	Vessel reinforcements			
Separatrix		Additional P1 coils	Separatrix dump plate supports		Separatrix dump plates	
Limiters	Eight carbon mid-plane limiters	Carbon belt limiters	Beryllium belt limiters	Modifications to Beryllium tiles		
Pellets	Single pellet injector	ORNL multiple pellet injector (1.5kms^{-1})			High speed pellet injector	
NBI	First NBI line (80kV)	Second NBI line (2x80kV)	One line modified to 140kV D		Second line modified to 140kV D	One line modified to 160kV T
ICRH	Three A_0 antennae	Eight A_1 antennae		Be antennae screens		
LHCD			Install Vacuum Chamber	Prototype system		Full system*
Disruption control						Saddle coils*
Tritium and Remote handling					Tritium plant and main RH modifications	Final modifications

* To go ahead only if New Phase of JET approved

New Phase Programme-Phase IVA (Nov 1991 - Dec 1993)

At the end of 1991, the Project will enter an extended shutdown, which will last until Spring 1993, in order to install the components relevant to the new pumped divertor phase. This will involve intensive in-vessel work to install the following equipment:

- lower divertor structure with inertially cooled beryllium target plates;
- pumping chamber and cryopump;
- internal poloidal divertor coils and corresponding power supplies;
- modified limiters;
- new ICRF heating antennae (A2);
- full Lower Hybrid Current Drive (LHCD) system with its modified launcher;
- divertor diagnostics;
- multiple high-speed pellet launcher;
- disruption control system using internal saddle coils.

The single-null X-point pumped divertor configuration should enable JET to progress towards extended high power operation with 40MW additional heating made of neutral beam and ICRF power (eg plasma currents of 6MA for up to 3s, 3MA for up to 5s). The control of disruptions using saddle coils system and the control of sawteeth using the full power LHCD system should also be studied.

The first operating period should focus initially on establishing reliable operation in this new configuration. Subsequently, attention should be devoted to the study of performance and effects of the pumped divertor in controlling impurities, plasma density and exhaust, and power loading on the target plates.

New Phase Programme-Phase IVB (Dec 1993-Dec 1994)

The proposed shutdown (~4 months) in late 1993 would be to provide an opportunity, in the light of information from the experimental programme and elsewhere, to implement modifications to the pumped divertor (eg enhanced cooling of the target plates). In addition, it should be possible to install other enhancements aimed at improving performance in the new configuration or for the D-T Phase (eg enhanced pellet injection or fuelling system, modifications to LHCD or additional heating systems, etc.).

The primary objective of this second operating period of the new phase (to end-1994) would be to provide information the full 40 MW power and to establish with confidence the key design features of the Next Step in relation to:

- impurity control;
- fuelling;
- helium transport and exhaust of ashes.

Another objective would be to optimise reliability and plasma performance in the divertor configuration in anticipation for D-T operations. In parallel, active commissioning of the Active Gas Handling System and Remote Handling preparation should be completed.

Tritium (D-T Operations) - Phase V (Jan 1995-Dec 1996)

Subject to the approval of the JET Council and to necessary official consents, and when it is clear that the results in deuterium and general levels of system reliability justify it, the D-T phase would start in 1995, after a short shutdown to complete final modifications required for active operations.

During D-T operations, it would be possible to study in depth the physics of α-particle production, confinement and heating and thermal excursions. In addition, the real experience of tritium operation in a relevant scale tokamak (ie tritium handling and recovery, fuel mixture control, confinement properties of D-T plasmas, and remote maintenance and plasma diagnostics with large neutron and gamma backgrounds) will provide essential information for the Next Step.

JET Programme with 1992 as end date

As noted previously, for the present, the Project is proceeding in a manner compatible both with pursuing the New Phase programme towards 1996 and with completing its experimental life with D-T operations in 1992. Plans have been developed for a campaign of D-T pulses which could be managed with a minimum of modification to the machine and existing subsystems. In order to keep the tritium inventory low, the plans involve a limited number of D-T pulses at the end of each operating day, immediately followed by cryo-panel regeneration. The exhaust would be collected in the Active Gas Handling System and isotopically separated for re-use after a few weeks of operation. This would entail the full operation of the AGHS, albeit not on a continuous basis and not using its capacity.

Work necessary to prepare for such a campaign is proceeding, including:

- preparation for formal submission to the UKAEA Safety and Reliability Directorate of an overall safety analysis;
- activation and shielding calculations for the limited D-T scenario;
- modifications to diagnostic and ancillary systems, (eg conversion of one NI box for tritium injection, reduction of diagnostic windows, etc.).

It is unlikely that, in the time available, multiple high-speed injection of tritium pellets will be brought into operation.

The 1992 and 1996 possible JET experimental programmes diverge at the end of 1991. However, as the JET Council has recognised, it is becoming increasingly difficult to maintain both options within the constraints in staff, money and time available. Before mid-1991, the Project will be forced, in the absence of a decision on the extension of the Project, into making choices which will adversely affect one or probably both paths.

Appendix I

JET Task Agreements 1990

Title	*Associations (JET Responsible Officer)*	*Duration of Agreement*
RF HEATING DIVISION		
LOWER HYBRID CURRENT DRIVE ON JET • Exchange of knowledge • Design and construction of special item • High power tests	EUR-CEA CADARACHE (CEA/TA4) (J. Jacquinot)	Completed. The prototype launcher built by CEA has been installed and operated successfully
PHYSICS OF LOWER HYBRID CURRENT DRIVE ON JET • set-up predictive and interpretive codes • participation in the LHCD programme at JET	UNIVERSIDAD DI LISBOA (UTL/TA1) (J. Jacquinot)	Completed
LH AND ICRF EFFECTS ON JET • CD efficiency including transport • Synergistic effects between FWCD and LHCD • Modulated heating modelling • Minority CD experiments • Effect of RF CD on MHD stability	EUR-UKAEA Culham (J. Jacquinot)	In progress: Radial transport of the fast electrons has been included in the Bandit code
EXPERIMENTAL DIVISION I		
PHYSICS OF SHAPED CROSS-SECTIONS	CULHAM UK (CUL/TA4) (P.E. Stott)	Started March 1983
EDGE PLASMAS & PLASMA SURFACE INTERACTIONS	CULHAM UK (CUL/TA2) (P.E. Stott)	Started June 1983
PLASMA WALL INTERACTIONS	GARCHING, FRG (IPP/TA2) (P.E. Stott)	Started Jan. 1984
NEUTRON PRODUCTION RELATED PHYSICS AND ASSOCIATED DIAGNOSTICS	SWEDEN (NFR/TA1) (P.E. Stott)	Started Jan. 1984
PLASMA SURFACE INTERACTIONS	SWEDEN (NFR/TA2) (P.E. Stott)	Started July 1987

Title	*Associations (JET Responsible Officer)*	*Duration of Agreement*
NEUTRON PRODUCTION RELATED PHYSICS	HARWELL UK (HAR/TA1) (P.E. Stott)	Started Aug. 1985
NEUTRON PRODUCTION RELATED PHYSICS AND ASSOCIATED DIAGNOSTICS	FRASCATI ITALY (ENEA/TA3) (P.E. Stott)	Started Jan. 1986
PHYSICS OF TURBULENT AND CONVECTIVE TRANSPORT, MHD AND RELATED DIAGNOSTICS	FOM NETHERLANDS (FOM/TA2) (P.E. Stott)	Started Nov. 1987
EXPERIMENTAL DIVISION II		
BULK IMPURITY PHYSICS AND IMPURITY RELATED DIAGNOSTICS	EUR-IPP FRG (P.R. Thomas)	Started Feb. 1983
SPECTROSCOPIC MEASUREMENTS: INTERPRETATION AND IMPURITY ANALYSIS	EUR-CEA CADARACHE, FRANCE (P.R. Thomas)	Started July 1984
PHYSICS OF ION AND ELECTRON ENERGY TRANSPORT AND RELATED DIAGNOSTICS	EUR-ENEA CREF, Italy (P.R. Thomas)	Started Oct. 1983
CHARGE EXCHANGE RECOMBINATION SPECTROSCOPY	FOM, AMOLF, NETHERLANDS (M. von Hellerman)	Started June 1983
IMPURITY ANALYSIS AND PLASMA DIAGNOSTICS USING SPECTROSCOPIC MEASUREMENTS	EUR-NFR, SWEDEN (P.R. Thomas)	Started Jan. 1988
IMPURITIES AND OTHER TOPICS	EUR-AEA, CULHAM, UK (P.R. Thomas)	Started June 1987
THEORY		
TESTING THEORETICAL TRANSPORT MODELS AGAINST JET DATA	EUR-UKAEA CULHAM, UK (CUL/TA5) (T.E. Stringer)	Dec. 1986 - Dec. 1991
THEORY AND MODELS OF ANOMALOUS TRANSPORT	EUR-ENEA FRASCATI, ITALY (D.F. Düchs)	Started Jan. 1988

Appendix 2

Articles, Reports and Conference Papers Published in 1990

1. D-D fusion reactivity studies in high temperature JET plasmas.
Adams J M Balet B Boyd D Campbell D Challis C Christiansen J P Cordey J G Core W Costley A Cottrell G Edwards A Elevant T Eriksson L Hellsten T Jarvis O N Lallia P Lawson K Lowry C Nielsen P Sadler G Start D Thomas P von Hellermann M Weisen H
Joint European Torus JET. March 1990. 35p.
Report JET-P(90)10 Submitted to Nuclear Fusion.

2. A comparison between hypervapotron and multitube high heat flux beam stopping elements.
Altmann H Falter H D Hemsworth R S Martin D Papastergiou S Tivey R B
Fusion Engineering. IEEE 13th Symp., Knoxville, 2-6 October 1989. New York, IEEE. 1990. pp.931-936.

3. Peaked profiles in low q high current limiter plasmas in JET.
Attenberger S Balet B Campbell D J Christiansen J P Cottrell G A Edwards A Jones T T C Kupschus P Lomas P J Nielsen P O'Rourke J Pasini D Prentice R Sadler G Schmidt G Stubberfield P Taroni A Tibone F Weisen H
Controlled Fusion and Plasma Heating. 17th EPS Conf., Amsterdam, 25-29 June 1990. Contributed papers. Geneva, European Physical Society. 1990. pp.I-5 - I-8.(Report JET-P(90)14, pp.121-124.)

4. Nonlinear evolution of ideal internal kink modes in tokamaks with nonmonotonic q profiles.
Avinash K
Physics of Fluids B: Plasma Physics vol.2 no.10 October 1990 p.2373-2382.

5. Determination of local transport coefficients by heat flux analysis and comparisons with theoretical models.
Balet B Bartlett D Cordey J G Gowers C Hammett G W von Hellerman M O'Rourke J Morgan P Nielsen P Sadler G Stubberfield P M Weisen H
Controlled Fusion and Plasma Heating. 17th EPS Conf., Amsterdam, 25-29 June 1990. Contributed papers. Geneva, European Physical Society. 1990. pp.I-162 - I-165. (Report JET-P(90)14, pp.61-64.)

6. Determination of local transport coefficients by heat flux analysis and comparisons with theoretical modes
Balet B Cordey J G Stubberfield P M
Submitted to Plasma Physics and Controlled Fusion, October 1990. JET Report JET-P(90)51. 48p.

7. Extrapolation of the high performance JET plasmas to D-T operation.
Balet B Cordey J G Stubberfield P M
Controlled Fusion and Plasma Heating. 17th EPS Conf., Amsterdam, 25-29 June 1990. Contributed papers. Geneva, European Physical Society. 1990.pp.I-106 - I-109. (Report JET-P(90)14, pp.65-68.)

8. High temperature L- and H-mode confinement in JET.
Balet B Boyd D A Campbell D J Challis C D Christiansen J P Cordey J G Core W G Costley A E Cottrell G A Edwards A W Elevant T Eriksson L-G Hellsten T Jarvis O N Lallia P P Lawson K Lowry C Morgan P D Nielsen P Sadler G Start D F H Thomas P R Thomsen K von Hellermann M Weisen H
Nuclear Fusion vol.30 no.10 October 1990 p.2029-2038. (Report JET-P(89)81.)

9. Double crystal X-ray spectroscopy at JET
Barnsley R
Submitted to Rev. Sci. Instrum. and JET Report JET-P(90)39.

10. Electron impact ionization of neutral chromium.
Bartschat K Reid R H G Burke P G Summers H P
Joint European Torus (JET). October 1990. Report JET-P(90)48 (Preprint of paper to be submitted for publication in J. Phys. B).

11. Risk assessment methodology for the JET active gas handling system (AGHS) and the significance of the exhaust detritiation system in meeting design safety targets
Bell A C Ballantyne P R
16th Symposium on Fusion Technology, London, UK, 3-7 September 1990. JET Report JET-P(90)56 - Volume II, pp.151-156.

12. Deposition of carbon and beryllium and retention of deuterium on probes in the scrape-off layer of JET.
Bergsaker H Coad J P Behrisch R Clement S Lama F Prozesky V M Rover G Simpson J C B
Journal of Nuclear Materials, 176 & 177, pp.941-947. Joint European Torus (JET). 1990. (JET papers presented at 9th Int. Conf. on Plasma Surface Interactions and Controlled Fusion Devices, Bournemouth, 21-25 May 1990). pp.299-311. Report JET-P(90)41-II

13. JET design, construction and performance.
Bertolini E
Nuclear Energy vol.29 no.1 February 1990 p.31-45.

14. Supplying JET from the UK 400kV supergrid: a major engineering achievement relevant to the next step.
Bertolini E Cleobury E Dwek M Jervis B Marchese V Mondino P L Murphy G
16th Symposium on Fusion Technology, London, UK, 3-7 September 1990. Contributed papers. JET Report JET-P(90)56 - Volume I, pp.1-6.

15. Fast wave current drive in the ion cyclotron range of frequencies.
Bhatnagar V P Jacquinot J Moreau D Rimini F Start D F H
Joint European Torus (JET). October 1990. 24p. Report JET-P(90)22 Preprint of an Invited Paper presented at the Joint Varenna-Lausanne Int. Workshop, Varenna, Italy, August 1990.

16. ICRH produced H-modes in the JET tokamak.
Bhatnagar V P Bures M Campbell D Clement S Hatayama A Jacquinot J Start D F H Stork D Tanga A Tibone F Tubbing B J D
Controlled Fusion and Plasma Heating. 17th EPS Conf., Amsterdam, 25-29 June 1990. Contributed papers. Geneva, European Physical Society. 1990. pp.I-255 - I-258. (Report JET-P(90)14, pp.13-16.)

17. ICRH produced H-modes in the JET tokamak.
Bhatnagar V P Jacquinot J Tubbing B J D Stork D Tanga A Balet B Bosia G Bures M Campbell D Clement S Hatayama A Lawson K (Culham) Tibone F Start D F H
Joint European Torus (JET). July 1990. 33p. Report JET-P(90)44 Submitted to Plasma Physics and Controlled Fusion

18. JET ICRH antenna for pumped-divertor geometry.
Bhatnagar V P Jacquinot J Kaye A
JET contributions to the Workshop on the New Phase of JET: The Pumped Divertor Proposal (25-26 September 1990). Joint European Torus JET. 1989. pp.146-164. Report JET-R(89)16

19. Beamline duct gas release conditioning and the upgraded duct wall protection system of the JET neutral injectors.
Bickley A J Jones T T C Papastergiou S Challis C D Davies J F de Esch H P L Stork D Altmann H
Fusion Engineering. IEEE 13th Symp., Knoxville, 2-6 October 1989. New York, IEEE. 1990. pp.1438-1443.

20. An optical scanning diagnostic for neutral beam alignment on JET
Bickley A J Jones T T C Norman T Stork D Wight J
16th Symposium on Fusion Technology, London, UK, 3-7 September 1990. JET Report JET-P(90)56 - Volume I, pp.55-60.

21. Problems and methods of self-consistent reconstruction of tokamak equilibrium profiles from magnetic and polarimetric measurements.
Blum J Lazzaro E O'Rourke J Keegan B Stephan Y
Nuclear Fusion vol.30 no.8 August 1990 pp.1475-1492. (Report JET-P(89)63.)

22. An analytic procedure for currents and forces calculations in JET
Bobbio S Bertolini E Garribba M Miano G Noll P Senatore E
16th Symposium on Fusion Technology, London, UK, 3-7 September 1990. JET Report JET-P(90)56 - Volume I, pp.85-90.

23. Feasibility of diagnostic of JET LHCD plasmas by means of X-ray crystal spectroscopy.
Bombarda F Brusati M Giannella R Rimini F
Controlled Fusion and Plasma Heating. 17th EPS Conf., Amsterdam, 25-29 June 1990. Contributed papers Geneva, European Physical Society. 1990. pp.IV-1713 - IV-1716.

24. MHD modelling of density limit disruptions in tokamaks
Bondeson A Parker R Hugon M
Submitted to Nuclear Fusion, and JET Report - JET-P(90)73.

25. Beryllium related maintenance on JET
Booth S J Celentano G Newbert G Pick M Tesini A
16th Symposium on Fusion Technology, London, UK, 3-7 September 1990. JET Report JET-P(90)56 - Volume II, pp.133-138.

26. Automatic VSWR control in JET ICRH transmitters
Bosia G Lamont B Sibley A Schmid M Wade T
16th Symposium on Fusion Technology, London, UK, 3-7 September 1990. JET Report JET-P(90)56 - Volume I, pp.67-72.

27. High power tests of the JET prototype LHCD launcher
Brinkschulte H Rey G Brusati M Ekedahl A
Gormezano C Kaye A Lennholm M Pain M
Panissié H Plancoulaine J Schild P
16th Symposium on Fusion Technology, London, UK, 3-7 September 1990. JET Report JET-P(90)56 - Volume I, pp.91-96.

28. Simulation of propagation, absorption and current drive efficiency of lower hybrid waves in reactor relevant JET discharges.
Brusati M Gormezano C Knowlton S
Lorentz-Gottardi M Rimini F
Radio-frequency power in plasmas. 8th Topical Conf., Irvine, U.S.A., 1-3 May 1989. New York, American Institute of Physics. 1989. pp.122-125.

29. Global influx impurity behaviour during ICRF heating in JET with beryllium limiters.
Bures M Jacquinot J Campbell D Lawson K
Stamp M Start D F H Thomas P
Journal of Nuclear Materials, 176 & 177, pp.387-391. Joint European Torus (JET). 1990. (JET papers presented at 9th Int. Conf. on Plasma Surface Interactions and Controlled Fusion Devices, Bournemouth, 21-25 May 1990). pp.107-121. Report JET-P(90)41-I

30. ICRF heating/plasma edge interaction in JET with beryllium gettering. (Invited paper).
Bures M Jacquinot J Stamp M Lawson K Thomas P
Fusion Engineering and Design (Procs. IAEA Technical Committee Meeting on ICRH/Edge Physics, Garching, F.R.G., 2-5 October 1989) vol.12 nos.1&2 April 1990 pp.251-259.

31. Impurity release from the ICRF antenna screens in JET.
Bures M Jacquinot J Lawson K Stamp M
Summers H P D'Ippolito D A Myra J R
Submitted to Plasma Physics and Controlled Fusion, October 1990. JET Report JET-P(90)49.

32. Role of the antenna screen angle during ICRF heating in JET.
Bures M Jacquinot J J Start D F H Brambilla M
Nuclear Fusion vol.30 no.2 February 1990 pp.251-263.

33. The JET in-vessel inspection man-machine interface
Businaro T Junger J F
16th Symposium on Fusion Technology, London, UK, 3-7 September 1990. JET Report JET-P(90)56 - Volume II, pp.109-114.

34. Design features of the JET vacuum enclosure for safe operation with tritium.
Caldwell-Nichols C J Usselmann E
Fusion Engineering. IEEE 13th Symp., Knoxville, 2-6 October 1989. New York, IEEE. 1990. pp.716-719.

35. Methodology of tritium and radiation compatibility assessments for JET diagnostic and other systems and the preliminary results
Caldwell-Nichols C J
16th Symposium on Fusion Technology, London, UK, 3-7 September 1990. JET Report JET-P(90)56 - Volume II, pp.145-150.

36. Confinement and stability in JET: recent results.
Campbell D J and the JET Team
Plasma Physics and Controlled Fusion vol.32 no.11 November 1990 (Controlled Fusion and Plasma Heating. 17th European Physics Society Plasma Physics Division Conf., Amsterdam, 25-29 June 1990. Invited Papers. Edited by F C Schuller). pp.949-964. (Report JET-P(90)34)

37. The independent assessment of planned tritium operations at JET
Campbell H E Rowbottom M D
16th Symposium on Fusion Technology, London, UK, 3-7 September 1990. JET Report JET-P(90)56 - Volume II, pp.163-169.

38. Sawteeth and their stabilization in JET
Campbell D J and the JET Team
Nuclear Fusion Supplement (13th IAEA Conference on Plasma Physics and Controlled Nuclear Fusion Research, Washington, U.S.A., 1-5 October 1990, IAEA-CN-53/A-6-3), JET Report - JET-P(90)62, pp.119-131.

39. Proposal to measure the q profile on JET by Thomson scattering.
Carolan P G Forrest M J Gowers C W Nielsen P
Review of Scientific Instruments vol.61 no.10 pt.II October 1990 (Procs. 8th Topical Conf. on High Temperature Plasma Diagnotics, Hyannis, Massachusetts, 6-10 May 1990). pp.2926-2928.

40. Measurements of the energy distribution of fast tritons and helium atoms escaping from the plasma in JET.
Carruthers E V Zhu J Stangeby P C McCracken G M
Coad J P Erents S K Goodall D J H Simpson J C B
Partridge J W
Journal of Nuclear Materials, 176 & 177, pp.1027-1031. Joint European Torus (JET). 1990. (JET papers presented at 9th Int. Conf. on Plasma Surface Interactions and Controlled Fusion Devices, Bournemouth, 21-25 May 1990). pp.313-326. Report JET-P(90)41-II

41. Octant removal at JET for a toroidal field coil exchange
Celentano G Macklin B Booth S Last J R
Papastergiou S Pick M A Presle P Scott S Tesini A
16th Symposium on Fusion Technology, London, UK, 3-7 September 1990. JET Report JET-P(90)56 - Volume II, pp.169-174.

42. High β_p plasmas in DIII-D.
Challis C D and others
Bulletin of the American Physical Society vol.35 no.9 October 1990 (Program of the 32nd Annual Meeting of the Division of Plasma Physics, Cincinnati, Ohio, 12-16 November 1990). (Selected abstracts). p.2024, Paper 5F10.

43. Stability of high $\varepsilon\,\beta_p$ discharge in DIII-D.
Challis C D and others
Bulletin of the American Physical Society vol.35 no.9 October 1990 (Program of the 32nd Annual Meeting of the Division of Plasma Physics, Cincinnati, Ohio, 12-16 November 1990). (Selected abstracts). p.1972, Paper 3P2.

44. Transport modelling of high β_p plasmas in DIII-D.
Challis C D and others
Bulletin of the American Physical Society vol.35 no.9 October 1990 (Program of the 32nd Annual Meeting of the Division of Plasma Physics, Cincinnati, Ohio, 12-16 November 1990). p.1979, Paper 3Q16.

45. MHD analysis of peaked pressure profiles produced by pellet injection in JET
Charlton L A Baylor L R Houlberg W A Milora S L Lynch V E Kupschus P Edwards A O'Rourke J Schmidt G L Hammett G W
Submitted to Nuclear Fusion, and JET Report - JET-P(90)65

46. The role of current profile broadening in L-mode and H-mode plasmas.
Christiansen J P Cordey J G
Nuclear Fusion vol.30 no.4 April 1990 pp.599-610.

47. A unified physical scaling law for tokamak energy confinement.
Christiansen J P Cordey J G Thomsen K
Nuclear Fusion vol.30 no.7 July 1990 pp.1183-1196. (Report JET-P(90)05)

48. Unified physical scaling laws for tokamak confinement.
Christiansen J P Cordey J G Kardaun O Thomsen K
Controlled Fusion and Plasma Heating. 17th EPS Conf., Amsterdam, 25-29 June 1990. Contributed papers. Geneva, European Physical Society. 1990. pp.II-797 - II-800. (Report JET-P(90)14, pp.33-36.)

49. The conversion and operation of the neutral beam power supplies up to 160kV
Claesen R Mondino P L Baigger P Bertoldi P Binder D Jensen F Rushton R
16th Symposium on Fusion Technology, London, UK, 3-7 September 1990. JET Report JET-P(90)56 - Volume II, pp.187-192.

50. Edge fuelling scenarios and scrape-off layer parameters in JET with beryllium limiters.
Clement S Tagle J A Erents S K de Kock L Sartori R Saibene G
Journal of Nuclear Materials, 176 & 177, pp.432-437. Joint European Torus (JET). 1990. (JET papers presented at 9th Int. Conf. on Plasma Surface Interactions and Controlled Fusion Devices, Bournemouth, 21-25 May 1990). pp.155-166. Report JET-P(90)41-I

51. Effect of ICRH on the JET edge plasma with carbon and beryllium coated limiters.
Clement S Erents S K Tagle J A Brinkschulte H Bures M De Kock L
Fusion Engineering and Design (Procs. IAEA Technical Committee Meeting on ICRH/Edge Physics, Garching, F.R.G., 2-5 October 1989) vol.12 nos.1&2 April 1990 pp.261-266.

52. Scrape-off layer parameters at JET during density limit discharges.
Clement S Campbell D Erents S K de Kock L Saibene G Sartori R Tagle J A
JET Papers contributed to 17th EPS Conf. on Controlled Fusion and Plasma Heating, Amsterdam, 25-29 June 1990. Joint European Torus JET, 1990. pp.109-112. Report JET-P(90)14

53. Effect of limiter composition on Z_{eff} and recycling in JET.
Coad J P Behrisch R de Kock L Ehrenberg J Lama F Martinelli A P Partridge J Saibene G Sartori R Simpson J C B Stamp M F Summers D D R
JET Papers contributed to 17th EPS Conf. on Controlled Fusion and Plasma Heating, Amsterdam, 25-29 June 1990. Joint European Torus JET, 1990. pp.21-24. Report JET-P(90)14

54. Evolution of Be-containing layers in JET boundary region.
Coad J P Burch S Kaveney G Lama F Neill G F Partridge J Simpson J C B Vince J
Journal of Nuclear Materials, 176 & 177, pp.145-149. Joint European Torus (JET). 1990. (JET papers presented at 9th Int. Conf. on Plasma Surface Interactions and Controlled Fusion Devices, Bournemouth, 21-25 May 1990). pp.25-37. Report JET-P(90)41-I

55. Operation and reliability of a pneumatic hydrogen pellet injection system on JET.
Combs S K Jernigan T C Baylor L R Milora S L Foust C R Kupschus P Gadeberg M Bailey W
Fusion Engineering. IEEE 13th Symp., Knoxville, 2-6 October 1989. New York, IEEE. 1990. p.1305.

56. A regime showing anomalous triton burnup in JET.
Conroy S Jarvis O N Pillon M Sadler G
Controlled Fusion and Plasma Heating. 17th EPS Conf., Amsterdam, 25-29 June 1990. Contributed papers. Geneva, European Physical Society. 1990. pp.I-98 - I-101. (Report JET-P(90)14, pp.85-88.)

57. Tokamak stray field compensation system for JET neutral beam
Cooper D Altmann H Carwardine J Challis C de Esch H P L Stork D
16th Symposium on Fusion Technology, London, UK, 3-7 September 1990. JET Report JET-P(90)56 - Volume I, pp.79-84.

58. Preliminary analysis of the ITER energy confinement H-mode data base.
Cordey J G
Bulletin of the American Physical Society vol.35 no.9 October 1990 (Program of the 32nd Annual Meeting of the Division of Plasma Physics, Cincinnati, Ohio, 12-16 November 1990). (Selected abstracts). p.1922, Paper 1P15.

59. Assessment of transport models on the basis of JET ohmic and L-mode discharges.
Corrigan G Duchs D F Nocentini A Sack Ch Springmann E Stringer T E Taroni A Tibone F
Controlled Fusion and Plasma Heating. 17th EPS Conf., Amsterdam, 25-29 June 1990. Contributed papers. Geneva, European Physical Society. 1990. pp.II-801 - II-804. (Report JET-P(90)14, pp.77-80.)

60. Electron density and temperature measurements on large tokamaks.
Costley A E
Joint European Torus (JET). July 1990. 19p. Report JET-P(90)35 Paper presented at 5th National Topical Meeting on High Temperature Plasma Diagnostics, Minsk, U.S.S.R.,June 1990.

61. Electron cyclotron emission and electron cyclotron resonance heating
(Report on the 7th Workshop and the IAEA Technical Committee Meeting (EC7), Hefei, China, 9-11 May 1989).
Costley A E
Nuclear Fusion vol.30 no.10 October 1990 pp.2185-2190.

62. Evidence for fine-scale density structures on JET under beam heated conditions.
Costley A E Cripwell P
Bulletin of the American Physical Society vol.35 no.9 October 1990 (Program of the 32nd Annual Meeting of the Division of Plasma Physics, Cincinnati, Ohio, 12-16 November 1990). (Selected abstracts). p.1999, Paper 4P25.

63. Measurements of the electron temperature and electron density in the edge plasma of JET by ECE and microwave reflectometry.
Costley A E Bartlett D V Porte L Prentice R Salmon N A Sips G
Journal of Nuclear Materials, 176 & 177, pp.1064-1069. Joint European Torus (JET). 1990. (JET papers presented at 9th Int. Conf. on Plasma Surface Interactions and Controlled Fusion Devices, Bournemouth, 21-25 May 1990). pp.327-340. Report JET-P(90)41-II

64. Recent developments in microwave reflectometry at JET.
Costley A E Cripwell P Prentice R Sips A C C
Review of Scientific Instruments vol.61 no.10 pt.II October 1990 (Procs. 8th Topical Conf. on High Temperature Plasma Diagnotics, Hyannis, Massachusetts, 6-10 May 1990). pp.2823-2828. (JET Report JET-P(90)19) pp.7-28

65. A large-orbit model for ICRH heating: Comparison with JET data.
Cottrell G A Start D F
JET Joint Undertaking Joint European Torus JET. May 1990. Report JET-P(90)17
Submitted to Nuclear Fusion.

66. Maximum entropy and plasma physics.
Cottrell G A
Joint European Torus JET. January 1990. Report JET-P(90)04

67. Transport and gyrokinetic effects on heating and current drive in tokamaks
Cox M Dendy R O Fuchs V Lashmore-Davies C N McKenzie J S O'Brien M R
Presented to 13th IAEA Conference on Plasma Physics and Controlled Nuclear Fusion Research, Washington, USA, 1-5 October 1990. JET Report JET-P(90)25.

68. Toroidal plasma rotation in JET.
de Esch H P L Stork D Weisen H
Controlled Fusion and Plasma Heating. 17th EPS Conf., Amsterdam, 25-29 June 1990. Contributed papers. Geneva, European Physical Society. 1990. p.I-90 - I-93. (Report JET-P(90)14, pp.141-144.)

69. Reionised power deposition in the JET neutral beam duct and plasma facing components
de Esch H P L Jones T T C Stork D
16th Symposium on Fusion Technology, London, UK, 3-7 September 1990. JET Report JET-P(90)56 - Volume I, pp.49-54.

70. Interpretation of heat and density pulse measurements in JET in terms of coupled transport.

de Haas J C M O'Rourke J Sips A C C
Lopes Cardozo N J
Joint European Torus JET. 1990. 29p. Report JET-R(90)04

71. Impurity production and recycling in JET.
de Kock L Bures M Clement S Denne B Erents S K Ehrenberg J Giannella R Harbour P Hugon M McCracken G M Pitcher S Summers D Stamp M Tagle J von Hellermann M and the JET Team
Impurity control in toroidal devices. Technical Committee Meeting, Naka-gun, 13-15 February 1989. Vienna, IAEA, 1990. pp.37-42.

72. Damage to JET beryllium tiles.
Deksnis E Cheetham A Hwang A Lomas P Pick M Summers D D R
Journal of Nuclear Materials, 176 & 177, pp.583-587. Joint European Torus (JET). 1990. (JET papers presented at 9th Int. Conf. on Plasma Surface Interactions and Controlled Fusion Devices, Bournemouth, 21-25 May 1990). pp.181-193. Report JET-P(90)41-II

73. Design of high heat flux components for the JET pumped divertor
Deksnis E Garribba M Martin D Sborchia C Tivey R
16th Symposium on Fusion Technology, London, UK, 3-7 September 1990. JET Report JET-P(90)56 - Volume I, pp.31-36

74. Beryllium in JET - A report on the operational experience.
Dietz K J Pick M A Peacock A T Sonnenberg K Ehrenberg J Saibene G Sartori R
Fusion Engineering. IEEE 13th Symp., Knoxville, 2-6 October 1989. New York, IEEE. 1990. pp.517-521.

75. Effect of beryllium on plasma performance in JET.
Dietz K J and the JET Team
Plasma Physics and Controlled Fusion vol.32 no.11 November 1990 (Controlled Fusion and Plasma Heating. 17th European Physics Society Plasma Physics Division Conf., Amsterdam, 25-29 June 1990. Invited Papers. Edited by F C Schuller). pp.837-852. JET Report JET-P(90)53.

76. Problems of the vacuum in JET.
Dietz K J
Joint European Torus JET. 1990. 11p.
Report JET-P(90)24 Submitted to Procs. of The Euro. Conf. on Vacuum Technology, Bordeaux, May 1990. In French, with English and French abstracts.

77. Impurity separation. A review of plasma exhaust purification methods.
Dombra A Haange R
Tritium and Advanced Fuels in Fusion Reactors. Course and Workshop, Varenna, 6-15 September 1989. Bologna, for Societa Italiana di Fisica by Editrice Compositori, 1990. pp.463-514.

78. On diffusion of magnetic field lines.
Duchs D F Montvai A Sack Ch
Controlled Fusion and Plasma Heating. 17th EPS Conf., Amsterdam, 25-29 June 1990. Contributed papers. Geneva, European Physical Society. 1990. pp.II-691 - II-694. (Report JET-P(90)14, pp.101-104.)

79. Tokamak global confinement data: Joint European Torus (JET).
Duchs D F Corrigan G Gottardi N A O Kardaun O J W F Lazzaro E Pacco M G Smeulders P Tibone F and the JET Team
Nuclear Fusion, vol.30 no.9 September 1990 pp.1961-1967.

80. Impurity release by ICRF antennas in JET.
D'Ippolito D A Myra J R Bures M Stamp M Jacquinot J
Fusion Engineering and Design (Procs. IAEA Technical Committee Meeting on ICRH/Edge Physics, Garching, F.R.G., 2-5 October 1989) vol.12 nos.1&2 April 1990 pp.209-216.

81. Analysis of deuterium recycling in JET under beryllium first wall conditions.
Ehrenberg J Philipps V de Kock L Causey R A Hsu W L
Journal of Nuclear Materials, 176 & 177, pp.226-230. Joint European Torus (JET). 1990. (JET papers presented at 9th Int. Conf. on Plasma Surface Interactions and Controlled Fusion Devices, Bournemouth, 21-25 May 1990). pp.53-65. Report JET-P(90)41-I

82. Edge measurements in JET during the L-H mode transition.
Erents S K de Kock L McCracken G M (Culham) Reichle R
Journal of Nuclear Materials, 176 & 177, pp.533-537. Joint European Torus (JET). 1990. (JET papers presented at 9th Int. Conf. on Plasma Surface Interactions and Controlled Fusion Devices, Bournemouth, 21-25 May 1990). pp.167-179. Report JET-P(90)41-I

83. An investigation into high ion temperatures in the JET plasma boundary.
Erents S K Clement S Harbour P J von Hellerman M de Kock L McCracken G M Stamp M F Stangeby P C Summers D D R Thomas P R Weisen H
JET Papers contributed to 17th EPS Conf. on Controlled Fusion and Plasma Heating, Amsterdam, 25-29 June

1990. Joint European Torus JET, 1990. pp.177-180. Report JET-P(90)14

84. Scrape-off layer parameters in JET with beryllium limiters.
Erents S K Clement S Harbour P J de Kock L McCracken G M Tagle J A Thomas P R
Journal of Nuclear Materials, 176 & 177, pp.301-305. Joint European Torus (JET). 1990. (JET papers presented at 9th Int. Conf. on Plasma Surface Interactions and Controlled Fusion Devices, Bournemouth, 21-25 May 1990). pp.67-78. Report JET-P(90)41-I

85. Calculations of ICRF driven current profiles caused by TTMP and ELD.
Eriksson L-G Hellsten T
Presented at the Joint Varenna-Lausanne International Workshop: Theory of Fusion Plasmas, Vareena, 27-31 August 1990. JET Report JET-P(90)50.

86. Time dependent self-consistent calculations of ICRH-power deposition and ion velocity distributions
Eriksson L-G Willen U Hellsten T
Presented at the Joint Varenna-Lausanne International Workshop: Theory of Fusion Plasmas, Varenna, Italy, 27-31 August 1990. JET Report JET-P(90)42. 10p.

87. Observations of toroidal plasma rotation induced by ICRF in JET
Eriksson L-G Giannella R Helsten T Källne E Sundström
Submitted to Nuclear Fusion Letters and JET Report - JET-P(90)38.

88. A high resolution Lidar-Thomson scattering system for JET.
Fajemirokun H Gowers C Hirsch K Nielsen P Salzmann H
Controlled Fusion and Plasma Heating. 17th EPS Conf., Amsterdam, 25-29 June 1990. Contributed papers. Geneva, European Physical Society. 1990. p.IV-1692.

89. A high-resolution Lidar-Thomson scattering diagnostic for JET.
Fajemirokun H Gowers C Nielsen P Salzmann H Hirsch K
Review of Scientific Instruments vol.61 no.10 pt.II October 1990 (Procs. 8th Topical Conf. on High Temperature Plasma Diagnotics, Hyannis, Massachusetts, 6-10 May 1990). pp.2843-2845. (JET Report JET-P(90)19 pp.39-48

90. A new method for estimating and identifying systematic error in Thomson scattering diagnostics.
Fajemirokun H Gowers C Nielsen P Salzmann H Hirsch K
Review of Scientific Instruments vol.61 no.10 pt.II October 1990 (Procs. 8th Topical Conf. on High Temperature Plasma Diagnotics, Hyannis, Massachusetts, 6-10 May 1990). pp.2849-2851. (JET Report JET-P(90)19 pp.29-37

91. Implantation and re-emission of hydrogen and helium in the beam stopping panels of a 10MW ion beam line.
Falter H D Deschamps G H Hemsworth R S Massmann P
Journal of Nuclear Materials, 176 & 177, pp.678-682. Joint European Torus (JET). 1990. (JET papers presented at 9th Int. Conf. on Plasma Surface Interactions and Controlled Fusion Devices, Bournemouth, 21-25 May 1990). pp.269-282. Report JET-P(90)41-II

92. Power loading tests of the JET pumped divertor plates
Falter D Massmann P Al;tmann H Deschamps G Deksnis E Hemsworth R S Martin D Tivey R Thompson E
16th Symposium on Fusion Technology, London, UK, 3-7 September 1990. JET Report JET-P(90)56 - Volume I, pp.37-42.

93. Sawtooth triggered disruptions at the density limit on DITE.
Fishpool G M Morris A W Controlled Fusion and Plasma Heating. 17th EPS Conf., Amsterdam, 25-29 June 1990. Contributed papers. Geneva, European Physical Society. 1990. pp.I-347 - I-350. (Report JET-P(90)14, pp.169-172.)

94. A numerical model for the gas dynamics of a fast pellet injector
Flory D Zacchia F
16th Symposium on Fusion Technology, London, UK, 3-7 September 1990. JET Report JET-P(90)56 - Volume II, pp.121-126.

95. Feasibility of alpha particle diagnostics for the active phase of JET, using charge exchange recombination spectroscopy.
Frieling G J Hoekstra R de Heer F J Mandl W Boileau A Summers H P von Hellermann M
Controlled Fusion and Plasma Heating. 17th EPS Conf., Amsterdam, 25-29 June 1990. Contributed papers. Geneva, European Physical Society. 1990. pp.IV-1664 - IV-1667.

96. Specific features of the control and data acquisition for the JET pellet injector
Gadeberg M Krom J G Kupschus P Parker S B
16th Symposium on Fusion Technology, London, UK, 3-7 September 1990. JET Report JET-P(90)56 - Volume II, pp.103-108.

97. ICRF power deposition profile and determination of the electron thermal diffusivity by modulation experiments in JET.

Gambier D J Evrard M P Adam J Becoulet A Corti S Hennequin P Jacquinot J Start D F H Thomsen K Tubbing B J D Zanza V
Nuclear Fusion vol.30 no.1 January 1990 pp.23-34.

98. Transport of impurities during H-mode pulses in JET.
Giannella R Lauro Taroni L Barnsley R Gottardi N Hawkes N C Lawson K Mompean F Morsi H Pasini D Stork D
Controlled Fusion and Plasma Heating. 17th EPS Conf., Amsterdam, 25-29 June 1990. Contributed papers. Geneva, European Physical Society. 1990. pp.I-247 - I-250. (Report JET-P(90)14, pp.57-60.)

99. Fusion relevant performance in JET.
Gibson A and the JET Team
Plasma Physics and Controlled Fusion vol.32 no.11 November 1990 (Controlled Fusion and Plasma Heating. 17th European Physics Society Plasma Physics Division Conf., Amsterdam, 25-29 June 1990. Invited Papers. Edited by F C Schuller). pp.1083-1100. (Report JET-P(90)33)

100. The JET project - a review of progress.
Gibson A Smeulders P and the JET Team
Paper presented to International Plasma Physics Conference, New Dehli, India, November 1989. (Report JET-P(90)12) 28p.

101. Determination of tokamak plasma behaviour and parameters from tomographic analysis of soft X-ray camera data
Gill R D Edwards A Pasini D Wolfe S
IAEA Technical Committee Meeting, Nagoya, Japan, 19-22 November 1990, and JET Report - JET-P(90)69, pp.11-23.

102. Impurity control in JET using fuelling.
Gondhalekar A Erents S K Morgan PD O'Rourke J Olsson M Pasini D Stamp M F Stangeby P C Thomas P R von Hellerman M
Journal of Nuclear Materials, 176 & 177, pp.600-605. Joint European Torus (JET). 1990. (JET papers presented at 9th Int. Conf. on Plasma Surface Interactions and Controlled Fusion Devices, Bournemouth, 21-25 May 1990). pp.225-241. Report JET-P(90)41-II

103. Inversion methods for analysis of neutron brightness measurements in tokamaks.
Gorini G Gottardi N
Joint European Torus (JET). February 1990. 62p. Report JET-R(90)03

104. Lower hybrid current drive experiments in JET.
Gormezano C Brusati M Dobbing J Ekedahl A Jacquinot J Kaye A Lennholm M Pain M Rimini F Schild P
Bulletin of the American Physical Society vol.35 no.9 October 1990 (Program of the 32nd Annual Meeting of the Division of Plasma Physics, Cincinnati, Ohio, 12-16 November 1990). (Selected abstracts). p.1986, Paper 3S8.

105. Radio frequency heating and current drive status and prospects for the next step
Gormezano C
Submitted to Fusion Engineering and Design. Invited paper at 16th Symposium on Fusion Technology (London, U.K., 3-7 September 1990), JET Report - JET-P(90)64

106. Radiation asymmetries and H-modes.
Gottardi N Mast K F Thomas P Corrigan G Giannella R Sack C
Controlled Fusion and Plasma Heating. 17th EPS Conf., Amsterdam, 25-29 June 1990. Contributed papers. Geneva, European Physical Society. 1990. pp.I-263 - I-266. (Report JET-P(90)14, pp.153-156.)

107. High power ruby and alexandrite lasers for LIDAR-Thomson scattering diagnostics.
Gowers C Gadd A Hirsch K Nielsen P Salzmann H
Joint European Torus JET. March 1990. 12p. Report JET-P(90)09 Paper submitted to Procs. SPIE 1277 'High Power Solid State Lasers and Applications'.

108. JET experimental results.
Green B J
Nuclear Energy vol.29 no.1 February 1990 p.21-29.

109. Experiments with high voltage insulators in the presence of tritium.
Grisham L R Stevenson T Wright K Falter H Causey R Christman W
Joint European Torus JET. February 1990. 14p. Report JET-P(90)07
Submitted to Review of Scientific Instruments.

110. Pumping of tritiated plasma exhaust.
Haange R Hemmerich J L
Tritium and Advanced Fuels in Fusion Reactors. Course and Workshop, Varenna, 6-15 September 1989. Bologna, for Societa Italiana di Fisica by Editrice Compositori, 1990. pp.407-418.

111. FALCON - A program for fast analysis of local confinement in JET
Hamnen H Tibone F Corrigan G Düchs D F Galway A Maddison G P Stringer T E
Joint European Torus (JET), December 1990. Report JET-R(90)06

112. Comparisons of the current decay during carbon-bounded and beryllium-bounded disruptions in JET
Harris G R

Joint European Torus (JET), December 1990.
Report JET-R(90)07

113. Modelling and experimental studies of impurity control in JET X-point configurations.
Harbour P J Simonini R Tagle J A Gottardi N von Hellermann M Keilhacker M Lawson K (Culham) O'Brien D O'Rourke J Reichle R Spence J Summers D D R Taroni A Watkins M L
Journal of Nuclear Materials, 176 & 177, pp.739-745.
Joint European Torus (JET). 1990. (JET papers presented at 9th Int. Conf. on Plasma Surface Interactions and Controlled Fusion Devices, Bournemouth, 21-25 May 1990). pp.283-297.
Report JET-P(90)41-II

114. Modelling and experimental studies of impurity control in JET X-point configurations.
Harbour P J Simonini R Tagle J A Gottardi N von Hellermann M Keilhacker M Lawson K O'Brien D O'Rourke J Reichle R Spence J Summers D D R Taroni A Watkins M L
Procs. of Satellite Workshop of the 9th Int. Conf. on Plasma Surface Interactions, Cadarache, France, 28-30 May 1990. Association Euratom-CEA. Departement de Recherches sur la Fusion Controlee, Cadarache. September 1990. pp.161-181.
Report EUR-CEA-FC-1403

115. Electrostatic wave generation by the Faraday shield in ICRF heating.
Heikkinen J A
Joint European Torus JET. November 1989. 17p.
Report JET-P(89)74 Submitted to Physics Letters.

116. Fast wave antenna coupling to slow waves and ion Bernstein waves during ICRF heating of tokamak plasmas.
Heikkinen J A Bures M
Plasma Physics and Controlled Fusion vol.32 no.3 March 1990 pp.173-188.

117. Fast wave absorption at the Alfven resonance in ICRF heating.
Heikkinen J A Hellsten T Alava M J
Joint European Torus JET. 1990. 23p.
Report JET-P(90)28

118. Local analysis of mode conversion at $S=n^2$, resonances in the ion cyclotron range of frequencies
Heikkinen J A Alava M J
Submitted to Plasma Physics and Controlled Fusion, October 1990. JET Report JET-P(90)21. 12p.

119. On the decay of a dipole pump to half-harmonics
Heikkinen J A Pattikangas T J H Devillers G
Submitted to Journal of Plasma Physics and
JET Report JET-P(90)76.

120. The cryogenic diffusion pump and its implementation in a complete fusion reactor forevacuum system.
Hemmerich J L Kussel E
Journal of Vacuum Science & Technology A: Vacuum, Surfaces, and Films vol.8 no.1 January/February 1990 p.141-144.

121. Concluding remarks.
Hemsworth R
Production and Neutralization of Negative Ions and Beams. 5th Int. Symp., Brookhaven, New York, 1989. New York, American Institute of Physics, 1990. pp.786-793.

122. High energy and high power ion and neutral beam source development
Hemsworth R S Holmes A J T
Submitted to BNES, October 1990.
JET Report JET-P(90)52. 61p.

123. Summary of the 16th Symposium on Fusion Technology
Hemsworth R S
Submitted to Nuclear Fusion,
JET Report - JET-P(90)61, 15p.

124. Theoretical analysis of high-beta JET shots.
Hender T C Huysmans G T A Kwon O J Goedbloed J P Lazzaro E O'Brien D P
Controlled Fusion and Plasma Heating. 17th EPS Conf., Amsterdam, 25-29 June 1990. Contributed papers. Geneva, European Physical Society. 1990. pp.I-399 - I-402.

125. Long-wavelength magnetic dipole lines of highly ionized nickel measured in Tokamak Fusion Test Reactor plasmas.
Hinnov E Denne B Ramsey A Stratton B Timberlake J
Journal of the Optical Society of America B vol.7 no.10 October 1990 p.2002.

126. Some key technical developments for the fast ion and alph particle diagnostic system on JET
Hoekzema J A Hammond N P Taylor E F Stevens A L
16th Symposium on Fusion Technology, London, UK, 3-7 September 1990. JET Report JET-P(90)56 - Volume I, pp.61-66.

127. Evidence of coupling of thermal and particle transport from heat and density pulse measurements at JET.
Hogeweij G M D O'Rourke J Sips A C C de Haas J C M
Controlled Fusion and Plasma Heating. 17th EPS Conf., Amsterdam, 25-29 June 1990. Contributed papers. Geneva, European Physical Society. 1990. pp.I-158 - I161. (Report JET-P(90)14 , pp.45-48.)

128. Evidence of coupling of thermal and particle transport from heat and density pulse measurements at JET.
Hogeweij G M D O'Rourke J Sips A C C
Joint European Torus (JET). September 1990. 14p.
Report JET-P(90)45 Submitted to Plasma Physics and Controlled Fusion

129. Perturbative measurements of the electron transport matrix.
Hogeweij G M D O'Rourke J Rimini F Sips A C C Start D F H
Bulletin of the American Physical Society vol.35 no.9 October 1990 (Program of the 32nd Annual Meeting of the Division of Plasma Physics, Cincinnati, Ohio, 12-16 November 1990). (Selected abstracts). p.1999, Paper 4P26.

130. JET gas economy with C and Be first wall and implications for the gas introduction system
How J Usselmann E Saibene G Sartori R
Green B J Brelen H Rainford M Gondhalekar A
16th Symposium on Fusion Technology, London, UK, 3-7 September 1990. JET Report JET-P(90)56 - Volume II, pp.115-120.

131. Magnetic island self-sustainment by finite Larmor radius effect.
Hugon M Rebut P H
Controlled Fusion and Plasma Heating. 17th EPS Conf., Amsterdam, 25-29 June 1990. Contributed papers. Geneva, European Physical Society. 1990. pp.II-703 - II-706. (Report JET-P(90)14, pp.53-56.)

132. Self-consistent magnetic chaos induced by electron temperature gradient
Hugon M Rebut P-H
Nuclear Fusion Supplement (13th IAEA Conference on Plasma Physics and Controlled Nuclear Fusion Research, Washington, U.S.A., 1-5 October 1990, IAEA-CN-53/D-1-4), JET Report - JET-P(90)62, pp.132-144.

133. Technical status of JET and future prospects.
Huguet M Bertolini E
Fusion Engineering. IEEE 13th Symp., Knoxville, 2-6 October 1989. New York, IEEE. 1990. pp.491-496.

134. Technical aspects of impurity control at JET: status and future plans
Huguet M and the JET Team
Submitted to Fusion Technology, and JET Report - JET-P(90)70.

135. MHD stability analysis of high-β JET discharges
Huysmans G T A Hender T C Kwon O J
Goedbloed J P Lazzaro E Smeulders P
Submitted to Plasma Physics and Controlled Nuclear Fusion. JET Report JET-P(90)26.

136. The impurity spatial distributions, sputtering yields and power deposition at beryllium and carbon belt limiters in JET.
Hwang A Stamp M F Summers D D R Elder D
Forrest M J McCracken G M Morgan P D
Stangeby P C Summers H P
Journal of Nuclear Materials, 176 & 177, pp.588-592. Joint European Torus (JET). 1990. (JET papers presented at 9th Int. Conf. on Plasma Surface Interactions and Controlled Fusion Devices, Bournemouth, 21-25 May 1990). pp.195-208.
Report JET-P(90)41-II

137. Effect of berllium evaporation on the performance of ICRH on JET.
Jacquinot J Bhatnagar V Bures M Campbell D
Giannella R Lawson K Stamp M Tubbing B
Fusion Engineering and Design (Procs. IAEA Technical Committee Meeting on ICRH/Edge Physics, Garching, F.R.G., 2-5 October 1989) vol.12 nos.1&2 April 1990 pp.245-250. (Report JET-P(89)85.)

138. Retention of gaseous (Ar, He) impurities in the JET X-point configuration.
Janeschitz G Giannella R Jaeckel H J Taroni L
Stamp M Barnsley R Coulon J P Haas G
Harbour P J Hawkes N
JET Papers contributed to 17th EPS Conf. on Controlled Fusion and Plasma Heating, Amsterdam, 25-29 June 1990. Joint European Torus JET, 1990. pp.89-92.
Report JET-P(90)14

139. Determination of deuterium concentrations in JET plasmas.
Jarvis O N Adams J M Balet B Conroy S W
Cordey J G Elevant T Gill R D Loughlin M J
Mandl W Morgan P D Pasini D Sadler G Watkins N
van Belle P von Hellermann M Weisen H
Nuclear Fusion vol.30 no.2 February 1990 pp.307-315.

140. Use of the $^{28}Si(n,p)^{28}Al$ reaction for the measurements of 14MeV neutrons from fusion plasmas
Jarvis O N Sadler G van Belle P Pillon M
Paper presented at the 8th Topical Conference on High Temperature Plasma Diagnostics, Hyannis, Massachusetts, 6-10 May 1990
(JET Report JET-P(90)19 pp.62-72

141. Use of activation techniques at JET for the measurement of neutron yields from deuterium plasmas.
Jarvis O N Clipsham E Hone M Laundy B Pillon M
Rapisarda M Sadler G van Belle P Verschuur K A
Joint European Torus (JET). September 1990. 42p.
Report JET-P(90)46 Preprint of paper to be submitted for publication in Fusion Technology.

142. Vessel calibration of the JET Neutron Monitors using a ^{252}Cf Neutron Source: Difficulties Experienced

Jarvis O N Sadler G van Belle P Elevant T
Paper presented at the 8th Topical Conference on High Temperature Plasma Diagnostics, Hyannis, Massachusetts, 6-10 May 1990)
(JET Report JET-P(90)19 pp.50-59

143. The design and construction of the TARM - a crane-mounted remotely-controlled transporter for JET
Jones L P D F Galbiati L Gredel M Neddermeyer W
16th Symposium on Fusion Technology, London, UK, 3-7 September 1990. JET Report JET-P(90)56 - Volume II, pp.127-132.

144. The fusion performance of JET limiter plasmas using Be coated graphite and solid Be surfaces.
Jones T T C Lomas P J Attenberger S Christiansen J P Cottrell G A Gianella R de Kock L Kupschus P McCracken G Lowry C G Nielsen P Pasini D Prentice R Sadler G Stamp M F Summers D D R von Hellerman M Weisen H
Controlled Fusion and Plasma Heating. 17th EPS Conf., Amsterdam, 25-29 June 1990. Contributed papers. Geneva, European Physical Society. 1990. pp.I-9 - 112. (Report JET-P(90)14, pp.137-140.)

145. Transitions in Al-like, Mg-like and Na-like Kr and Mo, observed in the JET tokamak.
Jupen C Denne B Martinson I
Physica Scripta vol.41 no.5 May 1990 pp.669-674.

146. Tokamaks.
Kadomtsev B B Troyon F S Watkins M L
Nuclear Fusion (30th Anniversay Issue) vol.30 no.9 September 1990 pp.1675-1694.

147. Global H-mode scalings based on JET and ASDEX data.
Kardaun O Thomsen K Cordey J G Wagner F and the JET Team
Controlled Fusion and Plasma Heating. 17th EPS Conf., Amsterdam, 25-29 June 1990. Contributed papers. Geneva, European Physical Society. 1990. pp.I-110 - I-113. (Report JET-P(90)14, pp.69-72.)

148. Overview of results from the JET tokamak using a beryllium first wall.
Keilhacker M and the JET Team
Physics of Fluids B: Plasma Physics vol.2 no.6 pt.2 June 1990 (Special Issue: Invited and review paper from the 31st Annual Meeting of the Division of Plasma Physics of the American Physical Society Anaheim, Calif., 13-17 November 1989) p.1291-1299 (Report JET-P(89)83)

149. A scrape-off layer model for the study of impurity retention in the pumped divertor planned for JET
Keilhacker M Simonini R Taroni A Watkins M L
Submitted to Nuclear Fusion, August 1990. JET Report JET-P(90)37. 26p.

150. Modelling impurity control by plasma flows in the JET pumped divertor
Keilhacker M Deksnis E Harbour P Rebut P H Simonini R Taroni A Vlases G C Watkins M L
Nuclear Fusion Supplement (13th IAEA Conference on Plasma Physics and Controlled Nuclear Fusion Research, Washington, U.S.A., 1-5 October 1990 IAEA-CN-53/A-5-1), JET Report - JET-P(90)62 pp.79-96.

151. HECTOR: A code for the study of charged particles in axisymmetric tokamak plasmas.
Kovanen M A Core W G F
Joint European Torus (JET). August 1990.
Report JET-P(90)40

152. Finite orbit effects in ICRF heated tokamak plasmas
Kovanen M A Core W G F Hellsten T
Submitted to Nuclear Fusion, and
JET Report - JET-P(90)68.

153. Fuelling of magnetically confined fusion reactor plasmas.
Kupschus P
Tritium and Advanced Fuels in Fusion Reactors Course and Workshop, Varenna, 6-15 September 1989. Bologna, for Societa Italiana di Fisica by Editric Compositori, 1990. pp.343-362.

154. The JET high-speed pellet launcher prototype development, implementation and operational experience
Kupschus P Sonnenberg K Bailey W Flory D Gadeberg M Ge X Hedley L Helm J Novak A Romain R Twynam P Szabo T Watson M Willis B Zheng Z
16th Symposium on Fusion Technology, London UK, 3-7 September 1990. JET Report JET-P(90)56 Volume I, pp.7-12.

155. Upgrading the JET pellet injector with a two- stage light gas gun prototype and future planning.
Kupschus P Sonnenberg K Bailey W Gadeberg M Hardaker J Hedley L Helm J Flory D McCarthy P Nowak A Twynam P Szabo T Watson M
Fusion Engineering. IEEE 13th Symp., Knoxville 2-6 October 1989. New York, IEEE. 1990 pp.1293-1298.

156. JET TF coil fault-detection, diagnosis and prevention
Last J R Bonicelli T Cooke M Dolgetta N Huguet M Lanza R Noll P Presle P Sborchia
16th Symposium on Fusion Technology, London UK, 3-7 September 1990. JET Report JET-P(90)56 Volume II, pp.175-181.

157. The JET divertor magnetic configuration and coil design
Last J R Bertolini E Garribba M Huguet M Noll P Rebut P H Sborchia C
16th Symposium on Fusion Technology, London UK, 3-7 September 1990. JET Report JET-P(90)56 Volume II, pp.181-186.

158. H-mode confinement at low q and high beta in JET.
Lazzaro E Tanga A Huysmans G Nardone C O'Brien D P Smeulders P von Hellermann M
Nuclear Fusion vol.30 no.10 October 1990 pp.2157-2161.

159. Coupling of slow waves near the lower hybrid frequency in JET.
Litaudon X Moreau D
Nuclear Fusion vol.30 no.3 March 1990 p.471-484.

160. ICRF antenna for the JET pumped divertor configuration
Lobel R Bhatnagar V Jacquinot J Kaye A Panissié H Rebut P H
16th Symposium on Fusion Technology, London UK, 3-7 September 1990. JET Report JET-P(90)56 Volume I, pp.73-78.

161. Optimisation of performance in JET limiter plasmas
Lomas P J and the JET Team
Nuclear Fusion Supplement (13th IAEA Conference on Plasma Physics and Controlled Nuclear Fusion Research, Washington, U.S.A., 1-5 October 1990 IAEA-CN-53/A-6-2), JET Report - JET-P(90)62 pp.27-40.

162. Heat pulse analysis in JET limiter and X-point plasmas.
Lopes Cardozo N J de Haas J C M
Nuclear Fusion vol.30 no.3 March 1990 p.521-532 (Report JET-P(89)78)

163. A comparison of the plasma performance of JET with carbon and beryllium as target materials
Lowry C G Bures M Campbell D J Fessey J Giannella R Gottardi N Harbour P J von Hellermann M de Kock L Morgan P D Saibenne G Stamp M F Stork D Summers D D Tanga A Thomas P R Thomsen K Tubbing B J Ward D J
Bulletin of the American Physical Society vol.35 no.9 October 1990 (Program of the 32nd Annual Meeting of the Division of Plasma Physics, Cincinnati, Ohio 12-16 November 1990). (Selected abstracts). p.1998 Paper 4P22.

164. Density limits in JET with beryllium.
Lowry C G Campbell D J Gottardi N Lawson K Vlases G
Controlled Fusion and Plasma Heating. 17th EPS Conf., Amsterdam, 25-29 June 1990. Contributed papers. Geneva, European Physical Society. 1990 pp.I-339 - I-342. (Report JET-P(90)14, pp.125-128.)

165. Measurements of deuteron density profiles in JET.
Mandl W von Hellermann M Morgan P D Summers H P Weisen H Olsson M van BelleP Elevant T Sadler G
Controlled Fusion and Plasma Heating. 17th EPS Conf., Amsterdam, 25-29 June 1990. Contributed papers. Geneva, European Physical Society. 1990 pp.IV-1496 - IV-1499. (Report JET-P(90)14 pp.105-108.)

166. JET neutron emission profiles and fast ion redistribution from sawteeth.
Marcus F B Adams J M Cheetham A Conroy S Core W G F Jarvis O N Loughlin M J Olsson M Sadler G Smeulders P Van Belle P Watkins N
Controlled Fusion and Plasma Heating. 17th EPS Conf., Amsterdam, 25-29 June 1990. Contributed papers. Geneva, European Physical Society. 1990 pp.I-331 - I-334. (Report JET-P(90)14, pp.17-20.)

167. JET neutron emission profiles and fast ion redistribution during sawtooth crashes
Marcus F B Adams J M Cheetham A D Conroy S Core W G F Jarvis O N Loughlin M J Olsson M Sadler G Smeulders P van Belle P Watkins N
Submitted to Plasma Physics and Controlled Fusion November 1990. JET Report JET-P(90)55. 20p.

168. Proposal for 160keV He^3 injection and combined NBI/RF heating.
Marcus F B Bickley A J Campbell D J Challis C D Cordey J G Core W G F Corti S Cottrell G de Esch H P L de Kock L Hellsten T Hughes T P Jacquinot J Jarvis O N Jones T T C Lallia P Obert Sadler G Smeulders P Start D F H Stork D Tanga A Stott P E Thompson E van Belle P von Hellermann M
Joint European Torus (JET). August 1990. Report JET-R(90)01

169. Fishbone activity in JET.
Marcus M F F Campbell D Joffrin E Marcus F B Sadler G Smeulders P Thomsen K
Joint European Torus JET. 1990. 34p. Report JET-P(90)32

170. Tomographic analysis of data from the JET neutron profile monitor to deduce the 2-D spatial and temporary evolution of neutron emissivity
Marcus F B Adams J M Gill R Jravis O N Sadler G Smeulders P van Belle P Watkins N
IAEA Technical Committee Meeting, Nagoya, Japan 19-22 November 1990, and JET Report - JET-P(90)69 pp.1-10.

171. Simultaneous evolution of temperature and density perturbations following pellet injection in JET.
Martin-Solis J R Cheetham A Erents K Gondhalekar A
Controlled Fusion and Plasma Heating. 17th EPS Conf., Amsterdam, 25-29 June 1990. Contributed papers. Geneva, European Physical Society. 1990 p.I-219 - I-222. (Report JET-P(90)14, pp.73-76.)

172. Pumping of gaseous helium using argon frosted liquid helium cryo-condensation pumps.
Massmann P Romain R Deschamps G H Falter H D Hemsworth R Obert W
Fusion Engineering. IEEE 13th Symp., Knoxville, 2-6 October 1989. New York IEEE. 1990. pp.1156-1159.

173. Pumping of ^{3}He and ^{4}He gas using argon frosted liquid helium cryopumps at sub-condensation temperature
Massmann P Bickley A J Davies J F Deschamps G H de Esch H P L Falter H D Hemsworth R S Jones T T C
16th Symposium on Fusion Technology, London UK, 3-7 September 1990. JET Report JET-P(90)56 Volume I, pp.13-18

174. Experimental search for 'cold fusion' in the deuterium-titanium system.
McCracken G M Bailey M Croft S Findley D J S Gibson A Govier R P Jarvis O N Milton H J Powell B A Sadler G Sene M R Sweetman D R van Belle P Watson H H H
Journal of Physics D: Applied Physics vol.23 no.5 14 May 1990 p.469-475.

175. A comparison of global modelling of impurities in JET with experimental data obtained using carbon and beryllium limiters.
McCracken G M Matthews G F de Kock L Erents S K Gottardi N A Lowry C Morgan P D Stamp M F Stangeby P C
Journal of Nuclear Materials, 176 & 177, pp.392-397. Joint European Torus (JET). 1990. (JET paper presented at 9th Int. Conf. on Plasma Surface Interactions and Controlled Fusion Devices Bournemouth, 21-25 May 1990). pp.123-134. Report JET-P(90)41-I

176. Formation of detached plasmas during high power discharges in JET.
McCracken G M de Kock L Erents S K Gottardi N Harbour P J Hwang A Jones T T C Lawson K Lomas P J Lowry C Morgan P D O'Rourke J Pasini D Pitcher C S Stamp M Stott P E Summers D D R Bures M Tagle J A Thomas P von Hellerman M
JET Papers contributed to 17th EPS Conf. on Controlled Fusion and Plasma Heating, Amsterdam, 25-29 June 1990. Joint European Torus JET, 1990. pp.165-168 Report JET-P(90)14

177. Diffusion of ions in presence of nearly overlapping magnetic islands.
Mendonca J T Brusati M
Controlled Fusion and Plasma Heating. 17th EPS Conf., Amsterdam, 25-29 June 1990. Contributed papers. Geneva, European Physical Society. 1990 pp.II-719 - II-722.

178. Magnetic field structure at the onset of sawtooth relaxations.
Mendonca J T Porcelli F
Controlled Fusion and Plasma Heating. 17th EPS Conf., Amsterdam, 25-29 June 1990. Contributed papers. Geneva, European Physical Society. 1990 p.II-918.

179. The JET quality assurance programme and its associated system of technial documents
Meriguet P Evans C Green B Horn G Hurd F Rebut P H Sigourney D
16th Symposium on Fusion Technology, London UK, 3-7 September 1990. JET Report JET-P(90)56 Volume II, pp.157-162.

180. A practical experience of using special remote handling tools on JET.
Mills S F Schreibmaier J Tesini A Wykes M
Fusion Engineering. IEEE 12th Symp., Monterey CA, 12-16 October 1987. New York, IEEE. 1987 pp.186-189.

181. State diagrams of tokamaks and state transitions
Minardi E
Submitted to Plasma Physics and Controlled Fusion and JET Report - JET-P(90)71.

182. The high power, wide bandwidth disruption feedback amplifiers for JET
Mondino P L Tenconi S M Boselli A Carpita M Dolgetta N Gallandt C Marchese V Odone A Pittera L Rizzo E Santagiustina A Zannelli L
16th Symposium on Fusion Technology, London UK, 3-7 September 1990. JET Report JET-P(90)56 Volume II, pp.193-198.

183. Ion temperature measurements at JET.
Morsi H W von Hellermann M Barnsley R Ellis J J Giannella R Mandl W Sadler G Weisen H Zastrow K-D
Controlled Fusion and Plasma Heating. 17th EPS Conf., Amsterdam, 25-29 June 1990. Contributed papers. Geneva, European Physical Society. 1990 pp.IV-1608 - IV-1611. (Report JET-P(90)14 pp.157-160.)

184. Dynamic response of plasma energy and broad- band magnetic fluctuations to additional heating in JET.
Nardone C De Luca F Hansen P M Jacchia A Mantica P Thomsen K
Controlled Fusion and Plasma Heating. 17th EPS Conf., Amsterdam, 25-29 June 1990. Contributed papers. Geneva, European Physical Society. 1990 pp.I-166 - I-169. (Report JET-P(90)14, pp.161-164.)

185. Mode locking in tokamaks.
Nave M F F Wesson J A
Joint European Torus JET. February 1990. 22p.
Report JET-P(90)06 Submitted to Nuclear Fusion

186. Observation of MHD structures in JET temperature profiles
Nave M F F Edwards A Hirsch K Hugon M Jacchia A Lazzaro E Salzmann H Smeulders P
Submitted to Nuclear Fusion, November 1990. JET Report JET-P(90)57, 27p.

187. Vertical instabilities in JET.
Noll P Bonicelli T Garribba M
Controlled Fusion and Plasma Heating. 17th EPS Conf., Amsterdam, 25-29 June 1990. Contributed papers. Geneva, European Physical Society. 1990 pp.I-419 - I-422. (Report JET-P(90)14, pp.49-52.)

188. Performance of the cold ejector of the JET cryoplant.
Obert W Mayaux C Hemsworth R Jones A Parfitt A Peel T Ziegler B
Advances in Cryogenic Engineering vol.35 pts .A&B 1990 pp.1013-1021.

189. JET pumped divertor cryopump
Obert W Papastergiou S Rebut P H Barabaschi P Deschamps G Deksnis E Garribba M Mayaux Ch Perinic G Sannazzaro G
16th Symposium on Fusion Technology, London UK, 3-7 September 1990. JET Report JET-P(90)56 Volume I, pp.43-48.

190. Particle and heat deposition in the X-point region at JET. O'Brien D P Kovanen M A Reichle R Core W Lazzaro E Summers D D R Taylor T
Controlled Fusion and Plasma Heating. 17th EPS Conf., Amsterdam, 25-29 June 1990. Contributed papers. Geneva, European Physical Society. 1990 pp.I-251 - I-254. (Report JET-P(90)14, pp.5-8.)

191. The change in the safety factor profile at a sawtooth collapse.
O'Rourke J
Joint European Torus (JET). September 1990. 10p
Report JET-P(90)43 Submitted to Plasma Physics and Controlled Fusion

192. Faraday rotation measurements on JET, and the change in the safety factor profile during a sawtooth collapse.
O'Rourke J Lazzaro E
Controlled Fusion and Plasma Heating. 17th EPS Conf., Amsterdam, 25-29 June 1990. Contributed papers. Geneva, European Physical Society. 1990 pp.I-343 - I-346. (Report JET-P(90)14, pp.133-136.)

193. Feasibility study of bulk ion temperature measurements on JET by means of collective scattering of gyrotron radiation
Orsitto F
Paper presented to 8th Topical Conference on Plasma Diagnostics, Hyannis, USA, May 1990
(JET Report JET-P(90)19) pp. 1-6

194. Feasibility study of bulk ion temperature measurements on JET by means of collective scattering of gyrotron emission
Orsitto F
Joint European Torus (JET), October 1990.
Report JET-R(90)05

195. The 15 MW microwave generator and launcher of the lower hybrid current drive experiment on JET.
Pain M Brinkschulte H Bosia G Brusati M Dobbing J A Ekedahl A Gammelin M Gormezano C Idelon C Jacquinot J Jessop G Kaye A Lenholm M Plancoulaine J Schild P Sibley A Wade T Walker C Walton R Wilson G
Fusion Engineering. IEEE 13th Symp., Knoxville 2-6 October 1989. New York, IEEE. 1990 pp.1083-1088.

196. Reliability analysis of the JET neutral injection beamlines.
Papastergiou S
Fusion Engineering. IEEE 13th Symp., Knoxville 2-6 October 1989. New York, IEEE. 1990. pp.416-419.

197. Simulation of MHD activity during density limit disruptions in JET.
Parker R Bondeson A Hugon M
Controlled Fusion and Plasma Heating. 17th EPS Conf., Amsterdam, 25-29 June 1990. Contributed papers. Geneva, European Physical Society. 1990 pp.II-962 - II-965.

198. Enhanced carbon and beryllium influxes during high power operation in JET.
Pasini D Summers D Philipps V Weisen H de Esch H Jones T Deksnis E Lomas P Lowry C McCracken G Mandl W Nielsen P Reichle R Stamp M von Hellerman M
Journal of Nuclear Materials, 176 & 177, pp.186-190. Joint European Torus (JET). 1990. (JET paper presented at 9th Int. Conf. on Plasma Surface Interactions and Controlled Fusion Devices Bournemouth, 21-25 May 1990). pp.39-51.
Report JET-P(90)41-I

199. Impurity transport in JET using laser injected impurities in ohmic and radiofrequency heated plasmas.
Pasini D Mattioli M Edwards A W Giannella R Gill R D Hawkes N C Magyar G Saoutic B Wang Z Zasche D
Nuclear Fusion vol.30 no.10 October 1990 p.2049-2062. (Report JET-P(90)01

200. Measurements of impurity concentrations and Z_{eff} in JET using X-ray tomography.
Pasini D Weisen H Weller A Edwards A W
Bulletin of the American Physical Society vol.35 no.9 October 1990 (Program of the 32nd Annual Meeting of the Division of Plasma Physics, Cincinnati, Ohio 12-16 November 1990). p.1998, Paper 4P23.

201. Impurity coverage and deuterium inventory of beryllium and carbon first wall components after beryllium operation in JET.
Peacock A T Coad J P Lama F Behrisch R Gauthier E Martinelli A P Mills B E Pick M Partridge J Prozesky V Simpson J C B Zhu Y K
Journal of Nuclear Materials, 176 & 177, pp.326-331. Joint European Torus (JET). 1990. (JET paper presented at 9th Int. Conf. on Plasma Surface Interactions and Controlled Fusion Devices Bournemouth, 21-25 May 1990). pp.79-91. Report JET-P(90)41-I

202. Operational experience with the JET beryllium evaporators
Peacock A T Coad J P Dietz K J Israel G Jensen H S Pick M A Saibene G Bergsaker H
16th Symposium on Fusion Technology, London UK, 3-7 September 1990. JET Report JET-P(90)56 Volume I, pp.19-24.

203. Operational experience with the JET beryllium evaporators in the J1W test bed.
Peacock A T Dietz K J Israel G Jensen H S Johnson A Pick M A Saibene G Sartori R
Joint European Torus JET. 1989.Report JET-R(90)02

204. Large gyroradius m=1 Alfven modes and energetic particles.
Pegoraro F Porcelli F Schep T J
Joint European Torus JET. March 1990. 20p. Report JET-P(90)13
Submitted to Physics of Fluids B.

205. Large gyroradius m = 1 Alfven modes and energetic particles.
Pegoraro F Porcelli F Schep T J
Controlled Fusion and Plasma Heating. 17th EPS Conf., Amsterdam 25-29 June 1990. Contributed papers. Geneva, European Physical Society. 1990 pp.II-946 - II-949.

206. Experience with graphite in JET.
Pick M A Celentano G Deksnis E Dietz K J Shaw R Sonnenberg K Walravens M
Fusion Engineering. IEEE 12th Symp., Monterey CA, 12-16 October 1987. New York, IEEE. 1987 pp.137-140. Book

207. Neutron energy spectrum determination near the surface of the JET vacuum vessel using the multifoil activation technique.
Pillon M Jarvis O N Conroy S
Fusion Engineering. IEEE 13th Symp., Knoxville 2-6 October 1989. New York, IEEE. 1990. p.160.

208. Some effects of ion cyclotron resonance heating on the Joint European Torus boundary plasma.
Pitcher C S Bures M de Kock L Erents S K Gottardi N A McCracken G M Stamp M F Stangeby P C Summers D D R Tagle J A
Journal of Vacuum Science & Technology A: Vacuum Surfaces, and Films vol.8 no.3 pt.1 May/June 1990 (Procs. 36th National Symposium of The America Vacuum Society, Boston, Mass., 23-27 October 1989 pp.1760-1766. (Report JET-P(89)86)

209. Nonstandard trapped orbit analysis and the response of fast ions to m=1 perturbations.
Porcelli F Berk H L Eriksson L-G
Bulletin of the American Physical Society vol.35 no.9 October 1990 (Program of the 32nd Annual Meeting of the Division of Plasma Physics, Cincinnati, Ohio 12-16 November 1990). (Selected abstracts). p.2116 Paper 8R3.

210. Sawtooth stabilisation by fast ions: Comparison between theory and experiments.
Porcelli F Campbell D J Diachenko W D Eriksson L-G Jacquinot J Levin L S Start D F H Taroni A
Controlled Fusion and Plasma Heating. 17th EPS Conf., Amsterdam, 25-29 June 1990. Contributed papers. Geneva, European Physical Society. 1990 pp.I-327 - I-330.

211. Stabilisation of drift-tearing modes at the breakdown of the constant-ψ approximation.
Porcelli F Migliuolo S Pegoraro F
Joint European Torus JET. 1990. 13p. Report JET-P(90)08
Submitted as a letter to Physics of Fluids B.

212. Stabilisation of drift-tearing modes at the breakdown of the constant-ψ approximation.
Porcelli F Migliuolo S Pegoraro F
Controlled Fusion and Plasma Heating. 17th EPS Conf., Amsterdam, 25-29 June 1990. Contributed papers. Geneva, European Physical Society. 1990 pp.II-898-901. (Report JET-P(90)14, pp.129-132.)

213. The collisionless m=1 tearing mode
Porcelli F
Submitted to Physical Review Letters, October 1990
JET Report JET-P(90)23. 12p.

214. A method for the determination of the total internal magnetic field in JET.
Porte L Bartlett D V Costley A E Gowers C W
Controlled Fusion and Plasma Heating. 17th EPS Conf., Amsterdam, 25-29 June 1990. Contributed papers. Geneva, European Physical Society. 1990 pp.IV-1504 - 1V-1507. (Report JET-P(90)14 pp.173-176.)

215. First measurements of electron density profiles of JET with a multichannel reflectometer.
Prentice R Sips A C C Fessey J A Costley A E
Controlled Fusion and Plasma Heating. 17th EPS Conf., Amsterdam, 25-29 June 1990. Contributed papers. Geneva, European Physical Society. 1990 p.IV-1500-IV-1503. (Report JET-P(90)14, pp.25-28.)

216. Sawtooth stabilisation by fast ions: Comparison between theory and experiments.
Porcelli F Campbell D J Diachenko W D Eriksson L-G Jacquinot J Levin L S Start D F H Taroni A
JET Papers contributed to 17th EPS Conf. on Controlled Fusion and Plasma Heating, Amsterdam, 25-29 June 1990. Joint European Torus JET, 1990. pp.29-32 Report JET-P(90)14

217. Impurities in JET and their control.
Rebut P H Lallia P P Keen B E
Fusion Engineering. IEEE 13th Symp., Knoxville, 2-6 October 1989. New York, IEEE. 1990. pp.227-235.

218. The JET project and its impact on nuclear fusion research.
Rebut P H
ITER Newsletter vol.3 no.4 April 1990 pp.5-10.

219. A programme towards a fusion reactor
Rebut P-H Watkins M L Gambier D J Boucher D
Submitted to Physics of Fluids. Invited Review Paper at 32nd Meeting of the Division of Plasma Physics of the American Physical Society (Cincinnati, Ohio USA, 12-16 November 1990),
JET Report - JET-P(90)75.

220. Next step programme based on JET and other tokamaks.
Rebut P H
Bulletin of the American Physical Society vol.35 no.9 October 1990 (Program of the 32nd Annual Meeting of the Division of Plasma Physics, Cincinnati, Ohio 12-16 November 1990). (Selected abstracts). p.1917 Paper 1RV1.

221. Magnetic turbulence self-sustainment by finite larmor radius effect
Rebut P H Hugon M
Submitted to Plasma Physics and Controlled Fusion
JET Report - JET-P(90)58, 22p.

222. Recent JET results and future prospects
Rebut P H and the JET Team
Nuclear Fusion Supplement (13th IAEA Conference on Plasma Physics and Controlled Nuclear Fusion Research, Washington, U.S.A., 1-5 October 1990 IAEA-CN-53/A-1-2), JET Report - JET-P(90)62, pp1-26.

223. Future prospects for JET and next step tokamaks
Rebut P-H
Submitted to Fusion Engineering and Design. Invited paper at 16th Symposium on Fusion Technolog (London, U.K., 3-7 September 1990),
JET Report - JET-P(90)66.

224. Carbon yields and influxes as a function of target temperatures in JET X-point plasmas.
Reichle R Summers D D R Stamp M F
Journal of Nuclear Materials, 176 & 177, pp.375-380. Joint European Torus (JET). 1990. (JET paper presented at 9th Int. Conf. on Plasma Surface Interactions and Controlled Fusion Devices Bournemouth, 21-25 May 1990). pp.93-106. Report JET-P(90)41-I

225. Electron absorption of fast magnetosonic waves by TTMP in JET.
Rimini F Bartlett D V Bhatnagar V P Campbell D J Challis C D Cheetham A D Corti S Edwards A W Eriksson L-G Gill R D Gottardi N Hellsten T Jacquinot J O'Rourke J Mayberry M J Moreau Salmon N A Smeulders P Start D F H von Hellermann
Controlled Fusion and Plasma Heating. 17th EPS Conf., Amsterdam, 25-29 June 1990. Contributed papers. Geneva, European Physical Society. 1990 pp.III-1150 - III-1153. (Report JET-P(90)14 pp.37-40.)

226. D-D neutron production from JET plasmas.
Sadler G Adams J M Attenberger S Balet B Cordey J G Jarvis O N Jones T T C Kupschus P Laundy B Lomas P J Loughlin M J Marcus F B Olsson M Stubberfield P M Start D F H Tanga A Thomas P R Tubbing B van Belle P
Controlled Fusion and Plasma Heating. 17th EPS Conf., Amsterdam, 25-29 June 1990. Contributed papers. Geneva, European Physical Society. 1990 pp.I-1 - I-4. (Report JET-P(90)14, pp.117-120.)

227. Hydrogen recycling coefficient in beryllium experimental determination and test simulation of the density evolution in a JET plasma discharge.
Saibene G Sartori R Tanga A Peacock A Pick M Gaze P
Journal of Nuclear Materials, 176 & 177, pp.618-623. Joint European Torus (JET). 1990. (JET paper presented at 9th Int. Conf. on Plasma Surface Interactions and Controlled Fusion Devices Bournemouth, 21-25 May 1990). pp.243-253. Report JET-P(90)41-II

228. Deuterium release measurements in the Be phase of JET and determination of tritium content in the exhaust gas.
Sartori R Saibene G Goodall D H J (Culham) Usselmann E Coad P Holland D
Journal of Nuclear Materials, 176 & 177, pp.624-629. Joint European Torus (JET). 1990. (JET paper presented at 9th Int. Conf. on Plasma Surface Interactions and Controlled Fusion Devices, Bournemouth, 21-25 May 1990). pp.255-267. Report JET-P(90)41-II

229. Modelling impurity control in the JET pumped divertor.
Simonini R Keilhacker M Taroni A Watkins M L
JET Papers contributed to 17th EPS Conf. on Controlled Fusion and Plasma Heating, Amsterdam, 25-29 June 1990. Joint European Torus JET, 1990. pp.97-100. Report JET-P(90)14

230. High-beta regimes in JET.
Smeulders P Adams J M Balet B Campbell D Cheetham A Corti S Edwards A Gottardi N Gowers C Hender T C Huysmans G Jacquinot J Joffrin E Kwon O Lazzaro E Marcus F B Morgan P Nave F Nielsen P O'Brien D O'Rourke J Porcelli F Porte L Sadler G Sips G Start D Tanga A Ward D Weisen H
Controlled Fusion and Plasma Heating. 17th EPS Conf., Amsterdam, 25-29 June 1990. Contributed papers. Geneva, European Physical Society. 1990. pp.I-323 - I-326. (Report JET-P(90)14, pp.9-12.)

231. Hope for fusion fuelled:
Reports from the 13th IAEA Conf. on Plasma Physics and Controlled Nuclear Fusion Research, Washington, 1-6 October.
Smeulders P
Physics World vol.3 no.12 December 1990 pp.21-22.

232. High density regimes and beta limits in JET
Smeulders P and the JET Team
Nuclear Fusion Supplement (13th IAEA Conference on Plasma Physics and Controlled Nuclear Fusion Research, Washington, U.S.A., 1-5 October 1990, IAEA-CN-53/A-3-4), JET Report - JET-P(90)62, pp.70-78.

233. Plasma stored energy and momentum losses during large MHD activity in JET.
Snipes J A Campbell D J Hender T C von Hellermann M Weisen H
Nuclear Fusion vol.30 no.2 February 1990 pp.205-218. (Report JET-P(89)64)

234. Temperatures and densities in the JET plasma boundary deduced from deuterium and beryllium spectra.
Stamp M F Summers H P
JET Papers contributed to 17th EPS Conf. on Controlled Fusion and Plasma Heating, Amsterdam, 25-29 June 1990. Joint European Torus JET, 1990. pp.149-152. Report JET-P(90)14

235. Cross-field diffusion coefficients measured in the JET edge for constant plasma current.
Stangeby P C Erents S K de Kock L Tagle J A
Plasma Physics and Controlled Fusion vol.32 no.6 July 1990 p.475-480. (Report JET-P(90)11)

236. The magnitude and direction of forces on impurities near a divertor plate - an exploratory investigation.
Stangeby P C
Procs. of Satellite Workshop of the 9th Int. Conf. on Plasma Surface Interactions, Cadarache, France, 28-30 May 1990. Association Euratom-CEA. Departement de Recherches sur la Fusion Controlee, Cadarache. September 1990. pp.77-93.
Report EUR-CEA-FC-1403

237. The plasma contamination efficiency of different impurity generation mechanisms in limiter tokamaks.
Stangeby P C Farrell C
Plasma Physics and Controlled Fusion vol.32 no.9 September 1990 pp.677-702.

238. Subsonic and supersonic divertor solutions
Stangeby P C
Submitted to Plasma Physics and Controlled Fusion (Letter), JET Report - JET-P(90)60.

239. Electron absorption of fast magnetosonic waves by transit time magnetic pumping in JET.
Start D F H Bartlett D V Bhatnagar V P Campbell D J Challis C D Cheetham A D Corti S Edwards A W Eriksson L-G Gill R D Gottardi N A O Hellsten T Jacquinot J J O'Rourke J Mayberry M J Moreau D Rimini F G Salmon N A Smeulders P von Hellermann M
Nuclear Fusion vol.30 no.10 October 1990 pp.2170-2176. (Report JET-P(90)02)

240. Fast ion orbit effects in high power ICRH modulation experiments in the JET tokamak.
Start D F H Evrard M P Bhatnagar V P Bures M
Controlled Fusion and Plasma Heating. 17th EPS Conf., Amsterdam, 25-29 June 1990. Contributed

papers. Geneva, European Physical Society. 1990. pp.III-1019 - III-1022. (Report JET-P(90)14, pp.41-44.)

241. Physics of high power ICRH on JET.
Start D F H Bhatnagar V P Bosia G Boyd D A Mures M Campbell D J Christiansen J P Cordey J G Cottrell G A Devillers G Eriksson L G Evrard M P Heikkinen J A Hellsten T Jacquinot J Jarvis O N Knowlton S Kupschus P Lean H Lomas P J Lowry C Nielsen P O'Rourke J Sadler G Schmidt G L Tanga A Taroni A Thomas P R Thomsen K Tubbing B von Hellermann M Willen U
Radio-frequency power in plasmas. 8th Topical Conf., Irvine, U.S.A., May 1989. New York, American Institute of Physics. 1989. pp.205-213.

242. He^3-D fusion studies and alpha-particle simulations using MeV ions created by ICRH in the JET tokamak.
Start D F H Bhatnagar V P Bures M Campbell D J Christiansen J P Cordey J G Core W G F Cottrell G A Eriksson L-G Hellsten T Jacquinot J Jarvis O N Lallia P Lomas P J Lowry C Nielsen P O'Rourke J Rimini F Sadler G Tanga A Thomas P R Thomsen K Tubbing B van Belle P Wesson J A
Controlled Fusion and Plasma Heating. 17th EPS Conf., Amsterdam, 25-29 June 1990. Contributed papers. Geneva, European Physical Society. 1990. pp.III-1015 - III-1018. (Report JET-P(90)14, pp.1-4.)

243. ICRF heating in reactor grade plasmas
Start D F H and the JET Team
Nuclear Fusion Supplement (13th IAEA Conference on Plasma Physics and Controlled Nuclear Fusion Research, Washington, U.S.A., 1-5 October 1990, IAEA-CN-53/E-2-1-1), JET Report - JET-P(90)62, pp.107-118.

244. Systematics of density increase and recycling behaviour in JET H-modes.
Stork D Jones T T C Clement S Morgan P D Reichle R Saibene G Sartori R Summers D D R Tagle T
Journal of Nuclear Materials, 176 & 177, pp.409-417. Joint European Torus (JET). 1990. (JET papers presented at 9th Int. Conf. on Plasma Surface Interactions and Controlled Fusion Devices, Bournemouth, 21-25 May 1990). pp.135-154. Report JET-P(90)41-I

245. Neutral beam heating and current drive systems
Stork D
Submitted to Fusion Engineering and Design. Invited Paper at 16th Symposium on Fusion Technology (London, U.K., 3-7 September 1990), JET Report - JET-P(90)63.

246. Diagnostics for experimental fusion reactors.
Stott P E Costley A E
Tritium and Advanced Fuels in Fusion Reactors. Course and Workshop, Varenna, 6-15 September 1989. Bologna, for Societa Italiana di Fisica by Editrice Compositori, 1990. pp.385-406.

247. Recent results from JET.
Stott P E
Bulletin of the American Physical Society vol.35 no.9 October 1990 (Program of the 32nd Annual Meeting of the Division of Plasma Physics, Cincinnati, Ohio, 12-16 November 1990). (Selected abstracts). p.1992, Paper 4I5, and JET Report - JET-P(90)74.

248. Present status and future developments of JET diagnostics
Stott P E
Fifth National Meeting on High Temperature Diagnostics, Minsk, USSR, 18-22 June 1990, and JET Report - JET-P(90)72, 17p.

249. Neutron calibration techniques for comparison of tokamak results.
Strachan J D and others including Jarvis O N (JET)
Review of Scientific Instruments vol.61 no.11 November 1990 p.3501.

250. Experimental evidence on fluctuations and transport in tokamaks.
Stringer T E
Joint European Torus JET. April 1990. 46p.
Report JET-P(90)15 Submitted to Nuclear Fusion.

251. Inclusion of poloidal potential variation in neoclassical transport.
Stringer T E
Joint European Torus JET. 1990. 25p.
Report JET-P(90)29

252. Extrapolation of the high performance JETplasmas to D-T operation.
Stubberfield P M Balet B Cordey J G
Submitted to Plasma Physics and Controlled Fusion. JET Report JET-P(90)47. 52p.

253. Measurement of the temperature dependence of carbon and beryllium fluxes in the JET boundary plasma using a high heat-flux probe.
Summers D D R Erents S K Hugon M Hwang A Rebut P-H Reichle R Stamp M F Stangeby P C
Journal of Nuclear Materials, 176 & 177, pp.593-599. Joint European Torus (JET). 1990. (JET papers presented at 9th Int. Conf. on Plasma Surface Interactions and Controlled Fusion Devices, Bournemouth, 21-25 May 1990). pp.209-223.
Report JET-P(90)41-II

254. The characteristics of neutral and near neutral atom emission at plasma boundaries and their diagnostic exploitation - a theoretical view.
Summers H P Stamp M F
Joint European Torus (JET). 1990. (JET papers presented at 9th Int. Conf. on Plasma Surface Interactions and Controlled Fusion Devices, Bournemouth, 21-25 May 1990). pp.341-360.
Report JET-P(90)41-II

256. Atomic spectroscopy in highly ionised plasmas
Summers H P Thomas P Giannella R
von Hellermann M Dickson W Lawson K Mandl W Briden P and members of Experimental Division II, JET
Submitted to Zeitschrift fur Physik, September 1990.
JET Report JET-P(90)20.

257. Atomic data for fusion
Summers H P Thomas P Giannella R
von Helermann M
Submitted to Journal de Physique (Colloque), November 1990. JET Report JET-P(90)54.

258. Fast ion cyclotron wave heating and current drive system for ITER.
Swain D W Batchelor D B Jaeger E F Jacquinot J Bhatnagar V
Bulletin of the American Physical Society vol.35 no.9 October 1990 (Program of the 32nd Annual Meeting of the Division of Plasma Physics, Cincinnati, Ohio, 12-16 November 1990). (Selected abstracts). p.1923, Paper 1P26.

259. Electric field and radial transport during ICRF heating in the edge plasma of JET.
Tagle J A Maux M Clement S Erents S K (Culham) Brinkschulte H Bures M De Kock L
Fusion Engineering and Design (Procs. IAEA Technical Committee Meeting on ICRH/Edge Physics, Garching, 2-5 October 1989) vol.12 nos.1&2 April 1990 pp.217-222.

260. The compatibility of the JET H-mode with other regimes of improved performance.
Tanga A Balet B Bartlett D V Gottardi N Gowers C Harbour P J Jacquinot J Johnson M F Lazzaro E Morgan P Porcelli F Sack H C Schmidt G Stork D Thomsen K Tubbing B J Weisen H
Controlled Fusion and Plasma Heating. 17th EPS Conf., Amsterdam, 25-29 June 1990. Contributed papers. Geneva, European Physical Society. 1990. pp.I-259 - I-262. (Report JET-P(90)14, pp.113-116.)

261. The control of plasma parameters to avoid high current disruptions in JET.
Tanga A Lowry C Lomas P Garribba M Johnson M F Noll P Tubbing B
Fusion Engineering. IEEE 13th Symp., Knoxville, 2-6 October 1989. New York, IEEE. 1990. pp.1271-1273.

262. High performance H-modes in JET
Tanga A and the JET Team
Nuclear Fusion Supplement (13th IAEA Conference on Plasma Physics and Controlled Nuclear Fusion Research, Washington, U.S.A., 1-5 October 1990, IAEA-CN-53/A-4-1), JET Report - JET-P(90)62, pp.41-58.

263. Interpretation and modelling of energy and particle transport in JET
Taroni A Tibone F Balet B Boucher D Christiansen J P Cordey J G Corrigan G C Düchs D F Giannella R Gondhalekar A Gottardi N Hogeweij G M D Lauro-Taroni L Lawson K Mattioli M Muir D O'Rourke J Pasini D Rebut P H Sack C Sips G Springmann E Stringer T E Stubberfield P Thomsen K Watkins M L Weisen H
Nuclear Fusion Supplement (13th IAEA Conference on Plasma Physics and Controlled Nuclear Fusion Research, Washington, U.S.A., 1-5 October 1990, IAEA-CN-53/A-2-1), JET Report - JET-P(90)62, pp.59-68.

264. Tritium contamination studies involving test materials and JET remote handling tools.
Tesini A Jalbert R
Fusion Engineering. IEEE 13th Symp., Knoxville, 2-6 October 1989. New York, IEEE. 1990. pp.713-715.

265. Results of JET operation with beryllium.
Thomas P R and the JET Team
Journal of Nuclear Materials, 176 & 177, pp.3-13.
Joint European Torus (JET). 1990. (JET papers presented at 9th Int. Conf. on Plasma Surface Interactions and Controlled Fusion Devices, Bournemouth, 21-25 May 1990). p.1-23.
Report JET-P(90)41-I

266. Comparison of beryllium and graphite first-walls in JET
Thomas P R and the JET Team
Nuclear Fusion Supplement (13th IAEA Conference on Plasma Physics and Controlled Nuclear Fusion Research, Washington, U.S.A., 1-5 October 1990, IAEA-CN-53/A-5-3), JET Report - JET-P(90)62, pp.97-106.

267. Dimensionally correct scaling laws for local thermal transport in JET discharges.
Thomsen K Christiansen J P Cordey J G Muir D G
Bulletin of the American Physical Society vol.35 no.9 October 1990 (Program of the 32nd Annual Meeting of the Division of Plasma Physics, Cincinnati, Ohio,

12-16 November 1990). (Selected abstracts). p.1922, Paper 1P14.

268. A quantitative assessment of ∇T_i driven turbulence theory based on JET experimental data.
Tibone F Corrigan G Stringer T E
Controlled Fusion and Plasma Heating. 17th EPS Conf., Amsterdam, 25-29 June 1990. Contributed papers. Geneva, European Physical Society. 1990. pp.II-805 - II-808. (Report JET-P(90)14, pp.145-148.)

269. H-mode energy confinement scaling from the DIII-D and JET tokamaks.
Tubbing B J D Thomsen K Cordey J G Keilhacker M Stork D Stott P E Tanga A and the DIII-D Team
Bulletin of the American Physical Society vol.35 no.9 October 1990 (Program of the 32nd Annual Meeting of the Division of Plasma Physics, Cincinnati, Ohio, 12-16 November 1990). (Selected abstracts). p.2023, Paper 5F3. (Report JET-P(90)16)

270. H-mode confinement in JET with enhanced performance by pellet-peaked density profiles
Tubbing B J D Balet B Bartlett D V Challis C D Corti S Gill R D Gormezano C Gowers C von Hellermann M Hugon M Jacquinot J J Jaeckel H Kupschus P Lawson K Morsi H O'Rourke J Pasini D Rimini F Sadler G Schmidt G L Start D Stubberfield P Tanga A Tibone F
Submitted to Nuclear Fusion, and JET Report - JET-P(90)67, 24p.

271. Experimental set-up for gas balance measurement at JET.
Usselmann E Hemmerich J L Holland D Grobusch L Schargitz U Sartori R Saibene G
Vacuum vol.41 nos.4-6 1990 (Special Issue: Selected Procs. of 11th Int. Vacuum Congress (IVC-11) 7th Int. Conf. on Solid Surfaces (ICSS-7), Cologne, FRG, 25-29 September 1989). pp.1515-1518.

272. Level 1 software at JET: A global tool for physics operation.
van der Beken H Green B J Steed C A Farthing J W McCullen P A How J
Fusion Engineering. IEEE 13th Symp., Knoxville, 2-6 October 1989. New York, IEEE. 1990. pp.201-204.

273. Calibration of the JET neutron yield monitors using the delayed neutron counting technique
van Belle P Jarvis O N Sadler G De Leeuw S D'Hondt P Pillon M
Paper presented at the 8th Topical Conference on High-Temperature Plasma Diagnostics, Hyannis, Massachusetts, 6-10 May 1990
(JET Report JET-P(90)19) pp.74-83

274. Real time diagnostic data acquisition and plasma control using transputers
van der Goot E Edwards A W Ellis J O'Brien D
16th Symposium on Fusion Technology, London, UK, 3-7 September 1990. JET Report JET-P(90)56 - Volume I, pp.97-102.

275. JET high current disruptive pulses (I_p^{max} greater than or equal to 5 MA).
Vannucci A Gill R D
Joint European Torus JET. 1990.
Report JET-P(90)30

276. Visible charge exchange spectroscopy at JET.
von Hellermann M G Mandl W Summers H P Weisen H Boileau A Morgan P D Morsi H Koenig R Stamp M F Wolf R
Review of Scientific Instruments vol.61 no.11 November 1990 pp.3479-3486. (Report JET-P(90)31)

277. Investigation of Thermal and Slowing-Down Alpha Particles on JET using Charge Exchange Spectroscopy
von Hellermann M Mandl W Summers H P Boileau A Frieling J
Submitted to Plasma Physics and Controlled Fusion, JET Report - JET-P(90)59 24p.

278. Charge exchange spectroscopy measurements of light impurity behaviour in the JET beryllium phase.
Weisen H von Hellermann M Pasini D Morgan P D Mandl W Stamp M F Summers H P
JET Papers contributed to 17th EPS Conf. on Controlled Fusion and Plasma Heating, Amsterdam, 25-29 June 1990. Joint European Torus JET, 1990. pp.81-84.
Report JET-P(90)14

279. High ion temperature in the edge of JET H- and L-mode plasmas.
Weisen H Campbell D Erents S K de Kock L O'Brien D Tanga A Stamp M Thomas P von Hellermann M Zhu J
Bulletin of the American Physical Society vol.35 no.9 October 1990 (Program of the 32nd Annual Meeting of the Division of Plasma Physics, Cincinnati, Ohio, 12-16 November 1990). (Selected abstracts). p.1999, Paper 4P24.

280. Measurement of light impurity densities and Z_{eff} in JET using X-ray tomography.
Weisen H Pasini D Weller A Edwards A W
Joint European Torus (JET). August 1990.
Report JET-P(90)36 Preprint of a paper submitted to Nuclear Fusion.

281. Negative voltage spike in tokamak disruptions.
Wesson J A Ward D J Rosenbluth M N
Nuclear Fusion vol.30 no.6 June 1990 pp.1011-1014.

282. On sawtooth reconnection.
Wesson J A
Joint European Torus JET. 1990. 7p.
Report JET-P(90)27

283. Spontaneous m=1 instability in JET sawtooth collapse.
Wesson J A Edwards A W Granetz R S
Joint European Torus JET. January 1990. 10p.
Report JET-P(90)03
Submitted to Physics Review Letters.

284. Sawtooth reconnection
Wesson J A
Nuclear Fusion Supplement (13th IAEA Conference on Plasma Physics and Controlled Nuclear Fusion Research, Washington, U.S.A., 1-5 October 1990, Post-Deadline Paper), JET Report - JET-P(90)62, pp.145-152.

285. Development of interface for remote mass spectrometer
Winkel T Uselmann E Steed A Ferrari S Ziveri A
16th Symposium on Fusion Technology, London, UK, 3-7 September 1990. JET Report JET-P(90)56 - Volume I, pp.25-30.

286. The detailed topology for the m=1 instability in the JET sawtooth collapse.
Wolfe S W Edwards A W Gill R D Nave M F F Wesson J A
Controlled Fusion and Plasma Heating. 17th EPS Conf., Amsterdam, 25-29 June 1990. Contributed papers. Geneva, European Physical Society. 1990. pp.I-335 - I-338. (Report JET-P(90)14, pp.93-96.)

287. Safety analysis of potential loss of vacuum incident in JET.
Wykes M E P
Fusion Engineering. IEEE 13th Symp., Knoxville, 2-6 October 1989. New York, IEEE. 1990. pp.312-315.
Physics vol.41 no.3 I February 1990 pp.1427-1434.

288. Safety analysis of potential graphite oxidation effects in JET
Wykes M E P Deksnis E B Caldwell-Nichols C J
16th Symposium on Fusion Technology, London, UK, 3-7 September 1990. JET Report JET-P(90)56 - Volume II, pp.139-144.

289. Scalings for tokamak energy confinement.
Yushman P N Takizuka T Riedel K S Kardaun O J W F Cordey J G Kaye S M Post D E
Nuclear Fusion vol.30 no.10 October 1990 p.1999-2006.

290. Measurement and comparison with theory of the temperature dependence of satellite-to-resonance line ratios of heliumlike nickel from the JET tokamak.
Zastrow K-D Kallne E Summers H P
Physical Review A: Atomic, Molecular and Optical

291. Deduction of central plasma parameters from line-of sight average spectroscopic observations
Zastrow K D Moris H W Danielsson M von Hellermann M G Källne E Konig R Mandl W Summers H P
Plasma Physics and Controlled Nuclear Fusion (JET Report JET-P(90)18)

292. JET Annual Report 1989. JET Joint Undertaking, June 1990.
Edited by B.E.Keen and G.W.O'Hara.
EUR 12807 EN,(EUR-JET-AR12).

293. JET Progress Report 1989. JET Joint Undertaking, March 1990. 2 vols.
Edited and compiled by B.E.Keen.
EUR 12808 EN, (EUR-JET-PR7).